CONF-771053

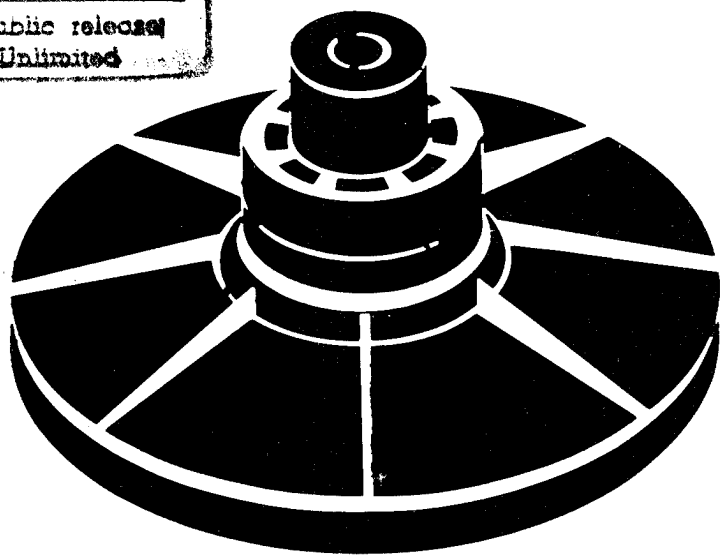
Add
425407 -
425424

1977 FLYWHEEL TECHNOLOGY SYMPOSIUM PROCEEDINGS

October 5-7, 1977
San Francisco, California

DISTRIBUTION STATEMENT A
Approved for public release;
Distribution Unlimited

DTIC
ELECTE
DEC 1 2 1995
F



Co-Sponsored By
U.S. DEPARTMENT OF ENERGY
Assistant Secretary for Energy Technology
Division of Energy Storage Systems

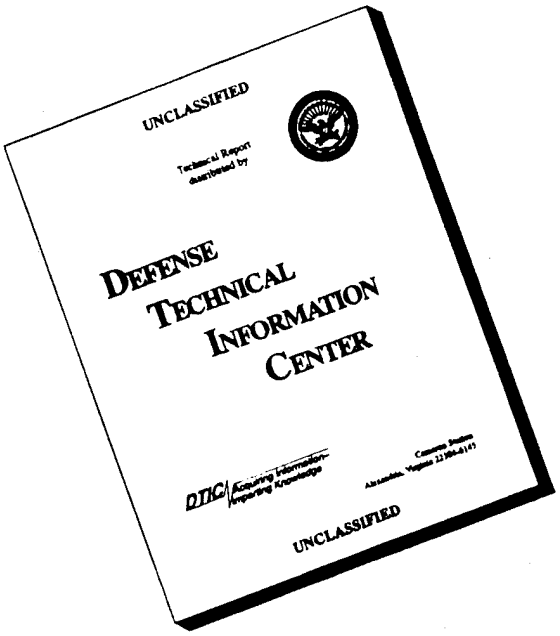
March 1978

19951128 163

DTIC QUALITY INSPECTED 5

UNCLASSIFIED
Standard Distribution

DISCLAIMER NOTICE



THIS DOCUMENT IS BEST QUALITY AVAILABLE. THE COPY FURNISHED TO DTIC CONTAINED A SIGNIFICANT NUMBER OF PAGES WHICH DO NOT REPRODUCE LEGIBLY.

CONF-771053
UC-94b, 96

1977 Flywheel Technology Symposium Proceedings

October 5-7, 1977
San Francisco, California

Accession For
NTIS GRA&I ☑
DTIC TAB ☐
Unannounced ☐
Justification
By
Distribution/
Availability Codes
Dist | Avail and/or Special
A-1

Co-Sponsored By
U.S. DEPARTMENT OF ENERGY
Assistant Secretary for Energy Technology
Division of Energy Storage Systems
Washington, DC 20545

March 1978

PROCEEDINGS

1977 FLYWHEEL TECHNOLOGY SYMPOSIUM

Co-Chairmen and Editors

G. C. Chang - U.S. Department of Energy
R. G. Stone - Lawrence Livermore Laboratory

Symposium Steering Committee

K. F. Barber - U.S. Department of Energy
J. F. Campbell - U.S. Department of Transportation
T. T. Chiao - Lawrence Livermore Laboratory
A. A. Frank - University of Wisconsin
E. L. Lustenader - General Electric Company
T. A. Norman - U.S. Postal Service
D. W. Rabenhorst - Applied Physics Laboratory
A. E. Raynard - Garrett AiResearch Manufacturing Co.

Sponsors

U. S. Department of Energy
U. S. Postal Service
U. S. Department of Transportation
Lawrence Livermore Laboratory

SAN FRANCISCO, CALIFORNIA
OCTOBER 5-7, 1977

TABLE OF CONTENTS

Page

PREFACE vii

WELCOME - A. Holzer 1

OVERVIEW OF FLYWHEEL DEVELOPMENT PROGRAM:

DEPARTMENT OF ENERGY'S FLYWHEEL PROGRAM 3
G. C. Chang, J. H. Swisher, and G. F. Pezdirtz

U.S. POSTAL SERVICE ELECTRIC FLYWHEEL VEHICLE 9
T. A. Norman

UMTA FLYWHEEL ENERGY STORAGE PROGRAM 13
J. F. Campbell

FLYWHEEL TECHNOLOGY PROGRAM IN THE NETHERLANDS 19
M. vanZanten

FLYWHEEL PROGRAMS IN OTHER COUNTRIES 27
D. W. Rabenhorst

SYSTEMS DEVELOPMENT PROJECTS

FLYWHEEL-CONTINUOUSLY VARIABLE TRANSMISSION SYSTEMS FOR AUTOMOTIVE AND TRANSIT PROPULSION SYSTEMS 39
A. A. Frank, N. H. Beachley, R. Harter, A. Dietrich, D. Stockman and K. Lau

FLYWHEEL ENERGY STORAGE SYSTEM DEVELOPMENT 47
E. L. Lustenader

ROCKETDYNE'S HIGH-ENERGY-STORAGE FLYWHEEL MODULE FOR THE U.S. ARMY . . . 55
D. Davis, D. Hodson and C. Heise

AN ADVANCED VEHICULAR FLYWHEEL SYSTEM FOR THE ERDA ELECTRIC POWERED PASSENGER VEHICLE 63
D. A. Towgood

AN ADVANCED ENERGY STORAGE UNIT FOR A U.S. POSTAL SERVICE DELIVERY VEHICLE 69
D. L. Satchwell

THE HIGH-ENERGY "FLYDRAULIC" ACCUMULATOR WITH HYDRO-COMPUTER MODULATED OUTPUT 75
R. C. Clerk

FLYWHEEL ROTORS - ANALYSIS

A COMPUTERIZED ANALYSIS OF AXISYMMETRIC FLYWHEELS 89
N. L. Newhouse

DESIGN OF SPOKED-RIM COMPOSITE FLYWHEELS 99344 99
E. D. Reedy, Jr. and F. P. Gerstle, Jr.

TABLE OF CONTENTS (Cont'd.)

Page

FLYWHEEL ROTORS - ANALYSIS (Cont'd.)

OPTIMIZATION OF HOOP/DISK COMPOSITE FLYWHEEL ROTOR DESIGNS 111
B. P. Gupta and A. F. Lewis

ON THE STRESS STATE IN QUASI-CIRCULAR BARE FILAMENT FLYWHEELS 119
G. Belingardi and G. Genta

OPTIMAL DESIGN OF ANISOTROPIC (FIBER REINFORCED) FLYWHEELS 127
R. M. Christensen and E. M. Wu

ANALYSIS OF THE DELTAWRAP FLYWHEEL DESIGN 131
C. E. Knight, Jr.

FLYWHEEL ROTORS - DEVELOPMENT

DEVELOPMENT OF THE "BANDWRAP" FLYWHEEL . . . . . 29345 . . . 137
C. E. Knight, Jr., J. J. Kelly, R. L. Huddleston and
R. E. Pollard

COMPOSITE FLYWHEEL ROTOR/HUB ATTACHMENT THROUGH ELASTOMERIC INTERLAYERS . . . . . 29346 . 155
D. P. McGuire and D. W. Rabenhorst

TENSION-BALANCED SPOKES FOR FIBER-COMPOSITE FLYWHEEL RIMS 161
F. C. Younger

THE PRESTRESSED LAMINATED FLYWHEEL AND ITS HYDROVAC AMBIENCE 167
R. C. Clerk

ALPHA-CROSS-PLY COMPOSITE FLYWHEEL DEVELOPMENT 181
B. D. Hatch

PRESTRESSED THICK FLYWHEEL RIMS . . . . . 29347 . 183
C. E. Knight, Jr. and R. E. Pollard

SYSTEMS APPLICATIONS AND ANALYSIS

FLYWHEEL PROPULSION FOR URBAN TRANSIT BUSES 193
L. J. Lawson

THE DESIGN OF A WIND ENERGY STORAGE SYSTEM WITH A CELLULOSIC FLYWHEEL . . 201
A. G. Erdman, D. A. Frohrib, T. P. Carlson, D. L. Hagen and
W. L. Garrard

UTILIZATION OF FLYWHEELS FOR THE EVOLUTION OF HIGH PERFORMANCE ELECTRIC VEHICLES 213
L. G. O'Connell, J. F. Cooper, A. B. Miller and H. W. Newkirk

HIGH SPEED FLYWHEELS OPERATING ON "ONE ACTIVE AXIS" MAGNETIC BEARINGS. 229
P. C. Poubeau

DESIGN DEFINITION OF A MECHANICAL CAPACITOR 241
E. W. Schlieben, R. D. Scott and T. D. Michaelis

TABLE OF CONTENTS (Cont'd.)

Page

SYSTEMS APPLICATIONS AND ANALYSIS (Cont'd.)

A FLEXIBLE FLYWHEEL CONCEPT. 249
J. M. Vance, E. H. Holtzclaw and R. T. Schneider

SPIN TESTING AND MATERIAL FAILURE MODES

SPIN TEST AND EVALUATION OF UCC-ND'S BAND-WRAP FLYWHEEL 259
J. J. Kelly

DESIGN, INSTRUMENTATION AND CALIBRATION OF AN EXPERIMENTAL FLYWHEEL CONTAINMENT ASSEMBLY 261
J. J. Kelly

FLYWHEEL DEVELOPMENT FOR THE ELECTRIC POWER RESEARCH INSTITUTE 263
W. M. Brobeck

FAILURE CHARACTERISTICS OF COMPOSITE FLYWHEELS 271
D. W. Oplinger and J. M. Slepetz

FAILURE MODES OF BI-DIRECTIONALLY REINFORCED FLYWHEELS 281
D. E. Johnson and D. W. Oplinger

PREDICTION OF CREEP BEHAVIOR FOR FILAMENTARY COMPOSITES UNDER STRESS CONDITIONS ENCOUNTERED IN FLYWHEELS 291
C. W. Bert and T. L. C. Chen

FLYWHEEL ROTORS - DEVELOPMENT (Cont'd.) and INPUT/OUTPUT SYSTEMS

CONSTANT RADIAL DISPLACEMENT, THICK WALL, FILAMENT WOUND FLYWHEELS . . 299
R. Z. Naar, R. A. Panora, Jr. and B. M. Halpin

SANDIA BASIC FLYWHEEL TECHNOLOGY STUDIES 315
R. O. Woods and F. P. Gerstle, Jr.

ADVANCED ELECTRICAL CONVERSION SYSTEMS FOR FLYWHEEL APPLICATIONS . . . 323
D. Eisenhaure, S. O'Dea and W. Stanton

AN ULTRA-WIDE RANGE HIGH EFFICIENCY HYDRAULIC PUMP/MOTOR POWER TRANSMISSION 331
R. C. Clerk

PROPERTIES OF MATERIALS

ROTOR DESIGN IMPLICATIONS FOR COMPOSITE MATERIAL PROPERTIES 345
R. H. Toland

EPOXY MATRICES FOR FILAMENT-WOUND FLYWHEELS 351
J. A. Rinde, E. T. Mones and T. T. Chiao

TRANSVERSE TENSILE CHARACTERISTICS OF FIBER COMPOSITES USING FLEXIBLE RESINS 355
R. M. Christensen, J. A. Rinde and E. T. Mones

COMPARATIVE PROPERTIES OF FIBER COMPOSITES FOR ENERGY-STORAGE FLYWHEELS. PART A: EVALUATION OF FIBERS FOR FLYWHEEL ROTORS 357
L. S. Penn

TABLE OF CONTENTS (Cont'd.)

Page

PROPERTIES OF MATERIALS (Cont'd.)

COMPARATIVE PROPERTIES OF FIBER COMPOSITES FOR ENERGY STORAGE FLYWHEELS. PART B: ENGINEERING PROPERTIES OF COMPOSITES . . . 29356 363
L. L. Clements

TIME-DEPENDENT PROPERTIES OF FIBER COMPOSITES FOR ENERGY-STORAGE FLYWHEELS 373
E. M. Wu and L. S. Penn

IMPROVED PERFORMANCE FOR HOOP-WOUND COMPOSITE FLYWHEEL ROTORS . 29357 377
R. E. Allred, R. F. Foral and W. E. Dick

BIBLIOGRAPHIC AND NUMERIC DATA BASES FOR FIBER COMPOSITES AND MATRIX MATERIALS 393
F. E. McMurphy and T. M. Quick

GLASS FIBER FOR ENERGY STORAGE FLYWHEELS . . . . . 29358 . . 403
S. N. Loud

THE PROPERTIES OF NATURAL CELLULOSIC MATERIALS PERTAINING TO FLYWHEEL KINETIC ENERGY STORAGE APPLICATIONS . . . . . 29359 . . 409
D. L. Hagen

ROTOR DYNAMICS AND ANALYSIS

CRITICAL SPEED FOR STANDING-WAVE INSTABILITY IN A FILAMENT-WOUND-COMPOSITE RING-TYPE FLYWHEEL 429
C. W. Bert

INFLUENCE OF BEARING STIFFNESS ON FLYWHEEL-ROTOR SYSTEM 435
J. S. Hickey

OVALIZATION CRITICAL SPEEDS IN ANISOTROPIC ROTATING DISKS 441
G. Belingardi, G. Genta and M. Gola

EFFECT OF HUB TO RIM STIFFNESS ON SPIN-WHIRL DYNAMICS OF PENDULOUS ROTORS 449
C. N. McKinnon, Jr.

ADVANCED FLYWHEEL DEVELOPMENT . . . . . 29360 . . 451
P. W. Hill, A. A. Vicario, T. C. White and T. L. Waltz

THE VARIABLE INERTIA FLYWHEEL (VIF), AN INTRODUCTION TO ITS POTENTIAL . . 463
D. G. Ullman and H. R. Velkoff

DESIGN SYNTHESIS AS APPLIED TO COMPOSITE FLYWHEELS 471
M. Vagins

PANEL DISCUSSION

A SUMMARY OF THE TECHNICAL TRENDS VERSUS R&D NEEDS 483
L. J. Lawson

TABLE OF CONTENTS (Cont'd.)

Page

PANEL DISCUSSION (Cont'd.)

OUTLINE OF AREAS IN WHICH INDUSTRY CAN ACT TO ADVANCE FLYWHEEL TECHNOLOGY 484
D. E. Davis

WAYS IN WHICH GOVERNMENT AGENCIES CAN ACT TO ADVANCE FLYWHEEL TECHNOLOGY 486
R. Taylor

THE BEST MEANS FOR COMMERCIALIZING FLYWHEELS 487
D. R. Phelps

LIST OF ATTENDEES 489

PREFACE

The 1977 Flywheel Technology Symposium brought together 150 of the leaders in the technology of flywheel energy storage systems from 10 countries representing industry, universities, and government.

The objectives of the three-day conference were twofold:

- To provide a forum for the exchange of information and stimulate ideas on the state of the art, new flywheel applications, and research needs of this energy storage technology.

- To offer an educational seminar for interested people to bring themselves up to date in the area of flywheels and their energy saving applications.

To some extent this was an update of the 1975 Flywheel Technology Symposium: Proposed ideas have been analyzed; selected materials have been evaluated; promising designs have been built and tested; and some systems under study have been operated and evaluated. In addition, many new ideas, analyses and proposals were presented.

The general progress of flywheel energy storage systems development over the past two years has been very impressive. The technology has evolved from fundamental investigations and coupon tests to high performance flywheel assembly development. Cost-sharing participation has been developed effectively to join and expand the programs of industry, universities and government. International technical interest in flywheels has also shown a significant increase. As the implementation process becomes imminent, funding requirements become more severe and competition with other energy storage technologies becomes more exacting. Progress during the next two or three years is expected to be most critical for successful introduction of flywheel technology to the vehicle industry.

These Proceedings have been reproduced from the best available copy. When papers were unavailable, the abstract as submitted earlier by the author has been included. For convenience, the papers are in the sequence of the printed symposium program, although a few sequence changes were made during the meeting.

G. C. Chang

R. G. Stone

WELCOME ADDRESS

Given By

Alfred Holzer
University of California
Lawrence Livermore Laboratory
Livermore, California

I would like to welcome you on behalf of the Lawrence Livermore Laboratory to the Second Flywheel Technology Symposium. I'm particularly glad to have this opportunity because I am personally extremely interested in both the technology and its application. To me it seems a very promising way to help alleviate our growing shortage of liquid petroleum for transportation.

I am sure many of you attended the first symposium held in Berkeley almost two years ago, where Dr. Street extended his welcome to you. At that time he remarked that he hoped the symposium would be the first of many to come. In looking over the abstracts for our present meeting, and having watched - and in some small way participated in - the developments of the past two years, I am convinced that this meeting will become a regular feature.

It strikes me that flywheels have some very important things going for them. We have here an exciting, developing technology - combining mechanical design, novel materials, unconventional fabrication procedures, and the opportunity for integration into a system with very early use. We also have a broad base of government interest providing impetus, and it is being enthusiastically and agressively implemented. I think we will see the results in this meeting.

This also gives me the opportunity to express my own thanks -- which I am sure you will share -- to Dick Stone, George Chang, and the others who have worked hard to put this symposium together. It also allows me the occasion to invite you to visit us at the Lawrence Livermore Laboratory to see what we are doing and to discuss mutual interests in more detail.

It is now time to get down to business. I hope your stay here will be profitable and enjoyable. I know mine will.

DOE'S FLYWHEEL PROGRAM

George C. Chang, James H. Swisher, and George F. Pezdirtz
Division of Energy Storage Systems
Department of Energy
Washington, D. C. 20545

INTRODUCTION

As the spokesman for the DOE Energy Storage Systems Division, I welcome all of you to the 1977 Flywheel Technology Symposium. The fact that we are here today holding a second meeting on the subject of flywheels, with international participation, is a good indication that you join me in the belief that flywheel technology is an important research and development activity. I fully expect that the papers presented here in the next three days and the discussion that will take place among the Symposium participants will prove to be mutually beneficial in achieving our individual and collective goals in the field of flywheel technology.

The basic purposes of this conference, like the first one in 1975, are to once again review the current state of the art in flywheel technology, and to facilitate technical exchanges among interested parties. We will be presenting DOE's progress and plans, and other govenment agencies and organizations in the private sector will be providing insights into their activities. The Conference should give us a good overall perspective and an opportunity to see how well the pieces fit together. We anticipate that the exposure and publicity brought about by this process will stimulate more industrial participation in the growing field of flywheel technology and will provide useful inputs to us at DOE as to desirable future roles for government involvement.

The first symposium in 1975 was, in fact, the formal announcement of ERDA's intention to pursue the development of flywheels for energy storage purposes. In my overview today, I will review where we were at that time. We will also talk about our goals and objectives for the flywheel program. Next, I will briefly summarize what ERDA accomplished since then, both at the ERDA laboratories and by our other contractors. Finally, I will discuss DOE's plans for the future as we see them now.

STATUS IN 1975

The people who attended the 1975 symposium were among the most knowledgeable individuals in this country, and maybe in the world, about the status of the development and application of flywheels at that time. Thus, we had a rare opportunity to get a clear picture of flywheel technology as of that moment. The papers presented at the first symposium discussed progress in testing of new designs for flywheels; the properties of materials in flywheels; the selection of flywheel design criteria; and how flywheels could be fit into the total environment through system considerations. Some of the users of the products containing flywheels which were then entering the market also provided comments. As you can see looking back, there was little cohesiveness in the work being done by independent researchers at that time.

The Rockwell Report (ERDA 76-65), which was done for ERDA was, you will recall, presented at the 1975 symposium; it was used in part in establishing ERDA's immediate and long-range goals and objectives for flywheel technology development effort. This was our first attempt to determine where the greatest needs were and what were the most practical approaches to meeting them.

Some of the report's conclusions were:

a. Flywheel energy storage systems (FESS) can be considered as feasible options for conserving energy resources in the transportation and utility sectors.

b. Costs will dominate technical considerations in determining feasible applications.

c. Development of composite rotors with densities of 40 to 60 Wh/lb should be carried out for both transportation and utility applications.

d. Safety of composite rotors should not be a problem.

e. FESS is practical but not cost-effective at current relative price levels for either residential, commercial or industrial applications.

Findings of this report and internal discussions at ERDA prompted us to focus our attention mainly on: 1) applications in the transportation sector, 2) the development of composite rotors, and 3) a search for means of reducing production costs in order to make flywheels cost-competitive with other storage devices. It goes without saying that budgetary considerations are always important in our planning but at least we had a sense of where program emphasis should be placed.

FLYWHEEL OBJECTIVES

The objectives of the flywheel program which were established after the first conference were intended to support ERDA's (and now DOE's) national objectives, as well as the more definitive objectives of the Energy Storage Systems Division.

The main objective today continues to be to provide safe and economical flywheel systems for transportation (electric and hybrid vehicles) and for stationary applications (initially wind energy storage and household electricity storage). To attain this objective, we need to develop composite rotors, advanced bearings, improved flywheel dynamics, and better input/output systems. Specific goals are 1) to achieve 70 percent storage efficiency, 2) to reduce system weight by one-half or more as measured against 1975 technology, 3) to improve rotor energy density from current values of 3 to 14 Wh/lb to 20 Wh/lb by 1980 and 40 Wh/lb by 1985, and 4) to reduce costs to $150/kWh for large units and to less than $800 for regenerative flywheels.

ACTIVITIES FROM 1975 to 1977

By the end of 1975, we had obtained initial funding to begin work on flywheel technology development for energy storage components. In early 1976, programs were begun to develop regenerative hybrid systems with flywheels combined with electric motors and heat engines, as well as an all-flywheel power pack for test purposes. The bulk of our work was clearly concerned with advanced component technology development.

In September 1976, 36 organizations attended a conference and participated in discussions of the status of hybrid cars and the R&D requirements for the future. Three prototype vehicles were displayed and demonstrated at the meeting in Albuquerque, New Mexico. Thus, the Energy Storage Systems Division began and is continuing in cooperative efforts with the DOE Transportation Energy Conservation Division in fulfilling the requirements of the Electric and Hybrid Vehicle Research, Development, and Demonstration Act of 1976.

During the first half of FY 1976, we planned to concentrate on determining the technical and economic feasibility of advanced systems for near-term applications and on developing high performance rotor technology. In particular, we planned to evaluate advanced fiber composites as the basis for developing rotors for practical applications. Rotor design was to be undertaken with fabrication and testing beginning in FY 1977. Some of the specific activities planned were:

- Select two composite rotor materials for further development in late 1976.
- Begin development of advanced concepts, input-out devices and advanced bearings in late 1977.
- Sponsor another state-of-the-art symposium in July 1977.
- Complete development of a prototype flywheel assembly for evaluation in postal jeeps by January 1978.
- Deliver industry-produced flywheel/inductor motor assembly by December 1977.

Obviously we missed the planned symposium date in July of this year, but not by much. October is probably a better time for such a meeting anyway. It will be interesting to see from the following presentations how close we came to other milestones. I feel safe in saying that overall we are making good progress in meeting our goals on schedule.

In 1976 and 1977, several contract awards were made. Our industrial contractors began hardware work on flywheel packages, while component technology work continued. Along with this, we continued to look for specific applications for

flywheels in the residential, commercial and industrial sectors because energy price changes could easily shift the cost-effectiveness balance.

The budget for FY 1975 through 1978 gives an indication of the level of effort of DOE involvement with flywheel technology development.

Fiscal Year	Total Outlays
1975	$110,000
1976	590,000
1976 Transition Quarter	225,000
1977	1,100,000 + 1,400,000*
1978	Approx.3,000,000 Total (Est.)

As I mentioned previously, the Division of Energy Storage Systems accomplishes development of flywheel technology through the DOE National Laboratories and private contractors. Many of the papers that follow will provide detailed information about these projects, however, I would just like to very briefly summarize some of the continuing project activities.

SANDIA LABORATORIES PROGRAM

The Sandia Laboratories' task is to upgrade all of the component technology associated with flywheel energy storage systems. In this respect, it is a generic program rather than one aimed at specific single achievements. Within its assignment, Sandia concentrates on five main areas:

- Bearings
- Input-Output devices
- Seals
- Vacuum Technology
- Composite Rotor development.

Most of the work during the last two years has been concerned with bearings and rotor mechanics. A major accomplishment has been the identification of fabrication and thermal stresses as the limiting factors affecting strength of the rotor. Up till the time of this discovery, it had been assumed that rotor dynamics would be the limiting factor. Sandia found that with high-speed rotation, transverse failure was the primary failure mode and that peripherally wrapped wheels tend to separate radially. This result led to design improvements.

Present plans for work on composite rotors are aimed at materials development to improve the transverse strength. Toward this end, various means of toughening the matrix are being studied. Analysis will be made of phenomena which degrade performance, and promising rotor designs will be fabricated and tested.

In the area of bearings, contracts have been or will be let to study various bearing types: hydrodynamic, passive magnetic, active magnetic, and rolling contact. As we discover potential advances, they will be reflected in design data.

High shaft speeds and vacuum-holding demands place unusual requirements on seal technology which are not met outside of flywheel technology. Sandia will be studying mechanical (friction) seals and ferrofluidic seals to meet this need.

Composite flywheels are particularly susceptible to aerodynamic heating and require "good" vacuums maintainable to near 10^{-4} torr. Particular problems in the vacuum systems which are being addressed at Sandia are:

- Outgassing rates of composite materials and lubricants.
- Vacuum failure sensors and automatic shutdown systems.
- Low-power vacuum pumps, and reliable and mechanically simple vacuum pumps.

It should be pointed out that the bulk of the flywheel work at Sandia is, and will continue to be, performed by outside contractors from industry and universities. The organizations involved include Rockwell, Garrett, Draper Laboratory, LMC Corporation, MTI, and Oklahoma State University.

One application of energy storage devices which has not received adequate attention has been its use with intermittent energy sources. To close this gap, Sandia Labs is conducting a study to identify

*For work directly applicable to meet requirements of the Electric and Hybrid Vehicle Research, Development, and Demonstration Act of 1976.

which combinations of solar energy source, mechanical energy storage and electrical demand appear most promising. If it is justified, hardware will be developed for at least one such system. In the meantime, plans are being made to conduct preliminary systems design with industrial participation.

LLL FLYWHEEL PROGRAM

LLL first became involved in the national flywheel program in February 1975 - shortly after ERDA was created. Their principal interest was and continues to be in the development of a good data base on composites. The goals set for LLL were:

- Provide composite design data that will be useful for many flywheel designs.
- Study prototype manufacturing processes and advanced rotor design.
- Disseminate information related to composite flywheels.
- Notable accomplishments toward achieving these goals can be summarized for each of the three areas:

1. Forty flywheels of different materials were tested to destruction to rank the materials. Kevlar 49/epoxy gave the best performance at moderate cost, whereas E-glass/epoxy gave moderate performance at the lowest cost. Details were published in a report from Livermore in April 1977. (Reference UCRL-79573, 4 and 5.)

2. The merits of various flexible resins were evaluated. Design data describing the effects of stresses in compression, tension and shear on the composites were published. A long-term performance test to establish flywheel life-times under sustained and cyclic loading was started during FY 1977 and will be completed in FY 1978.

3. In the search for good rotor designs, one in particular, the quasi-isotropic composite was found to be attractive. The design concept was described in an LLL publication (Reference: UCRL-79235, UCRL-50033-77-1). In examining various potential applications for flywheels, LLL found practical applications of the flywheel-battery hybrid for automotive use. LLL continues to make this and other information available through publications, symposia, and technical consultation.

As for the future, LLL plans to continue to acquire data on long-term flywheel performance. They are studying a new high-temperature matrix. Emphasis will be given to examining composite properties in vacuum and high temperature environments. As previously noted, they will be verifying some advanced rotor designs.

Consistent with requirements of the Electric and Hybrid Vehicle Research, Development, and Demonstration Act of 1976, LLL is to develop and demonstrate a mechanical energy storage module for use in electric and hybrid vehicles in a time frame consistent with the provisions of the Act. This effort started late in FY 1977 and is expected to continue at least through FY 1982. After establishing specifications for the mechanical energy storage module, the project will evaluate the current state of the art and identify areas requiring concentrated effort. When these have been identified, LLL will award contracts for the research, development and evaluation activities to provide the necessary technology development.

Several study groups have noted the increased range, enhanced performance, and improved battery life which result from the application of a flywheel module. These same groups noted the need for technology development to increase energy storage efficiency and thereby reduce its cost.

Specific tasks to be carried out are in the following areas:

a. Technology validation tests
b. Advanced component evaluation
c. System application assessment
d. Technical management of contracts and in-house activities.

Throughout the course of the project, as the technology is developed and demonstrated in these areas, it will be transferred to the vehicle systems group in the Transportation Energy Conservation Division. The major part of this work will be contracted to industry. Primary emphasis will be given to flywheel energy storage systems although other applicable mechanical energy storage devices, such as pneumatic and hydraulic accumulator systems, will also be investigated.

UNION CARBIDE Y-12 PLANT PROGRAM

The Union Carbide program was started somewhat later than those at the other labs, October 1976 to be exact. This project is directed toward a specific objective - to design, manufacture, and test a composite flywheel energy storage unit to be suitable for braking and load leveling. Emphasis is placed on the development of containment structures to ensure safe and efficient operation of the flywheel assembly.

A configuration for the filamentary composite flywheel rotor has been selected. Fabrication of the Kevlar-epoxy developmental units has essentially been completed and tests will be underway shortly.

Present plans call for completion of this work in FY 1978 at which time a total flywheel system will have been designed, fabricated and evaluated. This project will mark a significant step towards establishing a practical procedure for the design and development of a realistic flywheel system with a new optimum containment structure.

WORK WITH INDUSTRY

In addition to the work being performed at the National Laboratories, several contracts were awarded by ERDA between 1975 and 1977. The Rockwell contract was mentioned earlier. Others are:

Lear Motors

Component testing of rotors, bearings, and seals. The testing was part of the broader task to design, fabricate, and test a complete assembly for an all-flywheel car to be ready by the early 1980's. A final report was published recently. (Reference: LMC-770401B)

Garrett AiResearch

Design, fabricate, and test a flywheel module for an electric postal jeep in conjunction with the U.S. Postal Service. Work began in November 1976 with completion expected within four months.

General Electric

Design and fabricate a 1 kWh regenerative flywheel - inductor motor power pack to be tested by late 1977. Low-cost rotors are utilized.

Johns Hopkins University

The purpose of this contract work under negotiation is to design, manufacture, and test a low-cost staionary flywheel energy storage system rated at approximately one kilowatt-hour. Such flywheels will be designed for applications in a) night-time energy storage on a residential scale, b) stand-by power systems, or c) wind energy storage.

Another potential use for stationary flywheels is as a component of wind energy systems. At present, the designer does not have enough information available to conduct a proper analysis needed for optimizing system design. DOE is sponsoring the development of a dynamic systems simulation computer model which will allow the evaluation of candidate wind energy and storage systems. This work has been performed by Boeing Company of Seattle, Washington.

In general, our contractor work has been proceeding very well. Undoubtedly you will be getting a lot more detail from reports and papers to be presented by these contractors.

SUMMARY OF ACCOMPLISHMENTS

Since we have covered a lot of territory in a short time, perhaps it is wise now to summarize the major accomplishments of the past two years as we see them.

- Flywheel assemblies for regenerative braking have been designed and fabricated with successful testing expected within a few months.

- Two composite materials (Kevlar 49/epoxy and E-Glass/Epoxy have been characterized with respect to physical and mechanical properties.

- A nonhazardous failure mode of composite rotors has been verified.

- Initial investigations have begun in the area of input-output devices and bearings improvements.

- Oil savings potential achievable with flywheel systems in automobiles is now known.

PLANS FOR FY 1978

Finally, let me outline what we plan to be doing for the fiscal year we are now entering.

Continue design, fabrication and testing of components so as to advance the state of the art steadily. Component development will include advanced bearings, rotors, input-output devices, and vacuum systems.

Work on composite materials for advanced rotors will continue in order to achieve the goals of 20 Wh/lb by FY 1980 and 40 Wh/lb by FY 1985.

Accelerate the development and testing of upgraded flywheel systems designed for automotive regenerative braking.

Initiate laboratory testing of batteries that are load-leveled by flywheels employed in hybrid vehicles.

Begin laboratory development of low-cost flywheel systems for stationary applications including wind energy storage and household electricity storage.

Environmental issues will be identified and addressed with the goal of having these issues resolved within five years.

In conclusion, I wish to thank you for your interest and participation. During the next three days, I look forward to joining you in hearing the presentations on all the technical activities outlined in the program pamphlet. I am also interested in collecting any suggestions you care to offer on our flywheel development program plans.

U.S. POSTAL SERVICE ELECTRIC FLYWHEEL VEHICLE

Thomas A. Norman
U.S. Postal Service
11711 Parklawn Drive
Rockville, Maryland 20852

ABSTRACT

The U.S. Postal Service and the Energy Research and Development Administration have a joint effort for development and installation of a flywheel system in a 1/4 ton electric postal delivery vehicle. The completed vehicle is scheduled to begin operational test and evaluation in January 1978. Electric vehicles have the advantage over existing internal combustion engine vehicles of producing minimum pollution and requiring no oil based fuels. Preliminary test results show that adding a flywheel can significantly improve performance and increase the potential application of the electric vehicle for postal delivery service without an increase in energy consumption.

INTRODUCTION

The U.S. Postal Service and the Energy Research and Development Administration have a joint program effort to develop and install a flywheel system in a 1/4 ton electric postal delivery vehicle. Engineering tests on this completed vehicle is scheduled during November 1977. Operational tests and evaluation is scheduled to begin in January 1978. This, we believe, is a very significant undertaking which, to our knowledge, will represent the first flywheel system to be installed in an operational vehicle of this size. The results of this effort could have a very direct effect on the future application of electric delivery type vehicles.

This electric-flywheel vehicle is here on display and a paper covering the detail design of the system will be given later during this symposium.

My purpose here today is to discuss the potential benefits of an electri-flywheel system in an electric postal delivery vehicle and to compare the advantages of such a system with other competitive types of vehicle propulsion systems. Before I do this, it may be beneficial to give you a brief appreciation of the magnitude of our delivery vehicle fleet and the range of operational duty cycles.

POSTAL DELIVERY FLEET

The Postal Service owns and operates approximately 106,000 1/4, 1/2 and 1-ton vehicles. These are the vehicles that are used for the delivery and collection of mail. They may operate from five to 60 miles and make from 50 to 600 stops per day. These vehicles are equipped with gasoline engines and get from four to 13 miles per gallon while on delivery. It is evident that the gasoline engine is not highly efficient under this type of starting/stopping operation.

IMPROVED VEHICLE PROPULSION PROGRAM

Because of the high gasoline consumption, the potential scarcity and other limitations of oil based fuels, we have established a program to determine the feasibility of improved vehicles which will reduce life cycle cost, oil based fuel consumption and exhaust pollution. To accomplish this, we are evaluating, testing and developing a number of different propulsion systems for our delivery vehicles. These systems include smaller gasoline engines, diesel engines, stratified charge engines, hydrogen fueled engines, hybrids, electrics and electric/flywheels.

Most of our effort is being concentrated on the 1/4 ton delivery vehicle since we have approximately 75,000 of these vehicles in our fleet.

INTERNAL COMBUSTION ENGINES

The results of our tests and evaluations to date show that diesel engines

are the most efficient engines in terms of fuel consumption for postal delivery service. However, it like all other existing internal combustion engines require oil based fuels and produce exhaust pollution. Future internal combustion engines, such as the hydrogen fueled engines, do not require oil based fuel and produce very little exhaust pollution. Hydrogen engines are still under development and their operational application is still to be decided.

ELECTRIC VEHICLES

Electric vehicles have the very distinct advantage of producing little or no pollution, possibly requiring no oil based fuel and consuming no energy while at idle. Because of these advantages, the Postal Service has purchased 350 electric delivery vehicles which are now in operational use in various parts of the country. While these vehicles are operating satisfactorily on selected routes, they are quite limited in performance. They are limited in acceleration, gradeability, top speed and the number of starts and stops that can be completed on one battery charge. As a result, these electric vehicles can be used on only selected routes. Therefore, the total number of these types of electric vehicles that can be used for postal delivery service is limited.

IMPROVED ELECTRIC VEHICLES

We have been investigating a number of ways of improving the performance of these vehicles. The most obvious is to install a larger battery. We have tested an arrangement and found a significant improvement in performance. The problem is that a larger battery increases weight and cost. In addition, there is a limit to the size battery that can be installed in a vehicle of this type. Another approach is to install an improved type battery. Improvements are being made in lead acid batteries and newer batteries such as the nickel-zinc are being developed. We have tested an electric vehicle with a nickel-zinc battery and found that the number of starts and stops were almost doubled. The problem is that these batteries are still under development.

Flywheels have the very unique advantage of being able to improve performance of electric vehicles without an increase in energy consumption. This is accomplished by recovery and storage of the braking energy of the vehicle and making use of it in the next start up or drive cycle. In addition, a flywheel can be used with any improved battery that may be used.

ELECTRICS VS. FLYWHEEL/ELECTRICS

I would now like to discuss the electric vehicle flywheel system and describe the extent to which the flywheel system should improve the electric vehicle performance. The flywheel system that has been designed and installed in the postal delivery vehicle replaces the old drive motor and control system with new units which are much lighter in weight. The result has been a reduction of 200 pounds in the total weight of the delivery vehicle.

The flywheel system is designed to store the braking energy and use this energy to assist during acceleration and hill climbing. The results will be an increase in acceleration, gradeability and number of starts/stops that can be completed. In addition, there will be a reduction of battery peak current which should increase battery life and available energy.

The following Table 1 shows a comparison between the performance of the existing 1/4 ton electric delivery vehicle and that projected with the flywheel system.

ELECTRIC FLYWHEEL VEHICLE PERFORMANCE

	Present Electric	Electric Flywheel
Acceleration (sec)		
0 to 15	5.7	3
0 to 30	24.0	12
Top Speed (mph)		
Level	32.5	40
5% Grade	20.5	25
10% Grade	14.0	20
Range (Miles)	30.0	30.0
Simulated Route		
Starts/Stops	300	500
Miles	8.5	14.4

SUMMARY

Flywheels have the potential of significantly improving the performance of electric vehicles without increasing the energy consumption. They also increase the potential number of electric vehicles that can be used on postal delivery routes.

UMTA FLYWHEEL ENERGY STORAGE PROGRAM

James F. Campbell
Program Manager
Department of Transportation
Urban Mass Transportation Administration
2100 Second Street, S.W.
Washington, D.C. 20590

ABSTRACT

The Urban Mass Transportation Administration has been actively pursuing flywheel energy storage systems for transit application for the past eight years. A recent conceptual design has identified four flywheel energy storage transit vehicle application concepts to be in the competitive range of their conventional counterpart transit vehicles.

The Urban Mass Transportation Administration Act of 1964, with numerous subsequent amendments, provides for R&D activity to support the Nation's public transit systems. Prior to this legislation, the Nation's transit systems were giving way to the private automobiles and the freeway systems. Today, the public transit systems are not only seen as a major factor in conserving energy but by virtue of their multi-stop driving cycle, their massiveness and their common maintenance shed they appear to be the ideal test bed to begin the ground transportation-energy storage learning process.

The UMTA interest in energy storage systems closely resembles other transportation applications in that the interest is based on the application of two fundamental engineering principles, i.e., (1) regenerative braking and (2) load leveling.

It perhaps is unnecessary to dwell on the details of these two principles, but installed energy storage systems in the New York R-32 transit car do confirm a 30% improvement in range resulting from regenerative propulsion and a 50% reduction in the peak power demand resulting from load leveling.

UMTA studies indicate that the two principles can be applied to a broad range of urban multi-stop vehicles with perhaps considerable resultant success with respect to energy conservation.

Energy storage systems were considered and even applied in public transit prior to the energy crisis. The Swiss had designed and built the Oerlikon Gyrobus in the 1950's. They operated about 40 such buses over a 19-year period with considerable success. The R-32 energy storage transit car was conceived and demonstrated in the early 1970's and Lockheed had been contracted to install a flywheel energy storage system into a trolley coach to eliminate the need for overhead wires in San Francisco.

These programs all used the flywheel as an energy storage device. Other devices had been considered such as the hydraulic accumulator and batteries, but the flywheel appears to be the best all-around compromise available for today's applications.

So, in September 1976, UMTA awarded contracts to AiResearch and General Electric for conceptual design studies using flywheel energy storage in a broad range of transit applications. The ground rules for the study required each contractor to use state-of-the-art technology and employ a highly modular design approach. The latter requirement is essential in the small transit industry in order to establish a reasonable production base.

The bottom line numbers to determine viability of the respective concepts are the life cycle costs (LCC). Because of the importance of this parameter, a tremendous

effort was put forth to develop the methodology to compute the LCC for three baseline transit vehicles as well as the flywheel derivation concepts. The results of the conceptual design studies are now available.

Viewgraph #1 depicts the general schematic concept generated by both contractors. It can be pointed out that the flywheel motor concept is a spin-off of an ERDA development program -- both systems use electric transmissions, solid state controllers and separately excited field control traction motors.

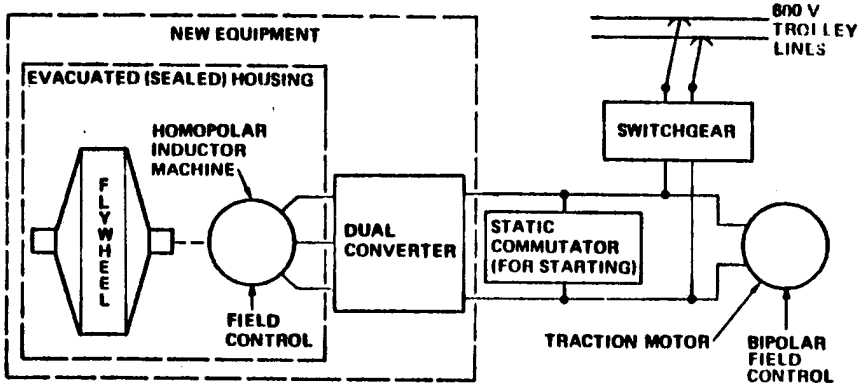
This approach does permit a high degree of modularity in the flywheel motor package in that the flywheel is comprised of a series of steel discs to match the energy requirement for a specific vehicle. The disc concept also provides a reasonable solution to containment in the event of a disc burst.

The second viewgraph conveys the four concepts for transit vehicle application that we feel are in the competitive range of their conventional counterpart systems. General engineering criteria are labeled with each concept.

The last viewgraph summarizes the LCC findings for each system and compares the initial costs as well as the maintenance and fuel costs of the conventional systems versus each of the flywheel derivative systems.

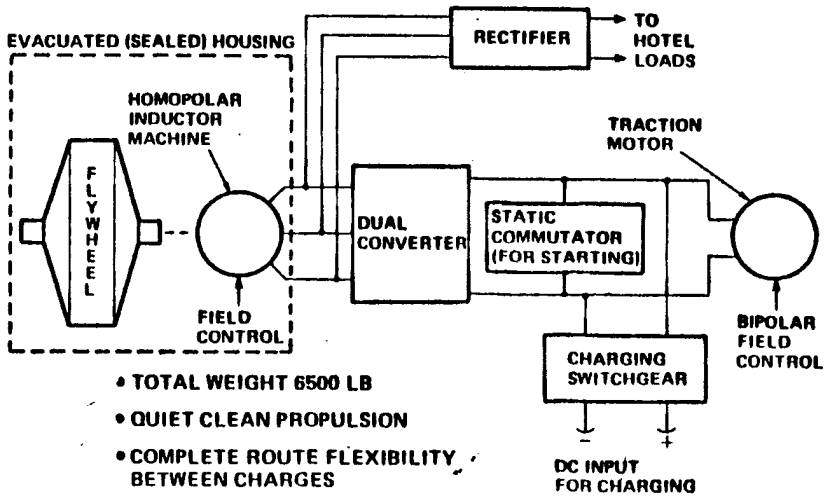
UMTA has recommended continuation of the second phase of the program which entails completing the design, hardware fabrication and test and evaluation. Assuming continued support from Congress, we all may see the flywheel operating transit buses in the next five to six years.

FLYWHEEL AUGMENTED TROLLEY COACH DRIVE



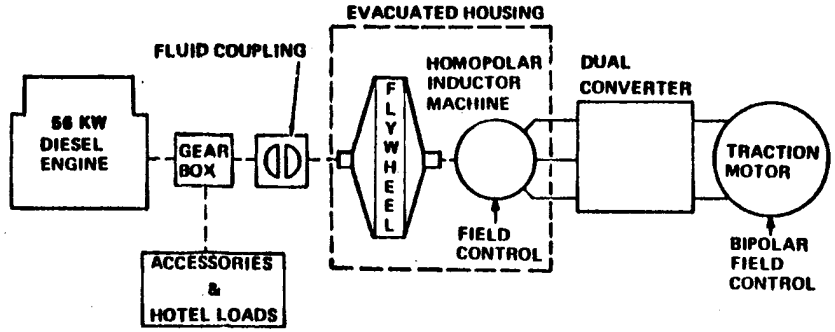
- TOTAL WEIGHT 2600 LB
- PEAK POWER LEVELING
- PROVIDES REGENERATIVE BRAKING
- INHERENT OFF-WIRE OPERATIONAL CAPABILITY

PURE FLYWHEEL BUS DRIVE



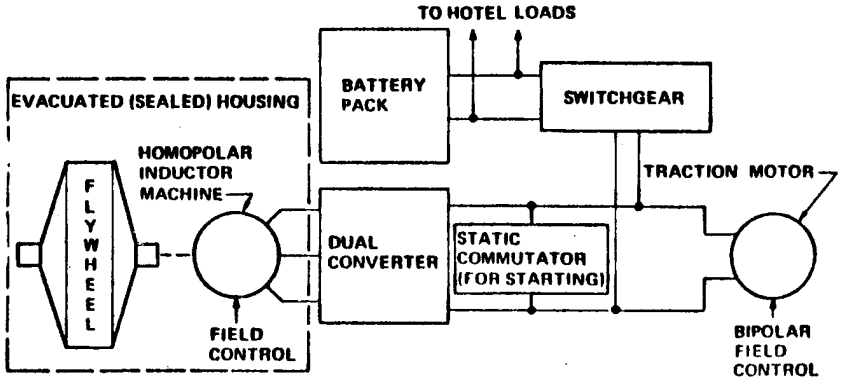
- TOTAL WEIGHT 6500 LB
- QUIET CLEAN PROPULSION
- COMPLETE ROUTE FLEXIBILITY BETWEEN CHARGES
- EXCELLENT ENERGY EFFICIENCY

FLYWHEEL/DIESEL ENGINE HYBRID



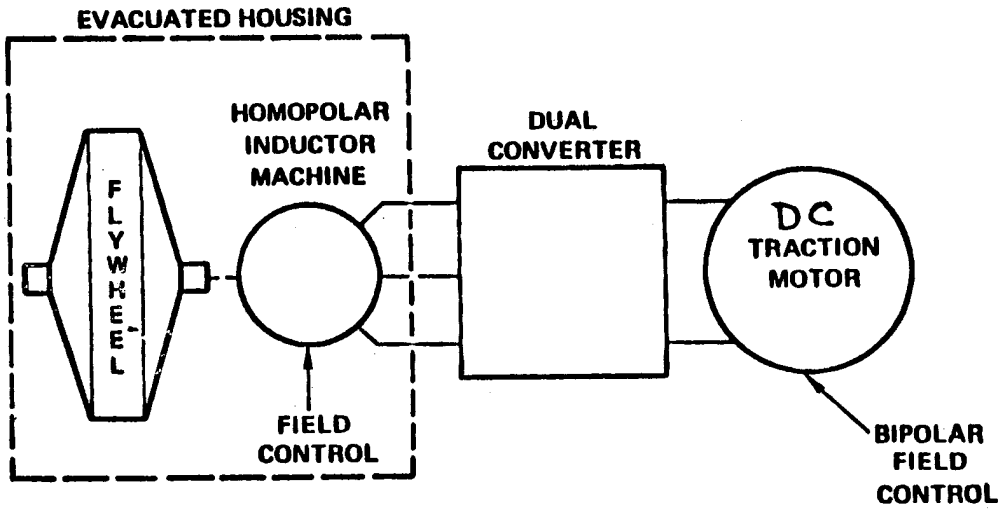
- TOTAL WEIGHT 5300 LB
- MINIMIZES FUEL CONSUMPTION
- REDUCES EMISSIONS
- LOWERS NOISE LEVEL
- PROVIDES REGENERATIVE BRAKING

FLYWHEEL/BATTERY HYBRID BUS DRIVE



- TOTAL WEIGHT 17,700 LB
- DOUBLES BATTERY CYCLE LIFE
- PROVIDES HIGH PERFORMANCE WITHOUT DAMAGING BATTERY

BASIC COMPONENTS
FLYWHEEL PROPULSION SYSTEM



- ELECTRIC TRANSMISSION
- DC TRACTION MOTOR
- BRUSHLESS DIRECT DRIVE SYNCHRONOUS MACHINE
- EVACUATED HOUSING
- SOLID STATE DUAL CONVERTER

PHASE I LCC RESULTS

(Costs in cents per mile discounted at 10% with 6 1/2% inflation)

BASIC SYSTEM	Base Line Standard	FLYWHEEL DERIVATIVE	Garrett	GE
I. CONTINUOUS WAYSIDE ELECTRIC		PURE FLYWHEEL		
LCC (cents/mile)	167.5	LCC (cents/mile)	146.0	157.7
Initial costs	33.9	Initial costs	23.7	27.5
Maintenance & fuel	29.5	Maintenance & fuel	18.2	26.1
Cost not affected by vehicle design	104.1	Cost not affected by vehicle design	104.1	104.1
II. DIESEL		FLYWHEEL/DIESEL		
LCC (cents/mile)	153.0	LCC (cents/mile)	143.5	N/A
Initial costs	20.8	Initial costs	20.5	N/A
Maintenance & fuel	28.1	Maintenance & fuel	18.9	N/A
Cost not affected by vehicle design	104.1	Cost not affected by vehicle design	104.1	N/A
III. TROLLEY COACH (T/C)		T/C AUGMENTED		
LCC (cents/mile)	167.5	LCC (cents/mile)	151.4	158.6
Initial costs	33.9	Inital costs	26.9	27.2
Maintenance & fuel	29.5	Maintenance & fuel	20.4	27.3
Cost not affected by vehicle design	104.1	Cost not affected by vehicle design	104.1	104.1
IV. BATTERY BUS		FLYWHEEL BATTERY		
LCC (cents/mile)	226.5	LCC (cents/mile)	196.8	194.0
Initial costs	30.1	Initial costs	30.5	30.8
Maintenance & fuel	86.1	Maintenance & fuel	57.9	55.2
Cost not affected by vehicle design	110.3	Cost not affected by vehicle design	108.4	108.0

FLYWHEEL TECHNOLOGY PROGRAM IN THE NETHERLANDS

Maarten van Zanten

Netherlands Energy Research Foundation ECN
Westerduinweg 3
Petten, N.H., Netherlands

ABSTRACT

The Netherlands Energy Research Foundation ECN has developed a national Flywheel Technology Research and Development Program in cooperation with industry and the electric utilities. The proposed program, if accepted by the Netherlands government, will start in 1978. It is based upon a study of potential applications of flywheel systems for energy storage. In the Netherlands, applications in the field of electricity supply could be attractive in the near future, i.e. based on proven technology, with optimum storage plant sizes corresponding with storage cycles in the order of hours. A short term demonstration of the technology in the utilities sector will serve the development of advanced systems.

The proposed program in the Netherlands would consist therefore of two main lines of activities.

The first line concerns the development of a flywheel system for demonstration at different places in the electrical network system within 5 years. The costs of this development are estimated at $ 8 million. The program will be executed by several companies including KEMA Research and Testing laboratories of the Netherlands electricity supply industry and will be managed by ECN.
The second line of activities consists of an optimisation of advanced flywheel design and materials, and of a systems analysis and development of other applications, in particular the transport sector. The R&D on specific components like composite rotor technology, electro-magnetic and permanent magnetic bearings, recently started at various institutes in the Netherlands may be incorporated in a national program.

INTRODUCTION

The study of energy storage systems is important for several reasons.[1,2] Firstly, the difficulties and costs resulting from the necessity to produce electrical energy at the moment of demand may be reduced. This may result in a reduction of the expansion of the installed capacity for electricity production, transmission and distribution, and in an improvement of the efficiency of the conversion of fuel. Secondly, a considerable energy conservation in the transportation field will be possible, combined with a decrease of environmental pollution.

As a result of an initiative from industry, the Netherlands Energy Research Foundation ECN set up a Project Group on "Energy Storage in Flywheels" which prepared a proposal for a research and development program on Flywheel Technology. This program has been submitted by ECN to the Netherlands Government. This research and development program aims at:

- on short term, the demonstration of flywheel applications in the field of electricity production and distribution,
- on the intermediate term, research and development of advanced flywheelunits for hybrid applications, and an analysis of the possibilities of purely flywheel-powered vehicles,
- on the intermediate and long term, R&D in the field of other flywheel - applications.

STORAGE APPLICATIONS IN THE NETHERLANDS

ELECTRIC UTILITY APPLICATIONS

In the Netherlands, the installed capacity is about 10.000 MW. The primary energy consumption for electricity production is about 20% of the total fuel consumption in

the country. As no use is made of any storage system, electricity has to be produced at the moment of demand. Thus, the installed capacity and the transport grid must be able to meet the peak demand in winter time. Variations in demand oblige the utilities to face the problems of starting and stopping units or to keep units in stand-by operation.

The application of a storage system can reduce the required maximum capacity and thus increase the load-factor of the production units. This results in lower investment costs and an increase in conversion efficiency. Dependent of the localisation of the storage system in the electrical network, the necessary transport capacity may also be reduced. The Netherlands electric utilities are connected to a national "coupling grid" so that they can be considered as one big power supplier. This enables them to optimise production to a considerable extent. For the assessment of central energy storage requirements it is worthwhile to distinguish the following possibilities:

a. Peak shaving. The energy needs during day-time peaks is supplied by a storage system which is loaded during low demand periods. In figure 1, the influence of storage is shown.

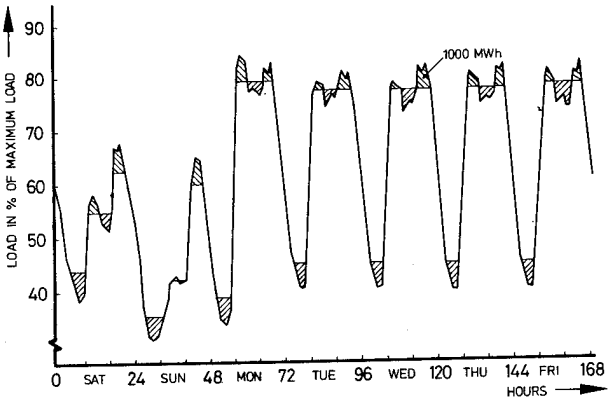


FIG. 1 STORAGE CAPACITY FOR PEAK-SHAVING APPLICATION

A storage system, with a capacity of 1000 MW hours reduces the installed capacity with 600 MW, or about 6% of total installed capacity. The increase of efficiency, i.e. fuel conservation in this case will be small.

b. Daily cycle. The capacity of the storage system in this case will be about 13000 MWh. In figure 2, it has been shown that the installed power can be reduced with 1900 MW which is about 19% of the total power installed.

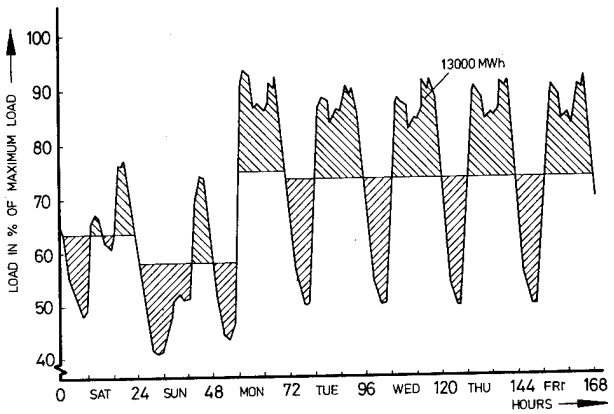


FIG. 2 STORAGE CAPACITY FOR DAY-NIGHT CYCLE APPLICATION

Here the increase of efficiency will be considerable. A conservative estimate gives an increase of efficiency from 37% to 39%. This corresponds with a yearly reduction of 0.4% of the Netherlands primary energy needs, which is about 3×10^{15} Joules. According to more optimistic estimates an increase to 41% should be possible, which would mean a yearly saving of about 6×10^{15} Joules.

c. Weekly cycle. A part of the demand during the five weekdays is supplied by the storage system, which is loaded during the weekend. In the case of a weekly cycle more reduction in installed power can be achieved but, compared with a and b this extra reduction will be small. A more detailed study is required in this case, but the costs of the storage system must be very low.

TRANSPORTATION APPLICATIONS

The energy consumption in the transportation field was about 11.5% of the use of primary fuel in 1975. In this field, the saving of energy by storage can become very important. If every car would have a storage system for hybrid applications the energy saving will be in the range of 2.5 to 5% of the Netherlands primary energy needs, which means 20×10^{15} Joules to 40×10^{15} Joules per year or 1.9×10^{13} Btu to 3.8×10^{13} Btu.

In the near future the hybride applications in urban transport systems are the most attractive from an energy-saving point of view. Measurements of acceleration-deceleration characteristics of public transport services in The Hague show that flywheels may be considered to have the most

favourable storage characteristics in this field. Besides the considerable energy saving, other important advantages may result from the use of a small flywheel (1-2 kWh):
- lowering of maximum installed power of the combustion engine,
- more efficient use of the braking system, resulting in less repair and less noise,
- a decrease of environmental pollution.

On the intermediate term systems analysis can result in R&D programs on purely flywheel-powered vehicles.

OTHER POTENTIAL APPLICATIONS

In the Netherlands several energy research and development programs are going on in which the availability of energy storage systems could play a decisive role. This is in particular the case for wind energy utilisation. In the framework of a national program, a vertical axis windturbine test facility has been commissioned this summer and in 1978 a 200 kW horizontal axis windturbine will be built. Flywheel systems development could practically be tied to these two facilities, both programs being managed by ECN.

COMPARISON OF STORAGE TECHNOLOGIES FOR PEAK SHAVING APPLICATIONS

According to the EPRI-report Assessment of energy storage suitable for use by electric utilities[3] storage systems with economic plant sizes in the range of 10-50 MWh are batteries, flywheels and hydrogen storage. Taking this result as a starting point a calculation, using Unsworth's method[4], has been made to determine the relative atractiveness of these systems in the case of more cycles a day i.e. peak shaving applications. Using cost and efficiency estimates from the EPRI-study, and Netherlands fuel costs of 0.017 $/kWh, it appears that for this application storage costs of flywheel systems are higher than those of advanced batteries but lower than those of lead acid batteries and hydrogen storage systems (figure 3). For shorter storage periods, the storage cost range of flywheel systems will overlap that of the advanced batteries systems because of a higher efficiency (90% instead of 70-85% from EPRI).

A fundamental remark has to be made with respect to this approach. The comparison of the costs per kWh of storage systems may give a first impression with respect to relative attractiveness of different systems,

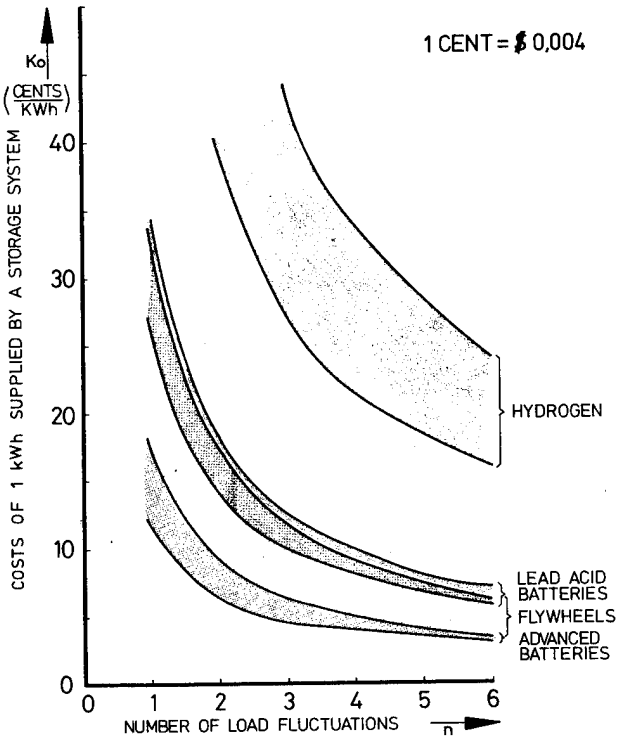


FIG.3 kWh-COSTS IN RELATION TO THE NUMBER OF LOAD FLUCTUATIONS FOR STORAGE CAPACITIES IN THE RANGE OF 10-50 MWh

but the comparison of these cost figures with the production costs of conventional electricity production can never be decisive for the economic attractiveness of the system as such. The reason is, that the storage system does not produce electricity, but replaces kWh's produced by the conventional system. On the contrary, it enables the utilities to replace the production of expensive kWh's during peak demand by less expensive kWh's produced during low demand periods. The profit of this operation cannot be expressed in simple terms of average production costs. To a large extent the real profit is qualified by other factors, e.g., the shape of the load curves and the investment costs of the saved production capacity. Therefore, a cost-benefit-analysis, i.e. the comparison of the production structure with and without insertion of storage systems, has been carried out at ECN.

COST-BENEFIT ANALYSIS OF A FLYWHEEL SYSTEM FOR UTILITY APPLICATIONS

In a cost-benefit analysis, two factors have to be considered: Investment saving and energy saving. Calculations have been made to determine the storage capacity needed for use by the Netherlands electric utility network. Starting point for the calculations is the Netherlands electricity demand on

characteristic days (figure 4): the maximum and minimum day load of the public network.

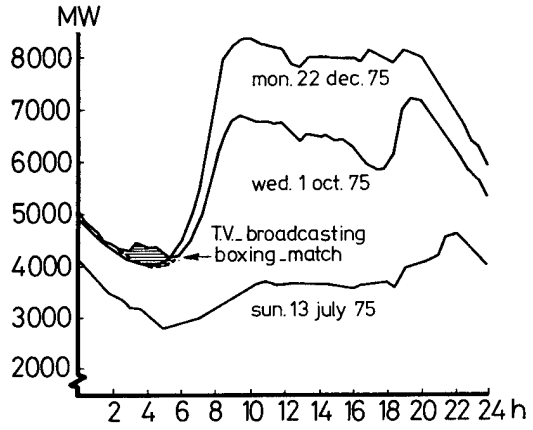


FIG. 4 MAXIMUM, MINIMUM AND AVERAGE LOAD CURVE OF THE NETHERLANDS ELECTRIC UTILITIES

INVESTMENT SAVING

In case of the use of a storage system, the maximum installed production capacity can be reduced, resulting in lower total fixed costs of electricity production. On the opposite the investment costs of the storage system have to be taken into account. In the case of one day-night-cycle, resulting in a nearly complete levelling out of the production curve, a storage capacity of about 13000 MWh is required. The investment costs of a flywheel system of that capacity, based on proven technology, are approximately 8 times higher than the financial savings in this case. However, in the case of smaller storage capacities benefits may counterbalance costs. This has been shown in an ECN study.[5] Decisive for this balance of costs and benefits is the way in which costs and benefits depend on the shape, i.e. the height and the surface, of the peak which is shaved off by the storage system: the height determines the saved investment, the surface the required storage capacity of the flywheel-system. In other words: if the stored capacity decreases, benefits decrease linearly with the height of the peak, whilst the costs decrease with the surface of the peak (figure 5).

Writing:
benefit: $B = Ax$,
costs : $K = mSx^2$,
the net saving will then be:
$B - K = Ax - mSx^2$.

The net saving will be positive for $mx < \frac{A}{S}$ and shows a maximum for $2\,mx = \frac{A}{S}$.

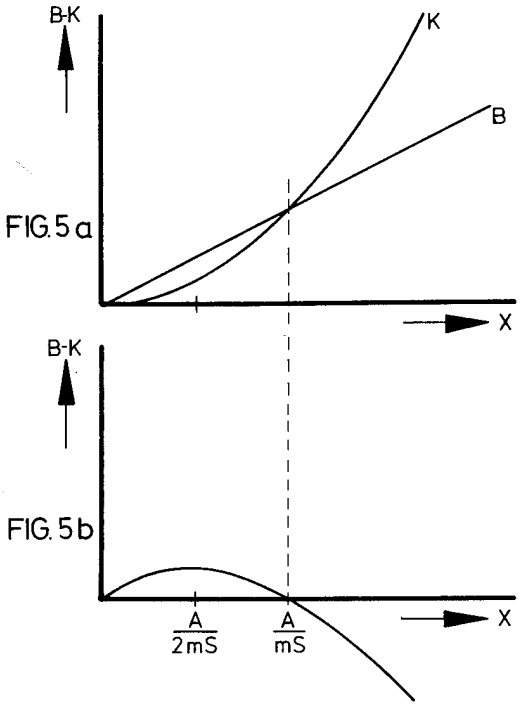


FIG. 5a BENEFIT AND COST IN RELATION TO THE HEIGHT OF THE PEAK

FIG. 5b NETT BENEFIT IN RELATION TO THE HEIGHT OF THE PEAK

The figures for investment- and capital costs of conventional power-capacity A and present flywheel technology S are:
A = f $1{,}5.10^5$/MW, based on f 10^6/MW investment and 15% capital costs,
S = f $1{,}5.10^5$/MWh, based on f $1{,}5.10^6$/MWh investment and 10% capital costs.

Under these circumstances, there will be a net saving if periods are not longer than two hours. The optimum period is one hour corresponding with a storage capacity in the region of 10-50 MWh (see figures 6 and 7). It should be noted that the steepness of the peak is a function of the factor m and will determine the necessary charge/discharge characteristics of the flywheel system.

ENERGY SAVING

Fuel conservation will result from a higher efficiency of electricity production. This efficiency-increase will however partly be offset by the losses of the storage system. In the Netherlands, the average efficiency of the electricity production in 1975 was about 37%. With the installation of a significant storage capacity, it is possible to raise the overall efficiency to 38 or 39%, including the losses in the storage system.

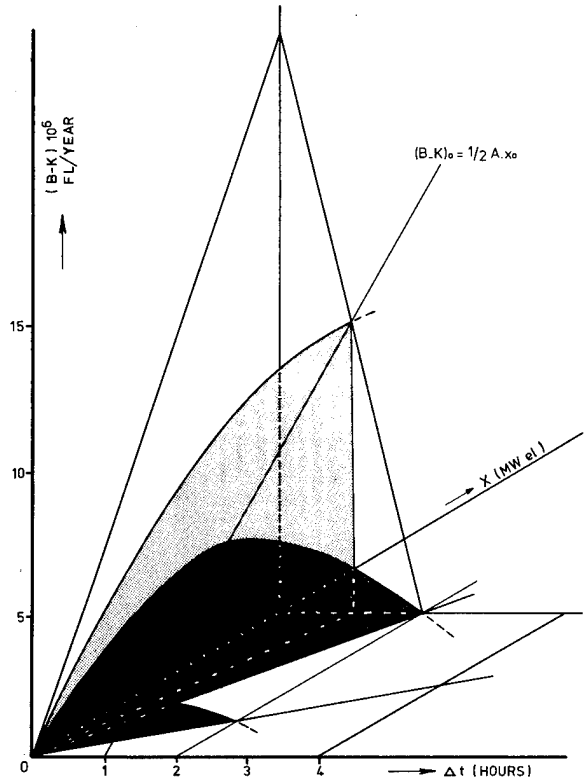


FIG. 6 THE NETT BENEFIT IN RELATION OF HEIGHT OF THE PEAK AND CYCLE PERIOD

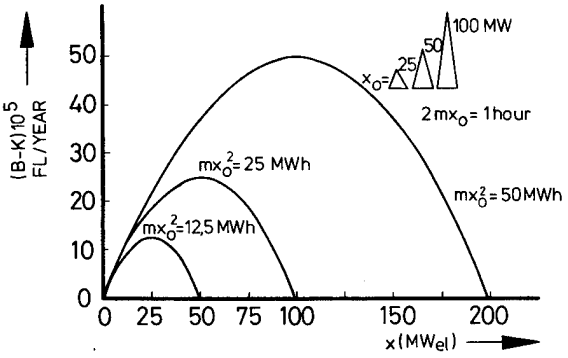


FIG. 7 THE NETT BENEFIT IN RELATION TO THE HEIGHT OF THE PEAK.

The scale of a storage system is mainly determined by the maximum power demand (figure 4) on the coldest day. But also during the rest of the year, storage can be of help to achieve a more regular production (and thus a higher efficiency), visualised by the load duration curves of the whole system (figure 8).

The calculations[6] are based on the case that the efficiency increases 1% respectively 2%, using a storage capacity of 10% of total electricity supply.

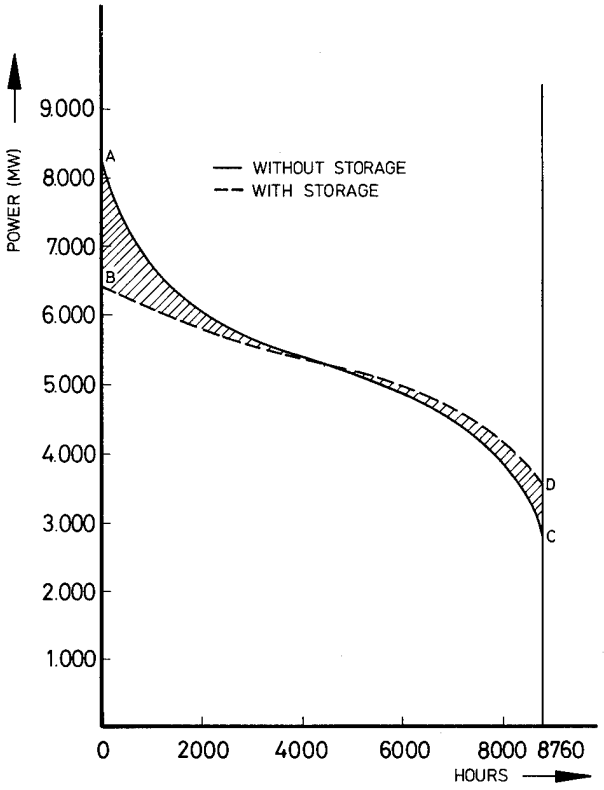


FIG. 8 LOAD DURATION CURVES

Assuming that the efficiency increases linearly with the percentage of stored energy, it can be seen that in the first case the efficiency of the storage system should be larger than 79% and in the second case larger than 65% in order to save fuel.

CONCLUSION

In our view it is not realistic to assess in general the economic feasibility of storage systems on the basis of the cost-benefit relation for the daily cycle. As regards the storage cycle periods to be considered there is a cost-minimum at much smaller storage capacities. This model shows an "inversed economy of scale"; this means that very moderate storage systems with short cycle periods can give a net profit, even when larger systems show a negative benefit. A shift of the optimum storage cycle period towards higher values may result from future development in technology and rising fuel prices.

Benefits related to capacity quality control and safeguarding of electricity transport and distribution systems have not been calculated.

RESEARCH AND DEVELOPMENT PROGRAM

GENERAL

The most favourable short term applications of energy storage in the Netherlands are found in electric power generation and in transportation. For both applications advanced batteries and flywheels turn out to be the main candidates for small to medium storage capacities. A comparison of flywheel systems and advanced batteries shows that flywheels have a number of advantages, i.e. high round trip efficiency, large number of cycles, temperature independence, high discharge depth and (dis)charge speed. Moreover the national industrial and scientific know-how and competence favour an R&D program on flywheel technology. Based on this view, the Netherlands Energy Research Foundation ECN has developed a national research and development program on flywheel technology in cooperation with industry and the utilities. The proposed program, if accepted by the Netherlands Government, will start in 1978. It consists of the following two lines of activities. The relation between these two lines is such that results from one line will be used for the other line.

FIRST LINE OF ACTIVITIES

The major goal of the program is to integrate a flywheel system at prospective locations in the electrical network within five years. This program will be based mainly on proven technologies and existing industrial know-how and concerns a flywheel module in the range of 1-3 kilowatthours of storage capacity. In figure 9, the development plan of this first line has been summarised. The five year period has been divided into four phases. In phase one, a pre-design will be made. In phase two, some experimental prototypes will be built into a test and demonstration facility. In phase three an industrial prototype will be designed and, in phase four, some small pilot plants will be built and tested in connection with a substation, a distribution station or the utility.

Phase one of the program comprises the following jobs:

Analysis of the functions of a storage system for peak shaving and load leveling applications: determination of the most favourable locations of a storage system in the electrical network.

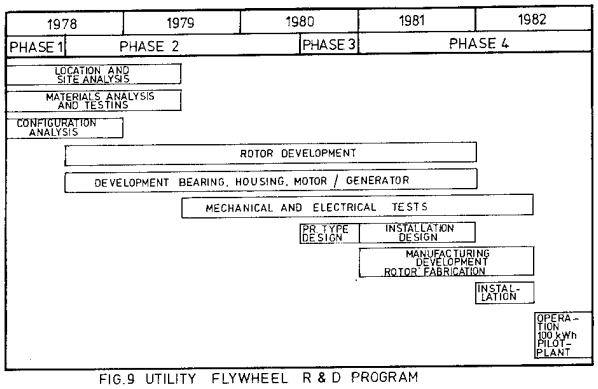


FIG.9 UTILITY FLYWHEEL R & D PROGRAM

Flywheel materials analysis.
Materials with proven characteristics will be chosen for determination of their energy storage capacity optimised with respect to theoretical energy density, rotor configuration and practical rotor energy density, costs of materials and their machining and manufacturing. Materials to be considered are high strength steel, and E-glass, S-glass, Kevlar, C-filament and boron-filament with epoxy-resin as matrix-material. Materials choice will thus depend on the physical properties of the starting material, its machinability and its expected behaviour under working conditions, including high vacuum operation.

Flywheel configuration analysis.
Analysis of existing national know-how leads to consider for short term development a thin wall cylinder and a single or multiple thin rim flywheel configuration. The energy storage characteristics will be determined in relation to wall or rim dimensions, taking into account the strength and dynamics analysis for candidate construction materials and the requirements for mass-production of 1-3 kWh modules. The results will indicate the rotor shape and material expected to provide the lowest storage costs over the system's operational life.

Bearings and damper system.
A spiral groove bearing is envisaged to serve as the bottom support and a magnetic bearing will be used at the top. The damping characteristics required will be determined by the dynamic behaviour of the rotor/bearing system. Extensive experience in the field of high speed high vacuum operated centrifuges suggest that the systems dynamics will pose neither technical nor economic problems.

Housing and siting requirements.
The principal functions of the housing are to provide a high vacuum environment for the rotor, protection against interior and exterior signals and safety under accident

conditions. The siting, above as well as underground will be considered in relation to safety requirements and costs.

Motor/generator and converter system.
Two different types will be analysed: a hysteresis motor/generator and a brushless DC motor/generator. Hysteresis motors with required characteristics are available, but the brushless DC motor has a better potential for higher conversion efficiencies and can be developed in the near future. In combination with available advanced converter systems, the energy losses of the motor/generator/converter system will be limited to a few percent.

Economic feasibility analysis.
The investigations mentioned, meant to verify the applicability of existing technology, will be executed in close relation to a costing analysis, which forms a part of the project management and tasks.

The continuation of this first design definition into a second phase of prototype testing will not only serve to verify whether a short term development with existing technology is possible. The resulting knowledge and experience will also offer guidance to the advanced systems R&D program, constituting the second line of activities.

SECOND LINE OF ACTIVITIES

The first phase of this advanced systems development program will include:

R&D for transport applications
Analysis of energy storage applications in transportation has shown that from an energy-saving point of view, the development of a hybrid flywheel for urban transport systems is the most promising for short term application. In this phase a more detailed analysis of different kinds of urban transport systems will be needed to define a development program. A cost-benefit analysis will result in the definition of the storage capacity required and the dimensions of the flywheel-units for different transport systems. To set up the program, automobile industry, public transport services and railway industry will be mobilized. The preparations in phase one will lead to a continuation in an R&D program to start mid 1978.

Advanced flywheel development plan. The research and development plan for the intermediate and the long term will concern:
- composite materials research (fibers and matrices),
- new materials research (amorphous metals, metallic glass applications),
- development of manufacturing processes for composite rotors,
- configuration analysis and testing,
- higher energy densities,
- evaluation of testing methods,
- development of electro-magnetic and permanent magnetic suspensions.

Systems analysis of future applications.
This part consists of evaluation studies of intermediate and long term applications, for instance in the field of:
- purely flywheel-powered vehicles,
- wind power production systems,
- industrial peak power supply,
- combined heat and power supply,
- solar electric production systems.

REFERENCES

[1] Energy 1976; Second Interim report of the National Energy Research Steering Group. The Hague, Staatsuitgeverij (1976).

[2] Outline programme; National Energy Research Programme. The Hague, Staatsuitgeverij (1976).

[3] Assessment of energy storage suitable for use by electric utilities, EPRI EM-264/ ERDA E (11-1)-2501. Vol I, II (1976).

[4] G.N. Unsworth, A Review of Pumped Energy Storage Schemes, Atomic Energy of Canada Limited Report, AECL-4926 (1975).

[5] A.A. de Boer, J. Smit, and M. van Zanten, Energiespectrum 1, 158 (1977).

[6] A.A. de Boer, J. Smit, De Ingenieur 89, 453 (1977).

FLYWHEEL PROGRAMS IN OTHER COUNTRIES

D. W. Rabenhorst
The Johns Hopkins University
Laurel, Maryland 20810

INTRODUCTION

Over the past 10 years, the author has received dozens of letters from more than 20 countries requesting information about the Superflywheel programs at the Applied Physics Laboratory, The Johns Hopkins University. Through continuing correspondence, and in many cases through personal contact, it has been established that nine of these countries have on-going programs in flywheel technology. Letters were sent to these countries requesting information on their respective flywheel programs. In an attempt to standardize the flywheel program information received, a guideline form was sent to correspondents in these nine countries along with appropriate covering letters. The typical information requested is illustrated in Fig. 1, whereas the addressees are listed in Fig. 2. Replies were received from eight of the countries contacted; however, the requested information was not included in all of the replies.

As would be expected in this relatively new flywheel technology, many of these R&D programs are barely in the embryo stage. A few are even still in the proposal stage. On the other hand, some countries have organized their flywheel programs within the past few months, whereas others have been engaged in this work for 10 or 12 years.

For the most part, the information reported herein is that received from specific correspondence as outlined above, however, there will be some cases where this information will be expanded by data from other sources, such as by personal contact or through the media.

The flywheel programs in the subject countries are presented in alphabetical order in the following discussion.

FRANCE

The bulk of the information on the French flywheel programs was provided through correspondence with M. Pierre Poubeau, who will be presenting a paper later in this symposium. Additional information was obtained from Aerospatiale literature and from the Washington, DC office of the company.

The principal R&D program concerning modern flywheel technology in France appears to be the one at Aerospatiale, under the direction of Mr. Poubeau. This work has been underway since about 1969, and has so far dealt mainly with spacecraft applications, although a number of ground applications have also been considered. The Aerospatiale external funds for this work have come from Intelstat; however, it is estimated that company funds have greatly exceeded the external funds. Total expenditure to date is of the order of $1,000,000 or less.

The Aerospatiale superflywheel* is one of the first (if not the first) to be used in service. It provides altitude control for current telecommunications satellites. The typical flywheel construction is shown in Fig. 3. It employs a wound rim of carbon fiber/epoxy encased in a cyclo-profile wound structure made from Kevlar.

The flywheel system performance is not spectacular in terms of energy-to-weight and energy-to-volume ratios. However, notable achievements have been demonstrated in the areas of reliability and low drag. These have been achieved through the use of the Aerospatiale-developed three-plane magnetic suspension system, of which the principal components are identified in Fig. 4. Energy storage levels of the order of 72 MJ/kg (20 wh/kg) are typical.

*The term "superflywheel" is used herein to designate those flywheels made predominately of modern filament materials.

GERMANY

The requested information about existing flywheel programs in Germany had not been received at the time this report was being written. However, the following comments are based upon information received from other sources.

Three German flywheel programs have been identified. The first is believed to have been conducted at the University of Stuttgart under the direction of Professor Gunter Scholl. This program apparently had as its main goal the feasibility demonstration of a flywheel-powered road vehicle, using fiberglass as the main flywheel constituent. The present status of this program is unknown, although it was stated during the European Flywheel Symposium in Biel, Switzerland, last year that this program had been abandoned.

The second program publicized in the media is an undefined mission sponsored by the German Federal Department of R&D. The work is apparently being done at the University of Aachen with total funds of approximately $230,000.

There is also an undefined (to the author) program at Daimler-Benz, under the direction of a Mr. Swinner who is in charge of all flywheel programs in that company. Details of the Daimler-Benz flywheel program are lacking at this time.

ITALY

The Italian superflywheel R&D program is a relatively well laid out national effort supported by the National Research Council (CNR) at an annual funding level of about $1,000,000. The two principal objectives of the overall program are to develop a flywheel/engine hybrid bus by 1979 and an industrial storage system within three years. A loosely knit organization of a dozen companies, universities and laboratories comprise the work force for this program. These organizations are listed in Fig. 5.

The flywheels for the Italian program are being developed under the direction of Dr. Giancarlo Genta at the Institutto della Motorizzazione of the Politecnico di Torino. The configuration which has been adopted is The Johns Hopkins University, Applied Physics Laboratory, bare filament superflywheel which will employ steel tire wire, coated fiberglass, or Kevlar, depending upon the application in question. An early version of the Italian Kevlar bare filament superflywheel is illustrated in Fig. 6. This can be compared with the APL/JHU version shown in Fig. 7. The latter configuration has exceeded 325 KJ/kg (90 wh/kg) in recent tests (including consideration of hub and spokes). Thus, it would appear that the Italian program goals of 20 to 60 wh/kg can be readily met with this configuration.

The main difference between the Italian and APL bare filament configurations is that the former type uses compression spokes, whereas the latter type uses tension spokes, which are an order of magnitude lighter and comparably lower in manufacturing cost.

In addition to the bare filament flywheels, various Italian organizations have engaged in other related R&D work involving hardware as well as flywheel applications studies. Fiat, for example, is investigating flywheel battery hybrid vehicles of several types from minicars to buses in several company-funded projects. Also, Pirelli is known to be experimenting with various flywheel configurations involving rubber matrices. Other flywheel configurations are being explored at the University of Cagliori. This work will be reported later in this symposium.

JAPAN

The information concerning the Japanese flywheel programs was obtained from Mr. Kozo Kitoh of the Japan Automobile Research Institute, Mr. S. Nakamura of the Mitsui Engineering and Shipbuilding Company, and Dr. Tsuneji Yada of the Mechanical Engineering Laboratory of the Agency of Industrial Science and Technology, Ministry of International Trade and Industry. Like the Italians, the Japanese flywheel program appears to be aimed at a combination of vehicles, as well as at the industrial energy storage application. Understandable communications problems make it difficult to accurately extrapolate the various bits and pieces of information received. However, the program characteristics appear to be as follows: The vehicle programs began in 1976, and the first test vehicle was completed in July 1977. This was a state-of-the-art vehicle made from off-the-shelf components. It utilized a more-or-less

conventional steel flywheel and an electrical power transfer system.

The details of this flywheel system are shown in Fig. 8 and the installation in the vehicle is shown in Fig. 9. Figure 10 is a photograph of the actual van-type vehicle.

The flywheel in this vehicle is a nickel-chrome-vanadium steel disk 50 cm in diameter by 3 cm thick. It is spun up by a 60-volt dc motor which is fed through an appropriate converter from a standard 200-volt ac commercial electric source. The 0.14 kW·h of energy stored in the flywheel is sufficient to drive this experimental car 1 km at a running speed of 10 km/h.

Seals for this unit are a special variety made from fluororubber especially shaped to withstand the 10,000 rpm operating rotational speed. A mist lubricated combination ball and roller bearing system is used. A pressure of 10^{-1} torr is maintained by a vacuum pump driven by a separate 12-volt power supply, which is said to allow a pump-down time of less than 1 min.

The funding level for the flywheel-powered car program is apparently at a level of 10,000,000 yen (approximately $35,000) for FY 1977. The eventual goal of this program is to develop a flywheel-powered bus by FY 1981.

A second Japanese program involves the eventual development of a 10 MW·h utilities peaking flywheel system with a completion date of 1985. This work is also being done under the guidance of the Agency of Industrial Science and Technology, Ministry of International Trade and Industry (MITI). This is part of the general Japanese program called "Sunshine Projects." The flywheels in this program have not yet been defined in detail in the literature. They could be made from steel, fiberglass, carbon fibers, or Kevlar, etc.

The current funding for this program is about 28,000,000 yet (about $100,000) per year, which appears to be about 1% of that required to accomplish the utilities peaking flywheel R&D mission.

THE NETHERLANDS

Although Dr. Maarten Van Zanten has prepared a separate presentation on the proposed flywheel programs for The Netherlands, the following additional comments regarding the related work being accomplished in that country may be of interest. This work, which is being done at the University of Utrect and at Groningen University, deals with two relatively new materials which could have considerable impact on future superflywheels.

The first of these is amorphous metal, or metglass as it is otherwise known. While this material is not new, the development of useful flywheel-related properties is relatively new. Mr. W. C. Emmens of the University of Utrect described amorphous metals properties at the first European Flywheel Conference in Biel, Switzerland in September 1976. Tensile strengths of more than 3.5 GN/m^2 (500,000 psi) were reported for this material, which generally has a density slightly less than that of steel. The material form is usually a thin ribbon having a thickness of about 50 μm (0.002 in.) and a width of about 2 mm (approximately 0.050 in.). Although it is not readily structurally bondable, it would appear that this material is applicable to the bare filament superflywheel configurations described in the foregoing section.

The second applicable material described by Mr. Emmens concerns the work of Dr. A. J. Pennings at the Groningen University. This material, crystalline polyethylene, is reported to have a tensile strength of 4 GN/m^2 (580,130 psi). It is apparently theoretically capable of reaching 10 GN/m^2 (1,450,000 psi). Since the density of this material is that of polyethylene, its strength-to-weight ratio has already exceeded twice that of Kevlar, and could eventually exceed five times that of Kevlar. Typically, the crystalline polyethylene fibers are about the same range of diameters as fiberglass, and experimental lengths up to several hundred meters have been produced in the laboratory.

As with many other prospective flywheel materials, the key to the eventual success of this new material will be its cost of production.

It should also be noted that the author was advised during a visit to AKZO corporate headquarters in Arnhem, The Netherlands in 1975, that this company

has developed a fiber having similar properties to Kevlar. AKZO is basically a textile company grossing more than a billion dollars per year.

SOUTH AFRICA

Professor Gordon L. Bredenkamp of the Electronic Department of the University of Pretoria is reported to be conducting the only flywheel R&D program in South Africa. This program, which is currently funded at a level of $30,000 a year, has as its immediate objective the satisfactory demonstration of a flywheel-powered electric vehicle. Other objectives are aimed at solar and wind applications and eventually at the utility application.

At the present time, the principal immediate objective is to develop a satisfactory fiberglass flywheel having a performance in the range of 180 MJ/kg (50 W·h/kg). The configuration is identical to one proposed by the author to the National Science Foundation in 1975. However, it is the method of manufacture which distinguishes the South African superflywheel from its Johns Hopkins counterpart.

This is accomplished through wet winding the filaments in a conventional manner and selectively inserting thin films of typical mold release material at various preselected radii and quadrants. In this manner the flywheel when completed consists of discrete thin rings which are bonded together only at the spoke areas. In addition to this, the rings are wound in a subcircular configuration in order to minimize the outward radial loads at the bonded spoke areas resulting from ring expansion during operation of the flywheel.

The University of Pretoria effort to date has concentrated on flywheel development, although some work has also been accomplished in the areas of high speed electric motor design and magnetic suspension.

Professor Bredenkamp has provided slides describing his work.

SWITZERLAND

The superflywheel program in Switzerland is described by Dr. Hans Asper of Conergy, Ltd., who was largely responsible for organizing the first European Flywheel Conference in September 1976. The Swiss program for superflywheel energy storage system development is unlike any of the other programs reported in the foregoing, in that it is funded primarily by private capital rather than by government capital. Conergy, Ltd., represents a coalition of concerned citizens who are primarily interested in promoting the application and industrial use of superflywheel energy storage systems through international cooperation on various levels.

The first phase of the Conergy effort will be the development and evaluation of an industrial superflywheel energy storage system having a capacity of 100 to 1000 W·h at a power level of up to about 1 kW.

UNITED KINGDOM

The report on flywheel activity in the United Kingdom is based upon information received from Mr. Robert C. Clerk of Glenrothes, Scotland, who has authored many flywheel-related activities since about 1965.

There are four flywheel energy storage programs on which information has been received. All of these make use of Mr. Clerk's patented prestressed laminated steel flywheel which is illustrated in Fig. 11. Depending upon the application and consequent material type, the general performance of the overall system ranges from about 14 to 26 W·h/kg.

The first program involves a 25 kW·h storage system to power a nonhazardous locomotive. This program is currently funded at a level of $250,000 and has a nominal completion date of late 1978. Design power output is 125 kW via the patented Clerk high performance hydraulic transmission, which is to be described elsewhere in this symposium by Mr. Clerk.

The second program is somehow related regeneratively to an offshore oil rig, and is also scheduled for completion in late 1978. It is included as part of an overall funding of $4,000,000 for the program, so it is difficult from this information to ascertain just how much funding is allocated for the flywheel system.

The third flywheel energy storage program reported deals with a general line of units for industrial and heavy transport systems. Performance for these is

reputed to be about 25 kW·h energy storage at a maximum power of 3000 kW (hydraulic). Funding level for this work is apparently $1,600,000, and a completion date of September 1978 was reported.

The fourth program involves the flywheel and hydrostatic transmission development work, which is supported by Mr. Clerk himself, and which he thinks should be completed by early 1979.

USSR

The author had not received a response to his questionnaire from the USSR by the time this article was in preparation. However, it was possible to assemble the information in the following discussion from the numerous Soviet reports, patents, books, magazines, photographs and letters which have been received on this subject over the past seven years.

The flywheel-related accomplishments in the Soviet Union cover nearly every aspect of modern superflywheel technology and are, indeed, so extensive that it would be entirely impractical to attempt to detail these activities in this presentation. The principal achievements are limited in Fig. 12, and the known machines employing flywheel storage systems are listed in Fig. 13. A few of these are worthy of special comments as follows: the main flywheel configuration described in the Soviet literature is the thin strip which is illustrated in Fig. 14. While not possessing particularly high specific performance, this configuration appears to be a near optimum combination of low cost and high safety — with performance exceeding that of a lead acid battery. This flywheel configuration was developed by Dr. Nurbei Gulia and Dr. M. Ochan at the Central Scientific Research Institute for Machine Building Technology.

A second notable USSR achievement is the intermediate flywheel rotating container illustrated in Fig. 15 which, all things considered, can result in aerodynamic drag reductions of more than a factor of two in some cases.

A novel mechanical infinitely variable, discrete range transmission having a reported efficiency as high as 97% has also been developed. The basic element of this unit is shown in the sketch in Fig. 16, while Fig. 17 illustrates how this basic unit is employed in the transmission. An actual transmission is shown in Fig. 18, and the test vehicle used in its evaluation is shown in Fig. 19.

A remarkable achievement in Soviet flywheel technology is the apparent discovery of a process for reducing bearing friction to a negligible amount. This process is best described by the following direct quotation from Dr. Nurbei Gulia's recent book, "Flywheel Engines," Mashinostroyeniye Press (1976): "The greatest promise for flywheel bearings operating in a vacuum, particularly a deep vacuum, is provided by the phenomenon of super low friction, recently discovered by a group of Soviet scientists. They discovered that a number of well-known materials, including many previously used for bearings with solid lubrication in a vacuum, if suitably irradiated, for example by helium nuclei or simply by an electron flux, show a reduction in coefficient of friction practically to zero. It was discovered that a vacuum is not only no problem, but actually may even be a necessary condition for the achievement of super low friction. Private conversations which I have had with the inventors, particularly with Doctor of Technical Sciences A. A. Silin and with Y. A. Dukhovskiy, have confirmed the technical possibility of creating super low friction bearings for flywheels operating in an evacuated spin chamber. When this is done, flywheel engines will have practically no internal energy losses, giving them almost 100% efficiency. Those are exciting words for flywheel engine designers!"

It can be seen from the table in Fig. 13 that the Soviets have incorporated flywheel energy storage systems in a large variety of machines. Notable among these is the wind energy storage system by Georgianovitch Ufimtsev in the early 1930's, which is illustrated in Figs. 20 and 21. The Ufimtsev system apparently also included a variable transmission.

Also remarkable are their flywheel-powered hand tools, typical of which is the hand drill shown in Fig. 22. And, finally, the most recent Soviet flywheel-powered vehicle is the miniature car shown in Figs. 23 and 24, which is currently in mass production as a driver education device. Later versions of this car will have a range of several kilometers on one charge.

It is important to note that while more than a dozen different Soviet flywheel-powered machines are covered here, not one of them requires a specific energy much greater than that of a lead acid battery!

The message here, which is also that which has been voiced by this author, is that it is not always necessary to have a flywheel with high performance to have high utility — just low cost and, above all, SAFETY.

FLYWHEEL MATERIALS	APPLICATIONS AND GOALS
FLYWHEEL CONFIGURATIONS	SCHEDULES
SYSTEM DETAILS	FUNDING LEVELS
PERFORMANCE	DOCUMENTS AND PHOTOS

Fig. 1. Information requested.

COUNTRY	INDIVIDUAL	ORGANIZATION
FRANCE	PIERRE POUBEAU	AEROSPATIAL
GERMANY	HUBERTUS CHRIST	DAIMLER-BENZ
ITALY	GIANCARLO GENTA	POLITECNICO DE TORINO
JAPAN	KOZO KITOH S. NAKAMURA TSUNEJI YADA	JARI MITSUI E&S MITI'
NETHERLANDS	MAARTEN VAN ZANTEN	ECN
SO. AFRICA	GORDON L. BREDENKAMP	UNIVERSITY OF PRETORIA
SWITZERLAND	HANS ASPER	CONERGY, LTD.
UNITED KINGDOM	ROBERT C. CLERK	(CONSULTANT)
USSR	NURBEI GULIA	COM. ON THEORETICAL & APPLIED MECH.

Fig. 2. Flywheel program correspondents.

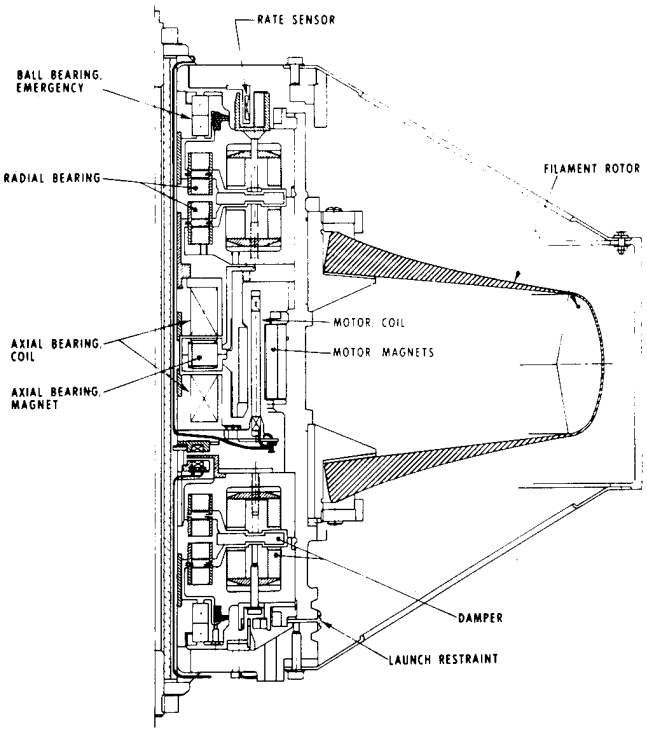


Fig. 3. Aerospatiale flywheel system diagram.

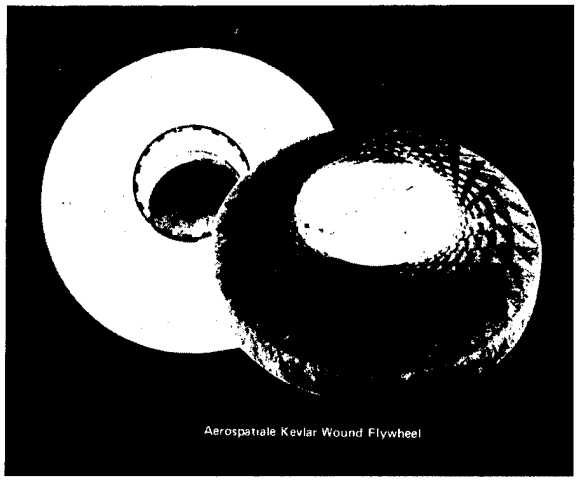


Fig. 4. Aerospatiale flywheel.

INDUSTRY AGENCIES	
FIAT	CISE
PIRELLI	ANSOLDO
RTM	ENEL

UNIVERSITY AND RESEARCH INSTITUTES		
UNIV. OF PADOVA	–	INSTITUTE OF ELECTRONICS
UNIV. OF PAVIA	–	INSTITUTE OF ELECTRONICS
UNIV. OF ROMA	–	INSTITUTE OF ELECTRONICS
UNIV. OF CAGLIARI	–	INSTITUTE OF APPLIED MECHANICS
UNIV. OF NAPOLI	–	INSTITUTE OF TECHNOLOGY
POLITECNICO OF TORINO	–	INSTITUTE OF MECHANICS
POLITECNICO OF TORINO	–	INSTITUTE OF MOTORIZZAZIONE

Fig. 5. Italian flywheel organizations.

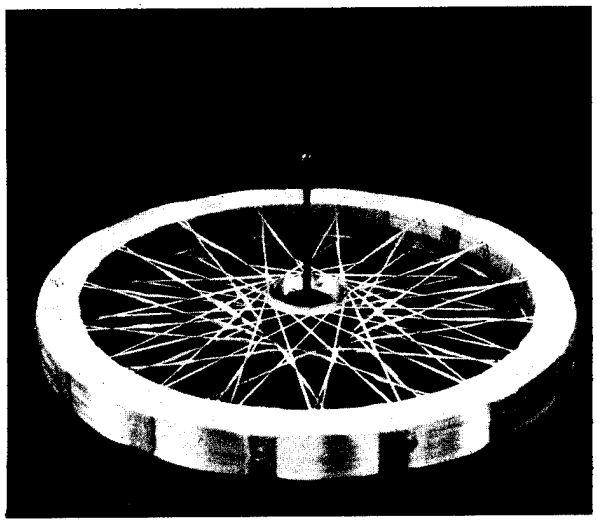


Fig. 6. Italian bare filament flywheel.

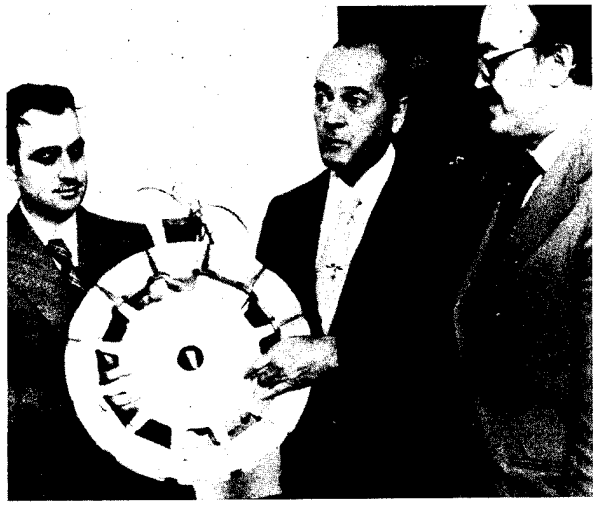


Fig. 7. APL-type 3 rotor.

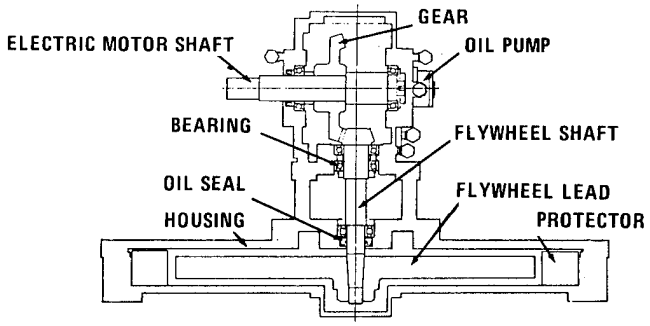


Fig. 8. Japanese flywheel design.

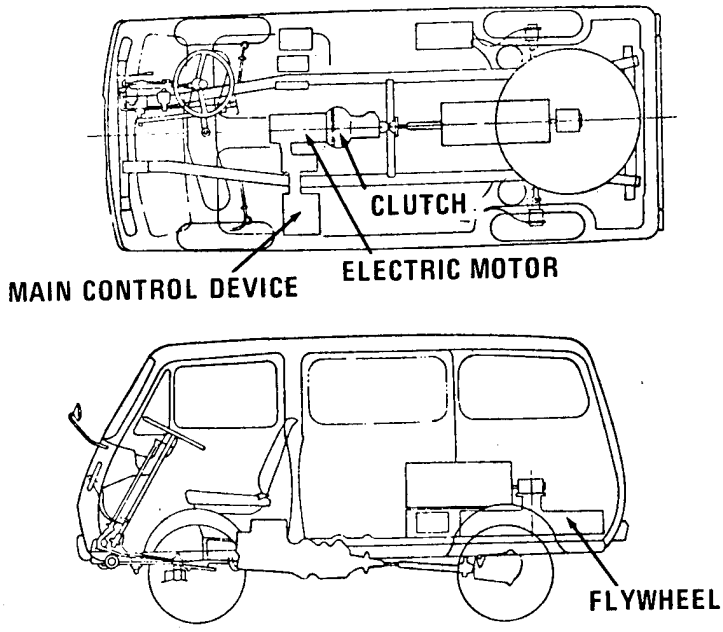


Fig. 9. Diagram of Japanese flywheel car.



Fig. 10. Photo of Japanese flywheel car.

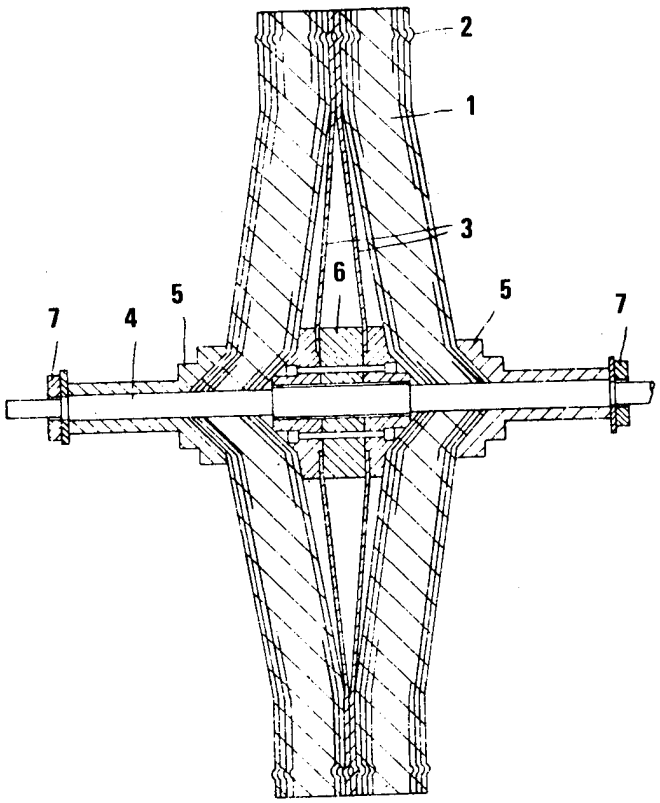


Fig. 11. Robert C. Clerk flywheel.

- THIN STRIP FLYWHEELS
  FIBERGLASS FLYWHEELS
  VARIABLE INERTIA FLYWHEELS
- DUAL CONTAINERS FOR REDUCED DRAG
  MAGNETIC BEARING UNLOADING
  TOTAL MAGNETIC SUSPENSION
- HIGH PERFORMANCE TRANSMISSIONS
- VERY LOW DRAG LUBRICANTS
  RUBBER RING SUSPENSION
  MANY FLYWHEEL APPLICATIONS
  (SEE FIGURE 13)
  EXTENSIVE FLYWHEEL DESIGN THEORY
  FLYWHEEL PUBLICATIONS
- DETAILED IN TEXT

Fig. 12. USSR flywheel achievements.

- BUS ACCEL-DECEL SYSTEM
  - SWITCHING AND MINE ENGINES
- WIND ENERGY STORAGE
  - TRUCKS
  - ROAD SCRAPER
- SMALL CAR
- HAND TOOLS
  - VARIOUS INDUSTRIAL STORAGE UNITE
    - PERSONNEL AND MATERIAL HANDLING
    - WELDERS
    - MACHINES
    - INDUSTRIAL PEAK LOAD
  - ONE HAULING TRUCK
- DETAILED IN TEXT

Fig. 13. USSR flywheel machines.

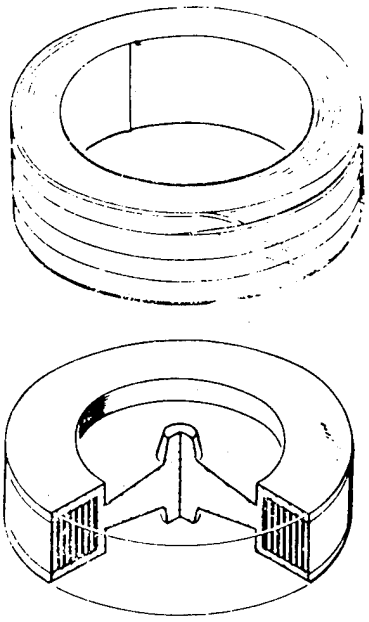


Fig. 14. USSR thin strip flywheel.

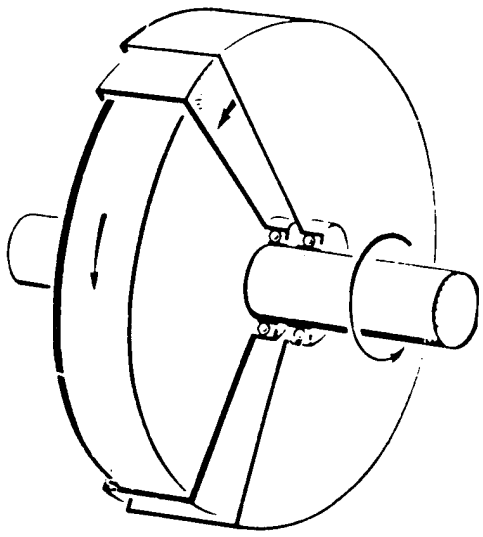


Fig. 15. Flywheel with intermediate case.

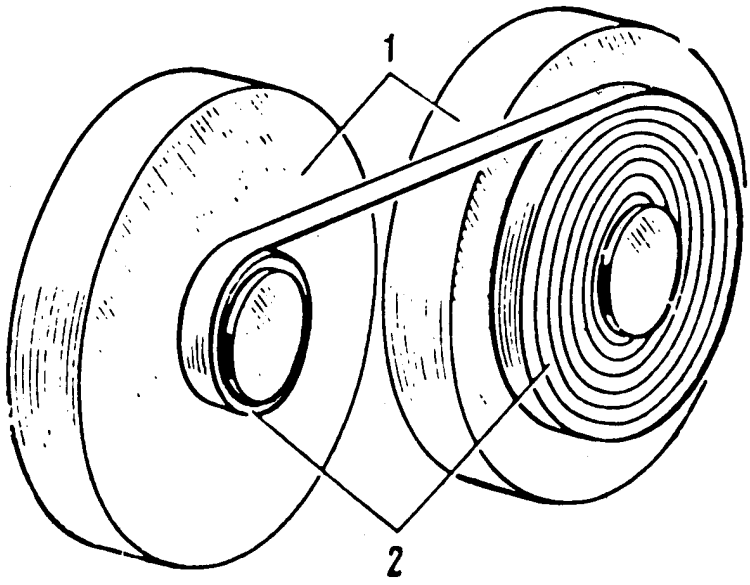


Fig. 16. Soviet transmission concept.

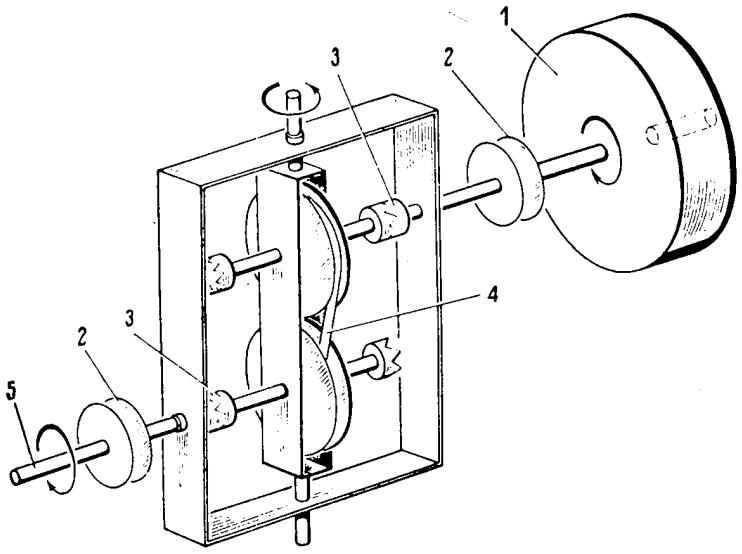


Fig. 17. Diagram of Soviet transmission.

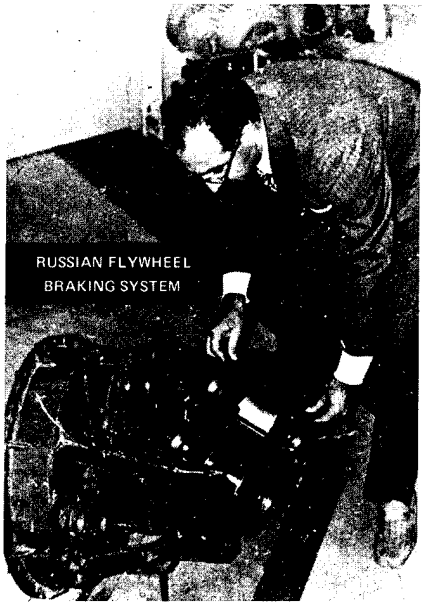


Fig. 18. Photo of Soviet transmission.



Fig. 19. Bus with Soviet transmission.

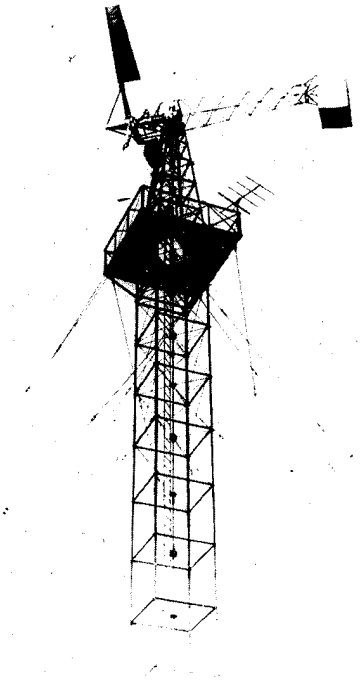


Fig. 20. Soviet flywheel windmill, 1931.

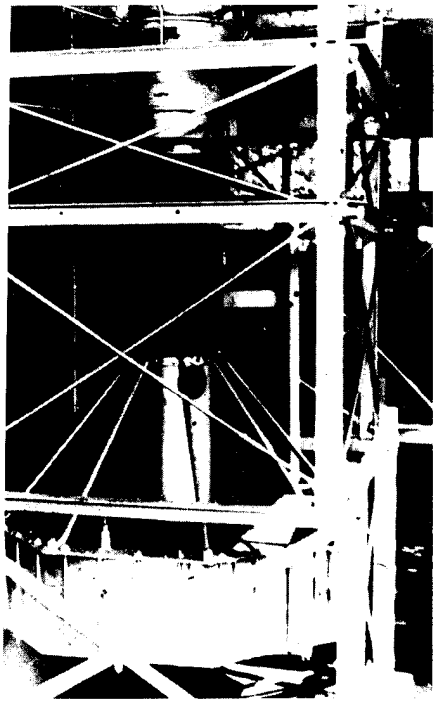


Fig. 21. Flywheel system in windmill.

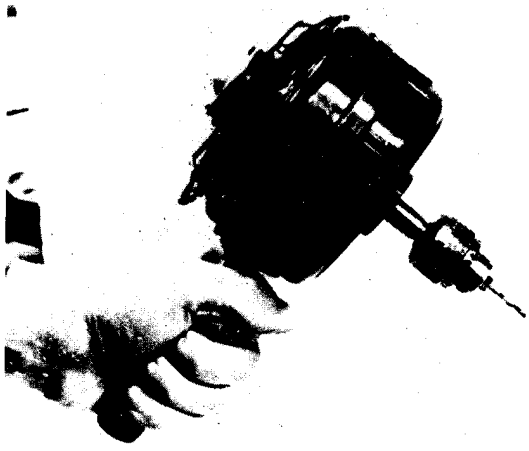


Fig. 22. Soviet flywheel hand drill.

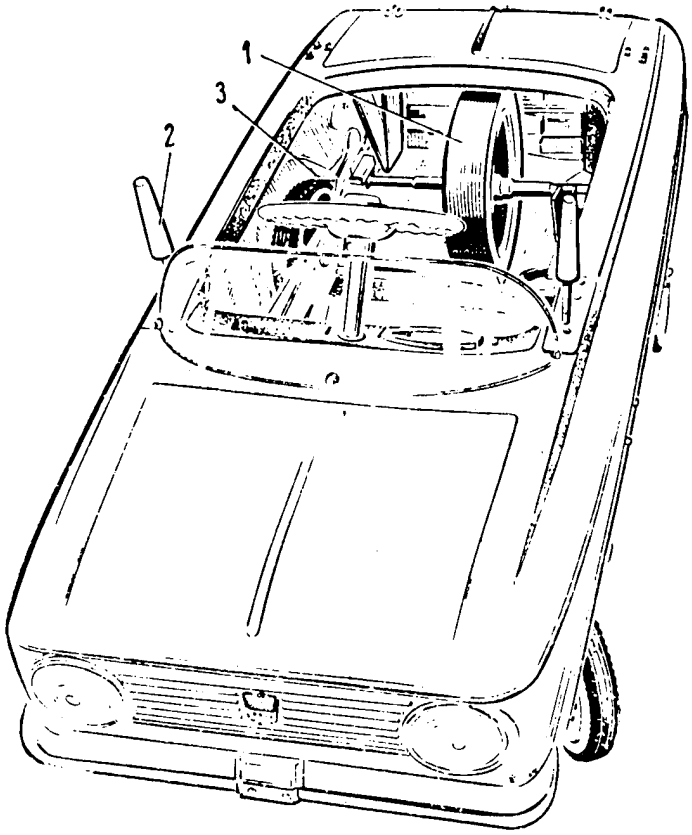


Fig. 23. Sketch of small flywheel car.

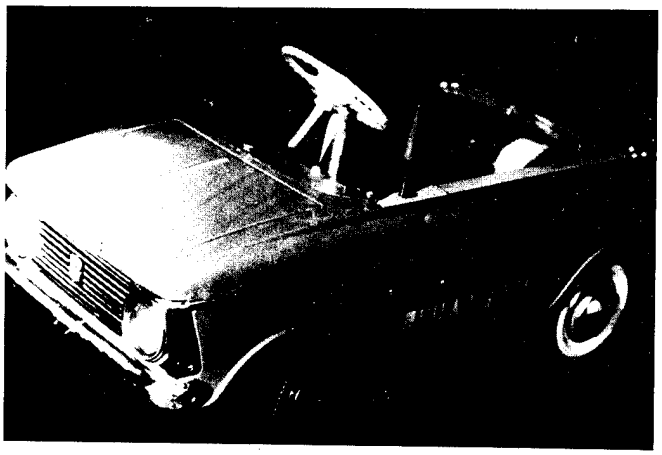


Fig. 24. Photo of small flywheel car.

FLYWHEEL-CONTINUOUSLY VARIABLE TRANSMISSION SYSTEMS FOR AUTOMOTIVE AND TRANSIT PROPULSION SYSTEMS

A.A. Frank, N.H. Beachley, R. Harter, A. Dietrich, D. Stockman, & K. Lau
University of Wisconsin-Madison
College of Engineering
Madison, Wisconsin 53706

ABSTRACT

The purpose of this paper is to discuss the characteristics of a transmission system necessary for automotive and transit propulsion in conjunction with a flywheel. The necessary characteristics, and especially the required efficiency of the transmission system are presented. It is demonstrated that the efficiency need only be good for certain combinations of torque and speed. The areas where high efficiency is required are dependent upon the driving cycle. The ones used as examples are the EPA standard driving cycles for automobiles. Four separate transmission configurations are presented and discussed.

INTRODUCTION

A flywheel drive automobile has been studied by many in the past.[1 2 3 4] Such an automobile may be either pure-flywheel, or a hybrid vehicle in which a prime mover such as a gasoline engine or electric motor is also incorporated. The objective of flywheel drive for automotive propulsion is improved fuel economy and performance. Thus, any concept proposed using a flywheel and the associated drive system must show sizable improvements over a conventional automobile driven from petroleum-based fuel to be attractive.

The concept of the flywheel drive vehicle, ignoring for the moment how the flywheel is charged, is shown in Fig. 1. The flywheel may be charged by an internal combustion engine,[5 6 7 8] external combustion engine, or electric motor[9 10] carried on-board the vehicle; or it may be charged from an external source located at a stationary point. The latter concept implies a vehicle range dependent upon the amount of energy stored in the flywheel package and therefore the size of the flywheel package. The former three concepts utilize the flywheel to provide the prime mover with a fixed or consistent load so that the prime mover can operate at its best efficiency conditions. Thus, with this concept, the flywheel effectively isolates the prime mover from the requirements of the road.

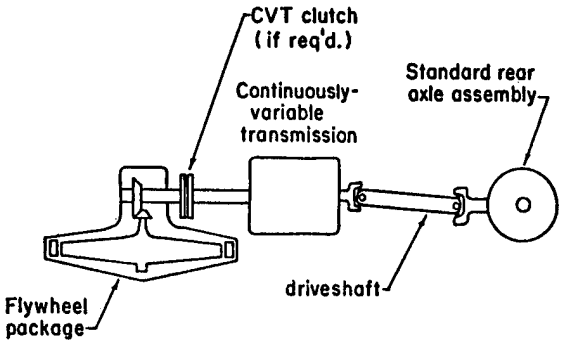


Fig. 1. Basic Configuration of a Flywheel Transmission Drive System.

The concept of isolation of the prime mover from the road is one of the attractive features of a flywheel drive. Because of this isolation, it is for the purposes of this paper possible to consider only a flywheel-transmission automobile.

The first aspect to be considered is the requirements of a transmission between the flywheel package and the drive wheels of the vehicle. There have, in the past, been many toys constructed which are flywheel driven. However, the one important feature that seems to be missing from all of these toys is a method of control. When a man drives an automobile, he wishes the automobile to respond to his commands or controls. When he wants to accelerate, he desires more torque to come from the drive system to the wheels.

If he wants to slow down, he desires to have negative torque provided to the wheels of the automobile. With a flywheel as the main energy source in an automobile, it is therefore necessary for the transmission to provide the control aspects to the automobile in place of the engine throttle as used in conventional cars. In addition, the transmission must provide any speed ratio required to continuously match the vehicle and flywheel speeds. Thus, the characteristics necessary for a transmission are the following:

(1) the transmission must be continuously variable,
(2) the transmission must be torque controllable,
(3) the transmission must be bi-lateral; that is be capable of torque transmission from the flywheel to the wheels or from the wheels back into the flywheel.

On top of these fundamental requirements, there is the general overall objective of the program, fuel economy, that dictates high efficiency of drive. This last point must be emphasized because if a transmission does not have the proper efficiency characteristics for a flywheel drive, then it makes the concept of a flywheel drive non-competitive with conventional drive systems. That is, even though in a conventional automobile the engine is asked to operate most of the time at areas of low efficiency, it may still be better than a concept in which the engine operates at best efficiency but the flywheel-continuously variable transmission system has consistently high friction losses.[1 2 3]

In order to study this problem, however, it is necessary to understand the manner in which an automobile is typically driven. In the United States, automobiles are assessed according to standard government cycles. These driving cycles are standardized and designed to represent average characteristics of people's behavior while driving their personal automobiles. Because of the existence of these standard driving cycles, the problem of designing a drive system is somewhat simplified. A fixed cycle implies that the driveshaft torque and speed are completely defined for the vehicle. This means that the transmission can be viewed as a device which supplies the required driveshaft torque and speed over this driving cycle with the main design objective of efficiency.

Having defined somewhat the requirements of a flywheel drive transmission system, the next aspect to be considered is the techniques for implementation for such a drive. Four concepts appear attractive for this application:

(1) electric drive,
(2) hydraulic drive,
(3) traction drive,
(4) clutch or torque converter drive.

All four types of transmissions have been studied and evaluated at the University of Wisconsin. In addition, we have constructed an experimental flywheel hybrid automobile with an internal combustion engine, flywheel, and hydromechanical continuously variable transmission. Figure 2 shows the configuration of this vehicle.

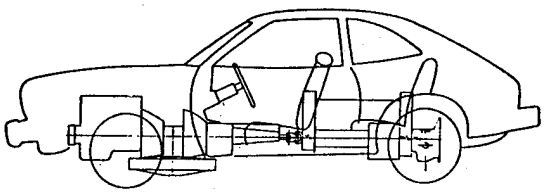


Fig. 2. Location of the Flywheel Energy Management Powerplant (FEMP) in the Pinto Chassis.

CHARACTERISTICS OF CONTINUOUSLY VARIABLE TRANSMISSIONS

We have outlined above the basic requirements of a transmission for flywheel drive vehicles. It has been shown by past research that the flywheel drive concept is most applicable to stop-and-go, or city driving conditions. Thus, most of the discussion will be centered around the EPA-CVS city driving cycle as defined by the U.S. government.

A plot of the city driving cycle is shown in Fig. 3. The driveshaft torque and driveshaft speed requirements for this cycle for a 1361 kg (3000 lb) standard vehicle are shown in the lower section of Table 1. The percentage of time spent at various speeds and torques is given by this table. The majority of the time, relatively low torque and medium speeds are required for city driving. It should be further noted that a good percentage of the time, approximately 15%, is spent in the idle mode, e.g., at stop signs waiting for traffic before one can proceed. By viewing the torque-speed requirements, one is able to immediately deduce areas of required good drivetrain efficiency.

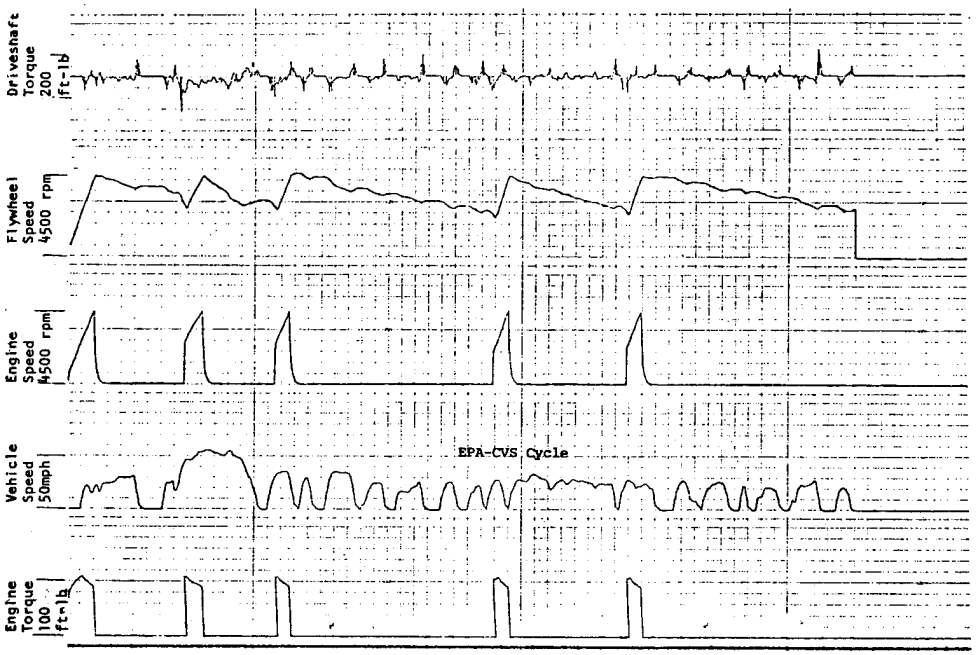


Fig. 3. Recorder Traces of a Flywheel Vehicle Simulation over the EPA-CVS City Driving Cycle.

Table 1. Digital Simulation of a 3000 lb Hybrid Car - EPA Driving Cycle 8/22/76 (upper table - highway cycle; lower table - city cycle).

TORQUE INTERVALS	SPEED INTERVALS																			
	0 130	130 260	260 390	390 520	520 650	650 780	780 910	910 1040	1040 1170	1170 1300	1300 1430	1430 1560	1560 1690	1690 1820	1820 1950	1950 2080	2080 2210	2210 2340	2340 2470	2470 2600
-194--168	.00	.00	.00	.00	.00	.00	.00	.00	.00	.00	.00	.00	.00	.00	.00	.00	.00	.00	.00	.00
-168--140	.03	.03	.00	.00	.02	.00	.00	.00	.00	.00	.01	.00	.00	.00	.00	.00	.00	.00	.00	.00
-140--112	.00	.00	.00	.03	.10	.00	.00	.10	.00	.07	.02	.12	.12	.08	.00	.00	.00	.00	.00	.00
-112- -84	.00	.00	.03	.10	.07	.15	.16	.02	.19	.08	.05	.00	.00	.05	.08	.00	.00	.00	.00	.00
-84- -56	.00	.09	.19	.00	.00	.00	.00	.00	.00	.00	.00	.00	.00	.08	.19	.12	.08	.18	.00	.00
-56- -28	.00	.00	.00	.00	.00	.00	.00	.00	.00	.00	.00	.01	.23	.27	.18	.18	.12	.00	.00	.00
-28- 0	.73	.32	.07	.07	.00	.05	.00	.07	.00	.17	.49	.46	.13	.30	1.12	.69	.74	.25	.35	.00
0- 28	.00	.00	.00	.00	.00	.00	.00	.00	.00	.13	.00	.99	1.34	.52	1.76	6.05	8.30	9.16	9.69	9.27
28- 56	.00	.00	.00	.00	.00	.00	.00	.00	.00	.13	.47	1.01	1.13	1.05	3.62	8.04	6.99	9.20	10.23	14.75
56- 84	.12	.00	.00	.00	.00	.00	.00	.00	.12	.37	.03	.00	.00	.54	.64	.08	1.20	.84	.58	.27
84- 112	.00	.00	.00	.00	.00	.00	.00	.02	.11	.01	.22	.06	.17	.09	.00	.00	.00	.00	.00	.00
112- 140	.07	.06	.09	.00	.00	.00	.10	.18	.00	.00	.00	.13	.00	.00	.00	.00	.00	.00	.00	.00
140- 168	.00	.02	.00	.00	.00	.09	.04	.00	.00	.00	.00	.00	.00	.00	.00	.00	.00	.00	.00	.00
168- 196	.00	.00	.05	.00	.00	.00	.00	.00	.00	.00	.00	.00	.03	.00	.00	.00	.00	.00	.00	.00
196- 224	.00	.00	.01	.04	.00	.00	.00	.00	.00	.00	.00	.00	.00	.00	.00	.00	.00	.00	.00	.00
224- 252	.00	.01	.01	.03	.07	.01	.00	.00	.00	.00	.00	.00	.00	.00	.00	.00	.00	.00	.00	.00
252- 280	.00	.03	.01	.00	.00	.01	.00	.00	.00	.00	.00	.00	.00	.00	.00	.00	.00	.00	.00	.00
280- 308	.00	.00	.01	.00	.00	.00	.00	.00	.00	.00	.00	.00	.00	.00	.00	.00	.00	.00	.00	.00
308- 336	.00	.00	.00	.00	.00	.00	.00	.00	.00	.00	.00	.00	.00	.00	.00	.00	.00	.00	.00	.00
336- 364	.00	.00	.00	.00	.00	.00	.00	.00	.00	.00	.00	.00	.00	.00	.00	.00	.00	.00	.00	.00
TORQUE INTERVALS																				
TOTALS,	.95	.55	.32	.28	.20	.31	.31	.36	.37	.96	1.27	2.27	3.15	2.97	7.59	16.12	16.93	9.62	15.85	19.27

TORQUE INTERVALS	SPEED INTERVALS																			
	0 125	125 250	250 375	375 500	500 625	625 750	750 875	875 1000	1000 1125	1125 1250	1250 1375	1375 1500	1500 1625	1625 1750	1750 1875	1875 2000	2000 2125	2125 2250	2250 2375	2375 2500
-196--168	.00	.00	.00	.00	.00	.00	.00	.00	.00	.00	.00	.00	.00	.00	.00	.00	.00	.00	.00	.00
-168--140	.34	.35	.00	.28	.30	.27	.19	.07	.12	.07	.02	.00	.00	.00	.00	.00	.00	.00	.00	.00
-140--112	.00	.41	.83	.61	.59	.45	.39	.30	.29	.12	.09	.00	.00	.00	.00	.00	.00	.00	.00	.00
-112- -84	.00	.05	.15	.12	.12	.21	.25	.39	.18	.29	.07	.02	.00	.00	.00	.00	.00	.00	.00	.00
-84- -56	.00	.15	.19	.00	.09	.20	.41	.50	.49	.09	.13	.16	.04	.02	.00	.00	.00	.00	.00	.00
-56- -28	.00	.07	.01	.01	.01	.20	.46	.50	.54	.27	.09	.20	.09	.11	.12	.07	.00	.00	.00	.00
-28- 0	18.62	.92	.12	.60	.51	.58	.84	1.72	1.48	2.18	1.09	.41	.29	.00	.09	.11	.22	.07	.16	.07
0- 28	.36	.00	.00	.37	.29	.53	.82	2.00	4.86	5.47	3.48	.57	2.98	.00	.00	.00	.51	.73	.95	.88
28- 56	.50	.07	.09	.18	.16	.33	.30	1.68	2.62	2.69	1.27	.62	.65	.00	.00	.00	.36	.41	.77	1.74
56- 84	.58	.23	.15	.11	.20	.49	1.08	1.12	1.04	.60	.25	.31	.07	.00	.00	.06	.16	.00	.26	.18
84- 112	.46	.18	.12	.23	.61	.61	.41	.56	.38	.28	.19	.05	.08	.13	.19	.09	.00	.00	.00	.00
112- 140	.46	.99	.20	.30	.11	.08	.30	.15	.00	.07	.07	.00	.00	.00	.00	.00	.00	.00	.00	.00
140- 168	.05	.61	.85	.70	.54	.31	.29	.18	.13	.05	.00	.05	.03	.00	.00	.00	.00	.00	.00	.00
168- 196	.00	.00	.00	.00	.08	.11	.05	.07	.08	.01	.01	.00	.00	.00	.00	.00	.00	.00	.00	.00
196- 224	.00	.00	.00	.00	.01	.09	.01	.00	.00	.01	.05	.01	.00	.00	.00	.00	.00	.00	.00	.00
224- 252	.00	.00	.00	.00	.01	.05	.06	.03	.00	.00	.00	.00	.00	.00	.00	.00	.00	.00	.00	.00
252- 280	.00	.00	.00	.00	.01	.09	.02	.01	.00	.00	.00	.00	.00	.00	.00	.00	.00	.00	.00	.00
280- 308	.00	.00	.00	.00	.00	.01	.00	.00	.00	.01	.00	.00	.00	.00	.00	.00	.00	.00	.00	.00
308- 336	.00	.00	.00	.00	.00	.00	.00	.00	.00	.00	.00	.00	.00	.00	.00	.00	.00	.00	.00	.00
336- 364	.00	.00	.00	.00	.00	.00	.00	.00	.00	.00	.00	.00	.00	.00	.00	.00	.00	.00	.00	.00
TORQUE INTERVALS																				
TOTALS,	21.36	3.42	2.65	3.51	3.54	4.37	5.89	9.25	12.18	12.17	6.65	2.41	4.23	.26	.30	.33	1.25	1.21	2.14	2.87

Summarizing the data of Table 1, one can say that the flywheel transmission system must have:

(1) low or zero idling spin loss,
(2) good efficiency at low torque-low speed conditions,
(3) good efficiency at low torque-medium speed conditions.

However, the speed of the flywheel connected to the input shaft of the continuously variable transmission is not fixed, but will vary as energy is taken out and put back in. The transmission must therefore have good efficiency over a range of ratios while operating at any given driveshaft torque-speed condition. The required overall range of transmission ratios has been found by extensive studies in the past[5 6 7 8] to be a minimum of 12 to 1. While good efficiency is not required over the entire range, it is required over a range of about 9 or 10 to 1. If this concept is to be used on the highway, it is further necessary for the continuously variable transmission to have low losses at high speeds and low torque (see the upper section of Table 1, which applies to the EPA highway cycle).

It may be instructive to consider the meaning of efficiencies at the various driveshaft torques and speeds over a driving cycle at this time. The comparison should be made between a standard transmission vehicle and the proposed flywheel-continuously variable transmission system. If we look at a certain driveshaft torque and speed requirement, we may find that the standard vehicle has a transmission efficiency of about 95% between the engine and driveshaft, but its engine is not operating at its best efficiency (at cruise the fuel efficiency is about 55% of the best). We could then say that the engine-transmission system is operating at 52% of its potential maximum efficiency (55% x .95 = 52%). If we consider a flywheel-continuously variable transmission at the same driveshaft torque and speed, we see that the engine can be run at essentially its best efficiency (with an on-off system) so that the net loss is attributed to the flywheel system and the continuously variable transmission. However, in the flywheel system, because the flywheel speed is varied over a range of approximately 2 to 1, the continuously variable ratio transmission at this particular point must also vary over a range of 2 to 1. Some suitable average ratio or average loss must be used to compare with the standard vehicle. If the engine-transmission system is transmitting 5 hp with a 1 hp average flywheel loss and a 3 hp average transmission loss, it is operating at 56% of its potential maximum efficiency (5/9 = 0.56), just slightly better than the conventional vehicle.

By studying Table 1, it is also clear that there is an appreciable amount of energy that can be recovered in the city cycle by regenerative braking if the transmission is efficient in the deceleration mode. It should also be apparent that driving the vehicle in the city requires, on the average, quite low driveshaft torque (seldom more than 20% of the maximum available) and relatively low driveshaft speed (seldom more than 30% of maximum). Thus it is seen that the transmission should have best efficiency at these low load conditions. Further, the magnitude of the spin loss when the car is motionless is extremely important, since this represents almost 15% of the time. Because of this, the transmission flywheel system should be designed so that the transmission becomes entirely stationary, or decoupled by a clutch, when the vehicle comes to a stop.

The four transmission concepts investigated have been "optimized" for city driving with the summarized losses over the city cycle given in Tables 2, 3, 4, and 5. The results are based on optimization studies in which each transmission concept was investigated to obtain the best gear ratios, component sizes, and other system parameters and operating procedures to take advantage of the characteristics of the components over the city driving cycle. The energy analyses have been based on component data as supplied to us from various component manufacturers. For example, for the hydraulic transmission, the configuration was a power-split as shown in Fig. 4, in which the various ratios between the hydraulic components and the gear differential system were selected to give maximum fuel economy over the city cycle.

The University of Wisconsin experimental flywheel vehicle, also based on the configuration of Fig. 4, is currently demonstrating only a modest improvement in fuel economy. This is due to excessive spin losses in the clutches, higher than planned losses in the hydrostatic components, and a non-optimum transmission design in terms of gear ratios, etc. Data from the experimental vehicle were

advantageously used in the study of the advanced hydrostatic power-split design, as well as the other systems studied.

Table 2. CVT Parameters and Simulation Results -- Flywheel Hybrid Car with Advanced Hydrostatic Power-Split CVT

Pump: bent axis, variable displacement, 2.0 in^3/rev max displacement

Motor: bent axis, fixed displacement, 2.0 in^3/rev

Ratios of 4-speed gearbox (in front of basic CVT): 0.237, 0.382, 0.611, 1.00

Rear axle ratio: 2.364/1

Speed ratio, pump/CVT main shaft: 0.6537/1

Speed ratio, motor/differential input: 2.116/1

CVT ratio range (theoretical) excluding gearbox: 1.894/1

Max speed of flywheel package output shaft: 4000 rpm

Energy generated by engine =	9729 hp-sec
Energy recovered in regenerative braking =	1666 hp-sec
Energy left in flywheel =	1413 hp-sec
Road load energy =	3685 hp-sec
Energy lost in non-regenerative braking =	443 hp-sec
Energy lost in CVT =	1255 hp-sec
Energy used by hydrostatic charge pump =	320 hp-sec
Energy lost in transmission gears =	573 hp-sec
Energy lost in rear axle =	530 hp-sec
Energy lost in clutching =	280 hp-sec
Flywheel package and clutch spin loss energy =	953 hp-sec
Energy lost in flywheel gears =	177 hp-sec
Energy lost to engine inertia =	198 hp-sec

Corrected fuel consumption = 41.8 mpg

Table 3. CVT Parameters and Simulation Results -- Flywheel Hybrid Car with Electric Drive CVT

Electric drive: for 100 hp engine

Ratios of 4-speed gearbox (in front of basic CVT): .274, .508, .730, 1.00

Overall rear axle ratio: 3.27/1

CVT ratio: 1/2.5

Table 3. (Cont'd)

Maximum speed of flywheel package output shaft: 4000 rpm

Energy generated by engine =	10160 hp-sec
Energy recovered in regenerative braking =	1552 hp-sec
Energy left in flywheel =	598 hp-sec
Road load energy =	3709 hp-sec
Energy lost in non-regenerative braking =	208 hp-sec
Energy lost in CVT =	3208 hp-sec
Energy lost in transmission gears =	571 hp-sec
Energy lost in rear axle =	556 hp-sec
Energy lost in clutching =	84 hp-sec
Flywheel package and clutch spin loss energy =	909 hp-sec
Energy lost in flywheel gears =	188 hp-sec
Energy lost to engine inertia =	198 hp-sec

Corrected fuel consumption = 36.5 mpg

Table 4. CVT Parameters and Simulation Results -- Flywheel Hybrid Car with Toroidal Drive CVT

Toroidal drive: 100 hp nominal rating

Ratios of 4-speed gearbox (in front of basic CVT): 0.237, 0.382, 0.611, 1.00

Overall rear axle ratio (toroidal reduction x differential ratio): 3.3/1

CVT ratios used (excluding gearbox): in first gear 0.5 to 2.5; in second, third and fourth gears 1.0 to 2.5

Maximum speed of flywheel package output shaft: 4000 rpm

Energy generated by engine =	10092 hp-sec
Energy recovered in regenerative braking =	1746 hp-sec
Energy left in flywheel =	1408 hp-sec
Road load energy =	3713 hp-sec
Energy lost in non-regenerative braking =	133 hp-sec
Energy lost in CVT =	2135 hp-sec
Energy lost in transmission gears =	724 hp-sec
Energy lost in rear axle =	547 hp-sec
Energy lost in clutching =	133 hp-sec
Flywheel package and clutch spin loss energy =	957 hp-sec
Energy lost in flywheel gears =	182 hp-sec
Energy lost to engine inertia =	198 hp-sec

Corrected fuel consumption = 40.3 mpg

Table 5. CVT Parameters and Simulation Results -- Flywheel Hybrid Car with Slipping Clutch CVT

Ratios of 5-speed gearbox: .184, .303, .452, .611, 1.00

Ratios of 2-speed gearbox: .85, 1.00

Overall gear ratios: .128, .152, .212, .250, .316, .372, .438, .503, .700, .824

Rear axle ratio: 3.27/1

Top speed (with flywheel package output speed of 4500 rpm): 80 mph

Minimum speed (in low gear with no clutch slip
(a) flywheel package output speed of 4500 rpm: 12.4 mph
(b) flywheel package output speed of 1500 rpm: 4.1 mph

Maximum speed of flywheel package output shaft for EPA-CVS run: 4000 rpm

Energy generated by engine =	8750 hp-sec
Energy recovered in regenerative braking =	2013 hp-sec
Energy left in flywheel =	704 hp-sec
Road load energy =	3631 hp-sec
Energy lost in non-regenerative braking =	271 hp-sec
Energy lost in transmission gears =	560 hp-sec
Energy lost in rear axle =	536 hp-sec
Energy lost in clutching =	1781 hp-sec
Flywheel package and clutch spin loss energy =	948 hp-sec
Energy lost in flywheel gears =	168 hp-sec
Energy lost to engine inertia	173 hp-sec

Corrected fuel consumption = 42 mpg

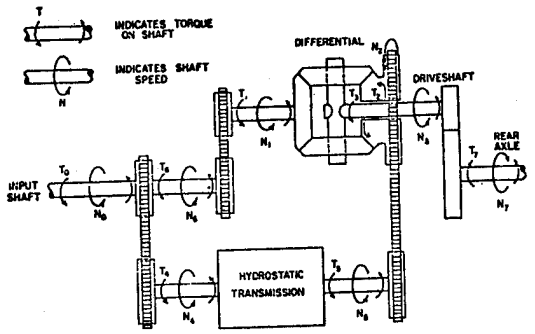


Fig. 4. Schematic of Power-Split Hydrostatic Transmission Used for Vehicle Simulations.

The electric transmission system investigated was an electric power-split, very similar to that of the hydraulic system. Characteristics of electrical machines were compared with hydraulic component characteristics and it was found that while the peak efficiencies of the electrical motors and generators can be as good as those of the hydraulic counterparts, the overall average efficiency, especially for part load operation, is not as good. As pointed out, for city driving, the part load efficiency is crucial.

Another concept which appears promising is traction drive, with either a rubber or steel belt system, or a steel-on-steel toroidal drive system, as illustrated in Fig. 5. The efficiency characteristics of these devices are somewhat difficult to obtain from manufacturers because they do not normally design them for automotive drive systems. With data supplied to us from a toroidal drive manufacturer, the simulated results of Table 4 were generated. The optimized arrangement required a 2-speed gearbox ahead of the drive system.

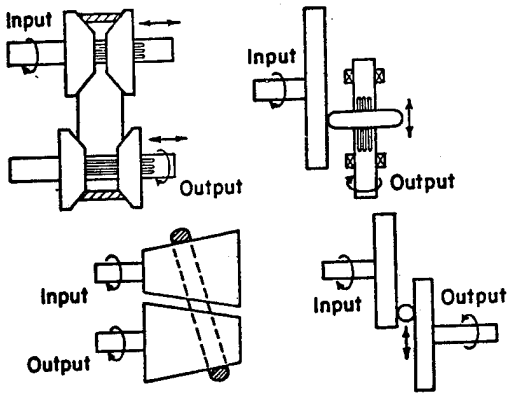


Fig. 5(a). Various Traction Drive CVT Concepts.

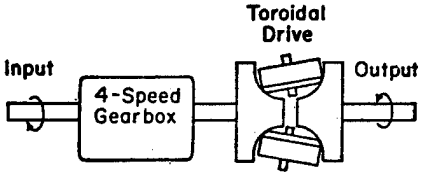


Fig. 5(b). Schematic of Traction Drive CVT Used for Vehicle Simulations.

The fourth transmission system may be termed a slipping clutch system (Fig. 6). An attempt was made to design a transmission in which most of the energy is carried via a gearbox since gear losses

are generally less than for other drive schemes. The number of speeds selected for this concept was 10-speeds forward. Then to obtain intermediate speed ratios, a clutch would be slipped. If there were 15% maximum difference between the gearbox speeds, then if the clutch slippage were the only CVT energy loss, in the worst case the transmission should be 85% efficient. And further, on the average, the efficiency should be much better than 85%. Implementation of this concept is extremely simple with a multi-disc clutch, as in standard automatic transmissions. A disadvantage of this concept is the high frequency of required gear shifts. However, because of the slipping clutch nature, this may be a relatively small factor since:

(1) the driver does not know whether or not a transmission shift has occurred, and
(2) the configuration shown in Fig. 6 allows the transmission shift to occur without hesitation.

The results of an "optimized" version of this transmission are shown in Table 5.

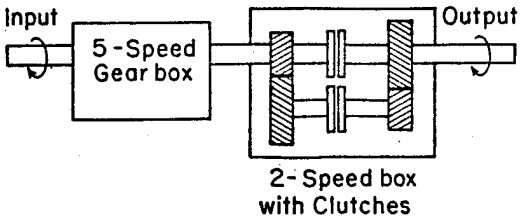


Fig. 6. A CVT Consisting of a 10-Speed Gear Transmission with Slipping Clutches.

It should be noted that the resultant fuel consumption of three of the concepts, after the optimization exercise, is approximately the same, about 17 kilometers per liter (40-42 mpg). This can be compared with the standard production vehicle which obtains about 10 kilometers per liter (24 mpg). The electric transmission is somewhat poorer because of the narrow efficiency range. Comparisons of these tables should be made to see the differences where the various energies are lost. For example, the slipping clutch transmission lost 1781 hp-sec in the clutches themselves, while the toroidal traction drive system lost 2135 hp-sec in the CVT. Thus, the traction drive loss was approximately equivalent to the slipping clutch. All items within an operating vehicle have been modeled based on our experience with the constructed flywheel vehicle, with losses for the flywheel system as measured and road load compared with realistic road test data.

SUMMARY AND CONCLUSIONS

While the flywheel drive concept has the potential of dramatically improving the fuel efficiency of prime movers in automobiles, it must be implemented with due regard to the requirements of automotive drive. Our studies show that automotive drives do not require good efficiency in high power areas. Efficiency of automotive drives is most important in two main areas (referred to the driveshaft) -- the low speed-low torque area for city driving, and the low torque-high speed area for cruising on highways. If a flywheel transmission system can be designed to operate efficiently in these two areas and to have very low idle losses, substantial fuel economy gain can be made with a flywheel drive system. It is anticipated that a 1300 kg (3000 lb) vehicle should be able to have its fuel consumption reduced by one-half with a properly developed flywheel drive transmission and the current prime movers. Such improvements will be obtained only with continued component and system research and development, however. It should be pointed out, in addition, that the vehicle performance can be greatly improved with respect to acceleration (0-100 km/hr in about 6-8 seconds). Advanced prime movers, such as a Stirling engine or a gas turbine, might improve this fuel consumption characteristic even further.

One of the most advantageous features of a flywheel drive transmission system is that the problem of part load efficiency of the engine is translated to a transmission problem. That is, the engine or prime mover can be asked to operate in an on-off mode, i.e., only to operate when the flywheel is low on charge. This concept allows the prime mover designers much greater flexibility in the design of their equipment. For example, to be able to control the power or torque out of the engine in a smooth and immediately responsive fashion is one of the main problems of the Stirling and gas turbine engines. With a flywheel transmission system attached to such an engine, it would be required to operate only at full power. In addition to solving the problem of prime mover part load operation, the flywheel acts as a constant load absorber to the prime mover and as a starter for the prime mover.

While high efficiency is not required for all conditions of torque and speed of the driveshaft, it is required in certain select areas as pointed out by this paper. We are talking in terms of about 95% efficiency in the areas discussed, dropping off to perhaps as low as 80% efficiency in the high power-high torque regions. These requirements pose a severe requirement for the transmission designer, since it is generally quite difficult to obtain very high efficiency at low load conditions.

Studies by ourselves and others[11] show that even though substantial fuel savings are possible on medium sized automobiles, greater gains are possible for larger classes of vehicles. Further, a flywheel system tends to equalize the fuel efficiency of all vehicles, i.e., heavier vehicles will have lower fuel penalties with the same performance.

REFERENCES

1. "Should We Have a New Engine? An Automobile Power Systems Evaluation," Jet Propulsion Laboratory, California Institute of Technology, Pasadena, CA, JPL SP43-17, Vol. I, II.

2. Gilbert, R.R., et al., "Flywheel Drive Systems Study," Lockheed Missiles and Space Co., Report LMSC-D246393 to EPA, July 1972.

3. "Feasibility Analysis of the Transmission for a Flywheel/Heat Engine Hybrid Propulsion System," Mechanical Technology Inc., November 1971.

4. Helling, et al., "Hybrid Drive with Flywheel Component for Economic and Dynamic Operation," Institute fur Kraftfahrwesen Technische Hochschule, Aachen, Proc. 3rd International Electric Vehicle Symposium, February 1974.

5. Beachley, N.H. and Frank, A.A., "Final Report -- Increased Fuel Economy in Transportation Systems by Use of Energy Management -- Third Year's Program," Report #DOT-TST-77-21, prepared for U.S. Dept. of Transportation, December 1976.

6. Frank, A.A., et al., "The Fuel Efficiency Potential of a Flywheel Hybrid Vehicle for Urban Driving," Proc. 11th Intersociety Energy Conversion Engineering Conference, September 1976, pp. 17-24.

7. Scott, D., "Flywheel Transmission Has Variable Speed Gear," Automotive Engineering, Vol. 85, No. 3, March 1977.

8. Beachley, N.H., et al., "Experimental Evaluation of Flywheel Energy Management Automobile," Proc. 4th International Symposium on Automotive Propulsion Systems, April 1977.

9. Rowlett, B.H., "New Battery Flywheel Power System for an Urban Automobile," Proc. 4th International Symposium on Automotive Propulsion Systems, April 1977.

10. Davis, D.D. and Epps, R.C., "The Flywheel Battery Hybrid Power System: A Concept to Improve Electric Vehicle Performance," Proc. 4th International Symposium on Automotive Propulsion Systems, April 1977.

11. Larson, G. and Zuckerberg, H., "Hybrid Heat Engine Propulsion for Urban Buses," Proc. 4th International Symposium on Automotive Propulsion Systems, April 1977.

FLYWHEEL ENERGY STORAGE SYSTEM DEVELOPMENT

E.L. Lustenader
General Electric Company
1 River Road
Schenectady, N.Y. 12345

ABSTRACT

The development of low cost, high efficiency drives is critical for the application of flywheels to electric propulsion systems. A synchronous machine drive appears to be particularly suited for this application. One reason is that a synchronous machine can be made self commutating so that the inverter becomes equivalent to a conventional phase control bridge converter without large commutating components.

General Electric has been evaluating a variety of drive systems for flywheel application. After numerous tradeoff studies, a solid rotor inductor machine with a load commutated inverter was selected for hardware development.

This paper describes a development of a small flywheel energy storage system of this type. The development is sponsored by the Energy Conservation Division of ERDA. The system consists of a 1 Kwh composite flywheel coupled directly to a 20 Kva, 15,000 rpm maximum solid rotor inductor motor/alternator unit. The motor/alternator/flywheel package is hermetically sealed, and receives power from a solid state inverter which is designed to provide the necessary frequency control from a fixed DC power source, such as a battery. The flywheel speed varies over a two-to-one range, thus full performance is achieved using a load commutated inverter. A simple auxiliary commutating circuit is provided for initial starting of the inductor machine.

The energy storage package under development is primarily aimed at small transportation applications; specifically a hybrid flywheel/battery electric vehicle in the 3000 pound weight class.

A battery/flywheel propulsion and control system is described. The same technology and basic propulsion concept can be scaled up to provide stored energy requirements for other applications such as an all-flywheel bus or a flywheel/battery bus.

INTRODUCTION

The use of flywheels to store energy has received renewed interest over the past few years. This is primarily due to the availability of new materials, both composites and steel, which promise high energy storage per pound for the flywheel rotor. The applications that have been proposed range from utility load leveling to both regenerative energy storage and total energy storage for ground transportation. For many of these applications, the system requires that electrical energy first be converted to mechanical energy, stored in the flywheel with minimum losses, and then reconverted upon demand back to electrical energy.

The development which is described here has been sponsored by ERDA's Division of Energy Storage Systems. The overall objective of this ERDA program has been to demonstrate new technology associated with a novel concept of a high speed flywheel energy storage system. This concept consists of a high speed composite flywheel directly coupled to a synchronous motor/alternator.

The energy storage package which is under development has been primarily aimed at a small transportation application, specifically a hybrid flywheel/battery electric vehicle which would weigh about 3000 pounds. However, the same technology and basic concept can be

scaled up to meet larger stored energy requirements for other applications such as an all-flywheel powered bus or a flywheel/battery hybrid bus.

There are several transportation applications where flywheel energy storage appears attractive. One is a flywheel/battery hybrid vehicle in which the battery pack provides the main propulsion energy and a small flywheel is used to recover braking energy of the vehicle. In this application, the flywheel load levels the battery and removes the peak current drains from the battery which would occur during vehicle acceleration.

Another application is the all flywheel powered vehicle where the flywheel provides the main propulsion energy and contains sufficient stored energy to provide the desired vehicle range. It also recovers the braking energy and reuses this during vehicle acceleration.

Flywheels can also be used in combination with diesel or internal combustion engines to load level and recover braking energy.

FLYWHEEL DRIVE

In the process of developing a complete flywheel energy storage system, various flywheel drive motors were considered ranging from DC to various forms of AC. The AC flywheel drive appeared to have several advantages over DC. Higher rotational speeds can be obtained which reduce the weight of the drive machine and allow a more optimum aspect ratio of the flywheel to be utilized. By combining the flywheel and a high speed motor into a single unit and hermetically sealing the rotating assembly, rotating seals and gears are eliminated. A disadvantage in comparison to DC is that more solid state power conditioning equipment is required to interface the flywheel drive with the power source.

After many tradeoff studies, a synchronous motor appeared to be the best choice for flywheel drive. One of the reasons is that a synchronous motor can be made self commutating so that the inverter becomes equivalent to a conventional phase controlled bridge converter without large commutating components. A solid rotor inductor type synchronous machine appeared to be ideal for the application since all windings would be in the stator and the solid rotor could contribute to the inertia.

The basic concept finally selected for development consisted of the flywheel package operating from a DC power source as shown in Figure 1. The main components are the inductor motor/alternator which is a synchronous machine with DC field control, and a composite flywheel which provides inertia over and above the inertia of the steel inductor motor rotor. The motor/alternator/flywheel package is coupled electrically to a load commutated inverter which allows power to pass in either direction, to or from the DC power source.

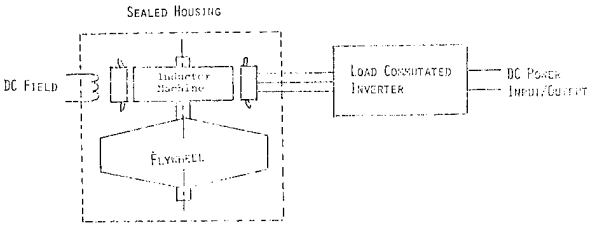


Figure 1. Basic Concept of the Inductor Motor/Alternator/Flywheel Package.

BATTERY/FLYWHEEL HYBRID PROPULSION SYSTEM

The application of this type of energy storage package to a hybrid propulsion system is shown schematically in Figure 2.

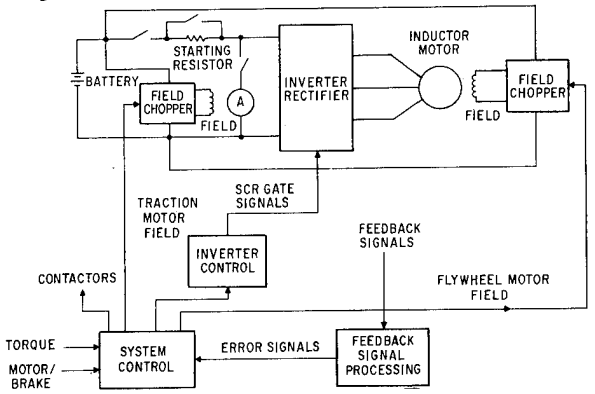


Figure 2. Battery/Flywheel Hybrid Propulsion System.

The main components are the traction battery package, the DC traction motor/generator, and the flywheel energy storage package (the synchronous motor/alternator/flywheel with its load commutated inverter). The battery supplies the main energy for propulsion. For the battery/flywheel hybrid application, the flywheel need store only enough energy to

accelerate the vehicle or provide for hill climbing. When the vehicle slows down, the traction motor operates as a generator and transfers vehicle kinetic energy back into the flywheel. System losses are made up from the main traction battery package. The short bursts of high power required for the vehicle acceleration are supplied directly from the flywheel. Thus, the battery need not supply the peak current demands of the system.

The control system shown senses the motor terminal voltage and AC line current to determine the motor internal operating conditions. This control method maintains the SCR turnoff time as a constant percent of the period of the generated back emf as speed and current are varied during operation. The inverter turnoff time is thus maintained by feedback control rather than the use of special function generators.

A 20 KVA drive system has been built on the ERDA program and successfully tested in the laboratory using this control strategy. A hybrid computer simulation of the drive and control system has been implemented for laboratory demonstration of the flywheel energy storage package.

The demonstration motor/alternator/flywheel energy storage package is shown in cross-section in Figure 3. It consists of the 20 KVA solid rotor induction type synchronous motor/alternator coupled directly to a multi-disk composite flywheel. The entire rotor assembly is hermetically sealed and operates in an atmosphere of hydrogen at 5 psia. The flywheel operates over a 2 to 1 speed range (1/2 to full speed) during its normal operation as an energy source or sink. The synchronous motor back emf is sufficient to provide for load commutation of the inverter thyristors.

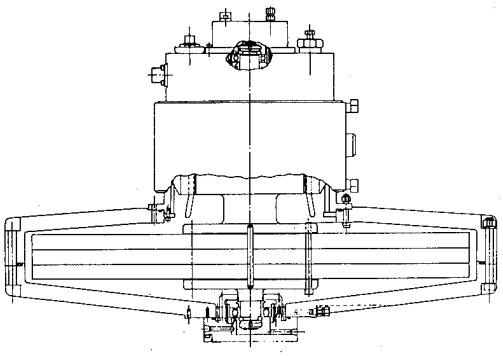


Figure 3. 20 KVA Inductor Motor/ Alternator/Flywheel.

INDUCTOR MOTOR/ALTERNATOR DESIGN

The function of the synchronous flywheel drive motor can best be explained by means of Figure 4. The cross-section shows a DC field coil between two stacks of stator laminations. A DC current in the field coil drives a magnetic flux as indicated through one stack of stator laminations, radially into the rotor, axially through the rotor, and radially out of the rotor through the second stack of stator laminations and the frame to close the loop. Large magnetic slots in the rotor interrupt the flux in the air gap and cause the flux through the AC windings to pulsate. This, in turn, generates an AC voltage in these windings. The windings are located in slots in the laminated stator stacks close to the air gap. In order to make the induced voltage add in both stator stacks, the magnetic rotor slots are offset by one-half mechanical pole pitch. The 20 KVA inductor rotor is shown in Figure 5. This is an 8-pole

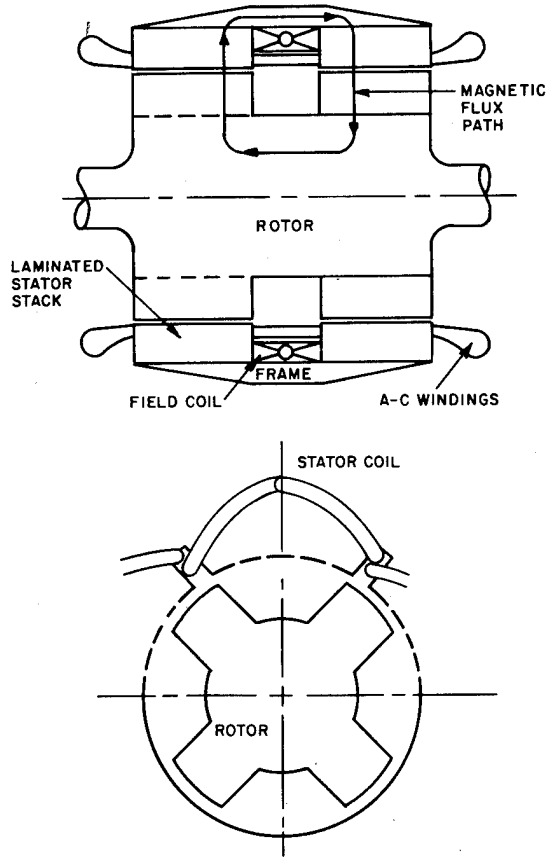


Figure 4. Cross Section of an Inductor/ Alternator (top) and End View of an Inductor/Alternator.

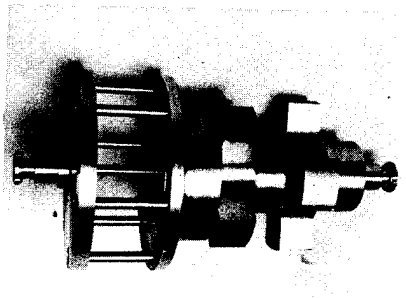


Figure 5. Inductor Motor/Alternator Rotor.

machine. The four poles on the left are north poles, the four poles on the right are offset and are south poles. The flux enters the north pole, flows axially through the rotor and returns through the south poles to the stator. Figure 6 shows a view of the stator windings. The lamination stacks with the central DC field coil are clearly visible.

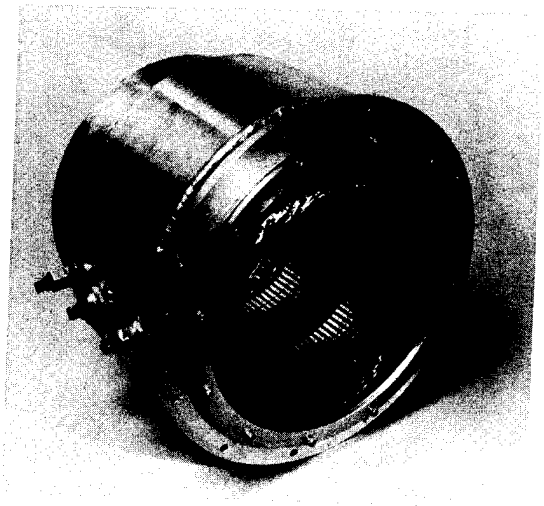


Figure 6. Inductor/Alternator Stator.

COMPOSITE FLYWHEEL

The flywheel consists of three one-inch thick 30" diameter disks. Each flywheel disk is a composite assembly made of laminated sheets of glass fibers and epoxy resin. The material selected is a scotch ply. Each wheel has a circumferential wrap approximately 1/2" thick of kevlar and epoxy tape. The flywheel construction is what we term "alpha 3" made by laying up a series of cross ply layers at 60° intervals. The "alpha" designation refers to the number of individual layers required for a 360° rotation. Alpha-3 has three layers at 120°, Alpha-5 has five layers at 72°, etc. The composite flywheel assembly is shown in Figure 7.

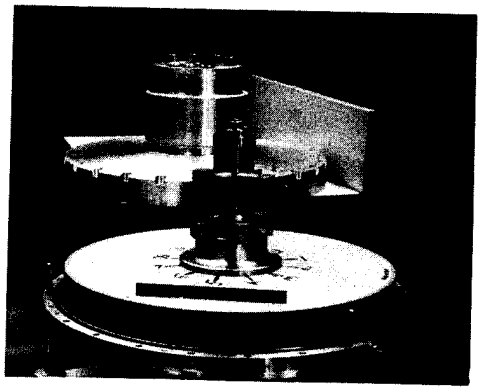


Figure 7. Composite Flywheel Assembly.

SOLID STATE POWER CONDITIONER

The solid state power conditioning equipment serves as an interface between the DC and AC portions of the propulsion system. The power conditioning equipment must have a bi-directional power control capability as it must provide power to the synchronous motor during vehicle braking and extract power from the inductor alternator during vehicle acceleration. This two-way power control need exist over the speed range which the inductor motor must operate at rated power, in this case a 2 to 1 speed range. The synchronous motor back emf is sufficient to provide for load commutation of the inverter thyristers. A starting resister is provided to limit the voltage applied to the synchronous motor during start up. A by-pass contactor removes the starting resistor from the circuit during normal operation of the system.

The load commutated inverter/rectifier consists of two three-phase thyrister bridges connected in inverse parallel so as to provide two-way power flow by reversing the direction of the DC current. The feedback processing circuit senses the three-phase AC current and voltage and supplies feedback signals representing motor operating conditions such as current, speed, and the phase feedback signal which synchronizes the inverter firing to the motor. The system control circuit receives the operator commands of torque required and a motor/brake signal in addition to

feedback signals. These input signals are compared to the motor operating conditions and appropriate commands are sent to the motor field exciters. In addition, the desired inverter frequency is sent to the inverter control. The inverter control then creates SCR gating signals at the desired frequency.

The control system described does not use shaft position sensing, but senses the motor terminal voltage and the AC line current to determine the motor internal operating conditions. The control method maintains the SCR turnoff time as a constant percentage of the period of the generated back emf as speed and current are varied during operation. The inverter turn off time is thus maintained by feedback control rather than the use of special function generators.

BREADBOARD POWER CONDITIONER

The power conditioner selected used 12 main SCR's. Figure 8 is the schematic diagram. The circuit was selected over a 6 SCR circuit because of the need to interface with a battery and the desire not to have to reverse the field current in the DC traction motor which would reverse its armature voltage polarity. Systems that are totally powered by a flywheel through an AC machine and power converter and whose traction motor is provided with reversable field current controller, can use a 6 SCR power circuit for two-way power flow. Another approach for polarity reversal is to provide mechanical reversing contactors rather than the equivalent function with the additional SCR's.

A breadboard of the power conditioner has been fabricated. The equipment shown in Figure 9 includes 12 main SCR's, two auxiliary SCR's, starting resistor, contactors and field current controller. The breadboard uses forced air cooled heat sinks and weighs 124 pounds. About 50 pounds of the total weight is attributed to structural supporting members and air ducts. A reduction in weight can be anticipated by using a 6 SCR power circuit and optimizing the heat sinks to bring the total power conditioner weight to 30 to 50 pounds. The power converter efficiency is computed as being greater than 90% at full power.

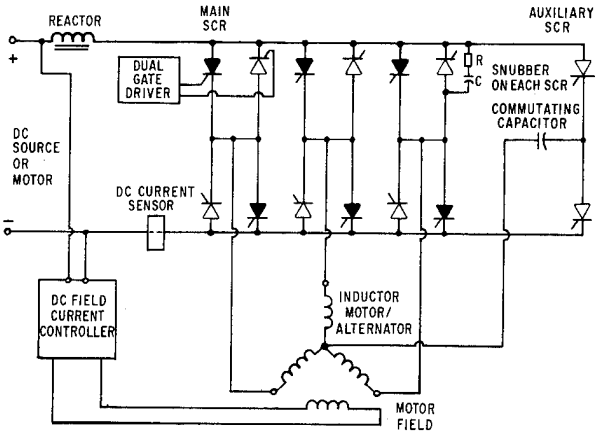


Figure 8. Power Circuit Schematic Diagram.

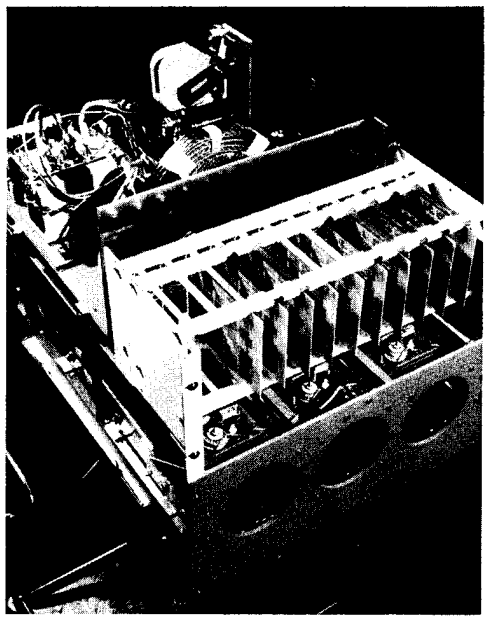


Figure 9. Complete Power Circuit Breadboard

SYSTEM TEST AND EVALUATION

The system is currently undergoing tests in the laboratory. Figure 10 shows the test arrangement. A hybrid controller composed of both digital and analog control elements is used to simulate the propulsion control. This controller provides the overall system control, acquires electrical signals from sensors, computes intermediate results, accumulates variables with respect to elapsed time, and stores results for later

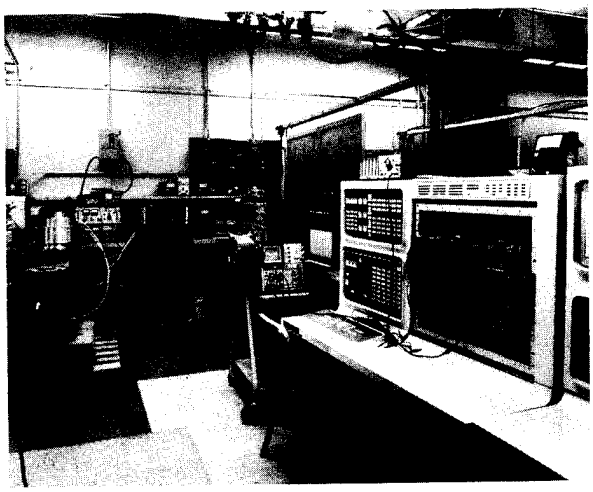


Figure 10. Laboratory Test Arrangement.

analysis.

During the test phase of the project important parameters such as the power conditioner efficiency, inductor machine efficiency, and overall energy storage efficiency will be evaluated.

HYBRID FLYWHEEL/BATTERY ELECTRIC VEHICLE PERFORMANCE

General Electric is currently developing under a separate contract with ERDA, a four-passenger all battery electric vehicle which will weigh approximately 3000 pounds. ERDA has elected to evaluate the performance of this vehicle under a typical urban driving cycle which is known as the SAEJ-227A Schedule D cycle. This SAE cycle requires that the vehicle accelerate from zero to 45 mph in 28 seconds, cruise at 45 mph for 50 seconds, coast for 10 seconds and then decelerate to rest in 9 seconds, followed by a dwell for 25 seconds. This duty cycle results in one stop per mile with an average speed of approximately 38 mph. Analysis has shown that with this type of flywheel energy recovery system, about 65% of the braking energy can be recovered which will have the effect of providing about a 22% improvement in range for the J227A Schedule D Driving Cycle. The range for the 3000 pound vehicle with two passengers will increase from 39 miles to approximately 49 miles. For the analysis, vehicle weight was held constant by removing batteries in the hybrid vehicle to offset the additional weight of the flywheel propulsion system. Analysis has shown that as the number of stops per mile increase, the greater will be the increase in range when a flywheel is used for regeneration. Calculations have shown that with eight stops per mile it is possible to double the range of a non-regenerative battery vehicle.

Figure 11 shows an artist's concept of a four-passenger flywheel/battery hybrid vehicle. The flywheel energy storage package would be located in the front of the vehicle, ahead of the DC traction motor. The solid state load commutated inverter and its control and relay group would be located on the fire-wall of the vehicle. The battery pack, would be located in a tunnel in the center of the vehicle.

General Electric is also conducting a study with the Urban Mass Transportation Administration of the U.S. Department of Transportation on a flywheel powered transit bus. Approximately 27 different flywheel & hybrid bus propulsion systems have been evaluated in this study. The inductor motor flywheel system with load commutated inverter was found to be ideally suited to both hybrid and all-flywheel powered buses. Figure 12 schematically shows the inductor DC flywheel system applied to an all-flywheel powered bus. The system would be charged from a wayside DC substation and the bus would retain its proven DC traction motor which is currently used in electric trolley buses in a number of cities. The on-board power conditioning unit would be the load commutated inverter. A steel flywheel would be used to store the necessary energy to propel the bus over its normal duty cycle.

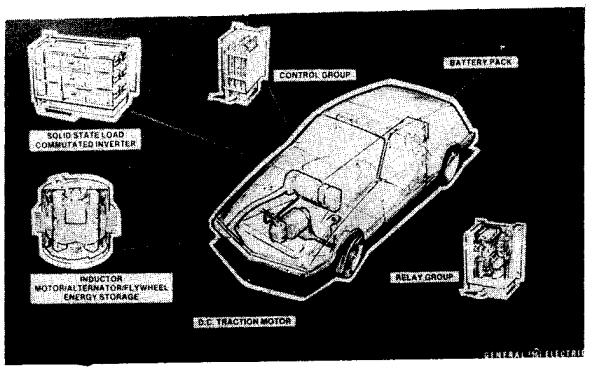


Figure 11. ERDA Battery/Flywheel Hybrid Electric Vehicle.

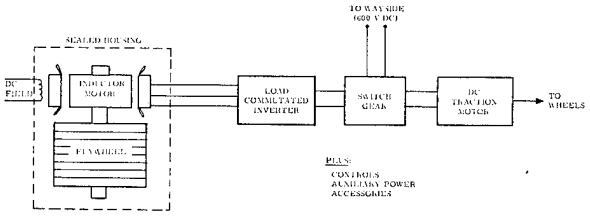


Figure 12. Schematic of Inductor/DC Flywheel System.

The same propulsion system can be used either with a wayside station for an all-flywheel powered bus or in combination with overhead wires to give off-line capability to present trolley buses. The same system is also compatible with a battery hybrid. Figure 13 shows an artist's concept of the flywheel propulsion package installed in an urban transit bus.

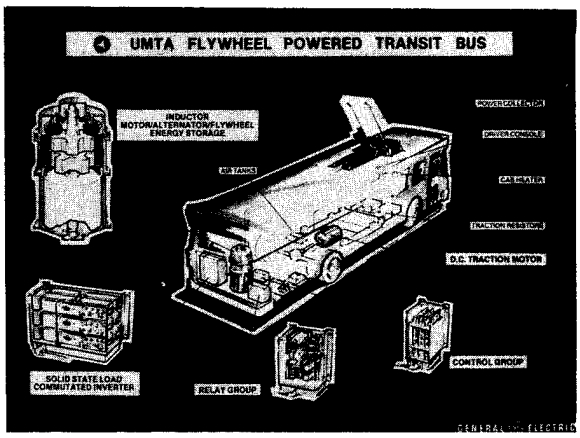


Figure 13. All Flywheel Powered Transit Bus.

CONCLUSIONS

The current ERDA program is expected to demonstrate the inductor motor/alternator/flywheel energy storage system in the laboratory and provide data to confirm the performance predictions relating to various transportation applications - flywheel hybrids and all-flywheel powered vehicles. Analyses which have been made indicate that an energy storage and recovery system of this type can significantly increase the range of a multi-stop battery electric vehicle. The technology is expected to have wide application for hybrid propulsion systems.

REFERENCES

1. Richter, E., "New Developments in Very High Speed Electrical Alternator," Intersociety Energy Conversion Engineering Conference, Boston, 1971.

2. Guess, R.H. and Lustenader, E.L., "Development of a High Performance and Lightweight Hybrid Flywheel/Battery Powered Electric Vehicle Drive," Fourth International Electric Vehicle Symposium, Dusseldorf, Germany, Aug., 1976.

3. Bedford, B.D. and Hoft, R.G., Principles of Inverter Circuits, John Wiley & Sons, N.Y., 1965, Ch. 3.

4. SCR Manual, 5th Edition, General Electric Co., Syracuse, N.Y., 1972.

5. Pelly, B.R., Thyristor Phase-Controlled Converters and Cyclo-converters, Wiley-Interscience, N.Y., 1971, Ch. 3 and 5.

6. Moltgen, G., Line Commutated Thyristor Converters, Pitman, London, England, 1972, Ch. 4.

7. Bakharerskŭ, V.P. and Utevskii, A.M., "A Circuit for Two-Stage Artificial Commutation of an Inverter," Direct Current, 3, No. 5, June, 153-159 (1957).

8. Steigerwald, R.L. and Lipo, T.A., "Analysis of a Novel Forced Commutation Starting Scheme for a Load Commutated Synchronous Motor Drive," 1977 IEEE/IAS Annual Meeting Conference Record.

9. Plunkett, A.B. and Turnbull, F.G., "Load Commutated Inverter/Synchronous Motor Drive Without a Shaft Position Sensor," 1977 IEEE/IAS Annual Meeting Conference Record

10. Lustenader, E.L., Chang, G., Richter, E., Turnbull, F.G., Hickey, J.S., "Flywheel Module For Electric Vehicle Regenerative Braking," 12th Intersociety Energy Conversion Engineering Conference, Washington, D.C., August, 1977.

ROCKETDYNE'S HIGH-ENERGY-STORAGE FLYWHEEL MODULE FOR THE U.S. ARMY

Dr. D. Davis and D. Hodson
Rockwell International/Rocketdyne Division
6633 Canoga Avenue
Canoga Park, California 91304

and

C. Heise
U.S. Army MERADCOM
Ft. Belvoir, Virginia 22060

ABSTRACT

The Rocketdyne Division of Rockwell International Corporation is developing an advanced 30 kW-hr high-energy-storage flywheel module for the U.S. Army. The module is designed to utilize the Rocketdyne-modified constant stress isotropic rotor system with a disc energy of 11.6 W-hr/lb at its rated speed. The flywheel system incorporates two counter-rotating assemblies connected through a common gearbox with each rotating assembly being comprised of two flywheel discs. The Rocketdyne-modified constant stress flywheel system has been fully tested on a subscale basis with the results of an energy storage density at disc failure in excess of 21 W-hr/lb. A significant advantage of the rotor system is the fail-safe mode of failure which has been demonstrated through subscale testing.

INTRODUCTION

Rockwell International has been actively involved in flywheel development programs since 1964,[1,2] at which time a composite rotor system was designed and tested for helicopter "quick getaway" assistance.

Rocketdyne's flywheel system approach is based on a foundation of over 20 years in the design and manufacture of high-speed rotating machinery. Operating speeds of 30,000 to 40,000 rpm have been used on almost all Rocketdyne rocket engine turbomachinery. This expertise has been used directly to develop advanced flywheel systems. Although parallel efforts concerning both isotropic and anisotropic flywheel programs have been pursued, the major emphasis to date has been the intensive development of the isotropic (steel) flywheel system due to its near term reliability for large flywheel assemblies. Based upon the more than 10 years of Rockwell International experience in research, design, fabrication, development, and delivery of flywheels for land-based systems, aircraft and space systems,[3,4,5] Rocketdyne has introduced a highly optimized patent-pending flywheel rotor system. The rotor system is characterized by high-energy storage efficiency at reduced levels of hub stress resulting in a comparably higher safety margin for any given application. Equally significant attributes of safety are emphasized by providing capability in the design for accurate sensing of disc strain during operation by providing a means for mechanical restraint to overspeed and disc growth and for limiting and/or containing burst modes of failure. These design characteristics have been demonstrated by rotor test to destruction with precise verification of strain, yield, and burst predictions.

The present U.S. Army program[6] involves the design, fabrication, test, and delivery of a 30 kW-hr isotropic flywheel module.

An extensive series of experimental rotor failure tests of the Rocketdyne flywheel system has been completed on a subscale basis. The purpose of the experimental tests were to verify failure modes and to increase the competence level with respect to the projected subtle and fail-safe mode of rotor failure.

Included in this paper are the results of subscale rotor testing, performance requirements of the large flywheel module, as well as rotor and profile approaches being pursued by Rockwell International.

DESIGN APPROACHES

U.S. ARMY MERADCOM MODULE

The U.S. Army high-energy flywheel is an isotropic rotor system, each rotor disc having the capacity for storage of 7.5 kW-hr. There are four individual flywheel discs of which two each are mounted on counter-rotating shafts interconnected to a gearbox. The flywheel module is powered by a Lycoming gas turbine which supplies power to each successive counter-rotating shaft through the gearbox, which is mounted as an interface between the gas turbine and flywheel module casing. The flywheel module as shown in Fig. 1 incorporates Rocketdyne's unique flywheel profile which incorporates a failure mechanism which, if failure does occur, the flywheel system is designed to minimize destructive release of energy. Each disc of the flywheel module is designed with energy storage capacity in excess of 11.6 W-hr/lb of disc weight. The 11.6 W-hr/lb is at a peripheral speed of 2420 ft/sec. At rated speed, a factor of safety in excess of 1.6 based upon ultimate of material is experienced by the isotropic material. The flywheel discs are attached to the hub section by the incorporation of a unique attachment configuration which does not compromise the integrity of the disc proper. The flywheel module is designed to accommodate high vacuum and incorporate braking rings which surround each of the four discs within the module. The purpose of the braking ring is to limit the flywheel overspeed based upon the radial growth of rotor versus speed conditions. Due to the fact that the rotor is operating at a rate of speed well below the material yield point, an elastic condition occurs throughout the rpm duty cycle up to and exceeding the rated speed by 30 percentile. The proper utilization of this elastic nature of the isotropic rotor allows for precise prediction of rotor speed based upon radial growth and also allows for overspeed protection by utilization of the braking ring. Experimental verification of the braking ring concept and failure modes have been accomplished successfully with data providing information exceeding theoretical predictions.

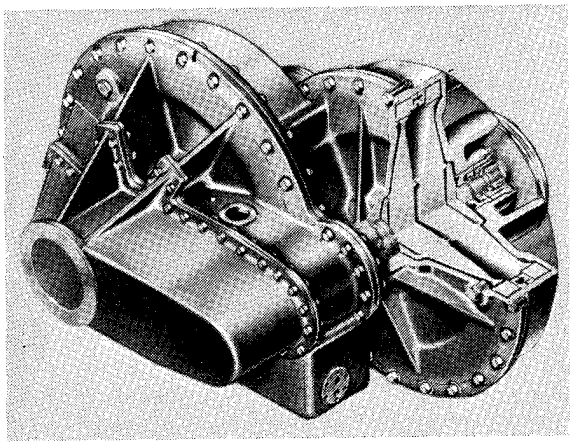


Fig. 1. U.S. Army 30 kW-hr Module

ISOTROPIC MATERIAL SELECTION

Candidate materials for applications for high-strength, high-energy density steel flywheels must have the capability of being fully hardened to high yield and ultimate strength levels, and possess good ductility, fatigue strength, and fracture toughness. Additionally, the material must be amenable to the standard fabrication processes such as forging, machining, heat treating, and welding, without undue distortion. It must also be capable of being inspected by ultrasonics, and magnetic particle or placement penetrant procedures. Consequently, only materials with known characteristics that could be applied to the design, fabrication, and testing of the flywheel system were considered.

The need for high strength to permit the use of as high a design allowable stress as possible is illustrated in Fig. 2. This figure shows that the energy that can be stored per pound of flywheel weight increases directly as the increase in allowable design stress. Also, higher allowable stresses tend to dictate higher operational speeds.

Good ductility in conjunction with high strength is required to permit localized plastic yielding at unavoidable stress concentrations. High fatigue strength is mandatory especially in the high-stress, low-cycle life range to minimize possible damage resulting from recharging and discharging duty cycles.

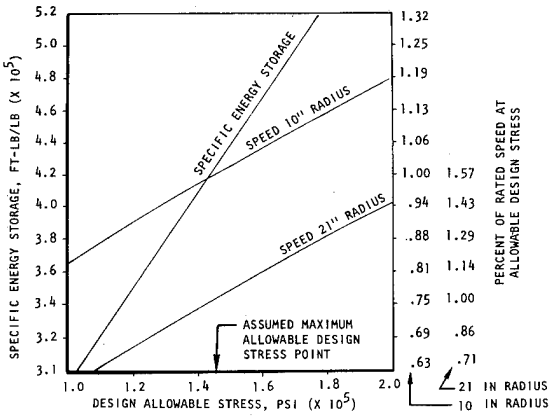


Fig. 2. Percent of Design Allowable Stress and Specific Energy of the Optimized Disk Flywheel (Steel)

Of prime importance in the selection of flywheel materials is the basic steel hardenability. Unless a material can be fully hardened to 100 percent martinsite in the thickest section of the flywheel where the stress are very high, the full capability of the material is not being utilized. Lower strength and lower power fatigue strength results when less than full hardening is attained.

High fracture toughness is important from both the threshold stress intensity levels and crack growth rates due to the magnitude of surface and subsurface flaws that can be undetectable by the best non-destructive test methods.

A survey of flywheel projects was conducted to verify materials being used on flywheel projects other than those being conducted by divisions of Rockwell International. One very important point must be made at this time. There have been no complete life cycle tests and evaluations of high-strength, high-energy density flywheels to date. Several high-strength flywheels have been constructed and tested for a limited number of cycles, but none of these units have been noted to undergo the high cyclic life testing necessary to ensure flywheel life and establish safety margins.

Of the four candidate materials that have been considered, AISI 4340-grade steel has undergone the greatest amount of high-strength flywheel testing. A steel flywheel forged from a billet of 300 M(VAR) steel, a modified AISI E4340 chromium nickel molybdenum alloy, was an end result of the Environmental Protection Agency Contract No. EHS 7-104 and has experienced limited testing. Properties of the four candidate materials that have been closely studied for flywheel application are listed in Table 1.

Table 1. Candidate Isotropic Flywheel Materials

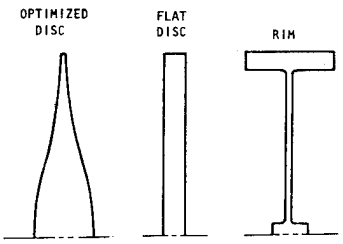
	4340 Steel	18Ni-250 (Maraging Steel)	hp-9-4-20	hp-9-4-30
Density, lb/in.^{3}	0.283	0.289	0.283	0.283
Poisson's Ratio	0.32	0.30	0.296	0.296
Tensile Ultimate, F_{tu}, ksi	260	270	190/215	220/240
Tensile Yield, F_{ty}, ksi	217	265	180/195	190/215
Weldability	poor	fair	best	good
Fatigue Strength	poor	fair	good	best
Impact Strength	fair	fair	best	good
Availability	good	good	good	good
Elongation, percent in 2 inches	poor	6	14/19	10

Additional candidates including, but not limited to, the following were reviewed: 300 M (carbon and silicone modified 4340) Hy 180 (10 percent Ni modified).

The 9-4 series alloy steels[7,8] are currently in use at Rockwell International for flywheel programs at the Los Angeles Division (hp-9-4-20) and at Rocketdyne (hp-9-4-30). Based upon extensive sample and rotor tests of the hp-9-4-30, Rocketdyne has identified the hp-9-4-30 as the optimum isotropic flywheel material. This material is being utilized in the U.S. Army MERADCOM flywheel module.

ROTOR PROFILE APPROACH

Flywheel Characteristics. Figures 3 and 4 graphically illustrate another point. There is a persistent belief that a rim-type flywheel will store more energy than any other type. Intuitively, it seems logical that this is true because the rim-type concentrates the mass near its outer radius where, presumably, it will do the most good. Therefore, it seems that this must be the most effective cross section. The data listed in Fig. 3 and 4 demonstrate that this is not the case. Figure 3 compares equal weight and equal diameter flywheels of the "optimized," flat disc, and rim types for relative energy storage capability. It can be seen that the optimized type stores more than one and one-half times as much as the flat disc type and nearly two times as much as the rim type. On the other hand, if it is assumed that the rotational speed and energy of the

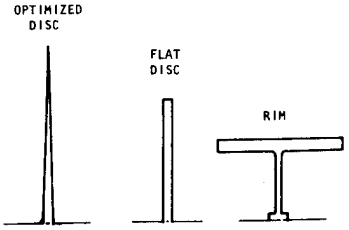


OUTSIDE DIAMETER, INCHES	10	10	10
WEIGHT, POUNDS	12.4	12.4	12.4
KINETIC ENERGY, IN.-LB	5.09×10^6	3.7×10^6	2.74×10^6
SPECIFIC KINETIC ENERGY, IN.-LB/LB	410,000	298,000	220,000
ANGULAR VELOCITY, RAD/SEC	6,584	4,280	2,750

ASSUMPTIONS:

1. FOR RIM TYPE, 90 PERCENT OF WEIGHT IS EFFECTIVE AT OUTSIDE DIAMETER, 10 PERCENT IS INEFFECTIVE AS A FLYWHEEL
2. SPEED IS LIMITED BY MAXIMUM STRESS AT ANY POINT
3. MATERIAL PROPERTIES: (STEEL)
   - 140,000 PSI MAXIMUM STRESS
   - 0.3 POISSON'S RATIO
   - 0.285 LB/IN.^{3} DENSITY
4. STRESS CONCENTRATION POINTS IN RIM FLYWHEEL DESIGN ARE NEGLECTED.

Fig. 3. Equal Weight and Equal Diameter Flywheels



OUTSIDE DIAMETER, INCHES	20	13	8.38
WEIGHT, POUNDS	14.9	20.5	27.7
KINETIC ENERGY, IN.-LB	6.1×10^6	6.1×10^6	6.1×10^6
SPECIFIC KINETIC ENERGY, IN.-LB/LB	410,000	298,000	222,000
ANGULAR VELOCITY, RAD/SEC	3,292	3,292	3,292

ASSUMPTIONS

1. FOR RIM TYPE, 90 PERCENT OF WEIGHT IS EFFECTIVE AT OUTSIDE DIAMETER, 10 PERCENT IS INEFFECTIVE AS A FLYWHEEL
2. SPEED IS LIMITED BY MAXIMUM STRESS AT ANY POINT
3. MATERIAL PROPERTIES: (STEEL)
   - 140,000 PSI MAXIMUM STRESS
   - 0.3 POISSON'S RATIO
   - 0.285 LB/IN.^{3} DENSITY
4. STRESS CONCENTRATION POINTS IN RIM FLYWHEEL DESIGN ARE NEGLECTED.

Fig. 4. Equal Speed and Equal Energy Storage Flywheels

three types of flywheels are to be equal (as shown in Fig. 4), then the weight of the optimized type is nearly one-half that of the rim type and less than three-fourths that of the flat-disc type. The only set of circumstances in which the rim type could prove superior would be one wherein the allowable outside diameter and the rotational velocity were simultaneously restricted. Usually this would make it impossible to stress the material in the truncated conical disc flywheel anywhere near its capabilities and would, thus, reduce its energy storage efficiency disproportionately.

Essentially, the specific energy storage capabilities (ft-lb/lb) of the truncated conical disc flywheel are directly porportional to the strength density ratio. Since specific energy is the best available measure of the basic energy storage efficiency of the flywheel, every effort should be made to use a material that has the highest possible allowable design strength and/or lowest possible density.

Figure 5 shows the position that the truncated conical disc flywheel takes in a family of known flywheel shapes[9,10] in terms of "shape factor." Shape factor is a measure of energy storage efficiency in which a shape factor of 1.000 means that all material in the disc is being stressed perfectly uniformly and, hence, is being

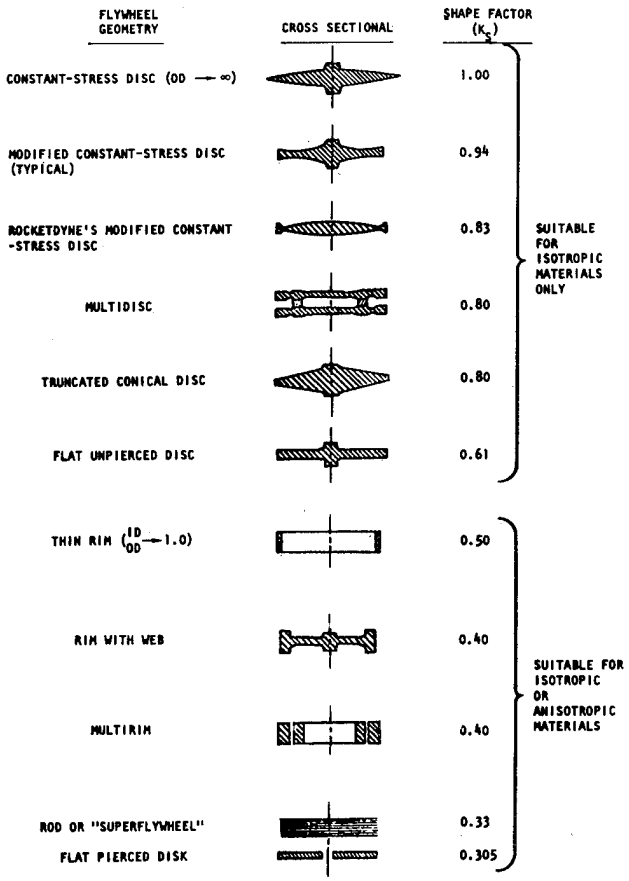


Fig. 5. Flywheel Shape Factors for Various Geometries

used efficiently. It can be seen from the figure that the optimized disc is at the top of the achievable configuration.

Modified Constant Stress Disc. At Rocketdyne, a modified form of the constant stress disc has been formulated to use the best features of both the rim type of flywheel and the truncated conical disc. Modified constant stress discs with a shape factor as high as 0.85 to 0.90 have been fabricated successfully by others; however, in the interest of achieving definable containment of the disc failure, Rocketdyne has chosen to trade off some of the spatial advantage for safety. In actual practice, the few points of difference achieved at the flywheel disc is overcompensated by the accessory design and casing arrangements that vary with each application. Rocketdyne has formulated a 7.5 kW-hr modified constant stress disc configuration under U.S. Army MERADCOM Contract DAAG55-75-6-0278, wherein a shape factor of 0.83 is achieved. This specific disc has been characterized by computer programs to formulate the capability to adapt the configuration for multiple wheel sizes and power requirements. The resulting disc configuration in combination with a relatively light, thin barrier ring offers what is believed to be the optimum state-of-the-art system in terms of safety and performance efficiency.

SUBSCALE ROTOR TESTS

The Rocketdyne flywheel rotor system was successfully tested on a subscale basis to verify failure modes and factor of safety based on overspeed tolerances. There were five successive tests of the subscale rotor system (Fig. 6), of which the final test was to demonstrate actual rotor failure modes and energy storage density at failure.

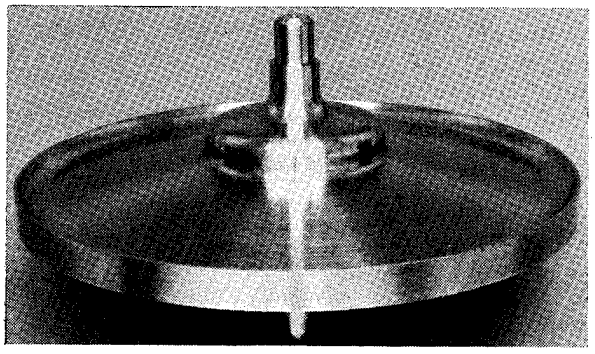


Fig. 6. Subscale Rotor, Pretest

The subscale rotor was designed to provide the exact one-on-one stress profile that the full-size rotor will experience. To accomplish this, the subscale rotor was rated at 39,750 rpm. At rated speed, the rotor energy storage density for both the full size and subscale rotor was designed at 11.6 W-hr/lb of rotor weight.

TEST NO. 3 (BRAKING RING VERIFICATION)

During Test No. 3, the subscale rotor was allowed to overspeed to verify the braking ring concept. The braking ring was designed to limit an overspeed condition at 20% of rated speed. This concept was verified when the rotor obtained 47,760 rpm (120.15% of rated speed) and it ceased to rotate at higher speed. After successive attempts to overspeed past 120.15% of rated speed failed, the rotor was removed for inspection. The wheel was examined posttest showing a rub mark over a local area of the outer rim face about 5 inches long circumferentially. The hardness reading in this area was found to have increased from the machined value of 50 to a local hardness of 55 slightly increasing local strength and brittleness but of no significant consequence to further test. Penetrant inspection was passed and the rotor was returned for Test No. 4. The barrier ring also showed local rub marks in two adjacent areas of about 5 inches each around its 14-inch ID. Both parts remained within their fabricated tolerance of ±0.001 inch radially with no evidence of rotor permanent deformation. The barrier ring was then resized to 14.117-inch ID preparatory to Test No. 4.

TEST NO. 4 (ELASTIC/PLASTIC TEST DATA)

During Test No. 4, speed was momentarily brought to 51,060 rpm and then held between 50,000 and 50,500 rpm for 7 minutes. During this period, rotor-to-ring gap was recorded and compared to elastic and plastic growth predictions and it was concluded a small permanent deformation of about 0.002 had been encountered. The possibility of uneven thermal growth influence was considered in estimating whether or not yield had occurred. As a check, speed was then reduced to 45,460 rpm. Figure 7 shows the traverse up and back to 45,460 rpm. Rotor radius enlargement was recorded at all reduced speeds relative to the initial upramp. From 46,000 rpm, rotor speed was increased to 51,500 rpm, where further yield was evident. At this level, the deviation

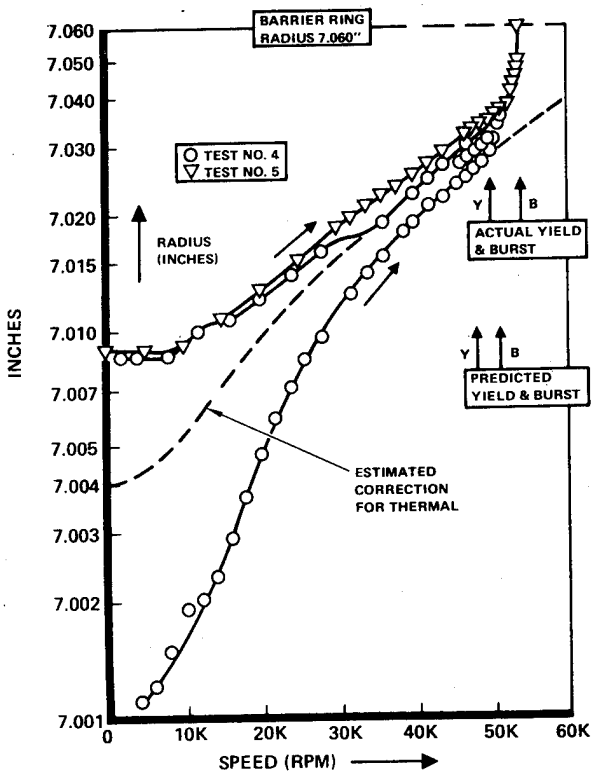


Fig. 7. Subscale Rotor Experimental Radius vs Speed Data

appeared to be 0.005 inch; however, at speeds between 35,000 and 40,000 rpm, a value of 0.004 to 0.0035 inch radial growth was indicated. After the test, rotor measurements were taken verifying that the pretest gap of 0.0585 was reduced to about 0.055 indicating about 0.0035 inch growth. The data of Fig. 7 indicates that the first yield occurred about 50,000 rpm. A reacceleration from 40,000 rpm seems to pass 50,500 rpm and reach 51,000 rpm before further yield is evident. In subsequent Test No. 5, the data indicates that speed was brought to about 52,000 rpm before the growth rate accelerates.

TEST NO. 5 (BURST TEST)

Rotor growth was displayed on a digital meter and recorded manually as the speed was increased. As speed passed 53,000 rpm, it was recognizable to the observer that growth was accelerating and that failure was imminent some 80 seconds before rim loss occurred. At 53,790 rpm, the gap detect circuit output was seen to surge, indicating that the rotor rim was contacting barrier ring. Four seconds later, failure at 53,800 rpm was clearly audible. Based on test data and posttest evaluation of hardware, the mode of failure is characterized as follows:

1. Rotor yield accelerated between 52,500 and 53,800 rpm until barrier ring contact was noted.

2. At 53,800 rpm frictional heating of the rubbing rim accelerated weakening and caused fracture 360 degrees around the rotor at the neck region (Fig. 8).

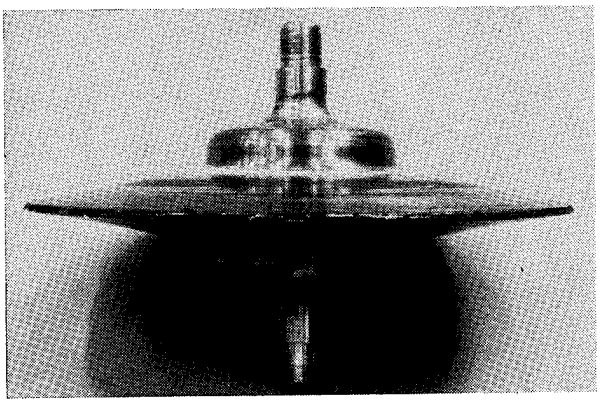


Fig. 8. Subscale Rotor, Posttest

TEST CONCLUSIONS

1. Restriction of barrier ring clearance is an effective safety measure for ensuring that the rotor can not grow beyond the elastic limit whether due to overspeed or overheating. This conclusion is derived from results of Test No. 3 where a 20% overspeed condition was safely concluded by braking action of the barrier ring.

2. Rotor operation to 125.8% of rated speed (50,000 rpm) was accomplished safely using gap detect monitoring. Although operation to this point of initial yield should not be allowed, it served to dramatize the margin of safety at rated speed.

3. The flywheel material and physical design strength was conservatively predicted and the mode of failure of the rim without disc fracture was correctly projected so that in the extremely unlikely event of overstress to the failure point only about 20% of the stored energy is released in centrifugal momentum.

4. The selected material, hp-9-4-30, can be machined and electron beam welded in the fully heat treated state to obtain a product of high quality and predictable performance.

5. The anticipated material properties of hp-9-4-30 such as strength and elongation were demonstrated to be valid, qualifying this material for high performance flywheel design and construction.

6. In the case where conditions are allowed to proceed to burst, the flywheel failure mode results in less destructive energy than alternative configurations yet has a higher performance index in terms of stored energy per pound of material at any given stress level.

7. Energy storage efficiencies for the disc and rotor assembly were computed as follows:

	Speed, rpm	Efficiencies ($\varepsilon_d/\varepsilon_r$), W-hr/lb
Design	39,750	11.6/10.1
Yield	50,000	18.4/16.0
Failure	53,000	21.2/18.5

TEST ACCOMPLISHMENTS

1. The highest speed of operation without permanent deformation was identified during Test No. 4 as 49,500 rpm (24.5% over rated speed).

2. During Test No. 4, it was indicated that permanent deformation in amounts as small as 0.001 to 0.002 can be detected during rotor operation.

3. The capability of monitoring rotor operation at 95 to 96% of burst speed was demonstrated during Test No. 4 as speed was safely varied from 0 to 50,520 rpm, reduced to 45,460 rpm, returned to 51,520 rpm and reduced to 0 rpm without loss of integrity.

4. Test No. 5 served to verify the precision of stress analysis employed in the design of the flywheel rotor wherein failure of the rim was planned and demonstrated without incurring loss in integrity in the hub section which was stressed to 97% of the neck load.

REFERENCES

1. Energy Storage Substation Concepts for Aircraft Actuation Functions; Rockwell International Contract No. AF33(615)-2971, completed 1 March 1966.

2. Experimental Demonstration of Energy Storage Substations; Rockwell International Contract No. AF33(615)-5173, completed 31 December 1967.

3. Integrated Power/Attitude Control System (IPACS) Study; Rockwell International Contract No. NAS1-11732, completed October 1973.

4. "Emergency Pump Systems are Bootstraps to Power," Product Engineering, 20 May 1968.

5. Helsley, C. W., "Weight is Saved When Flywheel Energy Storage Unit Supplements Aircraft Secondary Power Systems," SAE Journal, January 1969.

6. Davis, D. E., "The USA-MERADCOM High Energy Storage Flywheel Module," 1975 Flywheel Technology Symposium, 11 November 1975.

7. Properties of Production Product of HP 9-4-30 (CR, Mo); Republic Steel Research Center, 8 December 1965.

8. Fatigue Properties of HP 9NI-4CO Steels; Republic Steel Research Center, 30 December 1968.

9. "Design and Testing of High Energy Density Flywheels for Application to Flywheel/Heat Engine Hybrid Vehicle Drives," SAE 1971 Intersociety Energy Conversion Engineering Conference Proceedings, p. 38.

10. Dann, R. T. "The Revolution in Flywheels," Machine Design, 17 May 1973.

AN ADVANCED VEHICULAR FLYWHEEL SYSTEM FOR THE ERDA ELECTRIC POWERED PASSENGER VEHICLE

D. A. Towgood
AiResearch Manufacturing Company of California
Torrance, California

ABSTRACT

The purpose of this paper is to establish a rationale for the feasibility of composite material flywheels for use in urban vehicles. Comparisons in terms of safety, weight, and costs will be made between steel flywheels and composite material flywheels. This paper will also review pertinent results of the MERADCOM flywheel development program. An operating energy density of 21 w-hr/lb has been achieved in this test program. The results of this program have led to the selection of a composite material flywheel in the Energy Research and Development Administration (ERDA) electric powered passenger vehicle. Pertinent aspects of the energy storage unit design will be discussed.

INTRODUCTION

This paper discusses the feasibility of composite material flywheels for urban vehicle use; in particular, it will discuss the ERDA electric powered passenger vehicle.

AiResearch has been involved in the study, design, and manufacture of energy storage systems for over 8 years. As shown in Fig. 1, AiResearch has designed and built steel flywheel rotors for the R-32 and ACT-1 flywheel systems for rail mass transportation and for the University of Wisconsin automotive flywheel installed in a Ford Pinto.

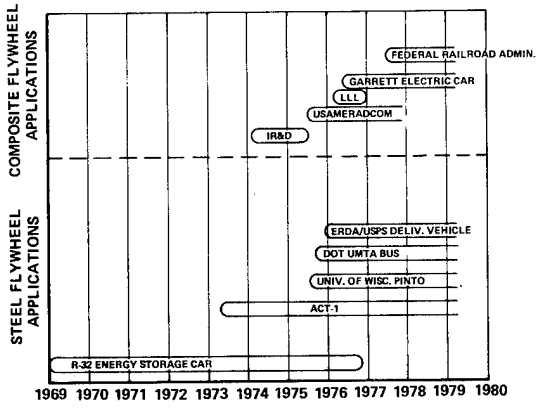


Fig. 1. AiResearch flywheel energy storage systems.

AiResearch has been actively involved in the field of composite material flywheels since 1974. The initial studies and testing were accomplished in a company-funded research program on a multirim E-glass rotor. The next major program involved the U.S. Army MERADCOM composite flywheel rotor, which utilized a multirim Kevlar-49 (Dupont Trademark) rim. The results of this program have been used to help establish the design for the ERDA electric car flywheel rotor.

COMPOSITE MATERIAL FLYWHEEL BACKGROUND

COMPOSITE MATERIAL IR&D FLYWHEEL

The design and testing of the initial composite flywheel was undertaken by AiResearch in 1974. This program verified the feasibility of the AiResearch multiring rim flywheel design. As shown in Fig. 2, the flywheel rim comprised four layers or rings of filament-wound E-glass in an epoxy matrix. Each layer was 1/4-in. thick by 2 in. wide, with an outside rim diameter of 26 in. This rim was mounted on a 4-spoke aluminum hub, and the assembly was run in an evacuated spin pit to 1920 fps rim speed. At this speed, the rim energy density was 16.8 w-hr/lb. The hub, which was a heavy test hardware piece (24 lb), reduced the overall energy density to 8.8 w-hr/lb. This rotor was cycled 1035 times between 1870 and 1070 fps to establish that this design could withstand cyclic loading. Subsequent inspection revealed no obvious signs of deterioration.

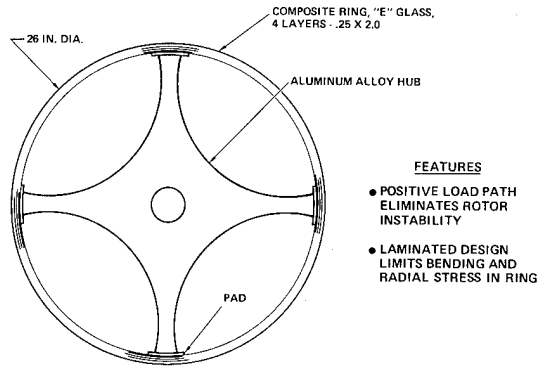


Fig. 2. Composite ring flywheel-IR&D.

MERADCOM FLYWHEEL

The next composite flywheel program by AiResearch was the MERADCOM composite flywheel. This program initially involved the design and testing of 16-in.-dia. Kevlar-49 epoxy rings to evaluate processing and material properties prior to fabricating and testing a full-size flywheel rotor module. Two basic tests were run on the 16-in. rings. First, the rings were loaded hydraulically in a hydrostatic test fixture. Both cyclic and burst tests were run on the hydraulic rig. In the second test, rings were spun to burst speed in a spin pit, shown in Fig. 3. The spin arbor and ring is shown in Fig. 4. Good correlation was found between the composite strengths determined by the hydro-burst and spin tests, with a demonstrated average ultimate strength of 260 ksi.

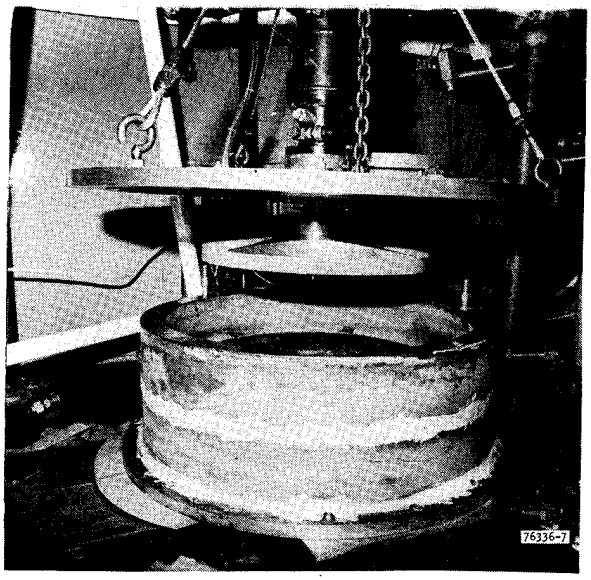


Fig. 3. Spin facility.

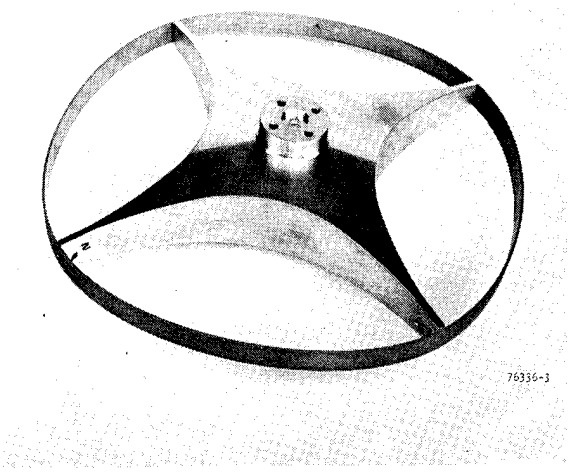


Fig. 4. Spin test flywheel.

The extremely high peripheral velocities achieved (up to 3846 fps) were very encouraging. The average energy density of the single 16-in. rings in these tests was 84 w-hr/lb at failure. The energy density of a complete energy storage rotor will be considerably less due to required margins of safety on stress and the diluting effect of the hub and shaft weight.

The final MERADCOM flywheel submodule shown in Fig. 5 was an 8-ring rim, with a 42-in. outside diameter. The rings were

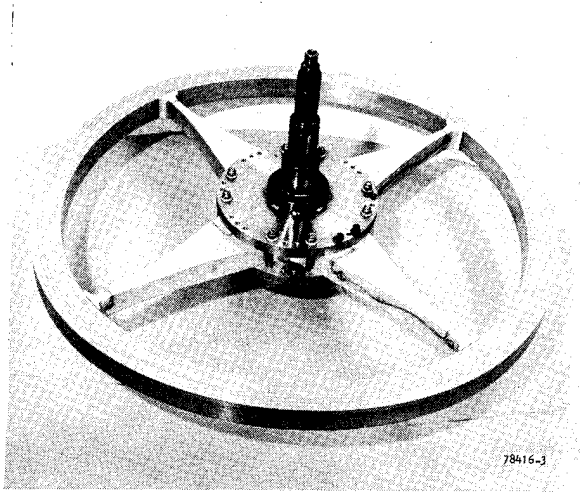


Fig. 5. MERADCOM 8-ring rim.

wound of Kevlar-49 in an epoxy matrix. The rim was mounted on a 4-spoke aluminum hub and successfully run to an operational tip speed of 2750 fps. Subsequent inspection of the rotor revealed no sign of degradation. At this speed, the energy density of the rim was 39 w-hr/lb and the energy density of the rim-hub assembly was 21 w-hr/lb.

Besides demonstrating these energy densities, this rotor demonstrated successful operation on a two-bearing rotor configuration of the type required in a vehicle. Previous testing of composite material flywheels had been performed on a rotor suspended on a flexible damped quill shaft system that is relatively insensitive to rotor radial and moment unbalance. Although the flexible quill shaft system is ideal for laboratory testing, it would be unable to support a flywheel under the maneuver and gyroscopic loads experienced in a vehicle.

ELECTRIC POWERED PASSENGER VEHICLE

PROGRAM DESCRIPTION

Under the Electric Powered Passenger Vehicle (EPPV) program, AiResearch has contracted with ERDA to design and develop a complete electric powered vehicle. Basically the objectives of the ERDA EPPV program are to define and develop a 4-passenger electric vehicle that will meet minimum urban range with acceptable performance, cost, and safety. The major objectives of the program are shown in Table 1.

Table 1. AiResearch EPPV design goals.

MIN. PASSENGER CAPACITY	4 ADULTS
MAX. CURB WT., LB	2566
MIN. URBAN RANGE (J227D), MI	75
MAX. INITIAL COST, PROJECTED, 1975$	5000
MIN. LIFE, MI	100,000
MAX. LIFE-CYCLE COST, PROJECTED, 1975$/MI	0.15
MAX. ELECTRIC RECHARGE ENERGY IN URBAN DRIVING, KW-HR/MI	0.391
MAX. RECHARGE TIME, HR	6
MIN. TOP SPEED, MPH	70
MIN. ACCESSORIES	HEATER/DEF. ONBOARD CHARGER
SAFETY FEATURES	ALL FMVSS REQUIREMENTS
MIN. ACCELERATION (0 TO 30 MPH), SEC	6
MIN. MERGING TIME (25 TO 55 MPH), SEC	10
SUSTAINED SPEED ON 5% GRADE, MPH	50
BATTERY TYPE	LEAD-ACID
MIN. AMBIENT TEMP. RANGE, °F	-20 TO + 125

The present state-of-the-art electric vehicles have marginal range, and they also have low acceleration capability, which could be dangerous for urban driving. Table 2 compares the present electric vehicle characteristics with those of the future. The use of the flywheel-augmented power system offers promise of overcoming the major shortcomings of the present electric vehicles: short range, poor acceleration performance, and limited battery life. The flywheel can provide high power for acceleration, thus eliminating high current demands from the batteries. In this way both vehicle performance and battery life are improved. Additionally, the vehicle range is improved by enabling the battery to discharge at a near-optimum rate as well as by recovering energy through regenerative braking.

Table 2. Electric vehicle performance (4-passenger vehicles).

	PRESENT TECHNOLOGY	ERDA STUDY REQUIREMENTS	AIRESEARCH DESIGN
DRIVING RANGE, MILE (ERDA CITY CYCLE)	40	75*	75*
ACCELERATION TIME, SEC (0-55 MPH)	32	32	17
BATTERY WEIGHT, LB	1200	–	1040

* BASED ON 1978 LEAD-ACID BATTERIES

The battery current load leveling is shown in Fig. 6 for the LA-4 Driving Cycle (Federal City Driving Cycle). The cycle covers 7.5 miles at an average speed of 19.6 mph with 2.4 stops per mile. The battery current is adjusted to the change in average power requirements, while the flywheel absorbs the peak power demands for acceleration and braking. Thus, both battery efficiency and life are improved. Figure 7 shows the effect of load leveling and regenerative braking on battery life. Not only are the total miles per pack increased by over 50 percent but the miles per charge cycle (range) are more than doubled. The system without regeneration and load leveling must not exceed a depth of discharge (DOD) much beyond 80 percent since power demand requirements cannot be met.

The flywheel can provide power levels to give the vehicle good acceleration capability, adding to driver acceptance of the vehicle. Figure 8 shows the maximum flywheel-powered acceleration of the vehicle. Note that 0 to 55 mph can be achieved in approximately 17 seconds.

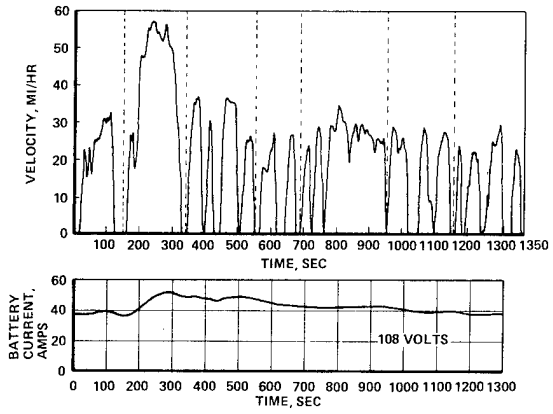


Fig. 6. Power system load leveling, LA-4 driving cycle.

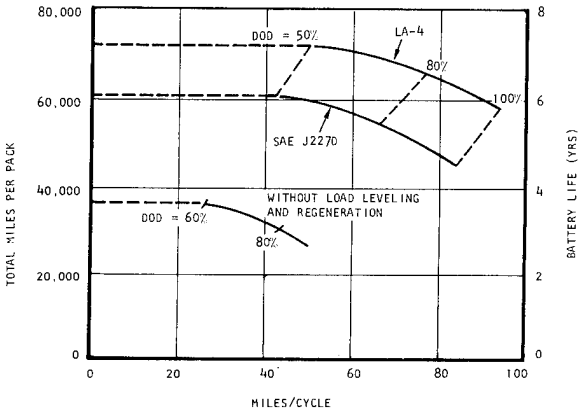


Fig. 7. Total battery pack miles vs nominal miles per charging cycle.

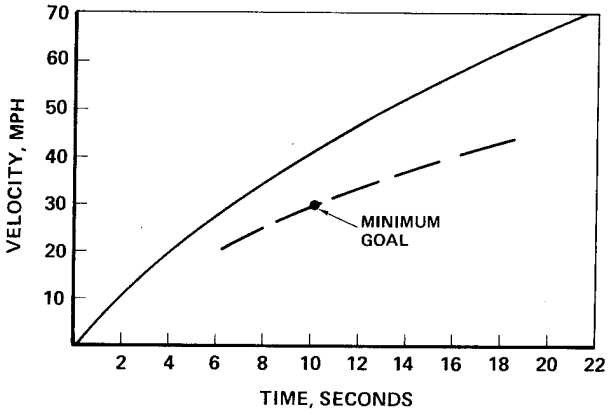


Fig. 8. Acceleration characteristics.

The power unit concept is shown schematically in Fig. 9. This is an electromechanical system in which the torque is split into two paths, one electrical and one mechanical. The main features of this system are:

Infinitely variable gear ratios

High efficiency

Reversible output shaft

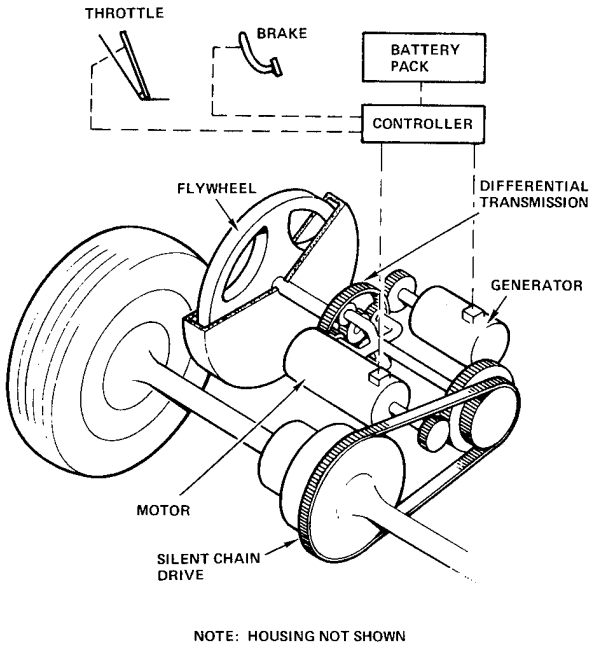


Fig. 9. Power system schematic.

The flywheel rotor will store 1 kw-hr of energy at a high flywheel rotor energy density level (22 w-hr/lb) for a duty cycle of 100,000 miles. Deliverable energy is three-fourths of this, or 750 w-hr, since the flywheel cycles between 50 and 100 percent speed during operation. The flywheel rotor chosen is a multi-ring rim mounted on a 4-spoke aluminum hub. The characteristics of the rotor are summarized in Table 3.

Table 3. Summary of flywheel characteristics.

Parameter	Value
Flywheel 100 percent speed, rpm	25,000
Energy storage at 100 percent speed, w-hr	1000
Available energy (down to 50 percent speed), w-hr	750
Flywheel size	
Rim OD, in.	23.0
Rim length, in.	4.2
Polar moment of inertia, ft-lb-sec^2	0.775

FLYWHEEL CONTAINMENT AND WEIGHT

The weight of a flywheel system is primarily dependent on materials (strength), rotor shapes, and safety containment requirements. A comparison of flywheel types (both isotropic and composite material) is shown in Table 4. These parameters are based on typical data for comparison purposes. The stress levels are based on long-term high-cycle operation.

Table 4. Flywheel comparisons, equal life designs.

	LAMINATED ROTOR	SHAPED DISC	MULTI-DRUM	MULTI-DRUM	MULTI-DRUM
MATERIAL	STEEL	STEEL	E-GLASS	S-GLASS	KEVLAR
SHAPE FACTOR K	0.30	0.85	0.30	0.30	0.30
MAX. STRESS/DENSITY (IN.-LB/LB)	0.49	0.49	1.25	1.90	2.4
PERIPHERAL SPEED (FT/SEC)	1260	2300	1950	2200	2500
ROTATIONAL SPEED	1.0	1.0	1.0	1.0	1.0
ROTOR SPECIFIC ENERGY (W-HR/LB)	5.6	13.1	11.8	17.9	22.6
ROTOR ENERGY/SWEPT VOLUME (W-HR/IN.^{3})	1.3	2.2	0.50	0.75	0.68
ROTOR WEIGHTS (RELATIVE)	1.0	0.43	0.45	0.31	0.25
APPROX. CONTAINMENT WEIGHT RELATIVE TO CORRESPONDING ROTOR	0.40	5.0	0.55	0.81	1.0
FLYWHEEL ASSEMBLY SPECIFIC ENERGY (W-HR/LB)	4.0	2.3	7.6	9.9	11.3
FLYWHEEL ASSEMBLY ENERGY/SWEPT VOLUME (W-HR/IN.^{3})	1.0	1.6	0.39	0.58	0.52

The composite rotors all show a high specific energy, with the Kevlar epoxy rotor the highest by a significant margin at 22.6 w-hr/lb. The composite rotors require more swept volume for the same energy. Although the rotor specific energy characteristics are of interest, the system specific energy is the main concern for a vehicle propulsion system. For this comparison the motor, gears, and other ancillary equipment are assumed constant for all types of flywheels. The remaining significant weight component is the rotor safety containment housing. As seen in Table 4, the composite flywheels have a much higher flywheel assembly specific energy than the steel flywheels; in fact, the Kevlar flywheel assembly has almost three times the specific energy of the laminated disc assembly. The reason for the low value on the shaped steel disc is the very high containment shield weight required for safety.

Based on this study the composite flywheel, especially the Kevlar system, will provide the lightest flywheel assembly.

FLYWHEEL SAFETY

The nature of a flywheel system requires special safety considerations, as outlined in Table 5. AiResearch recognizes this and addresses these problems both analytically and experimentally.

Table 5. Flywheel safety considerations.

- Flywheel Rupture
  - Minimized through low stress design
  - Containment - steel vs composite
  - Test evaluation
- Collision
  - Energy management structure
  - Test evaluation
- Gyroscopic moments
  - Rotor stiffness and strength
  - Vehicle stability

The basic philosophy used at AiResearch for the safety of public transportation flywheel rotors is that even with conservative design stress levels to minimize the probability of rotor failure, a failed rotor must be contained in the surrounding housing and the housing structure must not separate from its mounting structure.

It is much easier to contain composite flywheel rotors than steel flywheel rotors. The failure mechanism of the composite is such that no large homogeneous sharp-edged fragments are produced that require piercing containment. Instead, small fiber-epoxy fragments rub the wall, dissipating energy thermally, and the remaining energy is contained by designing for a hydrodynamic burst. The required containment weight for a composite flywheel is estimated to be between 15 to 30 percent of that required for an equal energy solid steel disc that fails in a tri-hub burst. In addition, the mount forces caused by momentum transfer from the rotor to the stationary housing have been found to be significantly less for composite rotors than for steel. The containment integrity of the composite flywheel rotor will be confirmed by laboratory test before initiation of flywheel testing in a vehicle.

Another safety concern with passenger vehicles containing flywheels is the impact of another vehicle or stationary barrier

into the flywheel housing. AiResearch recognizes this hazard and minimizes it through crash energy management design of the flywheel mount and the vehicle structure. Final evaluation will be made by crash testing.

Another special phenomenon associated with the safety of high-energy flywheels in vehicles is the gyroscopic effect. The magnitude of the gyrosopic moment is proportional to the product of the flywheel angular momentum and the precession rate of the spin axis. The flywheel hub, shafts, and bearings must withstand the gyroscopic moments due to the angular velocities caused by vehicle maneuvers. Sufficient stiffness must be present to minimize rotor deflections, and sufficient strength must be present to provide fatigue life. The flywheel spin axis in the electric powered passenger vehicle has been oriented in the transverse direction and the direction of rotation chosen so that the gyroscope moments due to turning (yaw) will roll-stabilize the vehicle.

FLYWHEEL COST

The cost of a flywheel assembly is based on two main factors: material costs and fabrication costs. For preliminary comparison, the fabrication costs per unit weight are assumed to be the same for all systems, and comparisons are made on the basis of material costs of the flywheel rotor and containment housing only.

Using the same flywheels previously discussed in Table 4, an estimate of the material cost for each system has been made as shown in Table 6. For all systems the containment housing cost is assumed to be 90 cents per lb. The rotor material costs shown in Table 6 are based on high-volume projections in the 1980's; however, estimated costs are in current dollars. Kevlar fiber, especially the Kevlar-29 that is being used in automobile tires, is expected to drop in cost. The composite flywheel assemblies are estimated to cost less than the steel flywheels when fabricated in mass-production quantities.

Table 6. Flywheel cost comparisons.

	LAMINATED ROTOR	SHAPED DISC	MULTI-DRUM	MULTI-DRUM	MULTI-DRUM
MATERIAL	STEEL	STEEL	E-GLASS EPOXY	S-GLASS EPOXY	KEVLAR EPOXY
ROTOR SPECIFIC ENERGY (W-HR/LB)	5.6	13.1	11.8	17.9	22.6
ROTOR WEIGHT (RELATIVE)	1.0	0.43	0.45	0.31	0.25
APPROX. CONTAINMENT WEIGHT RELATIVE TO CORRESPONDING ROTOR	0.40	5.0	0.55	0.81	1.0
FLYWHEEL ASSEMBLY SPECIFIC ENERGY (W-HR/LB)	4.0	2.3	7.6	9.9	11.3
ROTOR MATERIAL COST ($/LB) (COMPOSITE 70% FIBER, 30% EPOXY)	1.00	1.00	1.20	1.90	3.13(1)
FLYWHEEL ASSEMBLY MATERIAL COST ($/W-HR)(2)	0.24	0.42	0.14	0.15	0.18

(1) ASSUMES KEVLAR-29 AND KEVLAR-49 MIXTURE

(2) CONTAINMENT HOUSING, $0.90/LB

CONCLUSIONS

Flywheel weight has a cascading effect in terms of the overall vehicle weight. For example, a heavier vehicle requires a larger flywheel and a larger flywheel adds to vehicle weight if performance is to be maintained, Therefore, the composite flywheel assembly (including rotor containment) has a significant advantage over the steel flywheel, which resulted in its choice for the ERDA electric powered passenger vehicle.

AN ADVANCED ENERGY STORAGE UNIT FOR A U.S. POSTAL SERVICE DELIVERY VEHICLE

D.L. Satchwell
AiResearch Manufacturing Company of California
Torrance, California

ABSTRACT

This paper reviews steel flywheel technology as used in the R-32 Energy Storage Cars for the New York Metropolitan Transit Authority, the Advanced Concept Train for the U.S. Department of Transportation, and the Ford Pinto Conversion for the University of Wisconsin and the Department of Transportation. It presents the rationale that led to the energy storage unit design for the U.S. Postal Service Delivery Vehicle, provides details of the system, and tells how such considerations as safety, weight, and cost affect the design.

INTRODUCTION

This paper discusses the scope of the AiResearch flywheel energy storage experience, reviewing in particular the steel flywheel energy storage unit that AiResearch is developing for a U.S. Postal Service Delivery Vehicle.

AIRESEARCH FLYWHEEL ENERGY STORAGE SYSTEMS

Figure 1 shows the flywheel energy storage programs that have been conducted or are being conducted by AiResearch. AiResearch involvement in flywheel energy storage systems began in 1969 with the R-32 rail commuter car program. Two R-32 New York subway rail cars were retrofitted with flywheel energy storage devices. These cars were run on the Department of Transportation (DOT) Pueblo test track in 1974, and were run in revenue service in New York in 1976. In 1974 AiResearch also began composite flywheel development under a research and development program that concluded with a 1000-cycle test of a composite rotor. These programs led to development of the successful U.S. Army Mobility Equipment Research and Development Command (USAMERADCOM) Kevlar 49 composite flywheel in 1977, and the composite flywheel for the Garrett electric car that will be developed for the Energy Research and Development Administration (ERDA). AiResearch conducted hydraulic pressure burst tests and spin burst tests of 16-in.-diameter flywheel test rings for materials properties analysis conducted by Lawrence Livermore Laboratory (LLL). Also being studied is the application of composite flywheels for downhill energy storage for the Federal Railroad Administration.

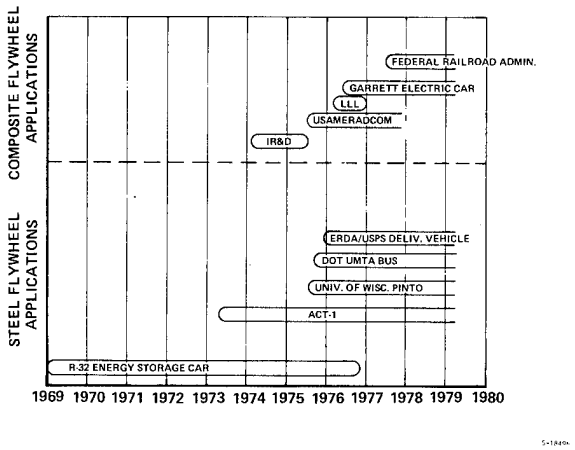


Fig. 1. AiResearch Flywheel Energy Storage Systems.

MULTIPLE DISC FLYWHEELS

Following development of the R-32 rail car flywheel, AiResearch introduced the multiple thin-disc steel flywheel design and applied it to the Advanced Concept Train (ACT-1), the University of Wisconsin automotive (Ford Pinto) flywheel system, and the Department of Transportation Urban Mass Transit Administration (UMTA) bus study. The U.S. Postal Service (USPS) Jeep delivery vehicle flywheel developed for ERDA also uses this concept.

Four-Disc Steel Flywheel. Figures 2, 3, and 4 show the NYC R-32 transit car, the energy storage unit (ESU), and the actual energy savings. The ESU for this car incorporates a flywheel with four shaped

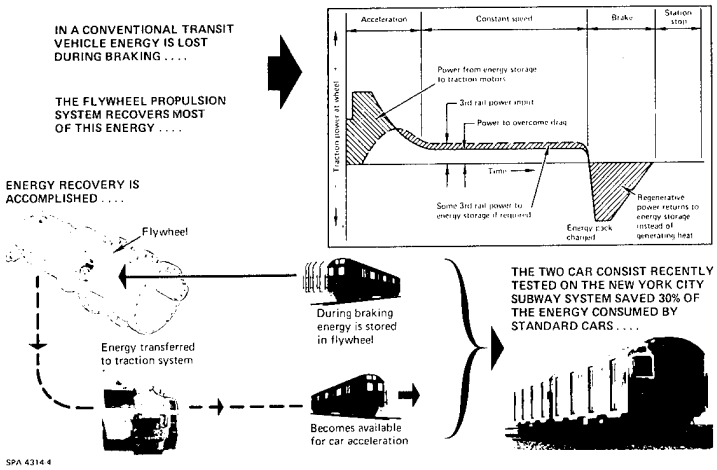
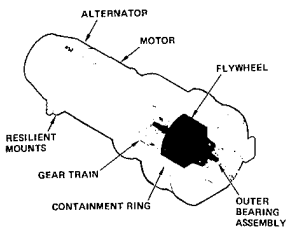


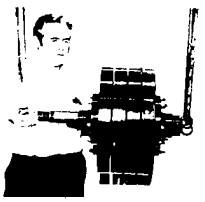
Fig. 2. How R-32 energy storage car saves energy.



FEATURES

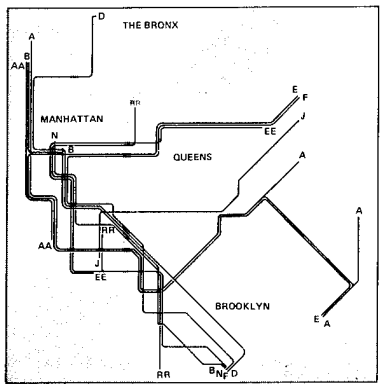
- TOTAL ONBOARD REGENERATION CAPABILITY
- PROVIDES CONTINUOUS AUXILIARY POWER SOURCE
- ELIMINATES NEED FOR POWER ELECTRONICS
- CAPABILITY OF MOVING CAR TO SAFETY IN EVENT OF POWER OUTAGE

Fig. 3. R-32 energy storage unit.



- ENERGY STORED = 3.0 KWH
- SPEED = 14,000 TO 9,800 RPM
- NO. OF CYCLES = 1.28×10^4 STOP-START, 3.1×10^6 100 TO 70 PERCENT SPEED
- SIZE = 20 IN. DIA BY 9 IN. LONG, 740 LB
- MATERIAL = 4340 STEEL FORGINGS, 156 KSI MINIMUM YIELD STRENGTH AT 300°F

Fig. 5. R-32 ESU four-disc steel flywheel.



TEST SCHEDULE		
LINE	ENERGY SAVINGS	MILEAGE
A	32%	188
N	26%	92
E	31%	65
EE	31%	82
AA	38%	79
B	28%	210
D	27%	155
F	28%	162
RJ	24%	87
RR	28%	35

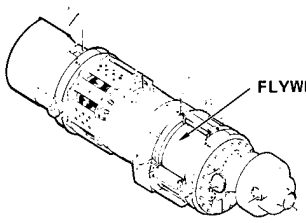
S-3150

Fig. 4. R-32 energy storage car demonstrated savings during New York City operations.

steel discs (Fig. 5); the housing utilizes a floating containment ring designed to fully contain the flywheel in the event of burst. The ESU, when used in conjunction with the other components of the system (traction motors and controls), results in a savings of one third of the energy required for a conventional transit car.

Multiple Thin-Disc Flywheel. Following the four-disc flywheel, AiResearch introduced the multiple thin-disc 4340 steel flywheel in the ACT-1. Figures 6 and 7 show a rotor with twenty-seven 0.4-in.-thick, 23-in.-diameter discs shrunk onto an 8-in.-diameter central shaft. A significant feature of this concept is that the containment ring required to completely contain all fragments of a possible burst flywheel can be made thinner and lighter than for the 4-disc flywheel or for a single flywheel of comparable energy storage capacity. Figure 8 shows a disc weakened to test containment capability. With the energy stored in 27 thin discs instead of a smaller number of thick discs, the energy per disc is greatly reduced.

The multiple thin-disc flywheel concept has been applied to the University of Wisconsin Pinto (Fig. 9) and the ERDA/USPS Delivery Vehicle.



- ENERGY STORED = 4.5 KWH
- SPEED = 11,000 TO 7,700 RPM
- NO. OF CYCLES = 1.28×10^4 STOP-START, 3.1×10^6 100 TO 70 PERCENT SPEED
- SIZE = 23 IN. DIA BY 11 IN. LONG, 1312 LB
- MATERIAL = 4340 STEEL PLATE, 156 KSI MINIMUM YIELD STRENGTH AT 300°F

S-18495

Fig. 6. Advanced concept train energy storage unit.

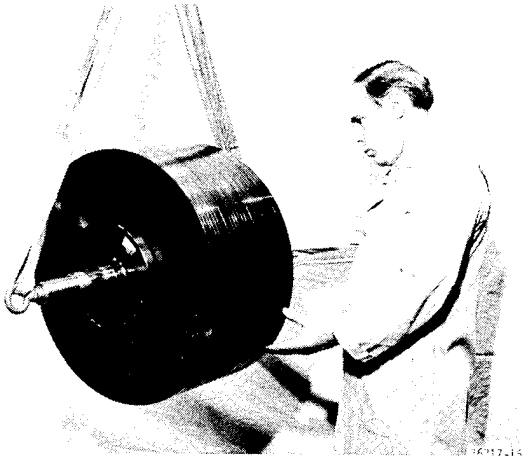


Fig. 7. ACT-1 multiple thin-disc flywheel assembly.

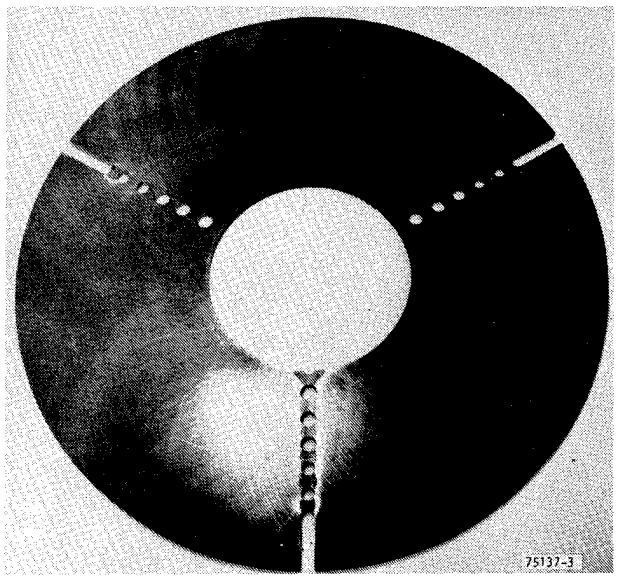


Fig. 8. ACT-1 flywheel disc weakened for tri-hub burst.

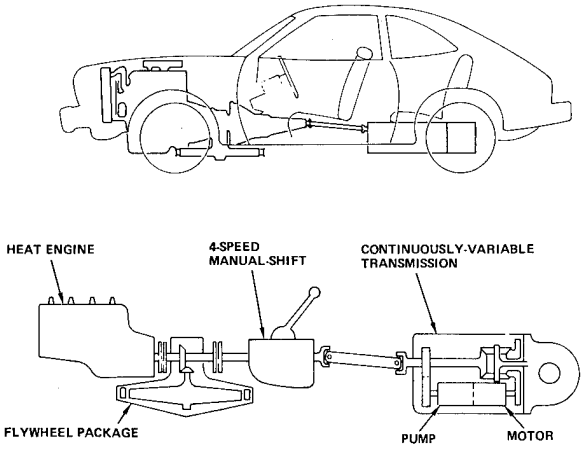


Fig. 9. University of Wisconsin Pinto conversion using multiple thin-disc flywheel.

COMPARISON OF STEEL FLYWHEEL CONCEPTS

Figure 10 shows that, in spite of the less favorable energy storage shape factor of the multiple thin-disc (laminated) rotor, the laminated rotor flywheel is the lightest configuration when the weight of the housing required for complete containment is considered.

EQUAL FATIGUE MARGIN DESIGNS	SHAPED DISC	MULTIPLE THICK DISC	MULTIPLE THIN DISC
MATERIAL	STEEL	STEEL	STEEL
SHAPE FACTOR K_S	0.85	0.43	0.30
PERIPHERAL SPEED (FT/SEC)	2300	1720	1360
ROTOR WEIGHT (RELATIVE)	0.4	0.8	1.0
APPROX. CONTAINMENT WEIGHT (RELATIVE)	4.1	2.1	1.0
APPROX. TOTAL WEIGHT (RELATIVE)	1.3	1.1	1.0

Fig. 10. Flywheel comparisons.

ERDA/USPS DELIVERY VEHICLE

In the ERDA/USPS Delivery Vehicle (Fig. 11) AiResearch is applying a multiple thin-disc flywheel energy storage system to a battery-powered vehicle to increase its useable stop-start capability, useful range, and acceleration into traffic, while reducing the maximum battery current demand from 600 amp to 270 amp.

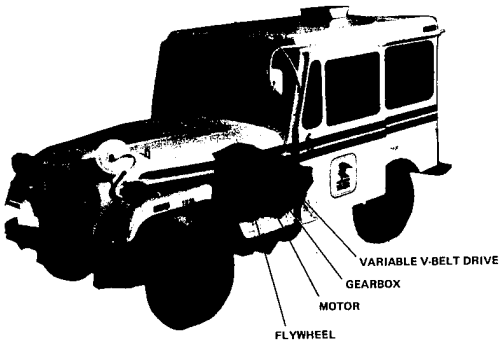


Fig. 11. ERDA/USPS delivery vehicle with multiple thin-disc flywheel ESU.

Figure 12 shows the system schematic. The flywheel power unit replaces the original electric motor, and the flywheel assists the electric motor in propelling the vehicle, reducing the power required from the battery during peak-demand transient operating periods. The flywheel is also used to regenerate the braking energy. Figure 13 shows the relation between flywheel speed, motor speed, and vehicle speed. The electric motor drives the vehicle to 7 mph, reaching its full 36,000-rpm speed. At that point the flywheel fluid coupling is engaged and the flywheel is used to drive the vehicle to its 33-mph cruise speed through the variable-ratio V-belt drive. The process is reversed during braking; the traction wheels supply energy to the flywheel while slowing to 7 mph. Below 7 mph and during emergency stops, the service brakes halt the vehicle. During idle, the fluid coupling is disengaged and the flywheel is the only component that is rotating. Figure 14 shows energy required and available to accelerate the vehicle to 33 mph.

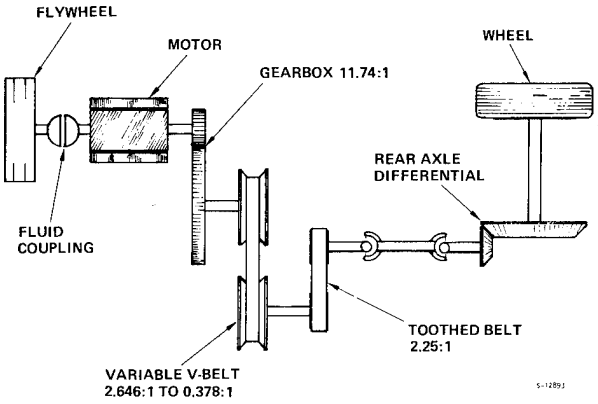


Fig. 12. ERDA/USPS delivery vehicle power train

Of particular interest is the high power feature. For added safety when entering lanes of moving traffic and for changing lanes, the flywheel system has the power to allow dashes up to 40 mph (Table 1).

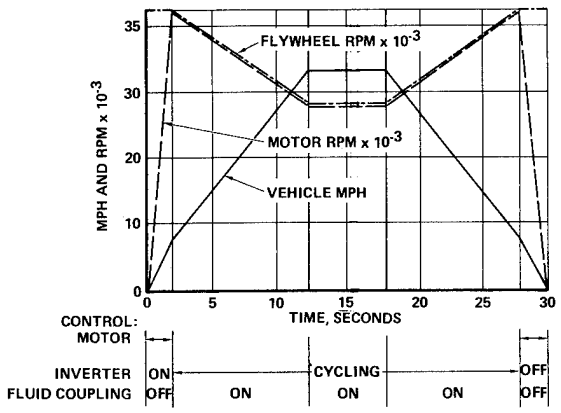


Fig. 13. ERDA/USPS delivery vehicle acceleration-deceleration.

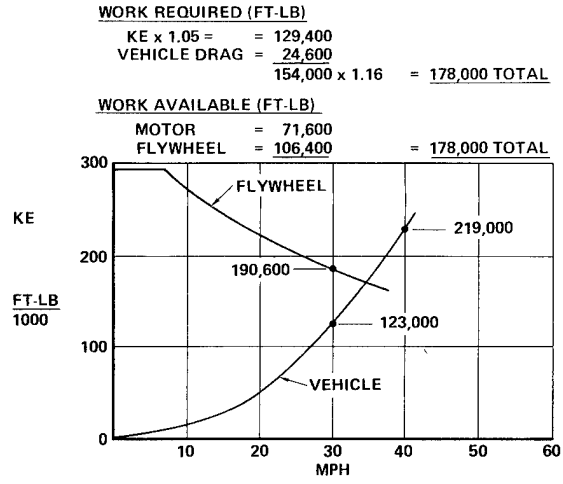


Fig. 14. Energy required to accelerate to 33 mph.

Table 1. ERDA/USPS delivery vehicle performance comparison.

	POSTAL SUPPLIED AM GENERAL DJ-5E	IMPROVED DESIGN
ACCELERATION	0-30 MPH IN 24 SEC	0-30 MPH IN 12 SEC
TOP SPEED	32.5 MPH	32.5 MPH (40 MPH DASH)
GRADEABILITY	10% GRADE @ 14 MPH	10% GRADE @ 20 MPH
SIMULATED POSTAL ROUTE	300 START/STOPS OVER DISTANCE OF 10 MILES	500 START/STOPS OVER DISTANCE OF 14 MILES
RANGE	27 MILES AT 30 MPH	27 MILES AT 30 MPH

By using the flywheel as a power booster, the vehicle can reduce its time required to accelerate to 33 mph by one half, increase its number of stops from 300 to 500, and provide a dash capability for lane changing in traffic. These performance improvements result in a more useful electric vehicle that overcomes some of the limitations imposed by existing electric propulsion systems.

"THE HIGH-ENERGY "FLYDRAULIC" ACCUMULATOR WITH HYDRO-COMPUTER MODULATED OUTPUT"

Robert C. Clerk
Research Consultant
20 Whitehill Road
Whitehill Industrial Estate
Glenrothes, Fife
Scotland

ABSTRACT

The Flydraulic high-energy accumulator involves association of a prestressed laminated steel flywheel with a specially developed hydraulic pump/motor having complementary characteristics and controlled in every aspect by a hydro-computing element which assures an output precisely as commanded by the operator or as demanded by the other system signals communicated in the same hydro-computing 'language'. The hydro-computer likewise controls regenerating input with negligible energy transformation loss, minimises no-load running losses, prevents overspeeding, and maintains constancy of performance throughout the operating speed range. The compact accumulator unit can incorporate up to six pump/motor elements, circuited and controlled separately or in combination, driven from the common flywheel sun-gear within the vacuum environment, and operated continuously in their overspeed range up to 200% above rated-power speed. It incorporates a diaphragm pressurised zero-ullage reservoir for the vacuum-stripped working fluid, and a scavenged and evacuated environmental enclosure for the flywheel and the gearing to the energy transducing hydraulic pump/motor within which is inserted the hydro-computing cartridge which controls the ultra-low loss idle running, the very high part and full load efficiencies, overspeed limits, energy regeneration and/or acquisition by integration with vehicle energy, and of course the smoothly modulated instantly responsive output of power.

PREFACE

As a result of protracted studies aimed at a rapid recharge short-term high-energy high-power accumulator with efficient energy/power transmutation it was decided that an inertia/hydraulic configuration offered the best commercial possibilities, granted optimised complementary elements might be available.

The Inertia Element To ensure minimum installed bulk as well as low weight the selected inertia element is a prestressed laminated flywheel, of high integrity but low production cost, rotating about a vertical axis within an evacuated casing as described in my other paper "The Prestressed Laminated Flywheel and its Hydrovac Ambience".

The Hydraulic Transmuting Element This drives or is driven by a variable displacement hydraulic pump/motor as the energy/power transmuting element capable of converting an incoming supply of hydraulic power into storable kinetic energy or conversely transmuting the stored inertia energy to a precisely modulated output of hydraulic power in response to demand or to internal hydraulically computed requirement.

The pump/motor researched and developed specially for this application and described in my other paper "An Ultra-Wide Speed Range High Efficiency Hydraulic Pump/Motor Power Transmission", had to meet criteria beyond current practice; ultra-low rotation losses, continuous operation at high overspeeds, low weight and cost, high efficiency and power throughput, quiet with low pulse signature, and lend itself to high-production manufacturing and assembly techniques. These features made it also ideally suited as complementary system elements, such as primary or prime mover pump, and output drive or propulsion motors identical save for the small inserted

programmable hydraulic function designator.

"Flydraulic" Accumulator Applications This "Flydraulic" (flywheel/hydraulic) high-energy accumulator will have application in many industrial spheres such as tidal barrage, tower cranes and elevators, peak-lopping storage alternators and "no-break" sets, rolling mills and heavy duty presses, haulage "donkey engines" and dragline excavators, suburban railway accelerate/regenerate boosters, airplane fast-taxi tractors and off-road vehicles but primarily to very high production automotive road vehicles to which it is particularly applicable, whether as non-polluting pure-storage propulsion systems or as regenerative-transmission performance-boosters in prime mover powered vehicles which are thereby endowed with perfectly modulated "stepless" full range acceleration and gradient surmounting of a very high order, without appreciable effort by the prime mover engine, management of which is controlled by the internal hydraulic computer to optimise its efficient operation.

Flydraulic Accumulator Propulsion Systems Such a system can vary all the way from the momentary boosting of an already high powered system, through systems having less installed power and using more boosting, through systems where the accumulator provides the prime power output and the installed power is used to provide more or less continuous "charging"; finally at the end of the line the accumulator provides the entire power output and, as power generation will have been deleted from the vehicle, recharging is effected from fixed service bases (sited say at normal filling stations), where a full recharge can be effected automatically in 2 or 3 minutes, or from an emergency service vehicle.

As this propulsion system provides controlled braking retardation with energy recovery returned to the accumulator at a high regenerative efficiency, the total energy degradation, or the energy which must be supplied by the installed or ancillary power, is entirely related to vehicle wind and rolling resistances and transmission efficiencies, and not at all to acceleration and deceleration which are generally accepted as prodigal of energy.

Of course for any system to be acceptable, high efficiency must go hand-in-hand with low noise, lower than existing hydraulic equipment standards and therefore an important development area. But for a total energy system the virtual elimination of idle running losses in the operating speed range is probably the most critical development characteristic.

Pre-history It should here be pointed out that my predilection for a flywheel-hydraulic system ante-dates our "Gyreacta" flywheel-mechanical transmission which was born into a national emergency of the 1950's which later evaporated. Unfortunately no suitable hydraulic equipemtn was available and the urgency of the situation would not allow of either time or money being diverted to hydraulic research; just a headlong rush to develop the mechanical solution.

It was more than 10 years before I was contractually free to review the project studies and again reached the conclusion that flywheel-hydraulic was the right approach and that the complementary hydraulic pump/motor, though still not procurable, was feasible and market research showed it would be worth the development effort.

This has proved to be so but it has also shown us that, however good the basic elements of any system are, they will be ineffective without complementary system integration and control best suited to operator requirements, convenience and comfort. Until now, hydraulic system controls have been bulky and clumsy whether viewed from the physical or sensory aspect.

Consequently considerable research was devoted towards the achievement of an integration and control system which, although far from straight forward in programming grasp, is mechanically so simple and small in size it can fit into any odd corner of each of the basic system elements endowing them with "identical twin" interrelationship although programmed for diverse function.

THE BASIC ACCUMULATOR

Fig. 1 shows a representative Flydraulic accumulator with prestressed laminated flywheel located vertically by hydrostatic footstep thrust support and inverted journal bearing in a radially convoluted casing

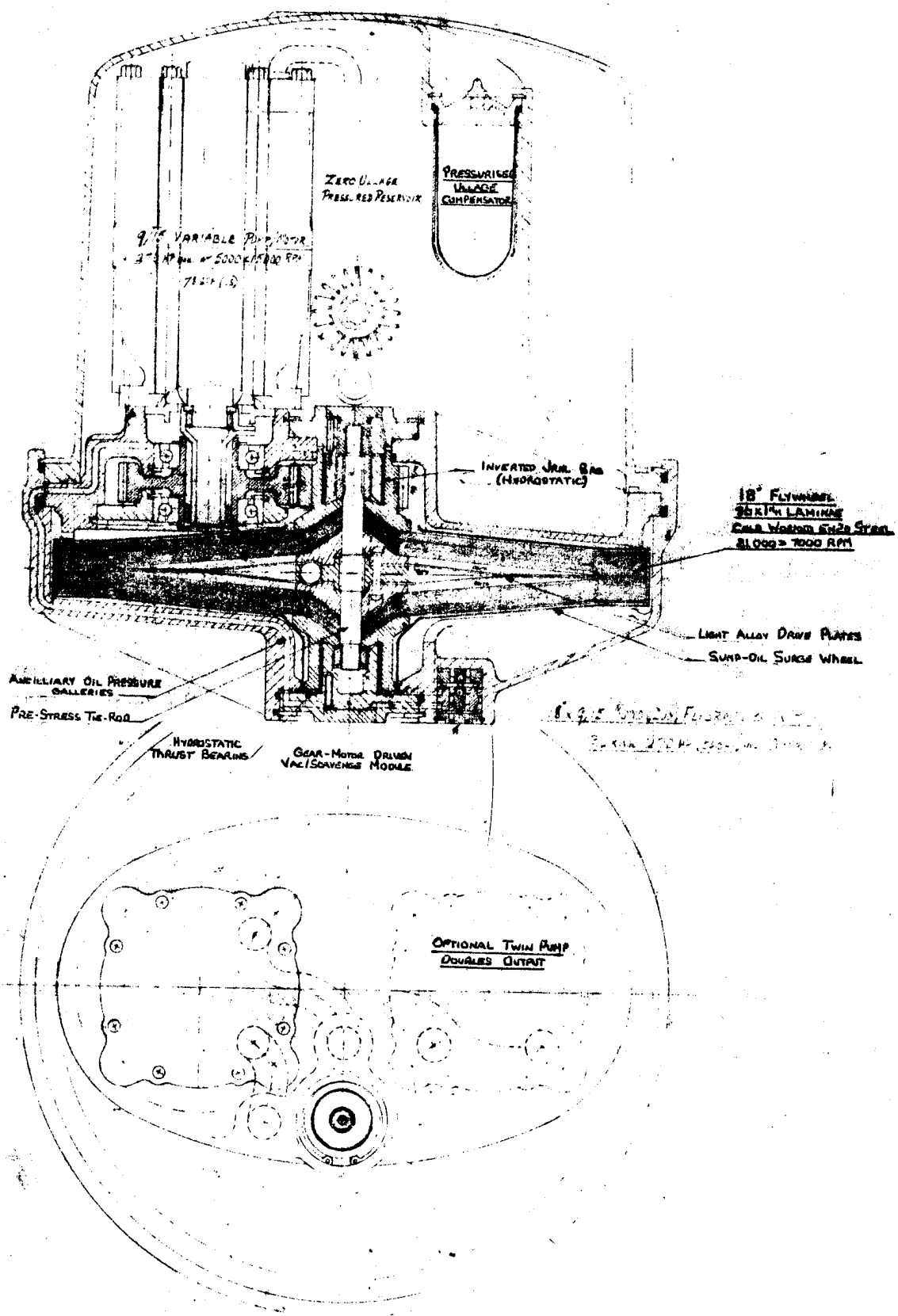


Fig. 1. "Flydraulic High-Energy Accumulator.

serving as a drainage sump from which effluent oil is scavenged and a vaccuity maintained by a modular gear-motor/gear-pump of minimal dimensions. The flywheel is close-shrouded by sheet-metal guards to prevent energy loss to the drainage oil, and its upper stubshaft is fitted with a driving gear which mates with one or more gearwheels journalled in the upper casing.

A quill sleeve connects the or each gear wheel to a vertical pump/motor without any sealing arrangement so that pump/motor leakage drains directly into the flywheel casing and the interior of the pump is subject to the vaccuous ambience. To conform with the 3 1 working speed range of the flywheel, the pump/motor is designed to operate continuously within the 200% overspeed limitation above rated power speed with its displacement fully variable from zero to rated delivery under control of a modular hydro-computing element which will have been programmed to accept the operator's command and a wide selection of other pertinent data for processing and activation as later described.

The pump/motor(s) is submerged within the oil reservoir the bottom of which is formed by the flywheel upper casing and otherwise closured by a bell casing incorporating a manifold facing(s) to mate with the top face(s) of the pump/motor(s). The reservoir has zero ullage, fluid expensions being taken care of by an insert flexible air-bag which also serves to pressurise the vacuum-stripped working fluid in the reservoir.

Although the flywheel and pump/motor casings are designed for diecasting in Aluminium alloys the shrinkage allowances and the scantling stresses allow substitution of Magnesium, cast-iron, steel or bronze from the same casting dies or sand patterns. In fact the first operational Flydraulic accumulator units will embody cast-iron external casings to comply with hazardous operational conditions, also aided by the fully hermetic casing envelope devoid of mechanical connections and their leak-prone seals.

The effective storeable energy rating of a Flydraulic accumulator is determined by the density, dimensions and speed range of the flywheel and the hydraulic power input/output capacity by the maximum displacement, pressure and rated speed of the pump/motor(s) which is (are) matched to the flywheel by the gearing such that rated pump speed equates to one-third of flywheel maximum operational energy speed at which the pump/motor would therefore be running 200% overspeed.

It is important to appreciate that the accumulator provides a hydraulic power output precisely as demanded, both as to pressure and delivery, so that there needs be no efficiency loss in accommodating the output to any pressure requirement of the recipient apparatus within the dictates of the operator. Conversely, incoming hydraulic power, regardless of its pressure/flow relationships, will be efficiently transmuted by the pump in motoring regime for acceptance into kinetic storage, thanks to the self-modulating control.

ACCUMULATOR SIZE RANGE

Being developed is a range of pressed lamination flywheels of diameters from 18" to 42" in 6" increments, with the possibility of 48" still being discussed, utilising both cold worked low Carbon steel and the more costly high-fatigue steels. These will offer effective energy capcities (8/9ths of maximum) of from ½ kWh to 44 kWh (or to 66 kWh nett for the 48") in Aluminium alloy casings which will accommodate one or more pumps of different sizes and outputs. For example, the 18" flywheel offering from ½ kWh to 3 kWh could be mated to pump/motors providing from 20 kW to 600 kW output whereas the 42" offering from 5 kWh to 44 kWh can provide up to 4000 kW output, and for a representative output of 500 kW weighs 4120 lb wet for highest energy.

Sizes above 48" diameter will be customised using flow-turned or explosively formed laminations in sizes up to 5 metres diameter (the limit of our present studies) for energies up to 4500 kWh. However, in general it would appear much more cost-effective to multiplex the smaller standardised unit programmed to operate in unison or in cascade, this offering the further advantage that individual unit can be pulled for servicing without disruption to normal operations.

The companion paper the planned range of pump/motors, customised above 9/25 size and this may be read in conjunction with Table A of my flywheel paper to gain some idea of the possible build variations, However consideration should be given to the fact that, in

going for low output capacity, the correspondingly low input capability will result in extended recharging time and/or inability to accept regenerated energy as quickly as the system retardation demands, this latter usually being the deciding factor in any regenerative transmission application.

APPLICATION ANCILLARIES

However, an overriding advantage in many such applications could be the production and spares commonality achieved by incorporating identical pump/motor units, individually programmed in their hydro-computer, inserts to perform the appropriate system function as work-load or vehicle transaxle motors, or as prime mover engine power pump, as well as flywheel pump/motor. We are developing such a transaxle in which identical motors, mounted side-by-side or siamesed to share a common distribution manifold, drive each wheel-driving half-shaft separately controlling wheelspin as well as wheel-lock during hydro-retarder or regenerative braking.

ENERGY RESERVES

In automotive application of the accumulator an allowance should be made, over and above the vehicle kinetic cycle, for the potential energy to surmount or be regenerated from roadway gradients of reasonable altitude difference. Usually expressed as a percentage reserve, additional to vehicle energy at maximum weight and operating speed, it serves to determine the accumulator net energy capacity (8/9ths of gross) for any application and the most appropriate flywheel dimensions as beascertained by reference to Table A.

The latitude in allowable laminar thickness can often be used to good effect in adapting the same basic accumulator to other vehicles in the model range. Fig. 1 shows a representative automobile accumulator using the same pump/motor unit as the engine driven pump and the transaxle motors of a hydrostatic automatic transmission which shows to advantage even without addition of the (optional?) accumulator. Incidentally, dimensionally identical pump/motors are designed to provide a similar cost-effective latitude in performance "stretch" (of the order of 87%) to accommodate to a model range, production changes being limited to alternative materials and surface finishes primarily affecting life.

ACCUMULATOR LOSSES AND EFFICIENCIES

The Flydraulic accumulator is subject to losses from three quite distinct operating aspects, charged idle running whilst awaiting a demand for power, power production, and regenerative charging.

Idle Running Losses For the first aspect, losses arise from three sources, flywheel "windage" drag and bearing losses already covered in my other paper, gearing lubrication and bearing losses which can be taken as 0.05% of installed output power rating as a good yard-stick, and pump/motor overspeed rotation and control priming losses. These last will of course depend upon the size of pump selected to meet the output requirement, but as pump speed is inversely related to size, the rubbing speeds are of the same order for pumps of all sizes at the same rating level and therefore the fluid film shear values will be the same but acting over an area greater as the square and at a torque radius varying directly with dimension and at a speed inverse to dimension. As a result shear power loss will increase as the square of pump dimension and as the 1.8 exponent of rated speed.

In the case of the 9/25 pump/motor, the power required to rotate it (exclusive of the temporary priming mini pump of proprietary manufacture) is 0.51 H.P. at 2500 Rpm at an oil viscosity of 4.5 micro-reyns, and 3.03 H.P. at 7500 Rpm. At the higher rated speed of 3000 Rpm it is 0.71 H.P. and at 9000 Rpm 4.2 H.P. In each case we feel we have optimised the losses at rated speed but that the overspeed losses will yield to further development of the swash-plate support thrust and the portface counter-thrust idle clearance control. Development of our high-helix priming mini-pump is not scheduled until February 1978 well in advance of first deliveries of the 18 kWh 400 H.P. accumulator, as against earlier pump/motors which demand no overspeed characteristic.

Power Production Losses During power delivery there are no additional losses attributable to the flywheel and its immediate ancillaries: in point of fact there will be a reduction of losses as the flywheel reduces speed with imparted energy. Power transmission loss for the low-helix gear contact and the

angled ball locating bearings as be taken as 1.15% of transmitted power, and for the pump/motor as 3.875% additional to the idle rotation losses.

Regenerating Power Losses Whilst recharging and during regenerative braking, the hydraulic power arriving at the accumulator will be subject to a similar transmutation loss of 3.875%, plus rotation 0.1% of installed rating rising to 0.6% at maximum energy speed; also a gearing loss of 1.15% rising to 1.2% before the residual power less the flywheel rotation loss is applied to accelerate the flywheel to higher energy. Installed rating is the power transmitted by a pump/motor at its median operating pressure limit and displacement when rotating at one third maximum geared speed; thus the installed rating of the 400 H.P. (specification) 9/25 pump/motor is 500 H.P. but program controlled to the specification limit.

NON-MOBILE ACCUMULATOR APPLICATIONS

Although high-pressure hydraulic accumulators have been available for decades, for the majority of applications the non-availability of a modulatable delivery pressure, and the consequent enormous losses in reducing the pressure to requirement, have lost such applications to alternative sub-disciplines. Even to make use of pressure accumulator delivery at the storage pressure, one is saddled with banks of back-up air bottles to minimise the reduction in storage pressure with delivery,

However, the Flydraulic accumulator provides the precise presure and delivery demanded of it with minimal loss. These losses are approximately 5% of power input/output plus a time-lapse loss of approximately 6% of instantaneous storage level.

Tower Cranes Tower cranes are usually electrically powered, with separate motors for luffing, reaching and lifting, the last demanding the highest power, over 100KW. They require a substantial counterweight to the jib; usually an idle lump of concrete. Tower cranes often operate in a pristine wilderness remote from 3-phase electricity mains, although a single-phase service line is usually brought in free. Tower cranes operate a work-duty (working load x time vs installed power) of seldom more than 6%

A counter-positioned Flydraulic accumulator is charged by a continuously running pump powered by a small single-phase electric motor. Hydraulic circuitry is simplified by incorporatin multiple satelite pumps in the accumulator, for luffing, reaching and lifting, plus one motor to accept the continuous hydraulic charge.

The accumulator reserve beyond unit work-cycle may be increased to cater for line breaks in the electricity service, which therefore will not inconvenience the all-hydraulic working of the crane. In fact, it would be practical to provide 12 hour/day working capacity, with 12 hour/overnight charging.

Flydraulic/Electric AC Storage AC storage is industrially attractive, both for peak lopping and "no-break" services. The equipments to achieve these are largely similar, comprising a prestressed laminated flywheel driving (or being driven by) a variable axial pump/motor coupled to a substantially identical motor/pump driving (or driven by) a synchronous alternator.

"No-Break" AC Sets Generally of smaller capacity than peak-lopping sets, the "No-Break" set can usefully take advantage of the byproduct accumulators of high-volume automotive production whose vertical axis construction advantages floor space requirement. Standard modules might provide 25 kWh storage 400 KW output, using a 42" 9/25 accumulator to power a 9/25 motor/pump and synchronous 2-pole alternator.

The synchronous alternator would be tied to mains frequency, motoring the set with just enough power to meet system losses. At mains failure it would without phase slip provide current to all the priority services in its circuit, maintaining frequency by memory unit until the mains were restored.

Used purely as a "No-Break" set the duty utilisation might be nil, so it would be economic to combine the "No-Break" facility with excess demand "peak lopping" thereby reducing electricity charges.

"Peak Lopping" AC Storage Systems

General sector applications rated in kWh storage capacity rather than public sector MWh are principally being studied. Early work was directed to large horizontally alignments, but subsequent work on "No-Break" sets showed advantages in vertical alignment of the flywheel/hydraulic accumulator elements, at least.

The laminations for large flywheels must either be flow-turned (machine spun) or explosive-formed as discussed elsewhere; however, it should be appreciated that sheer size is not necessarily an advantage as, due to the synchronous tie, any number of smaller units can be multiplexed to provide the same energy and output with better serviceability. Or multiplexed volume production accumulators could power fewer alternators, their hydraulic computing controls being programmed to cascade in response to changes in electrical demand.

Exemplary to the larger sizes, a 12 ft. flywheel might weigh up to 60 tons and have an effective storage capacity of 1000 KWh and say 800 KW electrical output. But forty size 42" accumulators driving four 250 kVA alternators would certainly cost less; and there is safety in numbers; and better serviceability.

Industrial Drives Some industrial processes with a high power requirement have an intermittent or cyclic peaking demand.

Rolling mills employ very costly Ilgner flywheel/electric sets to meet the peak demands when the cogged billets are introduced to the primary rolls. A hydraulic mill drive with Flydraulic accumulators would provide a vastly superior performance at greatly reduced capital cost and use only a fraction of the floor space.

Industrial Thrusters Hydraulic thrusting rams or cylinders pose a slightly different problem in applying the Flydraulic accumulator which is basically intended for circulatory flows.

To complement the pressure fluid transferred from the Flydraulic accumulator in displacing the ram or cylinder, a much larger hermetic reservoir is necessary, with a rolling diaphragm to fill the void left by the migrant fluid, without ingress of air.

Drag-Line Haulages Drag-Lines may be hauled either by motor driven cable-drum or by multi-reeved pulley blocks extended by a thrusting ram.

The former arrangement would be the more convenient to the standard Flydraulic accumulator, whereas the latter would demand the large reservoir with rolling diaphragm.

Barrage Sluice Control The juxtaposed semi-rotary sluices of an estuary barrage are preferably operated in unison, but the spasmodic power requirement can represent a considerable draw upon the electricity mains.

The Flydraulic accumulator provides a means whereby this high power draw can be isolated from the mains and by circuiting the sluice-driving hydraulic motors in series all the sluices would operate synchronously.

MOBILE ACCUMULATOR APPLICATIONS

These we will consider as three groups; those vehicles utilising service base charged pure accumulator propulsion, those hybridised with an on-board charging engine (A.P.U.), and those in which the accumulator is used to boost the output of a normal prime mover engine whose power is transmitted to the vehicle wheels by a hydrostatic automatic transmission comprised of an engine driven hydraulic pump and either a unitary hydraulic motor driving the Cardan shaft of a live rear axle, or, preferably, a remote frame mounted transaxle with two motors, each independently driving a half-shaft. All pumps and motors in the system will have an inserted hydro-computing module slaved to the accumulator pump/motor module as system master.

PURE ACCUMULATOR MOBILES

Where atmospheric levels of pollution are critical as within city limits, or where it is difficult or costly to install a secondary prime mover engine, it is possible to install energy storage capacity to meet all propulsion and ancillary needs of a vehicle excepting possibly air-conditioning.

City Bus (With Terminal Recharge)

There is no problem in providing high performance multi-stopping pure accumulator propulsion for a city bus over a route of up to 15 miles as the retard regeneration efficiency if such that the overall energy requirement will be less than non-stop at higher average running speed.

But lighting and air-conditioning over the longer journey time of multi-stopping become critical. At 12 miles between terminals the maximum lighting loads would be acceptable, but high temperature-differential air-conditioning would demand recharging every 4 night-time miles, or provision of a thermal generator for air-conditioning.

Terminal recharging would be fully automatic when the bus was driven into the charging bay of the service installation as described later.

City and Suburban Delivery Vans

Battery-Electric powered floats cover very short stage distances between protracted stops. Delivery vans operate over greater stage lengths where the Battery-Electric ceases to be cost-effective due to poor accelerative and regenerative performance and inability to operate a full day schedule without recharge or battery exchange.

A Flydraulic pure-accumulator powered delivery van would suffer no performance limitation, and when it needed recharging could be replenished in 2 minutes from an automatic drive-in hydraulic charging facility. It could be front mounted allowing a low loading floor area, the cab seats would be over the front drive transaxle and an 8" high step-in cab floor ahead of the driving wheels would obviate the operators hoisting their own weight at every re-entry.

Self Energising Trailers For transporting freight over poor roads, additional traction at the trailer wheels of a tractor/trailer haulage vehicle equipped with hydraulic transmission is possible merely by equipping the trailer with a hydraulic transaxle having hydraulic connections to the tractor's power system. Unfortunately such mainline connections (power and return) are a bugbear in service and unacceptable to operators.

However, replacing the mainlines to the trailer by a Flydraulic accumulator its self-computing control system could be programmed without any control connection, or with such that any acceleration gradient initiated by the tractor's propulsion system would be instantaneously imitated by the trailer's accumulator propulsion with a lag/lead accelerate/decelerate relationship to the trailer's accumulated energy.

From "dead" start the tractor will accelerate the vehicle without trailer assistance, but each brake application would regeneratively part-energise the accumulator which would then progressively increase its tractive contribution.

Alternatively the trailer can be precharged from the tractor by "jumper" connections. Conversely residual energy in the trailer could endow the parked trailer with self-motivated "positioning" capability.

Self Energising Automotive "Dead Axles"

Similarly to above, unassociated accumulator propulsion can be applied to the normally non-driven wheels of a vehicle without any power connection with worthwhile improvement to performance and fuel efficiency.

Golf Buggy A quick-charge hydraulic golf buggy is a fascinating prospect - but grossly overpowered even with our minimum equipment.

Underground and Safety Area Haulage An accumulator powered low-headroom tractor for mine haulage is under construction. Except for its lighting system it will be completely non-electric and therefore safe in hazardous atmospheres; also its smoothly modulated acceleration would obviate the sequential snatch normally evident with wagon-train couplings.

ENERGY CHARGING SERVICES FOR PURE MOBILES

Pure accumulator mobiles will only be acceptable if their recharging facilities are convenient, quick, clean and efficient. Convenient means strategically located according to operational usage: quick means comparable to a gas station fill-up; clean means no messing about; and efficient means effortless and cost-effective.

Automated Drive-In Charging

Applicable both to haulage terminal and gas station fore-court, the automated-connector drive-in charging bay with back-up oil conditioning, power production and energy storage, has been carefully studied.

As a result it was decided to break the system down into four areas. (1) the oil conditioning section; (2) hydraulic energy generation; (3) energy storage; (4) transfer connections.

Oil Conditioning Charging a Flydraulic accumulator from a service plant includes flushing the accumulator reservoir, so the conditioning plant comprises filtration, vacuum stripping, and a holding reservoir with vacuum environment.

Hydraulic Power Generation A reservoir feed pump passes fluid to an electrically driven high pressure pump equated to averaged vehicle charging service.

Energy Storage The pressure pump charges one or more Flydraulic accumulators some of which may be shut down during slack periods and reactivated by anticipatory time control associated with a demand integrator.

Transfer Connections: Self-Seeking Probe and Drogue Connection of hydraulic power delivery and return flow must be effected without ingestion of air, water or other pollutants, without oil leakage or dribble when uncoupling, and should be accomplished without human intervention or assistance, other than normal driving control of the vehicle requiring charge.

Any participating vehicle must be fitted with standarised complementary self-sealing connectors protected from weather and road detritus and located at the front of the vehicle which will be driven head on into the charging bay.

The servicing charge connectors are a pair of "probes" and the vehicle receptors become the "drogues" or female connections complete with terminal guidance cones. The probes are maintained parallel at standard centres allowing limited freedom in roll and in fore and aft compliance.

Articulating on a compound trapeze with underslung transverse beam carrying spaced vertical spindle waisted rollers for engagement by the vehicle fender and at extremities contra-linked flexible end-plates so centring the transverse beam horizontally, vertically and in azimuth, by the fender pushing against the beam.

Further pushing acts by leverage to force the probes through the flexible weather diaphragms to make coupling contact with the aligned self-sealing receptors, and to trigger the charging signal before reaching the limit buffers. An alternative arrangement uses hydraulic leverages and buffers.

Mobile Service Charger To cater for the usual circumstances or the "unwise virgins", a break-down "ambulance" carrying a charged Flydraulic accumulator with suitable jumper connectors can give a transferred charge in a very few minutes.

Alternatively any Flydraulic equipped vehicle fitted with appropriate jumper connections will permit a transferred charge.

Fleet "Trickle" Charging In a fleet park vehicles may be maintained at instant readiness by a low pressure charging circuit associated with feed pump of the main conditioning plant.

Domestic and Park "Trickle" Charging

Accumulator powered commuting vehicles in the domestic garage need a degree of charge to ensure their mobility. Their hydraulic propulsion motor is disconnectable from the axle drive in "Park" and is engaged by an on-board electric motor in regenerative pumping mode.

To mate with the A.C. outlet, a 3-pin plug with moulded cable axially aligned with the pins mean-centerline so as to be easily disconnectable. A self-reeling weatherproof connection at the front of the vehicle may plug into the domestic garage A.C. outlet or a weatherproof outdoor outlet.

ACCUMULATOR MOBILES WITH SELF-CHARGE FACILITY (HYBRIDS)

Basic pure accumulator mobiles in some cases have an operational requirement away from demanding an on-board hydraulic charging A.P.U. governed by energy level.

Flydraulic Commutacar Miniature accumulator powered "City" cars, with performance range handling disadvantages outside city limits are ineffective as a "second car". Flydraulic accumulator propulsion instead of Battery-Electric will overcome the performance handicap, and an A.P.U. charger will remove out-of-town range restraints. In town it will benefit from high regenerative efficiency and "instant charge" from a automated fore-court service base.

Airplane Fast-Taxi All-Services Tug

Jet engined airplanes are notorious for their high fuel consumption when taxying or idling on the ground, and resulting air pollution. Present tractor tugs are of low power suitable only for apron manoeuvring. A tractor should be capable of towing a 500 ton aircraft at 30 Knots for 2 miles against a headwind, ground-hold and up-queue for 30 minutes perhaps, meantime providing full air conditioning, 200 KW electrical supply and eventual engine starting; yet face the prospect of abort and return to apron.

Within the limited headroom and other dimensional constraints, multi-plexed Flydraulic accumulators can provide 320 kWh energy storage with 4400 H.P. tractive power and 550 H.P. (hyd) driving the ancillaries which have much the greater energy requirement. A 350 H.P. A.P.U. allows operation remote from charging base such as recovery of an off-runway airplane.

ACCUMULATOR-BOOSTED HYDROSTATIC PROPULSION

Here we can only examine in detail two vehicle cases involving Flydraulic accumulator boost. First a trans-continental heavy haulage roadway vehicle (tractor-trailer) and secondly a medium sized European automobile.

Trans-Am. Tractor-Trailer At 150,000 lb gross laden, powered by a 290 H.P. turbo-charged engine, these vehicles can attain 70 MPH, equivalent to 24.6 x 10 ft. lb. K.E. Allowing 100% reserve at 8/9ths effective, and adding 10% transmutation loss gives 23 kWh gross energy storage. A 42" diameter flywheel having 94 laminations (.080") runs at 8400 RPM derated for model range commonality.

Two 9/25 hydraulic motors drive the transaxle unit, identical size pump/motors are used in accumulator and as engine output pump computer controlled to match engine requirements. The accumulator pump/motor will be computer rated to 192 G.P.M. and 5140 p.s.i. (350 bar) limits, at all speeds between 2800 and 8400 R.P.M., giving 550 H.P. (hydraulic) maximum output and effectively trebling the engine-only power available at the vehicle wheels.

Maximum speed can be maintained up 1 in 5 gradient over at least one-sixth of a mile; this distance increasing as either or both speed and gradient decrease, down to 15 M.P.H. up 1 in 25 (4% gradient) which residual engine power could maintain indefinitely, yet with instantaneous availability of a relatively massive 3ft/sec. acceleration by drawing on the accumulator.

The adhesive weight will allow the maximum dynamic hydraulic braking to be applied by the wheel-driving transaxle motors, even on icy roads due to the instantaneous torque monitoring of the computing control system; but only one half of this can be regeneratively recovered by the accumulator unless this were fitted with twin pump/motors as allowed by its casing design. Otherwise the other half of the hydraulic retardation energy may be accommodated by the developed hydraulic retarder valve and dissipated by heat exchanger, also under control of the computing system.

A self-energising trailer would effectively double both tractive acceleration and deceleration without affecting the perfectly modulated two-pedal (Go and Slow) control of exquisite ease and convenience which is allied with oustanding fuel and maintenance economies.

European Medium-Sized Automobile Ford Granada 2500/300 The application of regenerative power boost to automobiles in high production will almost certainly be dependent upon the prior standardisation of hydrostatic transmission giving the effortless control which reduces tension and fatigue and provides a sensual ease to the occupants of an automobile.

This prototyping study is based on the Ford Granada 2500 which, apart from its smaller V-6 engine, is identical to the more usual Granada 3000.

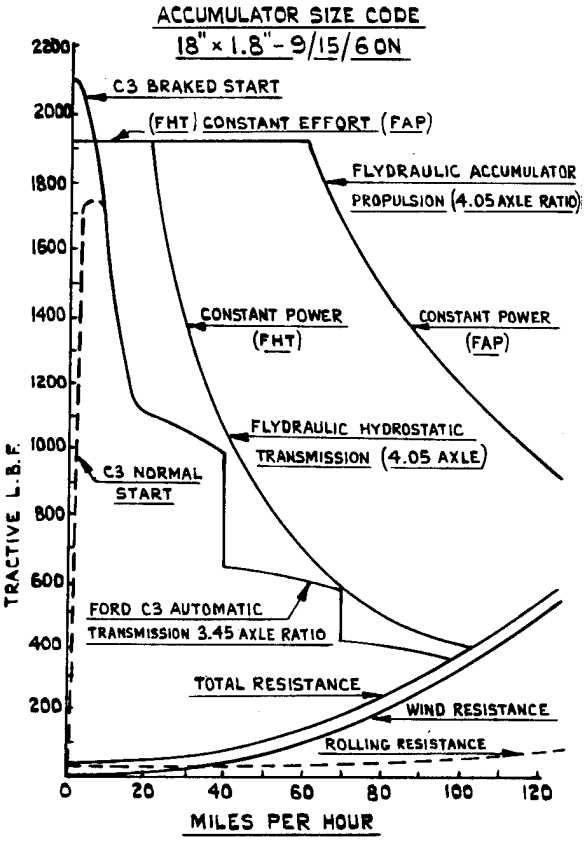
The smaller engine produces only 120 B.H.P. and makes for a 225lb lighter vehicle at 2800lb tare, but we have assumed full fuel and four occupants in the 3600 lb all-up weight, and 100 M.P.H. occasional cruising speed at which kinetic energy will be 1.2 x 10 ft. lb.

Due to the limited incidence of 100 M.P.H. cruising, we propose a stored energy reserve of 85% and transmutation allowance of 5% which at 8/9ths effective requires a gross flywheel energy capacity of 0.99 KWh. The most appropriate flywheel size is 18" diameter having 44 laminations 1 mm thick and running at 21,000 R.P.M. maximum, 7000 R.P.M. minimum operational, driving 1.52 ratio to a 9 x 15 mm pump/motor identical (other than the computing valve) with the pair of transaxle motors driving the rear wheels, and with the engine output pump. The installed weight (wet) of the flydraulic accumulator is then 194 lb.

At maximum displacement of 3.66 c.i.p.r. and 4600 R.P.M. the rated delivery is 60 G.P.M. (270 l/m) maximum maintained up to 13,800 R.P.M. so that at 5140 p.s.i. (350 bar) rated pressure the maximum power output is 216 H.P. (hydraulic) from the accumulator pump, and maximum torque 248 lb. ft. for each transaxle motor driving a half-shaft via a 4.05 ratio helical gear pair, giving a nett axle torque summation of 2010 lb.ft. maximum with 310 H.P. available at wheels.

The rolling diameter (25.4") of the rear tyres is 25.2" during maximum acceleration and tractive thrust 1918 lb. or 53.25% of gross weight. However, torque reaction weight transfer and inertia transfer increase the adhesive weight to 70%, and maximum tractive thrust can be maintained up to 62 M.P.H, then reduces inversely as speed increases.

Tractive resistances are shown on Fig. 2 which also shows tractive effort with the maker's C3 Automatic transmission, the Flydraulic Hydrostatic Transmission (without accumulator as Fig. 3) and with added accumulator propulsion (F.A.P.) as Fig. 4



FORD GRANADA 2500 AT 3600 LBS. LADEN

TRACTIVE EFFORT / RESISTANCE CURVES

FIG. 2.

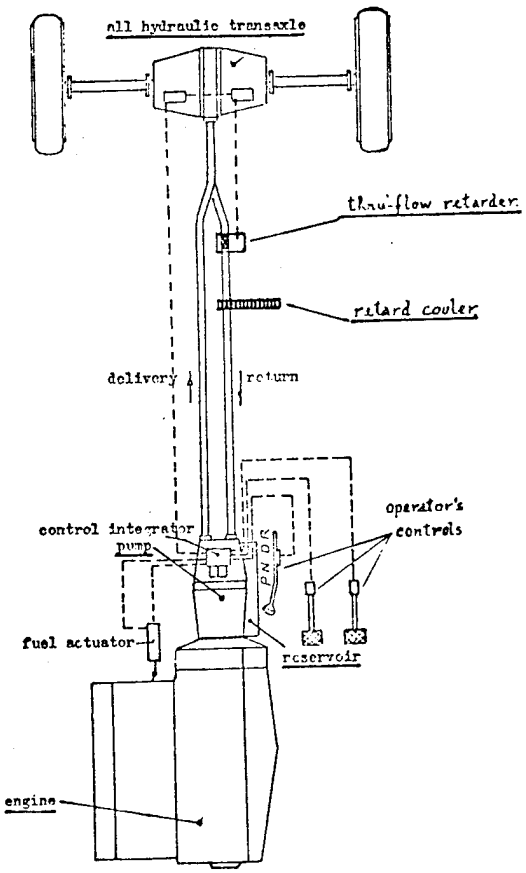


Fig. 3 Hydrostatic Automatic Transmission: Independent Axle Drive

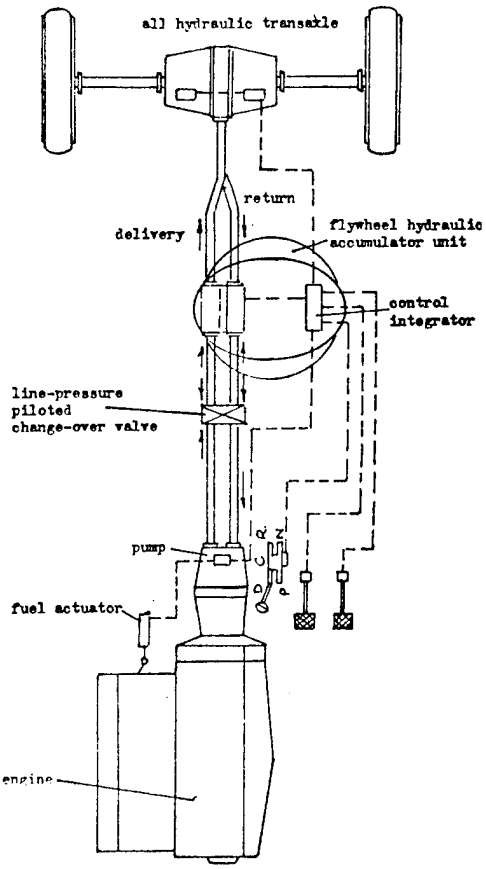
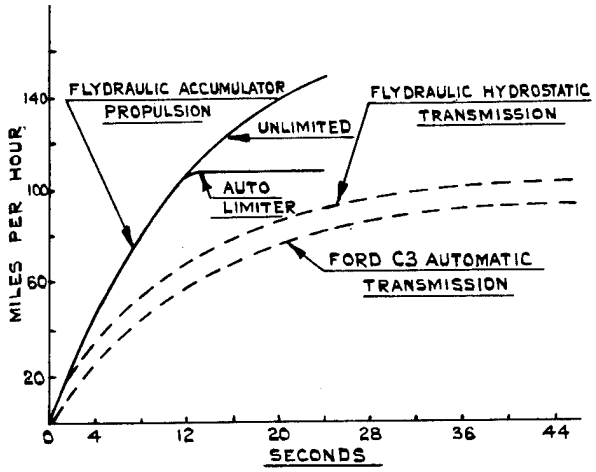


Fig. 4 "Flydraulic" Hybrid Regenerative Propulsion System.



FORD GRANADA 2500 AT 3600 LBS. LADEN

MAX. ACCELERATION GRAPH

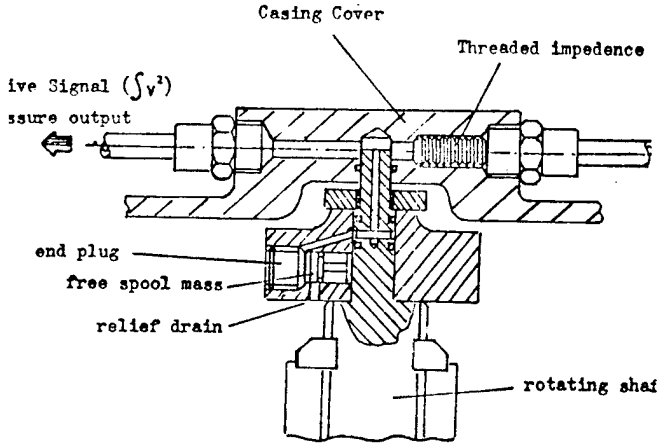
FIG. 5.

The C3 shows the highest tractive effort up to 5 M.P.H. and falling rapidly whereas FHT and FAP maintain their high constant effort to 22 MPH and 62MPH respectively before breaking to constant power. Indeed FAP at 100 M.P.H. has more effort available than does C3 at 15 M.P.H. in low gear, and could with a twin-pump accumulator maintain constant effort to 100 M.P.H.

The resulting acceleration curves Fig. 5 speak for themselves, showing the advantage of constant effort/constant power over stepped effort and "saw tooth" power. In fact the C3 transmission even with "3000" engine power is still no match for FHT with "2500" power (18 BHP difference) and bears no comparison to FAP even with "2000" power (40 BHP difference). Yet the very constancy of the acceleration reduces the sensation, with FAP even more than

with FHT, as the decay following the break to constant power is much more gradual - like an airplane at take off, after the first few seconds the acceleration ceases to be noticeable - until the hydro-computer phases it out above 100 MPH.

When driven more gently the same smooth control response exists but at reduced values of tractive effort proportional to accelerator pedal pressure.



Speed Responsive Signal Generator.

Front Wheel Drives and 4.W.D.

The same dual-motor transaxle as designed for the Ford Granada would be equally applicable to a front wheel driven automobile, or for that matter to both front and rear giving Four-wheel-drive without differentials or inter-differentials yet offering individual wheel slip control without reduction of effort at the other wheels: and conversely for wheel lock during regenerative braking. This applies to any rubber tired vehicle of any size but not at the moment to steel tired rail vehicles.

FUEL EFFICIENCY OF FLYDRAULIC BOOST PROPULSION

Although it is usual to determine overall efficiency of a system by itemising elemental power production and transmission efficiencies and summing these or their series products, the Flydraulic propulsion system goes much further by optimising the interaction of the elements to achieve much higher overall efficiency.

Even taking accumulator continuing loss at the present development state as 6% of instantaneous energy storage and hydraulic output transmutation loss as 5% of instantaneous power, prime-mover power loss as 4.1% and hydraulic trans-axle loss as 5%, the advantages conferred by hydro-computed interactive management are greater than the elemental loss summation and arises from four aspects.

BY VEHICLE INERTIA MANAGEMENT

By interchanging the inertias of vehicle and accumulator flywheel during acceleration and deceleration, the vehicle engine is reduced in purpose and function to overcoming resistance and efficiency losses, and the vehicle energy normally discarded as braking frictions is largely recuperated back to storage.

BY ENGINE SPEED AND B.M.E.P. MANAGEMENT

Engine output is managed, without human intervention, to accord with propulsive loss requirement but at optimised B.M.E.P. and lowest engine speed conducive to smooth running. This factor can improve engine efficiency by up to 30%

BY REDUCED RESPONSE REQUIREMENT

With existing systems fluctuating acceleration demands effect excessive enrichment by the carburettor fuelling system. But with Flydraulic propulsion acceleration demands are met instantly by the accumulator whereas engine power requirement accrues over a period of perhaps 10 seconds or more obviating any necessity for fuel enrichment and its adverse effect on engine wear and life.

BY SMALLER ENGINE

Without an accelerative requirement, prime mover engine power is determined by the designed cruising speed of the vehicle and the reduced size thus enabled by the accumulator will generate lower power production heat losses, will weigh less, cost less to manufacture, and be easier in development.

"STOP/START" ENGINE CYCLING

Although easily accommodated by the computing control and hydraulic cranking, the savings as against continuing optimised BMEP are negligible and not worth the psychological disturbance engendered by "sensory free-wheeling", not to mention its effect on air-conditioning and electrical ancillaries.

CONTROL FUNCTION AND DRIVEABILITY

It will have been gathered that the hydro-computers function as the brain and nerve system of Flydraulic propulsion, responding to the operator's requirements transformed to appropriate "pressure-language" as well as other system data, processed and presented as actuating functions to the driving motors, the accumulator pump/motor, engine pump and engine fuelling control.

OPERATOR'S COMMAND TRANSDUCERS

One transforms the accelerator pedal movement to a first stage pressure incremental to 480 p.s.i. max, (with feedback "feel" to pedal), transmitted to the accumulator master computing element commanding an increase in operating pressure and to a second stage which in association with a master signal instructs the:-

Drive Motor Computer (Slaved)

Which is basically simple and interprets the command signal for driving torque by setting the motor displacement to optimum for speed and operating pressure and if required for control of tractive wheel-slip. Additionally it accepts the brake pedal transformed signal to set the drive-motor as a pump, in collaboration with the accumulator pump acting as a motor for regenerative vehicle braking. It also responds to the Selector lever for "Neutral" location and for over center operation in "Reverse" and hydraulic locked "Park".

ACCUMULATOR (MASTER) COMPUTER

This receives the drive-motor generated vehicle speed signal in addition ot its own pump generated flywheel speed signal, both in square law, integrates them to an energy summation (moving) constant, controls braking regeneration with this varying flywheel energy limit and the hydraulic retarder (or vehicle wheel brakes) when the limit is exceeded, controls the prime mover engine pump to make an appropriate contribution when short of the limit, taper-cancels the acceleration energy-boost above a programmed (cruising?) speed, prevents flywheel overspeed, and overall ensures smooth build up of instantaneous responses and perfectly controlled modulation.

ENGINE PUMP COMPUTER (SLAVED)

This interprets the master-computer instruction in "Drive" and "Reverse" (or the bypassed operator command in "Neutral" and "Park") for more power (or more revolutions) which it resolves with its speed and displacement feedback signals pressure, to increase power against an increasing pump(displacement x system pressure) torque. The engine B.M.E.P. vs. speed can therefore be precisely controlled within a programmed envelope.

A COMPUTERIZED ANALYSIS OF AXISYMMETRIC FLYWHEELS

Norman L Newhouse
Brunswick Corporation
Defense Division
4300 Industrial Avenue
Lincoln, Nebraska 68504

ABSTRACT

A method is presented for analysis of axisymmetric flywheels with one or more circumferential layers. This method has been developed into a user efficient computer program. A closed form analysis is used for each layer and a finite element technique is used to provide for compatibility of sequential layers. Plane stress analysis gives exact solutions for axially thin disks and close approximations for thick disks and disks of non-uniform width. The analysis provides for flywheels of one or more layers, isotropic and orthotropic materials, and inertial and thermal loading. Stresses, strains, and displacements are calculated at the layer boundaries and intermediate points in each layer. In addition, rotational energy and energy density are calculated.

NOMENCLATURE

A,B,C,D	Arbitrary Constants
a	Outer Radius of a Layer
b	Inner Radius of a Layer
E	Energy
E_r,E_θ	Radial and Hoop Modulus of Elasticity
F	Force
F1	Force at Inner Boundary of a Layer
F2	Force at Outer Boundary of a Layer
F(r)	See Eq. (17)
G1 to G4	See Eq. (17)
g_c	Gravitational Constant
H(r)	See Eq. (17)
K	Stiffness Matrix
K11,K12,K21,K22	Elements of Layer Stiffness Matrix
M	Mass
m	See Eq. (6)
n	Number of Layers or nth Layer
Q_{rr},$Q_{r\theta}$,$Q_{\theta r}$,$Q_{\theta\theta}$	Elastic Constants, See Eq. (2)
r	Radius
S	See Eq. (16b)
ΔT	Change in Equilibrium Temperature
u	Radial Displacement
u_i,u_o	Radial Displacement at the Inner and Outer Boundaries of a Layer
u_h,u_p	See Eq. (7) and Eq. (8)
V	Volume
X	Displacement
α_r,α_θ	Radial and Hoop Coefficients of Thermal Expansion
ε_r,ε_θ	Radial and Hoop Strains
$\nu_{\theta r}$,$\nu_{r\theta}$	Poisson's Ratios, See Eq. (2)
ρ	Density
σ_r,σ_θ	Radial and Hoop Stresses
ω	Angular Velocity

INTRODUCTION

Brunswick Corporation has been active in the design and manufacture of filament wound flywheel rotors for several years. Design, analysis, material studies and manufacturing efforts have been carried out under contract to several organizations as well as with internal development funds.

To meet its design and analysis requirements, Brunswick needed a computer program which was versatile, precise and user efficient.

Analysis of a flywheel rotor has consisted primarily of defining rotational speed limits and optimizing the shape for a given material system. To optimize a flywheel for a given material system, the radial and hoop stresses should be uniform throughout the wheel and should both reach their respective ultimate stress levels

simultaneously. For flywheels with a single isotropic material system, the optimum shape may be calculated precisely. Solutions for a flat disk are also precise and readily available for an isotropic material.

Solutions for flywheels made of orthotropic materials are generally found only in current literature. Solutions for optimum shape are possible, but manufacturing considerations generally dictate limitations on the size and shape of the final part. Solutions which were found for flat disks generally considered only one material system and one layer of material, and they generally did not address thermal effects.

Brunswick has found from experience that thermal stresses develop during cure processes of fiber/epoxy flywheels and during exposure to varying environmental temperatures. These thermal stresses are significant to the point that the ultimate radial stress level can be reached before the flywheel is rotated for the first time.

In addition to closed form analysis methods, some general purpose finite element computer programs are capable of rotational/thermal analysis of flywheels. However, these programs are generally cumbersome and expensive in terms of man hours and machine time.

In view of the difficulty of using general finite element computer programs and in view of the narrow range of closed form techniques in current literature, Brunswick felt that an analytical method should be developed which would be precise, versatile, inexpensive and easy to use. A plane stress analysis was developed, which, in combination with finite element techniques, gives exact answers for axially thin disks and close approximations for thick or tapered disks. Any number of materials or layers may be used with a minimum of inputs. Stresses, strains, and displacements are calculated for isotropic or orthotropic materials under inertial and thermal loading.

ANALYSIS

GOVERNING EQUATIONS

Three sets of equations govern the stress analysis of an axisymmetric disk: equilibrium, Eq. (1); constitutive, Eq. (2); and geometry, Eq. (3). Substituting Eq. (2) and Eq. (3) into Eq. (1) results in an equation for deflection in terms of material properties, radial position, rotational speed and change in equilibrium temperature, Eq. 4.

Equilibrium

$$\frac{d\sigma_r}{dr} + \frac{(\sigma_r - \sigma_\theta)}{r} = -\rho\omega^2 r \tag{1}$$

Constitutive

$$\begin{Bmatrix}\sigma_r \\ \sigma_\theta\end{Bmatrix} = \begin{bmatrix}Q_{rr} & Q_{r\theta} \\ Q_{\theta r} & Q_{\theta\theta}\end{bmatrix} \begin{Bmatrix}\varepsilon_r - \alpha_r\Delta T \\ \varepsilon_\theta - \alpha_\theta\Delta T\end{Bmatrix} \tag{2a, 2b}$$

$$Q_{rr} = \frac{E_r}{1-\nu_{r\theta}\,\nu_{\theta r}} \tag{2c}$$

$$Q_{r\theta} = \frac{E_r\,\nu_{\theta r}}{1-\nu_{r\theta}\,\nu_{\theta r}} \tag{2d}$$

$$Q_{\theta r} = \frac{E_\theta\,\nu_{r\theta}}{1-\nu_{r\theta}\,\nu_{\theta r}} = Q_{r\theta} \tag{2e}$$

$$Q_{\theta\theta} = \frac{E_\theta}{1-\nu_{r\theta}\,\nu_{\theta r}} \tag{2f}$$

Geometry

$$\varepsilon_r = \frac{du}{dr} \tag{3a}$$

$$\varepsilon_\theta = \frac{u}{r} \tag{3b}$$

Result

$$\frac{d^2u}{dr^2} + \frac{1}{r}\frac{du}{dr} - \frac{Q_{\theta\theta}}{Q_{rr}}\frac{u}{r^2} = \frac{\rho\omega^2 r}{Q_{rr}} + \frac{\alpha_r\Delta T}{r} + \frac{Q_{r\theta}}{Q_{rr}}\left(\frac{\alpha_\theta\Delta T}{r} - \frac{\alpha_r\Delta T}{r}\right) - \frac{Q_{\theta\theta}}{Q_{rr}}\frac{\alpha_\theta\Delta T}{r} \tag{4}$$

SOLUTION

The solution to Eq. (4) is found by summing the homogeneous and the particular solutions. The homogeneous solution takes the form $u_h = r^m$, Eq. (5) being the characteristic equation, Eq. (6) the solution of m, and Eq. (7) the homogeneous solution where A and B are unknowns.

$$m(m-1)r^{m-2+m}r^{m-2} - \frac{Q_{\theta\theta}}{Q_{rr}}r^{m-2} = 0 \tag{5}$$

$$m = \pm\sqrt{\frac{Q_{\theta\theta}}{Q_{rr}}} = \pm\sqrt{\frac{E_\theta}{E_r}} \quad (6)$$

$$u_h = Ar^m + Br^{-m} \quad (7)$$

The value m is then a measure of the anisotropy of the material system. For isotropic materials m=1, and as the hoop modulus increases with relation to the radial modulus, as in a circumferentially wound fiber/epoxy flywheel, the value for m increases.

The particular solution of Eq. (4) is of the form of Eq. (8), which can be solved for the constants C and D, Eq. (9). The total solution is then Eq. (10). Note that the constant C pertains to rotation while D pertains to temperature.

$$u_p = Cr^3 + Dr \quad (8)$$

$$C = \frac{\rho\omega^2}{Q_{rr}(m^2-9)} \quad (9a)$$

$$D = \frac{\alpha_r\Delta T + \frac{Q_{r\theta}}{Q_{rr}}(\alpha_\theta\Delta T - \alpha_r\Delta T) - m^2\alpha_\theta\Delta T}{1 - m^2} \quad (9b)$$

$$u = u_h + u_p = Ar^m + Br^{-m} + Cr^3 + Dr \quad (10)$$

BOUNDARY CONDITIONS

When solving for the unknowns A and B in Eq. (10), it is necessary to define boundary conditions. In general, the boundary conditions for free boundaries, Eq. (11), or fixed inner boundary, Eq. (12), would be used. These conditions are necessary and sufficient for a single-layered disk. For a multilayered disk, the boundary conditions at the layer interfaces must also be defined, Eq. (13), where the subscript n identifies the nth layer. In order to use a finite element approach, however, we will define a set of boundary conditions for each layer with the deflections at the inner and outer layer boundaries being defined in terms of the radii at the inner and outer layer boundaries, Eq. (14).

$$\sigma_r(b) = 0 \quad (11a)$$

$$\sigma_r(a) = 0 \quad (11b)$$

$$u(b) = 0 \quad (12a)$$

$$\sigma_r(a) = 0 \quad (12b)$$

$$(u_o)_n = (u_i)_{n+1} \quad (13a)$$

$$((\sigma_r)_o)_n = ((\sigma_r)_i)_{n+1} \quad (13b)$$

$$u_i = Ab^m + Bb^{-m} + Cb^3 + Db \quad (14a)$$

$$u_o = Aa^m + Ba^{-m} + Ca^3 + Da \quad (14b)$$

FINAL EQUATION

Equations (14a) and (14b) represent two equations and two unknowns, so we can therefore solve for unknowns A and B. First multiply Eq. (14a) by a^{-m}, then multiply Eq. (14b) by $-b^{-m}$ and add. This eliminates B and results in the value for A shown in Eq. (15a). Multiplying Eq. (14a) by a^m and Eq. (14b) by $-b^m$ and adding results in the value for B shown in Eq. (15b). By substituting Eq. (15) and Eq. (9) into Eq. (10), and rearranging terms, we get the final equation for displacement as a function of radius, Eq. (16). Equation (16) is substituted into Eq. (3) to obtain the radial and hoop strains, Eq. (17). It should be noted that the term involving rotation becomes indeterminate when m=3 and the term involving temperature becomes indeterminate when m=1. The solutions when m=1 or m=3 may be found in one of two ways. L'Hospital's rule may be used on the current solution, or a term involving rlnr could be added when evaluating the particular solution. These two methods will, of course, yield identical solutions.

$$A = -\frac{(u_i a^{-m} - u_o b^{-m}) - C(b^3 a^{-m} - a^3 b^{-m}) - D(ba^{-m} - ab^{-m})}{(b^{-m}a^m - b^m a^{-m})} \quad (15a)$$

(15b)

$$B = \frac{(u_f a^m - u_o b^m) - C(b^3 a^m - a^3 b^m) - D(ba^m - ab^m)}{(b^{-m} a^m - b^m a^{-m})}$$

(16a)

$$u = \frac{-(u_f a^{-m} - u_o b^{-m}) r^m}{S} + \frac{(u_i a^m - u_o b^m) r^{-m}}{S}$$

$$+ \frac{\rho\omega^2}{Q_{rr}(m^2-9)S} \left[(b^3 a^{-m} - a^3 b^{-m}) r^m - (b^3 a^m - a^3 b^m) r^{-m} \right.$$

$$\left. + (b^{-m} a^m - b^m a^{-m}) r^3 \right]$$

$$+ \frac{\alpha_r \Delta T + \frac{Q_{r\theta}}{Q_{rr}} (\alpha_\theta \Delta T - \alpha_r \Delta T) - m^2 \alpha_\theta \Delta T}{(1-m^2)S} \left[(ba^{-m} - ab^{-m}) r^m \right.$$

$$\left. + (ab^m - ba^m) r^{-m} + (b^{-m} a^m - b^m a^{-m}) r \right]$$

(16b)

$$S = b^{-m} a^m - b^m a^{-m}$$

(17a)

$$\varepsilon_r = mG_1 r^{m-1} - mG_2 r^{-m-1} + G_3 \frac{dF(r)}{dr} + G_4 \frac{dH(r)}{dr}$$

(17b)

$$\varepsilon_\theta = G_1 r^{m-1} + G_2 r^{-m-1} + G_3 \frac{F(r)}{r} + G_4 \frac{H(r)}{r}$$

(17c)

$$G_1 = (u_o b^{-m} - u_i a^{-m})/S$$

(17d)

$$G_2 = (u_i a^m - u_o b^m)/S$$

(17e)

$$G_3 = (\rho\omega^2)/(Q_{rr} S)$$

(17f)

$$G_4 = \left[\alpha_r \Delta T + \frac{Q_{r\theta}}{Q_{rr}} (\alpha_\theta \Delta T - \alpha_r \Delta T) - m^2 \alpha_\theta \Delta T\right] / S$$

(17g)

$$\frac{F(r)}{r} = \frac{1}{m^2-9} \left[(b^3 a^{-m} - a^3 b^{-m}) r^{m-1} \right.$$

$$\left. - (b^3 a^m - a^3 b^{-m}) r^{-m-1} + (b^{-m} a^m - b^m a^{-m}) r^2 \right]$$

(17h)

$$\frac{dF(r)}{dr} = \frac{1}{m^2-9} \left[(b^3 a^{-m} - a^3 b^{-m}) m r^{m-1} \right.$$

$$\left. + (b^3 a^m - a^3 b^m) m r^{-m-1} + (b^{-m} a^m - b^m a^{-m}) 3r^2 \right]$$

(17i)

$$\frac{H(r)}{r} = \frac{1}{1-m^2} \left[(ba^{-m} - ab^{-m}) r^{m-1} \right.$$

$$\left. + (ab^m - ba^m) r^{-m-1} + (b^{-m} a^m - b^m a^{-m}) \right]$$

(17j)

$$\frac{dH(r)}{dr} = \frac{1}{1-m^2} \left[(ba^{-m} - ab^{-m}) m r^{m-1} \right.$$

$$\left. - (ab^m - ba^m) m r^{-m-1} + (b^{-m} a^m - b^m a^{-m}) \right]$$

when m = 3

(17k)

$$\frac{F(r)}{r} = \frac{1}{6} \left\{ \left[\left(\frac{b}{a}\right)^3 - \left(\frac{a}{b}\right)^3 \right] \left[r^2 \ln r\right] + \left[b^3 a^3\right] \left[\ln\left(\frac{b}{a}\right)\right] r^{-4} \right.$$

$$\left. + \left[\left(\left(\frac{a}{b}\right)^3 \ln a \right) - \left(\left(\frac{b}{a}\right)^3 \ln b \right) \right] r^2 \right\}$$

(17l)

$$\frac{dF(r)}{dr} = \frac{1}{6} \left\{ \left[\left(\frac{b}{a}\right)^3 - \left(\frac{a}{b}\right)^3 \right] \left[3r^2 \ln r + r^2\right] \right.$$

$$\left. - \left[b^3 a^3\right] \left[\ln\left(\frac{b}{a}\right)\right] 3r^{-4} + \left[\left(\left(\frac{a}{b}\right)^3 \ln a \right) - \left(\left(\frac{b}{a}\right)^3 \ln b \right) \right] 3r^2 \right\}$$

when m = 1

(17m)

$$\frac{H(r)}{r} = \frac{1}{2} \left[\left(\frac{b}{a} \ln b - \frac{a}{b} \ln a \right) \right.$$

$$\left. + \left(ba \ln\left(\frac{a}{b}\right) \right) r^{-2} + \left(\frac{a}{b} - \frac{b}{a}\right) \ln r \right]$$

(17n)

$$\frac{dH(r)}{dr} = \frac{1}{2} \left[\left(\frac{b}{a} \ln b - \frac{a}{b} \ln a \right) \right.$$

$$\left. - \left(ba \ln\left(\frac{a}{b}\right) \right) r^{-2} + \left(\frac{a}{b} - \frac{b}{a}\right) (1 + \ln r) \right]$$

Equation (17) is now substituted into Eq. (2) to get radial and hoop stresses at any radius. However, it is still necessary to find the displacements at the inner and outer surfaces of a layer.

FINITE ELEMENT METHOD

STIFFNESS MATRIX

The first step in obtaining the displacements at the boundaries is to build a stiffness matrix for the entire flywheel by using Eq. (18). The term 'X' in Eq. (18) is set equal to unity, and the radial stress due to that displacement is calculated using Eq. (17) and Eq. (2). The term 'F' in Eq. (18) is calculated by multiplying the radial stress and the area over which it acts. Since the displacement 'X' is unity, the 'F' and 'K' terms in Eq. (18) are then equal.

$$\{F\} = [K]\{X\} \tag{18}$$

As an example, Eq. (19) is used to evaluate the stiffness terms for any layer. The displacement X1 is set to unity, the displacement X2, the rotation, and the temperature are set to zero and the resulting radial stresses at the boundaries are calculated. Multiplying the stresses by the respective areas over which they act yields force F1 at boundary 1 and force F2 at boundary 2, both due to unit displacement at boundary 1. Since X2=0, Eq. (20) holds, where K11 is the stiffness term at boundary 1 due to a displacement of boundary 1 and K21 is the stiffness term at boundary 2 due to a displacement of boundary 1. Similarly, setting X1=0 and X2=1 will give the stiffness terms K12 and K22. The stiffness matrix is symmetric, i.e. K12 = K21.

$$\begin{Bmatrix} F1 \\ F2 \end{Bmatrix} = \begin{bmatrix} K11 & K12 \\ K21 & K22 \end{bmatrix} \begin{Bmatrix} X1 \\ X2 \end{Bmatrix} \tag{19}$$

$$K11 = F1 \tag{20a}$$

$$K21 = F2 \tag{20b}$$

The layer stiffness terms are then added into the global stiffness matrix, Eq. (21). This results in a square matrix with n+1 rows and n+1 columns where n is the total number of layers. The global stiffness matrix is symmetric with all terms zero except for the diagonal elements and those elements adjacent to the diagonal elements.

$$\begin{bmatrix} K11(1) & K12(1) & 0 & 0 & \cdots & 0 \\ K21(1) & K22(1)+K11(2) & K12(2) & 0 & \cdots & 0 \\ 0 & K21(2) & K22(2)+K11(3) & \cdots & \cdots & 0 \\ 0 & 0 & \vdots & & & \vdots \\ \vdots & \vdots & \vdots & \cdots & K22(N-1)+K11(N) & K12(N) \\ 0 & 0 & 0 & \cdots & K21(N) & K22(N) \end{bmatrix} \tag{21}$$

FORCE MATRIX

The force matrix is calculated in much the same way as the stiffness matrix, but now the boundary displacements are set equal to zero and the rotation and temperature are set to their proper values. The radial stress is calculated at the boundaries of the layer, multiplied by the area over which the stress acts, and the resulting force terms are added into the global stiffness matrix, Eq. (22).

$$\begin{Bmatrix} F1(1) \\ F2(1)+F1(2) \\ F2(2)+F1(3) \\ \vdots \\ F2(N-1)+F1(N) \\ F2(N) \end{Bmatrix} \tag{22}$$

DISPLACEMENT MATRIX

We now have the force matrix and stiffness matrix which are related by Eq. (18). In order to obtain the displacements at the boundaries, we must first invert the stiffness matrix and then multiply by the force matrix. The solution will now take the form of Eq. (23) and the displacements at the boundaries are explicitly solved for. They can then be substituted into Eq. (17) to calculate strains, and the resulting strains substituted into Eq. (2) to calculate stresses.

$$[K]^{-1}\{F\} = \{u\} \tag{23}$$

THICK OR TAPERED DISKS

The analysis which has been presented is based on a plane stress model, that is, the assumption is made that all stress is in the r-θ plane and no stress exists in the axial direction. This assumption is good in the case of axially thin disks with no external loads on the faces. As the part becomes axially thicker, axial stresses build as distance from the free surface increases. However, other solution methods show this is not significant for moderately thick parts.

Tapered disks cannot be analyzed directly by this method, but a usable approximation can be made by varying the width of each layer to approximate the desired contour. Radial stress will not be equal across a boundary, but the forces will balance. This is due to the assumption that radial stress is distributed uniformly over the layer boundary, which is not of equal width from layer to layer. The stresses at a boundary are therefore not correct but if one looks only at the stresses and strains at the middle of a layer, meaningful results can be obtained.

ENERGY

The energy available from a flywheel rotor is of primary importance to anyone concerned with a practical application. The energy stored in a solid disks is calculated by using Eq. (24). Applying this to a layered disk leads one to Eq. (25). Energy per unit volume is calculated by using Eq. (26) and energy per unit mass is calculated by using Eq. (27). The energy and specific energy are easily calculated for individual layers as well as for the total wheel, which is important when considering the effectiveness of each layer.

$$E = \frac{1}{2} I\omega^2 = \frac{1}{4} \pi \frac{\rho}{g_c} r^4 h \omega^2 \qquad (24)$$

$$E = \sum_{j=1}^{n} \frac{\pi}{4} \frac{\rho_j}{g_c} (a^4_j - b^4_j) h_j \omega^2 \qquad (25)$$

$$\frac{E}{M} = \frac{E}{\sum_{j=1}^{n} \pi(a^2_j - b^2_j) h_j} \qquad (26)$$

$$\frac{E}{M} = \frac{E}{\sum_{j=1}^{n} \pi\rho_j (a^2_j - b^2_j) h_j} \qquad (27)$$

RESULTS

SAMPLE RUN

All of the equations necessary for plane stress analysis of an axisymmetric flywheel have been presented. These equations have been programmed for solution on a digital computer. Figure 1 presents the input and output data for a sample run of the program on a time sharing computer system. All lines beginning with a question mark are inputs, all other lines are printed by the computer. Required inputs include basic geometry information, material properties, angular velocity, and temperature change.

Specificially, input 1 is a description of the run being made. Input 2 specifies the inside radius of the first layer and the number of materials and layers. Input 3 specifies the material properties for each material. Input 4 specifies the material, thickness (radial), and width (axial) of each layer. Input 5 specifies angular velocity, temperature change, and the number of points in addition to the boundaries where stress and strain will be calculated. Units on inputs and outputs are inches, psi, ^{o}F and RPM.

All input data is printed back as a check. Strain and stress in the radial and hoop directions and radial deflection are calculated at each radial position. Energy and energy density are calculated for each layer as well as for the entire flywheel. The layer and global stiffness and force matrices have been printed as a check for anyone writing their own computer program using the methods presented in this paper.

GEOMETRY EFFECTS

A study was made of the effect of wall thickness on the distribution of stresses within a Kevlar/epoxy flywheel. Figures 2, 3, 4, and 5 illustrate the nondimensionalized results of that study. Figures 2 and 3 show the hoop and radial stresses for inertial loading, while Figures 4 and 5 show the hoop and radial stresses for thermal loading. Note that the ratio b/a

```
INPUT *1* : PROJECT DESCRIPTION
?*** SAMPLE RUN ***

INPUT *2* : RI,NMT,NL
?.5,3,3

INPUT *3* : MT, EH, ER, PRHR, GAMA, ALPH, ALPR
?1,30D6,30D6,.3,.286,6D-6,6D-6
?2,8.8D6,1.7D6,.32,.078,3.7D-6,17D-6
?3,12.8D6,1D6,.34,.05,-1.1D-6,33D-6

INPUT *4* : LN,MT,TL,WL
?1,1,2,1
?2,2,3,1
?3,3,4,1

INPUT *5* : OMEGA, DELT, ISPL
?10000,100,-9


*** SAMPLE RUN ***


RI= 0.5000    NMT= 3    NL= 3    OMEGA= 10000.00    DELT= 100.00

        EH            ER            PRHR          PRRH          M             GAMA          ALPH          ALPR
 0.3000D+08    0.3000D+08    0.3000D+00    0.3000D+00    0.1000D+01    0.2860D+00    0.6000D-05    0.6000D-05
 0.8800D+07    0.1700D+07    0.3200D+00    0.6182D-01    0.2275D+01    0.7800D-01    0.3700D-05    0.1700D-04
 0.1280D+08    0.1000D+07    0.3400D+00    0.2656D-01    0.3578D+01    0.5000D-01   -0.1100D-05    0.3300D-04

LAYER STIFFNESS MATRIX AND UNIT FORCE MATRICES

L= 1
    0.25824D+08   -0.13736D+08   -0.55512D-03    0.12857D+03
   -0.13736D+08    0.45604D+08   -0.27756D-02   -0.64286D+03

L= 2
    0.36154D+07   -0.13498D+07   -0.23781D-02    0.67582D+02
   -0.13498D+07    0.47253D+07   -0.58717D-02   -0.18883D+03

L= 3
    0.34148D+07   -0.10427D+07   -0.79273D-02    0.23014D+03
   -0.10427D+07    0.41010D+07   -0.15282D-01   -0.25149D+03

GLOBAL STIFFNESS MATRIX AND FORCE MATRIX

 0.2582E+08   -0.1374E+08    0.            0.           -0.1225E+05
-0.1374E+08    0.4922E+08   -0.1350E+07    0.            0.6318E+05
 0.           -0.1350E+07    0.8140E+07   -0.1043E+07    0.1100E+05
 0.            0.           -0.1043E+07    0.4101E+07    0.4191E+05

 LN MT    WL      RI      TL      RO  IPN      R          EPR          EPH          SR           SH           U
  1  1  1.000   0.500   2.000   2.500   1   0.500   0.6023D-03   0.5924D-03   0.1697D-13  -0.2292D+03   0.2962D-03
                                       2   0.700   0.5973D-03   0.5944D-03  -0.1452D+03  -0.2106D+03   0.4161D-03
                                       3   0.900   0.5932D-03   0.5946D-03  -0.2790D+03  -0.2456D+03   0.5351D-03
                                       4   1.100   0.5889D-03   0.5940D-03  -0.4264D+03  -0.3092D+03   0.6534D-03
                                       5   1.300   0.5841D-03   0.5928D-03  -0.5949D+03  -0.3940D+03   0.7707D-03
                                       6   1.500   0.5787D-03   0.5913D-03  -0.7873D+03  -0.4971D+03   0.8870D-03
                                       7   1.700   0.5727D-03   0.5895D-03  -0.1005D+04  -0.6172D+03   0.1002D-02
                                       8   1.900   0.5659D-03   0.5874D-03  -0.1248D+04  -0.7537D+03   0.1116D-02
                                       9   2.100   0.5585D-03   0.5850D-03  -0.1518D+04  -0.9063D+03   0.1228D-02
                                      10   2.300   0.5503D-03   0.5823D-03  -0.1814D+04  -0.1075D+04   0.1339D-02
                                      11   2.500   0.5414D-03   0.5794D-03  -0.2136D+04  -0.1259D+04   0.1449D-02

  2  2  1.000   2.500   3.000   5.500   1   2.500   0.4014D-03   0.5794D-03  -0.2136D+04   0.1159D+04   0.1449D-02
                                       2   2.800   0.5107D-03   0.5667D-03  -0.1953D+04   0.1106D+04   0.1587D-02
                                       3   3.100   0.5748D-03   0.5647D-03  -0.1843D+04   0.1123D+04   0.1750D-02
                                       4   3.400   0.6068D-03   0.5672D-03  -0.1786D+04   0.1163D+04   0.1928D-02
                                       5   3.700   0.6140D-03   0.5708D-03  -0.1772D+04   0.1200D+04   0.2112D-02
                                       6   4.000   0.6001D-03   0.5737D-03  -0.1795D+04   0.1218D+04   0.2295D-02
                                       7   4.300   0.5675D-03   0.5745D-03  -0.1851D+04   0.1207D+04   0.2470D-02
                                       8   4.600   0.5175D-03   0.5725D-03  -0.1939D+04   0.1162D+04   0.2633D-02
                                       9   4.900   0.4509D-03   0.5672D-03  -0.2057D+04   0.1077D+04   0.2779D-02
                                      10   5.200   0.3681D-03   0.5581D-03  -0.2205D+04   0.9499D+03   0.2902D-02
                                      11   5.500   0.2696D-03   0.5452D-03  -0.2383D+04   0.7787D+03   0.2998D-02

  3  3  1.000   5.500   4.000   9.500   1   5.500   0.7153D-03   0.5452D-03  -0.2383D+04   0.7576D+04   0.2998D-02
                                       2   5.900   0.1080D-02   0.5495D-03  -0.2007D+04   0.8015D+04   0.3360D-02
                                       3   6.300   0.1383D-02   0.6117D-03  -0.1687D+04   0.8665D+04   0.3854D-02
                                       4   6.700   0.1645D-02   0.6658D-03  -0.1404D+04   0.9453D+04   0.4461D-02
                                       5   7.100   0.1877D-02   0.7276D-03  -0.1149D+04   0.1033D+05   0.5166D-02
                                       6   7.500   0.2086D-02   0.7946D-03  -0.9151D+03   0.1127D+05   0.5959D-02
                                       7   7.900   0.2275D-02   0.8648D-03  -0.6998D+03   0.1224D+05   0.6832D-02
                                       8   8.300   0.2447D-02   0.9370D-03  -0.5012D+03   0.1323D+05   0.7777D-02
                                       9   8.700   0.2604D-02   0.1010D-02  -0.3183D+03   0.1423D+05   0.8788D-02
                                      10   9.100   0.2744D-02   0.1083D-02  -0.1512D+03   0.1522D+05   0.9850D-02
                                      11   9.500   0.2870D-02   0.1156D-02   0.5271D-15   0.1620D+05   0.1098D-01

 LN     WATT-HOURS       W-HR/LBM       W-HR/CU IN          INCH-LBF      IN-LBF/LBM    IN-LBF/CU IN
  1   0.7803D+00    0.1447D+00    0.4140D-01    0.2486D+05    0.4612D+04    0.1319D+04
  2   0.4740D+01    0.8128D+00    0.6340D-01    0.1523D+06    0.2590D+05    0.2020D+04
  3   0.2529D+02    0.2683D+01    0.1342D+00    0.8056D+06    0.8550D+05    0.4275D+04

TOTAL 0.3085D+02    0.1491D+01    0.1091D+00    0.9829D+06    0.4749D+05    0.3476D+04
      ENERGY/*SWEPT VOLUME*       0.1086D+00                                0.3467D+04
```

FIGURE 1 TYPICAL COMPUTER PROGRAM INPUT AND OUTPUT DATA

approaches, but does not equal, zero. The material properties used for the Kevlar/epoxy composite are presented in Table 1.

TABLE 1. MATERIAL PROPERTIES OF A KEVLAR/EPOXY COMPOSITE

E_θ	12.8×10^6	PSI
E_r	1.0×10^6	PSI
$\nu_{\theta r}$	.34	
ρ	.05	LB./CU. IN.
α_θ	-1.1×10^{-6}	IN/IN/^oF
α_r	33.0×10^{-6}	IN/IN/^oF

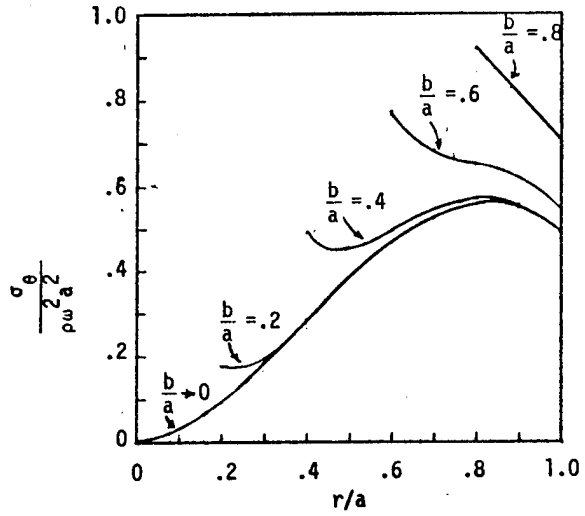


FIGURE 2. HOOP STRESS DISTRIBUTION IN A ROTATING KEVLAR/EPOXY DISK

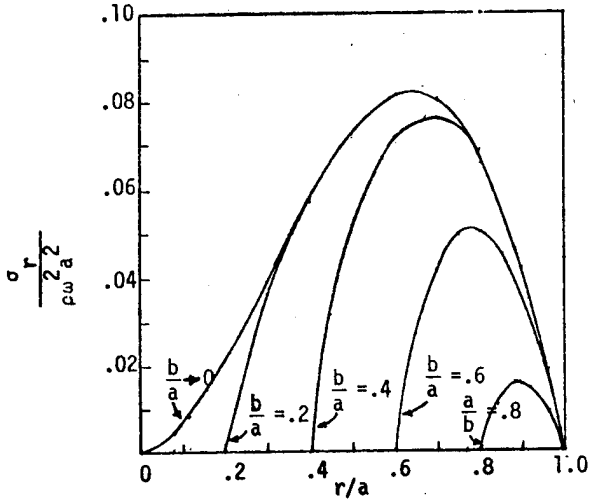


FIGURE 3. RADIAL STRESS DISTRIBUTION IN A ROTATING KEVLAR/EPOXY DISK

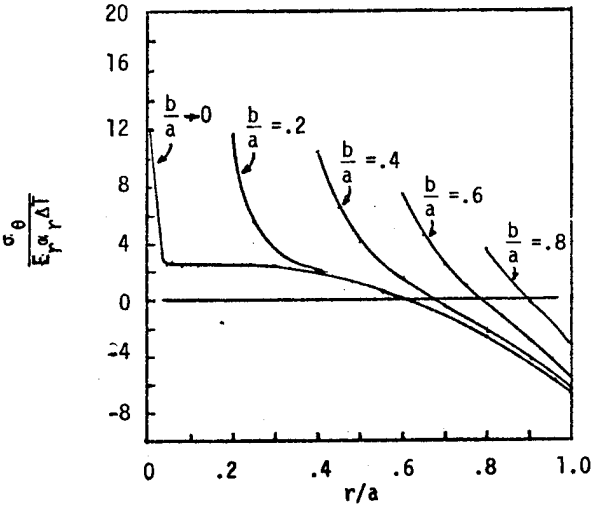


FIGURE 4. HOOP STRESS DISTRIBUTION IN A KEVLAR/EPOXY DISK SUBJECTED TO A CHANGE IN EQUILIBRIUM TEMPERATURE

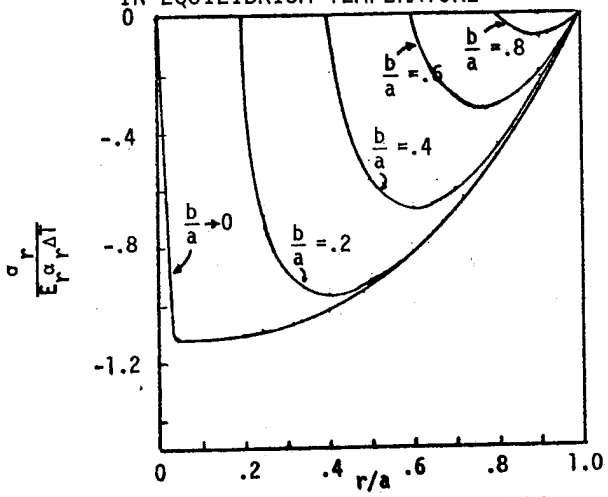


FIGURE 5. RADIAL STRESS DISTRIBUTION IN A KEVLAR/EPOXY DISK SUBJECTED TO A CHANGE IN EQUILIBRIUM TEMPERATURE

MATERIAL PROPERTY EFFECTS

A study was made of the effect of varying the material properties of an arbitrary set of materials. Figures 6, 7, 8 and 9 depict the hoop and radial stresses for a flywheel rotating at 10,000 RPM. The flywheel consisted of five layers, each one inch thick, with an inner radius of one-half inch. The curves labeled "1" correspond to the baseline material, which was given the material properties contained in Table 2. For curves "2" and "3" the outer layer consisted of the baseline material, with the density of the material in other layers increasing with decreasing radius. Using the radius at the center of each layer, the densities for each layer were arbitrarily chosen as $\rho=\rho_o(r_o/r)$ for curve "2" and $\rho=\rho_o(r_o/r)^2$ for curve "3". For curves "4" and "5", the inner layer consisted of the baseline material with the hoop and radial moduli increasing with increasing radius in subsequent layers. The moduli are chosen such that $E=E_i(r/r_i)$ for curve "4" and $E=E_i(r/r_i)^2$ for curve "5".

The curves in Figure 6 and 7 illustrate the effects of ballasting a composite flywheel. Radial strength is generally the limiting factor on energy storage in circumferentially wound flywheels. By adding weight to the inner layers, the radial stress becomes more evenly distributed, as shown by curve "2". Too much ballasting can result in excessive stresses at the inner layer, as shown by curve "3".

The curves in Figure 8 and 9 illustrate the effects of changing composite materials. By increasing the moduli with increasing radius, the radial stress decreases. However, this increases the hoop stress, which may eventually become the limiting factor.

The relative stresses and energy storage at 10,000 RPM are presented in Table 3, with a value of 100 given to the baseline curve.

TABLE 2. MATERIAL PROPERTIES OF AN ARBITRARY MATERIAL SYSTEM

E_θ	10.0×10^6	PSI
E_r	1.0×10^6	PSI
$\nu_{\theta r}$	.3	
ρ	.1	LB./CU. IN.

TABLE 3. RELATIVE STRESS AND ENERGY AT 10,000 RPM

	RADIAL STRESS	HOOP STRESS	ENERGY
#1 (BASELINE)	100	100	100
#2	105	116	123
#3	198	206	170
#4	68	122	100
#5	41	146	100

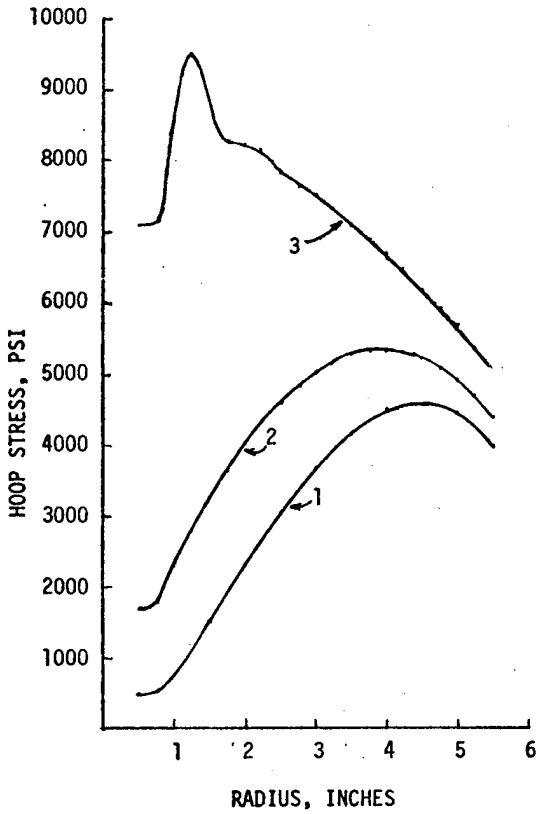


FIGURE 6

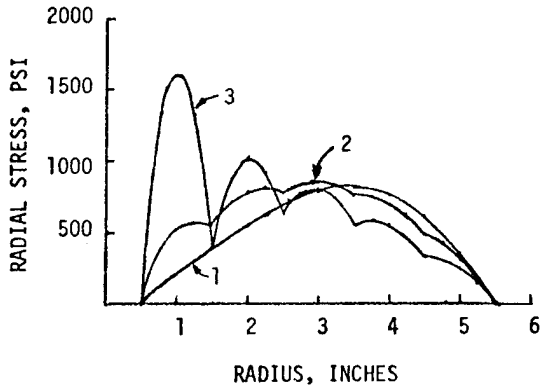


FIGURE 7

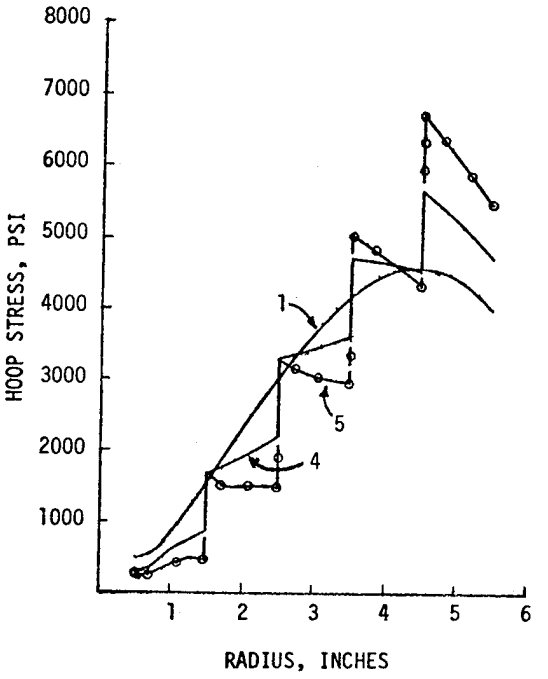


FIGURE 8

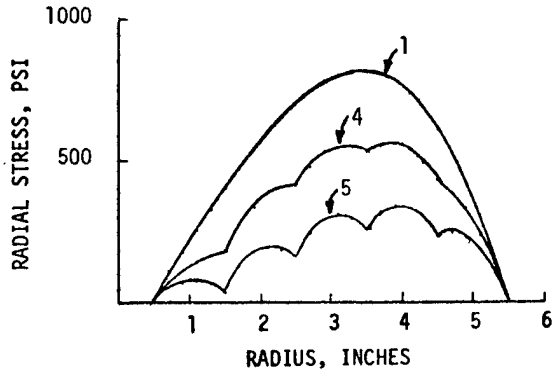


FIGURE 9

CONCLUSION

A precise, versatile, and easy to use computer program has been developed in response to a need for a design and analysis capability for axisymmetric flywheels. The mathematical development for this program has been presented so that others may write their own computer programs. A sample run has been included to aid in verifying such programs. Examples are given which describe several parameters which may be evaluated when designing a flywheel.

DESIGN OF SPOKED-RIM COMPOSITE FLYWHEELS*

E. D. Reedy, Jr. and F. P. Gerstle, Jr.
Sandia Laboratories
Albuquerque, New Mexico 87115

ABSTRACT

This study identifies design and material choices which optimize the energy storage capacity of a free-spinning, circumferentially wound rim. The rim designs considered were (1) a rim fabricated from a single material, (2) a rim with lead ballast uniformly distributed along its interior edge, and (3) a rim composed of two concentrically wound materials. The composite rims examined were reinforced with graphite, Kevlar 49, Kevlar 29, S-glass, and E-glass. The rims were required to satisfy weight, size and angular speed limitations which appear appropriate for a hybrid heat engine/flywheel propulsion system. A graphite/epoxy rim with an inner-to-outer-radius ratio of 0.775 was found to have the largest energy storage capacity.

INTRODUCTION

Based on mechanical properties, structural analysis, and a limited amount of prototype testing, filamentary composite rotors appear as likely candidates for use in hybrid (heat engine plus storage) vehicles. Filamentary composites have the potential of storing energy more efficiently and may fail in a more easily contained manner than metal rotors.[1] A rotor design incorporating a unidirectional composite must accommodate the large difference between longitudinal and transverse strengths, since the allowable transverse tensile stress will be as much as two orders of magnitude less. Most of the circumferentially reinforced rotor designs proposed to date have been limited by low transverse tensile strength in the composite. A complete listing of composite flywheel conceptual designs is given in Ref. 2. Of the circumferentially reinforced designs listed, the two simplest are the disk, either solid or multi-ringed, and the thick rim, attached to the hub with spokes or bands.

Solid, flat circumferentially wound disks have been built from glass-epoxy[3] and Kevlar-epoxy.[4] During spin testing these disks developed circumferential cracks (due to radial stresses) at rather low rotational speeds and circumferential stress levels. Tensile radial stresses are induced by the disks rotation. Furthermore, fabrication and temperature variations can add substantial radial tensile stresses into hoop wound disks.[5,6] Although the peak radial stress in a disk can be reduced by properly tailoring its thickness,[7,8] the low transverse tensile strength of all currently available resin composites appears to preclude the solid disk design. Multi-ring designs built to data have not achieved an adequate method to accommodate displacement incompatibility between rings and are subject to dynamic instability.[9]

A thick-rim design employing Kevlar 49 epoxy rim and bands was described in Ref. 2. This wheel also failed in radial tension (circumferential cracks), but did achieve a higher energy storage to weight ratio than did the solid disks. For a fixed outer radius, the peak radial stress in a rotating rim is reduced as the inner radius is increased. This effect is clearly demonstrated by Tang[10] (see his Figs. 8-10). Therefore, by careful choice of inner-to-outer-radius of a rim, the radial failure mode may be suppressed. Further, the restriction imposed by extremely low transverse tensile strength of Kevlar epoxy may be eased by using a different rim material, or by employing a ballast or second material on the inner radius. In this paper, feasible design and material choices which optimize the energy storage capacity of a rotating rim are identified. These choices can be used as a basis for developing thick rim designs.

* This work supported by the United States Energy Research and Development Administration.

RIM DESIGN APPROACH

Several different designs of circumferentially wound rims with constant axial height were considered. These designs were (1) a rim fabricated from a single material, (2) a rim with lead ballast uniformly distributed along its interior edge, and (3) a rim composed of two concentrically wound materials (Fig. 1). Designs 1 and 2 are special cases of the two-material rim (Design 3). The uniform lead ballast was modeled by requiring that the inner material of a two-material rim had a radial modulus E_r equal to that of lead, a vanishingly small circumferential modulus. E_θ, and a zero in-plane Poisson's ratio $\nu_{\theta r}$. The stress distribution induced in the spinning rim was determined from a plane stress analysis. The Appendix contains the solution of the plane stress field equations for the case of the two-material rim. Since the two-material rim is the most general design, the remaining discussion will be based upon this case.

The rims analyzed were required to satisfy weight, size, and operating speed limitations which appear appropriate for a hybrid heat engine/flywheel propulsion system which requires approximately 0.5 kWh storage capacity. The rim outer radius r_3 was set at 10 inches, with a constant axial height H less than 3 inches, a weight W less than 20 pounds, and an operating speed of less than 40,000 rpm. The inside radius r_1 and the radius at the material interface r_2 were treated as free parameters. They were chosen in a manner which optimizes the rim's energy storage capacity. A plane stress analysis was performed for a specified r_1 and r_2. The angular speed required for the rim to exceed a maximum stress failure criterion in the radial direction and also the speed required to fail the rim circumferentially were determined for each of the two rim materials. This was accomplished by searching the stress distribution for its maximum within each material and noting that the stresses are linear in the angular speed squared. The lowest of the four failure speeds was used as the rim's failure speed ω_f. Rim weight and polar moment of inertia per unit axial height were computed. The rim height necessary for a 20 pound rotor was then determined, subject to the 3 inch maximum. Rim weight and polar moment of inertia I were calculated based upon this height, and kinetic energy E found from

$$E = \frac{I\omega^2 f}{2}$$

A computer code was written to perform these parametric studies automatically. For a given input of geometry and materials, a plot of the energy storage capacity versus r_2 for incremented values of r_1 was obtained. The values of r_1 and r_2 which yield the greatest energy storage capacity can easily be identified from the plot.

RESULTS

In this study circumferentially filament wound rims reinforced with graphite, Kevlar 49, S-glass, and E-glass were examined. The nominal static properties were obtained from several sources[8,11,12]; these are displayed in Table 1. Each possible combination of rim design and material choice was examined with the design approach described above. Plots typical of those generated are shown in Figs. 2-4. Each symbol in these plots connotes a particular prespecified value of r_1/r_3, the inner-to-outer-radius ratio. The cross-plot of energy stored versus r_2/r_3 for fixed values of r_1/r_3 is displayed in Fig. 2 for a graphite/epoxy outer rim with an S-glass/epoxy inner rim. This plot shows that the highest energy occurs for $r_1/r_3 = \beta$, which corresponds to an r_1/r_3 value of 0.78, and r_2/r_3 approaching 0.78. This indicates that the optimum choice for this case contains only graphite/epoxy. For a rim with graphite/epoxy on the inside and Kevlar 49/epoxy on the outside, the optimum choices are $r_1/r_3 = \beta = 0.78$ and r_2/r_3 tending to 1 (Fig. 3). Therefore, the optimized rim contains no Kevlar 49. The optimization of a Kevlar 49/epoxy outer rim with an S-glass/epoxy inner rim retains both materials (Fig. 4). The optimum rim has $r_1/r_3 = \ ) = 0.77$ and $r_2/r_3 = 0.81$.

DISCUSSION OF RESULTS

Rims fabricated from a single composite material were analyzed first. For each composite material, the values of r_1 and H which optimize the rim energy storage capacity are shown in Table 2. This table also records the rim's angular speed, kinetic energy, kinetic energy per pound, and kinetic energy per swept volume at failure. The energy storage capacity of the optimum graphite reinforced rim exceeds that of any rim reinforced with S-glass, Kevlar 49, or E-glass. In turn, the optimum S-glass reinforced rim can store more energy than any filament wound rim containing only Kevlar 49 or E-glass. Finally, the energy storage

capacity of the optimum Kevlar 49 reinforced rim exceeds that of any E-glass reinforced rim. The optimum graphite reinforced rim weighed 20 pounds, has a 2.95 inch axial height and a 0.775 inner-to-outer-radius ratio, and should store 1.13 kilowatt hours at failure.

The effect of adding a uniform lead ballast to the inner edge of a one-material rim was next examined. The energy storage capacity of ballasted graphite, S-glass, or E-glass reinforced rims is always less than that obtainable in their optimal unballasted configurations. A lead ballast did improve the optimal energy storage capacity of a Kevlar 49 reinforced rim by 21% (Table 3). The optimum Kevlar 49 reinforced rim with ballast has an r_1 of 7.8 inches, an H of 2.99 inches, and has 30 mils of lead ballast. The energy storage capacity of such a rim exceeds that of any filament wound S-glass rim, but still is less than that of the optimum unballasted graphite reinforced rim.

Finally, rims fabricated from two concentrically wound composite materials were investigated. The six possible combinations of the composites listed in Table 1 were analyzed. The three combinations with a graphite composite as one of the materials showed no improvement over the optimum rim of graphite epoxy. Similarly, the optimization of a S-glass/E-glass reinforced rim reduced to all S-glass. Only a rim with a Kevlar 49 epoxy on the outside and either S-glass or E-glass composite on the inside proved to be a synergistic combination (Table 3). The energy storage capacity of the optimized E-glass/Kevlar 49 reinforced rim is 22% higher than that of the optimal Kevlar 49 reinforced rim, while the energy storage capacity of the optimum S-glass/Kevlar 49 reinforced rim is 25% higher. These results indicate (1) the inner material must have a hoop modulus lower than that of a Kevlar 49 composite and (2) the energy storage capacity of the rim increases as the density of the inner composite decreases. Therefore, a Kevlar 29 composite appears to be a promising choice for the inner material. Its hoop modulus of 7.25×10^6 psi[13] is significantly lower than Kevlar 49/epoxy and yet has the same density. The other mechanical properties of a circumferentially wound Kevlar 29 composite are not well documented. It was assumed that, except for circumferential modulus, Kevlar 29 and Kevlar 49 composites have the same mechanical properties. The energy storage capacity of the optimal Kevlar 29-Kevlar 49 composite rim is 31% higher than the optimal Kevlar 49 reinforced rim (Table 3). This rim stores 94% of the energy of the optimal graphite reinforced rim.

CONCLUSIONS

Design and material choices which optimize the energy storage capacity of a circumferentially wound rim were identified. The rims were required to satisfy weight, size, and speed limitations which appear appropriate for a hybrid heat engine/flywheel propulsion system. It was found that the optimal graphite reinforced rim has the highest energy storage capacity of all one-material rims. The addition of either a lead ballast or an inner layer of a second composite did not improve the maximum energy storage capacity of rims reinforced with graphite, S-glass, or E-glass, but it did improve the performance of a Kevlar 49 reinforced rim. This synergistic effect is undoubtedly possible because of the low transverse strength of Kevlar 49 composites. The energy storage capacity of the optimum Kevlar 29-Kevlar 49 reinforced rim is 31% higher than the optimal Kevlar 49 reinforced rim, but 6% lower than the optimal graphite composite rim. Therefore, it appears that the optimal graphite reinforced rim is the best choice for incorporation into a thick rim flywheel design.

APPENDIX - SOLUTION OF EQUATIONS

The governing differential equation for a rotating cylindrically orthotropic disk in plane stress is well known and is given by Gerstle[7] in terms of the radial displacement U. For a disk with a constant height the governing equation is

$$r^2 \frac{d^2U}{dr^2} + r \frac{dU}{dr} - \frac{Q_{\theta\theta}}{Q_{rr}} U = - \frac{\rho\omega^2 r^3}{Q_{rr}} \qquad (1)$$

where r = radial distance
ρ = density
ω = angular speed.

Stresses are related to the displacement through the constitutive relations (the strains are expressed in terms of U)

$$\begin{Bmatrix} \sigma_\theta \\ \sigma_r \end{Bmatrix} = \begin{bmatrix} Q_{\theta\theta} & Q_{\theta r} \\ Q_{\theta r} & Q_{rr} \end{bmatrix} \begin{Bmatrix} U/r \\ \frac{dU}{dr} \end{Bmatrix} \qquad (2)$$

where Q_{ij} are the components of the plane stress stiffness matrix. The appropriate boundary conditions for a two matrial rim (Fig. 1) are

$$\text{at} \quad r = r_1 \quad \sigma_r = 0$$

$$r = r_3 \quad \sigma_r = 0$$

and both the radial stress and the radial displacement distributions are continuous.

An equivalent non-dimensional form of Eq. (1) which is convenient for a two-material rim is

$$\bar{r}^2 \frac{d^2\bar{U}}{d\bar{r}^2} + \bar{r} \frac{d\bar{U}}{d\bar{r}} - \frac{Q_{\theta\theta}^{(i)}}{Q_{rr}^{(i)}} = -\bar{r}^3 \qquad (3)$$

with

$$\bar{r} = \frac{r}{r_3}$$

$$\bar{U} = \frac{Q_{rr}^{(i)} U}{\rho^{(i)} \omega^2 r_3^3} \qquad i = \begin{cases} 1 & \bar{r}_1 \le \bar{r} \le \bar{r}_2 \\ 2 & \bar{r}_2 < \bar{r} \le 1 \end{cases}$$

In this and all subsequent references to $Q_{\theta\theta}$, $Q_{\theta r}$, Q_{rr}, and ρ a superscript enclosed in parentheses will indicate if the quantity is defined for material 1 or 2.

The general solution of Eq. (3) for the case of a two-material rim can be written as

$$\bar{U} = \begin{cases} A\bar{r}^{n_1} + B\bar{r}^{-n_1} + \dfrac{\bar{r}^3}{d_1} & \bar{r}_1 \le \bar{r} \le \bar{r}_2 \\ C\bar{r}^{n_2} + D\bar{r}^{-n_2} + \dfrac{\bar{r}^3}{d_2} & \bar{r}_2 < \bar{r} \le 1 \end{cases}$$

where

$$d_i = n_i^2 - 9 \qquad i = 1,2$$

$$n_i^2 = \frac{Q_{\theta\theta}^{(i)}}{Q_{rr}^{(i)}}$$

The constants A, B, C, and D are chosen to satisfy the boundary conditions.

These constants can be expressed as

$$B = \frac{C_{22}X_1 - C_{12}X_2}{C_{22}C_{11} - C_{21}C_{12}}$$

$$D = \frac{C_{11}X_2 - C_{21}X_1}{C_{22}C_{11} - C_{21}C_{12}}$$

$$A = -BK_1\bar{r}_1^{-2n_1} - L_1\bar{r}_1^{(3-n_1)}$$

$$C = -DK_2 - L_2$$

where for i = 1,2

$$\bar{Q}_{\theta r}^{(i)} = \frac{Q_{\theta r}^{(i)}}{Q_{rr}^{(i)}}$$

$$K_i = \frac{\bar{Q}_{\theta r}^{(i)} - n_i}{\bar{Q}_{\theta r}^{(i)} + n_i}$$

$$L_i = \frac{\bar{Q}_{\theta r}^{(i)} + 3}{d_i\left(\bar{Q}_{\theta r}^{(i)} + n_i\right)}$$

$$S_i = \bar{Q}_{\theta r}^{(i)} - n_i$$

$$T_i = \bar{Q}_{\theta r}^{(i)} + n_i$$

and

$$P_1 = \frac{Q_{rr}^{(1)}}{Q_{rr}^{(2)}}$$

$$P_2 = \frac{\rho^{(2)}}{\rho^{(1)}}$$

$$C_{11} = \bar{r}_2^{-n_1} - K_1 \bar{r}_1^{-2n_1} \bar{r}_2^{n_1}$$

$$C_{12} = P_1 P_2 \left[K_2 \bar{r}_2^{n_2} - \bar{r}_2^{-n_2} \right]$$

$$C_{21} = S_1 \bar{r}_2^{-(n_1+1)} - K_1 T_1 \bar{r}_1^{-2n_1} \bar{r}_2^{(n_1-1)}$$

$$C_{22} = P_2 K_2 T_2 \bar{r}_2^{(n_2-1)} - P_2 S_2 \bar{r}_2^{-(n_2+1)}$$

$$X_1 = L_1 \bar{r}_1^{(3-n_1)} \bar{r}_2^{n_1} - L_2 P_1 P_2 \bar{r}_2^{n_2} + \bar{r}_2^3 \left(\frac{P_1 P_2}{d_2} - \frac{1}{d_1} \right)$$

$$X_2 = L_1 T_1 \bar{r}_1^{(3-n_1)} \bar{r}_2^{(n_1-1)} - P_2 L_2 T_2 \bar{r}_2^{(n_2-1)} + \bar{r}_2^2 \left(\frac{P_2 \left(\bar{Q}_{\theta r}^{(2)} + 3 \right)}{d_2} - \frac{\left(\bar{Q}_{\theta r}^{(1)} + 3 \right)}{d_1} \right)$$

Equations (2) can be used to determine the stress distribution in the rim.

REFERENCES

1. J. D. Cyrus, Editor, "Proceedings of the Hybrid Vehicle Interest and Capability Assessment Workshop," Sandia Laboratories, SAND 76-0645, March 1977.

2. R. L. Huddleston, J. J. Kelly and C. E. Knight, "Composite Flywheel Development (May 1-June 30, 1976)," Oak Ridge Y-12 Plant, UC-94b, January 1977.

3. G. F. Morganthaler and S. P. Bonk, "Composite Flywheel Stress Analysis and Materials Study," Advances in Structural Composites, 12th National SAMPE Symposium, Anaheim CA, Oct. 1967, paper D-5.

4. M. Moss and F. P. Gerstle, Jr., "Kevlar/Epoxy Flywheels: An Experimental Study," Proceedings of the 1975 Flywheel Technology Symposium, Lawrence Livermore Laboratory, Livermore CA, Nov. 10-12, 1975.

5. R. C. Reuter, Jr., "Thermal Stresses in Composite Flywheels," Proceedings of the 12th Annual Meeting of the Society of Engineering Science, Inc., Austin, TX, Oct. 1975.

6. F. P. Gerstle, Jr. and R. C. Reuter, Jr., "Thermal Stress Behavior in Cylindrically Orthotropic Structures," Failure Modes in Composites III, 105 AIME Annual Meeting, Las Vegas, NV, Feb. 1976.

7. F. P. Gerstle, Jr. and F. Biggs, "On Optimal Shapes for Anisotropic Rotating Disks," Proceedings of the 12th Annual Meeting of the Society of Engineering Science, Inc., Austin TX, Oct. 1975.

8. P. W. Hill and T. L. Waltz, "Near-Optimum Composite Flywheels," Society of the Plastics Industry, Conference of the Reinforced Plastics/Composite Institute, Washington, DC, Feb. 1977.

9. W. M. Brobeck and Associates, "Investigation of Multi-Ring Fiber-Composite Flywheels for Energy Storage," EPRI EM227, Sept. 1976.

10. S. Tang, "Elastic Stresses in Rotating Anisotropic Disks," Int. J. Mech. Sci., Vol. II, pp. 509-517.

11. R. E. Allred and F. P. Gerstle, Jr., "The Effect of Resin Properties on the Transverse Mechanical Behavior of High-Performance Composites," 30th Anniversary Technical Conference, Reinforced Plastics/Composite Institute, Washington, DC, Feb. 1975.

12. E. I. Dupont DeDemours, Inc., Kevlar 49 DP-01 Data Manual, 1974.

13. P. G. Riewald and C. Zweben, "Kevlar 49 Hybrid Composites for Commercial and Aerospace Applications," 30th Annual Technical Conference, Reinforced Plastics/Composite Institute, Washington, DC, Feb. 1975.

Table 1. Circumferentially wound composite properties

Property	Graphite/ Epoxy	Kevlar 49/ Epoxy	S-Glass/ Epoxy	E-Glass/ Epoxy
Circumferential tensile modulus 10^6 psi ($MPa \times 10^4$)	18. (12.4)	11. (7.6)	7.8 (5.4)	6. (4.1)
Radial tensile modulus 10^6 psi ($MPa \times 10^4$)	1.3 (0.88)	0.7 (0.45)	3. (2.1)	2. (1.4)
Poisson's ratio	.27	.34	.25	.25
Circumferential tensile strength ksi (MPa)	220. (1520.)	200. (1380.)	226. (1560.)	150. (1040.)
Radial tensile strength ksi (MPa)	4.8 (33.1)	2.3 (15.9)	5.8 (40.)	4. (27.6)
Density $lb/in.^3$ ($Kg/m^3 \times 10^3$)	.054 (1.50)	.05 (1.38)	.072 (1.99)	.075 (2.08)

Table 2. Optimal designs for rims made of a single material
$r_3 = 10$ in.

Reinforcement	r_1 in.	H in.	At Failure				
			W lb	ω_f rpm	kWh	$\frac{\text{w-hr}}{\text{lb}}$	$\frac{\text{w-hr}}{\text{in.}^3}$
Graphite	7.75	2.95	20.	39,850	1.13	56.7	1.22
Kevlar 49	8.35	3.00	14.3	38,680	.81	56.6	.86
S-Glass	8.40	3.00	20.	34,230	.90	44.5	.94
E-Glass	8.45	2.97	20.	27,300	.57	28.5	.61

Table 3. Optimal designs for synergistic combinations with Kevlar 49/Epoxy
$r_3 = 10$ in.

Inner Material	r_1 in.	r_2 in.	H in.	W lb	At Failure			
					ω_f rpm	kWh	$\frac{\text{w-hr}}{\text{lb}}$	$\frac{\text{w-hr}}{\text{in.}^3}$
Lead Ballast	7.8	7.83	2.99	20.	37,280	.98	48.9	1.04
S-Glass/Epoxy	7.7	8.1	2.93	20.	37,940	1.01	50.4	1.10
E-Glass/Epoxy	7.7	8.	2.96	20.	37,570	.99	49.5	1.07
Kevlar 29/Epoxy	7.5	8.5	2.91	20.	38,960	1.06	52.9	1.16

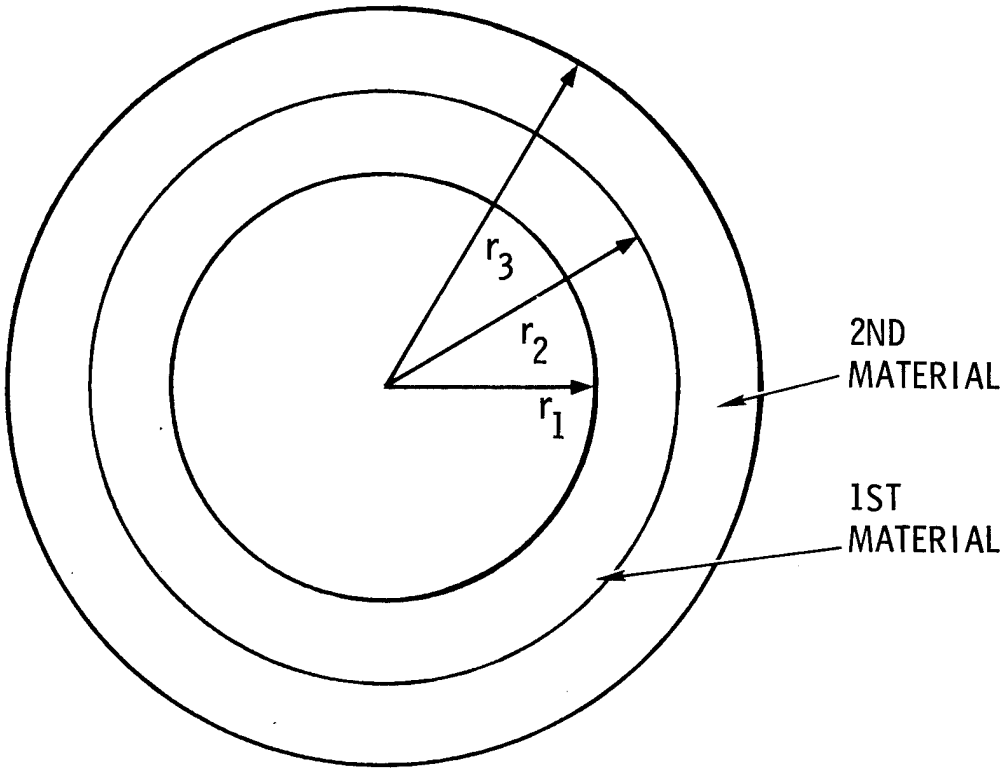


Fig. 1. Rim composed of two concentrically wound materials.

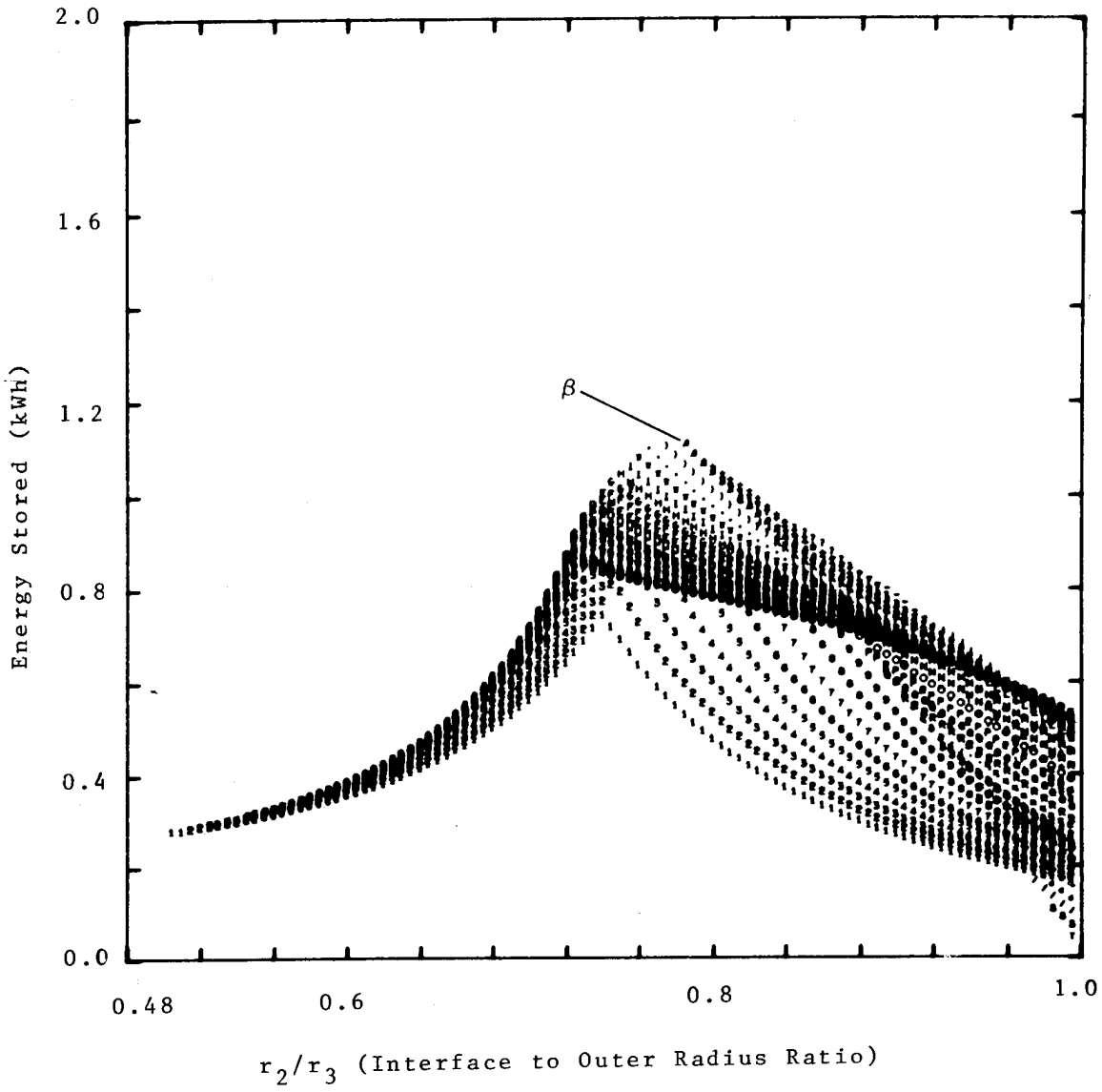


Fig. 2. Graphite/epoxy outer rim with S-glass/epoxy inner rim. Optimum choice of r_1/r_3 is β, which corresponds to 0.78, and r_2/r_3 tends to 0.78.

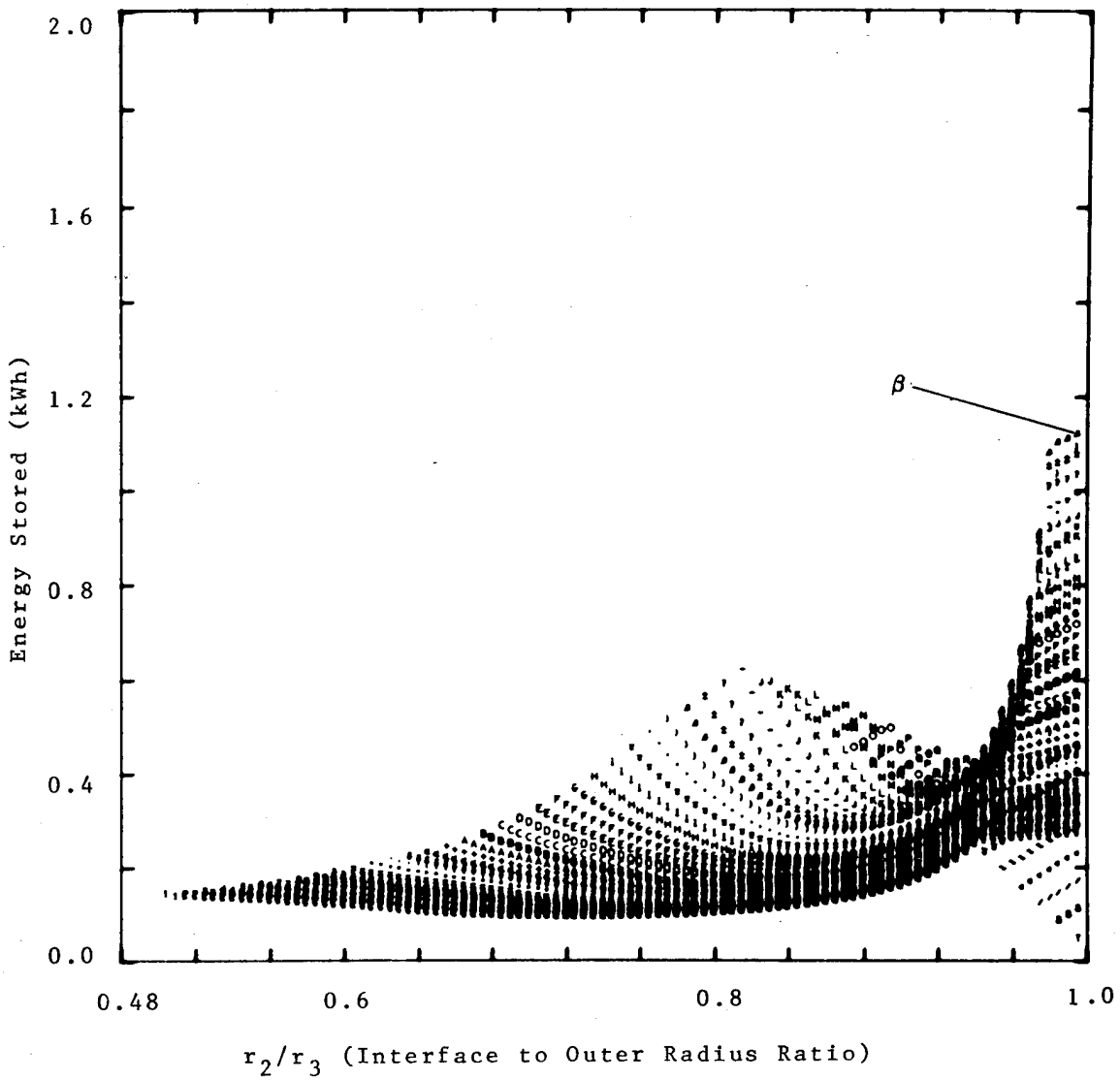


Fig. 3. Kevlar 49/epoxy outer rim with graphite/epoxy inner rim. Optimum choice of r_1/r_3 is β, which corresponds to .78, and r_2/r_3 tends to 1.0.

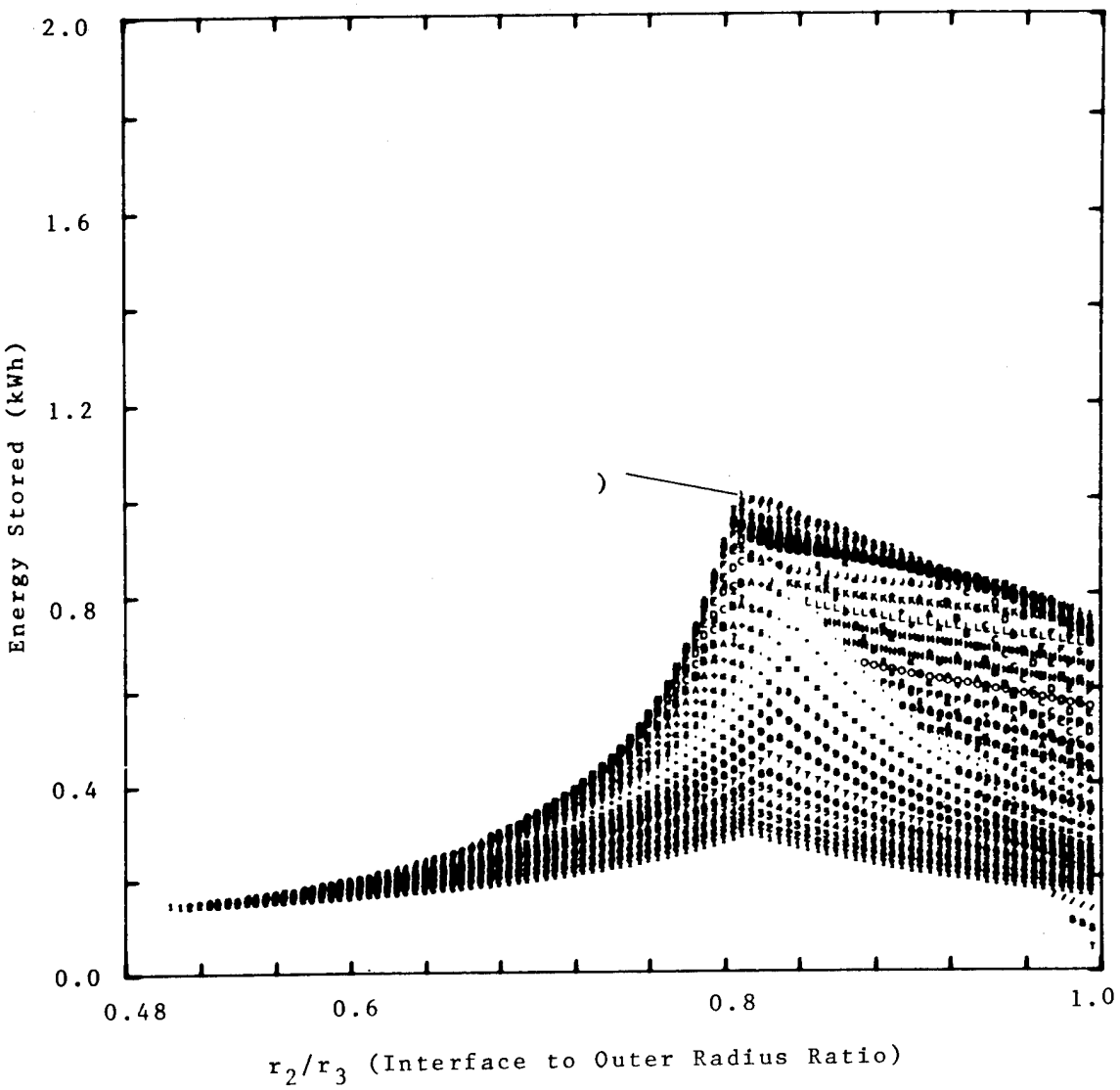


Fig. 4. Kevlar 49/epoxy outer rim with S-glass/epoxy inner rim. Optimum choice of r_1/r_3 is), which corresponds to 0.77, and $r_2/r_3 = 0.81$.

"OPTIMIZATION OF HOOP/DISK COMPOSITE FLYWHEEL ROTOR DESIGNS"

Bhagwati P. Gupta

and

Armand F. Lewis

LORD CORPORATION
ERIE, PA 16512

ABSTRACT

An energy storage flywheel rotor design comprising a disk of isotropic or quasi-isotropic composite material peripherally encapsulated in a hoop of circumferentially wound advanced fiber/resin composite material is proposed. Finite element analysis results on the effect of the modulus ratio and other materials parameters of the hoop and disk (fiber reinforced resin) materials on the maximum stresses in these components have been obtained. The closed form solutions for the stresses and displacements related to this functional composite rotor design have been established. Parametric studies were carried-out resulting in a series of nomographs leading to a method of optimizing this flywheel rotor configuration.

INTRODUCTION

During the past several years a variety of fiberous composite material based energy storage flywheel rotor configurations have been conceived, designed and to an extent been developed.[1,2] Each case or study has represented an attempt by the design engineer to optimize the structure in terms of efficient and effective materials utilization. Designing with regard to optimizing the energy storage capacity of the flywheel rotor per weight or volume have been some of the considerations.[3,4] More recently, the designs of energy storage flywheel rotors and rotor systems for optimized energy storage capacity per unit cost has become an important consideration.[5] It is evident that the design and development of energy storage flywheel systems of high energy storage capacity, low cost and occupy a small functional volume are needed if the wide spread commercial use of energy storage flywheels is to be realized; this is especially true in transportation and certain consumer product applications. Toward this end, therefore, the design and study of filamentary composite/resin based flywheel rotors is the active pursuit of a number of engineering researchers in the field of flywheel technology.

In this paper, a flywheel design is presented and mathematically analyzed with regard to optimzing its energy storage capacity per weight, volume and cost. This design can be referred to as a hoop-disk configuration (see Figure 1). It is composed of a central disk of low cost isotropic or quasi-isotropic material of low to moderate strength (and modulus) encircled by a peripheral hoop winding of high strength (and modulus) advanced fiber composite material.

One can demonstrate the principle of this hoop-disk flywheel rotor design by a specific example; if a disk of chopped glass fiber reinforced epoxy resin (10" radius, 1" thick) is spun to destruction, according to the equations for rotational dynamics of spinning disks of isotropic materials[6,7], the disk will fail at about 16,000 rpm (6 watt-hrs/lb) assuming the materials properties as tensile strength - 20,000 psi, poisson's ratio of 0.4 and a

density of 0.059 lbs/in^3. Now, if loop or hoop of higher modulus higher strength unidirectional composite, e.g. carbon fiber reinforced epoxy (unidirectional) hoop winding (modulus equal to 21 x 10^6 psi and a tensile strength of 180,000 psi) is wrapped around the outer edge of this disk, a compressive stress will be produced in the disk. This will reduce the tensile stress in the disk thus making the hoop-disk rotor system capable of higher rotational speeds before failure of the disk occurs. However, the strength of the hoop, through thickness optimization and/or materials property modification (selection of the proper composite hoop material) must be capable of sustaining the tension stresses produced by the centrifugally expanding disk as well as the tension stresses in the hoop itself. The rotationally induced stresses in the complete hoop-disk system must be considered.

In light of this argument, we have proceeded in this paper to:

1. Develop the closed form solution for stresses in a hoop-disk rotor configuration where the disk is considered an isotropic material and the hoop an orthotropic material.

2. Perform some mathematical parametric studies to optimize this design.

3. Establish some design parameters and nomographs for the convenient selection of the geometry of the hoop-disk rotor configuration that would be optimum for a given combination of disk and hoop materials.

DEVELOPMENT OF STRESS EQUATIONS

(See Appendix I)

OPTIMIZATION AND NOMOGRAPHS

Equations (8), (9), (10), and (11) give stress factors. Parameters on which these factors depend are the non-dimensional ratios, $M = (E\theta/Ed)$, $C = (a/b)$, $D = (\rho_d/\rho_h)$ and $R = (r/b)$.

For the determination of design stresses, the expressions for these stress factors are maximized with respect to r. Maximum stresses in the disk occur at its center and are given by:

$$\text{Max.}S_r^d = \text{Max.}S_\theta^d = -P + \frac{(3+\nu_d)}{8} DC^2 \qquad (12)$$

Maximization of stresses in the hoop, however, is somewhat complicated. An appropriate way to achieve this is by using Newton's method to find R for the maximum values of S_r^h and S_θ^h and then determine these values at the R so found. Maximum S_θ^d and max.S_θ^h are plotted in Figure 2, against C for different values of M (21, 30, 42, 50 and 60). Comparable values of max. S_r^h are plotted in the Figure 3.

Maximum tangential stress in the thick hoops ($a/b < 0.4$) occurs near the outer surface, at $R \simeq 0.84$; while for the thinner hoops ($a/b > 0.4$), it occurs at the inside surface. This is the reason why a discontinuity in the slope of these curves occurs at about $C = 0.4$. On the other hand, maximum radial tensile stress factor occurs always away from the inner surface, from $R \simeq 0.65$ for $C \simeq 0.0001$ to $R \simeq 1$ for $C \geq 0.8$.

We have found that the effect of $E\theta/ER$ and Poisson's ratios on these stresses is not very significant. But, the values of S_θ^h increase linearly with the density-ratio while those of S_r^h decrease. So a correction factor can easily be employed to account for this effect. Hence, the nomographs of major design utility are as given in Figures 2 and 3.

The use of the information presented in Figures 2 and 3 can best be demonstrated by describing a specific example:

Disk: material is 30% chopped glass fiber filled polycarbonate, for which the properties are:

E_d = 0.95 x 10^6 psi
σ_u = ultimate strength = 20,000 psi
γ_d = 0.0686 lb/in^3
νd = 0.4

Let us assume radius of the disk = 11 in., and run it at 25,000 rpm to develop 17 WH/lb (440 WH). But at this speed the disk will fail because it is developing a maximum stress of about 63,000 psi which is higher than the strength of its material. The safe speed it can take is about 14,000 rpm to yield about 5 WH/lb (138 WH). Now let us wind a hoop of an orthotropic material whose density is 0.055 lb/in^3 around the outer edge of this disk. The value of the quantity $\rho_h w^2 b^2$ = 120,000. For a stress of 20,000 psi in the disk S_θ^d = 0.1667. This will give, for D = 1.3722, a range of a/b from 0 to about 0.68, (from Figure 2), and a range of Eθ/Ed from 21 to 50. Consider, for example, the graphite epoxy composite, E_θ= 21 x 10^6 psi, γ_d = 0.055 lb/in^3, tensile strength = 180,000 psi and transverse strength = 6000 psi. We see from Figure 3 that for E_θ/E_d = 22, the maximum radial (transverse) stress does not exceed 2400 psi which is less than its transverse strength. So, the hoop is safe. This flywheel is then a combination of an isotropic disc of radius about 7.5 in.; and orthotropic hoop of outer radius equal to 11 in. It develops about 17 WH/lb. at 25,000 rpm; the disk hoop materials property combination and geometric considerations have therefore been optimized. By these nomographs we can now proceed to design other combinations such that both the disk and the hoop fail approximately at the same time. The above example comes quite close to this design aspect.

REFERENCES

[1] R. L. Huddleston, J. J. Kelly and C. E. Knight, "Composite Flywheel Development" - Union Carbide, Oak Ridge Y-12 Plant, Oak Ridge, TN, NTIS Report Y-2072, January 1977.

[2] G. E. Habercom, Jr., "Design and Application of Flywheels", Citations from NTIS Data Base. See NTIS/PS-76/0767 and PS 75/743, October 1976 and October 1975.

[3] G. C. Chang and R. G. Stone, "Proceedings 1975 Flywheel Technology Symposium" - Nov. 10-12, 1975. ERDA #76-85, released for publication July 1976.

[4] D. L. Hagan and A. G. Erdman, "Flywheels for Energy Storage: A Review with Bibliography", ASME Publication #76-DET-96, presentation at Design Engrg. Tech. Conference, Montreal, Quebec, Canada, September 26-29, 1976.

[5] D. W. Rabenhorst and T. R. Small, "Composite Flywheel Development: Final Report", Johns Hopkins University, Applied Physics Laboratory, Report # SDO-4616A, April 1977.

[6] F. Biggs, Sandia Laboratories Report (NTIS) SAND74-0113, November 1974.

[7] J. P. Den Hartog, "Advanced Strength of Materials", McGraw-Hill Book Co., New York, 1952, page 52.

[8] S. G. Lekhnitskii, "Anisotropic Plates" Gordon and Beach Science Publishers, New York, 1968; pp. 152-153.

ACKNOWLEDGEMENTS

Authors wish to express their gratitude to Mr. C. H. Parr for his continuous guidance and helpful contributions to the mathematical analysis. They would also like to thank Mr. Peter Barnhart for writing the computer program used in this work.

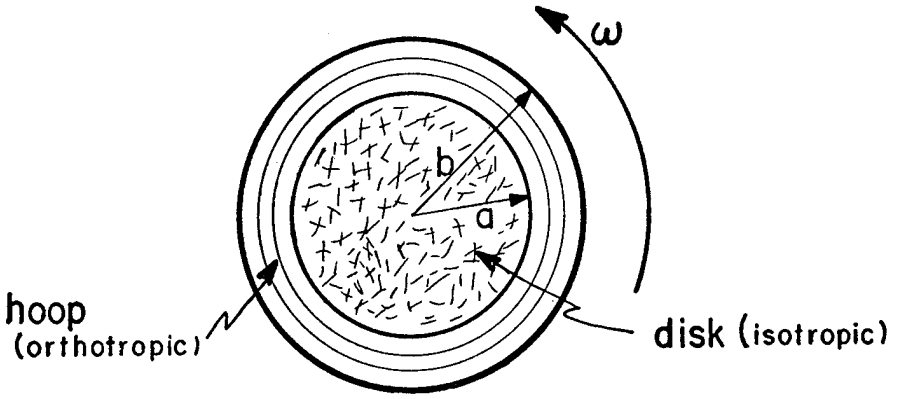


Figure I (a) Flywheel Configuration

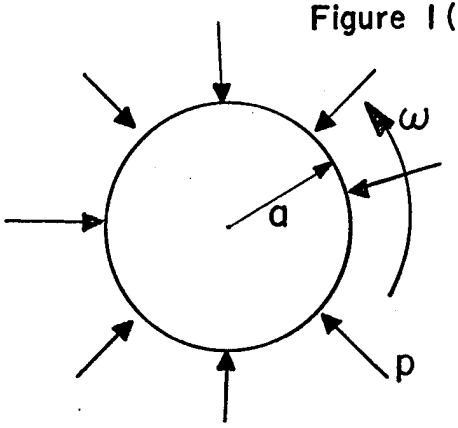


Figure I (b) Disk F. B.D.

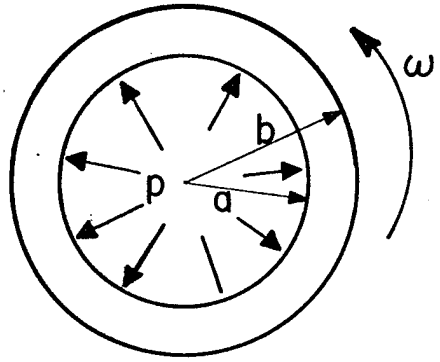


Figure I (c) Hoop F. B.D.

E_d = Modulus of Elasticity of disk Material

E_θ, E_R = Tangential and Radial Moduli of the hoop materials

ν_d, ν_θ = Poisson's ratios of the disk and hoop materials

γ_d, γ_h = Weight densities of the disk and hoop materials

ρ_d, ρ_h = Mass densities of the disk and hoop materials

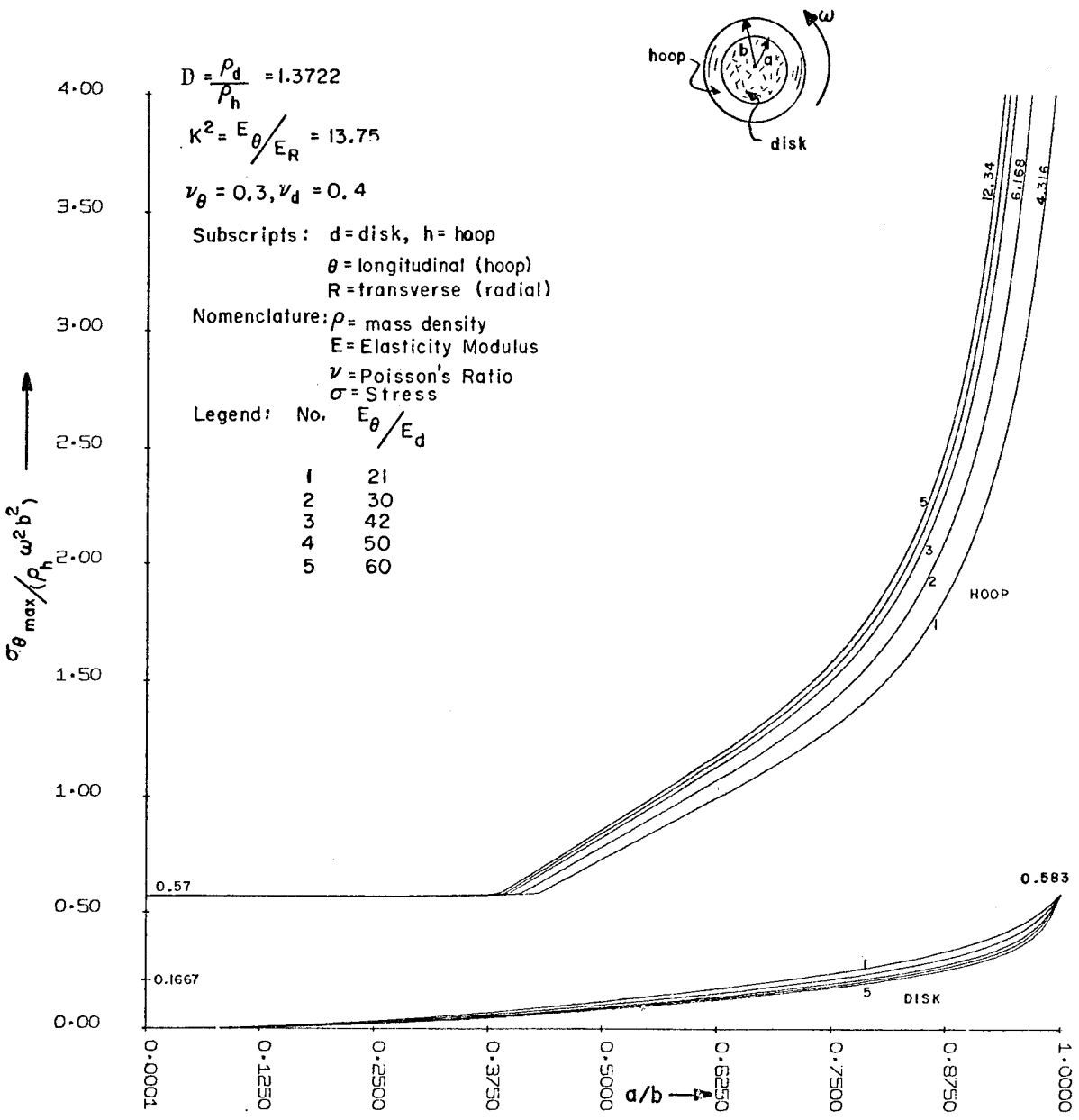


Figure 2 Tangential Tension Factor vs. Diameter - Ratio

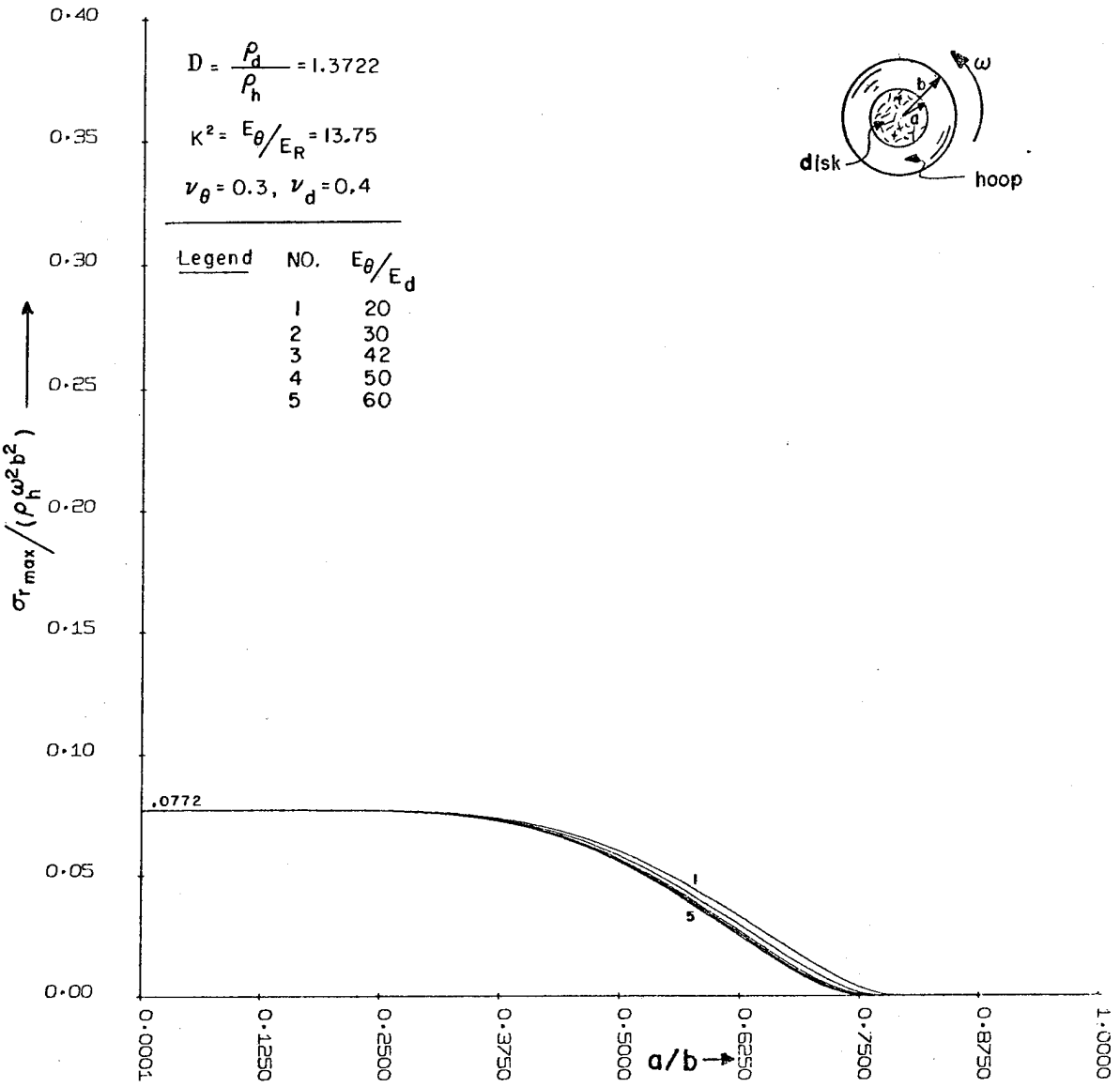


Figure 3 Radial Tension Factor in the Hoop vs. Diameter-Ratio

APPENDIX I - DEVELOPMENT OF STRESS EQUATIONS

According to mechanics theory[7], stresses and displacements in a disk at any radius r and angular velocity ω are given by:

$$\sigma_r = -p + \frac{(3 + \nu_d)}{8} \rho_d \omega^2 (a^2 - r^2) \tag{1}$$

$$\sigma_\theta = -p + \frac{(3 + \nu_d)}{8} \rho_d \omega^2 \left[a^2 - \frac{(1 + 3\nu_d)}{(3 + \nu_d)} r^2\right] \tag{2}$$

$$u = \frac{-p\,(1-\nu_d) r}{E_d} + \frac{(1 - \nu_d)}{8E_d} \rho_d \omega^2 r \left[(3 + \nu_d)a^2 - (1 + \nu_d) r^2\right] \tag{3}$$

where the symbols and terms are defined in Figure 1.

Furthermore, stresses and displacements in a hoop at any radius r and angular velocity ω are given by[8]:

$$\sigma_r = \rho_h \omega^2 b^2 \frac{(3 + \nu_\theta)}{(9 - K^2)} \left[\frac{1 - C^{2K+3}}{1 - C^{2K}} \left(\frac{r}{b}\right)^{K-1} + \frac{1 - C^{2K-3}}{1 - C^{2K}} C^{K+3} \left(\frac{b}{r}\right)^{K+1} - \left(\frac{r}{b}\right)^2\right] + \frac{pC^{K+1}}{1 - C^{2K}} \left[\left(\frac{r}{b}\right)^{K-1} - \left(\frac{b}{r}\right)^{K+1}\right] \tag{4}$$

$$\sigma_\theta = \frac{\rho_h \omega^2 b^2}{(9-K^2)} \left\{(3 + \nu_\theta) K \left[\frac{1-C^{2K+3}}{1-C^{2K}} \left(\frac{r}{b}\right)^{K-1} - \frac{1-C^{2K-3}}{1-C^{2K}} C^{K+3} \left(\frac{b}{r}\right)^{K+1}\right] - (K^2 + 3\nu_\theta) \left(\frac{r}{b}\right)^2\right\} + \frac{pC^{K+1}}{1-C^{2K}} K \left[\left(\frac{r}{b}\right)^{K-1} + \left(\frac{b}{r}\right)^{K+1}\right] \tag{5}$$

$$u = \frac{\rho_h \omega^2 b^3}{E_\theta (9-K^2)} \left\{(3 + \nu_\theta)\left[(K - \nu_\theta) \frac{1-C^{2K+3}}{1-C^{2K}} \left(\frac{r}{b}\right)^K - (K + \nu_\theta) \left(\frac{1-C^{2K-3}}{1-C^{2K}}\right) C^{K+3} \cdot \left(\frac{b}{r}\right)^K\right] - (K^2 - \nu_\theta^2) \left(\frac{r}{b}\right)^3\right\} + \frac{pbC^{K+1}}{E_\theta (1-C^{2K})} \left[(K - \nu_\theta) \left(\frac{r}{b}\right)^K + (K + \nu_\theta) \left(\frac{b}{r}\right)^K\right] \tag{6}$$

where $K = \sqrt{\frac{E_\theta}{E_R}}$, $C = \frac{a}{b}$ and $\nu_\theta = -\frac{\varepsilon_r}{\varepsilon_\theta}$

Imposing the boundary conditions $(u)_{r=a}$ in disk $= (u)_{r=a}$ in hoop, and employing equations (3) and (6) we can get the pressure, p, at the contact surface between the disk and hoop, into an equation of non-dimensional form given by:

$$P = \frac{p}{\rho_h \omega^2 b^2} = \left[\frac{(1-\nu_d)}{4} DC^3 - \frac{1}{M(9-K^2)} \left\{(3 + \nu_\theta)\left[(K-\nu_\theta)\left(\frac{1-C^{K+3}}{1-C^{2K}}\right)C^K - (K+\nu_\theta) \cdot \left(\frac{1-C^{K-3}}{1-C^{2K}}\right)C^3\right] - (K^2-\nu_\theta^2) C^3\right\}\right] \Big/ \left[(1-\nu_d)C + \frac{C^{K+1}}{M(1-C^{2K})} \left[(K-\nu_\theta)C^K + (K + \nu_\theta)C^{-K}\right]\right] \tag{7}$$

where $M = E_\theta/E_d$, and

$D = \rho_d/\rho_h$

Non-dimensional factors of σ_r and σ_θ are thus given by:

Disk

$$S_r^d = \frac{\sigma_r}{\rho_h \omega^2 b^2} = -P + \frac{(3+\nu_d)}{8} D \left(C^2 - \left(\frac{r}{b}\right)^2\right) \tag{8}$$

$$S_\theta^d = \frac{\sigma_\theta}{\rho_h \omega^2 b^2} = -P + \frac{(3+\nu_d)}{8} D \left(C^2 - \frac{(1+3\nu_d)}{(3+\nu_d)} \left(\frac{r}{b}\right)^2\right) \tag{9}$$

Hoop

$$S_r^h = \frac{(3+\nu_\theta)}{(9-K^2)} \left[\frac{1-C^{K+3}}{1-C^{2K}} R^{K-1} + \frac{1-C^{K-3}}{1-C^{2K}} C^{K+3} R^{-K-1} - R^2\right] +$$

$$+ \frac{P C^{K+1}}{(1-C^{2K})} \left[R^{K-1} - R^{-K-1}\right] \tag{10}$$

$$S_\theta^h = \frac{1}{(9-K^2)} \left\{(3 + \nu_\theta) K \left[\frac{1-C^{K+3}}{1-C^{2K}} R^{K-1} - \frac{1-C^{K-3}}{1-C^{2K}} C^{K+3} R^{-K-1}\right] -\right.$$

$$\left. - (K^2 + 3\nu_\theta) R^2\right\} + \frac{P C^{K+1} K}{(1-C)^{2K}} \left[R^{K-1} + R^{-K-1}\right] \tag{11}$$

where $R = r/b$

ON THE STRESS STATE IN QUASI-CIRCULAR BARE FILAMENT FLYWHEELS

Giovanni Belingardi - Giancarlo Genta
Istituto della Motorizzazione - Politecnico di Torino
Corso Duca degli Abruzzi 24 - Torino (Italy)

The present work was sponsored by C.N.R. (Italian Research National Council)

ABSTRACT

The problem of finding the stress state in quasi-circular (both sub- and supercircular) flywheels is here studied and solved with the following assumptions: both the hub and the wire show an elastic behaviour; the bending stiffness of the wire is negligible; the ratio between the cross sectional area of the winding and the one of the wires does not change with the speed (except for the effect of Poisson's ratio), the radial displacement of the hub is small enough to be neglected in the calculation of the centrifugal force.

Some spin tests already run gave results which are in good agreement with the calculations.

INTRODUCTION

Quasi-circular bare filaments flywheels consist of a hub, which is spoked or has a multilobe shape, and of a certain length of wire, or filaments, wound around it in such a way that each filament is laid, at rest, on a line lying between the circumference and the chord passing on the points on which it is supported. In this way the wire exerts a compression force on the hub when the disk in rotation (fig. 1)[1,2]

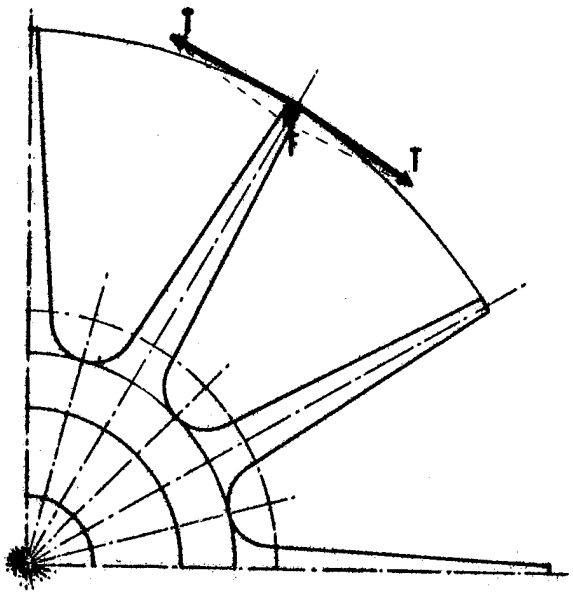


Fig. 1 - Basic principle of subcircular winding
T: stress in the wire
F: compressive force on the hub

Flywheels of this type can be regarded as a kind of the conventional rim - with - spokes flywheel; with the following advantages:

a) The rim is made of wires; the very high specific strength of wires and fibers can be fully used
b) The rim is not subject to bending loads
c) The spokes can be built using a material whose specific strength is lower than the one of the rim.

The advantages over composite material filament wound rotors are the following.

d) There is no matrix and no delamination problems.
e) It is possible to use low-cost well-known materials as steel wire.
f) If steel wire is used, very high energy/volume ratios can be reached at low speed. This can be useful for vehicular applications.
g) They are easy to build and, likely, they cost less than flywheels of other types, with similar performances.

ANALYSIS

SHAPE OF THE WIRE

The equilibrium equations for a wire of constant cross section A and of negligible bending stiffness in a centrifugal field (fig. 2) are:

$$TA \sin d\alpha + (T+dT)A \sin d\alpha = dF_c \sin \psi \quad (1)$$

$$TA \cos d\alpha - (T + dT)A \cos d\alpha = dF_c \cos \psi \quad (2)$$

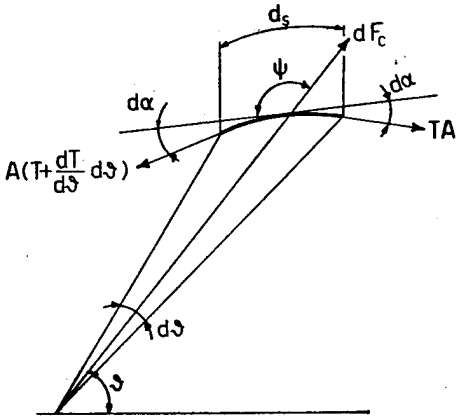


Fig. 2 - Forces on a wire in a centrifugal field

The length ds and the centrifugal force dF_c can be expressed as:

$$ds = d\theta \sqrt{r^2 + (dr/d\theta)^2} \qquad (3)$$

$$dF_c = \rho A \omega^2 r \, d\theta \sqrt{r^2 + (dr/d\theta)^2} \qquad (4)$$

Angles $d\alpha$, θ and ψ are linked by the relationship:

$$d\alpha = \frac{1}{2}(d\theta + d\psi) \qquad (5)$$

As:

$$\sin\psi = r \,/\sqrt{r^2 + (dr/d\theta)^2} \qquad (6)$$

$$\cos\psi = (dr/d\theta)\,/\sqrt{r^2 + (dr/d\theta)^2} \qquad (7)$$

eq. (1), (2), (3) and (4) yeld:

$$T\left(1 + \frac{d\psi}{d\theta}\right) = \rho\omega^2 r \qquad (8)$$

$$dT = -\rho\omega^2 r \, dr \qquad (9)$$

In eq. (8) and (9) all terms except the first in the Taylor series of sin $d\alpha$ and cos $d\alpha$ have been neglected.

Equation (9) can be integrated as:

$$T = \rho\omega^2 (K - r^2)/2 \qquad (10)$$

K is a constant to be calculated from the boundary conditions.

Equation (10) and (18) yield:

$$(K - r^2)\left(1 + \frac{d\psi}{d\theta}\right) = 2r^2 \qquad (11)$$

The derivative $d\psi/d\theta$ can be calculated from eq. (6) and (7):

$$\frac{d\psi}{d\theta} = -\left[r\left(\frac{d^2r}{d\theta^2}\right) - \left(\frac{dr}{d\theta}\right)^2\right] / \left[r^2 + \left(\frac{dr}{d\theta}\right)^2\right] \qquad (12)$$

Equations (12) and (11) give the equation which solves the problem:

$$r\frac{d^2r}{d\theta^2} = \left(\frac{dr}{d\theta}\right)^2 + \left[r^2 + \left(\frac{dr}{d\theta}\right)^2\right]\frac{3r^2 - K}{r^2 - K} \qquad (13)$$

As far as the A.A. know, eq. (13) cannot be integrated analitically (°). It can be adimensionalized, in such a way that a set of solutions (each one characterized by a value of K) can describe all possible filament configurations.

Putting:

$$\begin{cases} r = Rx \\ \frac{dr}{d\theta} = Ry \,, \end{cases} \qquad (14)$$

where R is defined in fig. 3, eq. (13) yield:

$$\begin{cases} \frac{dy}{d\theta} = \frac{x\,(3x^2 + K_1 + 4y^2)}{x^2 - K_1} \\ \frac{dx}{d\theta} = y \end{cases} \qquad (15)$$

(°) Only after having written this work the A.A. knew that eq. (13) can be transformed into the equation:[3]

$$\frac{dr}{d\theta} = \pm r\sqrt{\frac{r^2}{A}(r^2 - K)^2 - 1} \qquad (13a)$$

As $dr/d\theta = 0$ and $r = R$ for $\theta = 0$ (fig. 3), it is possible to evaluate A:

$$A = R^2 (R^2 - K)^2$$

Eq. (13a) can be adimensionalized as. eq. (13), yielding:

$$r = Rx \qquad (14a)$$

$$\frac{dx}{d\theta} = \pm \frac{x}{1 - K_1}\sqrt{x^2 (x^2 - K_1)^2 - (1 - K_1)^2} \qquad (15a)$$

As eq. (13a) leads to an elliptic integral, and must be integrated in a numerical way, the use of eq. (13) is equivalent to the use of eq. (13a).

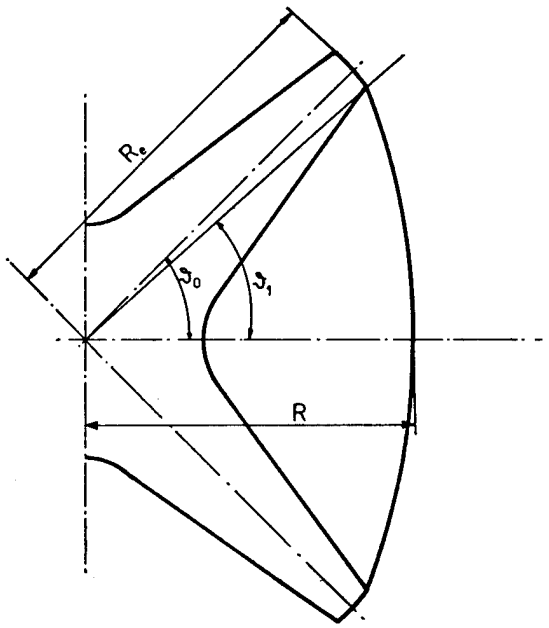


Fig. 3 - Definition of the angles θ_o and θ_1 and of R and R_e.

where $K_1 = K/R^2$.

For $\theta = 0$, the boundary conditions are:

$$\begin{cases} y = 0 \text{ (for simmetry)} \\ x = 1 \quad \text{(fig. 3)} \end{cases} \tag{16}$$

Angle θ_1 is given when the shape of the hub is known. Equation (15) can therefore be integrated for θ increasing from 0 to θ_1.

If $1 < K_1 < 3$ the line lies outside the circumference whose radius is R_e (supercircular shapes). If $K_1 = 3$ the circumference is obtained. For $3 < K_1 < \infty$ the solution lies between the arc and the chord (subcircular shapes). If $K_1 \to \infty$ it is possible to obtain the analytical solution $x = 1/\cos\theta$, i.e. the chord connecting the two spokes.

Once performed the integration $x_1 = x(\theta_1)$ and $y_1 = y(\theta_1)$ are known and it is possible to relate all parameters to R_e, which is one of the design parameters, instead of relating them to R, which is one of the unknowns.

The stress T and the radial force f on each spoke, and the stress T for $\theta = 0$ can be calculated as:

$$f = A \cos(\theta_o - \theta_1)\, \rho\, \omega^2\, R_e^2\, Q \tag{17}$$

$$(T)_{\theta=\theta_1} = \rho\omega^2 R_e^2\, P \tag{18}$$

$$(T)_{\theta=o} = \rho\omega^2 R_e^2 S, \tag{19}$$

where Q, P, and S are the following functions of K_1, x_1 and y_1:

$$P = (K_1 - x_1^2) / (2x_1^2) \tag{20}$$

$$S = (K_1 - 1) / (2x_1^2) \tag{21}$$

$$Q = -2P \cos\psi = y_1 (K_1 - x_1)^2 / (x_1^2 \sqrt{x_1^2 + y_1^2}). \tag{22}$$

The length L of the wire between two spokes and its stretching ΔL under the effect of T are:

$$L = R_e N \tag{23}$$

$$\Delta L = \rho\omega^2 R_e^3\, M/E, \tag{24}$$

where:

$$N = \frac{2}{x_1} \int_o^{\theta_1} \sqrt{x^2 + y^2}\, d\theta \tag{25}$$

$$M = \frac{1}{x_1^3} \int_o^{\theta_1} (K_1 - x) \sqrt{x^2 + y^2}\, d\theta \tag{26}$$

The five functions $M(K_1)$, $N(K_1)$, $P(K_1)$, $Q(K_1)$ and $S(K_1)$ allow to calculate all the possible configurations and stress states of a wire, wound around a given hub, or, better, all the hubs characterized by the angle θ_1.

Some of the possible configurations for a filament wound around a 12-spokes hub are shown in fig. 4.

It is possible to regard Q as the independent variable, and to express the remaining four functions M, N, P and S as functions of Q.

Those functions are plotted in fig. 5 for $\theta_1 = 15°$, $18°$ and $22{,}5°$.

As far as approximated calculations are concerned, the following simple expression can be used:

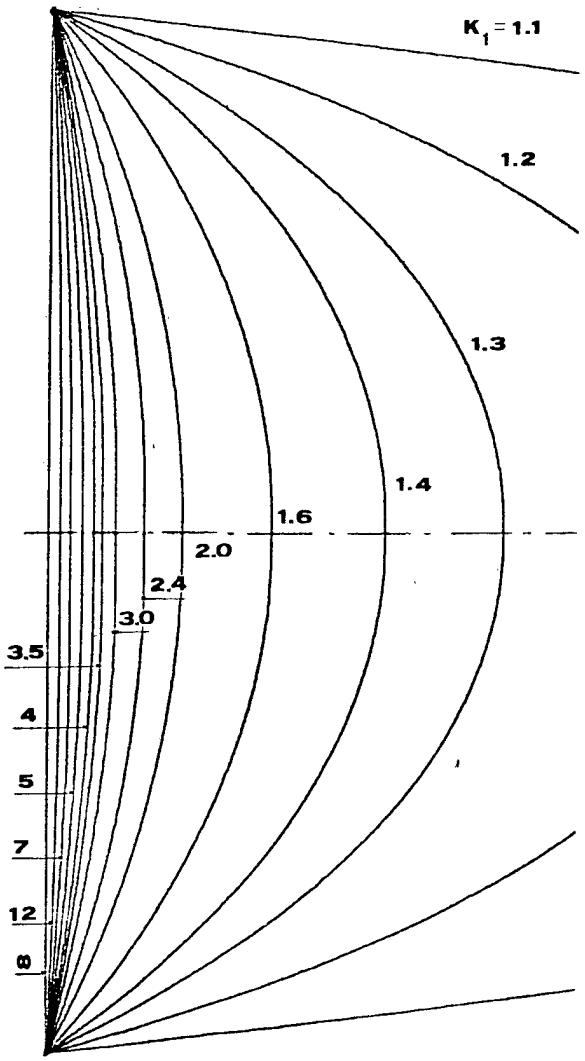


Fig. 4. Configurations of a wire wound around a 12 spokes hub (θ_1=15°).

$$\begin{Bmatrix} M \\ N \\ P \\ S \end{Bmatrix} = [a] \begin{Bmatrix} 1 \\ Q \\ Q^2 \\ Q^3 \end{Bmatrix} \qquad (27)$$

where $a_{11} = a_{21} = 2\theta_1$ and $a_{31} = a_{41} = 1$.

The remaining a_{ij} can be calculated from the numerical integration of eq.(15). If two different values of [a] are taken, according on the sign of Q, an approxima - tion better than .001% can be obtained on M, N, P and S for $-0{,}15 \leqslant Q \leqslant 0{,}15$.

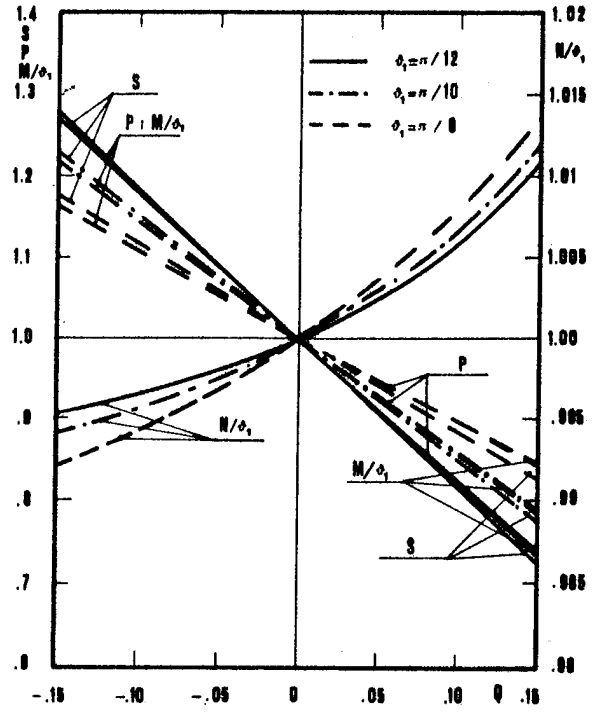


Fig. 5. Functions M(Q), N(Q), P(Q) and S(Q) for θ_1 = 15°, 18° and 22,5°.

INTERACTION BETWEEN THE HUB AND THE WIRE

The displacement u of the tip of the spokes can be written as:

$$u = B_1\omega^2 + B_2F \ , \qquad (28)$$

where B_1 and B_2 are constants (if the hub material has an elastic behaviour), which can be calculated from the hub geometry using any stress-analysis method (e.g. pla- ne stress disk theory and beam theory for simple cases, finite element method for the more complex ones).

If all wires in each layer behave in the same way, the force F due to n_1 layers of n_2 wires is:

$$F = \sum_{i=1}^{n_1} n_2 f_i \qquad (29)$$

If the displacement u is small enough that the variations of centrifugal force due to it can be neglected, assuming that no compenetration between layers is possi-

ble (°) (the ratio between the cross section of the winding and the one occupied by the wire $\xi = 4/\pi$), eq. (29) can be written as:

$$F = \pi\rho n_2 r_f^2\omega^2 \cos(\theta_o-\theta_1) \sum_{i=1}^{n_1} Q_i \cdot \cdot [R_e + (2i-1)r_f]^2 \quad (30)$$

Equation (28) together with eq. (30) gives the displacement of the tip of the spokes. The radius of the point in which the i^{th} layer of wire is supported is given by:

$$R_i = R_e+u+r_f(2i-1) - \frac{r_f\nu\rho\omega^2}{E} \cdot \left\{ 2 \sum_{j=1}^{i-1} P_j \cdot [R_e+(2j-1)r_f]^2 + P_i \cdot [R_e+(2i-1)r_f]^2 \right\} - \frac{2\rho\omega^2 r_f^2 \cos(\theta_o-\theta_1)}{\xi R_e(\theta_o-\theta_1)} \sum_{j=1}^{i-1} \frac{1}{E_j} \sum_{k=J}^{n_1} Q_k [R_e+(2k-1)r_f]^2, \quad (31)$$

where E_j is the elastic modulus in radial direction of the j^{th} layer, calculated taking into account all the possible stiffening effects of the matrix and ties which can be present over the spokes.

If spacers are put into the winding, the thickness of all spacers which are under the i^{th} layer must be added to R_e. If the wires are not isotropic, the ratio ν/E in eq. (31) is ν_{LT}/E_L, and E in eq. (35) is E_L.

If the filaments are wound around a circular mold, whose radius is R' (fig.6) with negligible stress; the length of each wire is, at rest:

$$L_{oi} = 2R' \operatorname{arsin}\left(\frac{R_e}{R'} \sin\theta_1\right) + 2r_f(2i-1)\theta_1 \quad (32)$$

(°) If there is compenetration, but the ratio ξ does not change with the speed, it is still possible to perform the calculation changing accordingly the value of n_1 in such a way that the expression $2 r_f n_1$ gives the total radial thickness of the winding.

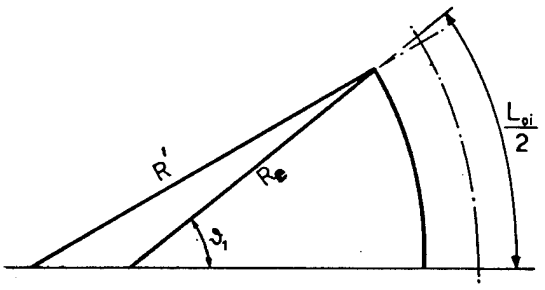


Fig. 6 - Geometry of the wires at rest.

When spacers are present within the winding, the length of the i^{th} layers which is over a spacer of thickness h put over n layers, is:

$$L_{oi} = 2\sqrt{(x_o-x_1)^2 + (y_o + mx_1)^2} + 2R \operatorname{atan} m + 2r_f\left[2(i-n) - 1\right]\theta_1 \quad (33)$$

where:

$$x_o = (2nr_f + h)\cos\theta + R'\cos\left[\operatorname{arsin}\left(\frac{R_e}{R'}\sin\theta\right)\right] \quad (34)$$

$$y_o = (R_e + 2nr_f + h)\sin\theta_1$$

$$m = \left[x_o y_o - (R'+2nr_f)\sqrt{x_o^2+y_o^2-(R'+2nr_f)^2}\right] / \left[(R' + 2nr_f)^2 - y_o^2\right]$$

if $x_o < R' + 2nr_f$ and

$m = o$ if $x_o \geq R' + 2nr_f$

$$x_1 = (x_o + my_o)/(1 + m^2)$$

If the expression under the square root in m is negative, the thickness of the spacer is too small. The length L_{oi} can also be calculated, taking into account the stretching of the wire over the spokes, as

$$L_{oi} = N_i R_i - \rho\omega^2 R_i^3 M_i/E + 2(\theta_o - \theta_1)\left[R_i(1 - \rho\omega^2 R_i^2 P_i/E) - R_e - r_f(2i-1)\right] \quad (35)$$

If there are spacers under the i^{th} layer,

their thickness must be added to R_e.

The calculation of the stress state starts taking a set of n_1 values of Q_i

Once the Q_i are known, the M_i, N_i and P_i can be easily calculated, and a set of n_1 L_{oi} can be obtained from eq. (30), (31) and (35). The values of L_{o_i} so obtained are compared with the ones calculated from eq. (32). If they are equal, the values of Q_i assumed are the correct ones, and the stress state in the wires and in the hub can be computed. If $Q_i < 0$ (subcircular, shape), the maximum stress in the wire is at $\theta = 0$, and S_i must be used. If $Q_i > 0$ (supercircular shape) the maximum stress occurs on the spoke, and P_i is used. If the two sets L_{oi} are not equal, new values of Q_i are taken, and the calculation is repeated.

RESULTS

The stress state in the hub and in the filaments of the flywheel sketched in fig. 7 is shown, in the same figure, as an example.

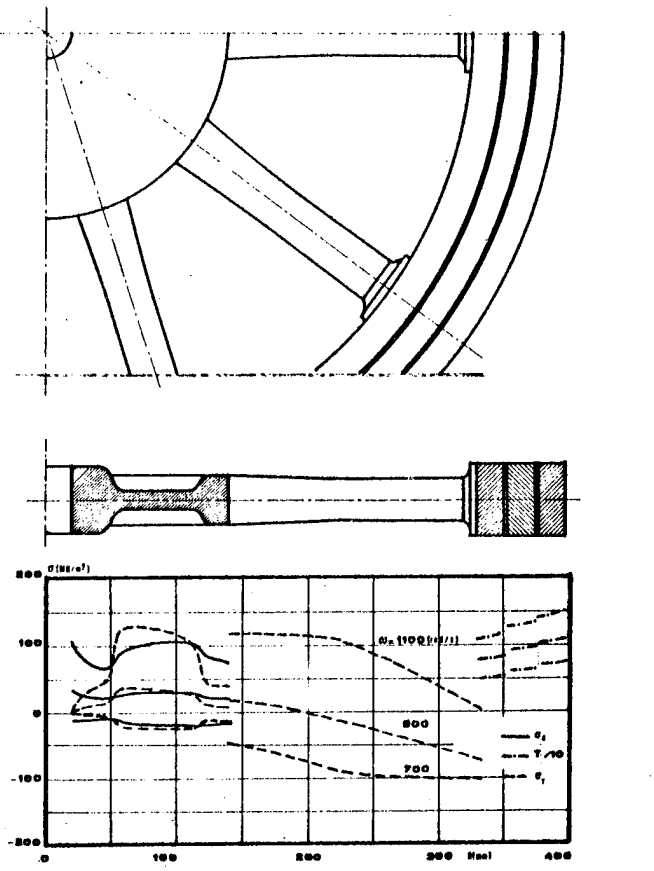


Fig. 7 - Geometrical parameters and stress state is a steel wire flywheel with aluminium alloy hub.

The stresses in some points of the same flywheel are shown as a function of the speed in fig. 8. The stresses are not proportional to the square of the speed; the hub is subject to compressive forces which are increasing with the speed; reach a maximum value, and then decrease, becoming eventually tensile.

Lines are dotted at low speed, where Q lies outside the values for which eq. (27) gives a very good approximation.

When the pressure P becomes positive the winding detaches from the hub. The speed at which this happens can be raised using an higher value of the radius R' but this raises also the maximum compressive stresses in the hub. The use of spacers in the winding can help to keep low the compressive stresses and to raise the maximum allowable speed.

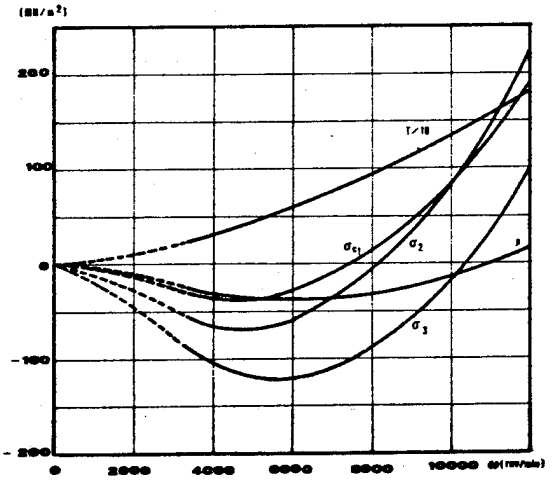


Fig. 8. Stresses in the hub and in the wires (σ_3 and σ_2 radial stresses at the outside and the inside of the spokes; σ_{c1} circumferential stress at the central hole; T maximum stress in the wire; P pressure between wires and hub) as a function of the speed.

CONCLUSIONS

The method here developed allows to perform the calculation of the stress state in quasi-circular bare filaments flywheels.

The only assumptions are that the behaviour of the materials is elastic, the displacements are small enough to be neglected in the calculation of the centrifugal loads; the bending stiffness of the wire is negligible, and that the ratio between the cross sectional area of the winding and the one of the wires doesn't change with the speed (except for the effect of Poisson's ratio).

It is possible to keep into account the effect of spacers put into the winding and of stiffeners which can be present over the spokes.

The results show that the stress state is not proportional to the square of the speed, and that the compression in the hub at low speed can be more dangerous than the stresses in the hub and in the wires at higher speeds.

Some early spin tests have shown results which are in good agreement with the theoretical ones.

SYMBOLS

- f radial force on the spoke exerted by one wire
- n_1 number of layers of wire
- n_2 number of wires in one layer.
- r radius.
- r_f radius of the wire or filament
- u radial displacement of the outside of the hub
- A area of the cross section of the wire
- E Young's modulus of the wires
- F radial force exerted on the spoke by the winding
- F_c centrifugal force
- L length of wire between two spokes
- R' radius of the mold used for the winding
- R_e outside radius of the hub.
- T stress in the wire
- θ polar coordinate
- ν Poisson's ratio of the wires
- ξ ratio between the area of the cross section of the winding and the one of the wires
- ρ wire density
- ψ angle between the radius and the wire
- ω angular velocity
- ΔL stretching of the wire.

REFERENCES

1 D.W. RABENHORST, Communication at the Ist European Flywheel Energy Storage Symposium, Thielle, Switzerland, September 14-15, 1976. Proceedings (to be published).

2 P. POUBEAU, Communication at the Ist European Flywheel Energy Storage Symposium. Thielle, Switzerland, September 14-15, 1976. Proceedings (to be published).

3 D.W. RABENHORST, T.R. SMALL, Composite Flywheel Development Program, Final Report. SDO-4616A APL/JHU, april 1977, appendix III, p. 21

OPTIMAL DESIGN OF ANISOTROPIC (FIBER-REINFORCED) FLYWHEELS*

R. M. Christensen and E. M. Wu

Lawrence Livermore Laboratory, University of California
Livermore, California 94550

EXTENDED ABSTRACT

In the case of isotropic material flywheel design, the optimal configuration is well known. The optimal shape is that of a radially tapered section, the thickness of which is governed by the exponential function. The criterion for optimazation is, relative to a prescribed weight or volume, that the flywheels should store the maximum amount of kinetic energy. Of necessity, the failure criterion for the material enters into the consideration because maximum energy could be stored only at the threshold of material failure. Furthermore, the maximum energy storage would occur only when all points of the medium are at the same stage of incipient failure, not just one point or a set of points. Thus the design criterion for isotropic materials is taken to be the maintenance of a uniform state of stress throughout the entire disk. The closed-form analyses are restricted to states of plane stress. In this context, the two principal stresses are required to be equal and constant throughout the disk; therefore the design often is referred to as the constant-stress flywheel. On the other hand, the corresponding problem of the optimal design of anisotropic flywheels has not been successfully treated. The objective here is to provide an optimal design strategy for the flywheel. The quantity to be optimized is the kinetic energy stored per unit mass. The variables to be adjusted to achieve the optimal configuration are the thickness of the disk as a function of radius and the degree and type of anisotropy. The analysis will be restricted to plane stress conditions. After having obtained exact, closed-form solutions for this problem, the practical questions of designing the wheel will be considered.

The material is taken to be cylindrically orthotropic and in a state of plane stress. The appropriate linear elasticity form of the stress/strain (σ/ε) relations is given by

$$\sigma_{rr} = Q_r \varepsilon_{rr} + Q_{r\theta} \varepsilon_{\theta\theta}, \tag{1a}$$

$$\sigma_{\theta\theta} = Q_{\theta r} \varepsilon_{rr} + Q_{\theta} \varepsilon_{\theta\theta}, \tag{1b}$$

where

$$Q_{r\theta} = Q_{\theta r}, \tag{2}$$

r and θ are the polar coordinates, and the constitutive coefficients are taken to be independent of position. The moduli Q_r, Q_θ, $Q_{r\theta}$, and $Q_{\theta r}$ will be related to the common engineering moduli measures later.

The appropriate Poisson ratios are given by

$$\nu_{r\theta} = \frac{Q_{r\theta}}{Q_r}, \tag{3a}$$

$$\nu_{\theta r} = \frac{Q_{\theta r}}{Q_\theta}, \tag{3b}$$

where $\nu_{r\theta}$ is the measure of contraction in the θ direction resulting from an applied load in the r direction.

There arises the necessity of specifying the failure criterion. There are many different criteria used for the development of fiber-reinforced composites. Many of them are quite complicated and preclude the type of analytical treatment sought here. A reasonably simple criterion is needed, and yet it is even more important that it be a realistic specification. To this end, we use the constant strain criterion. At this point, it is observed that the strain at failure may be taken to be that of the fiber phase at failure, if the matrix phase is sufficiently compliant. Thus the fiber phase characteristics become the governing factor for the composite.

*This report was abstracted from work of the same title to be published in the Journal of Composite Materials (Vol 11, 1977).

Maximum energy storage will be achieved when the material is used in the most efficient manner. Clearly, this corresponds to the condition of simultaneous material failure at all points of the medium (at the critical speed). A condition consistent with the use of the strain failure criterion is given such that the strain state is independent of radius r:

$$\varepsilon_{rr}(r) = \varepsilon_{\theta\theta}(r) = \varepsilon(\text{constant}). \quad (4)$$

Note that Eq. (4) requires more than the usual statement of a maximum strain criterion because both components of strain are specified to have the failure value.

Under plane stress conditions, the compatibility equation has the form

$$r\frac{d\varepsilon_{\theta\theta}}{dr} + \varepsilon_{\theta\theta} - \varepsilon_{rr} = 0. \quad (5)$$

Obviously, this governing condition is satisfied by Eq. (4). It remains to satisfy the equilibrium equation under steady-state conditions;

$$\frac{d}{dr}(hr\sigma_{rr}) - h\sigma_{\theta\theta} + \rho\omega^2 hr^2 = 0 , \quad (6)$$

where the thickness of the disk is an unknown function of radius,

$$h = h(r) ,$$

ρ is the density, and ω is the angular speed.

The preceding equations may be integrated to obtain the thickness function as

$$h = kr^{-(1-\alpha)} e^{-\lambda r^2} , \quad (7)$$

where

$$\lambda = \frac{\rho\omega^2}{2Q_r(1 + \nu_{r\theta})\varepsilon} , \quad (8)$$

$$\alpha = \frac{(1 + \nu_{\theta r})Q_\theta}{(1 + \nu_{r\theta})Q_r} , \quad (9)$$

and k is the constant of integration.

The objective is to maximize the kinetic energy stored per unit mass of the flywheel. The kinetic energy is given by

$$T = \frac{1}{2}\rho\omega^2 \iint h(r)r^2(r\, d\theta\, dr), \quad (10)$$

where the integral is over the plane of the disk. Similarly, the total mass is given by

$$M = \rho \iint h(r)(r\, d\theta\, dr). \quad (11)$$

Substituting Eq. (7) into Eqs. (10) and (11) gives

$$\frac{2\rho}{\varepsilon}\frac{T}{M} = Q_r + Q_\theta + 2Q_{r\theta} . \quad (12)$$

It is the right-hand side of Eq. (12) that is to be maximized by varying the degree of the anisotropy. The thickness variation already has been obtained through the restriction that the material must fail simultaneously throughout the entire disk. An examination of the terms in Eq. (12) reveals that there is, in fact, no further optimization to be performed. The combination of terms $Q_r + Q_\theta + 2Q_{r\theta}$ is an invariant with respect to coordinate rotation, even though the individual terms vary depending upon the orientation of an individual lamina relative to the given coordinate system.

This property of invariance has been derived by Tsai and Pagano* using the tensor transformation laws for anisotropic media properties. Thus, whether the entire reinforcement is radial, circumferential, or any combination, it is still the same maximum energy density that is attainable. Of course, to achieve this maximum energy density, the disk must have the thickness variation dictated by Eq. (7), and very different shapes are involved depending upon the type of anisotropy involved. The corresponding isotropic material results can be extracted from Eq. (12) by letting

$$\nu_{r\theta} = \nu_{\theta r} = \nu ,$$

$$E_r = E ,$$

*S. W. Tsai and N. J. Pagano, "Invariant Properties of Composite Materials," in Composite Materials Workshop, S. W. Tsai, J. C. Halpin, and N. J. Pagano, Eds. (Technomic Publication Company, Stamford, Connecticut, 1968).

with E and ν being the corresponding isotropic properties. Thus, for the isotropic (I) case, the result can be shown to be

$$\frac{T}{M_I} = \frac{E\varepsilon}{(1 - \nu)\rho} \quad . \tag{13}$$

The final results of the optimization analysis are both Eq. (12), which gives the kinetic energy stored per unit mass as a function of the material properties, and the corresponding shape solution, Eq. (7), which also depends upon the material properties. A remarkable result emerges in the derivation. As long as the appropriate optimum shape is used for a given ratio of radial to circumferential reinforcement, the corresponding energy storage capacity is the same for the entire spectrum of optimum shapes.

The next problem, then, is how to select the "best" shape with the corresponding type of anisotropy. The answer to this problem lies in the realm of practical design. Consider the shape solution of Eq. (7). For $\alpha < 1$, radial reinforcement dominates, and it is seen that the thickness solution is singular at $r = 0$. On the other hand, for $\alpha > 1$, circumferential reinforcement dominates and from (Eq. 7) it is seen that at $r = 0$, $h = 0$. It is only in the case of $\alpha = 1$, which corresponds to equal radial and circumferential stiffness, that there is not an unappealing and, in fact, an impossible design condition at $r = 0$. In the case of predominant circumferential reinforcement, it is interesting to note from Eq. (7) that the optimal shape involves a section that thickens with increasing radius near the origin, has a maximum thickness at some determinable radius, and thereafter tapers to vanishing thickness. Obviously the case of equal radial and circumferential reinforcement is the most practical configuration.

A flywheel could be constructed with equal radial and circumferential reinforcement. This certainly is more general than the isotropic case. However, it can be shown that identical results emerge for the energy storage, whether the system is isotropic or just of equal stiffness in the radial and circumferential directions. (The latter case is orthotropic but not, in general, isotropic.)

One question to be raised at this point is whether the fiber-reinforced flywheel, with fibers arranged to give an effectively isotropic property characterization, has any advantage over a ring-type fiber-reinforced flywheel. The limiting case of fiber effects only shows that these two configurations give the same energy storage. However, the solid wheel has a design advantage over the ring: it is more efficient in space use, having less swept volume. Second, it is likely to be more efficient and stable under conditions of acceleration and deceleration (the attachment of the ring-type wheel to spokes and hubs may cause problems).

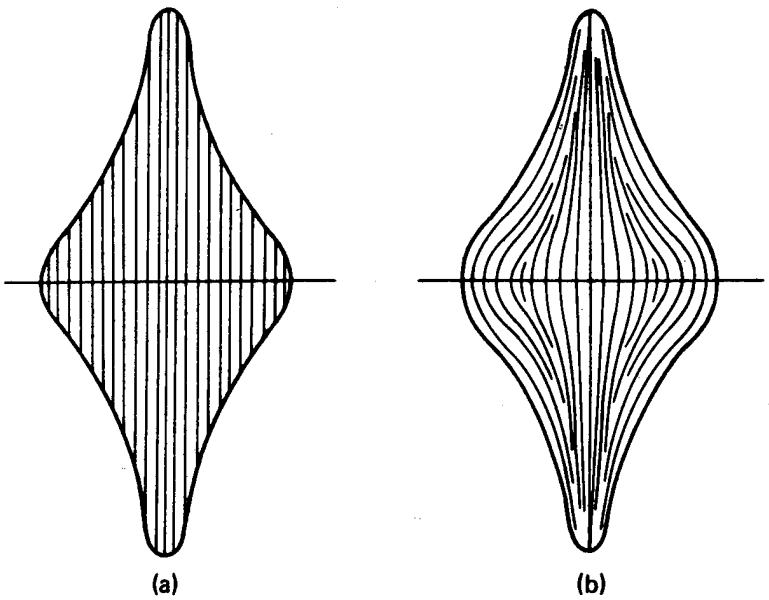


Fig. 1. Schematic diagram of isotropic flywheels: (a) parallel laminas where the prescribed flywheel shape is obtained by varying the planar size of the succession of laminas, and (b) laminas arranged at equal angles, possibly providing more effective stress transfer than the (a) design.

Finally, with regard to the question of the actual design layout of an isotropic fiber-reinforced flywheel, consider the schematic diagrams shown in Fig. 1. A flywheel can be constructed by laying up laminas at various angles to obtain the isotropic property distribution. In the example of Fig. 1a, all laminas are parallel; the prescribed flywheel shape is obtained by varying the planar size of the succession of laminas. This configuration has an appealingly simple means of fabrication. However, an alternative scheme also must be considered. An isotropic laminate composed of several laminas arranged at equal angles could be constructed; these laminates then could be placed in the configuration shown in Fig. 1b, possibly providing a more effective stress transfer system than that in the Fig. 1a design. Considerations such as these alternative schemes are best pursued through numerical studies using three-dimensional elasticity models.

Acknowledgements - This work was performed under the auspices of the U.S. Department of Energy under contract No. W-7405-Eng-48.

ANALYSIS OF THE DELTAWRAP FLYWHEEL DESIGN

C. E. Knight, Jr.
Union Carbide Corporation-Nuclear Division
P. O. Box Y
Bldg. 9998, MS-1
Oak Ridge, TN 37830

ABSTRACT

The higher shape efficiency of the isotropic constant stress disc profile is brought about by the transfer of body force loading in the outermost portions of the disc back to the disc hub region. This is difficult to accomplish with a fiber composite disc because of its low transverse strength. However, the same end might be accomplished in a rim type flywheel design through use of a full overwrap around the rim, tying back to the hub. This is an extension of the "Bandwrap" design but involves considerably more analysis complexities. A model and computer program developed at the Oak Ridge Y-12 Plant* calculates the thickness and elastic properties versus position on the overwrap. The thickness is calculated based on coverage per band, number of bands, and band thickness at a given radial coordinate. The elastic properties are derived assuming the overwrap material to be modeled by the properties of an angle ply laminate. The thickness and properties provide input to a finite element model. A linear, elastic finite element analysis provides an estimate of the energy storage potential for this design. The model was two-dimensionally axisymmetric and was analyzed using the ADINA finite element program.

CONCEPTUAL DESIGN

The "Deltawrap" flywheel design incorporates a rim, hub, and overwrap connecting the two. The elements of the design are illustrated in Figure 1. The rim is similar to rims used in other flywheel designs[1], and many of the rim considerations are independent of this design. The hub simply provides a connection between the overwrap and driving shaft. The hub must be designed in close relationship with the overwrap design.

The key element in the Deltawrap design is the overwrap. The overwrap performs several functions. The primary function is to connect the rim and hub and, thereby, the shaft. It also provides torque load capability, rigidity in the rim-hub coupling to reduce dynamic problems, and external pressure on the rim to lower the rim hoop stresses.

If sufficient advantage can be taken of the external pressure applied to the rim by the overwrap, then the energy storage capacity may be increased. The isotropic material flywheel may be fabricated in a shape derived to maintain a constant stress throughout. It is a more efficient energy storage flywheel because

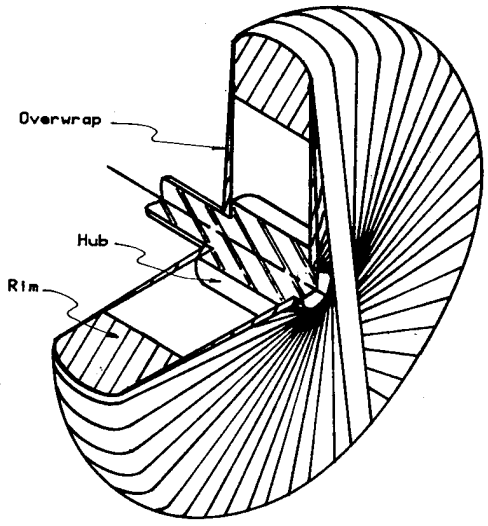


Fig. 1. DELTAWRAP FLYWHEEL CONCEPTUAL DESIGN.

*Operated by the Union Carbide Corporation's Nuclear Division for the US Department of Energy

the higher body-force loadings in the elements near the outside are carried by transfer back to elements near the hub. If the composite flywheel is fabricated by circ winding, most composites are too weak in transverse loading to carry the body forces back to inner elements. The fibers in the overwrap are near radial. It is easily shown that the radial rod has its highest stress at the center of rotation and, that for the same speed, has a lower maximum stress than the rotating rim. Therefore, the radial rod can carry some additional load before failure.

From a simplistic view, the rod has the same radial displacement capability as the thin rim since it is the same strain level; but it will not displace the same in the rotational gravity field because the radial rod is not uniformly stressed. Thus, there is automatically an interference condition when the radial fibers are wrapped around the rim and the assembly is spun. This applies additional tensile stress in the radial fibers and external loading to the rim. If the overwrap thickness is designed properly, the additional tensile stress in the radial fibers will not exceed failure levels. Furthermore, the external pressure on the rim will reduce its hoop stresses and allow the whole assembly to spin faster before it reaches the failure speed.

The rim element should have a radius ratio low enough to store the necessary amount of energy. If the radial strength is exceeded, then some design alternative such as those presented in a companion paper[2] must be selected. Of course, the rim design used must be analyzed in conjunction with the overwrap and hub to properly evaluate any proposed engineering design.

The hub simply connects the overwrap with the driving shaft. The design needs to be such that the hub is self-locking to both the shaft and overwrap during spin-up of the flywheel.

MODELING THE OVERWRAP

The overwrap is a variable-thickness, variable-fiber-orientation, structural component. This combination complicates the analysis and requires preparation of a computer program to calculate the thickness profile and fiber-orientation angle as a function of the radial position. The thickness profile is then modeled by the finite-element mesh for analysis. The varying fiber orientation causes the material properties to vary and must be accounted for in the model.

Calculation of thickness and fiber angle is based on the geometrical considerations illustrated in Fig. 2. At any given radial coordinate, r, the thickness calculation is based on the arc coverage of a band on the circle of radius, r, the number of bands, and the band thickness. The thickness is calculated by the equation:

$$t = r(\phi_2-\phi_1)\frac{2N}{\pi r}t_b \qquad (1)$$

where:

- t represents the thickness buildup
- ϕ_2 and ϕ_1 the angles shown (Fig. 2)
- N the number of bands in the set, and
- t_b the band thickness.

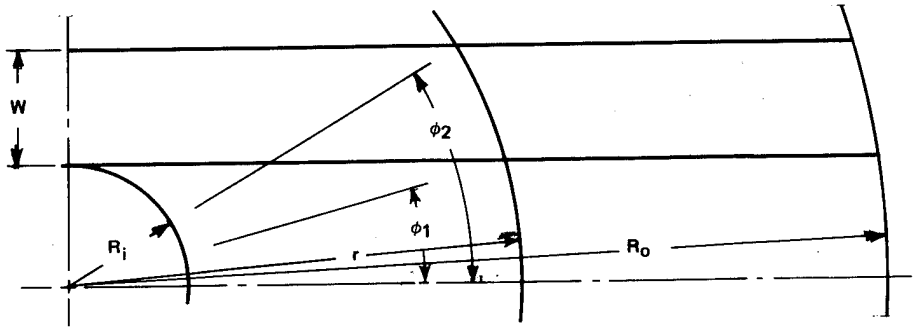


Fig. 2. GEOMETRICAL RELATIONSHIP FOR CALCULATING THE OVERWRAP-THICKNESS PROFILE AND FIBER ANGLE.

Along the inner band edge, the angle is:

$$\phi_1 = \sin^{-1} \frac{R_i}{r} \quad ; \qquad (2)$$

along the outer edge, the angle is:

$$\phi_2 = \frac{\pi}{2}, \text{ for } R_i \leq r \leq R_i + W, \text{ and} \qquad (3)$$

$$\phi_2 = \sin^{-1} \frac{R_i + W}{r}, \text{ for } R_i + W \leq r \leq R_o. \qquad (4)$$

where:

R_i represents the inner radius of the band set,

W the band width, and

R_o the outer radius of the band set.

The fiber orientation angle with respect to the radial direction varies between ϕ_1 and ϕ_2 at the radial position, r. The average of ϕ_1 and ϕ_2 is specified as the fiber angle at radius r. The thickness profile and fiber angle are plotted in Fig. 3 for the case of R_i = 0.750 inch, R_o = 10.0 inches, W = 0.750 inch, t_b = 0.003 inch, and N = 40 bands. The fiber-angle variation with the radial coordinate, of course, causes the material properties, with respect to the radial-hoop coordinates, to vary. The fiber-angle variation between ϕ_1 and ϕ_2 at a given radial coordinate also causes the properties to vary. There are

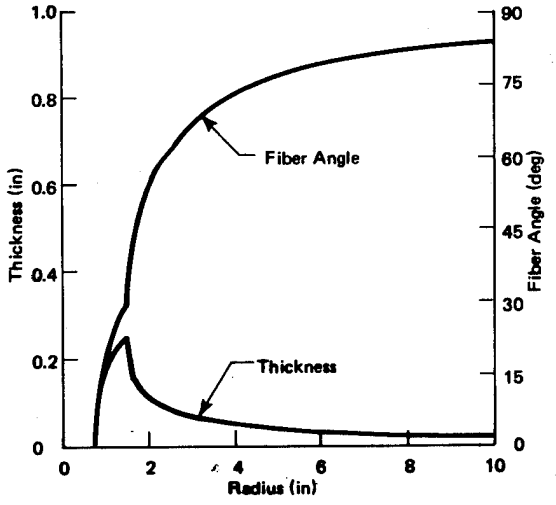


Fig. 3. THICKNESS AND FIBER-ANGLE PROFILE OF THE OVERWRAP ON THE DELTAWRAP FLYWHEEL.

a number of approaches to find the material-stiffness matrix which will represent the oriented material at the given radial position. The composite is modeled as a symmetric angle-ply laminate. The first option is between bonded plies and unbonded (shear-failure) plies. On initial loading, the plies are bonded; and prior experience with angle-ply wound structures indicates that they remain bonded up to the ultimate laminate strength.

The next option is whether to calculate the properties for the average fiber angle at a given radial position or calculate properties for the range of fiber angles at that position and average the material-stiffness matrices. Since the material-stiffness matrix transforms with the angle as a fourth-rank tensor, the resulting stiffness matrix for the two approaches will not be the same. The latter approach is more involved but should be more representative of the average material at a given position and is the approach used. This approach demands that the calculations be performed in the thickness and fiber-angle program rather than in the finite-element code. The average material properties are derived from this stiffness matrix and output with the thickness and average fiber angle for each specified radial coordinate. The computer program listing and the output corresponding to that in Fig. 3 are given in a quarterly progress report.[3]

FINITE ELEMENT ANALYSIS

The selected radii to output data from the thickness calculation program should correspond to the finite-element mesh used to analyze the structure. Since the material properties vary with the radial position, a different material type will have to be assigned at each radial position unless the property values are reasonably close for two or more positions.

A mesh generation program was utilized to prepare the finite element mesh shown in Fig. 4. Part (a) in the figure shows the boundaries of the hub, overwrap, and rim portions of the Deltawrap design. Thin interface layers are between the hub and overwrap and the overwrap and rim to represent the bond lines. Part (b) in the figure draws the actual quadrilateral mesh used in the analysis. The z-axis is the center of rotation for the axisymmetric model, and the model is symmetric about the r-axis.

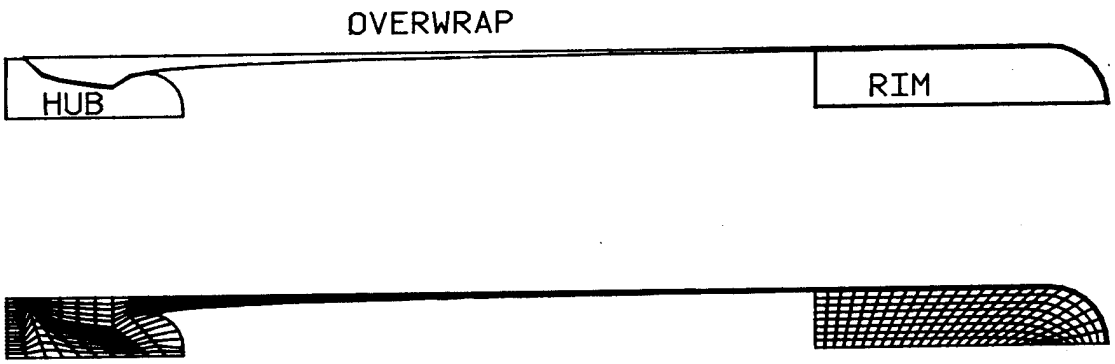


Fig. 4. DELTAWRAP FLYWHEEL FINITE ELEMENT MESH.

The hub is made of an isotropic metal such as aluminum. The overwrap is made of incrementally positioned parallel fiber bands resulting in full coverage of the rim circumference. The rim is made of circumferentially wound unidirectional composite. The interfaces may be modeled with epoxy bonds or rubber bonds.

The finite element code needs some special capabilities to properly analyze composite materials. The composite material is usually elastic and orthotropic. Most general finite element codes have the ability to input orthotropic material properties. There is no generally accepted failure criterion for composites, so most codes have not put any in their program. The failure criteria that can be used usually require either the strain components or stress components in the local fiber coordinate system. Unfortunately, these components are not usually output from any of the codes unless they are aligned with the overall coordinate axes or the element local axes. The components needed may be gained by altering the code or post processing.

A constant strain triangle finite element code in use for many years was modified to produce the fiber coordinate stress components. This code was used to analyze the model in Fig. 4. A new code called ADINA[4] was also used to analyze the model. This code has orthotropic material capability and uses the more refined isoparametric element. A post processor is necessary to determine the local fiber coordinate stress components. The analyses done with ADINA compare very closely with those done with the older code. This lends confidence to the results of both, but the ADINA code will be used in the future analysis because it has extensive dynamic and nonlinear analysis capability.

Results from the analysis of the model in Fig. 4 are presented in the next few figures. The amount of data generated by a finite element analysis can be enormous so the presentation of data becomes a significant problem. A post processing graphics program called MOVIE[5] is used to develop plots of the data. The model has been magnified ten times in the axial direction for presentation purposes.

A three-dimensional perspective view of the magnified Fig. 4 mesh is shown in Fig. 5. The hub, overwrap, and rim parts are exploded in this view.

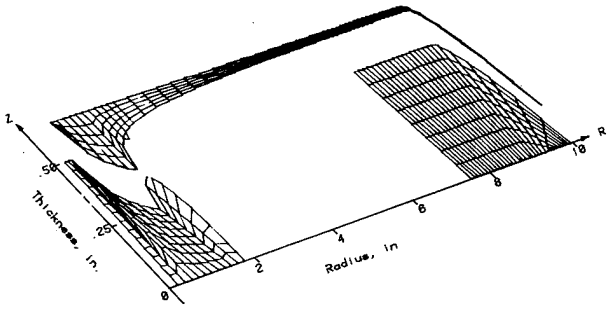


Fig. 5. MAGNIFIED AND EXPLODED DELTAWRAP FINITE ELEMENT MESH.

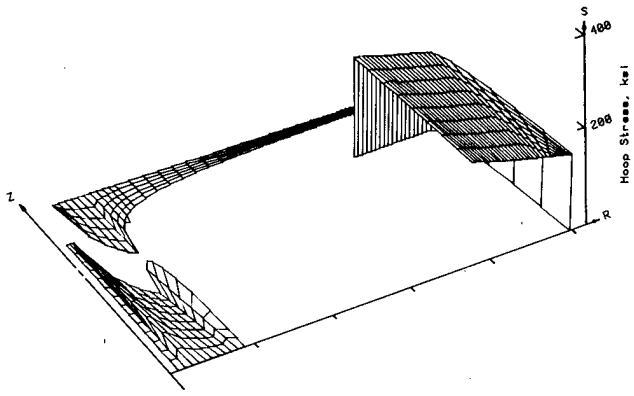


Fig. 6. RIM HOOP STRESS DISTRIBUTION.

The hoop or fiber direction stress component in the rim is shown in Fig. 6 plotted as a surface above the element mesh cross section. The maximum hoop stress is 215 ksi at the inner surface. The more critical radial stress is plotted in Fig. 7 above the mesh cross section. A prestressed rim would be necessary to prevent radial delamination at a low speed.

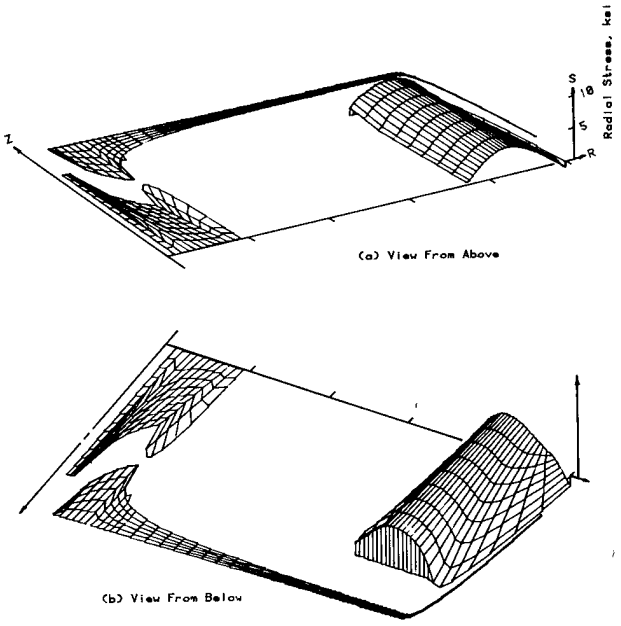


Fig. 7. RIM RADIAL STRESS DISTRIBUTION.

The overwrap stresses are plotted in Fig. 8 and 9. The component transverse to the fiber direction in the lamination plane is displayed in Fig. 8. This result indicates significant transverse cracking will occur at a relatively low speed. Transverse micro-cracking may not be a problem since it has been a common occurence in the filament-wound pressure vessel industry for years. If the composite had high enough transverse strain capability, there would be no cracking. The fiber direction stress component displayed in Fig. 9 indicates a peak stress on the outside surface at the position where the overwrap leaves contact with the hub. This component is relatively low at other locations, so the peak significantly reduces the overwrap performance.

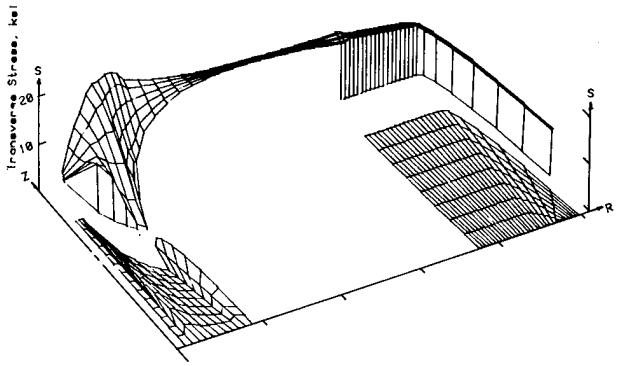


Fig. 8. OVERWRAP TRANSVERSE DIRECTION COMPOSITE STRESS PLOT.

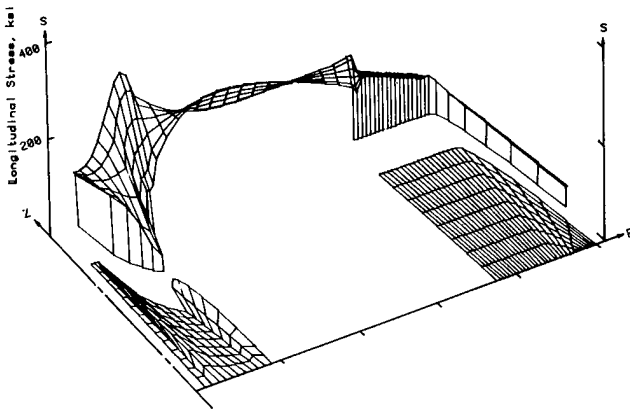


Fig. 9. OVERWRAP FIBER DIRECTION COMPOSITE STRESS PLOT.

Based on these results, some design changes should offer some improvement. The hub design could be changed to lower its stiffness where the overwrap and hub separate, thereby, reducing the overwrap peak stress. It may be better to allow the overwrap thickness variation to be symmetric about a mid-plane rather than forcing all the variation to the inside. These changes need to be evaluated by finite element analysis before any firm conclusions can be drawn.

REFERENCES

[1]R. L. Huddleston, J. J. Kelly, and C. E. Knight, Jr; Composite Flywheel Development Completion Report (May 1 - September 30, 1976), Y-2080; Union Carbide Corporation-Nuclear Division, Oak Ridge Y-12 Plant, Oak Ridge, Tennessee; May 11, 1977.

[2]C. E. Knight, Jr., and R. E. Pollard, "Prestressed Thick Flywheel Rims," Proceedings 1977 Flywheel Technology Symposium, October 5 - 7, 1977; San Francisco, California.

[3]R. L. Huddleston, J. J. Kelly, and C. E. Knight, Jr; Composite Flywheel Development (January 1 - March 31, 1977), Y-2087, Union Carbide Corporation-Nuclear Division, Oak Ridge Y-12 Plant, Oak Ridge, Tennessee; September 1977.

[4]K. J. Bathe, "ADINA - A Finite Element Program for Automatic Dynamic Incremental Nonlinear Analysis," Report 82448-1, Massachusetts Institute of Technology, Cambridge, Massachusetts; September 1975.

[5]H. Christiansen and M. Stephenson, "MOVIE - A General Purpose Computer Graphics System," Brigham Young University; December 1976.

DEVELOPMENT OF THE "BANDWRAP" FLYWHEEL

C. E. Knight, Jr.
J. J. Kelly
R. L. Huddleston
R. E. Pollard
Union Carbide Corporation-Nuclear Division
P. O. Box Y
Bldg. 9998, MS-1
Oak Ridge, TN 37830

ABSTRACT

A program for development of fiber composite flywheels and associated containment was started in May 1976 at the Oak Ridge Y-12 Plant.* This paper describes the development of the first test flywheel in the program. The flywheel design uses a thick rim element and unidirectional fiber composite bands which pass around the rim diameter and across a metal hub fitted to the drive shaft. The individual bands are meshed together at the hub and function similar to spokes on a wheel. The design is called the "Bandwrap" flywheel. The development leading to the first test flywheel is reported in the May to September 1976 Project Report.[1] In the development process, conceptual designs were selected for detailed study. After detailed study, the Bandwrap design was selected for fabrication and test. After fabrication, the flywheel was spun to 18,000 rpm where a predicted delamination occurred in the rim. At this speed, the energy stored was 0.25 kwh and the energy density was 10.1 Wh/lb.

CONCEPTUAL DESIGN STUDY

FLYWHEEL SPECIFICATIONS

The objective of this program is to develop a high efficiency, fiber composite-material flywheel and containment housing for energy storage. Based on discussion with DOE Advanced Physical Methods Branch staff, the most suitable starting point for development was a unit sized to the requirements of a heat engine/flywheel hybrid propulsion system for automobiles. This application requires a nominal storage capacity of 0.5 kwh. The flywheel specification and design objectives are summarized in Table 1. Assuming an operation speed range of three-to-one for energy input/output, a maximum stored energy of 0.56 kwh at maximum operating speed will suffice.

In establishing the program specifications and objectives, it was believed that no known fiber composite flywheel had been fabricated demonstrating this energy storage level. The state-of-the-art metal flywheels reach an operating storage efficiency of 15 wh/lb. The ultimate strength-to-density ratio of current Kevlar-49/epoxy composites project an ultimate efficiency of 80 wh/lb in a thin-rim flywheel configuration. A goal of 20 wh/lb operating storage efficiency was selected for the flywheel developed in this program. Achievement of this goal will fully demonstrate the ability of fiber composite flywheels to exceed the capabilities of metal flywheels. A 20 wh/lb efficiency requires a flywheel weighing a total of 28 lbs.

Table 1

DESIGN SPECIFICATIONS FOR AN AUTOMOTIVE SYSTEM FLYWHEEL

Available Stored Energy	- 0.50 kWh
Design Stored Energy	- 1.12 kWh (min)
Maximum Design Speed	- 40,000 rpm
Flywheel Weight	- 28 lb
Flywheel Size	- 20 " D (approx)
Torque Load Capacity	- 100 ft lb
Dynamic Characteristics	- Minimize the Number of Critical Frequencies in the Operating Speed Range

*Operated by the Union Carbide Corporation's Nuclear Division for the US Department of Energy

The overall size of the flywheel for an automobile application should be limited to minimize packaging problems. If the diameter is too small, the flywheel speed will be very high; and the weight must be attained by making the axial cylindrical dimension long. A disc-type configuration is preferred to reduce mounting and system stability problems. The nominal maximum diameter is 20 inches, which is suitable for an automotive installation and is compatible with existing composite winding equipment and facilities and existing spin-test facilities.

The design objective for dynamic characteristics is the elimination, if possible, of all critical frequencies in the operating speed range. Rigid body modes should be below the lower speed bound and elastic body modes above the upper speed bound, and preferably above the ultimate failure speed.

CONCEPTUAL DESIGNS CATALOG

In the conceptual study, 18 conceptual designs with design options on some were cataloged. These are illustrated in Fig. 1, 2, and 3 and are briefly described in the following paragraphs.

Designs A through E (Fig. 1) employ the rim configuration and devise various methods for attaching the rim and drive shaft. The rim design in each case is uncoupled from the arbor. The rim is designed to reach its own ultimate speed capability. The rim speed-displacement response is used to design the arbor so that the arbor will follow without significantly loading the rim. The rim design is controlled by the material properties, fabrication process, and design parameters and can usually be described by a dimensionless inside/outside radius ratio. Selection of either radius then determines the radial thickness, and the axial thickness is determined by the energy storage requirement.

Designs F through I (Fig. 2) employ the rod configuration. The rod elements of each design are fabricated of a continuous, unidirectional composite material. Most likely, the elements would be individually fabricated and then assembled in the flywheel form. The energy stored in each element determines the number of elements required. While the energy stored per unit weight is high, the primary disadvantage of these designs are their low volumetric energy densities.

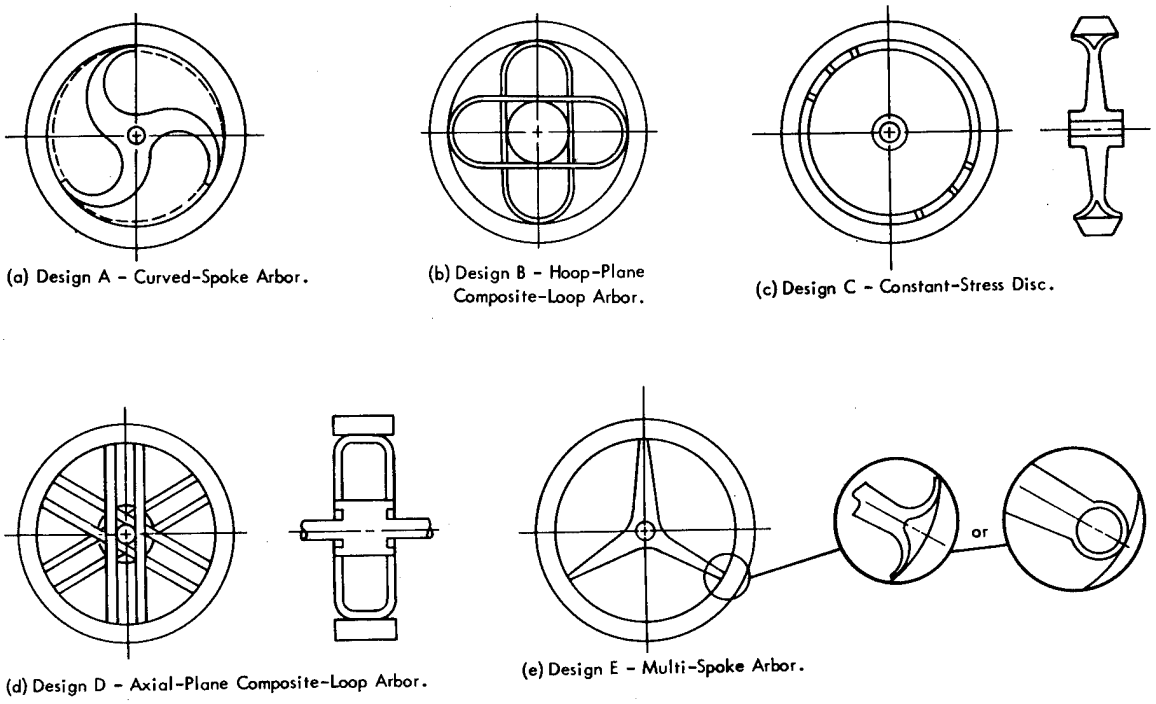
Designs J through R (Fig. 3) are categorized as solid disc configurations, although there are similarities to the rim designs. These designs would normally have the highest volumetric energy densities but usually with some sacrifice of the weight energy density. These designs attempt to either limit radial stresses in circumferentially wound composite sections or provide fiber orientations to accommodate the radial loads.

DESIGN EVALUATION AND SELECTIONS

A method has been established for rating the cataloged conceptual designs and selecting the design(s) for further analysis and hardware development. Each concept was studied and its strength and weaknesses listed. Based on these listings, a set of rating criteria was established as follows (numbers in parentheses represent the rating-scale value and the range for each criterion):

Rating Criterion Number	Criterion
1	Energy Stored/Unit Weight (0-10)
2	Energy Stored/Unit Volume (0-5)
3	Potential for Meeting the Objectives of this Program (0-10)
4	Ease of Fabrication (0-5)
5	Likelihood for Near-Term Successful Test (0-10)
6	Development Time Required (0-10)
7	Design and Analysis Complexity (0-10)
8	Economical End Product (0-5)
9	Potential of Significant Improvement with Further Development (0-5)
10	Likelihood of Minimal Dynamic Problems (0-10)
11	Torsional Strength and Stiffness Capability (0-5)

A decision table was formed and a subjective rating for each conceptual design estimated for all the criteria. Table 2 is a reproduction of the decision table. Some of the criteria and the rating-scale values were selected to meet the objectives of the FY 1976-1976T program. Thus, the final rating and selection of designs for development may be re-evaluated at a later time. The rating values were summed for each design to determine an overall ranking for each conceptual design and, from these values, the designs to be developed were selected.



(a) Design A - Curved-Spoke Arbor.

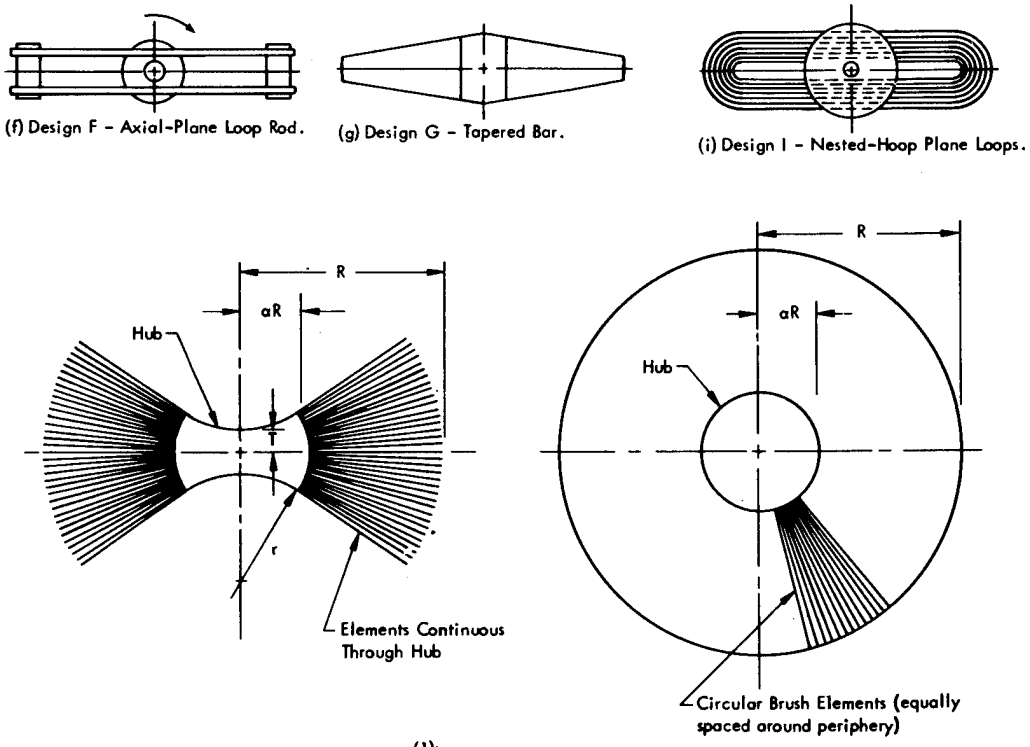
(b) Design B - Hoop-Plane Composite-Loop Arbor.

(c) Design C - Constant-Stress Disc.

(d) Design D - Axial-Plane Composite-Loop Arbor.

(e) Design E - Multi-Spoke Arbor.

Fig. 1. CONCEPTUAL DESIGNS FOR THE FLYWHEEL. (Rim Configuration)



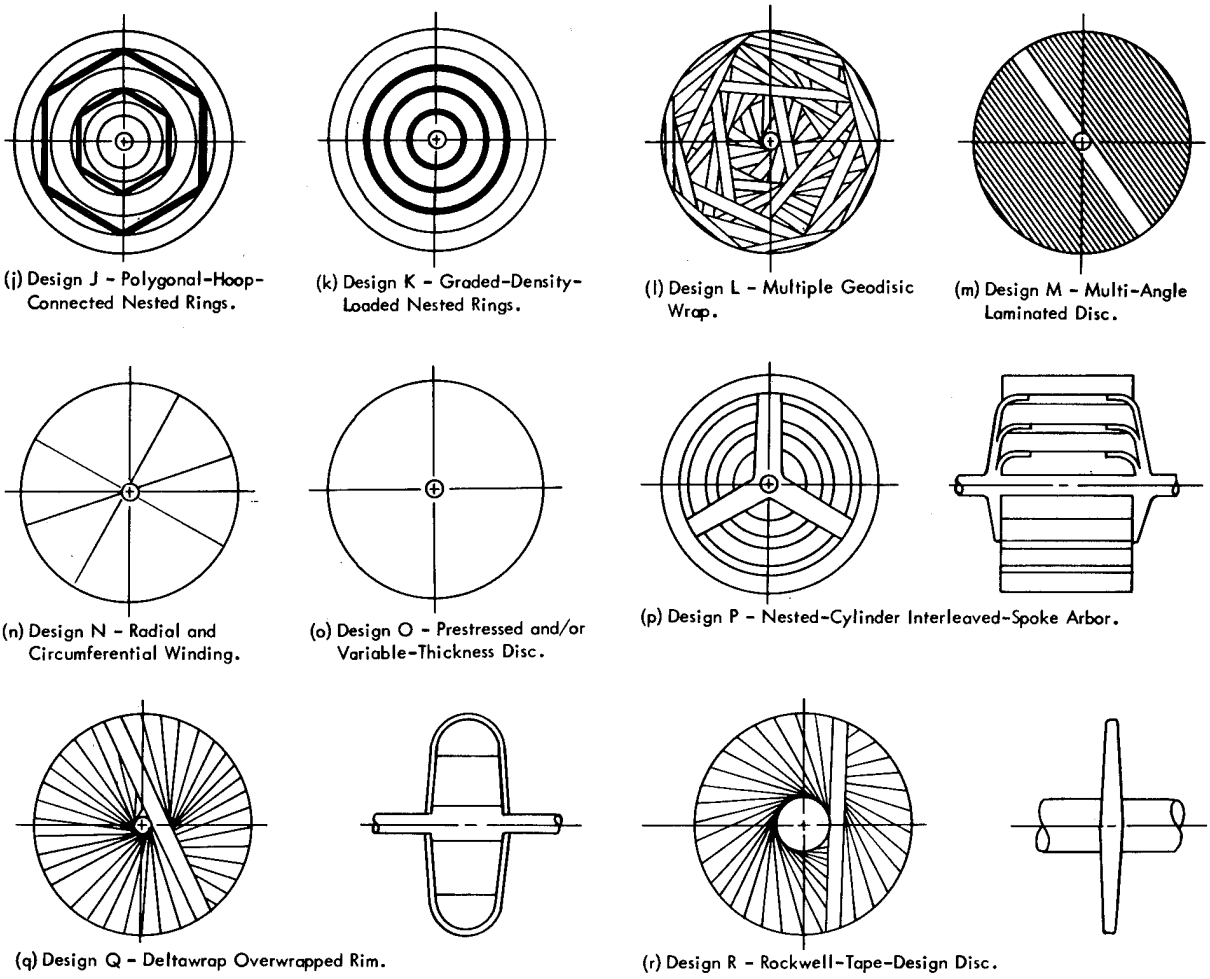
(f) Design F - Axial-Plane Loop Rod.

(g) Design G - Tapered Bar.

(i) Design I - Nested-Hoop Plane Loops.

(h) Design H - Brush Designs. (From Rabenhorst [1])

Fig. 2. CONCEPTUAL DESIGNS FOR THE FLYWHEEL. (Rod Configuration)



(j) Design J - Polygonal-Hoop-Connected Nested Rings.

(k) Design K - Graded-Density-Loaded Nested Rings.

(l) Design L - Multiple Geodisic Wrap.

(m) Design M - Multi-Angle Laminated Disc.

(n) Design N - Radial and Circumferential Winding.

(o) Design O - Prestressed and/or Variable-Thickness Disc.

(p) Design P - Nested-Cylinder Interleaved-Spoke Arbor.

(q) Design Q - Deltawrap Overwrapped Rim.

(r) Design R - Rockwell-Tape-Design Disc.

Fig. 3. CONCEPTUAL DESIGNS FOR THE FLYWHEEL. (Disc Configuration)

Table 2
DECISION TABLE FOR CONCEPTUAL DESIGN RANKING

Conceptual Design	Rating Criterion Number											Total Rating (85,max)	Rank
	1	2	3	4	5	6	7	8	9	10	11		
A	5	3	10	3	7	6	3	1	2	6	4	50	8
B	8	3	10	3	6	6	4	2	2	3	1	48	9
C	6	4	10	3	7	9	3	2	2	8	5	59	4
D	9	3	10	4	8	10	9	3	3	7	2	68	1
E	5	3	10	3	5	4	2	1	2	7	3	45	11
F	2	1	0	3	1	3	3	2	0	0	1	16	17
G	3	2	1	2	2	2	5	2	2	1	2	24	14
H	3	1	1	1	1	1	3	1	2	3	2	19	15
I	3	1	2	1	1	1	2	1	2	2	2	18	16
J	5	4	10	2	3	2	2	3	2	3	2	38	13
K	6	5	10	3	5	3	10	4	2	6	4	58	5
L	6	4	8	1	4	2	1	3	4	6	4	43	12
M	6	4	10	4	5	5	5	5	2	10	5	61	3
N	5	4	10	0	7	0	5	2	3	10	5	51	7
O	5	4	10	3	3	1	3	5	3	8	3	48	10
P	5	4	10	3	3	5	5	2	3	5	4	49	8
Q	10	3	10	4	7	6	3	4	5	9	4	65	2
R	6	4	8	3	6	5	3	3	3	10	5	56	6

The five highest ranking designs were selected from the decision table. These designs were: D, Q, M, C, and K, respectively. The ratings for Design D were based on the plan of having the composite loops pass around the rim exterior. This form of Design D looks like a natural forerunner of Design Q. Design Q has the highest rating for potential improvement with further development.

Design D was selected for initial development in the FY 1976-1976T program, possibly leading to development of Design Q in following programs. Designs M, C, and K will be carried at a low activity level as backup designs.

MATERIAL CHARACTERIZATION AND SELECTION

MATERIAL SELECTION

The design selected for development is of the rim configuration. Since most of the energy is stored in the rim, it must have sufficient mass at the design speed to store the desired level of energy. The rim, therefore, cannot be an ideal "thin" rim unless it has a large axial length. In order to maintain a disc-type geometry to minimize dynamic problems, the axial length must be limited.

The material chosen for fabricating the rim must have a high strength-to-weight ratio to give a high-energy-stored/unit-weight efficiency. The material must also have the properties and characteristics needed to form a relatively thick rim. The candidate material systems for use in this program have been limited to those systems with which the Y-12 Composite Structures Group has had fabrication experience.

Systems applicable to the flywheel are: graphite/epoxy, S-Glass/epoxy, E-Glass/epoxy, and Kevlar-49/epoxy. Of these, the aramid fiber (Kevlar-49) in an epoxy matrix has the highest strength-to-weight ratio. The graphite/epoxy systems were eliminated because the strength-to-weight ratios are too low to give an adequate margin of capability above the program objectives.

The epoxy resin was selected so that it could be room-temperature cured. This selection allowed the full rim to be wound and cured without delamination that would be expected with elevated temperature curing resins. The epoxy was Dow Chemical Co. DER 332 with Jefferson Chemical Co. Jeffamine T-403 hardener.

MATERIAL CHARACTERIZATION

The elastic properties of the Kevlar-49/epoxy composite have been published in the literature and have also been characterized in our laboratories. The strength properties of composites are sensitive to the material processing conditions, the selected constituents, and the laboratory where the materials and specimens are fabricated.

Tests performed in this program gave higher hoop strength results and lower transverse strength results than published in the literature. Hoop strengths were determined from hydroburst of circ-wound rings. The rings were 6.000 inches in I.D., 0.250 inch wide, and 0.125 inch thick. A circumferential wire was placed around the ring in the hydrotest fixture, and the prestress/elongation curve was recorded for the test ring. The load/strain curves were linear to failure. Hoop strength data are summarized in Table 3.

Table 3

STRENGTH AND MODULUS OF THE KEVLAR 49 ROVING USED IN THE RIM FABRICATION

Rim Number	Tensile Strength [ksi (CV)(1)]	Modulus [Msi (CV)]
1	263.5 (7.1%)	12.5 (3.1%)
2	225.6 (6.2%)	12.1 (1.7%)
3	262.7 (7.2%)	12.6 (3.5%)

(1) CV - coefficient of variation.

The transverse tensile strength is normally significantly dependent on the epoxy resin system used. A special test was set up to measure the radial tensile strength of a thick ring. A segment of a ring was mounted in an apparatus illustrated schematically in Fig. 4. A pure bending moment was applied to each end of the segment. This action produced a flexural hoop stress and a radial tensile stress if the moments were applied in the direction shown. The radial-stress distribution is similar to that in a rotating ring and should, therefore, be indicative of the expected ultimate radial strength in the flywheel rim. Small-scale thick rings wound, for residual stress

evaluation, provided specimens for this radial-strength measurement.

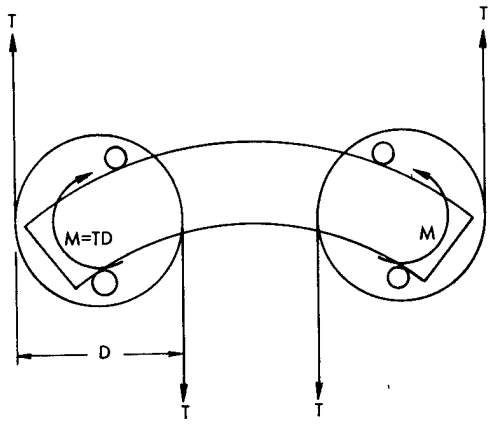


Fig. 4. SPECIAL-RING-SEGMENT TRANSVERSE TENSILE TEST.

The stresses generated by the flexure of a curved beam are derived in a number of texts, one of which is authored by Seely and Smith.[2] A curved beam of rectangular cross section is illustrated in Fig. 5. The bending moment generates both circumferential and radial stresses in the curved beam, but the radial stresses are of most concern here. The circumferential stresses may be approximated by the standard beam-flexure equation. The radial stress at any radial position through the section located by coordinate y is given by:

$$\sigma_r = \frac{Ma'}{Rta\,(R+y)}\left(1 - \frac{z'}{z}\right) \qquad (1)$$

For rectangular cross sections:

$$z = -\frac{1}{a}\int_{-c}^{+c} \frac{y}{R+y}\,da = -1 + \frac{R}{2c} \times \left[\ln\left(\frac{R+c}{R-c}\right)\right], \text{ and} \qquad (2)$$

$$z' = -\frac{1}{a'}\int_{-c}^{y} \frac{y}{R+y}\,da = -\frac{1}{c+y} \times \left[c + y - R\ln\left(\frac{R+y}{R-c}\right)\right] \qquad (3)$$

where:

σ_r represents the radial stress,

M the applied moment,

a' the cross-hatched area (Fig. 5),

R the radius of curvature to the section centroid,

t the beam thickness,

a the total section area, and

y the coordinate referenced to the centroid.

The maximum radial stress will occur at the location of the neutral axis. The y coordinate of the neutral axis is given by:

$$y_o = -zR/(z+1). \qquad (4)$$

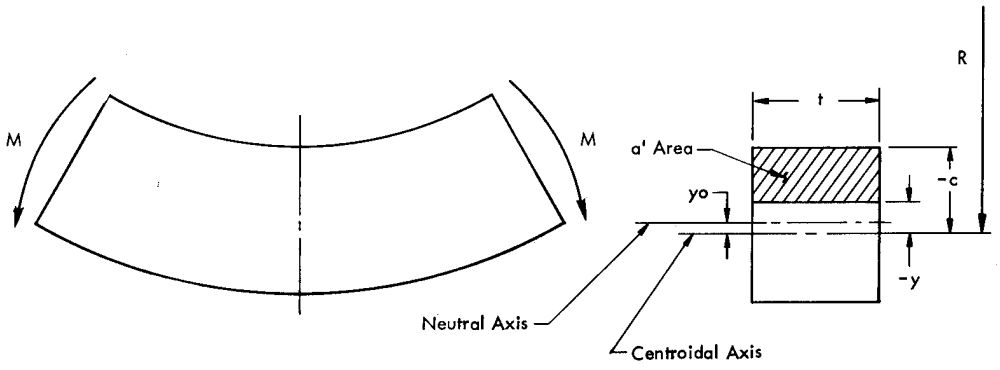


Fig. 5. CURVED-BEAM SEGMENT WITH THE RECTANGULAR CROSS SECTION LOADED IN PURE BENDING.

The negative sign indicates that the neutral axis is nearer to the inside radius. This value of y is used in Eq. (3) to find z′, then Eq. (1) to find $\sigma_{r\ max}$.

The composite system being used in this program was used to wind test rings, and the radial strengths were determined. The values shown in Table 4 were much lower than anticipated based on literature data. These data indicated the likelihood of premature failure in the first test flywheel, but the flywheel fabrication was well along when the data were obtained. Some other epoxy resins were also evaluated, as shown in Table 4, in an attempt to find a higher transverse strength composite, but none were found.

The characterization studies by the LLL[3] show similar results except their transverse tensile data is somewhat better. The reason for this is probably the lower void content in their composites due to vacuum impregnation. We have not developed a vacuum impregnation system that would work satisfactorily for winding full size rims; and, therefore, we chose to make the characterization specimens by the same process used for the rims so they would be representative of the final product.

RESIDUAL STRESS ANALYSIS

The residual stresses in a composite structure may be of critical importance, especially in the direction transverse to the fiber axis. The residual stresses present in the fabricated rims were determined to evaluate the potential flywheel performance.

The procedure for evaluating residual stresses is: a test ring is parted from the fabricated rim; the ring is instrumented with strain gages, and strain changes are recorded as thin layers of material are machined off the diameter. The strain changes are used to calculate the residual stresses that were present initially.

The stresses were calculated incrementally, corresponding to the strain change produced when an increment of material was removed. The ring is illustrated schematically in Fig. 6 after removal of the i^{th} layer. The radial stress, σ_{r_i}, was calculated from the equation for the tangential stresses in a thick-wall, orthotropic ring subjected to an external pressure and the total strain change from the initial reading. The first few rings examined were strain gaged on the inside radius. The tangential stress change on the inside radius produced by the strain change was determined by:

$$\Delta\sigma_\theta = \Delta\varepsilon_\theta E_\theta = \frac{2Ka^{(K-1)}r^{(K+1)}}{r^{2K} - a^{2K}}\,\sigma_{r_i}. \quad (5)$$

Table 4

TRANSVERSE TENSILE STRENGTH OF SELECTED COMPOSITES

Material System	Quantity (vol %) Fiber	Resin	Void	Tensile Strength (psi)	Maximum Hoop Compressive Stress (ksi)	Modulus of Elasticity (msi)
Kevlar-49/ (DER332/T403)	74.5	22.9	2.6	870 (CV = 18.2%)[2]	23	0.89
Kevlar-49/ (XD7818/D230/A398)	76.0	22.8	1.2	1000 (CV = 12.8%)	26	0.94
Kevlar-49/ (DER332/T403/A398)	72.9	24.6	2.5	960 (CV = 10.9%)	25	0.82
S-glass/ (DER332/T403)	74.0	22.2	3.8	2920 (CV = 1.3%)	75	2.95
S-glass/ (ERL2258/MPDA)	74.9	22.1	3.0	3380 (CV = 10.0%)	89	3.18
3M SP308 Kevlar-49 prepreg				1975 (CV = 24.6%)		0.72

(1) DER332 and XD7818 are products of Dow Chemical; T403, D230, and A398 are products of Jefferson Chemical; ERL2258 is a product of Union Carbide; MPDA is metaphenylenediamine, a standard chemical product; 3M SP308 is a product of 3M.

(2) Coefficient of variation, CV = (standard deviation/mean) x 100 percent.

Rearranging to yield the radial stress gives:

$$\sigma_{r_i} = \frac{r^{2K} - a^{2K}}{2Ka^{(K-1)}r^{(K+1)}} \qquad (6)$$

where:

σ_{r_i} represents the radial "initial" stress existing inside the i^{th} layer,

r the radius to Layer i,

a the ring inside radius,

K a constant equal to $\sqrt{E_\theta/E_r}$ (where E is the tangential modulus of elasticity and E_r the radial modulus of elasticity), and

$\Delta\varepsilon_\theta$ the tangential strain change from its initial zero reading.

Thus, the radial stresses were determined at all incremental points through the wall. The tangential stress in any layer, i, was found by calculating the membrane stress in the cylindrical layer due to the differential pressure $(\sigma_{r_{(i-1)}} - \sigma_{r_i})$, thus,

$$\sigma_{\theta_i} = (\sigma_{r_{(i-1)}} - \sigma_{r_i}) \frac{r}{\Delta r} . \qquad (7)$$

where:

σ_{θ_i} represents the tangential "initial" stress existing in the i^{th} layer, and r the layer thickness. The radial and tangential "initial" or residual stresses are plotted versus radial position to display their distribution.

Residual stresses were measured in two full-size rims wound for flywheel manufacture and test. A ring was parted from the rim and instrumented with strain gages mounted on the side of the ring so that the residual stresses on both the inner and outer surfaces could be determined with better accuracy. Machining of layers was conducted first from the outer surface incrementally toward the strain-gage location, then from the inner surface toward the strain-gage location. The data were reduced in a manner similar to the method described above. However, the strain increment that results when a layer is removed in this case depends on both the radial and tangential stress components at the strain-gage location.

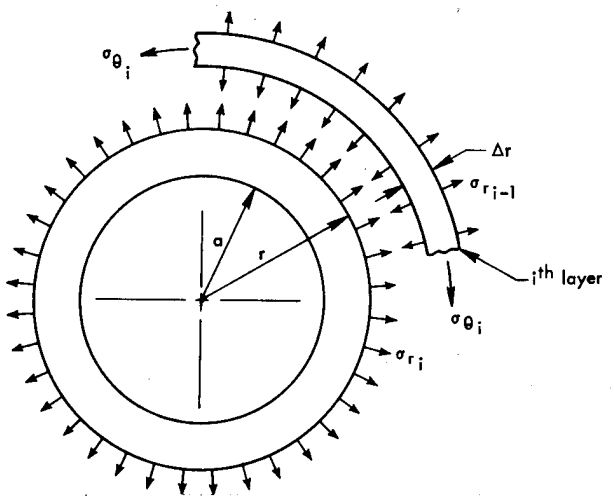


Fig. 6. TEST RING RESIDUAL STRESS ANALYSIS MODEL.

Results from the two rims were very close and similar to the results on earlier test rings. Stress distributions from the first full-size rim are indicated in Fig. 7. When the rim was used in a flywheel, the outer surface was machined to a contour and approximately 0.125 inch of stock removed. This removal also removes the high residual stress layers on the outside. On the tangential stress curve in Fig. 7, this removal occurs at approximately the 8-ksi stress level. Based on these results, the finished rim used in the flywheel did not have any significant residual stress problem.

STRUCTURAL ANALYSIS

Detailed stress analyses were performed by using the finite-element method. The computer code that was used solves two-dimensional axisymmetric or plane-stress problems with orthotropic, temperature-dependent, material properties. The analysis required both axisymmetric and plane-stress modeling. A code modification was inserted to apply the rotational-body-force loading to plane-stress cases. Minor modifications were made to allow the code to calculate the weight and moment of inertia of the input model.

A finite element model was prepared through the use of a mesh-generation

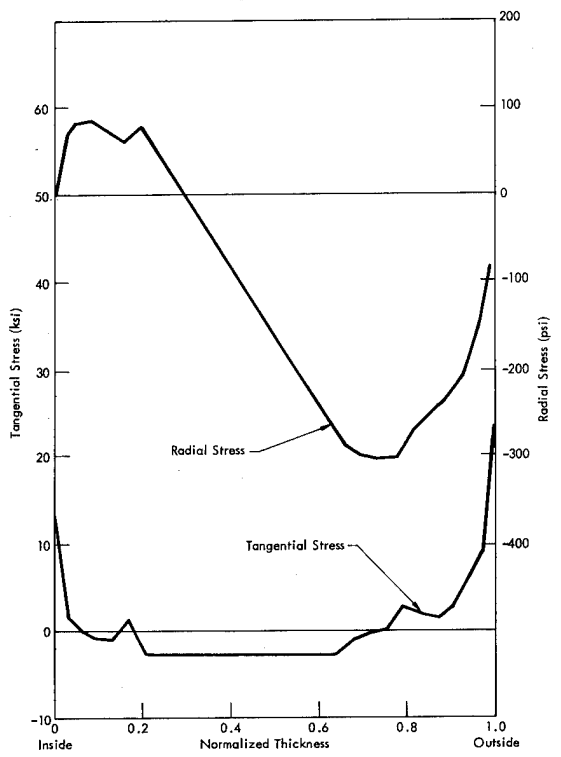


Fig. 7. RESIDUAL STRESSES IN THE FIRST FULL-SIZE RIM(A 15-inch-ID by 20-inch-OD Circ-Wound Kevlar-49 Composite).

program. One such model is reproduced in Fig. 8. The rim has a 7.500-inch inside radius and a 10.000-inch outside radius. The band has a 0.100-inch uniform thickness passing around the rim outer contour. A thin interface layer was placed between the rim and band in order to determine the required bond strength.

Results from the last analysis iteration are presented in Fig. 9 through 12. As mentioned, the model was run first in the axisymmetric mode. This run determines the stresses in the rim due to centrifugal loading and its corresponding displacements. In this step of the analysis, the material density of the band and interface materials was zeroed. The elastic properties were also factored down to allow for a free expansion of the rim. This procedure is probably a closer approximation to the real case than if the properties were unaltered in the full-rim-overwrap covering provided by the axisymmetric model. Computed stresses in the rim at an angular velocity of 2827 rad/sec (27,000 rpm) are given in the graph of Fig. 9. At this angular velocity, the flywheel stores 0.56 kWh of energy and has a theoretical weight efficiency of 22.8 Wh/lb. Figure 9, Graph a, is a plot of the hoop-stress distribution; Graph b is a plot of the radial-stress distribution.

Rim displacements in the axisymmetric computer code run were recorded and used as specified displacements on the rim cross section in the place-stress analysis. The band and interface-material densities and properties were restored and the plane-stress problem solved for the same angular velocity. The interface material may be represented in many different ways. It could be modeled as a bondline with average epoxy properties, low modulus epoxy adhesive properties; or portions of the interface could be free and other portions bonded. All of these may be plane-stress or plane-strain analyses with property transformations.

Results from two of the modeled interfaced schemes are presented here. The interface shear and normal stresses are plotted in Fig. 10 and 11. Figure 10 presents the shear-stress distribution and the normal-stress distribution when the interface is modeled by an average epoxy (E = 500,000 psi, ν = 0.35) in plane

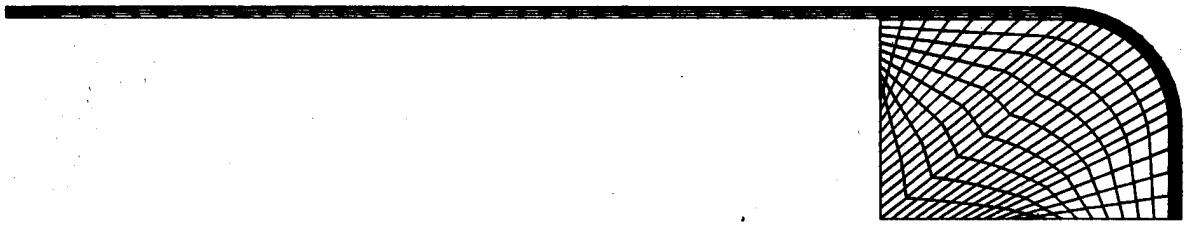


Fig. 8. FINITE ELEMENT MODEL OF THE DESIGN D FLYWHEEL.

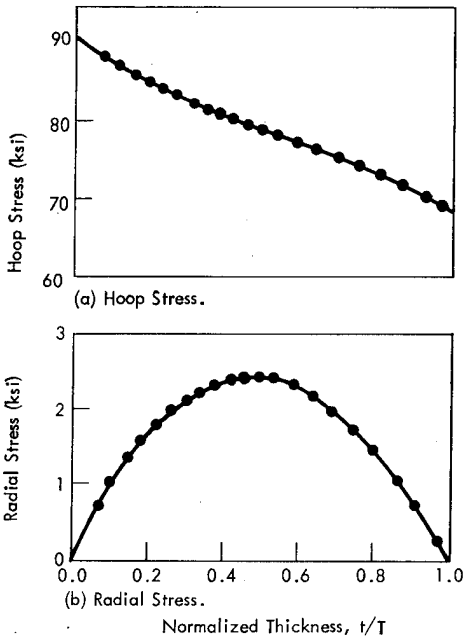


Fig. 9. STRESS DISTRIBUTIONS ALONG A RADIAL LINE IN THE PLANE OF SYMMETRY THROUGH THE RIM THICKNESS FROM THE FINITE ELEMENT ANALYSIS.

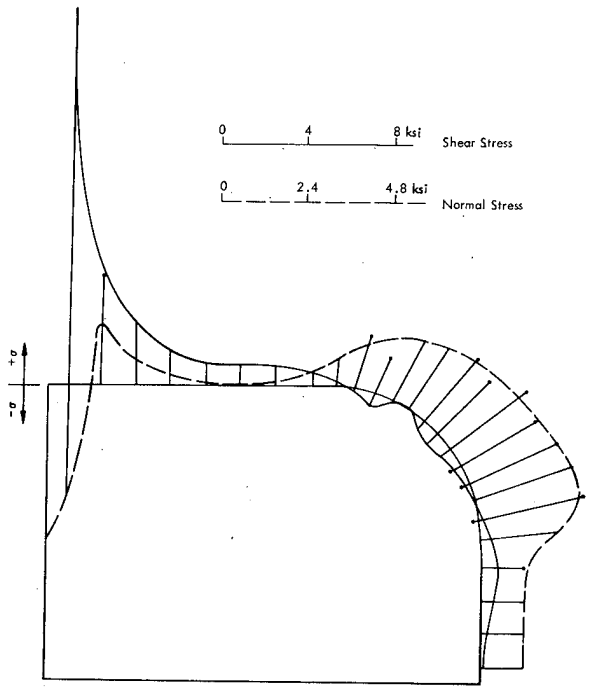


Fig. 10. SHEAR AND NORMAL STRESSES ALONG THE FULLY BONDED RIM/BAND INTERFACE WITH AN EPOXY BONDING AGENT MODELED IN PLANE STRAIN.

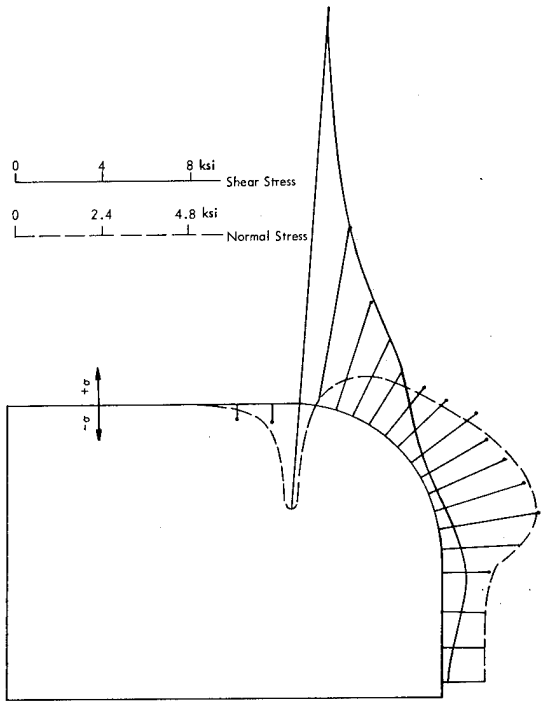


Fig. 11. SHEAR AND NORMAL STRESSES ALONG THE RIM/BAND INTERFACE WHEN THE RIM AND BAND ARE NOT BONDED ALONG THE FLAT RIM SIDE.

strain; Fig. 11 presents the shear-stress distribution and the normal-stress distribution when the interface is not bonded along the rim side out to the beginning of the corner radius, with the remainder at the interface modeled by an average epoxy in plane strain.

Stresses in the band are plotted in Fig. 12. The average longitudinal stress in the fully bonded band is plotted in Graph a, the average longitudinal stress in the band that is not bonded on the rim side is plotted in Graph b. These results from the analysis of Design D looked very promising. Based on preliminary property data, the design appeared to be more than adequate to reach the design operating goal. The radial tensile strength test data reported previously were not available until after the first flywheel of the design had been fabricated. These data indicated that the flywheel would likely fail by delamination, premature to the design level.

RIM DESIGN ALTERNATIVES

The Bandwrap flywheel stress analysis was performed for a fiber composite rim of

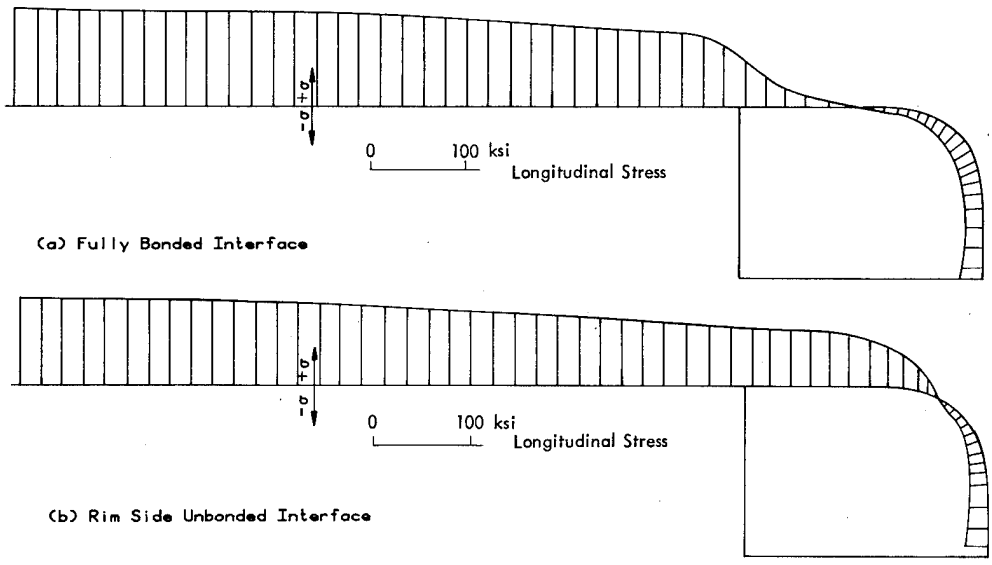


Fig. 12. LONGITUDINAL BAND STRESSES FOR TWO INTERFACE CONDITIONS.

homogeneous construction and negligible residual stress. Based on the transverse strength data, the Kevlar-49/epoxy composite performance is severely limited due to delamination failure.

The options for the Bandwrap flywheel are then to select a different composite material that has adequate strength or choose a rim design alternative that reduces the transverse strength requirement. Some rim design alternatives are: 1) dead weight loading on the inside radius, 2) varying material hoop moduli, 3) multiple nested rims with portions of the band set passing around each rim, and 4) radial compressive prestress distribution. Results on studies of some of these alternatives in the FY 77 Development program are presented in the quarterly progress reports.[4,5,6,7]

Dead weight loading on the inside radius has been analytically evaluated in a Bandwrap design. A layer of lead inside the Kevlar-49/epoxy rim of 0.75 radius ratio was shown to reduce the maximum radial tensile stress to 1 ksi at a speed which produces 260 ksi hoop stress and, thus, a simultaneous hoop and radial failure at an estimated 46 watt-hr/lb of total weight.

Varying the material hoop moduli has also been evaluated analytically for one specific case. It was shown that a rim whose inner half was Kevlar-29/epoxy and outer half was Kevlar-49/epoxy has a maximum radial tensile stress of 1.3 ksi at a speed where the maximum hoop stress is 260 ksi. The overall radius ratio was increased to 0.782 in order that the displacements of the two halves would match at the interface thus producing zero radial stress at the interface. A multiple nested rim design has not been analytically evaluated but should be straightforward. A prestressed rim design has been calculated, and the results are presented in another paper at this conference.[8]

FLYWHEEL FABRICATION

TOOLING DESIGN

The tooling required to fabricate the circ (circumferentially)-wound rims was relatively simple. A steel cylinder, 15 inches in diameter by 4.100 inches long, was fitted with two side plates. The side plates had a 0.050-inch recess for the cylinder and had an outside diameter of 22 inches. A two-inch-diameter shaft passed through the side plates. The side plates were 0.750 inch in thickness to provide adequate stiffness to resist the side pressure during winding. The wound rim could then be up to 22 inches in outside diameter by 4 inches wide.

The tooling for winding bands around the rim was more complex. A form had to be provided for each band to be wound. This form controlled the fiber-laydown position and the overall dimensions of the band. A multipiece disc was fitted between the hub described earlier and the rim. This disc positioned the rim concentric with the hub and aligned the band forms in the correct position relative to the hub features. Matched multipiece discs were required for each side of the flywheel.

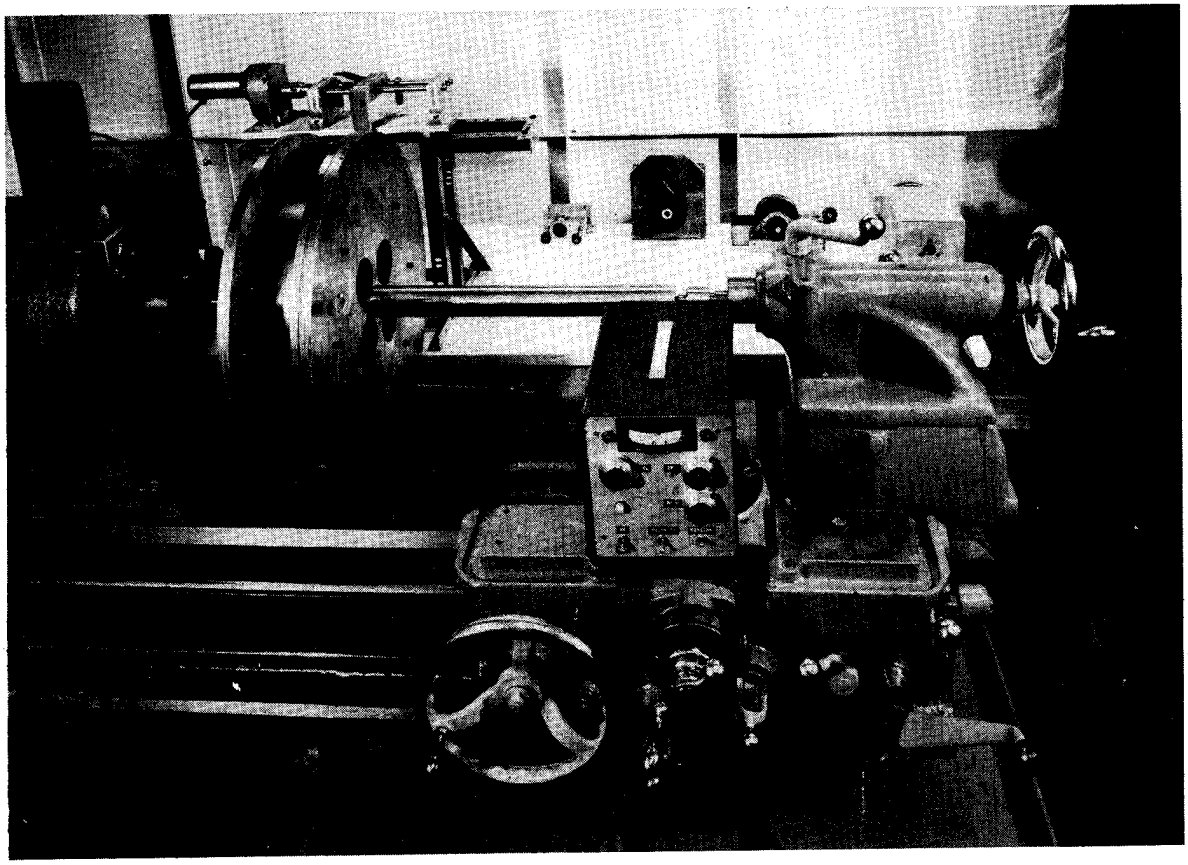
RIM FABRICATION

The rim tooling was received and the first full-scale rim was wound. The winding setup is shown in Fig. 13. The fiber was 1420-denier Kevlar-49 yarn, the resin system was DER 332/T403 cured at room temperature, and the winding tension was held constant at 1,800 grams. The rim was wound to approximately 20.2 inches in outside diameter so that the high residual stress region at the outside could be machined away. The total winding time was 28 hours at a laydown rate of 28 rpm. A view of the rim is seen in Fig. 14.

Two other rims were wound, one using 1420-denier Kevlar yarn and the other using 4560-denier Kevlar yarn. The second wound rim used 4560-denier yarn with 6,000 grams of winding tension. Winding time was seven hours at a laydown rate of 28 rpm. The third rim used 1420-denier yarn with an 1,800 gram winding tension. An insert placed on the mandrel reduced the part width to approximately 3.6 inches. The winding time was 19 hours at a laydown rate of 37 rpm. Pertinent data on the three rims are summarized in Table 5.

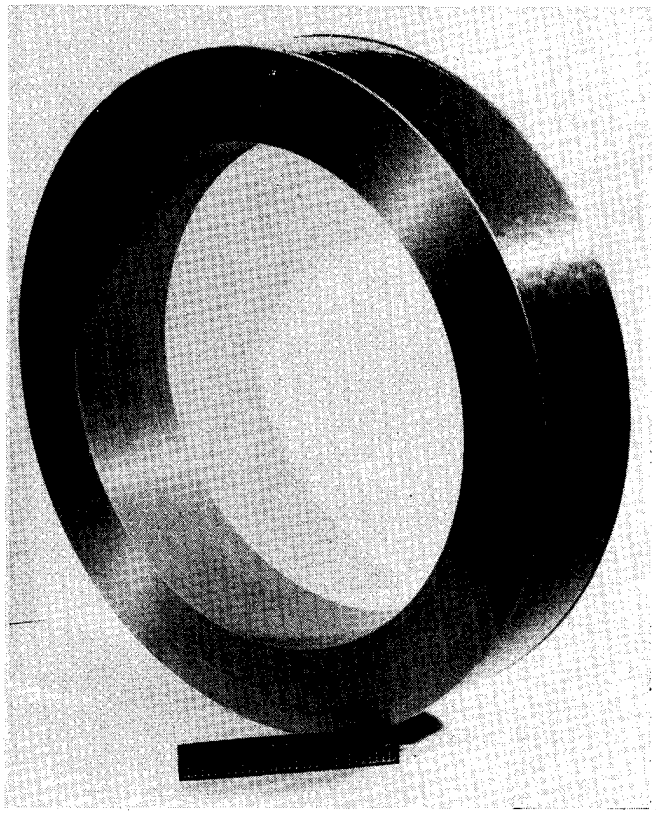
FLYWHEEL FABRICATION

Fabrication of a finished Design D flywheel for testing involved rim preparation, machine setup, rim and band tooling assembly, and alignment and winding of the band set. Rim preparation required machining of the sides and outer contour. A planar winding machine was set up with special alignment fixtures to



168735

Fig. 13. WINDING SETUP FOR FABRICATING THE FULL SCALE RIMS



166398

Fig. 14. COMPLETED AS-WOUND RIM AFTER REMOVAL FROM THE WINDING MANDREL.

mount the rim and provide the desired band orientations.

Machining of the as-wound rim presented some special problems. Composites, in general, are difficult to machine. It is particularly difficult to achieve a satisfactory surface integrity on Kevlar-49/epoxy composites. The usual surface condition after machining is a rough, hairy texture with many loose fiber ends raised on the surface. This condition is illustrated in Fig. 15, which shows a ring section cut from a test cylinder. A high-speed parting-saw operation with coolant flooding was used.

Obviously, the condition illustrated in Fig. 15 is not satisfactory for a flywheel, which must spin at high speeds. The machined surface must be on the same order of smoothness as the surfaces that are wound against a smooth mandrel. Fortunately, machining technology existed in Y-12 which was able to produce the desired surface.

A unique machining process has been developed in the Y-12 Plant for providing a super finished ($\sim$ 2 μin, peak to valley) surface on a machined part and has been used to produce mirrors for several laser research programs around the country. The process uses a special cutting tool called a "diamond knife" which is made from a single crystal diamond and is extremely sharp because of a near-perfect edge. The turning machine employs an air-bearing spindle and other very stiff and very precise components. The technique had been used exclusively on metal parts but was adapted to machine the Kevlar-49/epoxy composite.

A machined rim mounted on the turning machine is shown in Fig. 16. Machining is normally done wet with a coolant; but since the effects of coolant on the composite are unknown at this point, rim machining was done dry. Results were very good, as seen in Fig. 16, and were felt to be satisfactory for spin testing.

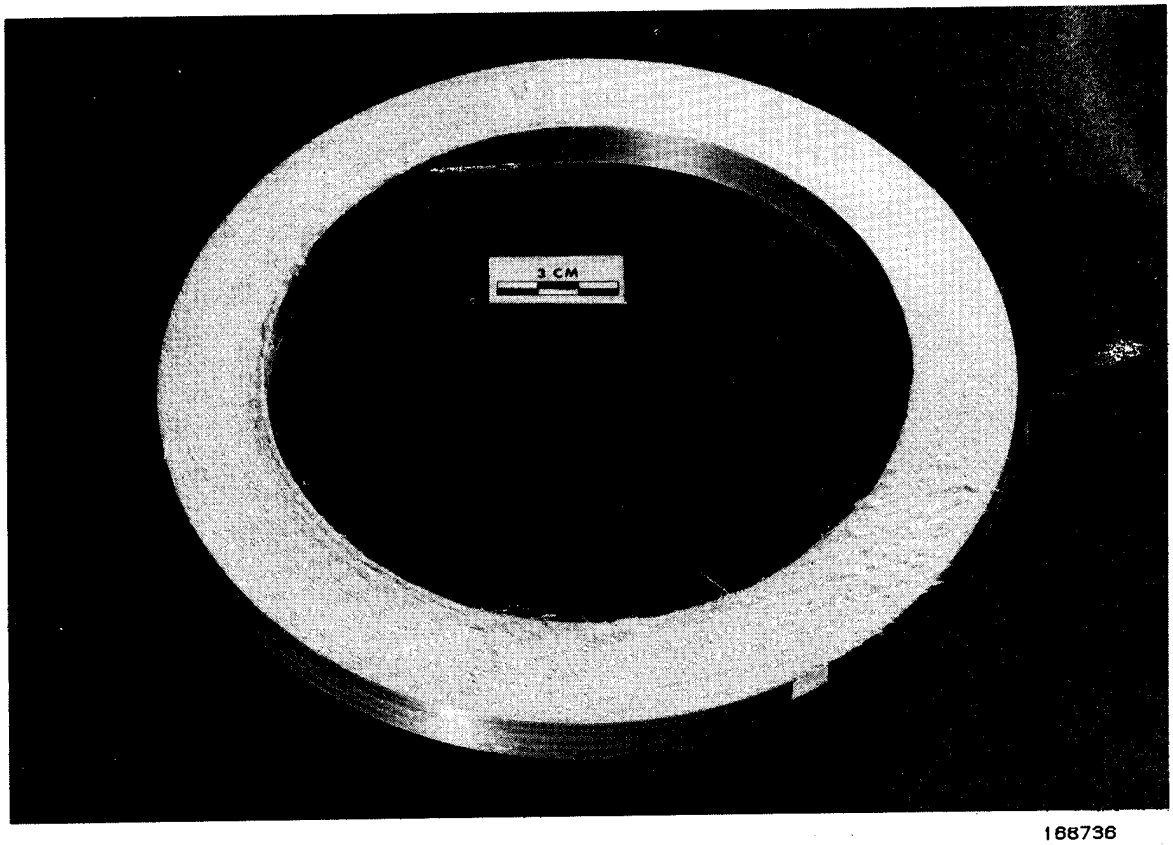
The procedure for winding bands across the hub and around the rim called for a planar winding machine. In addition, the planar path had to have a built-in motion normal to the plane of winding in order to generate a parallel fiber band of the desired width. An existing machine had these required features. A picture of the machine and flywheel setup is presented in Fig. 17.

The rim and band tooling assembly

Table 5

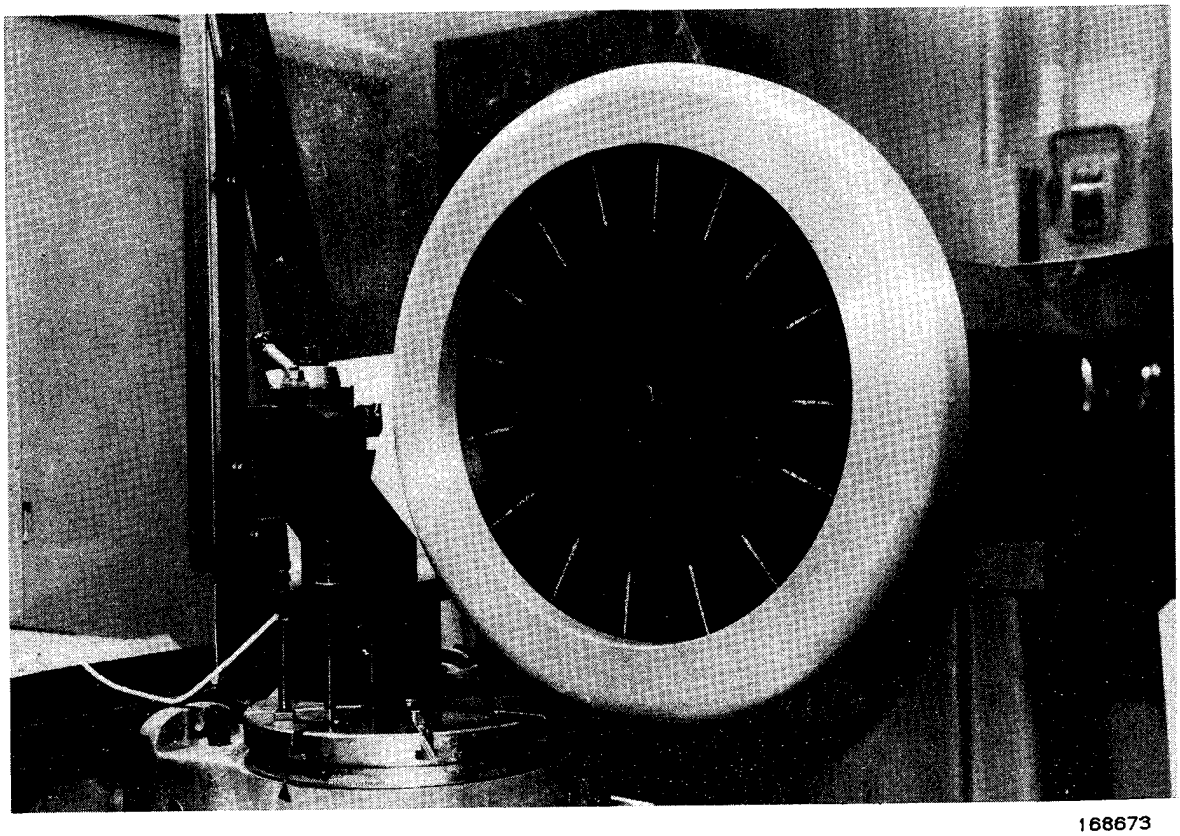
FABRICATION DATA ON FLYWHEEL RIMS MADE OF KEVLAR-49/EPOXY (DER 332/T403)

Rim Number	Yarn (denier)	Winding Tension (g)	Winding Speed (rpm)	Fiber Volume (%)	Resin Volume (%)	Void Volume (%)
1	1420	1800	28	73.0	23.9	3.1
2	4560	6000	37	73.2	23.6	3.2
3	1420	1800	37	73.1	23.6	3.3



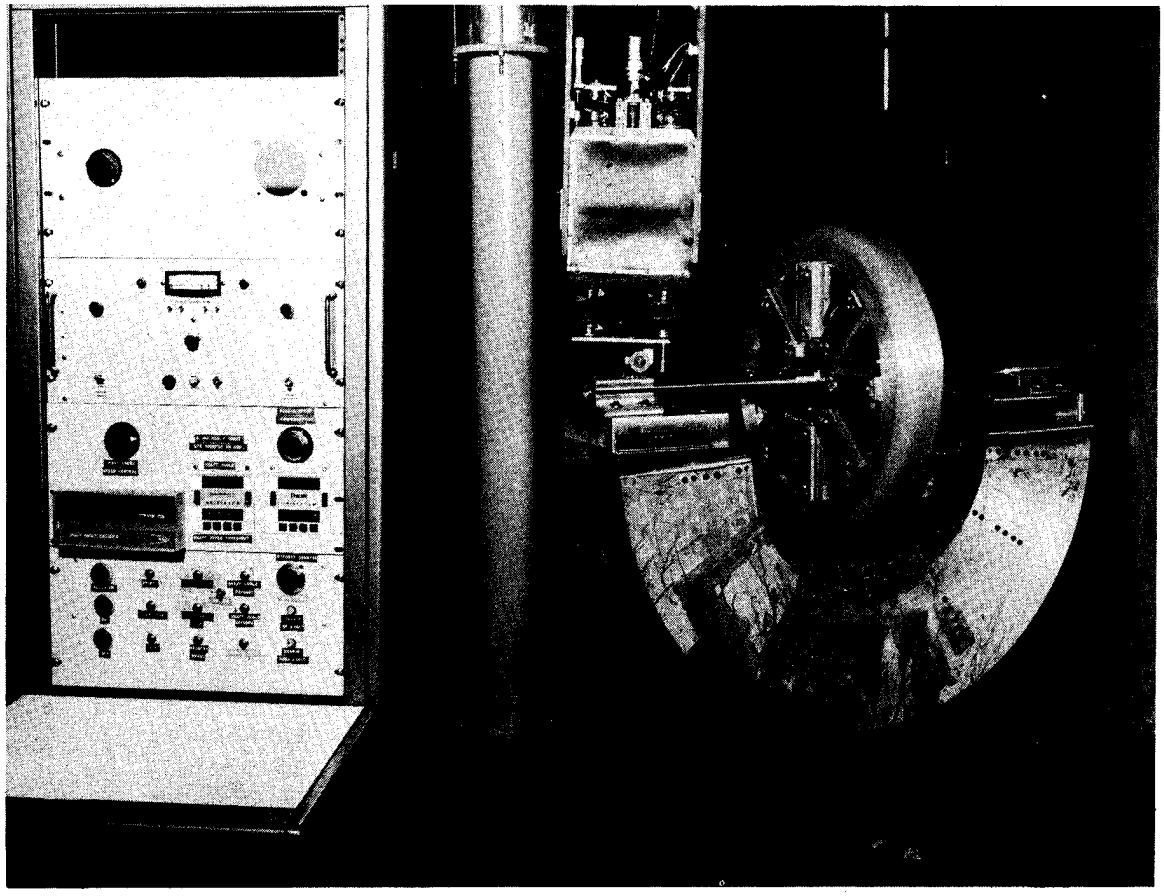
168736

Fig. 15. THE NORMAL AS-CUT KEVLAR-49/EPOXY COMPOSITE SURFACE.



168673

Fig. 16. DIAMOND-KNIFE-MACHINED FLYWHEEL RIM OF KEVLAR-49/EPOXY COMPOSITE.

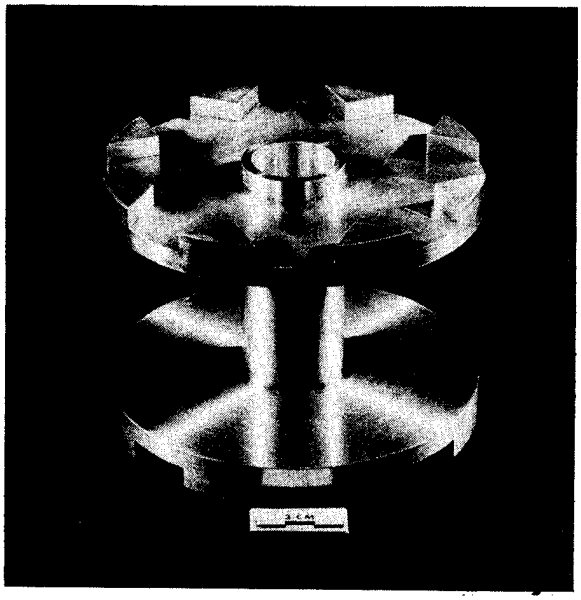


166665

Fig. 17. PLANAR WINDING MACHINE AND FLYWHEEL SETUP FOR WINDING BANDS.

was designed such that the multipiece tooling fitted between the hub and rim, holding the rim in position relative to the hub bore. A machined hub is shown in Fig. 18. The multipiece tooling was manufactured by mounting all the pieces assembled in a set on a face plate, then machining the band slots and inner and outer diameters simultaneously. The set was then match marked so that it could be reassembled in the same relationship. A gap was left between the hub and tooling-set diameters and between the tooling-set and rim diameters, so that shims could be used to adjust the alignment and provide for easier disassembly after the bands were cured.

This first flywheel had the hub and band tooling assembled to the rim with a 0.002-inch TIR on the rim OD and a 0.004-inch TIR on the rim face. The band set was wound with 380-denier Kevlar-49 yarn, and the same epoxy resin used in the rim. The first flywheel data are summarized in Table 6. The finished flywheel after



166734

Fig. 18. MACHINED ALUMINUM HUB WITH LUGS TO MAINTAIN BAND POSITION.

removal of the tooling and readied for spin testing is shown in Fig. 19.

Table 6

PHYSICAL DATA ON THE FIRST FLYWHEEL

	Weights (lb)	Moments of Inertia (in-lb-sec^2)
Rim	21.29	4.256
Bands	1.48	0.150
Hub	1.78	0.019
Total	24.56	4.425

FLYWHEEL TESTING

Spin testing of the composite flywheel entailed adapting an existing test stand to accommodate safe flywheel testing, low speed balancing, and spin testing. The flywheel was radial- and couple-balanced and, subsequently, spin tested to a speed of 18,000 rpm. At this speed, a predicted delamination occurred in the rim; and the flywheel was decelerated and stopped without catastrophic failure. The energy stored was 0.25 kwh, and the energy density was 10.1 Wh/lb at 18,000 rpm. These test results are presented in more detail in a companion paper.[9]

REFERENCES

[1]R. L. Huddleston, J. J. Kelly, and C. E. Knight, Jr; Composite Flywheel Development Completion Report (May 1 - September 30, 1976), Y-2080; Union Carbide Corporation-Nuclear Division, Oak Ridge Y-12 Plant, Oak Ridge, Tennessee; May 11, 1977.

[2]F. B. Seely and J. O. Smith, Advanced Mechanics of Materials; John Wiley & Sons, Incorporated (1966).

[3]R. G. Stone, et.al.; Fiber Composite Program for Flywheel Applications, Second Quarterly Progress Report, UCRL-50033-75; Lawrence Livermore Laboratory; Livermore, California; November 1975.

[4]R. L. Huddleston, J. J. Kelly, and



168760

Fig. 19. FIRST BAND-WRAPPED FLYWHEEL, COMPLETED AND READY FOR SPIN TESTING.

C. E. Knight, Jr; Composite Flywheel Development (October 1 - December 31, 1976), Y-2081; Union Carbide Corporation-Nuclear Division, Oak Ridge Y-12 Plant, Oak Ridge, Tennessee; May 11, 1977.

[5]R. L. Huddleston, J. J. Kelly, and C. E. Knight, Jr; Composite Flywheel Development (January 1 - March 31, 1977), Y-2087; Union Carbide Corporation-Nuclear Division, Oak Ridge Y-12 Plant, Oak Ridge, Tennessee; September 1977.

[6]R. L. Huddleston, J. J. Kelly, and C. E. Knight, Jr; Composite Flywheel Development (April 1 - June 30, 1977), Y-2097; Union Carbide Corporation-Nuclear Division, Oak Ridge Y-12 Plant, Oak Ridge, Tennessee; October 1977.

[7]R. L. Huddleston, J. J. Kelly, and C. E. Knight, Jr; Composite Flywheel Development - Completion Report (October 1, 1976 - September 30, 1977); Union Carbide Corporation-Nuclear Division, Oak Ridge, Y-12 Plant, Oak Ridge, Tennessee; (to be published).

[8]C. E. Knight, Jr., and R. E. Pollard, "Prestressed Thick Flywheel Rims," Proceedings 1977 Flywheel Technology Symposium, October 5-7, 1977, San Francisco, California.

[9]J. J. Kelly, "Spin Test and Evaluation of UCC-ND's Bandwrap Flywheel," Proceedings 1977 Flywheel Technology Symposium, October 5-7, 1977, San Francisco, California.

COMPOSITE FLYWHEEL ROTOR/HUB ATTACHMENT THROUGH ELASTOMERIC INTERLAYERS

Dennis P. McGuire
Lord Corporation
Erie, PA 16512

David W. Rabenhorst
Johns Hopkins University
Applied Physics Laboratory
Laurel, MD 20810

ABSTRACT

An adhesive bonded elastomeric interlayer has been found to be a very effective method for attaching composite flywheel rotors to shafts. Spin tests of quasi-isotropic glass fiber/epoxy discs have shown distinct advantages of this method of hub attachment relative to rigid adhesive bonding or the use of discrete fasteners. Thirteen discs with bonded elastomeric hubs were spin tested to burst. No failures occurred at the rotor/hub interface. Burst speeds were tightly grouped and consistent with values expected based on the ultimate strength of the rotor materials. The effect of the elasticity of the interlayer on the dynamics of the rotor has been considered. In addition to its primary function, the elastomeric hub attachment can be designed to damp resonances, relocate critical speeds, reduce gyroscopic moments, and isolate the flywheel from drive train torsional oscillations. Further development of this concept is planned.

INTRODUCTION

The quasi-isotropic disc is a potentially attractive configuration for low cost/moderate performance flywheel rotors. They can be easily fabricated by laminating multiple plies of a unidirectional fiber reinforced composite at different angles (Figure 1). Since the disc material is not uniformly stressed, only moderate performance levels, in terms of energy storage per unit weight, can be achieved. However, energy storage per unit volume is high, and the quasi-isotropic rotor is easier to balance and analyze than many other configurations.

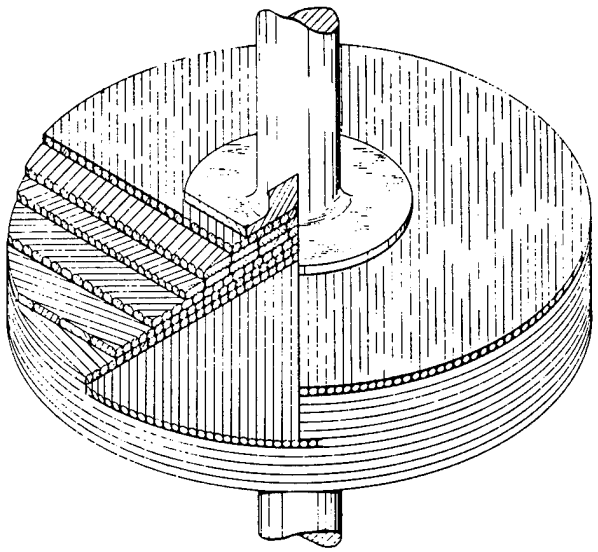


FIGURE 1 Quasi-isotropic Flywheel Rotor

A key factor in the performance of quasi-isotropic rotors is the method used to attach the rotor to the input/output shaft. Stress analysis of a rotating

isotropic disc shows that piercing the disc at its center doubles the maximum stress relative to a solid disc.[1] This is true regardless of how small the hole is made. Consequently, the energy storage capability of the pierced disc is only half that of the solid disc. Therefore, the use of a shaft passing through the flywheel rotor or bolted attachments is obviously undesirable. Adhesive bonding is the simplest and most obvious way to attach a rotor to a shaft without piercing it. This method was used by Dave Rabenhorst in his evaluation of materials and configurations for low cost flywheels.[2] A tapered hub was bonded to the quasi-isotropic disc using a high strength structural epoxy adhesive. This hub, which was about 1/4 of the rotor diameter, was then bolted to the driveshaft. A number of spin tests were performed using this configuration. The results were unsatisfactory. Typically, the bond between the hub and disc failed before the expected burst speed of the disc was reached. The disc then separated from the shaft at a speed much lower than that predicted by the strength of the disc material and was completely destroyed. Attempts to improve the bond by use of different adhesives and bonding procedures were all unsuccessful.

ELASTOMERIC INTERLAYER

To overcome the failures at the hub/disc interface, Lord Corporation proposed that an elastomeric interlayer be bonded between the hub and the disc. The elastomer having a very low shear modulus would minimize the shear stresses ordinarily induced in the epoxy adhesive by the difference in strain levels between the hub and disc. Peeling stresses due to gyroscopic moments could also be reduced.

Calculations indicated that an elastomer layer as thin as .020" would be adequate for these purposes. Thicker sections were actually used to provide favorable effects on the dynamics of the system by influencing critical speeds and introducing additional damping.

Diameter of the interlayer would ordinarily be determined by the required driving torque capability. Since the torque applied during the spin tests is very small, three different diameters were also tested to determine how this parameter might influence performance. A typical quasi-isotropic disc with the bonded elastomeric interlayer attachment is shown in Figure 2.

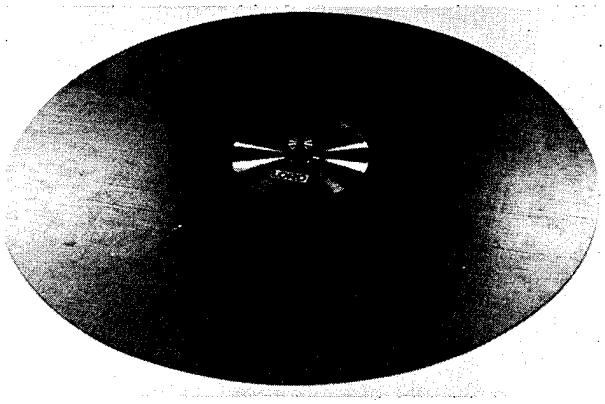


FIGURE 2 Quasi-isotropic Disc Flywheel Rotor With Bonded Elastomeric Hub Attachment

SPIN TEST ROTORS

Thirteen 24" diameter quasi-isotropic rotors with bonded elastomeric interlayers were fabricated for the initial series of spin tests.

The first nine of these consisted of seven plies of unidirectional glass fiber/epoxy prepreg in a 0°-90° cross-ply laminate. Elastomer thicknesses of .063", .125" and .250" were used along with diameters of 1.50", 3.00" and 6.00".

Four additional discs were fabricated using elastomeric interlayers .125" thick and 3.00" in diameter. One of these discs consisted of eight plies in a 0°-45°-90° orientation while the other three were six plies at

0°-60°-120°. All of these samples were fabricated by Lord Corporation and spin tested at the Johns Hopkins University - Applied Physics Lab.

SPIN TEST RESULTS

The initial spin tests using the elastomeric interlayer hub attachment showed dramatic improvement over previous tests. Burst speeds were much higher than previously attained and more repeatable as shown by the results for the 0°-90° cross-ply discs in Table 1.

Table 1. Spin test results for 24-inch diameter 90° cross-ply glass fiber/epoxy discs with bonded elastomeric hub attachment.

Test	Elastomer Diameter (in)	Elastomer Thickness (in)	Burst Speed (RPM)	Energy / Weight (W-hrs/lb)	Energy / Volume (W-hrs/in^3)	Nominal[a] Stress (psi)
1	3.00	.250	22290	15.9	1.04	54443
2	3.00	.125	22840	16.7	1.09	57162
3	3.00	.063	22000	15.5	1.01	53035
4	3.00	.125	22170	15.8	1.02	53858
5	3.00	.063	22680	16.5	1.07	56364
6	1.50	.125	22180	15.8	1.03	53907
7	6.00	.125	22300	15.9	1.04	54491
8	6.00	.125	23110	17.1	1.11	58522
9	1.50	.125	22920	16.8	1.09	57563
Average			22500	16.23	1.055	55483 psi

[a]Based on isotropic disc $S_{max} = \frac{1}{8} \frac{\rho\omega^2}{386.4} (3+\nu)R^2$

The nominal stress at burst and the close grouping of the burst speeds are consistent with the ultimate strength characteristics of the disc material. The mean burst speed corresponds to an energy storage of 16.25 W-hrs./lb. at burst. In all cases, the elastomer/composite bond remained intact (Figure 3).

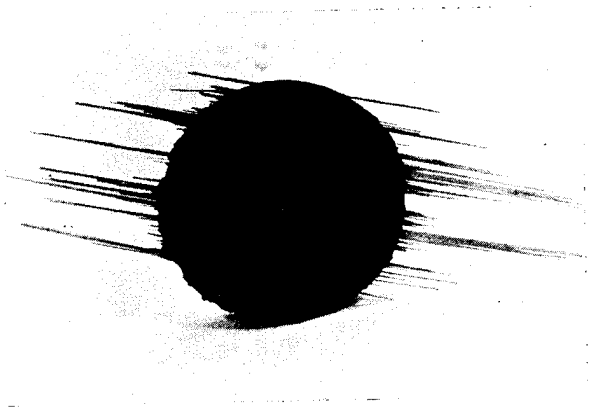


FIGURE 3 Elastomeric Interlayer/ Disc Interface After Spin Test

Neither the diameter or thickness of the elastomer layer appeared to influence the results. This was not particularly surprising since both of these parameters were deliberately made larger than the calculations indicated were necessary. They did however influence the dynamics of the rotor. Tests with the elastomeric interlayers ran much smoother than previous tests with no objectionable vibration. On this basis, the 3" diameter by .125" thick elastomeric interlayer was chosen as the standard for all further testing.

Solution of the hub attachment, problem by means of the bonded elastomeric interlayer, permitted the evaluation of the 0°-±45°-90° and 0°-60°-120° quasi-isotropic discs to proceed. Both of these configurations showed significantly higher energy storage than the 0°-90° cross-ply. The results are summarized in Table 2.

Table 2. Spin test results for 24-inch diameter quasi-isotropic discs with 3-inch diameter by .125 inch thick bonded elastomeric hub attachment.

Test	No. of Plies	Ply Orientation	Burst Speed (RPM)	Energy / Weight (W-hrs/lb)	Energy / Volume (W-hrs/lb^3)	Nominal Stress (psi)
10	8	0°-+45°-90°	24890	19.9	1.29	67884
11	6	0°-$\overline{60}$°-120°	26120	21.9	1.42	74760
12	6	0°-60°-120°	25490	20.8	1.35	71197

The 0°-60°-120° ply orientation gave the best results. Energy storage was 30% greater than the 0°-90° cross-ply discs.

An additional test was performed to empirically determine the effect which a small central hole would have on the energy storage capability of the quasi-isotropic disc. A .25-inch diameter hole was drilled in the center of a 0°-60°-120° disc after bonding of the elastomeric hub. This disc burst at a speed of 18,510 RPM with an energy storage of 11.0 W-hrs./lb. This value is 51% of the average for the unpierced discs and is consistent with the closed form solution for an isotropic disc with a hole.

Evaluation of the quasi-isotropic disc will continue with emphasis on evaluation of materials. Kevlar/epoxy, graphite/epoxy, and birch plywood discs have already been fabricated and prepared for testing.

ADVANTAGES OF THE ELASTOMERIC INTERLAYER HUB ATTACHMENT

In addition to overcoming the hub attachment problem and allowing quasi-isotropic flywheel rotors to develop their full energy storage capability, a bonded elastomeric interlayer can offer numerous other advantages in flywheel systems. Among these advantages are:

1. The damping inherent in the elastomer can help to control resonances which occur while passing through critical speeds. This effect was quite evident in the spin tests conducted at Johns Hopkins.[2] Tests with the elastomeric interlayer were much smoother than the others. Unlike viscous damping, hysteresis damping provides a force which is proportional to amplitude but not frequency. The equivalent damping factor is high at low speeds where resonances can occur but much smaller at the operating speed.

2. The stiffness characteristics of the elastomeric layer can be designed to favorably influence the critical speeds and modes of the system. Radial and cocking stiffnesses can be tailored for specific applications. Initial analysis of the rotor dynamics indicates that these characteristics can have a dominant influence on the system.[3] The wide variety of elastomers available would allow flexibility in adjusting the dynamic characteristics of a system after it is designed and tested. Modulus and loss factor of the elastomer layer could be readily changed to overcome unexpected problems.

3. The flexibility of the elastomeric layer provides a limited degree of gimballing of the flywheel rotor relative to the shaft. By allowing this motion, the loads on the shaft

and bearings due to gyroscopic moments can be reduced significantly while maintaining control of the flywheel position relative to the shaft. The degree of gimballing provided can be traded off against the time required for the rotor to achieve its new orientation when disturbed. This phenomenon is being investigated further.

4. The torsional stiffness of the elastomer layer about the shaft axis can be tailored to isolate the flywheel from drive train disturbances. Existing technology in elastomeric couplings could be applied to achieve this while maintaining sufficient torque transmission capability.

Thin bonded elastomer layers could also be applied in rim type flywheel configurations at the juncture of the spokes and rim to accommodate differential strains while transmitting the driving torque. Multi-rim flywheels could be fabricated using existing technology developed for laminated elastomeric bearings for helicopter applications. While the bonding and processing techniques developed for the quasi-isotropic discs would be directly applicable. Further discussion of these possibilities is beyond the scope of this paper.

Future work at Lord Corporation on the elastomeric interlayer hub attachment will closely parallel the development of the quasi-istropic rotor. Bonding techniques will be developed as required to evaluate new rotor materials. Scale-up to more practical rotor sizes is also anticipated.

REFERENCES

1. Roark, R. J., "Formulas for Stress and Strain," Fourth Edition McGraw-Hill, 1965, p. 360-361.

2. Rabenhorst, D. W., and Small, T. R., "Composite Flywheel Development Program: Final Report" Johns Hopkins University Applied Physics Lab, April, 1977, p. 42-54.

3. McGuire, D. P. and Gaitens, "Dynamics of a Superflywheel with an Elastomeric Hub" Unpublished Report AS77-008, Lord Corporation, March, 1977.

TENSION-BALANCED SPOKES FOR FIBER-COMPOSITE FLYWHEEL RIMS

Francis C. Younger
William M. Brobeck & Associates
1235 Tenth Street
Berkeley, California 94710

ABSTRACT

The tension-balanced spokes for supporting fiber-reinforced composite rims for flywheels satisfy the general requirements of providing a stable mechanical connection between the flywheel hub and rim. This connection maintains the concentricity and geometric alignment needed for static and dynamic balance and is rigid enough to resist the radial and gyroscopic forces which may be imposed. In addition, the spokes transmit the torque required for high rates of rim acceleration and deceleration. As the flywheel rim dilates under the action of the centrifugal force and the high circumferential tensile stress it produces, continuity will require that the spokes stretch by an amount equal the dilation of the rim in order that rim contact be maintained. Spokes directly attached to a rim will generally require a high radial force to stretch the spokes enough to maintain the contact. However, spokes simply fastened to the fiber-reinforced composite rim would produce an excessive radial force. To avoid this force, the centrifugal loading on the spokes is increased by the addition of weights to their outer ends so as to produce the required stretching without excessive radial loads being transferred to the rim. A spoke using this means of stretching is called a tension-balanced spoke. Preshaping of the spokes is required to avoid bending stresses. This shape has been found by solution of the equations for a force balance on curved elements of the spokes in a centrifugal force field.

INTRODUCTION

The very high strength-to-weight ratio of filament-wound fiber-wound composite materials indicate that such materials are ideally suited for use in high-speed flywheels for kinetic energy storage. The high filament strength and low weight will permit very high rotational speeds for filament-wound rings as the unidirectional filaments are oriented in such a way as to resist the centrifugal loading via hoop tension. However, a practical flywheel must withstand forces other than the centrifugal forces. These other forces are associated with the torque transmitted from the rim to the output shaft, the forces to maintain concentricity and the torque to resist gyroscopic moments. These other forces induce stresses such as shear, flexure and transverse tension, for which the fiber-reinforced composite material may be very weak.

A major problem in designing flywheels with filament-wound rings is to find a suitable means of support for the ring which will permit its dilation due to centrifugal force and at the same time will provide constraint against transverse and axial motion and will resist the torsional loads of acceleration and gyroscopic effects. Numerous means of solving this problem have been proposed. One means presented here involves a unique spoke arrangement which permits dilation of the ring without imposing significant radial forces upon the ring. Although the spokes have adequate elasticity to permit ring dilation, they can still have adequate rigidity to provide dynamic stability to maintain concentricity and to resist gyroscopic and acceleration torques.

CONCEPT OF TENSION-BALANCED SPOKES

The tension-balanced spokes for supporting fiber-reinforced composite rims for flywheels is shown in Fig. 1 and combine several basic concepts. The general requirement for flywheel spokes is that they provide a stable mechanical connection

between the flywheel hub and rim to maintain the concentricity and geometric alignment needed for static and dynamic balance and to resist the radial and gyroscopic forces which may be induced by external disturbances. The spokes must also transmit the torque required for high rates of rim acceleration and deceleration.

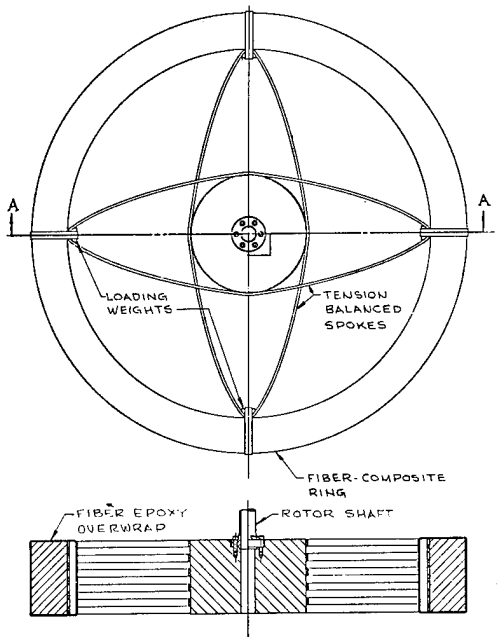


Fig. 1. Tension-balanced Catenary Spoke for Larger Rim.

Spokes for fiber-reinforced composite rims have some special requirements. Because such rims have very little strength to resist the shear and flexure stresses which spokes would normally impose upon rims, the spokes must not impose high radial forces at the point of attachment. Radial loads imposed by the spokes will produce shear and flexure stresses throughout the rim in addition to the local radial stresses at the attachment point. The flywheel rim dilates due to the high circumferential tensile stress produced by centrifugal force. The amount of dilation is dependent upon the circumferential tensile stress and the modulus of elasticity. Continuity requires that the spokes must stretch to maintain contact with the rim by an amount equal to the dilation of the rim. The radial stretch of the spokes is dependent upon the spoke stress and the spoke modulus of elasticity. Consequently, the average spoke stress required for continuity must equal the stress in the rim times the ratio of the modulus of elasticity of the spoke to the modulus for the rim. If the rim and spoke material have the same modulus of elasticity, the average stress in the spoke will equal that in the rim; however, because the centrifugal force on the spoke causes a stress variation along its length, the spoke will have a higher peak stress. If the rim has a higher modulus than the spoke, the stresses in the spoke will be lower. A rim of a fiber-reinforced composite with a high-modulus reinforcing material such as KEVLAR* or graphite could be supported by spokes made from a fiber-reinforced composite of lower modulus material such as E-glass. In these cases, the stress in the spokes would be less than that in the rim by the ratio of modulii.

Spokes directly attached to a rim will generally require a high radial force to stretch the spoke enough to maintain the contact. Fiber-reinforced composite spokes simply fastened to the rim would produce an excessive radial force on the rim. To avoid this force, the centrifugal loading on the spokes is induced by the addition of weights to their outer ends which produce the required stretching without excessive radial loads at the rim attachment. A spoke using this means of stretching is called a tension-balanced spoke. Figure 1 showed a possible arrangement. As shown, the loading on the tension-balanced spoke is due to the centrifugal force along the spoke in addition to the centrifugal force acting on the added weight required for matching the rim dilation. Thus, a variation in tension occurs along the length of the spoke.

In order to carry forces due to the torsional load on the rim without bending moments in the spokes, the spokes must be at some significant angle to the flywheel radii. Consequently, the centrifugal forces acting upon the spokes will have a transverse component, which can be resisted by a pure tension element if it has the correct curvature. The shape of the spokes required for pure tension has been found by a solution of the equations for a force balance on finite elements of the spokes in a centrifugal force field. Figure 2 shows shape and finite element with forces acting on it. The variation in tension along the spokes has also been determined.

*E. I. Du Pont de Nemours & Co. trademark for their poly aramide fiber.

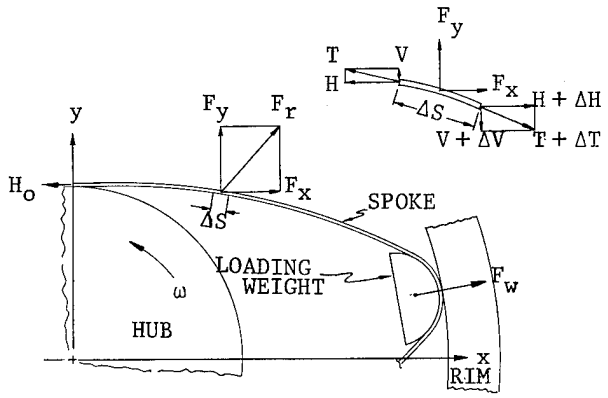


Fig. 2. Polar Catenary Force Diagram

A pure tension element such as a cable would assume the shape of a common catenary if it were supported at its ends and acted upon by a uniform gravitational load. If it is acted upon by a centrifugal force field characterized by a load radiating from a central point with a magnitude varying with the radius, the shape of the curve may be called a "polar catenary." The polar catenary has been examined numerically by finite difference methods. An equation of closed form for the curve has also been developed for a taut spoke.

The tension-balanced spoke should be preshaped to lie along a segment of a polar catenary. The radius of curvature and overall shape of the particular curve for connecting a specific rim and hub has been calculated and a spoke system based on such a curve has been built.

DERIVATION OF SHAPE OF HIGH SPEED SPOKES

Figure 2 shows the forces on an element of a spoke having length Δs along the spoke. The force F_r is the centrifugal force and is directed radially outward from the center of rotation, having a value:

$$F_r = \frac{w}{g} \Delta s \; r \; \omega^2 \qquad (1)$$

where w = spoke weight per unit length, lb/in
g = gravitational constant, in/sec^2
r = radius of element, inches
ω = rotational speed, rad/sec
Δs = incremental length, inches

The centrifugal force components in the x and y directions are as follows:

$$F_x = \frac{w}{g} \Delta s \; x \; \omega^2 \qquad (2)$$

$$F_y = \frac{w}{g} \Delta s \; y \; \omega^2 \qquad (3)$$

From a force balance on an element of length Δs in which the flexure stiffness is ignored, as it should be, the following relationships are found:

$$\Delta H = -F_x = -\left(\frac{w}{g}\omega^2\right) x \; \Delta s \qquad (4)$$

$$\Delta V = -F_y = -\left(\frac{w}{g}\omega^2\right) y \; \Delta s \qquad (5)$$

Letting

$$P = \frac{w}{g}\omega^2 \qquad (6)$$

then in the limit as Δs approaches 0

$$\frac{dH}{ds} = -P \; x \qquad (7)$$

and

$$\frac{dV}{ds} = -P \; y \qquad (8)$$

For completely flexible elements, it can be seen that:

$$\frac{V}{H} = \frac{dy}{dx} \qquad (9)$$

so that

$$\frac{dV}{dx} = \frac{d\left(H\frac{dy}{dx}\right)}{dx} \qquad (10)$$

Differentiating (10) gives:

$$\frac{dV}{dx} = \left(\frac{dH}{dx} \cdot \frac{dy}{dx}\right) + H\frac{d^2y}{dx^2} \qquad (11)$$

Equations 7, 8, and 11 can be solved by finite difference methods starting with initial conditions for T, Y, and dy/dx at x = 0; however, it would be of value to have an analytical solution. An approximate solution is obtained by substituting Δx for Δs. Such a substitution is quite reasonable for shallow curves where Δx is nearly equal to Δs.† Then Eqs. 7 and 8 become:

†Tilting the coordinates so that the x axis more nearly parallels the spoke improves this approximation!

$$\frac{dH}{dx} = -P\,x \qquad (12)$$

$$\frac{dV}{dx} = -P\,y \qquad (13)$$

Substituting (12) and (13) into (11) yields:

$$H\frac{d^2y}{dx^2} - Px\frac{dy}{dx} + Py = 0 \qquad (14)$$

Equation 12 can be solved to give:

$$H = H_o - \tfrac{1}{2}Px^2 \qquad (15)$$

which on substitution in (14) gives:

$$(\frac{2H_o}{P} - x^2)\frac{d^2y}{dx^2} - 2x\frac{dy}{dx} + 2y = 0 \qquad (16)$$

Equation 16 is the differential equation for the shape of a shallow curve of a flexible cord in a centrifugal force field. The equation has variable coefficients and can be solved to yield a power series solution by the method of Frobenius. The details of the solution will not be given here but the reader may make a back substitution to verify the solution. For convenience, a new parameter should be substituted.

$$\text{Let } q = \frac{P}{2H_o} = \frac{w}{2g}\cdot\frac{\omega^2}{H_o} \qquad (17)$$

then the general solution of (16) is:

$$y = C_1(1 - qx^2 - \frac{1}{3}q^2x^4 - \frac{1}{5}q^3x^6 \ldots . \ldots - \frac{1}{2n-1}q^nx^{2n} \ldots .) + C_2x \qquad (18)$$

where C_1 and C_2 are arbitrary constants to satisfy initial conditions.

A closed form for the series can be found using the known series††.

$$\text{Ln}(\frac{1+\beta}{1-\beta}) = 2(\beta + \frac{1}{3}\beta^3 + \frac{1}{5}\beta^5 + \frac{1}{7}\beta^7 \ldots) \qquad (19)$$

From Eq. 19 it can be shown that

$$\frac{\beta}{2}\text{Ln}(\frac{1+\beta}{1-\beta}) = \beta^2 + \frac{\beta^4}{3} + \frac{\beta^6}{5} + \frac{\beta^8}{7} \ldots \qquad (20)$$

Letting

$$\beta = \sqrt{q}\,x \qquad (21)$$

it can be shown that

$$y = C_2\,x + C_1\left[1 - \frac{\sqrt{q}\,x}{2}\text{Ln}\left(\frac{1+\sqrt{q}\,x}{1-\sqrt{q}\,x}\right)\right] \qquad (22)$$

For the initial value problem, the value of C_1 and C_2 can be shown from (18) to give:

$$C_1 = y \text{ at } x = 0$$
$$C_2 = \frac{dy}{dx} \text{ at } x = 0 \qquad (23)$$

DERIVATION OF STIFFNESS OF SPOKE

The spoke stiffness of the flywheel must be high enough to maintain the concentricity of the rim and hub when they are acted upon by a dynamic disturbance. This requires a high stiffness to insure that the natural frequency of the hub to rim vibration be significantly higher than the flywheel rotational speed. The relationship for this frequency is a well-known function of the masses and spring constant.

The stiffening of the spoke due to the transverse component of centrifugal force can be approximated with reasonable accuracy for the shallow curve by considering the transverse load per unit length as a constant and by treating the curve as a segment of a circle. Let the transverse force per unit length equal:

$$\frac{F}{\Delta L} = \frac{\omega}{g}\,y\,\omega^2 \qquad (24)$$

where y is the average transverse offset of the curve. Consider the curved spoke in Fig. 3 as a segment of a circle. The length is as follows:

$$L = 2\,\alpha\,R \qquad (25)$$

The tension required to support the transverse load is found from a force balance to be:

$$T = \frac{m\,y\,\omega^2\,L}{2\,\alpha} \qquad (26)$$

But

$$2\,\alpha = L/R \qquad (27)$$

So that

$$T = m\,y\,\omega^2\,R \qquad (28)$$

††Marks Handbook, 4th Edition, Page 160.

Differentiating gives

$$\Delta T = m\, y\, \omega^2\, \Delta R \qquad (29)$$

The cord length can be shown to be:

$$x = 2R \sin \alpha \qquad (30)$$

Expanding sin α as a series and keeping the first higher order term gives:

$$x = 2R\left(\alpha - \frac{\alpha^3}{6}\right) \qquad (31)$$

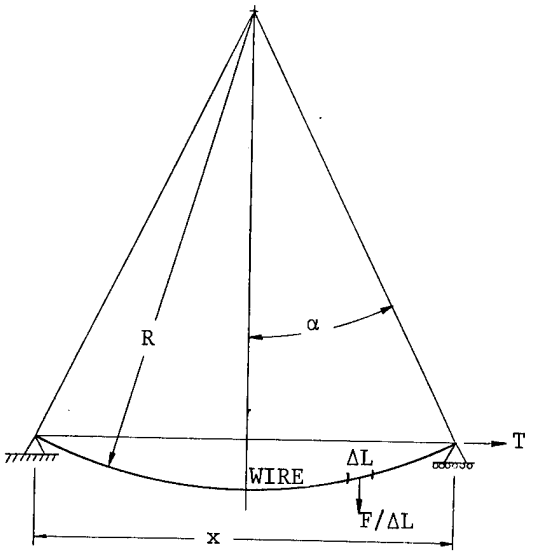


Fig. 3. Taut Wire with End Tension, T.

Thus,

$$L - x = \frac{R}{3}\alpha^3 \qquad (32)$$

Substituting and simplifying gives:

$$x = L\left(1 - \frac{\alpha^2}{6}\right) \qquad (33)$$

Since L is a constant,

$$\Delta x = \frac{-L\alpha}{3}\, \Delta\alpha \qquad (34)$$

$$\Delta\alpha = \frac{-L}{2R^2}\, \Delta R \qquad (35)$$

$$\Delta R = \frac{6}{4}\frac{\Delta x}{\alpha^3} \qquad (36)$$

Substituting gives:

$$\Delta T = m\, y\, \omega^2 \left(\frac{3}{2}\frac{\Delta x}{\alpha^3}\right) \qquad (37)$$

Then the effective spring constant:

$$k = \frac{\Delta T}{\Delta x} = \frac{3}{2}\frac{m\, y\, \omega^2}{\alpha^3} \qquad (38)$$

But

$$\alpha^2 = 6\,\frac{(L - x)}{L} \qquad (39)$$

Therefore,

$$k = \frac{3}{2}\,\frac{m\, y\, \omega^2}{\left(6\,\frac{(L - x)}{L}\right)^{3/2}} \qquad (40)$$

The spring constant increases with the square of the rotational speed, and inversely with the 3/2 power of the difference between arc length and the cord length. The spring constant also increases with the mass per unit length.

Calculations using finite step integrations for tension, shape, and path length have been used to check the validity of the above equation for the very shallow curved shape being considered for the spoke. These calculations show that the approximation is very good.

TEST OF TENSION-BALANCED SPOKES

A flywheel shown in Fig. 4 was assembled and tested to evaluate the tension-balanced spoke concept. The spokes for this flywheel were made from S-glass/epoxy prepreg which was filament-wound and cured on a curved form to produce the theoretical shape of a "polar catenary." Figure 5 shows a finished spoke unit of the type which was used to connect a 30-inch diameter fiberglass/epoxy ring to an 8-inch diameter aluminum hub. Two of these units were used to assemble the flywheel shown in Fig. 6. At the point where the spokes were bonded to the rim, a steel loading weight was installed to produce the centrifugal loading necessary to balance the spoke tension and prevent excessive tension in the bond at the spoke-to-rim joint. The loading weight and the joint were overwrapped with fiberglass/epoxy and cured. The spokes were bonded with epoxy to the hub with the bond extending over an arc of 19°.

The cured spokes provided adequate rigidity at low speed to maintain good rim centering so that very little vibration was observed in traversing the low speed resonance. Very little runout or oscillation occurred over the speed range of the test. Nothing of an adverse nature was

observed until a speed of 10,000 rpm was reached at which point the flywheel abruptly failed. The rim dropped to the bottom of the tank where it continued to rotate until stopped by friction. The hub broke loose from the support shaft and dropped to the bottom of the tank where it also rotated until stopped by friction.

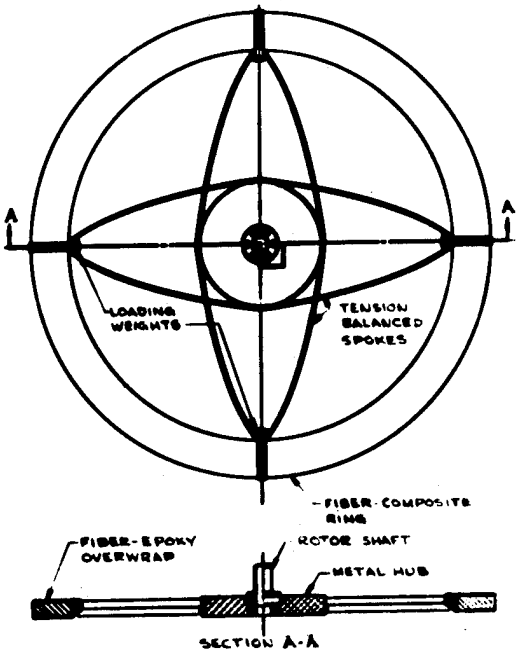


Fig. 4. Single Ring Using Tension-Balanced Catenary Spokes.



Fig. 5. Polar Catenary Spoke for Test Flywheel.



Fig. 6. Assembled Flywheel with Tension-Balanced Spokes.

On inspection after the test tank was opened, it appeared that the loading weights had been flung to the sides of the tank where they struck with high velocity causing dents in the tank wall and extensive deformation of the weights themselves. It seems probable that the centrifugal force on the weights, which was 3,000 lbs at 10,000 rpm, caused excessive bearing compressive stress in the spokes at the attachment point and that a failure of the spokes at this point resulted from this transverse loading. A larger radius of curvature for the loading weight appears to be necessary in order to keep the bearing stress within allowable limits.

CONCLUSION

The test results appear to validate the general nature of the design while uncovering a deficiency in its execution. Dynamic stability was maintained at speeds greatly in excess of the first critical frequency indicating that adequate rigidity had been achieved. Moreover, a radial dilation of about .090 inches due to the tensile stress induced by centrifugal force had been accommodated. The failure which occurred appeared to be the result of an inadequate load bearing area for the spoke-tension induction weights. There appears to be nothing to prevent the bearing area from being increased to such a point as required for an acceptable bearing stress.

ACKNOWLEDGMENT

This work was carried out under contract to the Electric Power Research Institute.

"THE PRESTRESSED LAMINATED FLYWHEEL AND ITS HYDROVAC AMBIENCE"

Robert C. Clerk,
20 Whitehill Road,
Glenrothes, Scotland.

ABSTRACT

The prestressed laminated flywheel seeks to retain the advantages of steel, in it low material cost, high specific inertia and low specific bulk, which serve to reduce ancillary weights of gearing and vacuum casings, while also extending the fatigue range and integrity beyond normal practice, so that when considered overall, the specific storage of the operating assemblage in Watt hours, is high.

The cold cross-rolled, low carbon steel sheets are pressformed as cymbal shaped "disc springs", assembled in opposed stacks enclasping the aluminium drive plate and spacer hub, and when pulled up by the tie rod and gripped by the stubshaft radial transfer concavities, thus prestresses in compression the critical central areas of the laminar assemblages. The peripheral nip on the low modulus drive plate ensures low centrifugal stress at the hub driving concentrarions. The Inverted stub-shaft journals counter normal production imbalance, have considerable effect on bearing power loss, noise and life expectancy, and like the support thrust bearing, are hydrostatic. The miniature vacuum/scavenge pump is hydraulic gear-motor driven, the casings are radially pleated to provide a baffled drainage sump, to increase thermal transfer area, and to reduce differential pressure deflection. The vacuum-stripped lubricant has a dissolved Helium residuum.

PREFACE

The history of flywheels and their usage up to 1963 has been embracingly covered in my SAE paper[1] of that year. Until then, higher energy flywheels were forged weld-fabricated or cast, but we would no longer categorise these as high-energy.

Feasibility studies then had shown that the promise of highest energy per pound of flywheel weight lay with light weight filamentary constructions but a large part of this advantage would be lost to the larger and stiffer casing demanded by the greater bulk, and to the higher gear reduction to compensate for the increased speed. Also there appeared at the time to be a seemingly intractable problem at the driving transition between flywheel and supporting shaft; not to mention the cost aspect.

In the circumstances we decided to research ways of utilising the capabilities of steel more efficiently and in doing so conceived the pressed laminar construction with compressive prestress to bring the critical stress areas to an initial state of compression. We also discovered that the fatigue range and integrity of the steel sheets could be advantaged by cold reduction and cold-work forming and that fortuitiously one of the lowest cost grades of steel was most responsive to this treatment.

FLYWHEEL DEVELOPMENT

Based on a long term background of unitary steel flywheels, extending from the war years, development of a laminated flywheel to the prestress theory progressed relatively quickly in the five defined areas :

(a) lamina contouring for optimised prestress gradient compromised to cold press forming and assembly stacking.

(b) application of prestress without unaccounted stress concentrations

(c) transmitting torque to and from the laminations without stress concentration.

(d) stability of the stacked assembly to limiting thickness/diameter ratios related to laminar vibration, gross out-of-balance, precession and journal vibrations

(e) optimising material specifications, production forming and stacking of laminations, and assembly and balancing of complete flywheels.

PRINCIPLES OF CONSTRUCTION

Normally, even a pin-hole at the center of a disc has a quite disproportionate effect on centrifugal stress, worsening progressively with increasing hole diameter. Yet a built-up construction, other than a fully adhesive structure, demands accommodation of at least a thru tie.

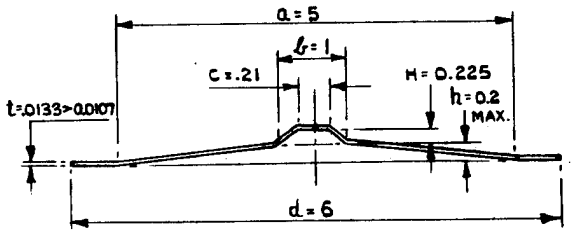
As the centrifugal tensile stress approaching the center of a laminar disc is approximately twice that at the periphery, whereas the deflection stress of an obtuse conical thin disc is highly compressive near the centre, balanced by mild tension at the periphery, at approximately 8:-1 ratio, this forms the basis of our prestress with opposed stacks of conical laminae contra-loaded by a tie-rod of minimum diameter, as Fig. 1.

ACCOMMODATING THE "SPINDLE":

To limit the applied preload, an interstack axial spacer is required, and to distribute the load application demands a concave "collar" matching the external convexity of the two outermost laminae, the "collars" being adapted as stub-shafts for supporting and locating the flywheel and effectively providing a built-up spindle.

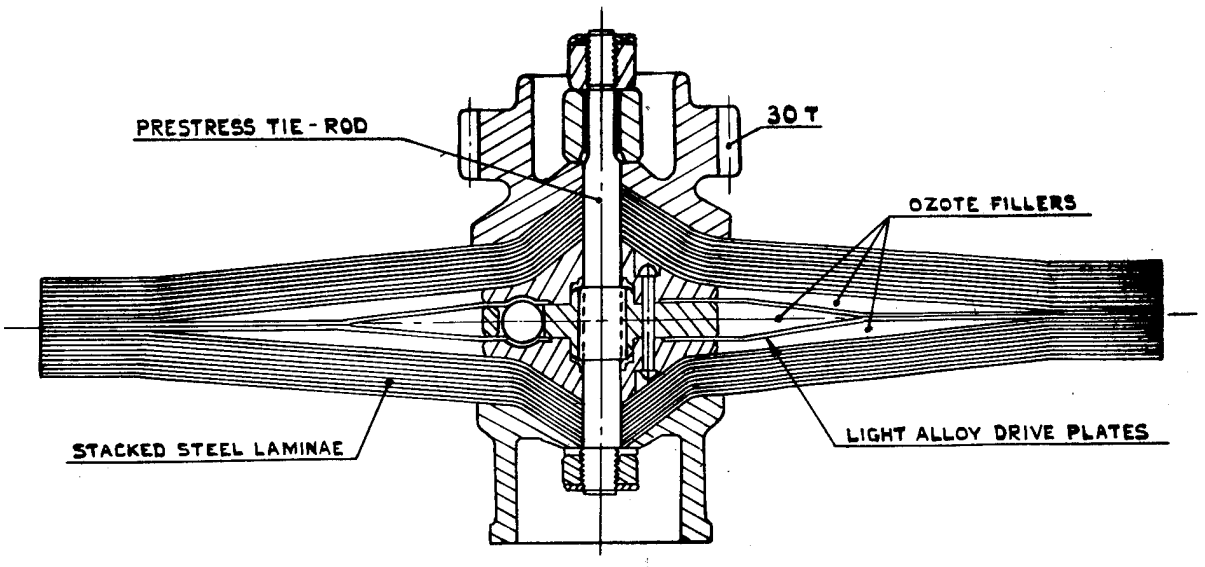
LAMINAR STRESS DISTRIBUTION:

Both to offset the concentration of stress around the central tie-rod hole and to provide positive centering of each stack of laminae, the central area of each lamina is formed to a very much more acute cone angle (ca. 110° incl.) than the obtuse cone angle (ca. 178° incl.) of main area of the disc Fig. 2.



DIMENSIONS OF FORMED LAMINA FOR PRESTRESSED FLYWHEEL

FIG. 2



PRESTRESSED LAMINATED FLYWHEEL

FIG. 1

The tierod-load distributing concavity of each stub-shaft matches the acute conical area of the laminae very closely both in diameter and inclusive angle, as does the double-convexity of the inter-stack spacer, but their inclusive angle is fractionally greater and the spacer is short of the unloaded stacks by a predetermined gap which, when closed by the tie-rod load, limits the compressive prestress of the unclamped inner area to the desired figure. Any centrifugal loading must first neutralise this compression stress before going tensile to a fatigue-safe tensile limit.

The slight angular mismatch of the acute conical clamped area further increases prestress approaching the tie-rod hole and under centrifugal conditions there is considerable shedding of the radial/tangential loads to the reinforced stub-shaft collar such that critical tensile stresses around the hole are alleviated.

TRANSMITTING DRIVE TORQUE

On the face of it, the conical clamping to the stub-shaft should allow transmission of substantial inertia driving torque between the laminae and driving stub, especially if the laminae are appropriately spray bonded during assembly. However, a mathematical analysis shows that such torque transmission is very limited and any initiation of slip could disastrously affect balance and rigidity. Of course, any attempt to positively couple the clamped centres would generate stress concentrations as would negate the prestress inter-relationships.

As the greater inertia of the stacked laminae is effective at the periphery, and as the powerful deflection loading of the opposed stacks also interact at the periphery, by leaving the near-periphery of the laminae flat when press-forming, a driving plate can be securely clutched between the stacks at such a great torque radius that the possibility of slippage is non-existent. But at its centre the driving plate would have to be securely fixed to the clamping spacer which in turn must be torsionally located within the stub-clamped assemblage.

Unfortunately, such a drive plate, if formed from steel sheet would be critically over-stressed at its drive centre. However, an aluminium alloy plate constrained to the same radial centrifugal strain expansion at its periphery as the steel laminae, will due to its very low Young's modulus be subject to a compressive rather than a tensile stress radially inwards of the clutched periphery, this compression reducing inwards to a nodal pitch circle which becomes the effective diameter for centrifugal stressing of the drive plate. This stressing is of course further minimised by the low specific weight of the aluminium alloy, such that liberties may be taken with the stress concentrations engendered by a secure driving connection to the clamping spacer.

At very high centrifugal loadings a single flat light alloy drive plate might be subject to compression buckling inwards of its periphery or radial creep of the clutched periphery, but this can be alleviated either by pressing wave rings around the compression area or by substituting slightly dished twin drive plates of lighter gauge.

The clamping spacer, which has now become a drive hub, must be torsionally located to the driving stub-shaft so that any incidental application of torque in excess of operational limits will not easily cause drive-hub slippage.

LAMINAR STRESSES AND FATIGUE

Actual laminar stress is engendered by the interaction of centrifugal (centripetal) forces with the assembly pre-stress. Fatigue is affected by integration of changes of tensile stress above the limit for infinite fatigue life and the number of times such changes occur. In a non-prestressed flywheel the greatest incidence of fatigue is that due to the flywheel running down to a standstill and subsequently accelerated back to

maximum operational speed. The energy differentials of normal operation will make a much smaller contribution to the total fatigue summation.

In a prestressed laminated flywheel, as the central areas which are subject to the greatest rate of change of stress will only be in fatigue effect when the rotation speed is exceeded beyond which centrifugal forces cancel the compressive prestress and exert themselves in tensile, only the peripheral area is subject to change of tensile stress over the entire speed range down to and upwards from standstill, and this at a low rate of change, unreversed and covering only a portion of the overall tensile stress. Consequently, as a general rule, the run down cycles can be neglected and the fatigue stress taken as effective only in operational differential energy cycling, the mean differential depth of each application determining the prestress necessary to effect fatigue balance between centre and periphery.

It is usual for flywheels to be used operationally in the upper two-thirds of their speed range, so utilising eight-ninths of their energy capacity. But in most applications the cycling mean is only 50% of this, the other 50% being reserved to cater for the less usual incidental demands.

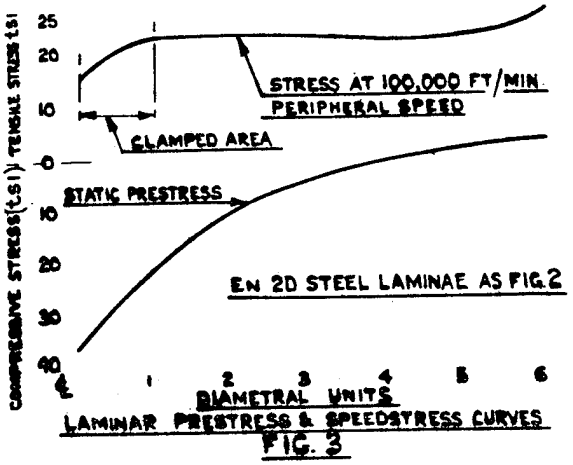
It is generally considered appropriate to stress for infinite fatigue, but there will be applications where advantage can be taken of a low operational cycle count or a short life requirement by using very high tensile alloys (possibly of higher density) despite known deficiency in fatigue limits. However, it has been found that a low-cost low carbon steel (EN 2D/E) cold worked in finish rolling and press forming to around 116,000 lbf/sq.in. effective (125,000 max.) can have a fully reversed fatigue limit of 60,000 lbf/sq.in., better than most of the more costly high alloys and, due to the very low scatter in the formed laminae, safe at ± 47,000 lbf/sq.in.

For higher specific energies at infinite life, high-fatigue stainless steel (FV 520s) laminae can safely be stressed at ± 80,000 lbf/sq.in. equivalent to 16 Watt-hours per pound, as against 9 Wh/lb for the cold worked mild steel. Some later modern steel formulations, which have not yet been assessed at infinite life, offer even higher specific energies; and for finite limited life applications can give up to 50 Wh/lb without excessive drive speeds and with low specific bulk.

STRESS METHOD

For static prestress calculation we neglect the Almen-Laszlo[2] method as, for reasons later discussed, our chosen laminar thickness/diameter ratio will be negligibly minimal; but Hertzer's[3] method is interesting in that it is concerned with the tensile fatigue aspect of the inner concave face resulting from deflection (our prestress), a condition only applying to our laminae at high centrifugal forces.

Although our prestress calculations are simplified by neglect of the stress differential between concave and convex faces of the laminae, they are complicated by the fact that deflection from static height is limited to the gently dished medial area, but the radial/tengential forces generated by deflection (Fig. 3) are accommodated additionally in the flat peripheral and the steemply coned central areas, the latter itself being subject to its own minimal clamped deflection and compressive load, and the former also sometimes being formed with a minimal dish so as to bear flat when subjected to the main deflection load.



LAMINAR PRESTRESS & SPEEDSTRESS CURVES
FIG. 3

DIMENSIONAL RELATIONSHIPS

Figure 2 shows typical dimensional relationships of a lamina, the frustro-conical height (h) being a compromise between the shallow height advisable to prevent tie-rod overstress at maximum laminar stacking and/or maximum laminar thickness (t. max.),and the depth appropriate to ensuring adequate drive-plate peripheral nip and to obviate peripheral wave vibrations at minimum stacking.

PERIPHERAL DYNAMIC VIBRATIONS

A single lamina or an opposed pair of laminae at high rotational speed develop a peripheral wave the amplitude of which increases with rotational speed, decreases with peripheral tension and also decrease inversely as the cube of laminar thickness, as has been shown reference Timoshenko[4], Lamb[5], Southwell[6] and Sandor/Broniarek[7]. The Peripheral pre-tension of conically prestressed laminae therefore has some slight effect in delaying the onset and reducing the amplitude of peripheral vibration, but the effect of multiple stacking not only provides a stiffening inter-reinforcement but more importantly affords inter-laminar frictional damping or viscous-bond shear damping which effectively prevent the wave-form from developing to significant proportions at stacking levels above the currently accepted minimum of nine laminations in each demi-stack.

FLYWHEEL STABILITY

The structural stability of built up assemblies is always open to question, especially where they may be subjected to out-of-balance or elastic vibrations.

The prestressed laminated flywheel assembly owes its structural stability to two quite separate sets of forces, the laminar deflection loads counter-reacting at a large base-circle diameter, and the clamping loads active over the much smaller diameter of the stub-shaft clamping flanges but enjoying a stabilising augmentation from their deep-cone pressure angle.

At very high speeds the tendency towards "flattening" of the laminae reduces the wide-based counter-reactive loads. This is not sufficient to affect the EN 2D laminations seriously but must be taken into account in determining the additional prestress to be applied to FV.520(s) or other highly stressed laminae, especially where the maximum stacking limitation is approached, increasing the cumulative deflection load applied by the centre tie-rod whose stress may become critical unless laminar thickness is reduced.

The conically clamped central area is directly affected by rotational speed only to the extent that the centripetal radial/tangential forces shed from the laminations to the coned stub-flange may strain the flange rim sufficiently to reduce clamping nip at the flange periphery: but again this applies more to high-stress laminations than to EN 2D except at maximum stacking. However, the greater effective length between stub-flanges at maximum stacking affects stability in whirling (radial) deflection much more, varying as the cube of length in relation to the relatively small effective moment of inertia of the central clamped area.

FLYWHEEL FAILURE MODES

Flywheel failure will be due to one of two possible causes, an over-stressed tie-rod or laminar crack propagation. Of these the former is less predictable, in absolute terms, as to the way its effects will act, but the bump/yump axial counterthrust would still maintain an overall hydraulic clamping force on a basically self-centring melange, and the relief of prestress would, at the more critical high speeds, be to some extent offset by centrifugal deflection of the laminae in the same sense as the original prestress.

Laminar failure, other than due to a flawed lamination escaping inspection will always commence with one of the outermost laminae.

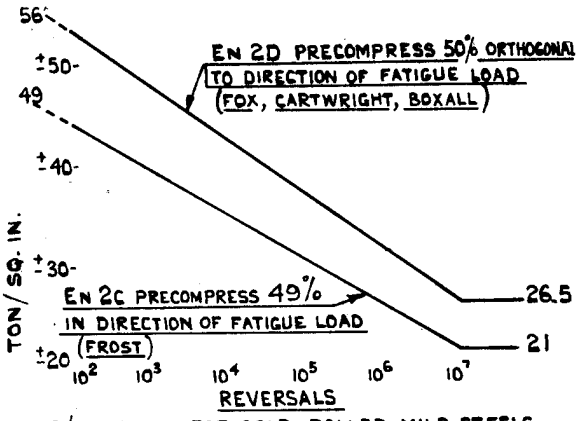
The energy possessed by the largest likely detaching segment would suffice

at worst to puncture the casing without possibility of escaping, but the collapsed vacuum environment would have immediate effect to slow the flywheel rapidly to below sonic peripherical speed, more than halving centripetally induced stresses. The out-of-balance effect on the flywheel would also act to increase retarding drag. As a result the possibility of a catastrophic failure is negligible.

For some applications added assurance may be provided by adopting a higher fatigue material for the outermost laminations of each demi-stack.

MATERIALS AND FORMING METHODS

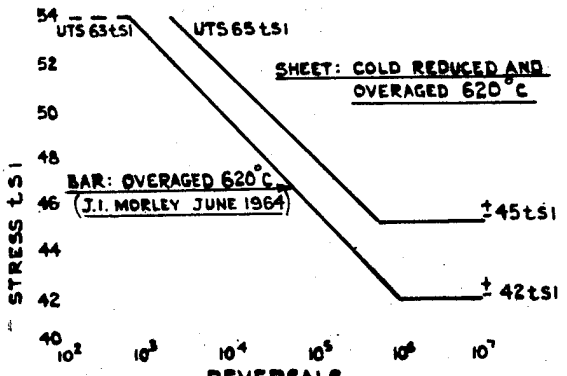
The preferred and most cost-effective material for lamination is EN 2D low-carbon steel work hardened by cold roll finishing in the strip mill to 215 Brinell (100,000 lbf/sq.in) max., cut square and cross rolled in a reversing mill 50% total reduction to gauge size at 240 Brinell (110,000 lbf/sq.in.) max., centre-spot flame softened before blank-holder centre-punch pressed to form raising the near-centre worked area to 250 Brinell (116,000 lbf/sq.in.) max. An upstroking press is preferred as this allows the formed lamina to be slid on to a ball-ended transfer finger contacting only the centre hole so that a striker will produce a true ringing note if the lamina is without flaw. Although not entirely comparable, the fully documented work of Frost shows the very considerable effect of compressive (axial) and torsional cold working prestrain on the fatigue limit of En2C stressed in identical direction to prestrain as shown on Fig. 4. Also shown is the result of later work by Fox, Cartwright and Boxall of British Iron and Steel Research Association, where En2D strip has been rolled/compressed 50% of thickness before stressing in the orthogonal plane, producing a higher fatigue limit and greatly reduced tendency to crack propagation.



S/N CURVES FOR COLD-ROLLED MILD STEELS

FIG.4

For higher energies, Firth-Vickers high fatigue stainless F.V. 520 (S) Steel in the Overaged 620 C condition exhibits the unusual characteristic that the fatigue limit (Fig. 5) coincides with the limit of proportionality and it's unaffected by any reasonable prehistory of excessive transgression, as may occur in the forming process. Although a considerable programme of explosive forming research was undertaken, it was not then practicable to assess possible damage to the fatigue characteristic due to shock, as has since been done for cold worked En2D which has been found to suffer quite severely as had been postulated. F.V.520 (S) is also less critical of the vagaries of powerspin forming than is En2D which latter would therefore appear to be at a lesser advantage for diameters beyond press-forming capability.



S/N CURVES FOR FV 520 HI-FATIGUE STEELS

FIG. 5

FLYWHEEL ANCILLARIES

Likewise, development of the flywheel containment, bearings and other ambient conditions, from that used successfully in earlier forged flywheel applications, was concurrently rethought in six areas which might directly or indirectly affect basic flywheel development :

(a) casings stiffness and casting dies

(b) inner sheet-metal close-shrouding and sump-shield to reduce kinetic losses to lubricant and residual atmosphere

(c) hydraulic powered modular vacuum/ scavenge mini-pump drawing down to low torr

(d) hydrostatic support thrust and inverted journal bearing to minimise bearing vibration losses

(e) input/output drive to the flywheel by gearing "invacuuo" despite the difficult lubrication conditions

(f) a fully hermetic zero-ullage inclusive system permitting expansion of the pressurised "vacuum-stripped" working fluid

An exemplary arrangement of a hydro-kinetic accumulator Fig. 6 provides reference for discussion of these facets which are covered fully in my other paper[9] presented in another session area.

FLYWHEEL COMPONENTS AND ASSEMBLY

As earlier mentioned, the prestressed laminar flywheel is a built-up assembly comprising, apart from the opposed laminar stacks, a drive-plate, centre spacer, stub-shafts and nutted tie-rod. It is sometimes advantageous to fill the inner voids of the flywheel with shaped cellular plastic elements as the air otherwise entrapped during assembly may later leak into the vacuum environment, upsetting the hermetic balance.

DRIVE PLATE(S)

Rather than a single Aluminium alloy plate which can cause problems, we prefer to use twin lighter gauge driving plates, slightly coned and pre-indented for ball-indent drive which has proved far superior to peg-hole drives when subjected to reversing overloads.

CENTRE SPACER

The 3-piece construction adopted to accommodate the ball-indent drive will be no more costly to produce than a one-piece peg-hole drive hub if the shoulder spigots are eliminated by pre-broaching the centre element and by use of a sophisticated assembly jig. Also a Loctite fit of the coaxial convexed elements on the tie-rod spindle makes for a more rigid flywheel assembly.

STUB SHAFTS

Each stub-shaft fulfils four functions. Firstly, the concave flange serves as the external clamping surface locating a laminar stack. Secondly, the stiffened flange periphery accepts the transferred radial component of centripetal forces acting on the laminar stack. Thirdly, the cupped outer end of the stub serves as the rotating outer race of an inverted journal bearing locating the flywheel axis. The fourth function is different for lower and upper stub-shafts, the lower cup-lip supporting the vertical-axis flywheel on a foot-step bearing, whereas the upper stub-cup carries the drive-transmitting gear.

TIE ROD

Splined for torsional location of the drive-hub and stub-shafts, the tie-rod can be very highly stressed in tension as it is not fatigue conscious in this aspect but it must be fully creep resistant.

For very high energies, the F.V. 520(S) laminar stacks will be plain broached at full deflection to a close fit on the tie-rod, as will the clamping members, with liberal use of anaerobic

Loctite at assembly. For some applications the splining may be deleted in a fully adhesive assembly, but the transmitted torque must be strictly limited.

FLYWHEEL BEARINGS

The high running speed, and precession forces due to vehicle movement, did not prove to be the most significant bearing problems; rather those due to excess lubrication and to flywheel out-of-balance effects. The lubrication problem could have been handled by a special high-angle-contact ball footstep bearing combining journal and thrust support, but the out-of-balance precession caused the bearing load to advance around the running clearance of the outer race, whether this was static as in the case of the footstep bearing or rotating at equal speed as was the upper pilot bush in the clutchable bevel-drive pinion, which suffered more when clutched than when running free in a static pinion bush.

INVERTED JOURNALS

At high running speeds the vibration precessions transmute considerable amounts of energy into noise and heat however "perfect" the balance and however close the original running clearance.

A study of the forces involved showed that the out-of-balance precession effect could effectively be nullified if the bearing configuration were inverted; that is, the outer race or bush revolved, with the flywheel, about the fixed journal pin locating the force reactions. A roller journal was ruled out by lubrication problems and a ball bearing generated and transmitted too much noise, even when mounted in resilient sleeves.

HYDRODYNAMIC BEARINGS

Although solving the noise problem, hydro-dynamic journal bearings were subject to shear-drag losses which appeared to be quite intractable even in the inverted configuration with its mildly regressive load angle. There appeared to be no "right" position to introduce the lubricant as the dynamic pressure wedge kept moving around and pumping back with drastic collapse.

RHEODYNAMIC JOURNALS

The application of hydrostatic pressure areas to the static stub "pin" of the inverted journal at least gave predictable and reliable results, with even lower noise transmission. But at efficient "leakage" flows the shear-drag loss was higher than was acceptable for a "total energy" system.

Two avenues of shear reduction were explored. First, as shear drag varied proportionally with differential surface speed, a half-speed floating bush carrying subjoined pressure areas on its outer surface was found to halve the drag. Secondly, boundary land clearances were tailored inversely to the pressure differentials across them and this had a dramatic effect on the shear drag, though with more deterioration of frequency response "stiffness" than would have been acceptable at the highest running speed. However this was easily corrected by retailoring the clearance inverse function.

Eventually both ploys were used in combination to good effect; and even the incorporation of both sets of pressure areas within and without the annular floating sleeve appears to make only a very small and quite acceptable difference to the response definition.

RHEODYNAMIC FOOTSTEP SUPPORT

A flat annular hydrostatic pressure area bounded by inner and outer lands provides a simple and effective supporting thrust bearing, with adequate response to high vehicle bump acceleration but lacking stability in rebound or zero-G yump conditions.

As a counteracting thrust of similar construction acting from above the flywheel unit is impracticable for a number of reasons, a non-dimensional hydraulic thrust equivalent to approximately 50% of flywheel weight is applied to stabilise the down-load during rebound or similar conditions.

FOOTSTEP THRUST WASHER

When the flywheel is going out of service its speed will run down to standstill. But before it runs right down, the footstep thrust supporting pressure will have reduced below the critical minimum for the bearing load, resulting in scored bearing faces. To obviate this a thrust washer is introduced having on one face the annular pocket and boundary lands for the hydrostatic support pressure, and on the other face Glacier DX anti-friction facing material which will provide the running surface at the low-run down speeds. It also has a toothed or vaned periphery which fulfils another function later described.

FLYDRAULIC PARASITIC ENERGY/LOSS.

Until magnetic thrust support and journal location are commercially feasible, flywheel ambience must be effected by a vacuum/scavenge ancillary pump with an energy-loss penalty substantially proportional to the through-flow of bearing effluent. Nevertheless this becomes a secondary priority in comparison with bearing losses related to lubricant through-flow, and even to driving gear lubrication and pump/motor leakage.

Taking first only the flywheel related losses, the ancillary pressure flow required to "lubricate" the hydrostatic bearings and to power the vacuum/scavenge pumping are related to flywheel size and weight and therefore a constant, whereas the bearing shear-drag losses vary with speed, as do the windage losses unless these are maintained low enough to be neglected.

RHEODYNAMIC BEARING LOSSES (SUPPORT)

Fluid film shear losses of rheodynamic thrust support bearings are a function of supported weight, bearing diameter, responsive land ratio, pressure drop and rotation speed. The pressure drop is effectively fixed by the designed level of ancillaries pressure in absolute units (Pabs = 520 p.s.i.a.): the land ratio should depend upon the application vertical acceleration characteristic, but in the interests of standardisation we work at 40%: the bearing diameters are determined, the inner by the journal pin (10% of flywheel diameter; see below) and the outer by the support area at 80% flotation, 1.5 g vertical bump acceleration plus 0.5 Mg counterthrust, giving an area equivalent to 3.75 Mg/Pabs, at a pre-impedenced normal support pressure of 0.5 Pabs for Mg maximum and higher impedences for lower flywheel weights.

Although the speed factor could be taken at the mean of the flywheel 3:1 speed range, the losses are more critical at maximum storage speed, and on the above basis the energy loss from this bearing source will approximate to 0.45% of max. energy.

RHEODYNAMIC BEARING LOSSES (JOURNAL)

The 3-pad journal bearings (one above and one below the flywheel) are determined sizewise by their intercept distance, by the allowable out-of-balance of production flywheels, by the operating speed, and by upset precession forces.

The inverted bearing construction has the internal bore of each cupped flywheel stubs-shaft rotating about a fixed journal pin through the intermediary of a "half-speed" bearing sleeve in which are formed the hydrostatic pad recesses fed by three radial holes in the journal pin, each separately impedenced from the ancillary pressure source.

This system is not ideal as compared with pad recesses formed around the journal pin but is adequate and has production advantages. The "half-speed" sleeve effectively halves the speed related shear drag which is further reducing by increasing the clearances at the inter-pad lands. The combined losses of the upper and lower journals at maximum storage speed approximate to 0.65% of gross energy for shear and leakage, at the present state of development.

VACUUM/SCAVENGE PUMPING LOSS

To scavenge the bearing leakages and to maintain a 10-1 torr vacuum requires 0.35% of gross which added to the bearing losses gives a total of 1.45% of gross energy. Therefore a 10 kWh flywheel would require 0.145 kW to keep it at maximum energy, exclusive of flywheel windage which, by using residual Helium in a cost-effective level of vacuum ambience, appears to be negligible.

FLYWHEEL CASINGS AND ANCILLARIES

The flywheel casings carry the flywheel journal and support bearing and provide an enclosed vacuum environment for the flywheel, a drainage sump for bearing effluent and pump leakage oil awaiting scavenge clearance, a location for the drive gearing, a mounting face for the hydraulic pump/motor, and finally a bottom to the oil reservoir.

THE LOWER (SUMP) CASING:

The relatively large diameter exposes the evacuated casings to a considerable atmospheric pressure loading, necessitating a stiff construction to avoid excessive axial strain deflection. Early casings had radial rib reinforcements but nevertheless were subject to excessive deflection which caused problems. A conical formation with inward projecting deep radial folds has since proved adequately stiff, reduced the internal cone volume, provided anti-surge baffles for any temporarily unscavenged sump drainage, and increased the external direct cooling surface area. This axial pressure/vacuum loading provides a uniformly distributed load at the joint-face requiring only a circlip for its location. The fixed journal bearing pin carrier and the vacuum/scavenge motor/pump modular assembly are separately inserted in the casings, and cast-in galleries service them with input power fluid and scavenge outlet.

UPPER (DRIVE-SIDE) CASING

The upper casing also serves as the bottom of the pressurised oil reservoir and will require to be adequately reinforced against collapse deflection. It carries the flywheel upper-bearing, spigot for the output/input pump/motor, and bearing housings for the drive gearing, symmetrically disposed to accept one or more pump/motor units to allow of greater power output or a multi-plexed circuit.

Cast-in galleries service the flywheel upper bearing and rebound stabiliser, the drive gear bearings, the gear tooth retreating spray, and if required a quill-driven hydraulic speed-signal generator for energy-level indication, duplicating that incorporated in the hydraulic pump/motor.

DRIP AND SURGE SHIELDS

As waste oil from the flywheel upper bearing and the drive gearing coming into contact with the flywheel would acquire kinetic energy and dissipate it as heat to the outer casing, a light-gauge pressed sheet drip shield is incorporated to deflect such waste oil, as well as the pump/motor internal leakage, to the sump scavenge.

Another shield closely surrounds the flywheel periphery and underface and the lower stub-shaft to protect against surge of any unscavenged oil temporarily resident in the sump, despite the sump baffles. It also shrouds the scavenge primer intake.

VACUUM SCAVENGE PUMP MODULE

The gear-motor driven vacuum/scavenge/mini-pump withdraws the sump oil and maintains a near absolute vacuum (10^{-1} torr) returning the extravasation to the hermetically pressurised oil reservoir. It is of the root-supercharged helical gear type, centrifugally primed by the vaned thrust bearing washer, and is combined with the gear-motor as a replaceable modular insert communicating with the ancillary pressure supply and reservoir return galleries in the flywheel casing.

WORKING FLUID

The advisability of using a vacuum-stripped oil has been mentioned earlier, for reasons by now apparent.

However other aspects of the oil specification benefit from the fully hermetic system with no requirement for additives directed to anti-foaming, anti-oxidation, anti-acid, anti-sludging, anti-thermal cracking and other "antis", but a measure of dissolved Helium and constancy of viscosity index between say - 20° to + 70° Centrigrade, approximating to 45 micro-reyns at 60°C. The residual Helium allows of a cost-effective level of vacuum (ca 10^{-1} torr) without fear of Hydrogen embrittlement.

FLYWHEEL/PUMP CONNECTING DRIVE

Early Flydraulic accumulator layouts incorporated a disconnecting drive, as the idle-running drag loss of the best available pump/motor was so excessive that the stored inertia energy would have been quickly dissipated. However, the pump/motor researched and developed over the past eight years has exhibited such an extremely low idle-running drag loss (excluding the proprietary miniature gear pump, temporarily used for priming the controls, which at present trebles the drag loss) that it is now practicable for the pump/motor to be direct connected.

However, "direct connected" to a coaxially disposed pump/motor would mean speed-matching a fairly big flywheel to a rather small pump/motor without alternative unless a planetary drive intervened.

But an offset gear drive offers several important advantages. First a substantial reduction in overall (vertical) height. Secondly, the gearing ratio is easily altered to match any size (or speed) flywheel to any size (or speed) pump/motor. Thirdly, the flywheel stub-shaft gear pinion can drive, not just the one but up to five not necessarily identical pumps separately circuited to power and control a number of individual machines or services from a single energy storage source.

The pump/motor shaft is connected to the driving gear-wheel by a sleeve quill so that the pump shaft can bend quite freely without affecting the drive gearing.

Gear lubrication is by cooling jets spraying the gear teeth immediately post-engagement, except for very high peripheral speeds at high power throughout, when near total fling may necessitate a finely atomised spray of lubricant to the pre-engagement faces, proportioned to pump/motor pressure, as there will be no floating oil mist in the vacuum environment.

FLYWHEEL ENERGY CAPACITY

In any application of the flywheel, possibly the prime determinant will be energy capacity to be provided. Almost certainly, there will be limitations in one or more directions prescribed by manufacturing, assembly, power transmission, installation, servicing, life expectancy or for a dozen other reasons.

FLYWHEEL SIZE DETERMINATION

Usually, the cyclic energy differential of a dynamic system divided by the power transmission efficiency plus a percentage reserve according to application establishes the energy capacity. Thus in the case of a motor vehicle the cycle to be considered is acceleration to maximum or operational speed and subsequent retardation to standstill; the efficiency say 90%; and to cater for the vehicle potential energy gained or lost up and down hills and inclines, say 100% reserve; these totalled must be equated to 8/9ths of flywheel energy capacity as the flywheel is operated exclusively in the upper two-thirds of its speed range. Installation confines will determine thickness/diameter ratio in association with the power transmission ancillaries.

PRESS-TOOL PRESCRIBED SIZE RANGE:

Press-formed flywheel laminations demand a costly combination press-tool which would suggest a diametrically stepped range of flywheels, each covering a wide energy range by multi-stacking variations, though minimum stacking makes inefficient use of the common components such as drive plates, stub-shafts and casings.

The range tentatively prescribed starts at 18 inches, progressing in 6 inch increments to 48 inches which is the largest diameter presently considered for press-forming.

Beyond this progression would be by 12 inch steps, and forming by power-spinning or explosive forming. Table A provides a guide to flywheel size factors.

Table A. Laminar Flywheel Range - Laminations Formed From Low Carbon Steel

Diam.	Max. Gauge	Weight(lb) 1" Thick	Drive Centre (lb)	R.P.M. Max.	kWh/1" Thick	Centre kWh	Stacked Laminar Thickness
18"	.040"	72	10	21,000	0.575	0.0216	0.75"/3.5"
24"	.056"	128	25	15,750	1.02	0.0384	1.0"/5"
30"	.064"	200	45	12,600	1.60	0.060	1.25"/6.5"
36"	.080"	288	80	10,500	2.3	0.0865	1.5"/7.5"
42"	.092"	392	126	9,000	3.13	0.118	1.75"/9"
48"	.104"	512	187	7,875	4.09	0.154	2"/10"
60"	.128"	800	360	6,300	6.39	0.240	2.5"/12.5"
72"	.160"	1152	645	5,250	9.2	0.345	3"/15"
84"	.192"	1568	1030	4,500	12.5	0.47	3.5"/17.5"
96"	.212"	2048	1525	3,940	16.4	0.628	4"/20"
108"	.232"	2592	2100	3,500	20.7	0.79	4.5"/22.5"
120"	.252"	3200	2820	3,150	25.6	0.96	5"/25"
144"	.324"	4408	4815	2,625	36.8	1.38	6"/30"
168"	.375"	6272	8000	2,250	50.0	1.88	7"/35"
197"	.433"	8630	11000	1,920	69.0	2.59	8.2"/41"

NB Gross Weight of Accumulator Assy. (less Pump & Oil) = Weight of Flywheel + 25 Laminae (Cast Iron Casings) or + 10 Laminae (Al. Alloy Casings).

FV 520(s) Laminations will run 35% Faster and Store 82% More Energy

FLYWHEEL APPLICATIONS

The prime application envisaged for this project has always been related to vehicle propulsion systems, although this has not prevented us from studying other application areas, some in quite considerable detail.

Even before our earlier work on the Gyreacta flywheel/mechanical transmission, our 1949 studies showed that the optimum flywheel power transmission should be hydraulic, except that we could nowhere find a suitable pump/motor complementary in characteristics to the flywheel. Consequent to the 1963 SAE paper, market research showed the need for a high energy hydraulic accumulator but we still could not find a pump/motor with performance and control characteristics remotely approaching the flywheel requirement.

Further market research in 1968 showed that a successful hydrostatic automotive transmission would demand a pump/motor and control system very similar in overall characteristic to that for the high-energy accumulator; so fundamental study, research and development programmes were instituted the results of which are chronicled in a paper[10] presented in another session of this symposium.

The union of the developed pump/motor and the laminated flywheel as a high-energy accumulator is covered in session paper[9] earlier mentioned and illustrated as Fig. 6.

References

1. R.C. Clerk, "The Utilization of Flywheel Energy," S.A.E. Paper No. 711A, Toronto, 1963.

2. J.O. Almen and Laszlo, "The Uniform Section Disc Spring," Transactions of the A.S.M.E., 58th year, pp.305-314.

3. K.H. Hertzer, "Fatigue Strength and the Setting of Disc Springs," paper read at the Brunswick Technical University, 1959.

4. S. Timoshenko, "Vibration Problems in Engineering," Second Edition, p.440.

5. H. Lamb and R.V. Southwell, "The Vibrations of a Spinning Disk," Proc. R.S.A., Vol.99(1921), pp 272-280.

6. R.V. Southwell, "On the Free Transverse Vibrations of a Uniform Circular Disk Clamped at the Center," Proc. R.S.A., Vol. 101(1922), pp. 133-153.

7. Drs. G.N. Sandor and C.A. Broniarek (R.P.I., Troy, N.Y.). "Nonlinear Vibration of Four-Wheel Surface Vehicle with Flydraulic Driving System" paper for 2nd International Congress on Theory of Machines and Mechanisms, Sept. 1969, Poland; and Journal of Mechanisms.

8. N.E. Frost, "The effect of Cold Work on the Fatigue Properties of Two Steels," National Engineering Laboratory paper.

9. R.C. Clerk, "THE HIGH ENERGY 'FLYDRAULIC' ACCUMULATOR WITH HYDRO-COMPUTER MODULATED OUTPUT" Companion paper presented at 1977 Flywheel Technology Symposium.

10. R.C. Clerk, "Ultra-Wide Speed-Range High-Efficiency Hydraulic Pump/Motor Transmission," Companion paper presented in another session area.

ALPHA-CROSS-PLY COMPOSITE FLYWHEEL DEVELOPMENT

Burton D. Hatch
Corporate Research & Development
General Electric Company

ABSTRACT

The conceptual developments, design, production and test of light-weight, high strength, alpha-cross-ply composite disk flywheels for vehicular applications are discussed. The test results of a 13-inch diameter preliminary wheel are presented. The subsequent design, production and testing of a 30-inch diameter multiple disk flywheel as a production prototype is then presented in greater detail and the stress analyses and preliminary test results are discussed.

(Paper Not Submitted)

PRESTRESSED THICK FLYWHEEL RIMS

C. E. Knight, Jr.
R. E. Pollard
Union Carbide Corporation-Nuclear Division
P. O. Box Y
Bldg. 9998, MS-1
Oak Ridge, TN 37830

ABSTRACT

A homogeneous fiber composite flywheel rim has a radial tensile stress distribution when spinning about its axis of cylindrical symmetry. A circ-wound rim is ideally suited to support the very high hoop stresses, but it can only support very low radial tensile stresses. This limits the allowable rim inside-to-outside radius ratio so that the energy stored per unit volume is low. It would be desirable to have relatively thicker rims with no radial tensile stresses at the ultimate design speed for hoop stress failure. The methods for calculating the prestress produced by a given schedule of winding tensions are given. The significant parameters to be controlled in the fabrication process are presented. Some tension schedules for balancing the radial rotational stress in rims of a specific size and material are also presented. Experimental development of prestress conditions in small scale test ring demonstrates the capability to achieve prestress levels that can effectively eliminate radial tensile stress in the composite thick rim. Successful experimental development led to the fabrication of a full scale prestressed flywheel rim and utilization of that rim in the Oak Ridge Y-12 Plant* FY 1977 flywheel test package.

THICK RIM FLYWHEEL ELEMENT

COMPOSITE FABRICATION

Given the properties of fiber composites, the most ideal flywheel form is the thin rim. However, the amount of energy stored in a thin rim is low even though the storage efficiency is high. Therefore, in order to be an effective flywheel, the rim must be relatively thick (i.e., thick enough that the simplifying assumptions on stresses and energy storage and efficiency do not apply).

The rim flywheel element is most naturally fabricated by circ winding with a continuous fiber composite. This type of winding is very simple and reproducible. The highest fiber composite properties are in the hoop direction where they are needed.

FAILURE MODE

Because the rim must be thick to be an effective flywheel element, the transverse properties of the composite also become very important. In the homogeneous spinning rim, there are high hoop tensile stresses and also radial tensile stresses produced. The rim failure is likely to be in the mode that has the highest stress fraction of the respective strengths. The primary objective is to utilize the hoop properties to the fullest. If a radial delamination occurs before hoop failure, then the objective is not met. Based on the longitudinal and transverse properties of a specific composite material, an overall rim radius ratio can be determined which should produce simultaneous radial and hoop failure. Unfortunately, for most of the popular composites, this ratio is too high to form an effective flywheel element. Table 1 shows some of the calculated radius ratios.

THICK RIM DESIGN ALTERNATIVES

Design alternatives must be established if the rim flywheel element is to be used with lower radius ratios than those

---

*Operated by the Union Carbide Corporation's Nuclear Division for the US Department of Energy.

Table 1

MINIMUM RADIUS RATIOS FOR SIMULTANEOUS HOOP AND RADIAL FAILURE IN CIRC-WOUND FLYWHEEL RIMS

Fiber Material[a]	Elastic Modulus(msi) Hoop	Radial	Tensile Strength(ksi) Hoop	Radial	Radius Ratio
Kevlar-49	12.6	0.6	260	1.0	0.91
Kevlar-29	6.5	0.6	260	1.0	0.91
S-glass	6.7	3.3	320	3.0	0.65
E-glass	7.3	2.8	220	3.0	0.62

[a]All composites used DER332/T403 epoxy resin.

shown in Table 1. Some alternatives were conceived when it became apparent that our first test flywheel would fail by delamination, and these are reported in a companion paper at this conference.[1] The alternatives that have received some study are illustrated in Fig. 1. They are deadweight loading of the inside radius, a bimodulus rim of Kevlar-29/Kevlar-49 epoxy composites, nested rims of Kevlar-49/epoxy composite with individual radius ratios of 0.91, and a ten-layer prestressed rim. One of the most significant advantages of the prestressed rim is that the flywheel operates with radial compressive stress, where the other alternatives all have some level of radial tensile stress.

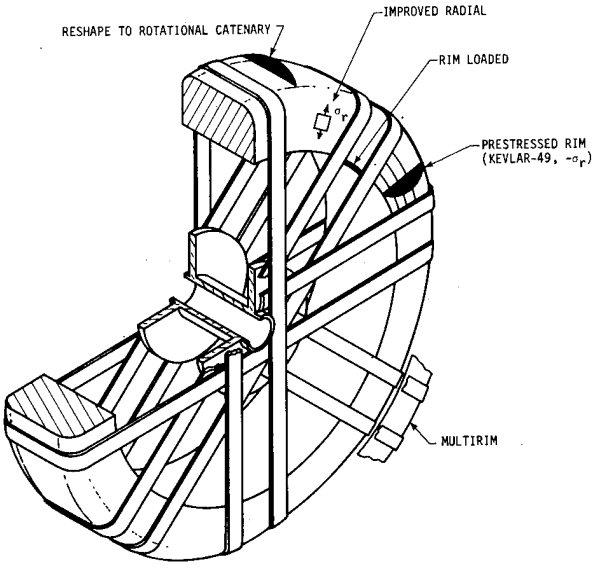


Fig. 1. RIM DESIGN ALTERNATIVES FOR THE BANDWRAP FLYWHEEL.

THEORY OF PRESTRESSED RIMS

The prestressed rim will allow lower radius ratio rims to be utilized in flywheels without premature delamination failure. From a safety standpoint, the delamination failure mode may be desirable if it does not precipitate catastrophic failure. If this mode is desired, then the design may be adjusted to fail by delamination at a suitable margin prior to hoop failure. This may be accomplished by building in the prestress just needed for the flywheel operating speed range.

REQUIRED PRESTRESS DISTRIBUTIONS

The rotational stresses in an orthotropic ring are illustrated in Fig. 2. These curves are for a Kevlar-49/epoxy composite of 0.75 radius ratio. This radius ratio is lower than that in Table 1; and, thus, the homogeneous ring with no prestressing would fail by delamination at a low speed.

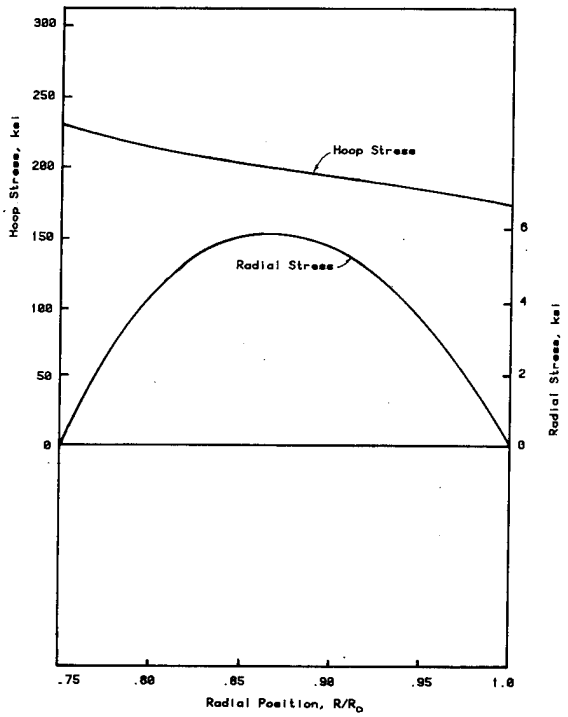


Fig. 2. ROTATION STRESSES IN AN ORTHOTROPIC RING CONSTRUCTED OF KEVLAR-49/EPOXY COMPOSITE.

The amount of prestress needed is that which balances the radial tensile stress at the desired rotation speed. If the desired speed is the point of hoop failure, then the magnitude is equal to the radial stress minus the radial tensile strength. At this level, there is simultaneous radial and hoop failure. The prestress needed to produce this condition in the ring of Fig. 2 is shown in Fig. 3. Also notice that the hoop stress distribution is not leveled but is reversed with the highest hoop stresses on the outer radius.

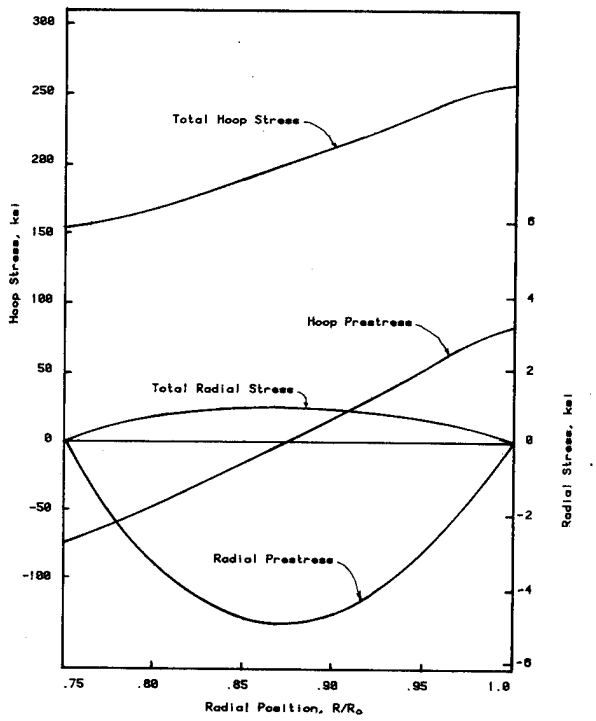


Fig. 3. IDEAL RADIAL PRESTRESS AND THE RESULTING TOTAL RADIAL AND HOOP STRESS DISTRIBUTIONS.

PRESTRESSING METHOD

A prestress distribution in a multi-region cylindrical pressure vessel is normally accomplished by interference-fit assembling of a set of thin cylinders, with the magnitude of interference for each cylinder determining the final pre-stress distribution. This approach would be difficult to carry out in practice with Kevlar-49/epoxy cylinders.

The most direct control on prestress in fiber composites is through variation of winding tension. A theory for residual stress control or elimination by programmed winding tension was presented by Liu and Chamis.[2] This theory assumed that the residual stresses were directly a result of winding tension alone and neglected other variables. In the normal filament-winding process, the other variables such as resin shrinkage, resin flow, and ortho-tropic thermal stresses usually dominate the generation of residual stresses. Furthermore, a significant portion of the winding tension is relaxed almost imme-diately upon application to the winding surface. Based on these facts, the theory could be applied if the ring was built up by winding and curing thin layers and using a winding tension that would result in the correct retained tension in each cured layer. The equations given by Liu and Chamis for the final stress state after cure and removal from the mandrel are:

$$\sigma_r = \frac{2sb^{2s}c^{s-1}\,f(b)}{c^{2s}-b^{2s}}\left[\left(\frac{c}{r}\right)^{s+1} - \left(\frac{r}{c}\right)^{s-1}\right] - b^{s-1}\left[\alpha\left(\frac{b}{r}\right)^{s+1} + \beta\left(\frac{r}{b}\right)^{s-1}\right] f(r), \text{ and} \quad (1)$$

$$\sigma_\theta = T(r) - \frac{2s^2b^{2s}c^{s-1}\,f(b)}{c^{2s}-b^{2s}}\left[\left(\frac{c}{r}\right)^{s+1} + \left(\frac{r}{c}\right)^{s-1}\right] + sb^{s-1}\left[\alpha\left(\frac{b}{r}\right)^{s+1} - \beta\left(\frac{r}{b}\right)^{s-1}\right] f(r), \quad (2)$$

where:

σ_r represents the radial stress,

σ_θ the hoop stress,

$T(r)$ the winding tension as a function of radius,

E_r the radial modulus of the composite,

E_θ the hoop elastic modulus of the composite,

E_m the elastic modulus of the mandrel material,

a the mandrel inside radius,

b the mandrel outside radius,

c the composite outside radius,

r the radial coordinate,

$\mu_{\theta r}$ the composite Poisson's ratio ($\varepsilon_r/\varepsilon_\theta$ for applied σ_ε), and

μ_m the mandrel Poisson's ratio.

In addition:

$$s = \sqrt{E_\theta/E_r} \quad (3)$$

$$B = \frac{E_\theta}{E_m(b^2-a^2)}\left[(1-\mu_m)b^2+(1+\mu_m)a^2\right], \quad (4)$$

$$\alpha = s - \mu_{\theta r} - B, \quad (5)$$

$$\beta = s + \mu_{\theta r} + B \text{ , and} \qquad (6)$$

$$f(r) = \int_r^c \frac{\rho^s T(\rho) d\rho}{\beta\rho^{2s} + \alpha b^{2s}} \qquad (7)$$

(where ρ represents the radial coordinate variable of integration).

These equations are developed assuming continuous variation of control variables, but they should reasonably approximate the conditions for step wise changes.

Another approach is to solve the simultaneous equations generated by the interference-fit assembly where the interference-fit of each layer is proportional to the retained average hoop tension in the layer. These equations have been used with optimization search methods to calculate parameters for prestressed multi-region high pressure cylindrical vessels in the pressure vessel industry.

EXPERIMENTAL DEVELOPMENT

Although the theory looks well developed and straightforward, it remains to be proven experimentally. As stated before, the prestress produced in a fiber composite ring is a function of several process variables, not just winding tension. The resin flow and shrinkage during cure, orthotropic thermal stresses if a heat curing resin is used, mandrel stiffness, winding speed, and tension relaxation are some of the factors affecting the resultant prestress.

EXPERIMENTAL APPROACH

Rather than develop a theory to account for all these variables, an experimental approach is taken here. This approach establishes the prestress that exists in a wound and cured layer as a function of applied winding tension while trying to hold the other variables reasonably constant. An empirical relationship between applied winding tension and average layer prestress is obtained. This relationship can be used with the theory of Liu and Chamis or with the equations developed for multiregion cylindrical vessels[3] to determine the applied winding tension schedule required for the needed prestress.

APPLIED WINDING TENSION - PRESTRESS RELATIONSHIP

A thin steel mandrel was instrumented with strain gages for measuring the tension relaxation during winding. A test winding was initiated, and mandrel strains were recorded at specific thickness increments. The average hoop tension versus wound thickness is plotted in Fig. 4. The tension change due to resin cure at the final wound thickness is also shown. A series of 6-inch rings, 0.125 inch thick, were wound at five different tension levels. The materials were 380-denier Kevlar-49 yarn and DER 332/T403 (100/43 pbw) epoxy resin, cured at room temperature. The mandrel was a rigid steel disc. The rings were strain gaged and then removed from the mandrel to measure the retained tension. The resulting relation is presented in Fig. 5.

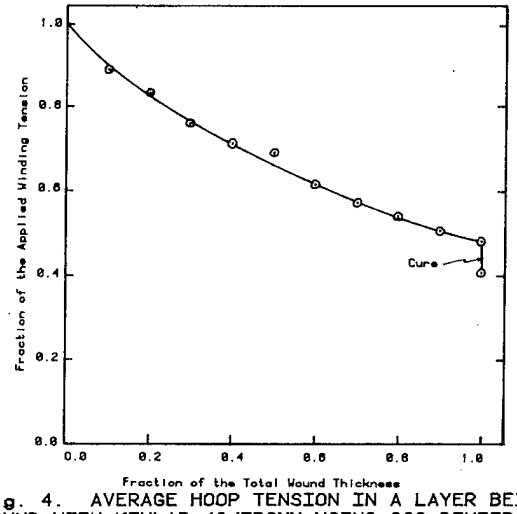


Fig. 4. AVERAGE HOOP TENSION IN A LAYER BEING WOUND WITH KEVLAR-49/EPOXY USING 380 DENIER YARN AT 1000 gm. WINDING TENSION.

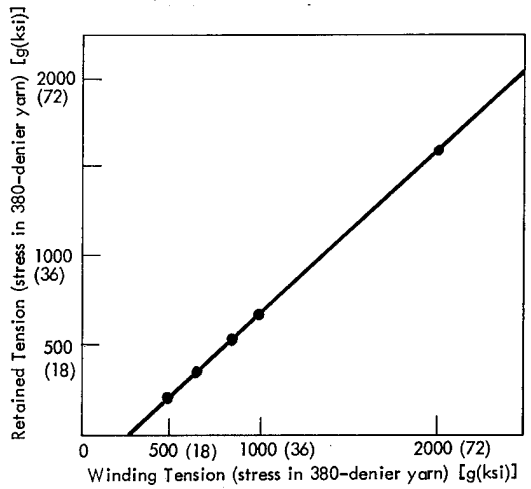


Fig. 5. RELATION BETWEEN THE APPLIED WINDING TENSION AND THE RETAINED TENSION IN WOUND AND CURED THIN RINGS OF KEVLAR-49/EPOXY COMPOSITE.

Several test layers were wound and cured on an instrumented mandrel to check the relation in Fig. 5. Several important factors in processing were discovered in these tests. The cylindrical mandrel needed to be free from edge restraint due to the side plates and yet stay centered in the assembly. This was accomplished by bonding rubber sheeting between the mandrel and side plates. There was also restraint of the composite layer edges because there was some bonding to the side plates even though they were coated with a mold release. This was solved by applying Teflon sheeting to the side plate faces. These factors help assure a uniform prestress across the layer width.

SMALL SCALE TEST RINGS

Three small scale test rings were wound and evaluated. Each ring was 6-inch inside diameter by 8-inch outside diameter and had 10 wound and cured layers. The first two failed by inner layer hoop compressive stress failure when the ring was completed or near completion. The third test ring was satisfactory and established the parameters to be used in a full scale rim fabrication.

The first test ring was wound on a 6-inch steel mandrel that was 0.040 inch thick. The mandrel dimensions and other parameters were used in Eq. (1) to (7), along with a winding tension schedule to determine the predicted prestress conditions.

The mandrel was a steel cylinder (6" OD x 0.040" T). The mandrel was strain gaged on the inside, and the strains were monitored as the layers were wound. Ten layers (each 0.100 inch thick) were wound. A layer was wound and allowed to cure at room temperature before winding the next layer. Strains were monitored when the layer was completed and still wet, and then when it was cured. There was only a slight relaxation during layer curing. The strain increment when a layer is applied and the properties of the composite-plus-mandrel cylinder to which the layer is applied are used to calculate the actual retained tensile stress in the applied layer. The calculation is performed for each layer and the results superimposed to find the resultant prestress distributions.

Table 2 summarizes the calculated-versus-realized parameters in the first test ring. The actual retained tensile stress in the layers deviated significantly from the desired levels. The reason for this deviation is not clear; but it could be due to a variation in the winding tension, variation in the resin viscosity, and/or inaccurate strain gage readings. The control seems to be much more erratic after the mandrel has yielded, which occurred as Layer 5 was applied. This result would seem to indicate inaccurate strain-gage readings due to plastic mandrel strain.

The theoretical-versus-experimental prestress distributions are shown by the graph of Fig. 6. The deviations previously mentioned appear in these distributions. If the strain gage readings are not reliable, then the actual distributions may be closer to the theoretical. The inner layers of the ring experienced a hoop-compressive microbuckling-type failure when the steel mandrel was removed. This

Table 2

PRESTRESS RESULTS IN TEST RIM 1
(380 Denier Kevlar-49 Yarn)

Applied Winding Tension (g)	Retained Layer Stress (ksi)		Layer Inside Radius (in)	Radial Stress (ksi)		Hoop Stress (ksi)	
	Theoretical	Experimental		Theoretical	Experimental	Theoretical	Experimental
275	0	2	3.0	0	0	-66.6	-69.0
600	11	11	3.1	-2.12	-2.23	-54.1	-53.7
925	22	20	3.2	-3.66	-3.83	-38.2	-37.0
1250	33	33	3.3	-4.61	-4.84	-21.2	-15.9
1600	44	41	3.4	-5.00	-5.17	- 3.5	1.2
1925	55	72	3.5	-4.84	-4.98	15.0	46.8
1925	55	50	3.6	-4.17	-3.54	23.2	32.6
1925	55	50	3.7	-3.33	-2.57	30.7	40.3
1925	55	27	3.8	-2.34	-1.43	37.7	20.6
1925	55	36	3.9	-1.23	-0.89	44.6	34.6
			at r = 4.0	0	0	51.3	34.6

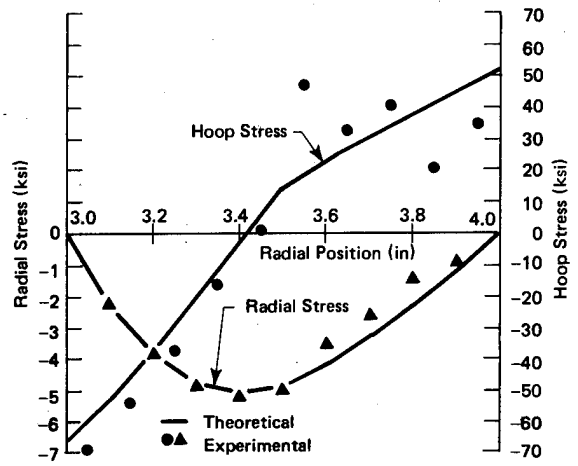


Fig. 6. THEORETICAL VERSUS EXPERIMENTAL RESIDUAL STRESS DISTRIBUTION IN TEST RING 1.

action occurred at a calculated stress level between 65 and 69 ksi. Measurement of the ring inside diameter compared well with the total strain readings, confirming this stress level. Failure of the inner layers prevented a residual stress analysis by incremental material-removal techniques.

By manipulation of parameters in the equations predicting the prestress, it is determined that a lower-stiffness mandrel produces the highest prestress level for a given maximum winding tension. Additionally, the best tension schedule to balance the radial-stress distribution in the 0.75 radius-ratio rim is a linear variation from zero tension in the inner layer to a maximum tension in the outer layer.

A second winding-tension schedule was developed for test and evaluation. Plexiglas was selected for the mandrel material to give a low stiffness as well as provide a linear stress/strain response through the strain range imposed during the test winding. The theoretical schedule limits the inner-layer compressive stress to 50 ksi and produces a maximum radial compressive stress of 4.1 ksi.

Table 3 summarizes the Schedule 2 parameters and gives the results of the test winding. The retained tensile stress in the wound layers, on the average, exceeded the desired levels by 19%. The resultant stress distributions are compared with the theoretical distributions in Fig. 7. The agreement is much better on this test ring, but the excess retained

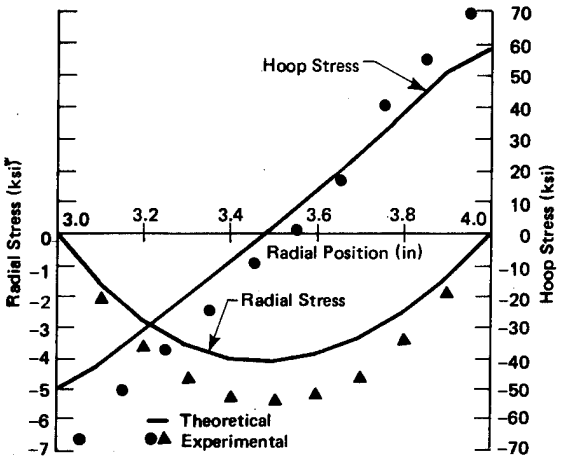


Fig. 7. THEORETICAL VERSUS EXPERIMENTAL RESIDUAL STRESS DISTRIBUTION IN TEST RING 2.

Table 3

PRESTRESS RESULTS IN TEST RIM 2
(380 Denier Kevlar-49 Yarn)

Applied Winding Tension (g)	Retained Layer Stress (ksi)		Layer Inside Radius (in)	Radial Stress (ksi)		Hoop Stress (ksi)	
	Theoretical	Experimental		Theoretical	Experimental	Theoretical	Experimental
250	0	0.7	3.0	0	0	−50.0	−66.2
475	6.5	8.3	3.1	−1.60	−2.14	−42.4	−50.2
650	13.0	14.4	3.2	−2.80	−3.64	−31.6	−37.5
850	19.4	21.4	3.3	−3.59	−4.67	−20.6	−24.3
1040	25.9	30.0	3.4	−4.02	−5.25	− 9.5	− 9.5
1250	32.4	34.8	3.5	−4.11	−5.37	1.7	1.1
1425	38.9	44.0	3.6	−3.87	−5.19	13.2	16.8
1625	45.4	59.5	3.7	−3.34	−4.60	25.2	40.6
1825	51.9	65.4	3.8	−2.51	−3.41	37.6	55.1
2000	58.4	75.0	3.9	−1.40	−1.91	50.7	74.3
			at r = 4.0	0	0	58.1	74.3

tension caused this ring to fail also by an inner-layer-microbuckling compressive failure. The failure occurred while the final layer was curing, and the inner layer stress was 65 ksi compression.

These two test rings demonstrate the capability to achieve prestress levels that can effectively eliminate radial tensile stress on the composite rim. The control as yet is not satisfactory but should improve with additional development.

A third test ring was fabricated and evaluated. The winding tension schedule was scaled down to prevent the hoop compressive failure of the inner layers which occurred in the first two test rings.

The third test ring was successfully fabricated with none of the inner layer compressive failure experienced on the prior rings. The winding tension schedule was scaled to produce a maximum inner layer hoop compressive stress of 35 ksi. However, the retained tensions, based on the strain gage results, again exceeded the expected values. The results calculated from the strain gage measurements during fabrication indicate an inner layer hoop compressive stress of 50 ksi and a maximum radial compressive stress of 4 ksi.

The theoretical and experimental prestress results from test ring No. 3 are shown in Fig. 8 and 9. The negative

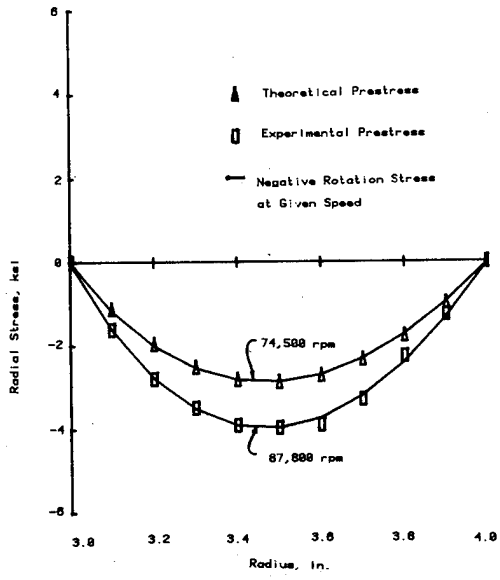


Fig. 8. THEORETICAL AND EXPERIMENTAL RADIAL STRESS DISTRIBUTIONS IN TEST RING 3.

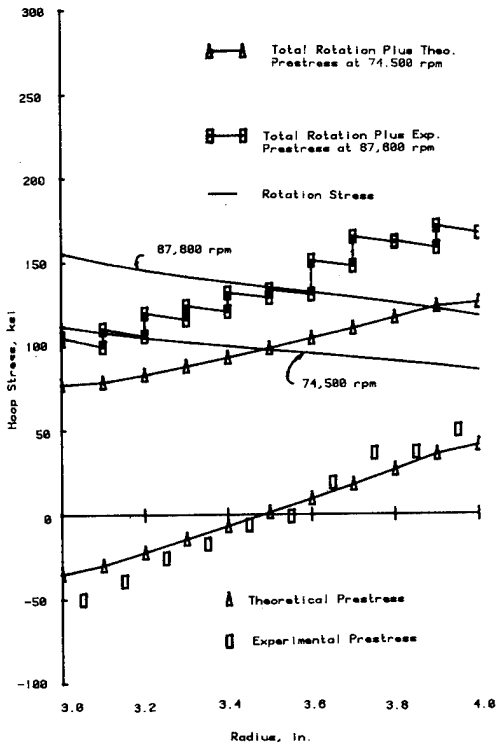


Fig. 9. THEORETICAL AND EXPERIMENTAL HOOP STRESS DISTRIBUTIONS IN TEST RING 3.

of the radial rotation stresses for two different rim speeds is also shown in Fig. 8. The lower speed is the point where the theoretical prestress results in a net zero radial stress. The higher speed is the point where the experimental prestress results in a net zero radial stress. The total hoop stresses (rotation plus prestress) are also shown in Fig. 9 for the same two speeds.

The total theoretical energy stored per unit weight based on the rim weight alone is 31 Wh/lb at 74,500 rpm and 44 Wh/lb at 87,800 rpm for a 6-inch inside diameter by 8-inch outside diameter rim (29,800 rpm and 35,100 rpm respectively for a 15- x 20-inch rim). Even though the failure mode in this case would still be by delamination, it offers a very significant improvement to the Bandwrap design performance.

FULL SCALE RIM FABRICATION

The successful completion of small scale ring No. 3 led to the fabrication of a full scale rim. A Plexiglas mandrel was scaled to the full size rim with the mandrel outside diameter oversized so that the rim inside diameter would be 15.000

inches when completed. A set of test layers were wound onto the mandrel and cured in succession with each layer 0.250 inch thick.

The purpose of this was to check the relation of Fig. 5 for the larger mandrel diameter and yarn denier. Tension levels were 1,900, 3,700, 5,600, and 7,500 grams. The resulting data points are plotted in Fig. 10 and compared with the relation from Fig. 5. Fiber buckling occurred while the first layer was being wound, due to the low mandrel stiffness. That probably caused the first data point to be low. Compressive fracture of the inner layer occurred while the fourth layer was being applied and causes the fourth data point to be invalid. The agreement with the relation of Fig. 5 is not outstanding, but there was not enough time to generate new data and the good data provides a reasonable confirmation of the relation.

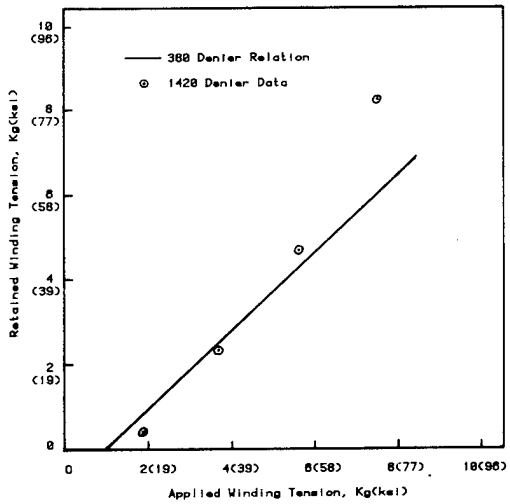


Fig. 10. APPLIED VERSUS RETAINED TENSION DATA FROM A TEST CYLINDER USING 1420 DENIER YARN.

The winding tensile stress schedule used in small scale ring No. 3 was factored down by 15 percent to be conservative and used for the full scale rim winding. The mandrel was 15.042 inches outside diameter by 13.793 inches inside diameter with strain gages mounted on the inside. There was rubber sheeting bonded to the side plates and mandrel, and the side plate faces were covered with Teflon film. The winding progressed smoothly with three layers wound each week.

The prestress condition calculated from the measured strains are plotted in Fig. 11. The calculations are a layer-by-layer determination of the stresses in the

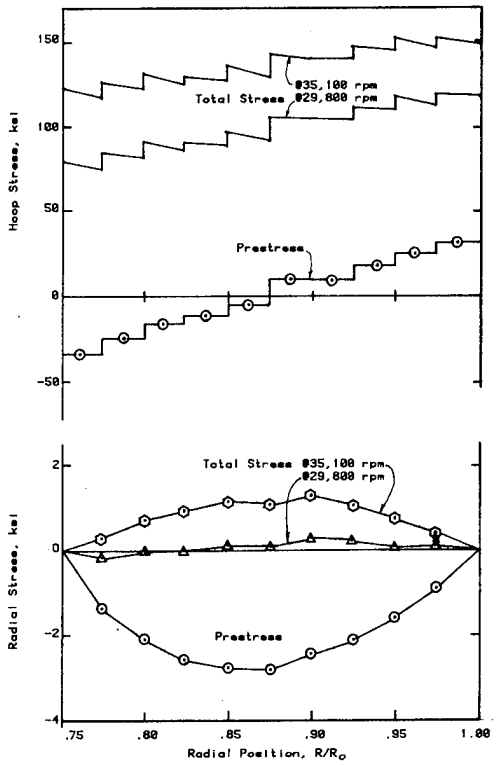


Fig. 11. PRESTRESS AND TOTAL STRESS DISTRIBUTIONS AT TWO SPEEDS IN THE FULL SCALE FLYWHEEL RIM.

existing and applied layers. The equations for the orthotropic ring with internal and external pressure were programmed on a hand calculator, and the data were reduced. The pressure at the mandrel-inner layer interface was calculated from the strain readings and the mandrel material properties. The external pressure on the existing layered ring applied by the new layer is determined from the strains and the average elastic properties of the existing ring. The internal and external pressures on the existing ring yield stresses to superimpose on the stresses already present. The external pressure on the existing ring is used to calculate the tensile stress held in the new layer.

This rim was used to fabricate an improved Bandwrap flywheel for the UCC-ND FY 77 Development Program. The rim was diamond knife machined with radiused outer corners and a rotational catenary-shaped outer contour. The rim was assembled with the band winding fixtures and the bands were wound. The flywheel will be tested late in FY 78.

A performance estimate can be made based on the prestress results in Fig. 11

and the rim rotational stresses. The estimate is that the rim's radial stress will remain compressive up to a speed of 29,800 rpm and that the delamination failure will occur at a speed of 35,100 rpm. This estimate assumes that there is no failure of the bands or hub. The finite element stress analysis indicates this to be a valid assumption. The rim energy density will be 31 watt-hr/lb at 29,800 rpm and 44 watt-hr/lb at 35,100 rpm.

This performance estimate is based on the current prestress condition. Since the flywheel will not be tested for approximately 9 months, there may be some creep and stress relaxation. A sample ring was parted from the as-wound rim for the purpose of doing a residual stress analysis by the incremental material removal method. This ring will be stored with the flywheel until the time of testing. The residual stress analysis done at that time will determine if there has been any significant creep problem. Of course, this problem would need more thorough investigation for deciding the lifetime suitability of prestressed rims in flywheels.

REFERENCES

[1]C. E. Knight, J. J. Kelly, R. L. Huddleston, and R. E. Pollard, "Development of the "Bandwrap" Flywheel," Proceedings 1977 Flywheel Technology Symposium; October 5-7, 1977; San Francisco, California.

[2]Y. Liu and C. C. Chamis, "Residual Stresses in Filament-Wound Laminates and Optimum Programmed Winding Tension," Proceedings, Section 5-D of the 20th Annual Meeting of the Society of the Plastics Industry (1965).

[3]R. L. Huddleston and B. R. Dewey, "Optimization of Elastic, Multilayer Cylindrical Vessels Loaded by Pressure and Radial Thermal Gradient," Journal of Basic Engineering, ASME, pp. 885-892, December 1972.

FLYWHEEL PROPULSION FOR URBAN TRANSIT BUSES

L. J. Lawson
AiResearch Manufacturing Company of California
2525 W. 190th Street, Torrance, California 90509

ABSTRACT

A comprehensive program was initiated in late 1976 by the U. S. Department of Transportation Urban Mass Transportation Administration (UMTA) directed toward the demonstration and ultimate production of energy efficient transit buses which overcome the limitations of present transit vehicles. The results of the initial study phase of this program have shown the viability of four flywheel-propulsion configurations that can match or exceed the performance and route requirements of typical transit properties. These new flywheel drives are: (1) a pure flywheel system; (2) a flywheel/battery hybrid system; (3) a flywheel/diesel engine hybrid system; and (4) a flywheel-augmented trolley coach. One or more of these concepts appears suitable to provide improved propulsion for a wide sector of urban transit operations.

INTRODUCTION

The urban transit bus offers a unique combination of characteristics that make it suitable for the demonstration of new propulsion concepts. In particular, the bus is an excellent candidate for evaluating the energy conservation made possible by the use of regenerative braking. First, buses are heavy vehicles that move at relatively high speeds, resulting in the availability of high values of kinetic energy for recuperation. Second, buses have frequent start-stop operations that increase the opportunities for energy recovery. Also, because of their size, buses are not very sensitive to the volume and weight of the new propulsion systems. In addition, reasonable control can be maintained over buses used for the demonstration of new propulsion concepts because the vehicles are generally operated over predictable routes and can be regularly inspected and serviced in the transit property maintenance facility. Also, the results of the tests and demonstrations of new energy-efficient propulsion systems conducted in transit buses can be extrapolated to a wide range of vehicles from small commuter cars to large trucks and vans.

The impetus for the new demonstration program is the transit industry desire for improved vehicles and the urgent need to reduce energy consumption, particularly petroleum fuel.

Over the past decade, many U.S. transit properties have indicated a need for rubber-tired transit vehicles that could provide clean, quiet, high performance operation like the electric trolley coach, but also offer the route flexibility of the diesel bus. Such vehicles should have the advantages of low maintenance cost and long service life, which are characteristic of electric transit, without the fixed cost and maintenance burden of a continuous energy collection system. In addition to these improvements, the new vehicles could help alleviate the energy shortage because of the improved regenerative braking energy efficiency and the compatibility with electric energy rather than petroleum fuel for propulsion. The most practical means of propelling such a new class of urban transit vehicles is by use of an onboard energy storage system in conjunction with an electric drive.

The multiphase flywheel-propelled transit vehicle program, which is now underway under UMTA sponsorship, is intended to expedite the deployment of new energy storage vehicles in revenue service. This will satisfy the user industry needs and at the same time demonstrate the energy economics of regenerative braking so that the concept can be applied to many vehicle types.

THE UMTA PROGRAM

PROGRAM OUTLINE

The UMTA flywheel-propelled vehicle program is divided logically into the four phases shown below with review points for assessment of technical progress and concept viability and marketability during and at the end of each phase.

Phase I - Design Study

Phase II - Development, Fabrication, and Test

Phase III - In-Service Demonstration

Phase IV - Production

PROGRAM OBJECTIVES

The overall purpose of the UMTA bus program is the demonstration and ultimate production of a new transit vehicle that can provide improved quality transit service while conserving energy, particularly petroleum fuel. The rubber-tired transit vehicle is considered to be important to petroleum fuel conservation because of the increasing scarcity (and cost) of oil. Thus, as more attractive public transit and the fuel shortage cause commuters to abandon their cars, highly efficient transit vehicles that can use electric energy will be available.

FLYWHEELS

The flywheel was selected by UMTA as the primary energy storage device for use in the recovery of braking energy and the enhancement of vehicle acceleration performance. In addition, the flywheel technology to be applied in the program was specified as current state-of-the-art which could be mechanized within one year. Table I is a comparison of battery storage systems, flywheels, and the energy storage required for transit buses. It may be seen from Table I that the present technology flywheel exceeds all transit bus requirements; therefore, it is a logical choice for use in an energy-conservation drive.

TRANSIT VEHICLE REQUIREMENTS

Because the flywheel study is based on the comparison of costs and performance between candidate flywheel-propelled vehicle configurations and standard transit buses, the characteristics of the standard vehicles were established as a basis for comparison.

The approach used in this determination was to analyze user industry data to establish the vehicle type that will have the highest demand over the next 15 years. The data used for this study came from a recent American Public Transit Association (APTA) survey[3]. This data shows the predominance of the 12-m bus demand through the eighties with an estimated average annual demand of 5,000 buses. From this market study, the conclusion was reached that the most significant transit market for application of flywheel-propelled vehicles is as a replacement (or modification) of the standard 12-m bus whether in the diesel bus, trolley coach, or battery bus configuration.

As a result of the APTA survey, the 12-m, 8-cylinder, air-conditioned diesel bus (similar to those now being produced by AM General, Flxible, and General Motors) was used as a baseline for comparative analyses with the new concept flywheel-propelled vehicles. Similarly, the Flyer Model 800, 12-m electric trolley coach with air conditioning (the only such vehicle now being delivered in the western hemisphere) was used as the baseline trolley coach for comparison to the new vehicles.

To compare the performance and costs of 12-m flywheel-propelled transit vehicles with those of a battery bus, it is necessary that the latter be of the same size and passenger capacity. The closest thing available is the West German M.A.N. Elektrobus, which is currently undergoing limited revenue service testing in Dusseldorf and Monchengladbach. The characteristics of a vehicle similar to the M.A.N. bus with the addition of electrically operated air conditioning and heating were assumed for comparison to the new concept vehicles

The required performance from the flywheel-propelled vehicles is expected to at least match that of the baseline vehicles. The top speed of the new vehicles will be the maximum legal speed level (88 km/kr), which is equivalent to that of the diesel bus. The initial acceleration of the flywheel-propelled vehicles will be held to 5.6 km/hr/sec, which is a passenger comfort limit that can be exceeded with the present diesel

bus. The required acceleration to speed with a full-seated load for the flywheel-propelled vehicle will be 10 sec to 48 km, which matches the present trolley coach performance, but exceeds that of the diesel bus. The new-concept vehicles will be required to match the electric braking of the trolley coach (5.6 km/hr/sec), although the new vehicles will use regenerative braking as contrasted to the trolley coach electric braking system that is principally dynamic. Finally, the gradeability of the new-concept vehicles will match the present 20-percent capability of the present diesel bus and trolley coach.

CANDIDATE FLYWHEEL CONFIGURATIONS

As a result of the Phase I study, four flywheel propulsion configurations have been defined. They match the transit user requirements and are suitable for operational performance and life-cycle cost comparisons with the three baseline vehicles. The new-concept propulsion systems are described in the following paragraphs.

PURE FLYWHEEL DRIVE

The optimum configuration of the pure flywheel drive for a 12-m transit vehicle was based on the premise of placing as much flywheel capacity as possible into the vehicle without exceeding the axle load limit while carrying a crush passenger load. The resulting pure flywheel drive system is shown in the block diagram of Fig. 1. This system has a weight of 3450 kg, which is compatible with the axle limit of 17200-kg with a 5,900-kg crush passenger load capability. The optimum pure flywheel system is configured with its 72 MJ steel flywheel and flywheel electrical machine enclosed within a sealed evacuated housing. The operation of the homopolar inductor machine in a vacuum is possible because the machine has a solid rotor (no rotating windings) with only minimal losses. The rejected machine heat from the stator winding and stationary field coil can be conducted out by an oil cooling system that is sealed, but operates out of the vacuum. The cooling lines are located in the laminated iron portions of the stationary structure of the machine. Operation of the flywheel machine within the sealed flywheel enclosure eliminates the need for a rotating shaft seal because energy can be transferred electrically into and out of the housing. The sealed housing can be pumped down to its 6 to 12 Pa vacuum level by an external vacuum pump and then left alone over an inspection interval of 1 to 2 months. The absence of the shaft seal also minimizes spinning losses and reduces the maintenance requirements of the flywheel assembly.

The operation of the pure flywheel system of Fig. 1 is relatively straightforward. Initial charging to base speed is accomplished by a front-end static commutator which provides reduced voltage, variable frequency power to the synchronous

Table 1. Energy Storage Comparison

	Present Lead-Acid Batteries[a]	Flywheels (Present Technology)[b]	Energy Storage Transit Bus Requirements[c]
Energy density	60-110 J/g	50-100 J/g	40 J/g
Power density	25-70 W/kg	220-440 W/kg	170 W/kg
Deep discharge Cycle life	500-1500	$>10^6$	> 250,000 (23-yr service)
Propulsion system Life-cycle-cost/mile (23-yr transit life)	137¢	29¢	44¢ (diesel bus)

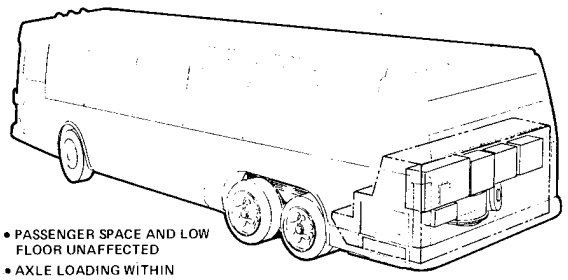
[a] See reference 1 (references are listed at the end of the text).

[b] See reference 2.

[c] Transit bus requirements are based on information obtained from 11 transit properties.

flywheel machine that is then brought up to base flywheel speed. Above base speed, the flywheel machine can provide sufficient voltage to self-commutate the dual converter so the front-end commutator is no longer required. When the flywheel is fully charged, propulsion is accomplished by controlled rectification of the flywheel machine output voltage to provide proper control of voltage applied to the separately excited field-type dc traction motor. This configuration is fully bilateral so that energy from vehicle braking operations can be coupled back to the flywheel by the load-commutated inverter operation of the dual converter and flywheel electrical machine, As shown in Fig. 1, the vehicle hotel loads are provided by rectifying the fixed voltage output of the flywheel machine.

PROPULSION SYSTEM LOCATION IN TRANSBUS (22 IN FLOOR)



- PASSENGER SPACE AND LOW FLOOR UNAFFECTED
- AXLE LOADING WITHIN PRESENT LIMITS
- MIN. STRUCTURAL MODIFICATION
- EASY ACCESS FOR INSPECTION AND MAINTENANCE

Fig. 2. Propulsion system location in low floor bus

PURE FLYWHEEL BUS DRIVE VERSION 2A

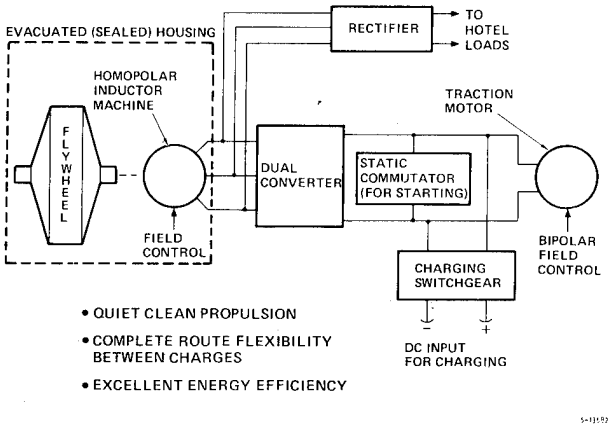


Fig. 1. Pure flywheel bus drive

The pure flywheel propulsion system may be installed in the Flxible 22 in floor Transbus by utilizing the rear engine and transmission compartment space made available by removing the conventional power plant. This space with the pure flywheel drive installed is shown in Fig. 2.

FLYWHEEL BATTERY HYBRID DRIVE

A block diagram of the flywheel/battery hybrid drive system for a 12-m bus is shown in Fig. 3. The operation of this system is the same as the pure flywheel system except that above traction motor base speed (about 32 km/hr), energy can be

FLYWHEEL/BATTERY HYBRID BUS DRIVE VERSION 4A

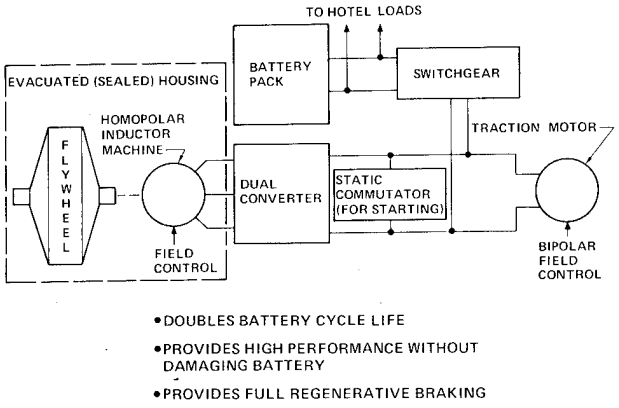


Fig. 3. Flywheel/battery hybrid bus drive

taken from the battery to augment the flywheel energy or to recharge the 22 MJ steel flywheel (during cruise). As in the pure flywheel system, regenerated braking energy is coupled back to the flywheel.

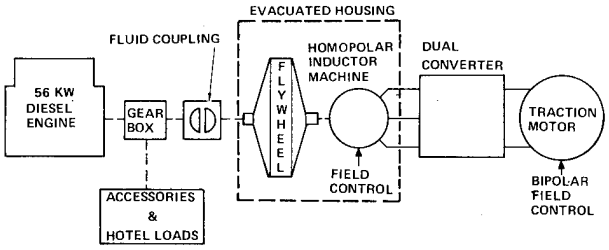
The weight of the battery pack required to provide a reasonable range between battery changes is 6,000 kg. This weight is excessive for a conventional two-axle bus, so the battery pack requires either a separate trailer or a modification of the basic

bus by addition of a third axle.

FLYWHEEL DIESEL ENGINE HYBRID DRIVE

The flywheel/diesel engine propulsion system block diagram is shown in Fig. 4. In this system, the diesel engine is coupled (through speed-increasing gears) by means of a fluid coupling to the flywheel. The 22 MJ steel flywheel can be brought up to engine speed by operating the engine at minimum speed and placing fluid in the clutch. The clutch will then transmit torque to the flywheel (although slipping), which will bring the flywheel up to speed. The engine can be slowly accelerated then to maximum speed to fully charge the flywheel. In operation, the dual converter either controllably couples the traction motor to the flywheel machine or vice versa, depending on the direction of power flow to or from the vehicle. All makeup power required for propulsion losses is then provided at a relatively low rate by the small 56-kW diesel engine. The engine is operated at high efficiency with minimum emissions and noise and provides power to the vehicle hotel loads and the engine accessories.

FLYWHEEL/DIESEL ENGINE HYBRID VERSION 6A



- MINIMIZES FUEL CONSUMPTION
- REDUCES EMISSIONS
- LOWERS NOISE LEVEL
- PROVIDES REGENERATIVE BRAKING

Fig. 4. Flywheel/diesel engine hybrid

FLYWHEEL-AUGMENTED TROLLEY COACH DRIVE

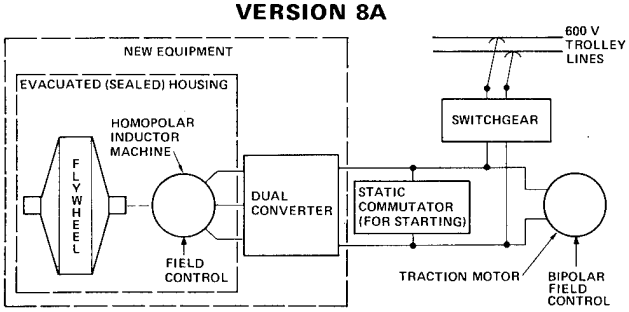
The flywheel-augmented trolley coach is a standard trolley coach with the new equipment added as shown in the block diagram of Fig. 5. When operating under trolley lines, the flywheel assembly and controls provide the following three important advantages:

(a) Capability of recuperating braking energy for reuse.

(b) Elimination of resistive (cam controller) speed control of traction motor by the use of a flywheel to supply power at low traction motor speeds and start-up. (Provides advantages similar to those of chopper control.)

(c) Reduces the peak demand on the overhead wires, thus minimizing the installed substation capacity required for trolley coach operation and reducing utility demand charges.

FLYWHEEL AUGMENTED TROLLEY COACH DRIVE VERSION 8A



- PEAK POWER LEVELING
- PROVIDES REGENERATIVE BRAKING
- INHERENT OFF-WIRE OPERATIONAL CAPABILITY

Fig. 5. Flywheel-augmented trolley coach drive

The flywheel-augmented trolley coach has the additional advantage of providing a limited offwire operational capability for the trolley coach. As a result, the trolley coach can operate in congested areas without overhead wires and can circumvent road obstructions. The 22 MJ steel flywheel shown in Fig. 5 could be increased in capacity if additional vehicle offwire range is required. The operation of the trolley coach system offwire is exactly the same as that of the pure flywheel vehicle. Charging after an offwire run is accomplished automatically from the overhead wires with the vehicle operating conventionally.

COMMONALITY AND MODULARITY

The design mechanization approaches used in the flywheel propulsion system study were intended to provide the widest possible commonality of components suitable for application to vehicles in the gross vehicle weight range from 1,300 kg to over 20,000 kg. Similarly, where commonality of components is not possible, the component designs were made to provide for the wide range of vehicles by modularity or other means for stretching (or shrinking) component capacities.

The recommended flywheel design approach is inherently modular in nature with the flywheel comprised of a stack of disks bolted together, similar to the AiResearch design used on the UMTA/New York MTA stored energy subway cars. This technique, which minimized the flywheel containment protection problem, also lends itself to the use of common flywheel parts for any capacity flywheel from 4 MJ up to at least 72 MJ. Common rotor and stator laminations can be used for a wide range of flywheel and traction machine sizes. In addition, the rear axle ratio used on various vehicles can be selected to provide the desired speed-torque range so that a single traction motor can be used for a wide range of applications. The power controls for various propulsion systems can use the same basic hardware except that the power rating of the semiconductors can be changed to meet the appropriate power requirements. The design of system controls for most flywheel propulsion configurations can be such as to be suitable for a wide range of vehicles. The flywheel/diesel engine hybrid systems for various size vehicles can make use of engines from the wide range of stock designs that properly match the vehicle energy requirements. Finally, the selection of the battery for a flywheel hybrid system can be made on the basis of the proper ampere-hour capacity for a particular application from the broad range of available designs.

COMPARATIVE ANALYSES

The four configurations of flywheel-propulsion systems installed in 12-m buses were subjected to a comparative analysis with the baseline buses (diesel, electric trolley coach, and battery bus) and with each other to determine their relative performance and cost merits.

OPERATIONAL PERFORMANCE

The results of the analysis showed that the flywheel-propelled vehicles in general compare very favorably with the baseline 12-m diesel bus. The improved energy efficiency, when coupled with the advantages of relative independence from petroleum fuel and absence of noise and emissions, appears to more than compensate for the excellent route flexibility offered by the baseline diesel bus. The flywheel/diesel engine hybrid offers an attractive intermediate step between the present diesel bus and the pure flywheel vehicle. In addition to route flexibility matching the diesel, this hybrid vehicle configuration offers the advantages of improved availability, use of presently available maintenance skills, and acceptable environmental impacts. Similarly, the flywheel-augmented trolley coach performance shows a substantial improvement in route flexibility, energy efficiency, and aesthetic considerations over the conventional trolley coach. The pure flywheel bus provides an added improvement over that of the flywheel-augmented trolley coach due to its greater range between charges. Finally, the flywheel/battery hybrid bus performance has a marked improvement in energy efficiency over the otherwise excellent operational performance of the pure battery bus.

The weighing factors for the performance comparison obviously are not the same and, furthermore, can vary widely from transit property to property. On this basis, it is not possible to assign absolute figures of merit to the various propulsion system configurations; however, based on the improvements noted, the conclusion has been reached that the flywheel propulsion systems are highly competitive with the baseline systems; and, in particular, the comparisons of like-type systems described in the preceding paragraph show a favorable comparison of the new concepts with the baseline systems.

LIFE-CYCLE COSTS

Life-cycle cost (LCC) comparisons were made for the four new-concept vehicles contrasted with the three baseline vehicles. The life-cycle costs (initial vehicle and facility costs along with operating and maintenance costs) per vehicle mile based on 23-year useful life of the new-concept

vehicles were calculated for the seven vehicle types. A tabulation of the undiscounted LCC is shown in Table 2. The total LCC values for the diesel bus ($2.13 per mile) and the trolley coach ($2.27 per mile) were found to compare favorably with the averages obtained from transit property cost records. In Table 2, the undiscounted LCC of the pure flywheel, the flywheel/diesel engine hybrid, and the flywheel-augmented trolley coach vehicles are seen to be clearly in the competitive range with the diesel bus and electric trolley coach. Also, it is seen that, although the LCC of the flywheel/battery hybrid appears higher than the other concepts, it compares favorably with the LCC of the pure battery bus.

CONCLUSIONS

The completion of the Phase I study of flywheel energy storage has resulted in the identification of an important area of initial application for flywheel energy storage. The study has shown the viability of flywheel-propelled buses, and a set of plans for successful deployment of these new vehicles has been prepared. The specific conclusions of the Phase I program are the following:

(a) Flywheel propulsion systems for transit buses are in the competitive range of life-cycle costs as contrasted with presently deployed baseline vehicles (diesel transit buses, electric trolley coaches, and battery buses).

(b) The flywheel/battery hybrid bus drive compares favorably in life-cycle cost with the pure battery bus.

(c) All four flywheel propulsion concepts developed in Phase I can meet or exceed transit property operating and maintenance requirements.

(d) The flywheel propulsion systems require substantially less energy for the same performance as that required by baseline vehicles.

(e) The pure flywheel bus, flywheel/battery hybrid bus, and flywheel-augmented trolley coach are all independent of petroleum fuel so long as electric energy generated from coal, hydroelectric, geothermal, nuclear, and solar sources is utilized.

(f) The flywheel/diesel engine hybrid bus reduces dependence on petroleum fuel.

(g) The flywheel-augmented trolley coach reduces peak power demand on the electric overhead when operating as a conventional trolley coach in addition to recuperating braking energy.

(h) All flywheel propulsion concepts offer substantial reduction in noise as compared with the baseline diesel bus.

(i) All flywheel propulsion configurations except the flywheel/diesel hybrid eliminate emissions. The emissions of the flywheel/diesel hybrid are substantially reduced below those of the standard diesel because the engine size is

Table 2. Life cycle costs in cents per mile.

	Undiscounted costs			
Vehicle	Maintenance and Fuel	Operating Cost	Initial Cost	Total Undiscounted LCC
Diesel bus	40.4	150.7	21.6	212.7
Trolley Coach	42.7	150.7	32.2	227.5
Battery Bus	124.3	159.6	30.8	318.4
Pure Flywheel Bus	26.0	150.7	20.9	201.3
Flywheel/Battery	81.4	157.0	30.9	273.0
Flywheel/Diesel Bus	27.4	150.7	20.9	200.9
Flywheel Trolley Coach	28.7	150.7	23.8	206.9

smaller and the operating range is tightly restrained.

(j) The major components of all four flywheel propulsion concepts developed in the Phase I study are essentially the same, thus providing a large production base if all four concepts are developed and deployed.

(k) A high potential exists for transfer of the flywheel-propelled bus technology to other urban vehicles such as commuter rail vehicles, para-transit vehicles, downtown people movers, delivery vans, school buses, and passenger cars.

REFERENCES

[1]Hagen H. and Zelinka, R., "The M.A.N. Elektrobus Experience Gained in Large Scale Tests," Fourth International Electric Vehicle Symposium, Dusseldorf, Germany, August 1976.

[2]Lawson, L. J., "Kinetic Energy Storage for Mass Transportation," Mechanical Engineering, Vol. 96, No. 9, September 1974, pp. 36-42.

[3]United States Transit Industry Market Forecast, American Public Transit Association, 1100 17th St., N.W., Washington, D.C., 1976.

THE DESIGN OF A WIND ENERGY STORAGE SYSTEM WITH A CELLULOSIC FLYWHEEL

Dr. Arthur G. Erdman
Dr. Darrell A. Frohrib
Mr. Thomas P. Carlson
Mr. David L. Hagen

Department of Mechanical Engineering

and

Dr. William L. Garrard

Department of Aerospace Engineering and Mechanics

University of Minnesota
Minneapolis, Minnesota 55455

ABSTRACT

The design of a wind energy storage system is discussed. The design and construction, in progress, of a small demonstration model is described. Suggestions for further study and development are presented. The development of a complete energy storage system which is cost competitive with other means of energy storage is addressed. Emphasis is placed on the development of a flywheel of a cellulosic material, such as wood or wood products, and on the implementation of mechanical transmissions for the input and retrieval of energy.

INTRODUCTION

Flywheel systems promise to be a practical means of storing wind energy. The availability of such energy is well documented but the variable supply and demand require energy storage. Cellulosic materials such as wood and paper, or related products, are worth considering in flywheel applications because they appear to be cost effective, are a renewable resource, and have desirable safety features.

This paper briefly describes work in progress aimed at developing an operational flywheel energy storage system of residential capacity. Such a system will store energy from the wind and produce electrical energy. To date this effort has concentrated on the flywheel system which stores and retrieves mechanical and/or electrical energy. This work does not address the design or development of wind energy generating equipment.

Design and construction of a small scale demonstration model of the system is near completion. Preliminary investigation of the pertinent mechanical properties of various wood and paper products is underway. This work is intended to evaluate the technical feasibility of the system and to identify areas for further research and design which will eventually lead to the development of an operational system with potential for commercial development.

Particular attention is being given to the development of the cellulosic rotor, and to the implementation of the mechanical transmissions in the input and output power systems. But the ultimate goal of this effort is to develop the entire storage system, including the requisite controls, supports, and vacuum housing, having a cost competitive with other means of energy storage.

DESIGN CONSIDERATIONS

CELLULOSIC MATERIALS

Kinetic Energy Storage. A residential flywheel energy storage system would be stationary (perhaps located underground) hence total volume and total mass of the

flywheel are not a primary design constraint. Ideally the flywheel will store maximum energy per unit mass and per unit cost of material. The energy storage capacity is directly proportional to the strength to density ratio of the flywheel material. Cellulosic fibers such as wood and bamboo have been suggested for flywheels by D. W. Rabenhorst of Johns Hopkins Applied Physics Laboratory because of their high strength to density ratios and low costs.[1] Rabenhorst has discussed the use of wood, extrapolated to vacuum conditions, and has suggested areas in which further research is needed. In addition, he has conducted dynamic failure tests of several sample wood disks.[2] These tests verify that wood has excellent potential for kinetic energy storage applications. These tests also demonstrate that wood fails by shredding thus making it much safer than steel, which fails by shattering into large, high speed fragments. A comprehensive review of current flywheel work by Hagen and Erdman has revealed that no research has been performed to establish the technical and economic feasibility of wood or cellulosic fibers as flywheel materials.[3]

The existing literature has been searched and reviewed by Hagen for basic information on relevant physical properties of wood.[4] Information is available on basic mechanical properties under ambient conditions but little data exists on the properties of wood at 0% moisture content. More than twenty-five species of wood have intrinsic specific energies* greater than 200 kJ/kg (25 w-h/lb). The tensile strength of individual fibers of summerwood Douglas fir have been measured as 776 MPa (113 kpsi) at zero moisture content. This represents an intrinsic specific energy of 520 kJ/kg. The tensile strengths parallel to the grain of bulk timber are typically an order of magnitude less, around 100 MPa, varying with species. The design challenge is to approach the strength of the individual fibers by reducing stress concentrations and improving fiber to fiber bonding.

The few studies of the fatigue of wood under cyclic tensile loading indicate high endurance. Experiments by Kellogg showed no loss in tensile strength at up to 100 cycles.[5] Tensile fatigue studies by Lewis on Douglas Fir parallel to the grain indicate that an average working tensile strength at 10^4 cycles was about 85% of the static strength and at 10^6 cycles was about 65%.[6] Lewis recommended working stresses of 50% of static strengths at 30 million cycles; 70% would probably be suitable at 10,000 cycles.

The literature of wood technology lacks extensive research on the mechanical properties of wood with negligible moisture content, as found under vacuum conditions. The available data show that the strength of wood increases significantly with decreasing moisture content from the saturation point, reaching maximum strength in the range of 8 to 12% moisture content. Strength then falls off, and wood becomes more brittle, as the moisture content is brought to zero. Further research is needed in this area before the effects of low moisture and vacuum conditions can be quantitatively treated as design parameters.

Flywheel Fabrication. Flywheels are usually considered in three major geometrical configurations: isotropic or pseudo-isotropic; radial, e.g., spoke or brush; and circumferential, e.g., wound fibers. Wood and paper technology are so versatile that cellulosic materials could be employed in any of these configurations, whether as veneers, paper, or cords. Wood veneers are commonly produced in a variety of widths and thicknesses; many wood processing mills can veneer sheets over 6 m (250 in.) wide, or produce veneers less than 0.2 mm (.01 in) thick but in smaller widths. Paper is commercially available in the U.S. in continuous rolls 72 in. (1.8 m) in width, and binder board is manufactured up to 0.24 in (6.1 mm) thick.

The pseudoistropic configuration is convenient for flywheel applications since it is well suited to plywood or veneers. In this design the grain of the wood is perpendicular to the axis of rotation, but the grains of adjacent layers are not parallel. The flywheel can be constructed by laminating plywood or veneers into a large block, then sawing and/or turning this to a cylinder.

The strength of wood increases with decreasing thickness, probably due to reduction of unequal stresses in the early and late growth sections of wood.

*The intrinsic specific energy of a material is characteristic of its rotary kinetic energy storage capacity on a mass basis, and is equal to the ratio of axial tensile strength to density.

However, below a critical thickness strength begins to fall off linearly with thickness due to cut fibers.

The strength of wood can also be increased by compression. Woods typically have a density on the order of 0.7 gm/cm^3. This can be doubled to almost 1.5 gm/cm^3 by applying pressure in the range of 7 to 27 MPa (1000 to 4000 psi), depending on the moisture content and temperature. This halves the volume, and gives some improvement in fiber to fiber bonding increasing the specific energy. The application of heat and pressure together will plasticize the cellulose composite enabling it to flow. This process appears to reduce stress concentrations in veneers by relaxing pre-existing strains. The technique of compressing wood laminates deserves further experimentation, especailly to determine if it can be cost effective in commercial production.

The ultimate strength, and therefore the maximum rotary kinetic energy, of a solid homogeneous cylinder is reduced by half if a hole is cut through the axis of rotation. Thus it is desirable to bond a separate shaft and hub to each end of a cylindrical flywheel. This procedure presents the challenge of accurate concentric and parallel alignment of the shafts while applying the pressure required for the bonding agent. This can be accomplished on a small scale in a lathe. Large flywheels will require special equipment, perhaps a customized hydraulic press. In addition, the rotor often fails dynamically at or near the bonding layer because of the different elastic moduli of wood flywheel and metal hub. An elastomeric bonding material recently developed by the Lord Corporation promises to mitigate this problem.[7]

Dynamic balancing of wood flywheels can be accomplished by removing material from the surface by drilling or sanding. The bonded hub and shaft configuration described above may allow more innovative and perhaps cost effective, balancing techniques. For example, proper adhesives could allow centrifugal bonding of hub to rotor above some critical speed. Because the flywheel will operate over a wide speed range, the speed at which dynamic balancing is executed may require identification based on the critical speeds realized by the total rotor-shaft-bearing system. Further analytical and experimental research is needed in this regard.

Cost. Solid birch plywood, used in patternmaking and other specialized industries, is commercially available at $1.00/kg for clear plywood and $0.50/kg for plywood with interior knots removed and plugged, based on purchase of carload quantities. Flywheels made of plywood with interior knots may have only half the energy storage capacity of clear plywood rotors since a knot near the axis of rotation will double the stress locally. Thus the unit cost for energy storage will be the same for either grade of plywood. Based upon the storage capability of 30 kJ/kg cited by Hagen[4], this cost is 30 kJ/$ (8.4 w-h/$) for material. Labor and processing might double this cost in actual production.

A similar analysis for Kevlar and S-Glass composites indicates equal or greater costs per unit of energy storage.[4] Thus wood appears to compete favorably with these much stronger but more expensive materials.

POWER TRANSMISSION

The duty cycle of a flywheel system which stores wind energy and subsequently generates electricity has two unique features. First, commercially available AC and DC generators require a constant shaft speed input.* Thus the system must employ a continuously variable transmission (CVT) in order to retrieve energy from the decelerating flywheel. Second, because the availability of wind energy is highly variable, the system must be designed for an erratic input power cycle.

The functional block diagram of the flywheel storage system may be viewed as a power source connected through a CVT to the flywheel; the flywheel is in turn connected to a constant speed electric generator through a second CVT, Figure 1. In practice, the same CVT may be used both to accelerate the flywheel and later to discharge the stored kinetic energy to the generator, Figure 2. Alternatively, the flywheel can be accelerated without a CVT using a variable speed input motor

*Electric genrators employing variable speed input are underdevelopment but are not considered here.

with electronic controls. This configuration, shown in Figure 3, is employed in our present demonstration model (discussed below). Gearing or belt-pulley systems for stepping the shaft speeds up or down and overspeed protectors are suppressed in these diagrams.

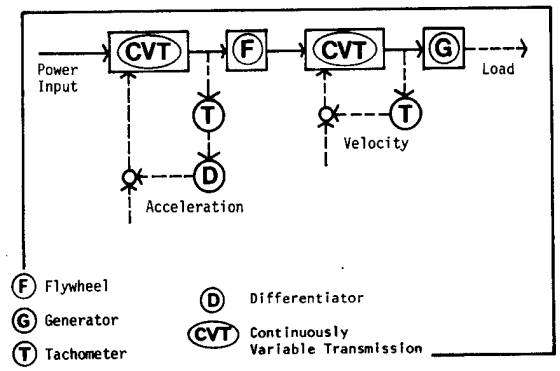


Fig. 1 - Functional Block Diagram

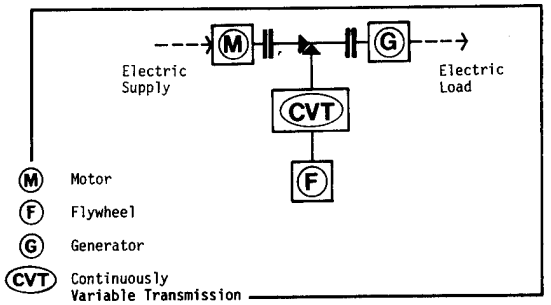


Fig. 2 - Mechanical Schematic of a System employing a single continuously variable transmission

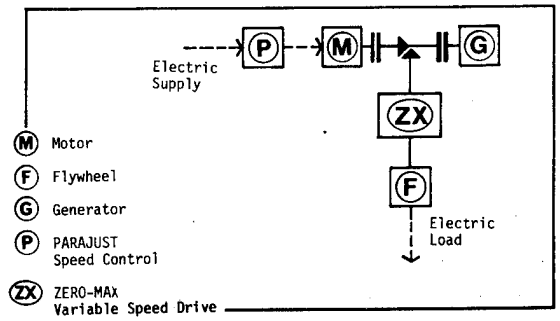


Fig. 3 - Mechanical Schematic of the demonstration model

A variety of electronic, hydraulic, and mechanical drives can provide continuously variable speed over the range to be considered in the proposed flywheel system. Mechanical drives seem to have an advantage due to cost (vs. electronic) and efficiency (typically 90% or better vs. 80-85% for hydraulic drives.) In addition, the control of mechanical drives is simpler than that of electronic drives, although electronic drives are generally more rapid and precise.

Input. The input power system must accelerate the flywheel to its maximum operating speed as the input power fluctuates. This can be accomplished with a CVT regulated by a feedback control loop as shown in Figure 1. The angular velocity of the flywheel input shaft is measured with a tachometer. This signal is differentiated and compared to signals proportional to allowable angular acceleration limits. If the input power is low it may be desirable to disengage the flywheel from the CVT in order to reduce friction losses. In particular, if the power falls off after the flywheel has been accelerated through a portion of its operating speed range the torque available to further increase the speed might be very small. Alternatively, if the angular acceleration, and hence the torque applied to the input shaft, exceeds some design value the flywheel must be disengaged to prevent damage to the shaft, hubs, or flywheel itself. Finally, when the angular velocity of the flywheel reaches its specified maximum value, the rotor is disengaged and the input power can be diverted away from the energy storage system.

Output. The angular velocity of the flywheel varies as the square root of the energy stored in the flywheel. Since a conventional constant-frequency generator requires a constant input shaft speed, a continuously variable transmission is located between the flywheel and the generator to provide a constant input velocity to the generator. As shown in Figure 1, the input shaft velocity to the generator is measured by a tachometer. The output of this tachometer is compared with a signal proportional to the desired input velocity for the generator. The resulting error signal is used to adjust the ratio of the continuously variable transmission in order to maintain the input shaft velocity at its desired value. In practice the

adjustment of the CVT, for both input and output, can be accomplished using an electronic feedback device which drives a servo motor attached to the CVT speed control mechanism.

Safety and Efficiency. In addition to the regulating system described above, control is necessary for safety assurance and efficient operation. It may be desirable to measure the vibration level of the flywheel housing so that if the flywheel begins to fail, the increased vibration levels can indicate an impending failure and the flywheel can automatically be disconnected to avoid damage to the rest of the system. It may also be desirable to measure bearing and flywheel housing temperatures to help detect incipent failure of the flywheel.

The control system can be used to maximize the efficiency of the various clutching sequences. Energy is lost as heat when a friction clutch engages rotary elements with different angular velocities. The controls could be used to match speeds before the clutch is engaged, e.g., use the motor to bring the generator to speed before discharging energy from the rotating flywheel. This operation, however, also requires an expenditure of energy.

The flywheel storage system described above consists of a large number of non-linear elements. Under certain conditions instabilities or limit-cycle oscillations which could damage the system may occur unless the control system is carefully designed. Thus it is necessary to analyze the proposed design using both analytical methods of control system synthesis and computer simulations to see if the systems perform as intended. Once the theoretical design has been completed, the control system can be constructed and tested as part of the overall system.

HOUSING AND SUPPORT

In general, design requirements for the housing and support of this system are not different than for other flywheel applications. The flywheel must rotate in an evacuated housing to reduce windage losses; the housing must be designed for safety in case of rotor material failure; bearings must be specified for efficiency and service life; and transient critical vibrations must be controlled. Some of the unique aspects of our system are here discussed briefly.

Evacuated Housing. Cellulosic flywheels 1 to 2 m (3 to 6 ft.) in diameter might rotate at up to 7,000 rpm and with surface speeds in the range of 200 m/s (Mach 0.6). A vacuum of 10^{-2} to 10^{-3} torr seems reasonable to sufficiently reduce windage losses in this speed range. This vacuum level is obtainable with commercially available cryogenic pumping systems. (Of perhaps equal concern in reducing windage is the production of a smooth surface on a wooden flywheel.) Under ambient conditions commercially available wood and wood products typically contain 7 to 10% moisture by weight. Thus initial outgassing may take considerable time. Because of this it may not be practical to permanently pump down a large cellulosic flywheel; periodic pumping may be preferable to maintain the desired vacuum level.

Many designs of rotary seals are commercially available having a wide range of (mechanical) efficiencies and costs. The trade off between these two factors will be an important design consideration for an operational, cost effective system. More important, the air leakage through the seals into the vacuum must be considered to compare the energy expended in pumping versus the windage losses for given vacuum levels. Such an analysis will facilitate proper design of the pumping system and selection of seals for optimum energy efficiency.

Because wood fails dynamically by shredding, burst containment for safety is not a critical design problem. Indeed, preliminary test results and analytical estimates of worst case failure indicate that a steel chamber sufficient to hold a vacuum will also sustain flywheel failure. The vacuum pumping system must be equipped with filters to contain the fibrous debris.

Bearings. The bearings for any flywheel storage system must be chosen for efficiency and long life, and, in many designs, be able to operate in a vacuum. As with the rotary seals, the cost effectiveness of the numerous available bearings must be considered. The total weight of a cellulosic flywheel may be greater than rotors of other materials because of the lower operating speeds.

This, in turn, would place the bearings under large static loads. It may prove most practical to mount such a heavy flywheel vertically on a gravity loaded thrust bearing. A spherical spiral groove hydrostatic bearing has been proposed as an extremely efficient and durable design. (This bearing is not currently commerically available.)

Vibration Control. Useful operation of any flywheel energy storage unit requires a wide range of operating speeds. Ratios of at least 2 or 3:1 between the maximum and minimum speeds are needed to withdraw 75% or 90% of the stored energy. However, residual unbalance and asymmetry in the rotor and shafts may cause vibration of the flywheel. Elasticity in the bearings, shaft and supports will give rise to the critical speeds and unstable regions which may lie in the operating range or which may be encountered to reach that range. Avoiding these speed regions, or controlling response as the flywheel moves through them is imperative for useful operation.

Careful study and design of the shaft, bearings, and supports are necessary to determine if passive isolators can accommodate the operating ranges and levels of acceleration. The modelling of the support system may require load-deflection and vibratory tests of the supporting components, coupled with finite element studies to ascertain parameters in a system model. Rotary inertia and rotational stiffness of bearings and isolators may be required as refinements to such a model. The range of solution instabilities has already been solved in the literature for certain parameters. If additional instability plots are required for a specific application they can be generated using automatic computation.

Active vibration control of the system may be necessary or preferable. This can be accomplished by either:

(1) Rapidly increasing power to or from the flywheel speed when approaching the unstable region so that the transition of the unstable region is rapid with the controlled vibration,
(2) changing the spring and damper coefficients of the isolators and thus rapidly changing and passing through the unstable regions.

ECONOMIC DESIRABILITY

The fixed costs and energy efficiencies of the various portions of the system must be considered in designing a storage unit suitable for commercial production. Cellulose appears to be cost competitive in kinetic energy storage per unit cost of material. Production of a cellulosic flywheel will raise these energy storage costs. Perhaps of greater interest is the cost of the associated input and output power systems. If the total cost of electronic controls, mechanical drive train and vacuum pumping equipment is on the same order as the cost of the flywheel, savings gained from cellulose may be negligible. On the other hand if the cost of supporting equipment can be made small compared to rotor costs, cellulosic rotors may prove to be highly cost effective. This will be particularly true if the cost of the supporting equipment is comparatively fixed as the size or operating speed of the flywheel is increased.

DEMONSTRATION MODEL

The design and construction of a small-scale demonstration model of the system cited above is currently in progress. The goals of this effort are to make a preliminary investigation of the technical practicality of such a system. This will provide a basic understanding of the functions of the various components within the whole system which, in turn, will facilitate the more sophisticated design of an efficient, operational system. This model will be completed and a preliminary evaluation made of its performance by the end of 1977.

This system is being constructed at modest cost using conventional, commercially available materials, hardware, and services. The following discussion briefly describes our design, indicating the level and scope of our effort. A comprehensive engineering analysis is not presented in this writing.

LAMINATED HARDWOOD FLYWHEEL

Flywheel Fabrication. A flywheel measuring 14 in. in diameter and 15 in. long has been constructed of solid birch plywood. It weighs approximately 60 lbs.

The plywood stock is 3/4 in., 7 ply, with 90° crossply. A block of material

was laminated using an epoxy adhesive. The necessary bonding pressure was applied with a 50 ton hydraulic press. The cylinderical shape was rough cut with a bandsaw, then turned smooth on a lathe.

Shaft Configuration. The shafts are of 0.75 in. hardened steel press fit into aluminum hubs 6.0 in. in diameter and 1.0 in. thick. Recessed walls were turned into the flywheel to receive the hub, and provide physical support in the event of adhesive failure. Each end of the flywheel is tapered to less than half the outside diameter to compensate for the increased stress at the hub recess.

The hubs are joined to the rotor with an epoxy suitable for wood to metal bonding. Concentric alignment and bonding pressure for this process were obtained using a lathe. After assembly the shafts were turned for true alignment.

POWER TRANSMISSION

The system is accelerated from rest by an electric motor regulated by a solid state speed control device. The stored energy is retrieved through a variable speed drive connected to an AC generator. This configuration is illustrated in Figure 3 above. The location of these components, their speeds, and the ratios of the belt drives are shown in Figure 4. In the operating range of 5,000 down to 2,000 rpm the indicated kinetic energy storage of the birch flywheel described above is approximately 1,000 w-min.

Input. The flywheel is accelerated by a 1.5 hp electric motor in conjunction with the Parajust AC motor speed control device. The Parajust is a solid state controller which converts single phase 220 VAC power to 3-phase 220 VAC. By adjusting the frequency and voltage of the output power the Parajust increases the motor speed to the rated maximum while maintaining a constant torque output.

Output. The CVT employed is the Zero-Max variable speed drive. This is a purely mechanical drive which obtains a stepless speed change by varying the distance a one-way clutch rotates an output shaft. This variation is accomplished by a six-bar linkage with an

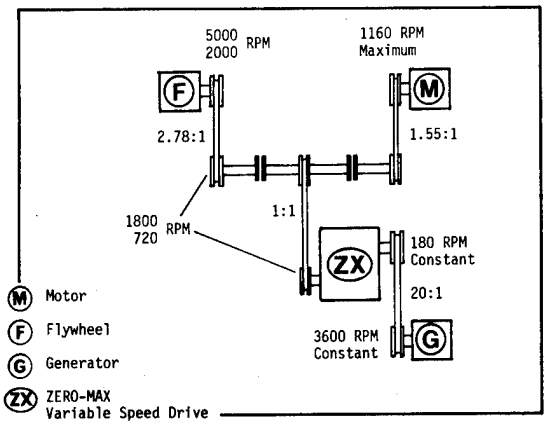


Fig. 4 - Operating Speeds and Drives Ratios of the demonstration model.

adjustable center pivot. In practice, several such clutch-linkage mechanisms are mounted in parallel, sequentially driving a common output shaft to provide smooth rotary motion. The linkage geometry is such that the Zero-Max varies the output shaft speed between zero and 25% of input shaft speed.

The generator in an Onan YCB with 120 VAC, 1250 watt capacity and requiring 3600 rpm shaft speed. The Zero-Max drive provides a constant shaft speed of 180 rpm which is stepped-up to 3600 rpm at the generator. The Zero-Max is equipped with a screw type speed control mechanism. A DC servo motor, regulated by a solid-state feedback control system, operates the mechanism to maintain this contant output speed.

Drive Train. Locations of pulley-belt drives and clutches are shown in Fig. 4. As an indication of the size of the system, the pulleys have pitch diameters ranging from 3.0 to 8.0 in.; the belts (cogged V-belts) have centers ranging from 16.0 to 24.0 in.

Two electromagnetic clutches are located on a central jack-shaft. In conjunction with the Zero-Max drive, a wide variety of clutching sequences are possible, including speed matching between the various components before engaging a clutch.

HOUSING AND SUPPORT

Vacuum and Burst Container. The vacuum container has been constructed from a steel air compressor tank. One end was cut off, pipe fittings were removed, and the interior sand-blasted. The tank has 18.0 in. outside diameter, with nominal wall thickness of 0.25 in., and is approximately 25 in. long outside including one bowl-shaped end of the original tank. The large end has been fitted with a steel flange 0.375 in. thick welded to the tank; the flange holds a steel end-plate. A static O-ring seal 21.0 in. in diameter is held between the plate and flange. A hole for the drive shaft is cut in the center of the plate. At the bowl shaped end a removable bearing mount with a static O-ring seal is inserted through a 5.0 in. diameter hole. This configuration allows convenient mounting of the flywheel in the container but does not require the shaft to protrude from both ends.

A burst containment ring 0.375 in. thick, 17.0 in. outside diameter, and 22 in. long is tack-welded to the inside of the vacuum container. This ring was rolled from hardened steel plate stock.

Vacuum Pumping System. A two-stage rotary vacuum pump capable of maintaining a vacuum of 10^{-2} torr will be used. This pump has a capacity of 5 cfm. A separate pump of larger capacity will be used, if necessary, to obtain a rough vacuum during outgassing. The filter will have several sizes of steel mesh to withstand dynamic flywheel failure and contain the debris of various particle sizes.

Bearings and Seals. Conventional, commercially available bearings and seals have been specified for the first assembly of the demonstration model.

Flange-mounted, self-aligning ball bearing units will support the shafts. They will be mounted inside the vacuum chamber, requiring special lubricating oil having low vapor pressure. At least two varieties of rubber-mounted bearings will be tested for vibration isolation.

A low cost rotary face seal will be mounted on the shaft immediately outside the vacuum chamber.

CONSIDERATIONS FOR FUTURE DEVELOPMENT

The design and construction of a residential size storage system will require more sophisticated components and methods of fabrication than those employed in the demonstration model. For example, a cylindrical hardwood flywheel possessing kinetic energy of 10^5 kJ (30 kwh) while rotating at 5,000 rpm would be approximately 2 m (7 ft.) long, 1.5 m (5 ft.) in diameter, and weigh 2500 kg (3 tons). Some significant topics requiring further research and development are discussed below.

FLYWHEEL

Material. Many cellulosic materials are worthy of consideration for flywheel applications. Laminating the flywheel from thin veneers, rather than plywood, seems especially promising. With this technique the interply angle between successive laminations can be specified for optimum strength. (The interply angle in commercially available plywood is 90°). Similarly, laminating rotors from paper or other pulp products may be desirable, particularly with regard to cost. The material properties and costs of various adhesives must be investigated.

Fabrication. Laminated flywheels are assembled under pressure sufficient for bonding; some adhesives require heat in addition to pressure. A large hydraulic press suitable for laminating rotors up to 1 m long and 1 m in diameter may be developed as part of the research described here. This press may also be modified to align the shaft-hub for bonding to the flywheel, as suggested above.

The technique of compressing wood in order to increase strength and specific energy will be investigated as part of the research in progress. Tensile testing of compressed wood samples is underway. Sample compressed wood and plywood disks will be dynamically tested. If this procedure proves technically advantageous for flywheel energy storage, consideration must be given to commercial production costs, especially if heat is required during the compression or bonding process.

The circumferential and radial geometrical configurations should be investigated for cellulosic flywheels. These

designs might be well suited to the long fibers of bamboo, which are not readily available in large sheets or veneers.

Reliable techniques for dynamic balancing and surface polishing of cellulosic flywheels must be developed.

POWER TRANSMISSION

Duty Cycle. The duty cycle of this storage system must be carefully considered before the design of an operational system can be completed. In particular, the availability of wind energy must be studied (for the geographic area under consideration) and compared to the demand so as to determine the typical duration of the storage cycle. This will place design constraints on the efficiency of the mechanical components. The control system for an operational residential storage unit must be capable of the various clutching and speed regulating sequences to store the wind energy when available and to retrieve it upon demand.

The input power source must be considered. Wind generating equipment can provide electricity or direct mechanical power through a drive shaft. Both provide challenges to the application of the wind generating device atop a tall tower, e.g. heavy electrical generators, long drive shaft, or hydraulic lines.

The control system might also be required to perform active vibration control, as discussed above.

Continuously Variable Transmission. The various CVT designs must be compared for suitability to this system. Three CVT designs will be tested in either the current demonstration model or in a larger (future) prototype. The three are: a modified Zero-Max drive, the Kopp variator traction drive, and a variable-pitch pulley-belt drive.

The Zero-Max drive, discussed above, is inexpensive yet has high precision of speed control. An important advantage is that the output speed can be brought to zero, thus allowing it to function as a clutch. Among its disadvantages are low rated speeds, 1800 rpm input, 450 rpm output; and low power rating, 1.5 hp, of the largest commercially available unit. Work is in progress to adapt the Zero-Max to the higher speeds and torques required for residential storage systems. One of the co-authors (A. Erdman) has consulted with the manufacturer and was instrumental in the design of the 1.5 hp unit, as well as a 5 hp prototype.[8,9] The intended improvements to the Zero-Max include implementation of materials and lubricants now used in other types of CVT's, and the strengthening of internal components of the drive.

The Zero-Max is not reversible, i.e., input and output shafts are distinct. This precludes using a single Zero-Max to both accelerate and subsequently decelerate the flywheel. This is not a major disadvantage since input power may be supplied electrically, as in the demonstration model. If direct mechanical power input is desired the cost of two separate Zero-Max drives may not be prohibitive. Moreover, this latter configuration may be preferable for implementing the separate input and output feedback control systems.

A traction drive transmits power between two rolling elements having smooth hard surfaces. Because the drive elements are smooth they can be moved freely, providing infinitely variable speeds. Until recently these drives were restricted to low power applications. Developments over the past few years have provided better steels and more sophisticated lubricants which, in turn, allow significantly higher rolling-contact pressures and greatly increased resistance to fatigue failure. Commercially available traction drives are now gaining popularity in industry, and are regarded as practical power transmission systems for heavy-duty applications with long service life. Traction drives, however, are more expensive than other types of CVT's.

The Kopp variator is among the most widely used traction drive geometries. Power is transmitted by rotating spheres held between bevelled discs connected to the input and output drive shafts. Tilting the sphere's axes of rotation varies the circumference of the contact path, and thus the speed ratio. This ratio ranges from 1:3 to 3:1 in commercially available units. A Kopp variator is manufactured and marketed in the United States by Eaton Corporation.

The maximum rated speed of the Kopp variator is high enough (5400 RPM) to allow direct coupling to the flywheel, thus eliminating the expense and

inefficiency of step-up belt or gears. Because it is reversible and has a symmetric speed ratio range about 1:1 it can be used both to accelerate the flywheel using the motor, and discharge stored energy to the generator. This configuration has great potential as an efficient and durable flywheel energy storage system.

Belt drives employing variable-pitch-pulleys have been widely used in industry for many years in moderate-power applications. They provide an inexpensive method of speed control where high precision is not essential and the range of speed ratios is not large. Recent experimental data indicate that well designed drives of this type operate at efficiencies over 90%.[10] Precise and rapid speed control of this device might prove difficult with a solid-state feedback controller. However, because this type of drive is inexpensive, durable, and readily available, testing its performance will provide at least a minimum standard with which other CVT's can be compared.

Diagrams of the Zero-Max and Kopp variator drives appear in the appendix.

Mechanical Efficiency. The power train must be designed and specified for optimum efficiency and cost. Gears may be preferable to belt drives depending on the speeds and torque loads of a given system design. The cogged V-belt employed in the demonstration model is an efficient belt drive for small loads but will probably not be suitable for a large operational system. The Poly-V belt, gaining wide popularity in recent years, appears to be an efficient and durable belt drive suited to heavy loads. Timing belts may be desirable because they do not slip at low speeds, a problem encountered by other belts during the complete flywheel system duty cycle. Various belt and gear drives should be tested for efficiency in flywheel storage applications.

A flywheel storage system employing a single CVT, per Fig. 2, may prove efficient by reducing the number and size of mechanical drive components. Such a system could be compact and could require a minimum number of step-up or step-down drive ratios.

If speeds greater than 10,000 rpm are desirable for a given application it may be desirable to have step-down gears inside the evacuated chamber so that the shaft speed at the rotary seal is low. While this design will increase the mechanical efficiency of the seal, it may prove difficult and expensive to assemble.

HOUSING AND SUPPORT

Evacuated Housing. The pumping cycle must be evaluated with regard to pumping capacity and energy consumption, outgassing time, seal leakage, and windage losses at the surface of the flywheel. Experimental data should be obtained for windage losses as a function of rotary speed and surface smoothness for wooden flywheels. Liquid type rotary seals, e.g. centrigual and ferro-fluidic, should be studied. These seal types have zero leakage and very high mechanical efficiencies. However, they present design challenges for other portions of the system. For example, the centrifugal seal must be operated above a threshold rotary speed before the chamber can be evacuated, placing a pressure differential across the seal. This imposes design constraints on the duty cycle of the flywheel. The ferro-fluidic seal employs colloidal particles of ferrous material suspended in the sealing fluid (oil), which in turn is held in place by the poles of a permanent magnetic housing. While this is an elegant and efficient design it has very low tolerance for shaft vibration, imposing constraints on the bearing tolerances and on vibration control needs.

Vibration Control. In the research in progress an analysis will be conducted regarding the flywheel as a rigid rotor suspended elastically at the hubs, shafts, and bearings. Empirical data from the demonstration model will be taken to determine if this analysis can accurately predict the critical speeds. Further study will be needed to refine this analysis in order to employ it as a design technique. For example, it may prove necessary to model a cellulosic flywheel as an elastic body.

Passive and active methods of vibration control should be investigated and compared for various flywheel storage applications. Vibration isolation appears most practical at the hubs and bearings; various materials should be tested for vibration isolation and service life in this regard.

SUMMARY

The design of an operational flywheel energy storage system requires the integration of several technologies. Further investigation, both analytical and empirical, is required for a practical storage system to be fully developed. Additional evaluation and refinement of the design will be needed to make such a system both energy efficient and cost competitive.

This paper has discussed the design of a stationary flywheel wind energy storage system of residential capacity. Among the more innovative aspects of the approach described are the development of a flywheel made of a cellulosic material, and the implementation of a mechanical continuously variable transmission for input and retrieval of energy. However, due consideration has been given to all other aspects of the design with the goal of producing a comprehensive, operational kinetic energy storage system.

ACKNOWLEDGEMENTS

The authors are grateful for financial support from the Minnesota Energy Agency under the auspices of the first biennial Alternative Energy Systems Demonstration Program; for graduate fellowship support at the University of Minnesota through the Department of Mechanical Engineering and the Institute of Technology Corporate Associate Fellowship Program; and for donations in kind of products and expertise from many businesses, including: Zero-Max Industries, Inc., and its Parametrics Division; 3M Company, Structural Adhesives Division; H. B. Fuller Company; Onan Corporation; Lord Corporation, Kinematics Division; Radke Veneer Mill; and Lenderink, Inc.

REFERENCES

1. Rabenhorst, D. W., "The Applicability of Wood Technology to Kinetic Energy Storage", Johns Hopkins University, Applied Physics Lab., APL/JHU Technical Digest, Vol. 11, No. 5, May/June 1972, pp. 2-12.

2. Rabenhorst, D. W., Smalt, T. B., "Composite Flywheel Development Program Progress Report: March-September, 1976", Johns Hopkins University Applied Physics Lab., 5DO-4616, APL/JHU, October 1976.

3. Hagen, D. L. and A. G. Erdman, "Flywheels for Energy Storage: A Review with Bibliography", Design Eng. Tech. Conf., Montreal, ASME Paper No. 76-DET-96 (Sept. 26-29, 1976).

4. Hagen, D. L., "The Properties of Natural Cellulosic Materials Pertaining to Flywheel Kinetic Energy Storage Applications", Paper at the 1977 Flywheel Technology Symposium, San Francisco, CA, October 5-7, 1977.

5. Kellogg, R. M., "Strain Behavior of Wood Subjected to Repetitive Stressing in Tension Parallel to the Grain", Forest Products Journal, Vol. 8, No. 10, 1958, pp. 301-7.

6. Lewis, Wayne C., "Fatigue of Wood and Glued Joints Used in Laminated Construction", Forest Products Research Society, Proceedings of the National Annual Meeting, Vol. 5, pp. 221-229.

7. Rabenhorst, D. W., "Composite Flywheel Development Program - Final Report", Johns Hopkins University, Applied Physics Lab., APL/JHU SDO-4616A, NSF Grant No. AER75-20607 (1977).

8. Erdman, A. G., "Dynamic Synthesis of a Variable Speed Drive", Proceedings of the 3rd Applied Mechanisms Conference, Paper No. 38, Stillwater, Oklahoma, November 1973.

9. Beer, R. and A. Erdman, "Time Response of a Variable Speed Drive", Proceedings of the 4th Applied Mechanisms Conference, Paper No. 29, Chicago, Illinois, November, 1975.

10. Palmer, R. S. J. and J. H. F. Bear, "Mechanical Efficiency of a Variable Speed, Fixed Center, V-Belt Drive", Journal of Engineering for Industry, Trans. ASME, Series B, Vol. 99, No. 3, August 1977, pp. 806-808.

APPENDIX

Figures A1 and A2 (next page) show the geometries of the Zero-Max and Kopp variator drives.

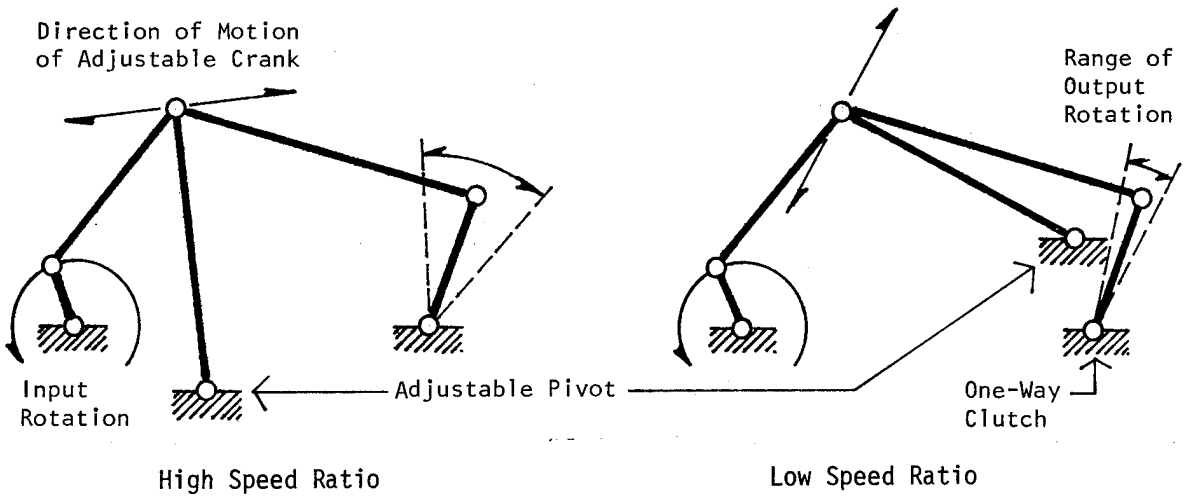


Fig. A1. Geometry of Zero-Max Variable Speed Drive

Range of output rotation depends on the direction of motion of the adjustable crank, which is controlled by the position of the adjustable pivot.

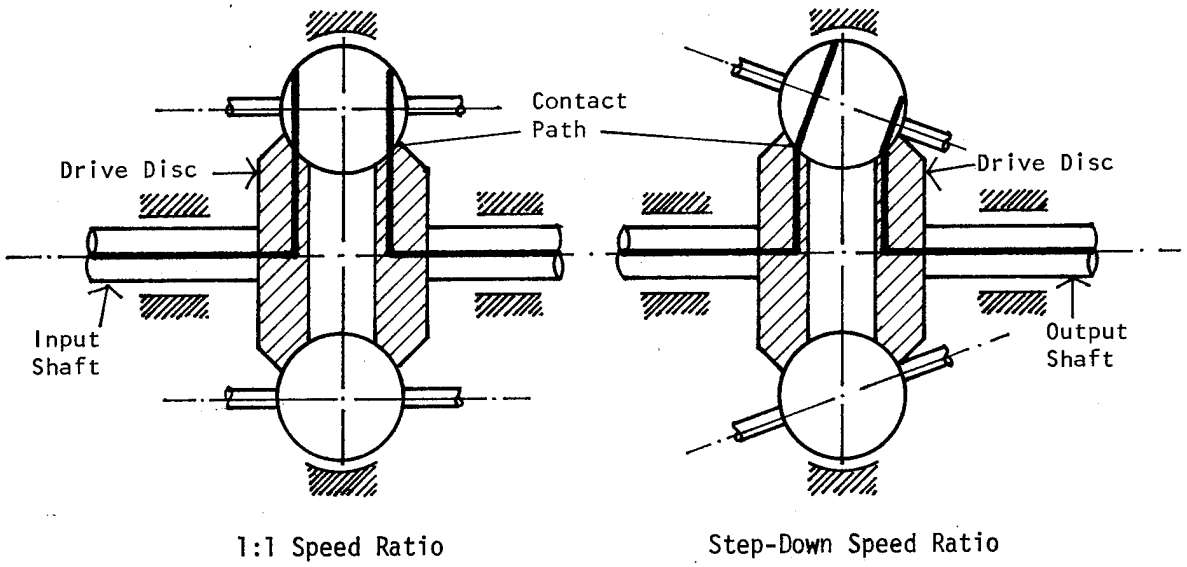


Fig. A2. Geometry of Kopp Variator Traction Drive

Tilting the axes of rotation of the spheres changes the circumference of the contact paths, thus varying the speed ratio.

UTILIZATION OF FLYWHEELS FOR THE EVOLUTION OF HIGH PERFORMANCE ELECTRIC VEHICLES

L. G. O'Connell, J. F. Cooper, A. B. Miller, H. W. Newkirk
University of California
Lawrence Livermore Laboratory
P.O. Box 808
Livermore, California 94550

ABSTRACT

The performance characteristics of current and future electric vehicles are examined and compared to projected heat engine vehicle parameters. The shortcomings of electric vehicles in the near-term time frame are discussed. It is predicted that the all-electric vehicle, even those utilizing flywheels for meeting transient power demand, will not gain wide acceptance in the near future because of degraded performance characteristics. It is indicated that the flywheel always improves performance and range under certain circumstances. Therefore, a hybrid concept is examined which the authors believe can give an enhanced performance level in the short range future. This type of vehicle is proposed as a much needed transition system to provide an evolutionary change from the heat engine system vehicle of today to electric vehicles with acceptable performance in the future.

INTRODUCTION

OVERVIEW

Electric vehicles (EV's) are being considered as one alternative to the internal combustion engine (ICE) automobile in an attempt to find a solution to our growing shortage of petroleum. In order for electric vehicles to have an effect on petroleum usage they must capture an appreciable share of the automotive market.

This paper will show that electric vehicles utilizing current and near-term technology cannot provide the performance comparable to their ICE counterparts and thus, their ability to make a major penetration in the automotive market place is questionable.

We also intend to show that this is not a static situation. The EV is likely to improve vis-a-vis the ICE and about 1990 may well be broadly competitive. What, then, can be done today, utilizing energy storage technology? The transportation research group at Lawrence Livermore Laboratory (LLL) has been concerned with this issue for some time. Last year our work led us to recommend combining storage devices, a battery and flywheel, into a hybrid electric power system.*[1] The resultant design utilized the key qualities of each storage device in an automotive power system. The flywheel addition provided the EV with performance acceptable by ICE standards, and in high speed urban driving profiles, the range was increased over that provided by the corresponding all-battery system utilizing today's lead-acid battery. While an improvement, the range was still far short of that achieved by an ICE vehicle.

LLL continued to address this problem and the transportation research group now believes there is a solution. The nation needs a transition vehicle to bridge the time gap from today's ICE vehicles to acceptable EV's of the 1990's. This transition vehicle should perform competitively with the ICE vehicle; it should bring about a dramatic reduction in petroleum consumption by automobiles, and it should pave the way to high performance electric vehicles. The concept of a transition is not new. Although the design approach was different from that in this paper Hoffman[2] did discuss such a transition vehicle in 1967.

Our transition vehicle is propelled by "QED", Quasi-Electric Drive. By "Quasi" electric, we mean a power system that is not quite all-electric. It is an electric drive system using a flywheel and battery as explained above which is augmented by a small heat engine when needed. The heat engine is utilized to provide only that energy required for range extension beyond that provided by the batteries and flywheel.

*A joint effort with the AiResearch Manufacturing Company of California.

As batteries improve, the heat engine system contribution can be reduced; by about the 1990's, it might be eliminated.

While we will explain the concept in more detail later in the paper, it should be understood that this concept differs from the usual concept of a hybrid. It operates as an electric vehicle most of the time. The battery and flywheel are recharged from offboard sources primarily. However, if at anytime the battery is discharged to a predetermined level, (e.g., 75% discharged) probably because of extended range trips, the system controller will switch on the engine and the vehicle operates as the normal hybrid.

SECTION I

PROSPECTS FOR ELECTRIC VEHICLES

Electric vehicles have existed for a long time. In fact, at the end of the last century, three types of personal transportation vehicles were on the market. They were the electric car, the steam car, and the internal combustion engine (ICE) car, the ICE was predominantly the spark ignition engine (SIE).

The history of the electric car goes back at least as far as 1839 when it is reported that a Mr. Anderson of Aberdeen attempted construction of such a car. In 1888 and 1891, respectively, efforts were made toward an electric car by Fred Kimball of Boston and by William Morrison of Des Moines. The first manufacturer to produce electric vehicles commercially was the Woods Motor Vehicle Company in Chicago. Sales of electric passenger cars peaked at more that 4,500 annually (possibly up to 6,000) in the period 1912-1914.[3,4] Estimates of annual sales between 1899 and 1933 are plotted in Fig. 1.[3] Electric vehicles for commercial applications sold at a rate of about 4,000 annually in 1912. The electric cars of those times had limited range because of the low energy density of the existing batteries; it was about 32 kilometers (20 miles). Their speed was low as well, even for those days - about 32 kph (20 mph) or less. Additionally it took from 8 to 12 hours to recharge the batteries. Electric cars were also expensive, well beyond the reach of the mass market.

The steam car was inconvenient. Range was limited by the need for frequent water refills. Starting the vehicle was a time-consuming chore. The vehicles were not as clean as the electric vehicle and the combustion process combined with the presence of a pressure vessel made the steam car appear to be less safe. They were also somewhat unreliable. Of course, all of these disadvantages were diminished as a result of considerable development work, but by then, the SIE car had taken a commanding lead.

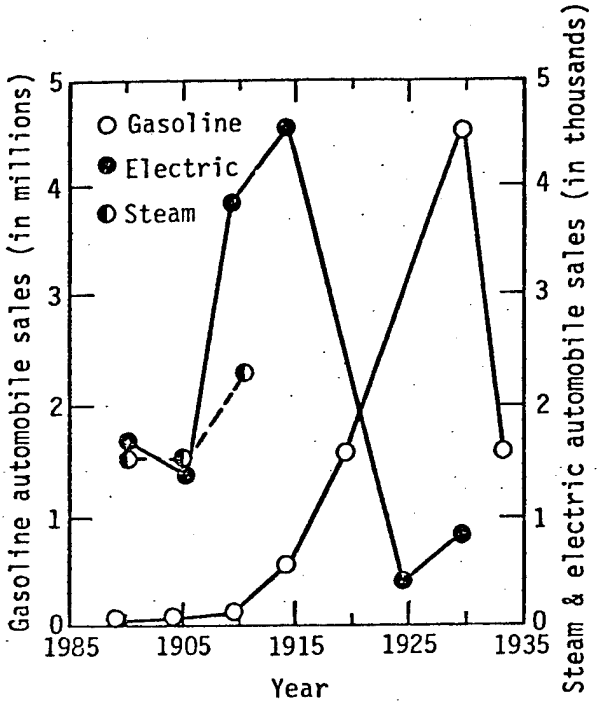


Figure 1. Relative marketability of steam, electric, and ICE cars during first third of 20th century.

The SIE also started out as a relatively dirty, cantankerous, unreliable power source but it had sufficient potential for long range and high performance at low weight and reasonable cost that it justified a lot of development effort. It was cleaned up and its reliability and ease of operation were improved. The self-starter and more recently the automatic transmission made it even more appealing. Accompanying the improvements in the SIE automobile were the developments in the highway system and in the service station infrastructure; the latter providing virtually unlimited range. As of this time, the SIE automobile has clearly outdistanced its competition.

The ICE vehicle gained market superiority over other types of propulsion on the basis of its superior performance. Since that time, the public has become thoroughly accustomed to its performance standards. Future electric vehicles will have to have performance good enough to attract consumers away from the ICE vehicles of the future in order to penetrate the automotive market.

HEAT ENGINE AUTOMOBILES-FUTURE PERFORMANCE

In order to determine the present and future viability of the electric vehicle it is necessary to understand the baseline product - the ICE vehicle - against which the proposed new product will be judged. This future baseline vehicle, itself a function of time, will consist of a future vehicle mix of various sizes, 4, 5, and 6 passenger automobiles.[5] We have chosen for purposes of this paper the 4-passenger car from reference 5 as our model.

In projecting the passenger car into the future, reference 5 contemplated a pattern of gradual change in the baseline product resulting from the conservative application of technology and of economic and marketing principles. Sensitivity analyses were made showing the effect upon various end-use characteristics (fuel economy, for example) resulting from various combinations of basic parameters such as acceleration performance, structural design and materials, engine design, type of transmission, safety and damageability criteria, and emissions criteria. In addition, a number of scenarios were studied assuming various times and rates of introduction of new design concepts. No single scenario was pointed to be the one, unique pattern of events. However, from our study of the results of that investigation, we have tentatively arrived at what follows as a description of the future 4-passenger, heat engine powered automobile (see Table I).

TABLE I

FUTURE VEHICLE CHARACTERISTICS

	CA 1980	CA 1985-87	CA 1995-2000
Fuel economy, km/ℓ (mpg)	10-14(24-32)	13-16(30-38)	16-19+(38-45+)
Power-to-weight ratio, kw/kg (hp/lb)	~0.07(0.04)	~0.05(0.03)	~0.03(0.02)
Acceleration performance, number of seconds, 0-97 km/h (0-60 mph)	12	15	20
Basic cruise speed, km/h (mph)	89(55)	89(55)	89(55)
Maximum cruise speed, km/h (mph)	129(80)	113(70)	105(65)
Curb weight, kg (lb)	1134(2500)	907(2000)	862(1900)
GVW, kg (lb)	1452(3200)	1225(2700)	1179(2600)
Fuel cost: cents/kilometer (cents/mile) (Assumes 16 cents/liter - 60 cents/gallon - for gasoline)	1.2-1.6(2-2.5)	1.0-1.2(1.6-2)	~1.0(~1.6)

Range . . . Limited between refuelings by size of gas tank and fuel economy. Assuming that some fuel is held in reserve, 320 Km (200 miles) is fairly typical. Existing infrastructure provides quick refueling at convenient stops, resulting in essentially unlimited range.

The hope would be that the heat engine car, with innovations in powerplant, transmission, and structure and with some sacrifice in performance and convenience (and probably comfort as well) would be able by the year 2000 or thereabouts, to provide personal transportation with an improvement in fuel economy of nearly 75% to 100% when compared to 1975 usage. This is based on today's composite 7.3 Km/l (17.1 mpg). Meanwhile, it is probably safe to say that the heat engine car will continue to set the standard of performance and utility against which other concepts must be measured.

SECTION II

THE FUTURE OF ELECTRIC VEHICLES

The Battery. The limiting factors in electric vehicle acceptance by the consumer are vehicle performance and cost where compared to their ICE counterparts. As we have shown earlier in this paper those were the same factors prevalent around the turn of the century. However, with the growing shortage of petroleum we must again search for alternative power systems. The battery as the primary energy source has always been the key to the success of the EV and fortunately better batteries appear to be coming. Of course the important question to be answered is whether these batteries will provide consumer acceptable automobiles in the near future and if not, when will competitive vehicles be available? In the last section we examined the performance expected for the ICE vehicle in the future; in this section we will examine the future performance of electric vehicles.

The battery is the key element. Table II lists the characteristics and costs of those batteries expected to effect the future of electric vehicles. These batteries range from current state-of-the-art to those in an early experimental stage of development. The relationship of specific power to specific energy for some of these batteries is plotted in Fig. 2 and Fig. 3. We have divided the future into three stages; near term (now to 1982), intermediate term (1982 to 1990), and long term (beyond 1990). These years indicate the time frame in which the batteries could conceivably be available to the public as electric vehicle batteries. The batteries and dates are indicated in Table II.

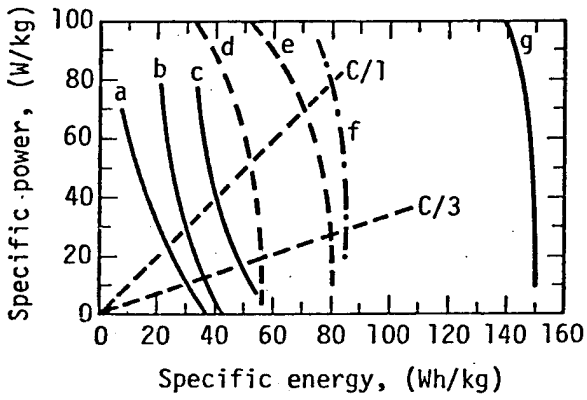


Figure 2.
Battery characteristics for selected near-term and intermediate term batteries.
a) lead acid - state-of-the-art
b) lead acid - improved
c) lead acid - projected
d) nickel zinc - near-term
e) nickel zinc - projected
f) lithium iron sulphide - near-term
g) lithium iron sulphide - advanced

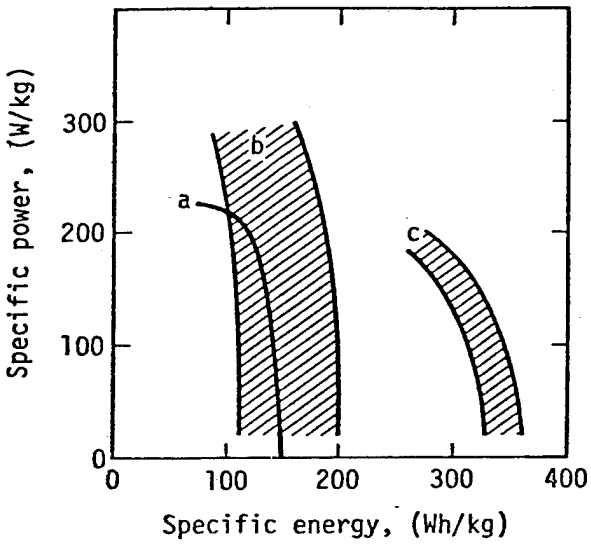


Figure 3.
Battery characteristics for selected long-range batteries.
a) lithium iron sulphide - projected
b) sodium sulphur
c) lithium air

TABLE II. BATTERY CHARACTERISTICS AND COSTS*

Battery Type	Specific Energy** Wh/kg	Specific Power** W/kg	Peak Specific Power, W/kg	Energy Efficiency,%	Cycle Life	Initial cost Cost/kWh $/kWh-cap	
			Near Term (1977 to 1982)				
1. Pb/PbO_2	24	24	70	65	400	40	6,7,8
2. $PbPbO_2$ improved	30	30	70	65	600	100	8,9
3. Fe/NiOOH	30-50	17	80	55	1000	500	10,6,7
4. Zn/NiOOH	55	20	100	65	200	?	10,6
			Intermediate Term (1982-1990)				
5. Pb/PbO_2 projected	40	40	140	65	800	50	6
6. Fe/NiOOH projected	60	20	100	60	1500	100	9
7. Zn/NiOOH projected	80	20	100	65	1000	100	8
8. Li-Al/FeS_x advanced	150	100	200	80	1000	30	9,10
9. Zn/Cl_2 improved	110	110	150	80	350	60	9, 6
			Long Term (beyond 1990)				
10. Li-Al/FeS_x projected	150	100	200	80	1000	30	9,10
11. Na/S projected	100-200	280	280	80	500-1000	30-50	6,11
12. Li/Air-advanced	350	100	200	35	-	-	9

*Inconsistencies abound in the literature concerning the projected performance characteristics of batteries.
**Specific energy at listed specific power.

Of necessity, we have left out a number of possible contenders either because the characteristics are not well reported in the literature or because there is little or no active development of the batteries for automotive applications in the United States. In all cases involving intermediate and long term batteries, the uncertainty of technical or economic success should be kept in mind. However, it can be seen that the specific energy and specific power of batteries is expected to increase considerably.

The Future Electric Vehicle. To determine the type of performance that can be expected of an electric vehicle, we chose as an example the 4-passenger automobile described in the previous section and calculated its performance as an electric vehicle using some of the batteries listed in Table II. The 4-passenger ICE automobile weighs 864 kg (1900 lb) curb weight and carries a payload of 318 kg (700 lb). This corresponds to the advanced design of the previous section (ca. 1995-2000). This was chosen because EV designers will likely attempt innovative concepts. The resulting GVW of the EV will be different, however. To determine this we allowed a ratio (α) of power system weight to GVW of 35%. Starting with the 1182 kg (2600 lb) ICE vehicle, stripping it of its ICE power system (including a mass compounding factor of 30%*[12]) provides a base structural weight. To this are added an electric power system (including the 30% mass compounding factor). For a ratio of power system weight to GVW of 35% the resultant GVW for the electric is 1585 kg (3486 lb). Following this we calculated the range of this vehicle over a modified SAE J227 Urban Driving Cycle† [13] and at a constant speed of 88 km/h (55 mph) for some of the batteries listed. The vehicle characteristics used in this calculation are shown in Table III. The LLL vehicle model was utilized to calculate range. The results are shown in Table IV. Since the value of α is a function of a more detailed design effort than is included in this paper and will have an effect on performance, we also list the results for an $\alpha = 0.4$ in Table IV. The resultant vehicle GVW at $\alpha = 0.4$ is 1800 kg (3960 lb).

*That structural weight added to support the power system; assumes some innovative design.
†See Table IV for explanation of driving cycle modification.

TABLE III ELECTRIC VEHICLE SPECIFICATIONS

Gross vehicle weight, kg (lb)	1585	(3486)
Payload weight, kg (lb)	318	(700)
Vehicle structure weight, kg (lb)	712	(1566)
Vehicle structure base weight, kg (lb)	545	(1200)
Power subsystem weight, kg (lb)	555	(1220)
Battery, kg (lb)	448	(985)
Storage System Components (Motor, Controller, Gearbox) kg (lb)	107	(235)
Power system to gross vehicle weight ratio, α	0.35	
Frontal area, $\overline{A}$, m^2 (ft^2)	1.86	(20)
Aerodynamic drag coefficient,	0.35	
Rolling friction coefficient,	*	

*Rolling Resistance, $R_R = \frac{T_R}{65} W (1 + 3.3 \times 10^{-3} V + 4.2 \times 10^{-5} V^2)$

T_R = Coefficient for tire resistance, Radial Tires = 0.9

W = Vehicle Weight (kg)

V = Vehicle Velocity (km/hr)

From these results it can be seen that in the near term, no electric vehicle is projected to match the range of the internal combustion vehicles over the same profile. In the intermediate term, ranges exceeding 320 km (200 mi) appear possible. Providing technically and economically successful introduction of Zn/Cl_2 or $Li-Al/FeS_x$ batteries* is accomplished, the competitive position of the EV will improve. The long term batteries however are expected to provide even more competition.

In this analysis the effect of regeneration was not included. Another study of the value of regeneration for near term battery systems such as the lead-acid[15] indicate a range improvement of 13.2% to 14.6% over similar driving profiles.

Adding a flywheel to the electric drive train allows batteries such as the above to be load leveled, because the flywheel can supply transient power.

Most batteries suffer a reduction in available capacity when subjected to elevated discharge rates. They provide highest energy at modest power demands. On the other hand, a flywheel can deliver or re-accept energy at high power levels without affecting its energy storage capacity. This capacity is limited only by the stress-bearing capability of the connected hardware, gearing, shafts, etc.

*Some doubt exists that fused salt batteries will be available before 1990.[11]

For the electric vehicle, the flywheel addition provides a means of satisfying the power demands of stop-and-go performance requirements that, time-averaged, represent only a modest continuous energy investment at low power levels.

In the flywheel/battery power system, the flywheel is called upon to augment the battery during periods of high current demand, i.e., starting, acceleration and hill climbing. The battery will supply cruise and control power plus the energy required to replenish some flywheel losses. This "split of energy demand is shown figuratively in Figure 4. With battery power demand stabilized at a low value, specific energy is maintained near maximum. The result is a vehicle with comparable acceleration to the ICE automobile and a range increase on the order of 33% over an all-battery system[15] such as the above (this advantage reduces to about 17% had the battery system employed regenerative braking) on high speed urban driving cycles such as the SAE J277a(D) cycle. The flywheel utilized was a fiber composite type with an energy density of 33 W·h/kg for the entire flywheel system.

Even though adding a flywheel will improve range, it will not be sufficient to change the overall result in the near term enough to make electric vehicles competitive. The value of flywheels in the future is expected to be appreciable, but depends on the development of advanced flywheels. This should be investigated.

SECTION III

HYBRID CONCEPTS

Previously in this paper, the QED concept was introduced as a transition vehicle which would allow advantageous use of state of the art batteries and which could provide an evolutionary change to

TABLE IV CALCULATED RANGE OF ELECTRIC VEHICLES

	SAEJ227 Modified Urban Cycle* km (mi)		Constant Speed 88 kph (55 mph) km (mi)	
	$\alpha = 0.35$	$\alpha = 0.4$	$\alpha = 0.35$	$\alpha = 0.4$
Near Term Batteries				
1.**Pb/PbO_2	42 (26)	58 (36)	39 (24)	58 (36)
2. Pb/PbO_2 -improved	63 (39)	82 (51)	60 (37)	82 (51)
3. Zn/NiOOH	124 (77)	161 (100)	122 (76)	163 (101)
Intermediate Term Batteries				
5. Pb/PbO_2 -projected	97 (60)	129 (80)	93 (58)	130 (81)
7. Zn/NiOOH -advanced	177 (110)	227 (141)	172 (107)	228 (142)
8. Li-Al/FeS_x-advanced	348 (216)	441 (274)	336 (209)	444 (276)
Long Term Batteries				
10. Li-Al/FeS_x-projected	348 (216)	441 (274)	336 (209)	444 (276)
11. Na/S	372 (231)	470 (292)	359 (223)	475 (295)
12. Li/Air	800 (497)	1015 (631)	794 (481)	1027 (638)

*The Modified Urban Cycle used is a combination of the SAE J227 Residential and Metropolitan Cycles. The combination was used to include both aspects of urban driving.

**Numbers refer to those in Table II.

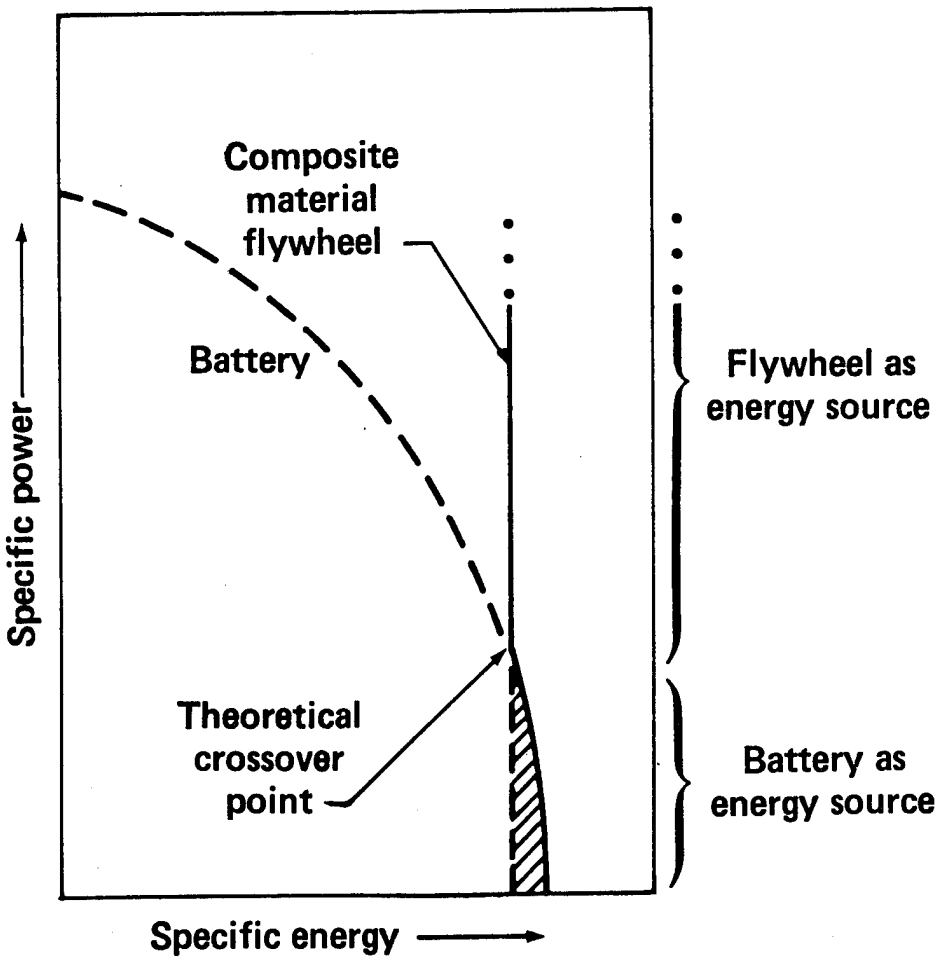


Fig 4. Specific energy as a function of specific power; battery and flywheel. Load leveling the battery at low power by allowing the flywheel to supply transient power demands has the effect of increasing the effective capacity of the battery.

high performance EVs of the 1990's. By definition, QED is a hybrid, but a hybrid concept that is quite different from most of the hybrid concepts of the past.

Historically the hybrid was born of the necessity to improve the performance of the ICE vehicle.[3] Early internal combustion engines had low torque characteristics. The parallel hybrid was conceived as a way around this. Since electric motors do not have similar torque limitations, an electric motor working in parallel with the ICE and energized by a battery or a flywheel (either can be used as the storage device) could be used to supplement low ICE torque when required. When available engine power is not needed some could be utilized to recharge the battery or flywheel.

Another problem with the ICE system was the need to shift a manual transmission periodically to match engine output to road load requirements. To avoid shifting a better way of load matching was required.

One form of continuously variable transmission consists of an electric generator driven by the engine where the generator output drives an electric motor; coupling between generator and motor is electric, not mechanical. Placing such a unit in series between the engine and the differential is the basis for the "series hybrid". The need for a mechanical clutch and gearbox are eliminated; good control at all speeds, forward and reverse, is possible. A storage battery is also utilized to supply power to the motor and thus provide the variable output desired.

The series hybrid provides flexibility of operation and control because the engine and the motor are not mechanically coupled, but all of the components must carry the full load and must be sized accordingly. In the parallel hybrid, the motor processes only enough power to enhance the engine torque when required for acceleration, hill climbing, and the like. This fact, combined with the speed variation obtained with the transmission, permits the parallel hybrid to use smaller electrical components than the series type.

As IC engine development continued, torque characteristics improved to the point where a hybrid assist was not required. Further, the introduction of the automatic transmission obviated the need for manual shifting. Thus hybrid concepts were not needed and never had a major impact in the market.

Interest in hybrids was renewed in the late 1960's as a result of the increasing concern over the emissions from the ICE and the resulting atmospheric pollution. Interest in the pure electric vehicle (EV) was also great at this time because it promised to eliminate the ICE. The advantages of the hybrid over the EV were superior range and performance, use of existing automotive technology and supporting infrastructure, and the offer of a gradual transition to the all-electric system.[2]

However, the attack on ICE emission control has been sufficiently successful so far, in spite of cost, complexity and performance penalties, that the development of a hybrid has not gained much support.

Now, increased awareness of the difficult petroleum situation has given impetus once again to a consideration of the hybrid-powered vehicle. Many other alternatives to the ICE and especially to the SIE, of course, are being considered. As mentioned earlier, the hybrid does offer good range and performance and the promise of a smooth transition to the all-electric system. Both the series and parallel hybrids offer savings in fuel consumption over a straight ICE vehicle[16,17,18,19] because they allow the ICE to be load leveled, or nearly so, depending upon the design. The electrical components supply power for transient demands and the ICE is then designed to operate at near minimum fuel consumption points.

The hybrids that have been discussed to date in the literature are thus designed to improve the operation of the heat engine system. Either they help reduce emissions, improve fuel economy or improve some other system characteristic. All these features revolve about the onboard combustion engine. The electric motor, generator and battery are used to enhance performance. The hybrid is generally more expensive when compared to the pure ICE system. Thus far, manufacturers have opted for other ways to improve performance.

Hybrids have not been designed to enhance electric vehicle performance.

QUASI-ELECTRIC DRIVE - QED

It has been shown that electric vehicles will begin to compete as alternatives to the internal combustion engine vehicle by the late 1980's or early 1990's when batteries with sufficient specific energy become available. Until then, electric vehicles propelled by batteries of lower specific energy are unlikely to be competitive. Recent LLL analyses of the flywheel-battery powered electric vehicle have indicated that a vehicle with competitive performance (acceleration, etc.) can be designed if a flywheel is added to the propulsion system. Therefore, though improved, the drawback to electric vehicles at this stage is lack of sufficient range. Since this lack of range is caused by the low specific energy of the battery, the problem then is to enhance this battery char-

acteristic. How can this be done? A transition vehicle is needed.

A promising way to accomplish this transition is with a car that is essentially an electric car powered by a hybrid flywheel-battery power system and that in addition, employs a compact heat engine to provide the features discussed above which cannot be supplied by today's storage devices. We call this power system QED, Quasi-Electric Drive, since it is essentially an electric system with a heat engine assist. The philosophy behind this concept would allow a gradual transition from ICE vehicles to EVs without any period of reduced performance - that is, limited performance vehicles - as would be required by any shift to today's EVs. The QED operates as an electric vehicle most of its operating life. This includes recharging the batteries by off-board sources, e.g., household electricity. The heat engine is only used when the storage devices are unable to propel the vehicle without exceeding preset limits on their energy consumption. This will normally occur in extended range missions. As batteries and flywheels improve, the range provided by these storage devices will increase and the heat engine contribution can be reduced accordingly.

Even though this proposed Quasi-Electric Drive vehicle would have a heat engine for extended range and emergency capabilities, the operation of the car, as previously stated, would be such as to maximize reliance on the storage devices. As shown in Fig. 5, most trips (approximately 75% of all vehicle miles traveled) made by the average individual are less than 80 kilometers (50 miles).[20] We will show later that a QED vehicle, without the use of its IC engine can achieve an 80 kilometer range in the near term. If the battery is fully charged after being plugged into a charger at home overnight, the heat engine need not be used at all for trips of 80 kilometers or less; and the benefits of using central power station electricity are obtained. If an emergency arises during the night, the heat engine and gasoline in the gas tank are available for immediate service. On a long trip, the battery would be used until it is discharged to an allowable level and then the heat engine would be activated and the propulsion system would operate as a hybrid; an "EV" without the usual range limits. As previously stated, statistics indicate that this hybrid use would only average about 25% of vehicle kilometers traveled. Thus, in principle, QED could provide a vehicle today that has a marketable performance and achieves 75% of the goal of the EV by reducing petroleum consumption accordingly.* This is depicted in Fig. 6.

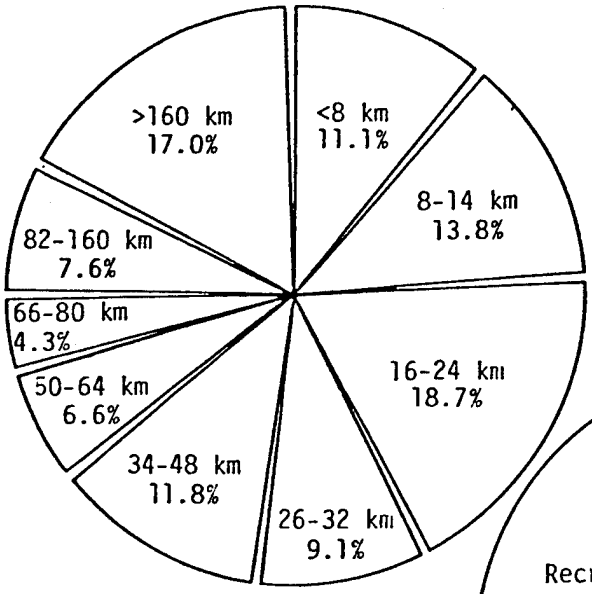
In the flywheel-battery power system the effective specific energy of the battery power system is improved because the flywheel acts as power booster and absorbs power transients, thus load leveling the battery at a low power demand. This effectively increases the battery's energy capacity and thus vehicle range in high speed urban driving cycles. This can be seen by examination of Fig. 4. The small flywheel addition can be accomplished without adding power system weight. With its utilization, other components can be reduced in weight.

The power system specific energy can be further improved by the addition of a small heat engine and fuel tank for an equal weight of battery removed so that again the power system weight remains the same. This is the essence of the Quasi-Electric Drive (QED).

This system is shown in Fig. 7. It is a hybrid system except for the philosophy of operation. It is an electric drive system with a heat engine range enhancer, whereas hybrid systems previously discussed were heat engine systems using storage devices as fuel economy enhancers or to reduce emissions. The object of the QED power system is to provide electric propulsion most of the time and extended range as needed through the use of a small heat engine.

The operating principle behind QED is simple enough. The vehicle will be operated as an electric as much as possible and the heat engine will only be utilized to provide energy when the battery is discharged to a preset level. Department of Transportation statistics indicate that trips of 80 km (50 miles) or less constitute 75% of the vehicle miles traveled in the United States.[20] If a QED vehicle can be designed to achieve this range electrically using near term storage technology and if the heat engine can provide the range boost when needed, then QED would appear to be an electric vehicle option today worth further investigation.

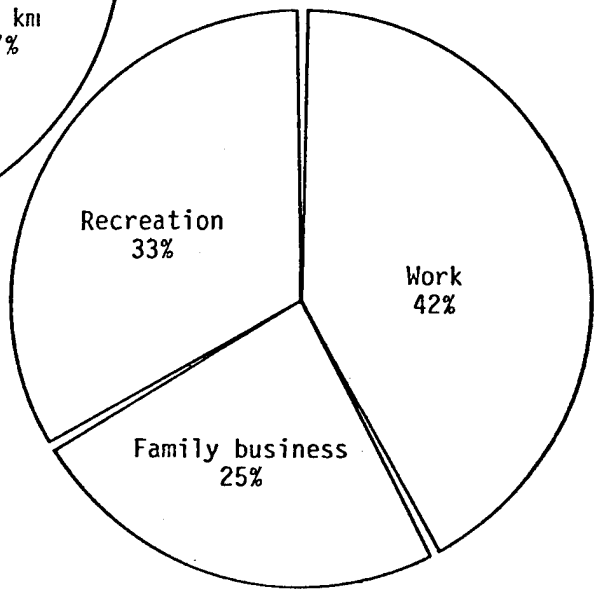
*We are assuming that electricity will not be produced from petroleum sources.



One-way trip length distribution for passenger autos. Percents listed are of vehicle kilometers traveled.

Conversion Table

km	mi
8	5.0
14	8.7
16	9.9
24	14.9
26	16.2
32	19.9
34	21.1
48	29.8
50	31.1
64	39.8
66	41.0
80	49.7
82	51.0
160	99.4



Passenger car use.

Figure 5. Analysis of passenger car use. Distance traveled is the measure of car use. Percentage distributions according to trip purpose and trip length are shown.

To determine possible QED performance we began with the electric vehicle described earlier which had a GVW of 1585 kg (3486 lb). We kept $\alpha = 0.35$ and added a small flywheel system as stated above. In addition, we then substituted a small heat engine and fuel tank for an additional weight of batteries removed. Thus, the GVW and α remain the same as before. The resultant vehicle is described in Table VI. The heat engine and fuel tank were sized to provide sufficient additional power system energy at 88 kph (55 mph) so that a range of 200 miles can be achieved before refueling is required. Battery depth of discharge is limited to 75% to prolong battery life. When this level of discharge is reached the power control unit would be programmed to switch on the engine. At this point the vehicle would operate as a hybrid with the engine system charging and discharging the storage devices* as determined by road load requirements. This would allow the heat engine to be load leveled thus improving its fuel economy. This operating principle makes QED different from other hybrid systems.

*Battery charge would be maintained at about the 25% level. Full recharge would be achieved by use of offboard energy.

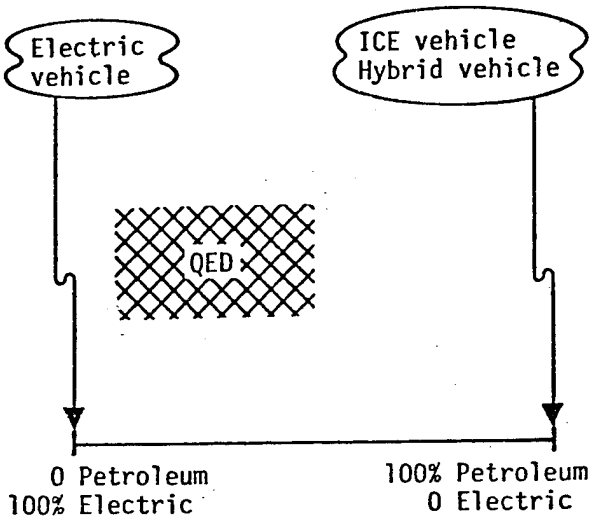


Figure 6. Relative position of vehicle types with respect to dependence on petroleum. QED vehicle is much closer to all electric than previous hybrids.

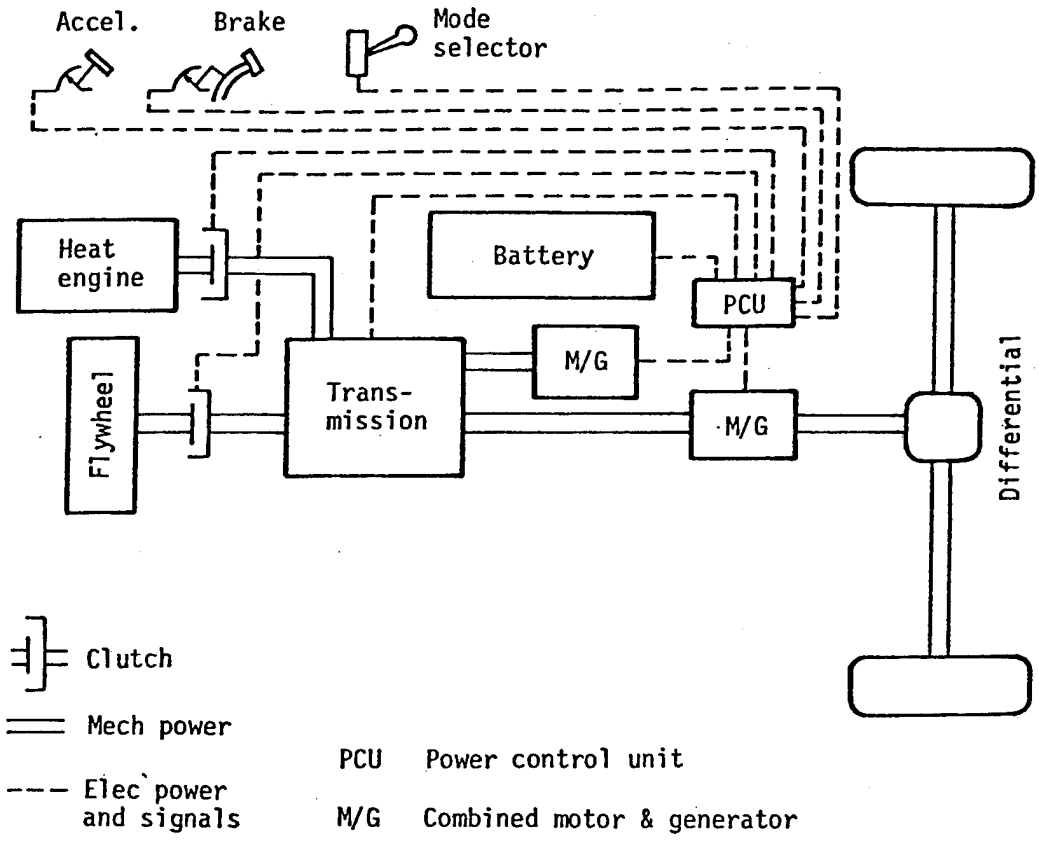


Figure 7. Block Diagram of Quasi-Eleectric Drive (QED)

Once the required heat engine system was determined the analysis was continued to determine if an "electric" range of 50 miles or more could still be obtained. Table VII gives the results of the analysis. Again, as with the electric vehicle analysis we have also included the results for a vehicle of $\alpha = 0.4$ weighing 1800 kg (3690 lb). An electric vehicle with an α of 0.35 can achieve the desired 50-mile range in the near term using QED. (If $\alpha = 0.4$, the range far exceeds 50 mi.)

The operating cost of this system is of course a combination of both electric and petroleum fuel costs. On the average the vehicle will travel 75% of the time electrically and 25% of the time on petroleum.[20] The effective fuel cost of the vehicle (α = 35%) electrically is 0.18 kW·h/km (0.29 kW·h/mi).[13] At 4 cents/kW·h, the cost is 0.72 cents/km (1.16 cents/mi). At 75% usage the cost is 0.54 cents/km (0.87 cents/mi). The cost of the petroleum increment per km (mi) is* 0.07 liters/km (0.03 gal/mi). At 16 cents per liter (60 cents/gal) and used 25% of the time, that is .28 cents/km (.45 cents/mi), the average fuel cost for this vehicle is 0.8 cents/km (1.3 cents/mi). This compares quite favorably with the ICE vehicle of ca 1990's - 1 cent/km (1.6 cents/mi) and the near term EV, 0.8-1.6 cents/km (1.3-2.6 cents/mi). Of course changes in fuel cost with time will alter these results.

QED can provide an electric vehicle with competitive performance today. As batteries improve, the heat engine contribution can be reduced until finally in the 1990's the vehicle can probably be all electric. QED can allow the evolutionary process needed to shift from ICE vehicles to EV's. It can act as a transition vehicle.

We have not addressed the vehicle cost. This can only be determined after a more detailed design has been accomplished. However, we expect it can be cost competitive with other EVs. The determination of specific performance parameters such as acceleration, gradeability, etc., also await the sizing of components in a detailed design. Previous design experience with systems involving flywheels as power boosters give us confidence that the vehicle can be designed to compete.

TABLE VI QED VEHICLE CHARACTERISTICS

GVW, kg (lbs)	1585	(3486)
Power Systems Weight, kg (lbs)	555	(1220)
Battery*, kg (lb)	386	(848)
Storage System Components**, kg(lbs)	107	(235)
Heat Engine Systems***, kg (lbs)	62	(137)
Power System Weight to GVW	0.35	-
Frontal Area, m^2 (ft^2)	1.86	(20)
Aerodynamic Drag Coefficient C_D	0.35	
Rolling Resistance Coefficient	****	

*Pb/PbO_2 No. 2 of Table II

**Motor/generator, gearbox, controller, and flywheel

***Engine (22HP) fuel tank, cooling, exhaust system, etc.

****See Table III

*The calculated fuel economy of the heat engine component is 14 km/l (32 mpg) for $\alpha = 0.35$ and 13 km/l (30 mpg) for $\alpha = 0.4$.

TABLE VII QED PERFORMANCE

		$\alpha = 0.35$	$\alpha = 0.40$
Range Electric			
SAE J227 Modified Urban Cycle	km (mi)	84 (52)	100 (68)

SECTION IV

CONCLUSIONS

Although only conceptual design work has been completed, QED appears to be a viable approach for near-term electric vehicles. It can provide electric vehicles today with competitive range compared to combustion engine vehicles. Performance using flywheel power boosting is expected to be acceptable although to determine actual values will require a more detailed sizing of components. The fuel operating cost at today's prices is equal to that of all battery electric systems using state-of-the-art batteries. If QED vehicles were employed today, they could dramatically reduce petroleum consumption by the automobile in the United States.

REFERENCES

[1]D. D. Davis et al., The Battery Flywheel Hybrid Electric Power Systems for Near-Term Application, Vol. I and II, Lawrence Livermore Laboratory, Report UCID 17098 (1976).

[2]G. A. Hoffman, Power Systems for Electric Vehicles, University of California Los Angeles for U.S. Dept. HEW, Public Health Service, Bureau of Disease Prevention and Environmental Control, National Center for Air Pollution Control, Cincinnati, Ohio (1967).

[3]C. Rosen,"Overview of Hybrid Vehicles," in Proceedings of the Second International Electric Vehicle Council, New York, New York (1971).

[4]Development of Electrically Powered Vehicles, Bureau of Power, Federal Power Commission (1967).

[5]The Report By The Federal Task Force on Motor Vehicle Goals Beyond 1980, Vol. I and II, for the Energy Resources Council (1976).

[6]F. J. Port,"Energy Sources," Electric Vehicle News, 6 (November 1976).

[7]Y. Ming-Chih and D. C. McCulloch, "Small Electric Vehicle Considerations in View of Performance and Energy Usage," in Proceedings of the Eleventh Intersociety Energy Conversion Engineering Conference, State Line, Nevada, 363 (September 1976).

[8]K. W. Mao and G. J. Hwang, "Development of Electric Vehicles in Taiwan," in Proceedings of the Eleventh Intersociety Energy Conversion Engineering Conference, State Line, Nevada, 357 (September 1976).

[9]L. G. O'Connell, Ed. The Role of Energy Storage Power Sytems in Transportation - Status Report, Vol. I and II, Lawrence Livermore Laboratory, Report UCID 17274 (1976).

[10]A. R. Landgrebe, "Secondary Batteries for Electric Vehicles," in Proceedings of the Symposium and Workshop on Advanced Battery Research and Design, Argonne National Laboratory, Report ANL-76-8 (1976).

[11]E. J. Cairns and Y. Ming-Chih, "Electric Vehicles Overview," in Proceedings of the Eleventh Intersociety Energy Conversion Engineering Conference, State Line, Nevada, 356 (September 1976).

[12]D. C. Sheridan, J. J. Bush, and W. R. Kuziak, Jr., A Study of the Energy Utilization of Gasoline and Battery-Electric Powered Special Purpose Vehicles, SAE Paper 760119 (1976).

[13]SAE Handbook, 1972 Edition, Society of Automotive Engineers.

[14]L. G. O'Connell et al., The Lithium-Water-Air-Battery: A New Concept for Automotive Propulsion, Lawrence Livermore Laboratory, Report UCRL 51811 (1975).

[15]D. D. Davis et al., Determination of the Effectiveness and Feasibility of Regenerative Braking Systems on Electric and Other Automobiles, Vol. I and II, Lawrence Livermore Laboratory, Report UCRL 52306 (1977).

[16]L. E. Unnewehr et al., Hybrid Vehicle for Fuel Economy, SAE Paper 760121 (1976).

[17]G. L. Dugger et al., Flywheel and Flywheel/Heat Engine Hybrid Propulsion Systems for Low-Emission Vehicles, Applied Physics Laboratory, The Johns Hopkins University (1971).

[18]J. Helling, H. Schreck, and B. Grera, Hybrid Drive with Flywheel Component for Economic and Dynamic Operation, presented at the 3rd International Electric Vehicle Symposium, Washington, D.C. (February 1974).

[19]P. D. Agarwal, R. J. Mooney, and R. R. Toipel, Stir-Lec I, A Stirling Electric Hybrid Car, General Motors Research Laborabory, Warren, Michigan, Research Publication GNR-840 (1969).

[20]1975 Automobile Facts & Figures, Motor Vehicle Manufacturers Association of the United States, Inc., Detroit, Michigan (1976).

HIGH SPEED FLYWHEELS OPERATING ON "ONE ACTIVE AXIS" MAGNETIC BEARINGS

P.C. Poubeau
Société Nationale Industrielle Aérospatiale
BP. n° 2 - 78130 LES MUREAUX - FRANCE

ABSTRACT

Since several years flywheels appear as attractive devices for storage of energy under kinetic form. The condition for the validity of such a system is to realise sufficient rotation and peripheral speeds. It présents two main aspects :
- the stresses in the materials of the rotor with the elongation and balance problems
- the bearings with wear, friction and power dissipation problems.

This lecture concerns a development which was made in the scope of satellite applications and oriented towards high speed momentum wheels realized with two possible applications :
- wide angular momentum for a low mass
- energy storage by utilisation of two counter rotating wheels.

The result of this development was to obtain several engineering models constituting small units able to store the energy under kinetic form with input and output of power under electric form. The successful operation of these models demonstrate the compatibility, for energy storage systems, of high speed rotors with a magnetic suspension. The particular characteristics of the magnetic suspension and of the rotors which were developed are described in this paper. These units appear as feasibility models for industrial application of energy storage.

1. INTRODUCTION

The flywheels which found utilization since the early times of human activity are always presenting high interest in many areas. Their present and foreseen possibilities cover a wide range of possibilitiesas well for space as, for ground applications.

The necessity for satellite flywheels to achieve very stringent characteristics gave birth to wide development efforts mainly oriented in two directions :

- the magnetic bearings which eliminate the wear problems and the main part of the power dissipation occuring with other types of bearings ; the effort described here was concentrated on "the one active axis" type of magnetic bearings with the radial centering performed passively, a single axial servoloop maintaining the rotor in the axial direction ; this concept is the simplest and the most reliable.
- the rotor with utilisation of fiber composite materials in different configurations ; the result was to obtain an interesting level of energy per mass unit involving sufficiently high periphal speeds ; the main problems to solve was to provide the compatibility of the rotor with stresses unduced by centrifugal forces and simultaneously the stability of the initial balancing in spite of the rim elongation.

* Part of this work was performed under the sponsorship of the International Telecommunications Satellite Organization (INTELSAT) under contract CSC-IS-555. Views expressed are not necessarly those of INTELSAT.

The result of this work was to obtain a completely integrated system including the rotor, the magnetic suspension, the motor-generator and associated to the electronics; it enable to introduce energy under electric form, to store it under kinetic form and to recover it under electric form. So it constitute at a small scale, a feasibility model of energy storage for industrial applications. In parallel the magnetic suspension can find other applications that flywhells and the developed rotors can be utilised on other types of bearings that magnetic bearings.

2 . MAGNETIC BEARING AND ASSOCIATED SUBSYSTEMS DESCRIPTION

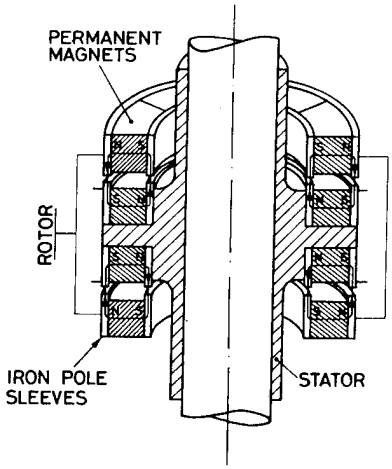
The dominant and most important feature is the essentially passive nature of the magnetic suspension systems employed. Passive magnetic suspension, i.e. based on maximal use of permanent magnets, is used in preference to alternative methods based entirely on electronically controlled electromagnets, in view of the primary objective to maximise reliability. The passive suspension configuration adopted employs permanent magnets operating in the attraction mode for radial centering of the flywheel hub, and a single servo driven electromagnets actuator for axial position control.

In this way, four out of the six degrees of freedom of the suspended rotor are constrained passively, and only one actively. The sixth degree of freedom is the desired rotational motion of the wheel which, of course, requires no constraint. The realisation of the various suspension and other elements involved are described separately below.

2.1 Passive permanent magnet radial bearings.

Radial centering of the rotor is effected by means of two permanent magnet radial bearings, the dimensions, geometry and design of which are chosen according to the specific requirements of each wheel. One possible configuration is shown in Figure 1. Each bearing comprises four radially magnetized Samarium Cobalt rings of segmented construction, fitted with soft iron pole sleeves on their inner and outer curved surfaces. Oppositely magnetized rings are attached to the flywheel rotor and stator respectively. The concentrated axial fields set up in the gaps between adjacent pole ring end faces give rise to appreciable radial centering forces for quite small radial displacements of the rotor with respect to the stator. Radial stiffnesses in the order of 1.5 to 5 x 10^5 N/m per bearing are easily achieved for quite small bearing dimensions, while ratios of radial stabilizing/axial destabilizing stiffnesses are in the order 0.5 to 0.25 are typical.

A number of constructional variations are possible. One possibility with some important constructional advantages is to employ radial instead of axially stacked ring pairs. The latter configuration has been adopted in more recently developed wheels.



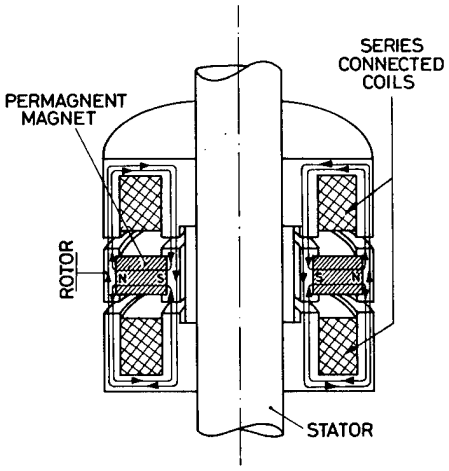
RADIAL BEARING

FIGURE 1

2.2 Active electromagnetic axial bearing

The attraction forces between the iron pole sleeves in the radial bearings give rise not only to a radial restoring effect but also tend to de-center the rotor in an axial direction.

In order to counteract these axial de-centering forces an electromagnetic axial bearing is employed. This bearing forms the power element of a servo-loop which automatically controls rotor axial position. Figure 2 shows the configuration adopted. A pair of series connected iron clad coils attached to the stator modulate the field produced by a radially magnetized Samarium Cobalt permanent magnet ring attached to the rotor. The direction of the resulting force depends on the direction of current flow in the coils. Compared with a straighforward electromagnet without permanent magnet bias, this arrangement produces much larger axial forces per ampere turn and exhibits a nearly linear force versus current relationship.



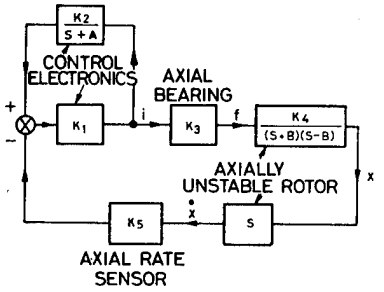
AXIAL BEARING

FIGURE 2

2.3 Axial servo loop

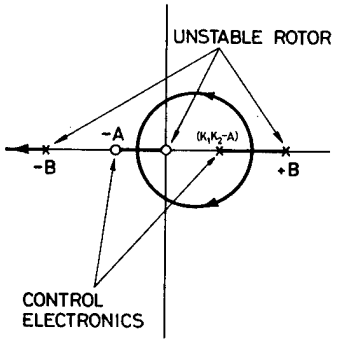
A block diagram of the electronic servo loop used for controlling the electromagnetic axial bearing is shown in Figure 3. The system employed is essentially a position control scheme which keeps the rotor at an axial position where applied forces (in 1g) are exactly compensated by lifting forces due to the permanent magnets in the radial and axial bearings. This system has the advantage of very low suspension power requirements in both 1g and 0g operating conditions as well as simplifying the electronic and mechanical realisation. The input signals used are the axial rate of the suspended rotor as measured by a small pick up coil mounted in the wheel stator and the current flowing in the axial bearing coils. A separate logic is used for initial lift off of the rotor.

The stability of the system is evident from the root locus plot shown in Figure 4. By appropriate choice of the electronic gain factors K_1 and K_2 all closed loop poles are brought into the left half plane.



AXIAL POSITION CONTROL SYSTEM

FIGURE 3



ROOT LOCUS OF AXIAL CONTROL SYSTEM

FIGURE 4

2.4 Radial dampers

The passive radial magnetic bearings described above may be likened to almost perfect lossless springs as far as their radial restoring characteristics are concerned. Together with the rotor mass they form an undamped second order vibratory system which is excited by unbalance forces during rotor spin up as well as precessional torques at normal operating speed. In order to prevent excessive amplitudes of rotor motion and the possibility of mechanical contact occuring between rotor and stator parts, radial damping of the rotor motion must be introduced. The radial damping devices employed are shown in Figure 5. Each wheel contains two dampers, each damper being made up of four permanent magnet rings attached to the rotor and a copper disc attached to the stator. Radial motion of the magnet rings with respect to the copper disc induces eddy currents in the latter which interact with the permanent magnet fields producing them to yield the required damping force. Rotational drag is small due to the azimithal continuity of the fields.

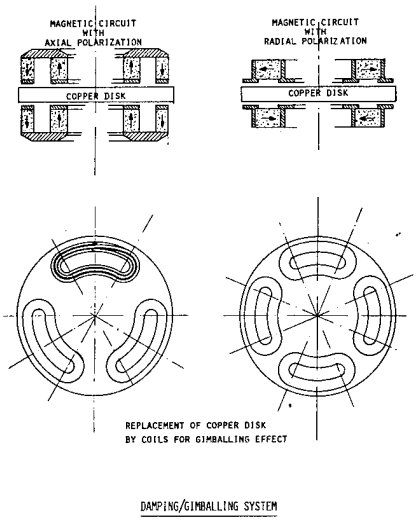


FIGURE 5

This type of damper was selected after extensive research involving a wide variety of alternative damping methods. Its chief advantages are its very effective damping characteristics, its nonreliance on structural deformation for its operation and its easy possible adaptation at a combined active damper/vernier alignment device by substituting the copper disc with a system of coils, if particular applications require such a vernier gimballing effect.

2.5 Motor

The motor is of the brushless d.c. type with electronic commutation based on high frequency sensing devices. The construction is shown in Figure 6. The rotating field structure consists of an iron ring fitted with a number of rare earth permanent magnet poles. The stationary armature comprises several coils of multistrand insulated conductors encapsulated in an epoxy resin cylindrical support. The use of ferrous materials in the stator armature is specifically avoided in order that no radial decentering forces due to attraction between the armature and field parts are introduced. In momentum wheels the motor is located at the flywheel hub while in reaction wheels location at the rim of the wheel has been found a more mass effective solution. In both cases, the motors are characterized by high efficiency, high delivered power to mass ratio and very smooth rational torque free of magnetic indent effects.

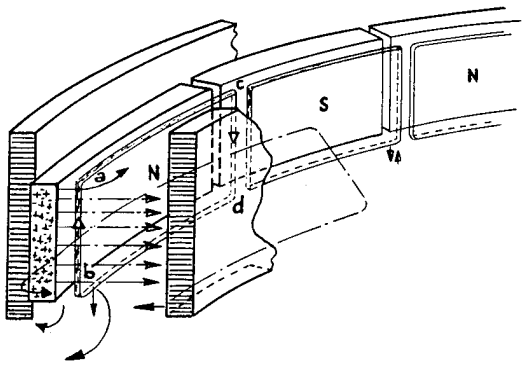


FIGURE 6

2.6 Emergency bearings

In order to avoid damage to the magnetic bearings in the event of a suspension failure at high wheel speeds or excessive slewing rates being applied, an emergency bearings system consisting of a dual pair of angular contact dry lubricated ball bearings is provided. These bearings act as both axial and radial excursion stops and only come into operation in case either axial or radial excursions become too great. The emergency bearings are attached to the rotor of the wheel and are fitted with contact touchdown pads. This configuration ensures consistently smooth touch-down behaviour even at very high rotor speeds.

2.7 Electronics

The electronics circuits control the current in the axial servoloop actuator and in the motor coils.

Three types of electronics have been developed :

- utilisation of operational amplifiers
- utilisation of discrete components
- utilisation of thick film hybrid electronics.

3. ROTORS DESCRIPTION

3.1 Overall concepts

The rotor is constitued of several functional parts :

- the central part which contains the elements of the magnetic bearings and the magnetic circuit of the motor,
- the rim which produces the main part of the inertia,
- the connexion between the central part of the rotor and the rim.

Two main problems are in relation with the rotor rim and its connexion to the centering rings :

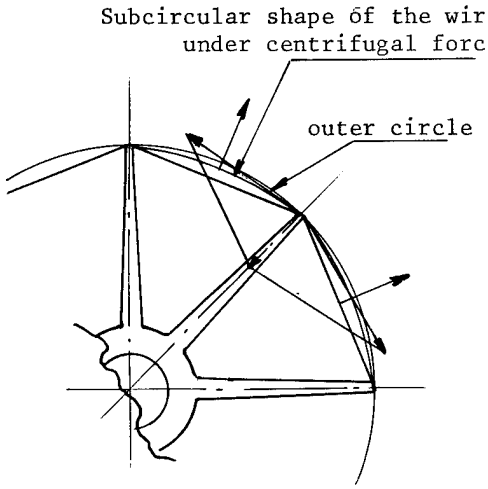
- to accept the stresses due to centrifugal forces
- to keep an accurate balancing : i.e. to maintain the coincidence between the axis of the rotor centering rings and the main axis of inertia, with a high level of accuracy. This accuracy will have to remain stable in spite of elongation due to centrifugal forces, of temperature variations, of time effect associated to the above indicated parameters.

Several types of rotors were developed. For medium speeds up to 15000 rpm and 250 m/sec of peripheral speeds light alloy rotors were developed. They are of interest for producing angular momentum (satellite applications) but they do not allow important levels of stored energy for a reasonable mass.

For high speed rotors, two main technics were utilized : the "subcircular rotor" and the "cycloprofile rotor"

3.2 Subcircular rotor

This type of rotor was developed many years ago. It is designed on the principles illustrated by the following picture.



APPLICATION OF FORCES IN A SUBCIRCULAR ROTOR

The central part of the rotor, shaft or hub, is equiped with several thick spokes. The filament material constituting the rim is wound along a polygonal shape. During the rotation, the elongation of the wire under centrifugal forces gives to the rim a shape between the polygone and the circle.

The resulting forces applied on the spokes are compressing the spokes. If the rim was initially circular, the force on the spokes should be a traction which for many reasons is not favorable to the stability of the balancing.

If necessary, the initial shape can be situated between the polygonal form and the circular form (winding over mandrels between spokes). Two rotors of that type were studied and designed in 1970 and 1971 manufactured in 1972 and tested up to 18000 rpm in 1973 and 1974. Their rim was made of steel wire for the one and of steel strip for the other ; the central shaft was in steel (rotation on ball bearings) and the spokes were in aluminium alloy).

3.3 Cycloprofile rotors

This solution was mainly utilized for rotors in which the mechanical connexion between the rim and the central hub has to be as hight as possible (high speed momentum wheels for satellites).

The rotor consists of three parts : an aluminium alloy hub that is used as interface between the filament rotor assembly and the rotor shaft, a circumferentially wound filament rim, and the cycloprofile envelope windings that attach the rim to the hub. The rim is wound about a mandrel. After curing, the mandrel and rim are finish machined. The envelope winding consists of two layers of filament tape. After the tape is cured, the mandrel is washed away. Several complete rotors have been fabricated, in glass fiber, in carbon fiber, and in KEVLAR 49*. These rotors were designed to be operated with the magnetic suspension described previously. Nevertheless, the same cycloprofile technics were applied to realize a 30000 rpm rotor in glass fiber epoxy adapted on a shaft ; it was designed for potential application to a hoist flywheel and tested up to 30000 rpm. It is presented in the annexed photo.

* Kevlar 49: Dupont de Nemours trade mark

3.4 Some magnitude orders for flywheels parameters

In a "thin rim" (thickness about one tenth of the diameter) as it is the case in the described concepts, the stress in the rim is :

$$\sigma = \rho V^2$$

were ρ is the specific mass of the rim material and V the mean peripheral speed. In addition, there is to consider, for a composite filament-resin rim, that the resin is the origin of an additional stress for the filament. The following table gives order of magnitude of the stresses and of the elongations for different peripheral speeds; the ultimate tensible strengh and elasticity modulus of the materials are also indicated (orders of magnitude).

PERIPHERAL SPEED Material	E hbar	U T S hbar	STRESSES 500m/s hbar	STRESSES 700m/s hbar	STRESSES 1000m/s hbar	ELONGATIONS 500m/s %	ELONGATIONS 700m/s %	ELONGATIONS 1000m/s %
Steel wire	20.000	300	200	-	-	1%	-	-
Glass fiber	7.000	350	75	150	300	1%	2%	4%
Carbon fiber	16.000	250	50	100	200	0,3%	0,6%	1,2%
Kevlar 49	12.000	350	45	90	180	0,4%	0,8%	1,6%

Another interesting order of magnitude is given by the comparison of the energy stored in a flywheel with another type of energy : for exmple let us suppose that a flywheel with a thin rim of 10 Kg on a diameter of 62 cm rotates at 30000 rpm and is utilised on a giant hoist operating without losses. The energy of the 10 Kg of rim rotating at a peripheral speed of 1000 m/sec would be able to take up to 5000 meters of height a mass of 100 Kg. Obviously this exemple is just given as a comparison of the two different physical aspects of this energy but it indicates clearly the wide amount of energy which can be stored in a small mass rotating at high speed ; even whith energy conversion efficiencies far under one, it appear many possibilities of application.

Several aspects are pointing out from these orders of magnitude :

- the concept of the rotor has to accomodate with the important elongations which are involved, particularly at the balancing point of view
- the long term operation which will be generally requested for energy storage systems will necessitate a relatively high safety margin between the working stresses and the ultimate tensile strengh.

4. CHARACTERISTICS OF HIGH SPEED FLYWHEEL DEVELOPED FOR SPACE APPLICATIONS

Stored energy	150 000 Joules
Recoverable energy	80 000 "
Rotation speed	24 000 rpm
Radial stiffness	$1.8.\ 10^5$ N/m
Axial stiffness	$1.1.\ 10^6$ N/m
Bearing critical frequency	25 Hz
Motor torque	0.05 N/m
Steady state power	20 Watts
Diameter	350 mm
Height	210 mm
Mass	10.5 Kg

The first flywheel with these characteristics (high speed momentum wheel) was developed under INTELSAT IS 555 contract and delivered to COMSAT Laboratories.

Three others are under in-house operation for preparing kinetic energy storage systems for satellites and for general Research and Development effort in high speed flywheels.

5. CONCLUSION

The main characteristic of the equipments described here is the availability of a complete unit able to store electric energy under kinetic form and to deliver this energy under electric form with two particular aspects :

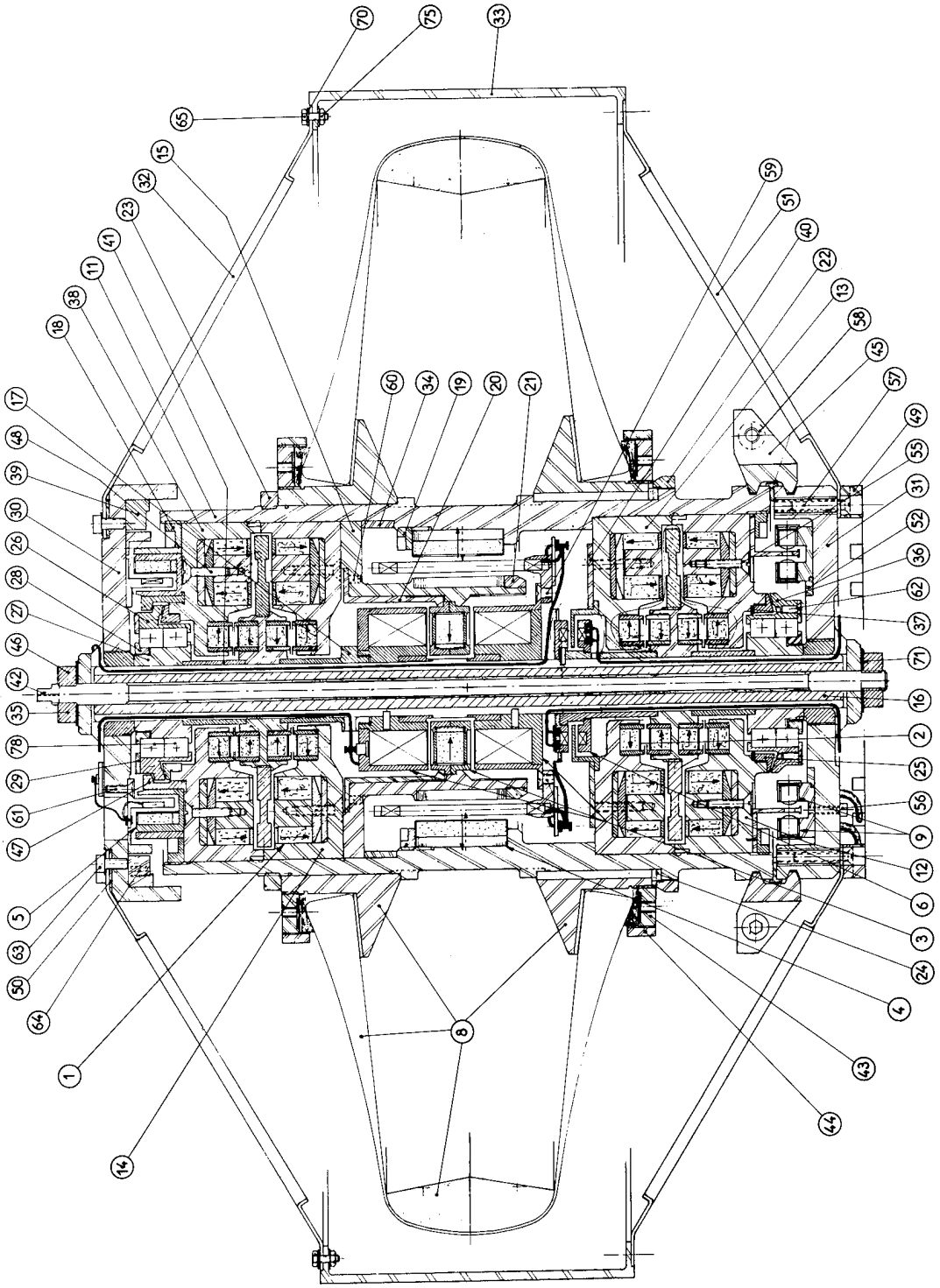
- the operation at angular and peripheral speeds in a range which is of interest for energy storage at industrial level
- the operation of the rotor with a magnetic suspension which eliminates wear and friction problem ; this magnetic suspension with only "one active axis" is the simplest and the most reliable which exists.

For these reasons, the models and subsystems were developed can give birth to industrial equipments with higher storing capacity, for a very wide range of applications.

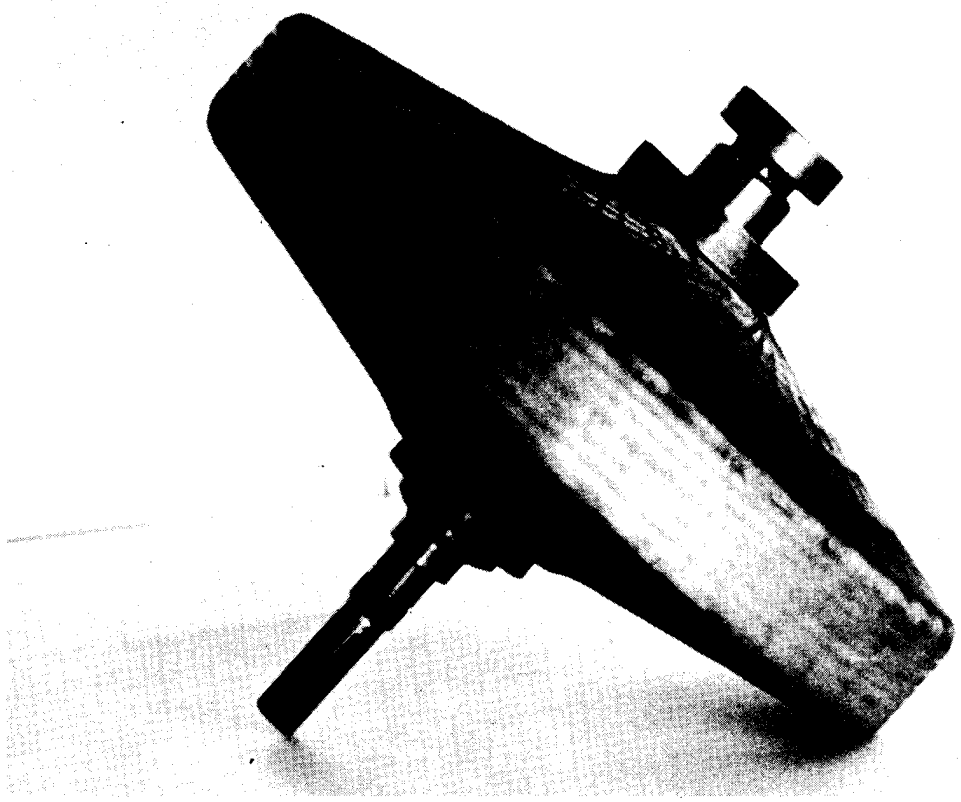
REFERENCES

1. Magnetic bearing momentum wheel
   by C.J. PENTLICKI - COMSAT Laboratories
   Clarksburg, Maryland
   and P.C. POUBEAU - AEROSPATIALE
   Les Mureaux, France
   AIAA/CASI - 6th Communications
   Satellite Systems Conference
   Montreal, Canada - April 5-8, 1976

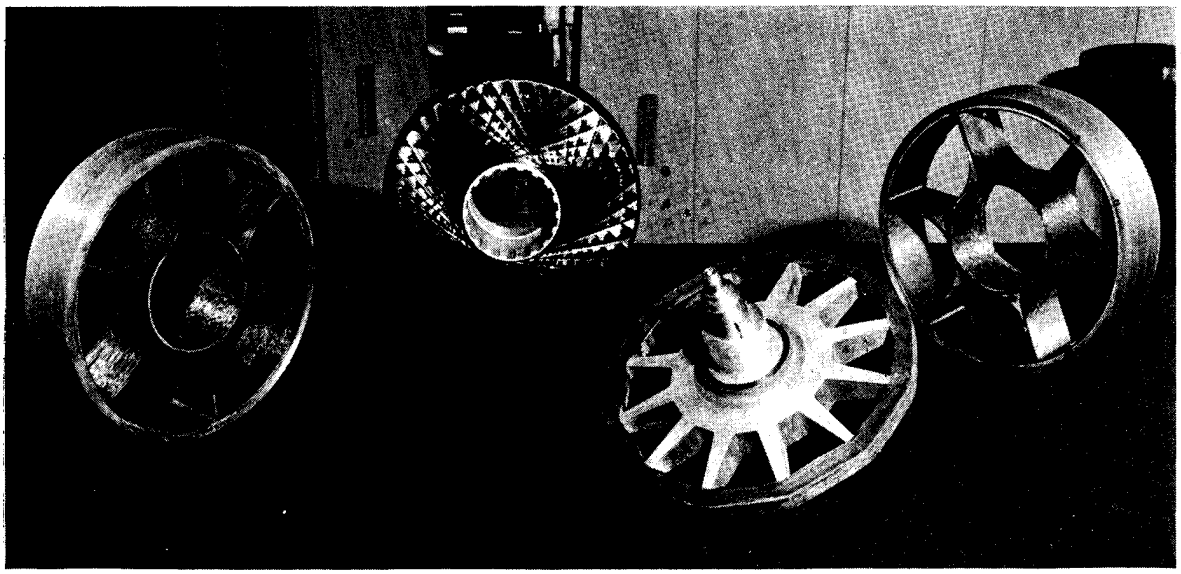
2. Development of a satellite flywheel family operating on "one active axis" magnetic bearings
   by P. C POUBEAU - AEROSPATIALE - France
   11th Aerospace Mechanisms Symposium
   NASA-Goddard Space Flight Center
   Greenbelt, Maryland - April 28-29, 1977



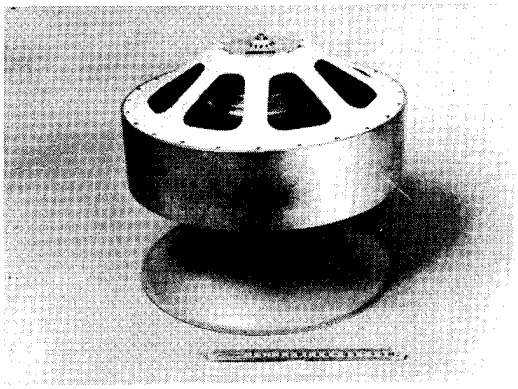
HIGH SPEED MOMENTUM WHEEL

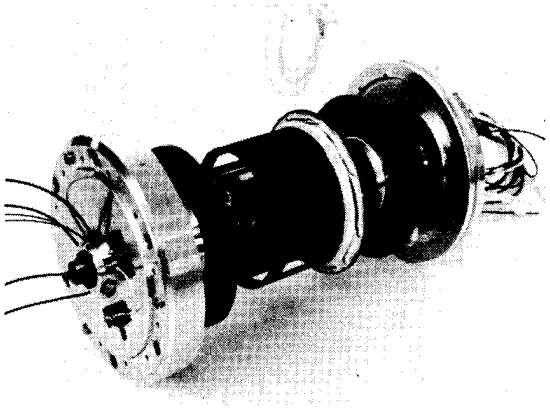


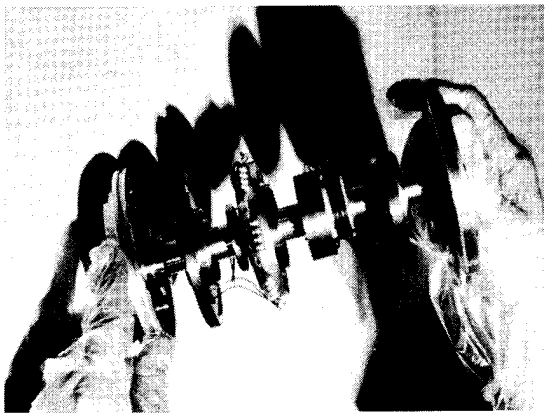
ROTOR FOR EXPERIMENTATION OF A HOIST FLYWHEEL

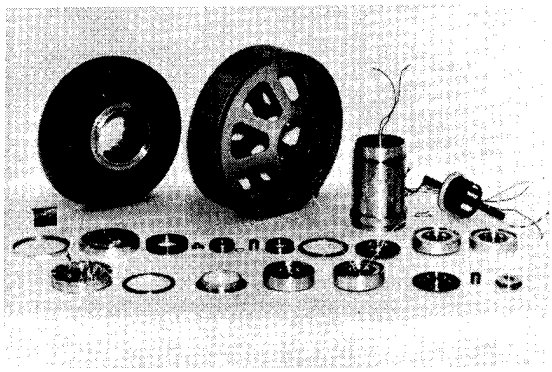


VARIOUS TYPES OF ROTORS
(subcircular and cycloprofile)

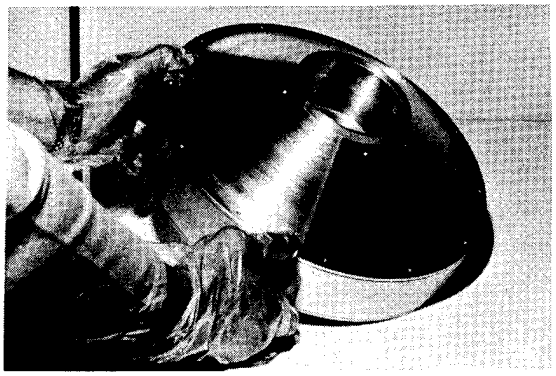


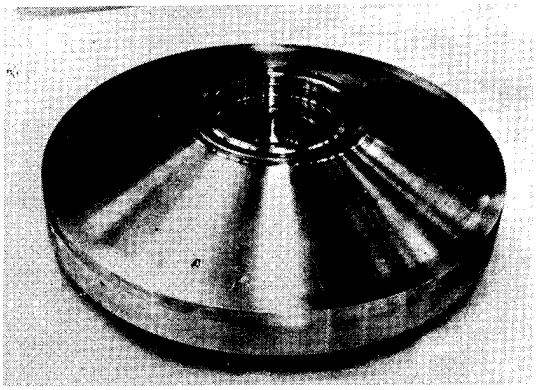








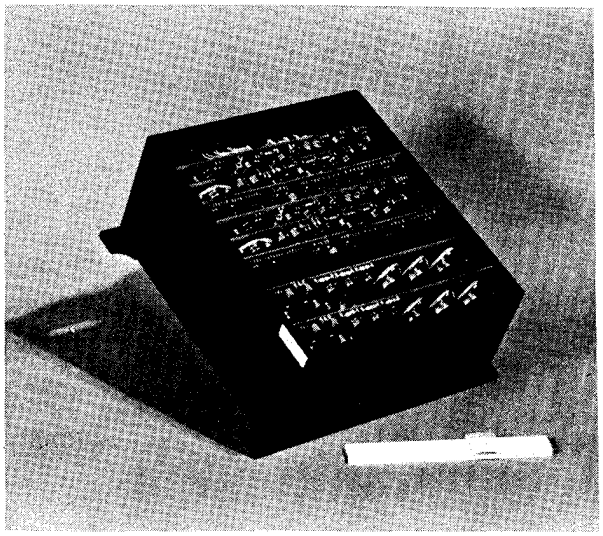


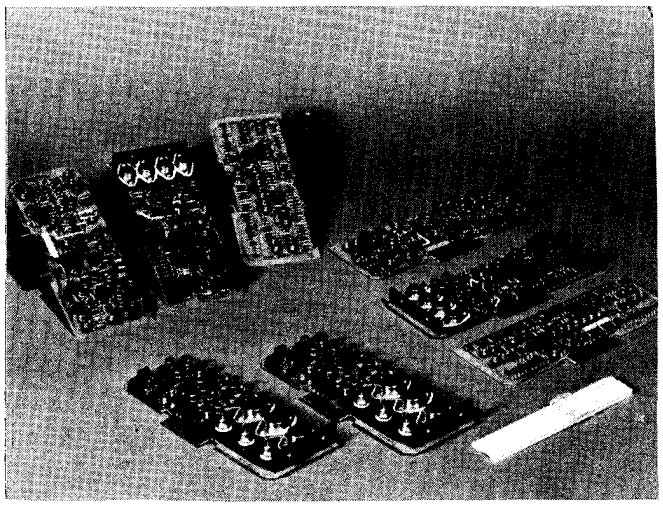


MAGNETIC BEARING MOMENTUM WHEELS

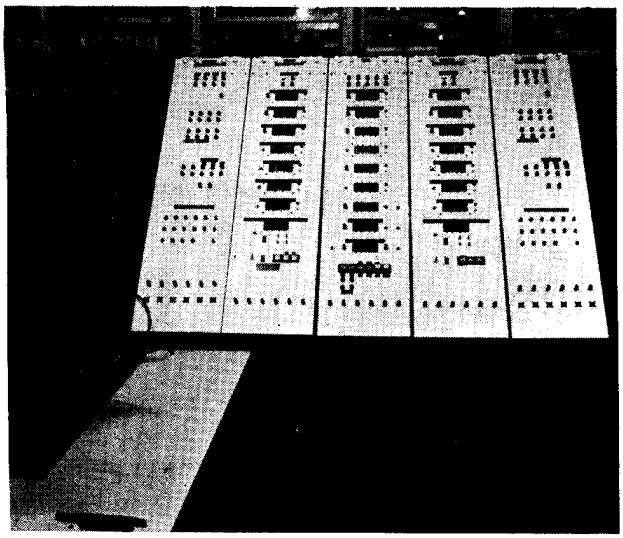
ASSEMBLY AND SEPARATE

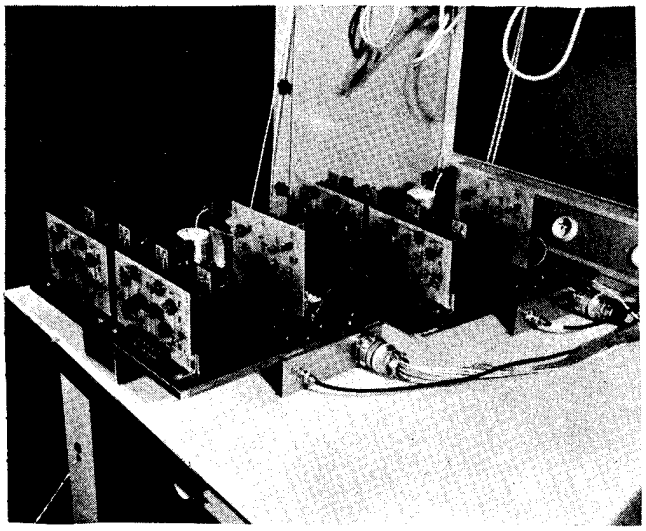
PARTS OF DIFFERENT MODELS





CONTROL ELECTRONICS FOR MAGNETIC SUSPENSION AND MOTOR COMMUTATION OF FLYWHEELS





TEST BENCH AND BREADBOARD MODEL FOR KINETIC ENERGY STORAGE

DESIGN DEFINITION OF A MECHANICAL CAPACITOR*

E.W. Schlieben
Von Research
Trenton, N.J.
R.D. Scott and T.D. Michaelis
RCA Corporation
Camden, N.J.

ABSTRACT

Mechanical Capacitor is a NASA originated descriptor for a special form of electro-mechanical energy-storage system, comprising a magnetically supported energy wheel (flywheel) coupled to the electrical supply and the load by an integral motor-generator and a separate power-conditioning system.

This paper contains the results and some details of a design study and supporting analysis, performed by RCA for the NASA-Goddard Space Flight Center, of a complete Mechanical Capacitor system for terrestrial application. The study addresses a system rather than the wheel component alone.

Two structural configurations, with energy densities of more than 40 Wh/lb, and four motor-generator configurations were analyzed. The wheel was treated as a gyroscopic body supported by a three-axis, active suspension system. Five degrees of freedom are controlled.

System power and energy losses were estimated for one cycle of operation.

INTRODUCTION

There is growing interest in the use of energy wheels (flywheels) as storage devices. This interest stems from the expectation that light, high-strength fibers can be used in specially designed wheels to store more energy per pound than flywheels made of high-strength steels or other stores, such as batteries. It is possible that lightweight mechanical energy stores may show significant cost savings because of the reduced weight of materials used, long life, and the economic advantage of weight savings in systems to which they may be applied.

NASA and RCA have addressed these possibilities in earlier studies and experimental programs. Their conclusions appear in technical notes and papers [1,2,3]. Briefly, these and other studies[4] indicated that the orthotropic thin rim is one of the most efficient types of rotating mechanical devices for energy storage, with energy densities (stored energy per unit weight) of 50 to 70 Wh/lb expected.

However, this conclusion arises from the examination and analyses of the rotating element only and does not include the total system performance of the energy store.

*This work was performed under the auspices of the NASA Goddard Space Flight Center, under Contract NAS5-23650, and reported in the Final Report for the period June 1976-April 1977.

The study reported here was established by NASA to examine a specific thin-rim energy wheel concept in detail and determine the technical and economic feasibility of its application in a baseline reference application. This paper summarizes the more significant conclusions from the study, including expected performance capabilities and limitations.

BASELINE PERFORMANCE REQUIREMENTS

In order to provide a framework within which to specify and evaluate the system design, a 24-hour cycle was defined for energy storage and power rate, as shown in Fig. 1. It describes a 10 kWh storage system, capable of discharging at a maximum rate of 15 kW. The wheel speed varies from full to 50% of full speed (75% depth of discharge). The charge period is 8 hours, at constant wheel acceleration. The coast period is 6 hours and intermittent loads are supplied with up to 10% maximum power during the next 9 hours. The wheel speed is then at 60% of full speed. In the last hour, full power is taken from the wheel for a short interval until the wheel speed is reduced to 50% of full speed.

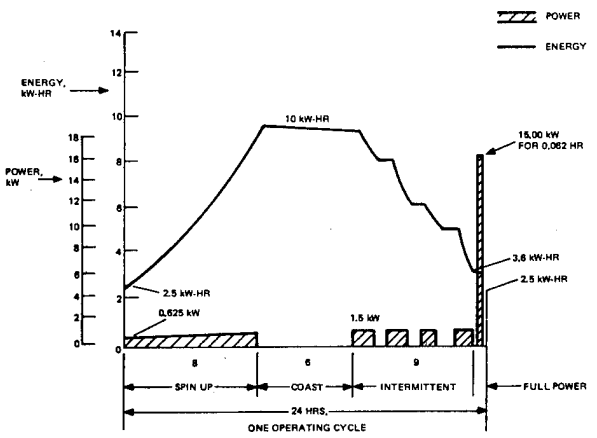


Fig. 1. Mechanical Capacitor power and energy profiles; 24-hour cycle.

In addition, other goals for system performance were set, including the following:

- Maximum energy density for the rotor, afforded by near-term technology.
- Turn around efficiency (energy out/energy in) over 60%.
- Overload survival (1 second) greater than 300% of rated power.
- Survival for worst-case seismic load.
- Minimum magnetic losses for support bearings and motor-generator.

REFERENCE DESIGN

GENERAL

In order to minimize the total volume, weight, and avoid the use of shafting, the motor-generator was designed to be an integral assembly with the rotor. The magnetic bearings were treated likewise. The inner diameter (ID) of the rotor was therefore sized to support the centrifugal load of the motor and bearings. Material selection included graphite fiber reinforcement at the ID to minimize radial growth. Conceptually, the structure was of the form shown in Fig. 2.

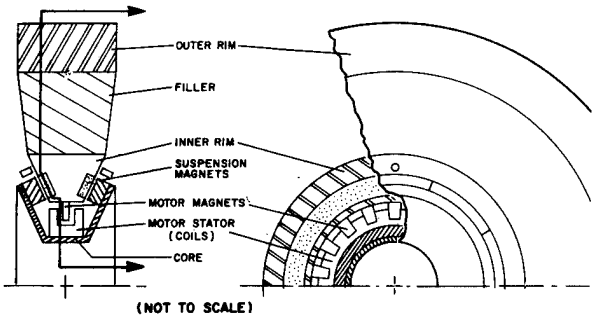


Fig. 2. Rotor concept.

The magnetic bearing acts on a chamfered surface, providing both radial and axial centering forces at the same surface. The motor-generator is a dc ironless armature type of construction.

An advantage of this approach is the inherent stiffness of the central annular mounting structure, which can be based on a tubular column. The central core may be hollow, and can be used to package electronic components if desired.

ROTOR AND MAGNETIC STRUCTURES

Two energy wheel structures were designed and analyzed:

1. A prestressed solid multi-ring wheel, which will be referred to as the NASA configuration[5].

2. A multi-ring wheel with light-weight fillers between the rings, which will be referred to as the RCA configuration.

The NASA configuration comprises prestressed circumferentially wound rims with no fillers. The RCA configuration comprises separate rims with honeycomb fillers. The honeycombs does not contact the rim directly but is bedded in an elastomer as shown in the detail in Fig. 3. The function of the elastomer is to accommodate changes in the radial direction between rims as the wheel speed changes.

With the prestressed construction, the radial tensile stresses can be reduced sufficiently so that the maximum fiber stress can be realized, even though the wheel may have an ID/OD path of the order of o.5.

By use of a very lightweight filler, on the other hand, the ID/OD ratio can be reduced to 0.5 - for structural reasons - while holding radial stresses to values allowable for honeycomb (order of 500 psi).

Both wheel designs show expected ultimate energy densities of approximately 50 Wh/lb, including the iron mass required for support and motor-generator elements. This value does not, however, reflect derating for allowances for manufacturing process, material property uncertainties, and the like.

SUSPENSION

The electromagnets, comprising part of the magnetic suspension subsystems, are shown in Fig. 4. These are biased electromagnets with integral permanent magnets that provide a 'bias' field across the gaps that can be modulated by coil currents. Coil currents variation with the electromagnet force is fairly linear. The suspension has the following features or capabilities:

- Support twice the rotor weight
- Conical bearing
- All-active axes
- Biased magnetic field
- Symmetrical surface sensing

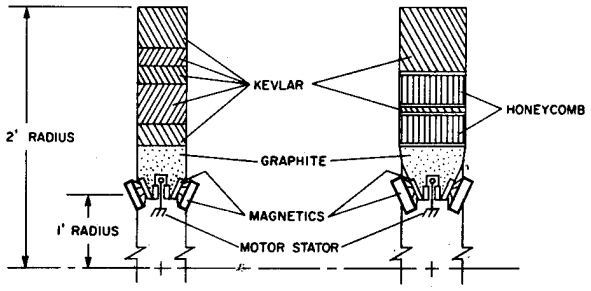


Fig. 3. Comparison of prestressed and honeycomb rims.

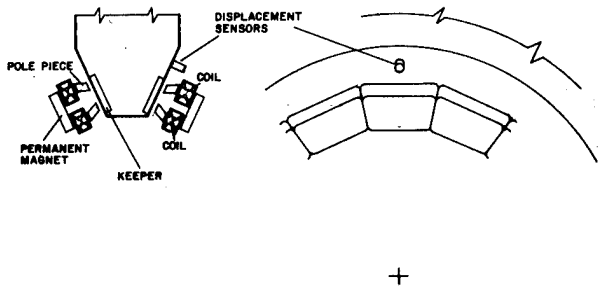


Fig. 4. Electromagnetic suspension

The block diagram of the system is shown in Fig. 5. Five degrees of freedom of the wheel are controlled by the system (three translation, two rotation). Six displacement sensors (five and one redundant) are needed to determine all motions. The sensors measure displacements (gaps) normal to the bearing surface. The system is stable for the rigid wheel. It is recognized that stability of the wheel as an elastic body will ultimately have to be determined.

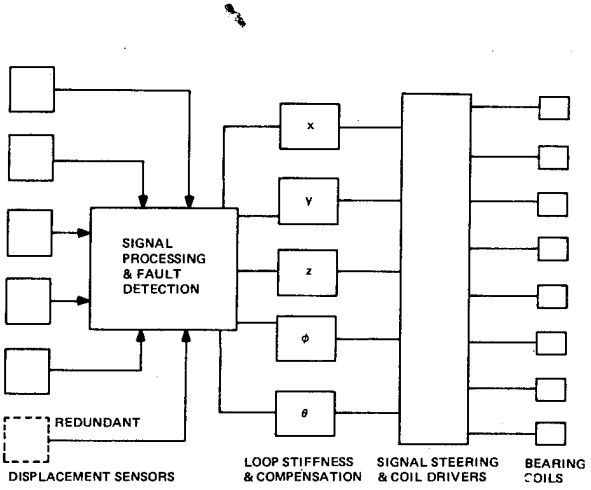


Fig. 5. Suspension system block diagram.

MOTORS

Four motor-generator configurations and four variants were examined instead of the two proposed configurations (a homopolar and a dc torquer). The basic configurations are shown in Fig. 6. The upper sketches are cross sections of the inner rim of the energy wheel. The lower sketches are views looking radially from the wheel axis of rotation. Two motor-generator configurations have fixed fields, and the others variable fields. In the first two, the generator voltage varies 2:1 with wheel speed. In the others, the field can be varied to maintain constant output voltage. A trade must be made, taking into account the effect on the power-conditioner subsystem design, motor-generator losses, wheel dynamic stability, weight, and cost. Configuration 2A-1 was considered as the optimum selection. This is a three-phase, delta-connected motor-generator operating at a high commutation rate with a permanent-magnet field structure carried on the wheel and the ironless armature supported by the fixed structure.

Power losses were estimated for each configuration; results of calculations for configuration 2A-1 (Fig. 6) are shown in Table 1.

POWER CONDITIONING SUBSYSTEM

The subsystem requirements were refined during the study to include the following assumptions and statements:

- Supply and load 3 ø, 110/220 V
- Supply has infinite tolerance for converter reactive volt-ampere demand and converter-injected harmonics
- Parallel tie-line operation
- Motor harmonic impedance high
- No filtering between converter and motor-generator

Motor configuration 2A-1 (Fig. 6) was used for the analysis.

The high frequencies involved and the high-efficiency requirement leads to a double-conversion transistor voltage and current fed scheme as shown in Fig. 7. The cost of this system in the 1980-1985 time frame is likely to be very high and becomes a principal consideration in the application of energy wheels.

SYSTEM EFFICIENCY

System efficiency is defined for a 24-hour cycle. The ratio of energy extracted to that supplied, for the 24-hour cycle, should be greater than 60%. The primary losses in the energy wheel system are caused by the magnetic suspension, the motor generator, and the power converter.

For the combined system, the operating energy loss can be derived as a function of the charge-discharge schedule. For the profile shown in Fig. 1, Table 2 results.

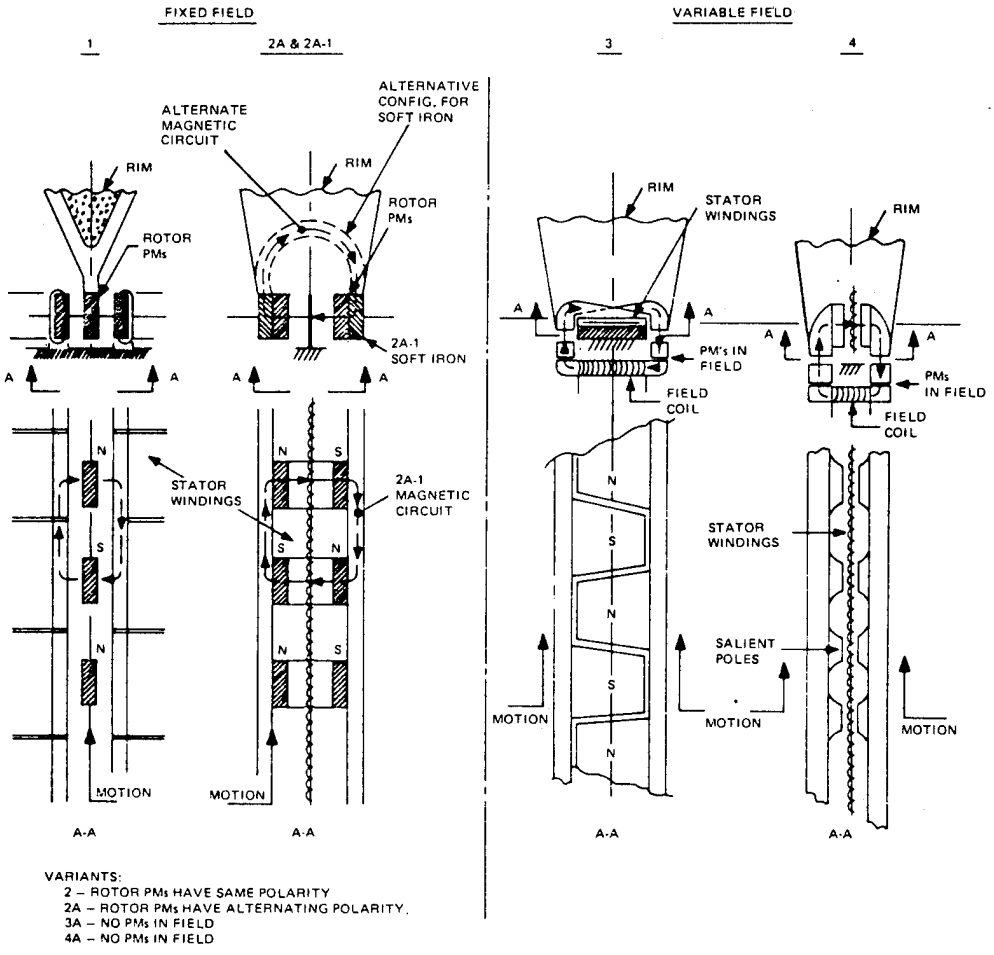


Fig. 6. Mechanical capacitor motor-generator configurations.

Thus, the turnaround efficiency is compromised severely by the power conversion equipment as presently available.

FURTHER DEVELOPMENT

The preliminary analysis and design of the mechanical capacitor required a number of assumptions concerning material properties and dynamic behavior for the rotor and magnetic systems. It is recognized that a number of technical issues must be addressed by analysis and experiment before a fully operating system can be developed as a general product. Following is a short review of the more important problem areas:

RHEOLOGICAL BEHAVIOR OF COMPOSITES

The behavior of some of the proposed materials (Kevlar, graphite fiber, and epoxy or elastomer composites) is not fully understood. Thus loads imposed on the wheel during cycling may cause plastic flow and consequent unbalance. If deformations are significant, wheel unbalance can increase with time, requiring constant monitoring and rebalancing.

MAGNETIC-STRESS INTERACTIONS

Both soft and hard magnetic metals exhibit changes in magnetic properties when stressed. The behavior of these metals must be determined to know whether the stresses impair their magnetic performance to an unacceptable degree.

MAGNETIC QUALITY

Rare-earth magnets are subject to manufacturing anomalies, including micro-cracks, non-uniform magnetic structure, variation in magnetic

Table 1. Power loss summary; M-G 2A-1 and suspension.

	Charge From 50% to 100% rated Speed in 8 hours	Coast Zero Input & Output Power for 6 hours	Low Power Intermittent Op. at 10% rated power to 60% Rated Speed in 9 hours	High Power 15 kW (rated power) During last hour down to 50% speed
1. Suspension				
- Electromagnets				
I^2R	11.31	11.31	11.31	11.31
Eddy Current	-	-	-	-
Hysteresis				
- Keepers				
Eddy Current	0.44-0.88	0.88	0.88-0.54	0.54-0.44
Hysteresis				
- Sensor & Electronics	6.0	6.0	6.0	6.0
Subtotal	18.0	18.0	18.0	18.0
2. M/G				
- Stator				
I^2R	0.16	-	0.32-0.90	86.9-125.2
Eddy Current (Armature)	3.8-7.5	7.5	7.5-4.5	4.5-3.8
Hysteresis				
- Rotor				
Eddy Current	-	-	-	-
Hysteresis				
Subtotal	4.0-7.7	7.5	7.5-5.4	91.4-129.10
Total loss, watts	22.0-25.7	25.5	25.5-23.4	109.4-147.1

strength, and varying stability with time. The effect of manufacturing variations must be related to their long-term performance in the energy wheel.

POWER LOSSES

Operational experience is necessary for reliable estimates of power losses, especially in coasting operations after the wheel is "charged." Such losses can determine the shelf life of the wheel to establish the competitive position of energy wheels versus batteries.

AGING

The long-term effects on all the wheel materials must be assessed to determine, for example, whether the polymer structure of the Kevlar fibers and the matrix resin will remain stable over 20 years, or whether the magnets will develop microcracks

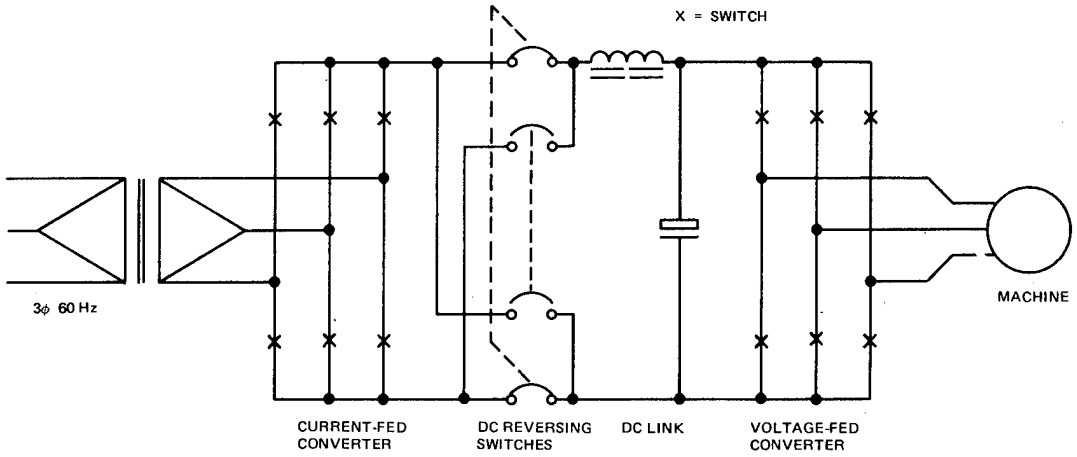


Fig. 7. Elemental schematic diagram of complete double conversion system.

Table 2. Operational efficiency.

	Charge	Coast	Intermit-tent Load	Full Load
Actual time (hr)	0.5/8.0	21/8	2.50/2.40	0.066
Losses -`wheel (kW-hr) (suspension & motor-generator)	0.09/0.403	0.402/0.153	0.050/0.048	0.009
Wheel Energy (kW-hr)				
Start of period	2.5	10.000	9.847/9.598	3.600
End of period	10.0	9.598/9.847	3.600	2.500
Loss-Power Conversion (kW-hr)				
(70% Efficiency)			1.987/1.91	
(90% Efficiency)	0.75 -			0.11
(55% Efficiency)	- 3.37			
Efficiency	80%/54%	96%/98.5%	68.20%/66.3	89.10%

Turnaround efficiency 8 hr charge = 46%

Turnaround efficiency 1/2 hr charge = 60%

that propagate with cycling stress, and destroy them or impair their strength.

POWER CONVERSION

Performance at partial power is of extreme importance to overall system performance and effect on cost because of low power conversion efficiency. This urgent problem warrants an independent program of research and development for development of solid-state switches with higher speed, greater power handling capabilities, and lower costs.

FABRICATION

The wheel configurations analyzed in this study pose fabrication problems. Composite material density and uniformity must be of a high order to attain the dynamic balance

required. Tight dimensional tolerances must be satisfied. And, in the prestressed wheel, ways must be found to achieve the initial stresses specified by the design. Finally, the cost of fabrication of these sophisticated structures must be reduced through innovations in tooling and fixturing.

REFERENCES

1. Kirk, James A., Studer, Philip A., and Evans, Harold E., "Mechanical Capacitor," Goddard Space Flight Center, National Aeronautics and Space Administration, NASA, TND-8185, March 1976.

2. Schlieben, E.W., "Systems Aspects of Energy Wheels," Proceedings of the 1975 Flywheel Technology Symposium, Lawrence Hall of Science, Berkeley, CA, ERDA 76-85, Nov. 10-12, 1975.

3. Schlieben, E.W., "System Aspects of Magnetically Suspended Energy Wheels," Second International Workshop on Rare Earth-Cobalt Permanent Magnets and Their Applications, University of Dayton, June 8-11, 1976.

4. Blake, Alexander, "Mechanical Design of a Composite Centerless Flywheel," Report UCRL-51978, Lawrence Livermore Laboratory, Livermore, CA, Dec. 1975.

5. Kirk, J.A., Huntington, R.A., "Energy Storage-- An Interference Assembled Multiring Superflywheel," 12th IECEC Vol I, pp 511-516, 1977.

6. Olson, E., Approach Magnetism - A Study in Quantities, New York, Springer Verlag, 1966.

7. "An Assessment of Energy Systems Suitable for use by Public Utilities," Final Report EPRI, EM-264, Project 225, ERDA E(11-1)-2501 in three volumes, prepared by Public Service Electric and Gas Co., Newark, N.J. for EPRI and ERDA, July 1976.

8. "Economic and Technical Feasibility Study for Energy Storage Flywheels," SO 75-SA-0166, by Rockwell International for ERDA, December 1975.

9. Cairns, Dr. Elton J. and Mc Breen, Dr. James, "Batteries Power Urban Autos," Industrial Research, June 1975.

10. Fulman, R.L., "Energy Storage by Flywheels," Record of the Tenth Inter-society Energy Conversion Conference, University of Delaware, Newark, Delaware, August 18-22, 1975.

11. Asher, Harold, "Cost-Quantity Relationships in the Airframe Industry," R-291, US Air Force Project Rand, July 1, 1956.

12. Grant, Eugene L. and Ireson, W. Grant, Principles of Engineering Economy, The Ronald Press Co., N.Y.

13. First Annual ERDA Battery Contractors Coordination Meeting, Collection of Vugraphs from Invited Guests, Germantown, MD, January 25-28, 1977.

14. Stoll, R.L. and Hindmarsh, R., "Turbogenerator Stator Windings Using Composite Subconductors," Proc. IEE, V123 No. 11, Nov. 1976, p. 1217.

A FLEXIBLE FLYWHEEL CONCEPT

J. M. Vance**, E. H. Holtzclaw and
R. T. Schneider*
University of Florida
*Department of Nuclear Engineering Sciences
**Department of Mechanical Engineering
Gainesville, Florida 32611

ABSTRACT

A new flywheel concept is described. The advantages of this new concept are claimed to be safety and economy. Preliminary testing at low rpm is reported. From the results obtained thus far, it can be concluded that the self centering feature of the concept allows one to operate the flywheel slightly unbalanced.

INTRODUCTION

There are two main forces which determine the direction of the development of technology. These forces are economy and practicality. Typically during the history of technology, an innovator had a new idea and offered it to the marketplace. The marketplace would accept it if: (1) the customers could afford it, and (2) if it was practical to deploy it, that is, if drastic changes in ways of life were not required. In very recent years a third force has been added to the traditional two: programmatic development by the government. Here, circumventing the tests of economics and practicality in the marketplace, the government decrees a certain way to solve an existing problem and a government funded program is, consequently, instituted. Decisions to institute and fund such a program are usually based on an engineering analysis rather than on a test involving reality. The logic of such an approach is that certain new technologies require a substantial threshold investment before a test involving reality can be made.

The advantages of such an approach to development of technology are obvious; unfortunately, there are also some disadvantages. The main one--from the standpoint of the innovator--is that a new idea may be rejected on the basis of an analysis which may be in itself correct but made on wrong assumptions. History is full of examples where correct analyses, based on wrong assumptions, proclaimed new ideas as impractical and uneconomic which later proved to be very successful. (The aircraft gas turbine is one famous example.)

In the area of storage of electrical energy, several ideas are waiting to be developed. Inertial energy storage by flywheels might be denied a vigorous development in favor of storage batteries on analytical grounds. It is the conviction of the authors of this paper that not all assumptions pertaining to flywheels are properly understood yet. It is the intention of this paper to make a contribution to the assessment of flywheel technology by showing that flywheels do not have to be necessarily dangerous and do not necessarily have to be expensive.

THE FLEXIBLE FLYWHEEL CONCEPT

The new flywheel concept uses a flexible flywheel; the required rigidity is achieved by centrifugal forces. Figure 1 shows a schematic diagram of the concept. A rope ring having a circular cross section, or any other cross section which is suitable, is suspended on individual strands

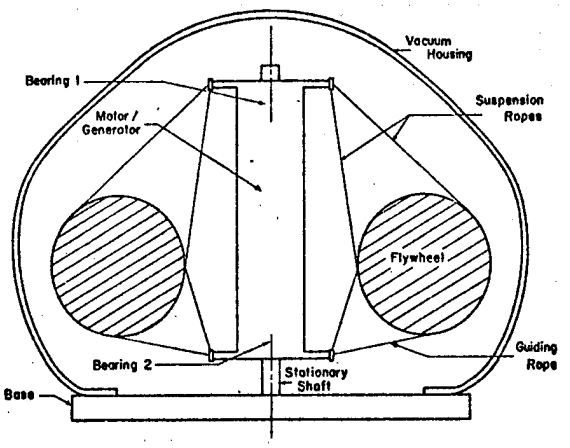


Fig. 1. Flexible Flywheel Concept

of rope or even a suspension net from an upper bearing. There is another lower bearing from which guide ropes lead to the flywheel.

Several safety features could be, but do not necessarily have to be, incorporated in such a concept. For example, in case a strand of the rope rings breaks, it will whiplash against the wall. A suitable detector, (e.g., a glass tube) could be located there to detect that a breakage has occurred. At the same time, the destroyed glass tube could be used to admit a braking fluid to brake the flywheel and dissipate its energy content in the form of heat (latent and vaporization) to the braking fluid. In case of rapid braking, the inertial momentum of the flywheel has to be accepted by the base. For this reason, it may be advantageous to transfer the momentum gradually to the base through a rotation brake. This means after contact between the flywheel and the housing wall has been made, friction will force the housing to rotate. This rotation will be slowed down by the rotation brake. Since the housing is already filled with braking fluid (e.g., water) at that time, due to the breakage of the glass tube detector, the fluid will lubricate the wall to ensure that the frictional force which tries to rotate the housing is minimized.

Energy is put into or taken out of the flywheel by a motor/generator connected to the flywheel supporting shaft by means of a clutch (unless the motor/generator is rated for low friction losses in a vacuum environment). It is intended to cool the motor/generator with oil which is also used to provide lubrication for the bearings. The access for the cooling oil to the rotating part of the motor has to be gained through these bearings.

The advantages of such a flexible flywheel concept are claimed to be the following:

1. The flexible flywheel can expand under stress without jeopardizing its integrity.
2. The flexible flywheel is self-centering (self-balancing).
3. The flexible flywheel can transmit vibrations to the shaft only through those suspension or guiding ropes which are under tension.
4. The flexible flywheel is inexpensive to manufacture.
5. The flexible flywheel is safe.

These advantages claimed above will be discussed as follows:

1. The flexible flywheel can expand under stress without jeopardizing its integrity. Since no resin is used and the rigidity of the flywheel is achieved by the centrifugal forces alone, the expansion will be uniform and, therefore, the effect on balance already established should be minimal.

2. & 3. The flexible flywheel is self-centering and self-balancing since due to its flexible suspension it is free to rotate around its center of gravity. A solid flywheel which is rigidly attached to a rotating shaft may be forced by this shaft to rotate around a center which is not exactly its center of gravity, thus making the flywheel housing a part of the system whereby the total system is trying to rotate around the common center of gravity, which manifests itself in vibrations. In case of the flexible flywheel, any vibrations to be experienced by the housing would have to be transmitted through those suspension ropes which are under tension. There will be other vibrations, however, which will be caused by the main bearing assembly and motor and transmitted through the stationary shaft.

4. The flexible flywheel is inexpensive to manufacture. One material which could be used is "DACRON," now popular for marine rope. The manufacturing process should operate along the traditional lines of rope making, although there needs to be some care taken to produce a homogeneous rope ring. Due to the lack of specialized machinery, the flywheels used in the investigations reported in this paper were made by hand imitating a weaving process which is usually used to produce braided rope.

5. The flexible flywheel is safe. This claim is based on the fact that it is highly unlikely that all the strands of a rope will break exactly at the same time. In the case of the rope ring, the many strands of which it is comprised are spliced individually to form endless rings. Therefore, the flywheel rope ring is really a composite of many endless thinner rope rings which are intertwined to form the big rope ring. If one strand should break, it will whiplash against the wall and the occurrence of this is easily detected and the flywheel can subsequently shut down.

Furthermore, the breaking of one or even several strands will not produce a catastrophic failure. Only whiplashing of the broken strands will occur.

Therefore, it can be said that the flexible flywheel concept is safe to use for individual household application. It is inexpensive to manufacture and it can be built using state of the art technology.

FLORIDA FLYWHEEL FACILITY

While in the previous paragraph the concept of the flexible flywheel for energy storage was described, an actual research facility dedicated to generate design information for the optimum configuration of such a flexible flywheel will look somewhat different since the emphasis is on research and not on energy storage per se.

Figure 2 shows the University of Florida research facility. The vacuum vessel has a diameter of 130 cm (51 inches), which determines the maximum size of flexible flywheels it can accommodate for testing.

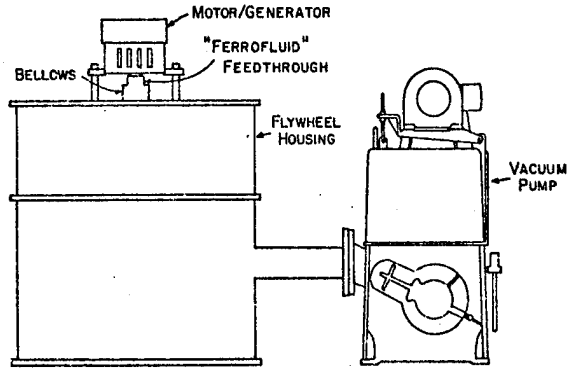


Fig. 2 University of Florida Flywheel Test Facility

For energy input, a 400 hz, 7.5 hp motor is used which can also be operated as an induction generator. The unit is intended for 11,000 rpm operation, although it will operate at higher rpms at a reduced hp rating. The power supply for this motor is a diesel-electric generator set with a nominal frequency of 400 hz. The frequency can be changed to any other desired value for variable speed operation.

Since the motor is not designed for operation in a vacuum, a rotary vacuum feedthrough has to be used. For this purpose, a commercially available "Ferrofluids" feedthrough rated for 11,000 rpm was selected. This unit has two ball bearings, a feature which would disqualify this particular unit for an actual flywheel storage device. However, for research purposes, which involves frequent opening of the vacuum vessel and frequent interchange of flywheels, such a unit seemed to be the best choice.

Due to the fact that both motor and vacuum feedthrough contain ball bearings, a clutch to disconnect these units from the main bearing is necessary. This clutch will allow the rope ring to freewheel for study purposes. Such a unit is not necessarily required in an actual flywheel storage facility.

Design of the main bearing assembly will be subject to further research. Therefore, as far as the design of the research facility is concerned, the only requirement here is that it is easily interchangeable to other bearing designs. For reasons of expediency, ball bearings were used for the initial investigations which are reported here with the intention to replace the bearings later in the program with hydrostatic oil bearings.

The main shaft of the facility is stationary (non-rotatory) and is hollow to allow for access of electrical and oil lines to the main bearing assembly for instrumentation (temperature and vibration) and lubrication. The main shaft is welded to a structure which is attached to the upper half of the vacuum housing, for easy removal of the total internal structure of the flywheel assembly. This allows for maintenance and modification work, without having to disconnect the motor, feedthrough or clutch and will conserve the alignment of these units.

Vacuum pumps, diesel generator sets and other auxiliaries are standard commercially available items which need not be discussed here any further. Table 1 lists the pertinent data of the Florida Flywheel Facility.

The internal structure is designed in a way that it can be set up outside the vacuum housing and the flywheel can be operated in the open atmosphere for easier access. In this case, operation has to be limited to a few thousand rpm, and it is better to use a dc motor for this purpose. Figure 3 shows the flywheel stationary and Figure 4 shows it in operation in the open

atmosphere. The results reported in this paper were obtained by open atmosphere runs only.

Table 1. Florida Flywheel Facility

Housing:

Diameter	129.54 cm (id)	51 in. (id)
Height	140.97 cm (id)	55.5 in. (id)
Volume	1857.85 liters	75.51 cf

Pump:

End Vacuum 10 micron
Pumping Rate 150 (325 gm) liters/sec

Motor: (Westinghouse Type 939D228-4)

Frequency	400 hz nominal
Power	7.5 hp
Speed	11,000 rpm nominal

Vacuum Feedthrough: (Ferrofluids Type SB-500-A-N-069)

Shaft dia : 1.27 cm 0.5 in.
Rated speed: 11,000 rpm

Diesel Generator: (USMC Type Pu-6681G, Consolidated Diesel Electric Co., Model 4251, 1968)

Frequency	400 (cps)
Power	5 (Kw) @ 18 amps 12 hp-diesel engine

RESULTS

MANUFACTURING TECHNIQUES

The manufacturing of a continuous rope ring still needs to be developed. It will require specialized machinery; however, the development of these should not be a major problem. For research purposes, where only a few are required, it is more expedient to make them by hand. It turns out that a better uniformity can be achieved by a knitting type procedure rather than twisting individual strands. Figure 5 shows the appearance of the second layer of such a wheel. The core or first layer is made of four individual strands, while the second layer employs eight individual strands. The third layer will be sixteen and so forth. This technique depends more on interlocking and less on friction as opposed to the twist which depends entirely on friction increasing with tension. Therefore, there was some concern if the same breaking strength could be achieved by the braid. Static break tests were made with a number of single strands (1/4" dacron twist) and a number of braids involving four identical strands. The single strands broke at 540-650 pounds; the braid broke between 1480-1650 pounds, which is 20% below the value to be expected for four strands. The reason for this may be explained by the fact that the interlocking mechanism gives way when the weakest strand breaks; while in a twist, friction distributes the forces more evenly. Therefore, for mass production, a twist would be

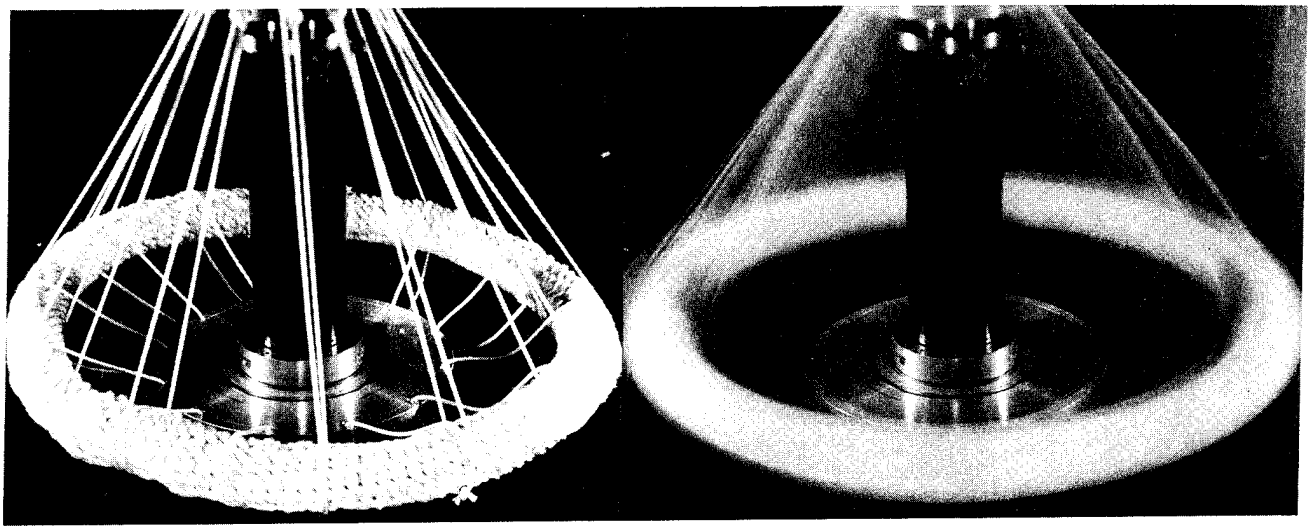


Fig. 3. Flexible Flywheel Stationary

Fig. 4. Flexible Flywheel Operating

preferable. For research involving studies of vibrations and balance problems, the braid will be adequate as long as it is understood that it will break sooner than a comparable twist will.

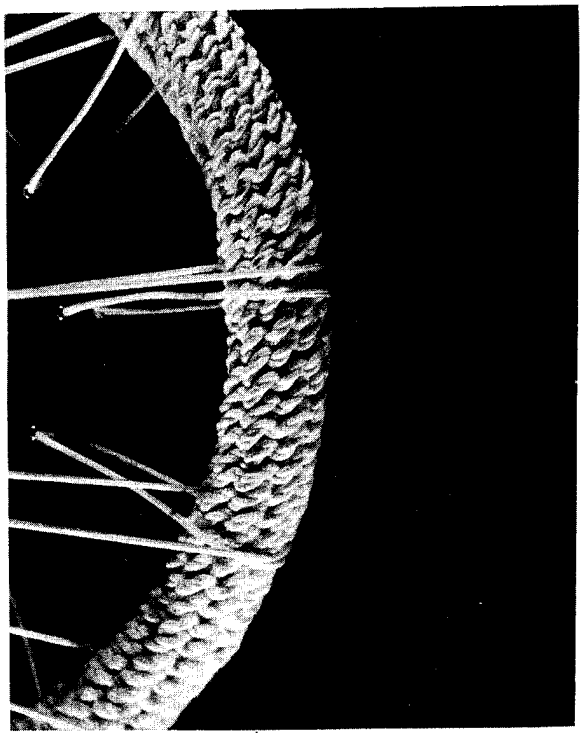


Fig. 5. Second Layer of Braided Wheel

DISTORTION

It has been proposed that an imbalance in a flexible flywheel would lead to a geometric instability. An inhomogeneous flywheel would then increasingly lose its circular shape until it becomes inoperable. To simplify the problem without loss of generality, assume that the flywheel is formed by four masses joined by some anonymous, semi-rigid material. (Two masses would, of course, be unstable as shown in Fig. 6.)

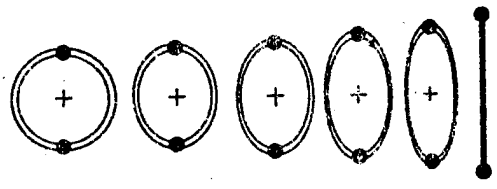


Fig. 6. Instability With Two Masses Only

Further, assume that this structure is supported by a frictionless assembly which provides only torque and in no way impedes shape change. Opposing weights have equal mass. The flywheel now appears as in Fig. 7.

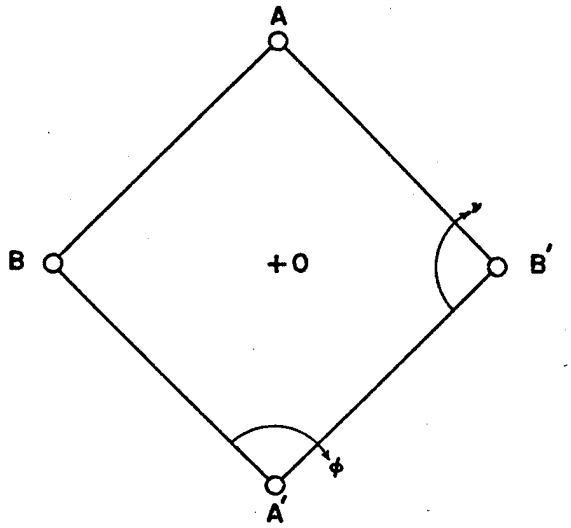


Fig. 7. Idealized Flywheel involving 4 Masses

Assume that a stable configuration exists at some rotational speed w. The forces on any of the four weights may be examined one at a time. (See Fig. 8.)

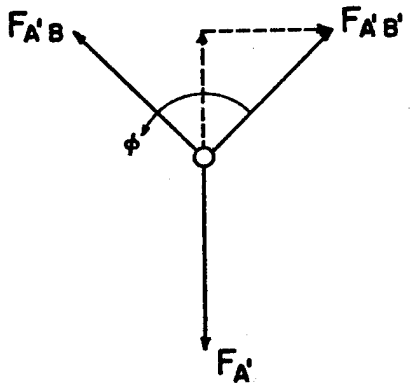


Fig. 8. Forces on One Mass

$F_{A'}$ → centrifugal force

F_{xy} → the force from x to y

$$\vec{F}_{A'} = \vec{F}_{A'B} + \vec{F}_{A'B'} \quad (1)$$

$$|\vec{F}_{A'}| = |\vec{F}_{A'B}| \cos(\tfrac{\phi}{2}) + \vec{F}_{A'B'}|\cos(\tfrac{\phi}{2}) \quad (2)$$

Assume

$$M_B = M_{B'} < M_A = M_{A'}, \text{ then}$$

$$|\vec{F}_{A'}| = 2|\vec{F}_{A'B'}|\cos(\tfrac{\Phi}{2}) \quad (3)$$

Similarly, via symmetry:

$$|\vec{F}_{A'}| = 2|F_{AB'}|\cos(\tfrac{\phi}{2}) \quad (4)$$

$$|\vec{F}_{B'}| = 2|F_{A'B'}|\cos(\tfrac{\nu}{2}) \quad (5)$$

$$|F_B| = 2|F_{AB'}|\cos(\tfrac{\nu}{2}) \quad (6)$$

Obviously, if it can be shown that a singular solution exists for ϕ and ν with any chosen w, then the configuration is stable.

Taking Eqs. (4) and (6):

$$|\vec{F}_{A'}| = 2|\vec{F}_{A'B'}|\cos(\tfrac{\phi}{2}) \quad (7)$$

$$|\vec{F}_{B'}| = 2|\vec{F}_{A'B'}|\cos(\tfrac{\nu}{2}) \quad (8)$$

$$M_{A'}r_{A'}w^2 = 2|\vec{F}_{A'B'}|\cos(\tfrac{\phi}{2}) \quad (9)$$

$$M_{B'}r_{B'}w^2 = 2|\vec{F}_{A'B'}|\cos(\tfrac{\nu}{2}) \quad (10)$$

By Eq. (1), $M_A \quad M_B$

therefore let

$$x = \frac{M_A}{M_B} \quad (11)$$

Further, if the structure has attained a stable configuration, then the rotational inertia of all weights will be identical.

$$M_{A'}wr_{A'}^2 = M_{B'}wr_{B'}^2 \quad (12)$$

$$x\, r_{A'}^2 = r_{B'}^2$$

$$\sqrt{\frac{r_{A'}^2}{r_{B'}^2}} = \sqrt{x}$$

$$\frac{r_{A'}}{r_{B'}} = \sqrt{x} \quad (13)$$

Now, divide Eq. (10) by Eq. (11)

$$\frac{M_{A'}r_{A'}w^2}{M_{B'}r_{B'}w^2} = \frac{2|\vec{F}_{A'B'}|\cos(\frac{\phi}{2})}{2|\vec{F}_{A'B'}|\cos(\frac{\nu}{2})} \quad (14)$$

$$x\sqrt{x} = \frac{\cos(\frac{\phi}{2})}{\cos(\frac{\nu}{2})}$$

Geometrical considerations yield $\Phi + \nu = 180$. Then:

$$\text{Const} = \frac{\cos(\frac{\phi}{2})}{\cos(90 - \frac{\phi}{2})}$$

Thus, there exists a singular solution for the configuration for any chosen w. The flywheel will not collapse.

DYNAMIC MEASUREMENTS

In order to get familiar with the most important problems of the flexible flywheel a small model was manufactured using the braided technique (See Fig. 3) and it was spun at a few thousand rpm only at the open atmosphere. The flywheel mass was 2087.5 gr. It had a large diameter of 21 inches and a small diameter of 2.25 inches. All measurements reported in this paper were made at a standard 1000 rpm. A Hewlett-Packard 3580 A spectrum analyzer was used to record the vibrations transferred to the frame. The vibrations were picked up by a transducer attached to the stationary shaft. Figure 9 shows typical recordings of vibrations transferred to the frame by the flywheel compared to the vibrations of the shaft without the presence of the flywheel. The flywheel was artificially unbalanced by attaching between one to four weights (25 gr. each) to one point on the rim. A superficial examination shows that with one weight attached, the amplitude of most frequencies are close to a minimum which means the wheel is close to being balanced.

Prominent frequencies on Fig. 9 are around 5 Hz, 35 Hz, and 100 Hz. The 5 Hz, which is lower than the rotational frequency of 17 Hz, is related to nonsynchronous succession of the rope ring. The 35 Hz frequency is twice rotational speed, and probably has its source in the shaft coupling. (A slight misalignment in many types of couplings produces a 2N frequency). The 100 Hz frequency is very likely related to the cyclic jerking of the support ropes as the rope ring whirls nonsynchronously.

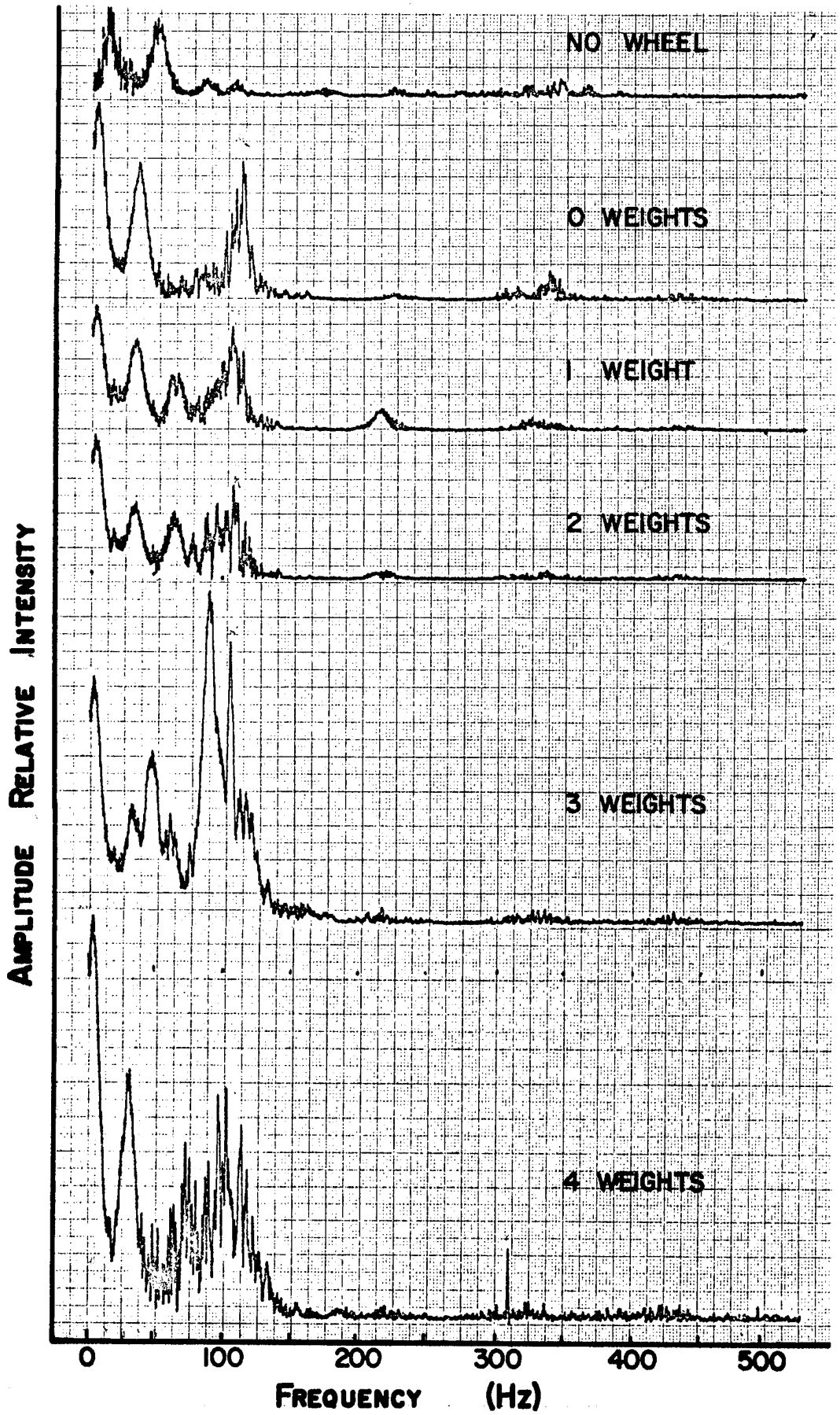


Fig. 9. Vibration Spectrum Emitted by Frame

It is significant that there was no vibration measured synchronous with shaft speed (17Hz), which shows that the flexible flywheel truly is self-balancing, at least at the low speeds run to date.

The one frequency which is potentially critical to successful operation of the flywheel at high speeds is the 5 Hz nonsynchronous precessing. This frequency is almost certainly caused by internal friction in the rope ring (see References 1 and 2).

To see how internal friction drives the subsynchronous whirling, refer to Fig. 10 which shows an instantaneous configuration of the whirling ring. Only four of the "spoke" support ropes are shown, for clarity. The dashed curve shows the path of the centroid of the rope ring as it precesses with angular velocity $\dot{\phi}$. The rotational speed (shaft speed) is $\Omega > \dot{\phi}$.

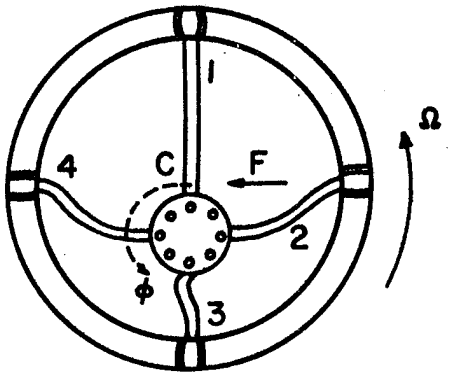


FIG. 10

Instantaneous Configuration of Rope Ring

Internal friction in the rope ring produces a resistance to the rate of change of deformation. Consider spoke number 2 at the instant shown. It is in the process of changing from a loose state (position #3), and simultaneously deforming the rope ring in the region of attachment. The rate of change of deformation is a maximum at position number 2, there producing a maximum of spoke tension from internal friction. Conversely, the spoke at position #4 would be compressing against the force of internal friction, if it were structurally possible. The unbalanced spoke force F is in the direction tangential to precession, driving the whirl.

It can be seen that the driving force F is proportional to the internal friction or hysteresis coefficient, and may also increase with the difference in angular velocities, $\Omega - \dot{\phi}$ (if the internal friction is velocity dependent). This is actually the same type of self-excited whirl described in References 1 and 2 for "solid" rotor shafts, but the mechanism is more easily understood in the flexible flywheel. It is common knowledge in the field of rotor dynamics that this type of instability can be suppressed by the use of external (non-rotating) dampers. An example of the hardware configuration typically used with rolling-element bearings is the squeeze-film damper shown in Fig. 11. In the flexible flywheel application, the rolling-element would be replaced by a fluid film for minimum rotational friction. The ideal location for such a damper would be under the lower guide bearing, where the forces are radial.

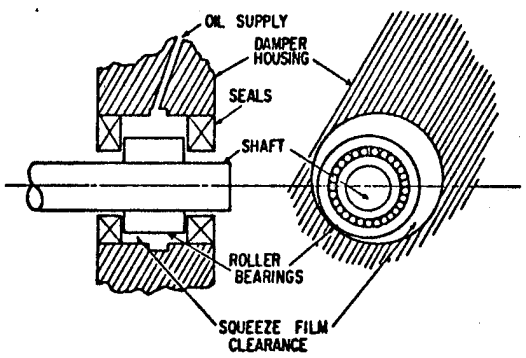


Fig. 11. Squeeze-Film Damper

Figure 12 shows that the 5 Hz precessional amplitude varied with mass unbalance. This result is contrary to rotor dynamic theories based on small amplitude assumptions, and shows that the flywheel was operating in a non linear region where even the nonsynchronous whirling is affected by unbalance.

Figure 13 shows how the amplitude at 100 Hz varied with unbalance. As previously explained, vibration at 100 Hz is completely dependent on the amplitude of the 5 Hz whirling and, therefore, would also be suppressed by the use of a damper.

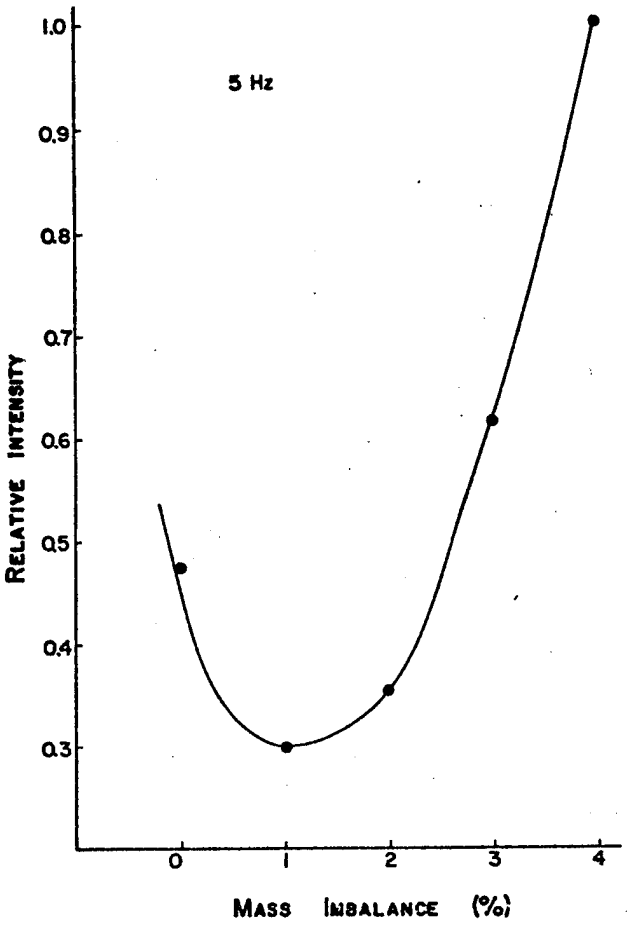


Fig. 12. 5HZ Precessional Amplitude

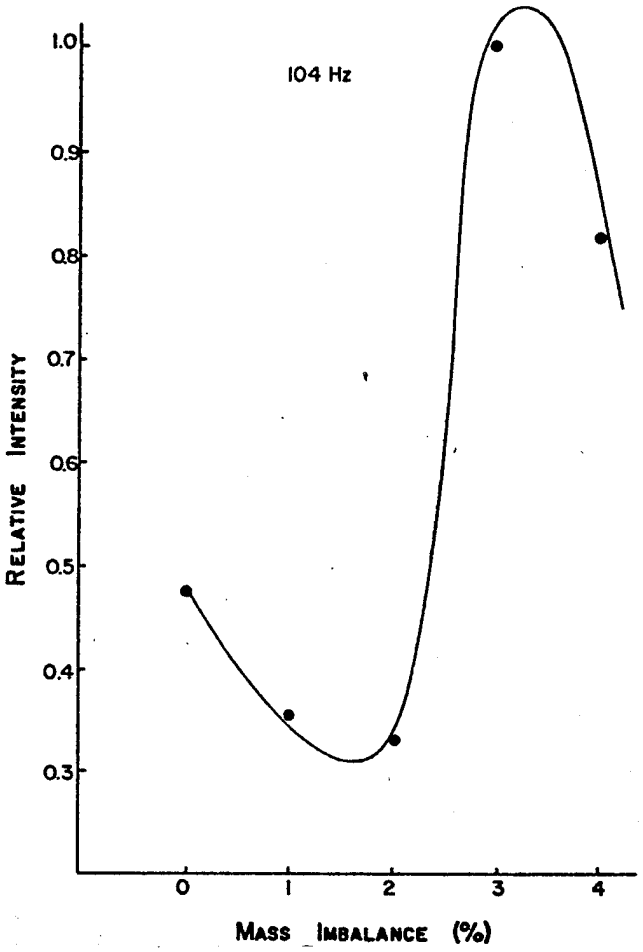


Fig. 13. Amplitude of 100 Hz Vibration

POWER EXTRACTION

As energy is removed from the flywheel, a counter torque is produced which tends to life the wheel via its flexible spokes. This lift can be mathematically related to the rate of energy removal.

Figure 14 illustrates a two dimensional projection of a flywheel section which is being decelerated due to energy extraction.

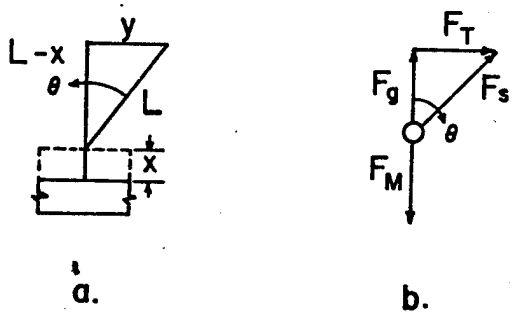


Fig. 14. a. Geometric Diagram b. Vector Diagram

Figure 14a depicts initial and final flywheel segment positions. Figure 14b depicts the vector force diagram of the flywheel segment. It can be seen from Fig. 14a:

$$(L-x) = L\cos\theta$$
$$x = L(1-\cos\theta)$$
$$\frac{x}{L} = 1-\cos\theta$$

and from Fig. 14b:

$$F_T = M_g \tan\theta = F_S \sin\theta$$

Assume that $|\vec{F}_S|$ is less than or equal to one fourth of the tensile strength of one spoke. Further, assume that the wheel has twelve spokes. Then:

$$|\vec{F}_S| = 3|\vec{F}_B|$$

where F_B is the tensile strength of one spoke. Taking the specifications of the ultimate flywheel towards which this project aspires:

Large radius - 80 (cm) = 31.5 in.
Samll radius - 20 (cm) = 7.9 in.
Total weight - 632(kg) = 1394.3lb.
Spoke tensile strength-1800(lbf)=403.56(NTS)

then:

$$\sin\Theta = .966,$$

$$\Theta = 75° .$$

This is a rather large angle, and it seems more reasonable to limit the lift of the rope ring x to not more than the ring diameter. Then, taking L = 160 cm gives

$$\cos\Theta = 1 - x/L$$

$$= 1 - 40/160 = .75,$$

$$\Theta = 41°,$$

$$F_T = F_S \sin\Theta$$

$$= (5400)\ .66 = 3564 \text{ lb.}$$

The torque of the couple formed by $\vec{F}_T$ at the wheel's radius is:

$$T = |\vec{F}_T| \times R$$

$$= (3564) \times 31.5/12$$

$$= 9355 \text{ ft-lb.}$$

The power output at 11,000 rpm is then:

$$W = Tw = 9355 \text{ ft-lb.} \times 11{,}000 \left(\frac{\text{rev}}{\text{min}}\right)$$

$$\times 2\pi \left(\frac{\text{rad}}{\text{rev}}\right) \div 33{,}000 = 19{,}594 \text{ HP}$$

$$= 14{,}617 \text{ KW.}$$

This is, of course a theoretical maximum which will not be reached for other reasons not covered in this simple analysis. However, it can be concluded that the power extraction is no serious concern.

CONCLUSIONS

A new flywheel concept was described The advantages of this concept are claimed to be safety and economy.

What can be learned from the preliminary studies at low rpm described in this paper is that it is probably possible to live with slight imbalances in the 1% range at high rpms. This would facilitate the mass production of flexible flywheels considerably. A problem which needs closer attention is the control of precessing movements. However, the present results seem to be encouraging enough to proceed with the more complex testing in vacuum at high rpm. It should be understood, however, that the described flywheel is a concept and will undergo some metamorphosis before the end product, a small, inexpensive storage unit for individual households, is obtained.

REFERENCES

1. F. F. Ehrich, "Shaft Whirl Induced by Rotor Internal Damping," ASME Journal of Applied Mechanics, June, 1964, pp. 279-282.

2. H. F. Black, "The Stabilizing Capacity of Bearings for Flexible Rotors With Hysteresis," ASME Paper No. 75-DET-55, Design Engineering Technical Conference, Washington, D. C., September 17-19, 1975.

SPIN TEST AND EVALUATION OF UCC-ND's BAND-WRAP FLYWHEEL

J. J. Kelly
Nuclear Division
Union Carbide Corporation

ABSTRACT

Testing methods and observed behavior of the band-wrap flywheel are presented. Prebalancing of the flywheel revealed force and couple imbalances which were correlateable with observed assembly misalignments. Subsequent high speed testing revealed stable performance up to and including the radial delamination speed ($\sim$ 18,000 rpm), at which time, the system monitors indicated problems and the flywheel was successfully driven down.

(Paper Not Submitted)

DESIGN, INSTRUMENTATION AND CALIBRATION OF AN EXPERIMENTAL FLYWHEEL CONTAINMENT ASSEMBLY

J. J. Kelly
Nuclear Division
Union Carbide Corporation

ABSTRACT

A test assembly has been designed which will be used to evaluate containment rings and measure the torsional and shaking loads occurring during flywheel failures. Removable containment rings permit the evaluation of various types of materials and thicknesses. The failure loads are determined by measuring the transient torsional and bending deformations occurring in the mounting pedestal during flywheel failures. It is intended that the test assembly be used to provide design data for the UCC-ND flywheel system.

(Paper Not Submitted)

FLYWHEEL DEVELOPMENT FOR THE ELECTRIC POWER RESEARCH INSTITUTE

William M. Brobeck
William M. Brobeck & Associates
1235 Tenth Street
Berkeley, California 94710

ABSTRACT

This paper covers two years of development work on flywheels for peak power shaving in the electric utility system. Single and multi-ring, E-glass composite wheels were spun at surface speeds up to 500 meters/sec. Considerable work was done on the stability of the pendulous support used. Both elastomeric and mechanical inter-ring attachments and a single ring with composite spokes were tested. Mechanical difficulties, overcome by the end of the project, limited speeds to considerably less than the ultimate strength of the material.

INTRODUCTION

In the summer of 1974, the Electric Power Research Institute began a program to investigate the technical feasibility of flywheel energy storage as a means of supplying the peak power requirements of electric utility systems. It appeared possible that flywheels could be cost-effective for this purpose because of the relatively high energy storage capability per dollar of epoxy-fiberglass composite flywheel materials. Moreover, because flywheel storage stations could be located in the distribution system close to the load, credit could be given the flywheel for the cost of the distribution and generating capability which would otherwise have been required to carry the load peaks. The type of flywheel station visualized is shown in Fig. 1. Such a station was expected to have an energy rating of the order of 10 MWh and a power rating of 1 to 5 MW.

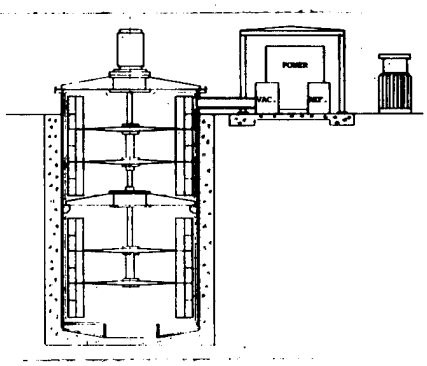


Fig. 1. Full Scale Flywheel Storage Station Concept.

The basic philosophy of the work was to build and test flywheels on as large a scale as practical in order to encounter and, hopefully, solve the practical problems which would arise. The presently lowest cost material, E-glass epoxy, was to be used. Material development was not an object of the work.

FLYWHEEL DESIGN

The design apporach followed for the wheels to be tested was that described and patented by Post and Post.[1,2] This was a series of concentric rings separated by spacers of elastic material bonded to the ring surfaces.

The ring type of flywheel, as distinguished from disk or brush designs, was chosen primarily because it placed the largest part of the mass at the largest radius. As the rings were to be wound of roving with no attempt to use the fiberglass to carry radial loads, the ratio of longitudinal to transverse strength limited the radial thickness of the rings to about 15 percent of the outer radius. Several rings were, therefore, to be used to make good use of the swept volume.

The multi-ring design has the serious problem of support of the rings, both the inner ring from the shaft and each succes-

sive ring from the one inside it. Following the design of Post and Post described in Ref. 1 and in the referenced patents, it was planned to attach the rings to the hub and to each other by means of elastic material bonded to the ring surfaces. Some work had already been done on the modes of vibration of a series of rings supported by elastic separators. This work indicated that the lowest frequency mode, in which the rings vibrated in two groups of about equal mass, could be kept above the operating speed. It was realized that the separators which must be stiff enough to hold the vibration frequency high and to resist the acceleration field of approximately 200,000 times gravity and still flexible enough to accommodate the ring expansion of 2 to 3 percent would be a formidable design problem.

FLYWHEEL SUSPENSION

Because of the nature of fiberglass and the plan to use elastic spacers between the rings, it was felt that it would be impossible to maintain the high degree of balance ordinarily required of high speed rotors to hold bearing loads within reasonable limits. Accordingly, a pendulum support was planned which enabled the wheel to spin around its center of gravity at all speeds above a few hundred rpm. This method also introduced problems in the form of unwanted modes of vibration. These modes, which are well described by Den Hartog[4], are referred to as whirl modes. They can be excited by energy fed from the rotation. If energy flows into whirl and is not absorbed, the whirl amplitude increases without limit until something breaks. Figure 2 shows a wheel rotating in a whirl mode in a test mock-up built to observe this phenomena at low speeds.

A whirl mode can be excited as a result of hysteresis of the shaft supporting the flywheel. The energy entering the whirl mode equals the hysteresis energy. This is a particularly obnoxious effect because as the whirl amplitude increases so does the hysteresis loss due to the increased bending of the shaft. The result is that the amplitude increases in an exponential way causing the shaft to break before the increase in whirl amplitude can even be detected. Fortunately, the hysteresis loss in the shaft is small and only a small amount of damping must be present to prevent the onset of whirl as we learned from both theory and experiment.



Fig. 2. Demonstration of Whirl Motion.

THE TEST FACILITY

With the above background, a test facility was built capable of spinning wheels up to one meter in diameter, weighing 100 kilograms at a maximum speed of 22,000 rpm. Figure 3 shows the tank with the cover removed but with the bearing support in place. The tank walls are of 2-inch steel plate. The drive and support, which is mounted in the tank so that all adjustments can be made before putting the cover in place, are shown in the figure.

The tank is provided with a mechanical pump of 10 cubic feet per minute capacity and a 4-inch oil diffusion pump. The usual operating pressure was about 100 microns which could be obtained with the mechanical pump alone.

As shown in Fig. 4, two sets of two bearings each are used. The upper set supports the weight of the flywheel and the lower set carries the damper. The shaft between the bearings is made as

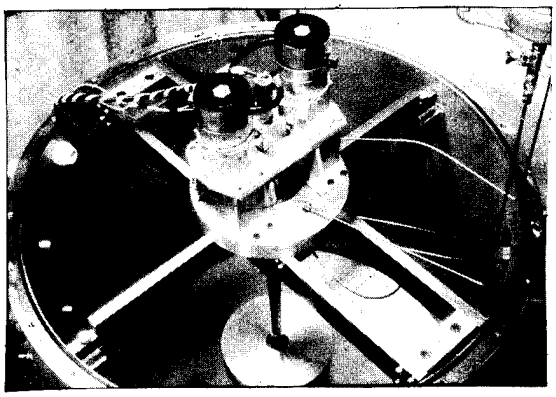


Fig. 3. Flywheel Test Tank and Support.

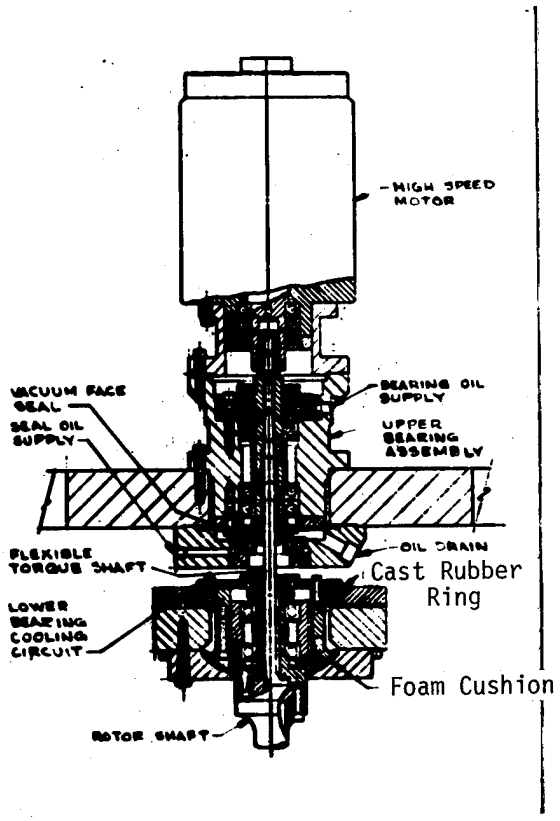


Fig. 4. Flywheel Bearing Support Shown with Induction Motor.

flexible as possible to allow the pendulum motion by reducing its diameter to 11 mm for a length of 190 mm. Damping is provided by a sheet of neoprene foam between the spherical surface of the lower bearing housing and the spherical socket in the stationary frame.

Precision angular contact bearings are used in both bearing sets. The upper set is lubricated by oil which also cools the vacuum seal and the lower bearing is grease-lubricated. The lower bearing housing is water-cooled.

The vacuum seal is a mechanical face seal running immersed in oil. Its inside diameter determined by the diameter of the flexible shaft is 28 mm.

The shaft is driven by a pair of alternating current series-wound motors (designed for wood routers) coupled through cog belts to pulleys on the shaft. Two motors were used to increase the power and reduce belt loads on the bearings. A 1-to-1 ratio with 3/4-inch pitch-diameter pulleys was used in all the testing. Power was adequate to accelerate a 10-kg wheel to 22 krpm in about 30 minutes which was quite fast enough for the operators.

The rotating speed was obtained from an optical pick-up on the shaft near the drive pulleys and read on a strip chart recorder. The recorder was automatically reset every 1000 rpm so that the speed could be read to about 10 rpm from the chart. An operator marked the chart to show which thousand was being recorded. An indicating tachometer reading directly was also used.

A very useful instrument sensed and recorded the position of the center of the wheel with respect to the bottom of the tank. This permitted continuous monitoring of the vibration of the wheel and the appearance of incipient trouble. Changes in the wheel while spinning appeared as changes in the amplitude of the motion of its center. The pick-up consisted of a ball bearing attached to the wheel which pressed against a group of four leaf springs, mounted at 90 degrees, to which strain gages were attached.

Other conventional instruments measured the tank pressure, the bearing temperature, and the motor current and voltage.

A television link was used to observe the wheel as it spun. It was found that a strobe light stopped the motion in the television picture as well as with direct visual observation. The TV pictures were recorded and could be played back to observe the wheels at the brief periods during which changes occurred. Although the causes of wheel failures (as distinguished from support failures) were usually ob-

vious, the TV pictures did assist in the diagnoses.

EXPERIENCE WITH THE SUSPENSION

Much of the effort during the two years of the project was spent on mechanical problems not associated with the flywheels themselves. The plan was to test each wheel design at a succession of speeds, stopping to examine the wheels after each run. This was done because the experience of others who had tried to reach full speed on the first run was that it was often difficult to determine the cause after a wheel had failed catastrophically. In the first runs at speeds up to about 10 krpm, there was little difficulty. At higher speeds, however, bearing heating became a problem and numerous changes in the bearing mounting, cooling and lubrication were made. Many runs were made spinning an aluminum disk to test the performance of the bearing support.

About two months after testing started, a failure occurred while spinning a bare hub at 19 krpm. The failure was believed to have been caused by a defective weld at the end flange of the support shaft where it attached to the hub. The design was changed to reduce possible stress concentration at the weld.

Tests continued until close to the end of the first year's work, about five months after the first failure, another occurred while spinning a two-ring rotor at about 16 krpm. The rotor fell to the bottom of the tank where it came to a stop after about half an hour. This time there was no question of weld failure; the cause seemed clearly to be the appearance of the whirl mode.

It had been believed that prevention of whirl was well understood but this apparently was not the case. Accordingly, all effort was placed on studying the mechanics of the motion. Whirl must be prevented if testing were to continue with the existing apparatus.

The whirl work proceeded on two fronts, theoretical and experimental. The theoretical work consisted of a) calculation of the whirl motion with damping and b) the investigation of higher frequency whirl modes. The work under a) is described in an ASME paper[3], which covers that part of the problem. A re-analysis of the mechanics of the support also showed that the conventional critical speed of the shaft was lower than had been calculated. The flywheel to which the shaft was rigidly attached did not constitute a built-in support as had been assumed.

The experimental work consisted of measurements of the damping and observations of the motion of metal wheels while spun under various conditions of imbalance. Several months before the second failure, the neoprene damping cushion had been removed and the spherical surfaces held together under spring pressure, lubricated with heavy grease to provide the damping required. Observation of the wheel eccentricity while spinning showed erratic motion of considerable amplitude with the grease damping compared to the relatively smooth motion of smaller amplitude with the cushion.

As a result of these investigations, the shaft length was reduced by about 100 mm and the neoprene cushion reinstalled. To verify the stability of the system, a disk was built that contained a weight designed to shift radially when a speed of about 10 krpm was reached. When the weight shifted, it moved the center of gravity of the spinning disk about 0.3 mm and caused the center of the disk to jump 30 mm. The resulting oscillation was damped out in about ten seconds. In all subsequent tests, the damping was observed on the motion recorder by striking the wheel under test with a rubber hammer before starting its rotation.

FLYWHEEL TEST PLAN

The plan was to design a series of concentric rings for which various ring-hub and inter-ring supports would be tested. Accordingly, 5 rings were specified with ID to OD ratios of .85. The maximum diameter of the outer ring was 760 mm which at 22 krpm would reach what was expected to be the ultimate strength of the material. The inside diameter of the smallest ring was about 300 mm. At this diameter, the stress would be small even at full speed. The objective of the first year was to test the first two of these rings to the full speed. This objective was not met until the end of the second year.

A total of twenty-seven E-glass rings were ordered and received from suppliers. In general, the quality of these rings was good except for the inside surface of one group which was not well impregnated with

the epoxy. Because of the delay caused by the support trouble, only the first two rings of the series were tested at full speed and so the strength limit of the composite was not apporached. Tension-spoke wheels of full 760 mm diameter were spun[5] but not to full speed. A 760-mm hub-supported ring was under construction when the work stopped.

ELASTOMERICALLY-SPACED WHEELS

In the approach to be followed, the first problem faced was the hub-to-ring attachment. As the initial plan was to use inter-ring spacers of elastomeric material, a similar method was used for the attachment of the first ring to the hub. Although centrifugal stresses at this point were small, the relative motion between the aluminum hub and the composite ring due to their different moduli of elasticity was considerable. Many runs were made with different designs of this joint. Finally, a design consisting of alternate elastomer and fiberglass layers which allowed appreciable shear deflection was successful in reaching the full 22 krpm. The design is shown in Fig. 5.

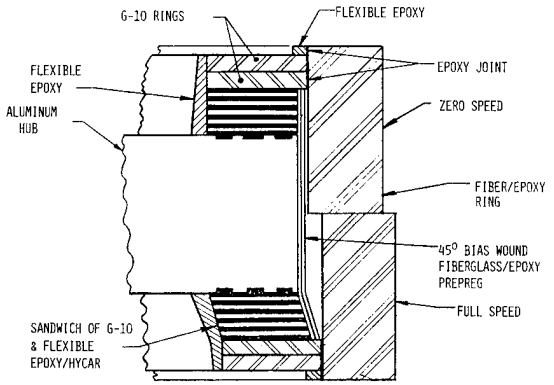


Fig. 5. Laminated Elastomeric Hub-to-Ring Joint.

Concurrently with the work on the hub-to-ring joint, work was also done on an elastomeric spacer between the first and second ring. This consisted of a layer of rubber grooved to allow lateral expansion of the rubber and bonded to both ring surfaces. Machining the grooves is shown in Fig. 6. Very little testing was done on the two-ring elastomeric spacer wheel because of the problem of the hub-to-ring joint which was not solved until near the end of the project.

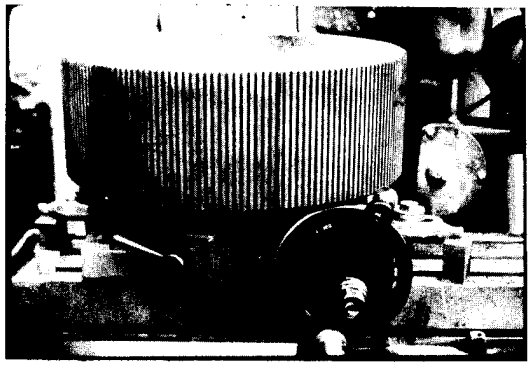


Fig. 6. Slots Being Ground into Nitrile Rubber Separator.

MECHANICALLY SPACED WHEELS

The difficulty with the elastomeric joints lead to consideration of alternate supporting schemes. One of the most obvious was to machine grooves in the rings and to separate and support them by flexible metal bands having mating teeth. In this approach, the hub would be a toothed disk. This design was analyzed in considerable detail and many runs were made on versions of it. The first inter-ring spacer of this type was a continuous band, slotted to allow it to expand with the ring against which it was held by centrifugal force and provided with inward and outward projecting teeth. Later designs as shown in Fig 7 used individual "tabs" which were much easier to make.

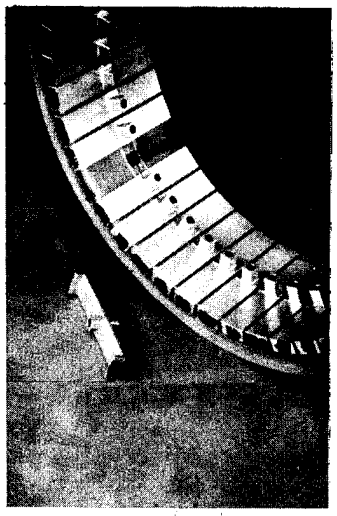


Fig. 7. Inter-ring Spacers.

The rings shown in Fig. 8 were of this "tooth-and-groove" type. Its testing showed up an important problem

with this design. When the grooves are machined in the faces of the rings, circumferential fibers passing through the lands between the grooves are necessarily cut. The lands, therefore, must be supported by shear between their root surfaces and the uncut part of the ring. By holding the groove depth to 3 mm, the shear stress is not excessive. However, the radial hoop tension causing the ring to dilate is not present in the lands. The dilation of the ring must be transmitted to the lands by circumferential shear stress which is too large for the epoxy material of the ring to withstand. For this reason, spinning the grooved wheels above about 10 krpm caused the lands to break off the rings. The lands broke one at a time, each sounding like a pistol shot when it struck the wall of the tank. The remedy was to make the lands of a different material from the ring and to cast them in place on the ring surface. The land material was compounded of epoxy and hycar to obtain an allowable deformation equal to that of the ring. This change worked successfully up to the maximum surface speed tested, approximately 500 meters per second where the acceleration is about 60,000 times gravity.

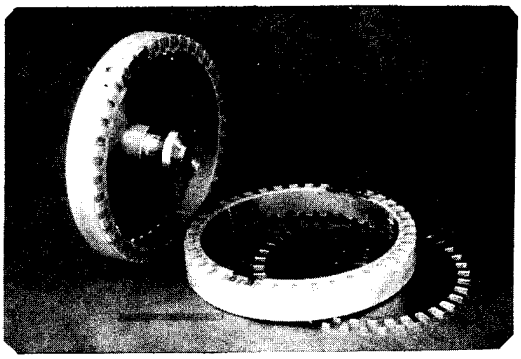


Fig. 8. Toothed Ring-to-Hub Assembly.

The hub teeth and tab teeth are fitted closely in the grooves in the composite rings. However, as the rings expand during rotation, the clearances of the teeth in the grooves increases allowing an increase in eccentricity between the rings. The effect of the eccentricity is to load the teeth by the centrifugal force between the rings. This effect is increased as the number of rings is increased and is significant for five rings. It was also realized that the inner rings contributed little to the stored energy. A two or three ring set would be more economical if a larger hub diameter were feasible.

About this time, it was realized that following the theory described by Stodola[6], a metal hub could be designed that would support even the largest 760-mm diameter ring, provided its rim thickness was made small. Accordingly, an aluminum hub of this design was built for the number two ring and tested with that ring. This wheel reached the highest energy density of any test during the project, 14 watt-hours per pound at 512 meters per second, surface speed.

TENSION SPOKES

The third design approach was the use of spokes of composite material to attach the ring to the hub. A wheel of this type is shown in Fig. 9. The principle involved is to design the spokes so that their shape does not change under the application of centrifugal force. Only a few runs could be made on this configuration before the work was stopped. However, 10 krpm was reached with the 760-mm OD wheel shown before failure of the spoke attachment. This corresponds to 8.6 watt-hours per pound. The design and performance of this type of wheel is covered by another paper[5] at this meeting.

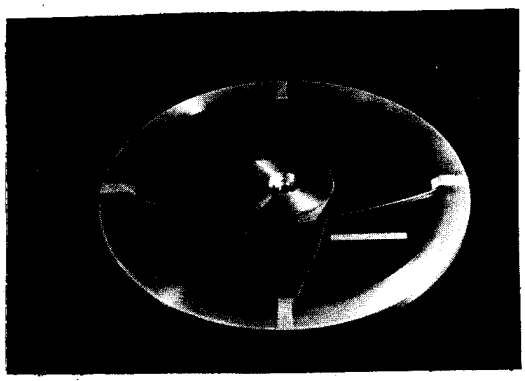


Fig. 9. Tension-Spoke Wheel.

CONCLUSIONS

In spite of the interruptions by support problems, it is felt that sufficient work was done to justify certain conclusions. These can be stated as follows:

1. Flywheels can run stably with pendulum support provided damping is provided and critical speeds are kept out of the operating range.

2. It is unlikely that isotropic elastic materials will be satisfactory for hub-to-ring or ring-to-ring joints. On

the other hand, anisotropic materials such as the fiberglass elastomer laminations used in the last tests may be suitable.

3. Fiber-composite multiple rings can be built that will reach useful energy densities. Although tests were limited by the diameter of the wheels, an energy density of 14 watt-hours per pound was reached with an 11-kg flywheel.

4. The tension spoke design is very promising for single rings.

5. Solutions were found for all the difficulties encountered at the stress levels reached. It is believed that these solutions will be applicable up to the ultimate strength of the flywheel material. Further testing will be required to confirm that opinion.

DETAILED REPORTS

The work described is reported in detail in two EPRI reports[7,8] covering the first and second year, respectively.

REFERENCES

1. R. F. Post and S. F. Post, "Flywheels," Scientific American, vol. 229, no. 6, pp. 17-23, December 1973.

2. U. S. Patent 3,683,216 to R. F. Post, "Inertial Energy Storage Apparatus and System for Utilizing the Same," August 8, 1972.

3. W. T. Thompson, H. S. Gordon, and F. C. Younger, "Whirl Stability of the Pendulously Supported Flywheel System." Paper No. 77-APM-20. Presented at the Applied Mechanics/Bioengineering/ Fluids Engineering Summer Conference, Yale University, June 15-17, 1977, of the American Society of Mechanical Engineers.

4. J. P. Den Hartog, Mechanical Vibration, 4th Edition, McGraw-Hill Book Co., New York, 1956, p. 253 et. seq.

5. F. C. Younger, "Tension-Balanced Spokes for Fiber-Composite Flywheel Rims," presented at the 1977 Flywheel Technology Symposium, San Francisco, California, October 5-7, 1977.

6. A. Stodola (translated by L. Loewenstein), "Steam and Gas Turbines," Volume I, McGraw-Hill Book Co., New York, 1927, p. 376.

7. "Development of High Density Inertial Energy Storage," Electric Power Research Institute Report No. 269-1, July, 1975. Prepared by Wm. M. Brobeck & Associates, Berkeley, California.

8. "Investigation of Multi-Ring Fiber Composite Flywheels for Energy Storage," Electric Power Research Institute Report No. EM-227, September, 1976. Prepared by Wm. M. Brobeck & Associates, Berkeley, California.

FAILURE CHARACTERISTICS OF COMPOSITE FLYWHEELS

D.W. Oplinger
and
J.M. Slepetz
Army Materials and Mechanics Research Center
Watertown, MA 02172

ABSTRACT

This paper discusses the various failure modes that can be expected to play a role in limiting the performance of composite flywheels, including fiber breakage, matrix failure due to transverse strain limitations and interlaminar shear failures. The role of radial strain failure in hoop wound wheels and the use of high-strain matrix materials in avoiding such failures are discussed. Also discussed is the need for adequate characterization of the composite with respect to fatigue and stress rupture. Fracture toughness considerations in composites are described. Finally, the relation of fracture characteristics to containment requirements is considered.

INTRODUCTION

Performance estimates for composite flywheels are usually based on ultimate tensile strength data on unidirectional composites obtained in short-term monotonic loading tests. In order to provide more realistic assessments of performance, account must be taken of strength degradation under cyclic and long term steady loading so that a knowledge of fatigue and creep rupture properties must be factored into the performance estimate. In addition, a useful discussion of failure modes must allow for the fact that the reinforcement may be bidirectional, as in the Avco approach, in contrast to all-circumferential reinforcement found in simple rim wheels and solid discs. The simplest types of failures are probably those in the case of radial spoke and dry hoop wound configurations where failure is restricted to fiber breakage. In the case of pure circumferential windings, failures include fiber failures associated with the hoop stresses and transverse splitting associated with radial stresses which arise when the radial thickness of the winding is not small (i.e. outer-to-inner radius ratio appreciably greater than unity). With bidirectional reinforcement, interlaminar shear stresses constitute a primary mode of transferring load support from hoop reinforcements to radial reinforcements so that fatigue and creep rupture properties with respect to interlaminar shear stressing must be accounted for in evaluating long-term performance. Beyond the effect of interlaminar shear stressing, interaction of layers in multi-directional laminates has long been a stumbling block to composites designers in that the usual failure theories tend to predict excessively low strength levels due to transverse straining of individual plies, whereas damage associated with transverse straining may in fact be quite benign and of a non-propagating variety. Benign damage also shows up in notched specimens subjected to both steady state and fatigue loading where it is sometimes found that residual strength is higher after cycling than before.

If it is established that the role of the matrix is only for providing dynamic stability through structural stiffness, thought should be given to relieving the matrix from contributing to failures by use of high-strain, low stiffness matrix materials. The radial failure problem in hoop wound wheels may be an artificial one associated with use of too rigid a resin, although the dangers of pushing the "soft matrix" approach too far may lead to a wheel which is so "limp" as to make dynamic instabilities intractable.

Failure considerations play a role not only in establishing a realistic level to which to de-rate proposed materials, but also in providing a standpoint from which to consider potential safety hazards and minimum requirements for protecting against

them. Expectations have generally been prevalent that failures of composite flywheels will be benign and easy to protect against. This is likely to be true if low interlaminar strengths of composites which are usually encountered lead to very fine-structured break-up of the wheel material. If interlaminar strengths are raised above some level not known at present, failure could take place in the form of large chunky fragments as is the case with metals, making the containment problem more serious than is presently anticipated.

The following discussion will address itself to these areas of consideration.

RELATION OF EXPECTED FAILURE MODES TO DESIGN CONCEPTS

GENERAL OBSERVATIONS

The following are composite reinforcement concepts which have been considered[1].

TABLE 1
COMPOSITE FLYWHEEL CONCEPTS

1. Radial and fanned brush
2. Rim-type (fixed radial spokes or connectors)
3. Rim-type (flexible rim connectors)
4. Pure circumferential wound (may be shaped)
5. Laminated bi-directional reinforcement
6. Radial-wrapped core
7. Pseudo-isotropic disc (laminated layups may be shaped)
8. Geodesic wound
9. Rods or bars
10. Concentric rings

Little experience has been met to date with achieving clear-cut overspeed failures in composite wheels since performance limitations have been associated with dynamic instabilities, deficient hub/attachment design, and similar features not related to stress failure of the composite. Moss and Gerstle[2] state that for a pure circumferentially wound Kevlar epoxy wheel which they produced, radial cracking corresponding to transverse strain failure of the Kevlar epoxy was the performance limiter. Apparently, such cracking was not actually observed in their wheel because of the low operating speeds they confined their experiments to (1.7 Watt hr/lb). Thus, any discussion of expected failure modes in composite flywheels cannot help but be somewhat speculative and is usually not backed up by hard data. One of the obvious deficiencies in current state of the art is the need for clear-cut demonstration of valid failure modes. The following discussion is based on general experience with composites together with rational guesses as to what failure modes are likely to be associated with particular reinforcement configurations.

DISCUSSION OF PARTICULAR FAILURE MODES

1) Pure Fiber Breakage

In the case of such configurations as radial and fanned brush, radial rods and bars, and dry wound circumferential winds (Table 1, items 1, 4, and 9), simple tensile failures due to longitudinal tension in the filaments would be the only failure mode to be expected. Design relatively close to static ultimate strengths could probably be achieved in this case. Due allowance for fatigue degradation and creep rupture of the fibers would be required in the form of some de-rating from measured ultimate strength values. In addition, safety margins would have to be chosen to allow for statistical variability of static ultimate strengths.

2) Radial Strain Failure

Figure 1 shows typical radial and hoop stress distributions in simple hoop wound wheels with various ratios of hoop-to-axial modulus. (Figure 1 applies to an outer-to-inner radius ratio of 21). More pertinent to the understanding of radial failures is the comparison of hoop and radial strain distributions. Table 2 gives the ratio of maximum radial strain, $\varepsilon_r)_{max}$ to maximum hoop strain, $\varepsilon_\theta)_{max}$ which is deduced from the curves of Figure 1 for the three cases considered. Using the data of Table 3 for Kevlar 49 epoxy[4], the allowable transverse strain is less than 0.153 times the allowable longitudinal strain for typical epoxy matrix materials, so that none of the radial strain levels in the cases shown in Table 2 could be tolerated.

Methods for elimating radial strain failures include reducing the outer-inner radius ratio of the hoop wound wheel, use of elastomeric matrix materials capable of large strain and addition of reinforcement in directions other than the hoop direction. For thin rim wheels, using the notation

$$t = r_t - r_i$$

(r_t = outer or "tip" radius, r_i = inner radius)

it can be shown* that for a relatively rigid matrix the stress ratio is

$$\frac{\sigma_r)_{max}}{\sigma_\theta)_{max}} \simeq \frac{3}{4}\left(\frac{t}{r_t}\right)^2 \qquad (1)$$

and the corresponding strain ratio is

$$\frac{\varepsilon_r)_{max}}{\varepsilon_\theta)_{max}} \simeq \frac{3}{4}\,\frac{E_\theta}{E_r}\,\left(\frac{t}{r_t}\right)^2 \qquad (2)$$

so that if the strain ratio is given, the upper limit on the rim thickness is given by:

TABLE 2

RELATIVE RADIAL STRAINS IN HOOP WOUND WHEELS DETERMINED FROM FIG. 1- ($\frac{r_t}{r_i} = 21$)

σ_t = "tip stress" for thin rim wheel = $\rho\omega^2 r_t^2$

r_t = tip radius; r_i = inner radius

$\frac{E_\theta}{E_R}$ ($\equiv \rho_E$)	0.825	16	64
$\frac{\sigma_\theta)_{max}}{\sigma_t}$	1	0.56	0.70
$\frac{\sigma_R)_{max}}{\sigma_t}$	0.412	0.08	0.02
$\rho_E \frac{\sigma_R)_{max}}{\sigma_\theta)_{max}} \simeq \frac{\varepsilon_R)_{max}}{\varepsilon_\theta)_{max}}$	0.36	2.28	1.82

*See Appendix to this paper.

$$\frac{t}{r_t} < \left(\frac{4}{3}\,\frac{\sigma_R)_{ult}}{\sigma_\theta)_{ult}}\right)^{1/2} \qquad (3)$$

For Kevlar epoxy, Table 3, this leads to

$$\frac{t}{r_t} < 0.105$$

This is a severe limitation on rim thickness but might be gotten around by constructing a thicker ring from a series of concentric non-communicating thin rings. Post and Post[5] discussed a concept of this type in which fiber layers were separated by soft elastomeric layers.

The route of elastomeric matrices has been discussed by Post and Post,[5] by Lewis and Natarajan[6] for hoop wound wheels and in radially overwrapped wheels with hoop wound cores[7]. It should be noted that even for very soft matrices the ratio of radial to circumferential strain will be no greater than 3.* For fiber materials like Kevlar which have ultimate strains on the order of 1-2% then, transverse strains in the unidirectional composite are not required to be greater than about 5-6% to eliminate radial failures. On the other hand the radial strain problem is a problem of limited matrix strain aggravated by strain concentrations associated with close approach of fibers embedded as hard inclusions in the matrix. Excessively high fiber densities (i.e. greater than about 65%) must be avoided to prevent such strain concentrations from getting too large.

Multidirectional reinforcement as exemplified by the Avco wheel which involves hoop wound disks reinforced with petal-shaped radial strips will help to eliminate the problem of radial strain failure.

In summary, the radial strain failure problem appears to be one which lends itself to a number of straight forward solutions.

3) Interlaminar Shear Failure

In the case of the Avco bi-directional concept care must be taken that interlaminar shear stresses do not jeopardize the integrity

*For cases where $E_r << E_\theta$, the hoop strain is almost exactly equal to $\rho\omega^2 r^2/E_\theta$. With the kinematic relations $\varepsilon_\theta = U/r$ and $\varepsilon_r = dU/dr$ we are led to $U = \rho\omega^2 r^3/E_\theta$ and ε_r ($\equiv dU/dr$) $= 3(\rho\omega^2 r^2/E_\theta)$ i.e. $\varepsilon_r = 3\,\varepsilon_\theta$

TABLE 3

MECHANICAL PROPERTIES OF KEVLAR 49 EPOXY[4]

Load Orientation/sign*	L/c	L/t	T/c	T/t
Modulus, G Pa	73	87.6	4.5	4.65
Strength, G Pa	0.254	1.5	0.053	0.0123
Ult. Strain, %	0.0035	0.017	0.017	0.0026

*Load Orientation: L = longitudinal (parallel to fiber)
T = transverse; Load Sign: c = compression, t = tension

of bonding between hoop and radial elements since release of this bond would quickly lead to overstressing of hoop reinforcements. Proper design of the radial elements can reduce the level of interlaminar shear stresses to safe values provided that the bond is adequately characterized with respect to fatigue and stress rupture. In general, it should be recognized that multidirectional laminated configurations including quasi-isotropic laminated lay-ups (Table 1, item 7) could be subject to interlaminar strength requirements.

4) Transverse Ply Splitting in Multi-Directional Laminates

Laminates reinforced in more than one direction, especially 0/90° cross ply laminates, tend to exhibit incipient matrix damage at low stress levels because the transverse strain of the plies tends to be less than the ultimate strain of the fibers. This phenomenon is signalled by the presence of one or more "knees" in the stress strain curve. There is a wide divergence of opinion as to whether or not this should be considered incipient failure and used as a limiting stress for design calculations. Acceptance of such a limitation may be over-conservative and an unnecessary sacrifice of the full range of performance of the composite. The decision to accept the incipient damage level as a design limit should be based on observations concerning the propagation of fatigue and/or creep rupture failures at such levels. In the usual applications of composites initial damage sites may constitute paths of access to adverse effects of humidity or other environmental factors. In the flywheel case, where operation in a vacuum is expected to be normal procedure, this should not be a consideration.

FATIGUE AND STRESS RUPTURE OF COMPOSITES

To perform satisfactorily as flywheel materials composites must possess favorable stress rupture properties. There is a scarcity of data on this aspect of composite behavior, and such data as exists do not pertain specifically to the vacuum environment of flywheel operation. Limited data for a few laminate configurations of boron/epoxy are available in the AFML Composites Design Guide[8]. Even more limited data are given for several graphite/epoxy systems. Lawrence Livermore Laboratories have completed several years of study of S-glass/epoxy and Kevlar/epoxy tested in air[9]. In these tests resin impregnated fiber strands were subjected to sustained loading at room temperature. In the case of S-glass strands the average one-hour strength was about 76% and the 10^4 hour strength was 57% of the static ultimate strength. The absolute short and long term average values were about the same for Kevlar strands but these corresponded to relative values of 92 and 72%, respectively, based on the static strength of the strands. It is questionable whether or not the strand tests are actually representative of behavior in unidirectional composites inasmuch as the fiber strength is seldom fully realized in standard tension tests, either because of test deficiencies or degradation of the fibers during composite fabrication. There is also reason to believe that stress rupture performance in vacuum of S-glass composites may be substantially better than in air due to the absence of moisture absorption which often degrades mechanical properties. Sustained loading data published for unidirectional boron/epoxy shows similar characteristics to Kevlar[9], i.e., 100 minutes sustained life at 90% of static ultimate and long term life ($\simeq 10^4$ hrs.) at about 70% of ultimate.

Published data for unidirectional graphite/epoxy are difficult to find but data for angle-ply laminates are comparable relative to static strength to that for boron/epoxy[11].

Medium cycle fatigue strength ($\simeq 10^5$ cycles) is another requirement of flywheel materials. Generally speaking, unidirectional composites exhibit good fatigue properties at all ranges in tension-tension loading. The exception to this, as in the case of sustained loading, is S-glass/epoxy. This material has the steepest S-N curve of all the advanced composites[12-14]. Mean fatigue strength at 10^5 cycles has been found to be as low as 30% of static ultimate in zero-tension tests conducted in air on one type of S-glass composite[10]. There is some contradiction in test results that have been published, however. For instance, the 10^5 cycle fatigue strength of $\pm 5°$ S-glass/epoxy specimens subjected to fully reversed loading was observed to be about 35% of static ultimate while that of [0-90] cross-ply specimens was nearly 60% of ultimate[11]. This is still relatively low compared to 85% for unidirectional boron/epoxy[8] and about 75% for graphite/epoxy[8] and Kevlar/epoxy. The reason for the relatively low performance of S-glass may again be the susceptibility of S-glass fibers to attack by moisture, and judgement regarding the use of this material for flywheel applications should be reserved until testing has been conducted in vacuum. The fatigue resistance of metal matrix composites such as boron/aluminum is similar in character to that of boron/epoxy at room temperature and substantially better at elevated temperature[8]. Behavior of metal/matrix composites under fatigue loading depends to a large extent on the heat treatment characteristics of the matrix and fabrication induced residual stresses. Some studies have indicated that fatigue strength may be enhanced by thermo-mechanical cycling to rearrange the residual stress state[13].

Fatigue failure in composites is a process of randomly occurring failure mechanisms starting with microcracking in the matrix, proceeding to fracture of the weakest fibers and subsequent debonding of fibers and matrix. There seems to be even more statistical variation inherent in this process than in the fatigue failure process of metals, and reliable design of composite flywheels will require extensive fatigue testing to establish material design parameters. This should be done by way of a test methodology which does not obscure behavior characteristics in actual flywheel operating conditions. For instance, in the usual repeated load testing of polymer matrix composites, considerable heat is generated through hysteresis and friction believed to occur in regions of damage. The temperature increase observed may influence the subsequent behavior of the composite under cyclic loading. In a flywheel operation this temperature rise may or may not be present since the time interval between recharging of the flywheel will be relatively long compared to the time between maximum loads in the fatigue test. At the same time, the absence of a medium for heat transfer could have just the opposite effect on temperature rise and subsequent behavior. In any case, the disparaties between testing and operational conditions will have to be resolved if intelligent selection of composites for flywheel materials is to be made on the basis of fatigue tests.

TOUGHNESS CONSIDERATIONS

Design configurations considered to be efficient for flywheel applications mostly employ either hoop wound, unidirectional or, as with the Avco concept, [0-90] cross-ply fiber reinforcement. The question as to whether catastrophic fracture could occur during operation is important to the safety assessment of such composite flywheels. As there has been little experience with testing flywheels to failure, recourse must be had to the large store of fracture test data collected on composites in recent years. Numerous test methods, including center and edge-notched tension, compact tension, and slow, edge-notched bend tests have been employed on a wide variety of composite types and laminate configurations. The various tests have generally been implemented within the framework of fracture mechanics despite the fact that the failure phenomena involved seldom resemble crack propagation as such. Measurements have been made of such parameters as fracture energy, strain energy release rate and critical stress intensity factor. The results obtained have depended on specimen configuration and test method, and there has seldom been correspondence between parameter values measured on the same material by different test methods. Factors related to an inherent characteristic size, to edge effects, and to growth of a subcritical damage region adjacent to the notch contributed to the complexity of fracture behavior. Test results are also statistically variable with a standard deviation of 20% not uncommon for carefully measured parameters. While general fracture criteria for composites are not yet state-

of-the-art, there are nonetheless, some pertinent observations regarding unidirectional and cross-ply laminates, which may have some bearing on their safe use in flywheels.

In the case of unidirectionally reinforced polymer composites, experience has shown that crack propagation invariably tends to occur parallel to fibers rather across them regardless of the orientation of flaws, notches, or applied loads. This behavior is due both to material heterogeneity and anisotropy. The toughness of polymer based composites is low in the transverse direction so that a crack tip is inevitably deflected to run parallel to fibers. Even in cases where fracture is constrained to occur across fibers, as in a severely side grooved compact tension specimen, some parallel slitting usually occurs before the main crack tip jumps across fibers. The critical strain-energy release rate in the transverse direction typically ranges from about 0.2 kJ/m^2 for graphite/epoxy to about 2 kJ/m^2 for S-glass/epoxy. In the latter, there is evidence that the transverse toughness increases with crack length due to crack bridging action of the fibers. Few valid toughness measurements have been accomplished for fracture across fibers in unidirectional composites, but such data as are available indicate this to be of the order of 55 $MN/m^2 \sqrt{m}$ * in high strength graphite/epoxy. It is estimated to be several times higher than this in S-glass/epoxy; however, valid measurements have yet to be obtained. No published fracture data are available for Kevlar reinforced composites, and it is difficult to speculate on fracture behavior of this material based on its unidirectional tension properties alone. Unidirectional metal matrix composites such as boron/aluminum exhibit a behavior somewhere between metals and polymer matrix composites. The crack trajectory may proceed in a tortuous, zig-zag fashion, parallel to and across fibers, but generally the test specimen is fractured perpendicular to the load direction. Fracture toughness values as high as 120 $MN/m^2 \sqrt{m}$ have been obtained.

*For typical steels, fracture toughness levels on the order of 57 $MN/m^2 \sqrt{m}$ (4340 steel, 20°C) are obtained by way of comparison.

The fracture behavior of some cross-ply composites resembles fracture in metals. [0-90] Graphite/epoxy and boron/epoxy are examples of this as evidenced by their relatively flat crack trajectory transverse to the load. Various damage mechanisms occur in addition to crack propagation, which seem to have significant influence on the laminate toughness. Toughness values for graphite/epoxy [0-90] laminates are typically of the order of 30 $MN \sqrt{m}/m^2$. The magnitude of toughness seems to depend primarily on the ratio of ply tension strength in the fiber direction to the interlaminar shear strength. When this ratio is high, a large damage zone can develop ahead of the crack tip, effectively blunting it. The nature of damage in this zone appears to be primarily in-ply parallel fiber splitting and debonding between plies. The damage zone in a cross-ply laminate acts similarly to the crack-tip plastic zone in a metal, but appears to be significantly larger. In cross-ply S-glass/epoxy the tensile to interlaminar strength ratio is so high that it is virtually impossible to propagate a sharp crack. Instead, the damage zone itself increases in size, giving this material a very high apparent toughness. Perhaps because of a lower tensile-to-laminar strength ratio, cross-ply E-glass/epoxy is much less tough measured values of toughness being of the order of 20 $MN\ m/m^2$.

In assessing the relative safety of composites to sudden fracture during operation, it is necessary to consider the laminate configuration and damage mechanisms. It is also important to remember that the toughness parameters generally used to characterize the behavior of metals do not always have a conceptual basis with regard to composites, and that toughness values quoted may have meaning only in comparison with other composites. In general, it would not seem likely that sudden fracture would occur in a unidirectionally constructed flywheel. Cracks that might initiate at internal flaws or stress raisers would tend to be deflected parallel to fibers in a relatively benign rather than catastrophic fashion. This will probably be true of any of the advanced fiber composites (S-glass, Kevlar, graphite, boron). The cross-ply configuration, however, sacrifices much of the toughness inherent in the unidirectional case, because adjoined plies parallel to the applied stresses tend to prevent crack deflection and permit propagation across rather than parallel to the load carrying area. Nevertheless, the development of a characteristic damage zone by in-ply splitting and

delaminating does tend to give a reasonably high degree of toughness to composites fabricated with S-glass and perhaps, Kevlar fibers, to the extent that sudden fracture should not be a major consideration.

RELATION OF CONTAINMENT REQUIREMENTS TO FAILURE MODES

Resin matrix composites are characterized by numerous planes of weakness interspersed between excessively high strength fibrous elements, making fine-structured failures likely. Observed failures which have occurred in both the Garrett multiple ring and Avco radially reinforced wheels tend to confirm the expectation that, because of this fine structure, failures of composite flywheels will be "soft" and easy to contain. By contrast, experience with turbine disks[15] shows that metal flywheels will tend to fail in large chunks having excessively high momentum levels which makes containment extremely difficult for flywheels weighing more than a few pounds. The problem is brought home by considering the fragment velocities of various flywheel concepts. Since these are approximately equal to the tip speed of the wheel, they can be estimated by the relation between maximum wheel speed and strength, i.e.,

$$\sigma_{ult} = K_s \frac{\rho_w}{g} \omega^2 r_t^2 = K_s \frac{\rho_w}{g} (12\ v_t^2) \quad (4)$$

where K_s is the geometric shape factor ρ_w is the weight density (lb-in^{-3}), g is gravitational acceleration (386 in/sec^2) and r_t (in) and v_t (ft/sec) are outer radius and tip speed, respectively, from which

$$v_t = \frac{1}{12} \left(\frac{\sigma_{ult} g}{K_s \rho_w} \right)^{1/2} \quad (5)$$

Table 4 shows a comparison of tip speeds predicted from equation (5) for a thin rim (K_s = 0.5) configuration in 4340 steel vs. Kevlar epoxy.

Since rifle bullets typically travel at speeds on the order of 1,000-3,000 ft/sec the fragment velocities shown in Table 4 can be considered to be representative of ballistic speeds. For steel fragments impacting steel targets, contact pressures on the order of 0.7 x 10^6 psi will be realized for short periods of time for impact velocities on the order of 800 ft/sec, using the acoustic impedance relationship

$$P = \frac{Z_c Z_f}{Z_c + Z_f} v \quad (6)$$

where Z_c = acoustic impedance of containment material, Z_f = acoustic impedance of fragment; for a given material, Z is calculated from E, Young's modulus, and ρ_w, weight density, by

$$Z = \left(\frac{E \rho_w}{g} \right)^{1/2} \quad (7)$$

For Kevlar epoxy fragments impacting a steel target the same type of calculation gives early contact pressures on the order 285 ksi for 2000 ft/sec impact velocities. Small particles impacting thick targets tend to realize the same initial pressures as large particles but unload more quickly due to wave reflection from free surfaces, so that the duration of the contact pressure pulse is shorter. This is a rough way of characterizing the mechanism by which the finer structure of composite failures can lead to reduced containment requirements. An additional consideration is the fact that harder projectiles tend to maintain small areas of contact against targets for long periods of times whereas soft projectiles tend to undergo lateral flow, increasing areas of contact and thereby engaging more of the target available for resisting the projectile. Whereas the steels being considered for flywheel applications have static ultimate strengths on the order of 300,000 psi, strengths of typical composites for impact transverse to fibers are an order of magnitude less. The ability of hard (though brittle) armor materials such as ceramics to cause early break up and blunting of sharp-tipped projectiles is a reflection of the fact that such blunting is equivalent to spreading the load exerted by the projectile over large target areas, thereby reducing the contact stresses.

It appears that the most important requirement of the containment shield is to resist early ballistic penetration by flywheel fragments. Areal density of the fragments defined as mass of the projectile divided by area of contact with the containment shield is an important parameter controlling the outcome of the impact situation, and small fragments will obviously have low areal densities. In addition to fine structure of fragments, low mass density of composites is an important factor in limiting

TABLE 4

TYPICAL FRAGMENT VELOCITIES IN FLYWHEEL FAILURES

Material	4340 Steel*	Kevlar Epoxy*
σ_{ult} (lb/in^2)	140,000	170,000
(G Pa)	1.00	1.21
ρ_w (lb/in^3)	0.29	0.052
ρ (gm/cm^3)	7.8	1.4
v_t (ft/sec)	804	2035
(m/sec)	245	619

*Properties from Ref. 14

fragment areal densities.

Penetration resistance of armor materials against fragments is normally tested by ballistic firing of "fragment simulators" of various designs against the candidate protection material. However, actual fragments such as debris recovered from a failed flywheel can be launched in sabots contained in test rounds. Determination of the containment thickness required to resist penetration can be thus established emperically.

REFERENCES

Note: The following abbreviations for sources are used below:

F.S. - Proceedings of the 1975 Flywheel Technology Symposium, ERDA Report, ERDA 76-85. (Nov 1975)

ERDA - "Economic and Technical Feasibility Study for Energy Storage Flywheel", ERDA Report, ERDA-76-65, (Dec 1975). Prepared by Space Division, Rockwell International

1. ERDA, p. 4-25.

2. Moss, J. and Gerstle, F.P., Kevlar/Epoxy Flywheels; An Experimental Study", F.S., pp. 59-61.

3. Gerstle, F.P. and Biggs, F., "On Effective Uses of Filamentary Composites in Flywheels", F.S., pp. 146-150.

4. Clements, L.L., "Engineering Design Data for Composite Materials", F.S., pp. 229-233.

5. Post, F.P. and Post, S.F., Scientific American, V. 229, No. 6, pp. 17-23.(Dec 1973).

6. Lewis, A.F. and Natarajun, R.T., "Engineering Properties of Elastomer/Advanced Composite Laminar Structures", F.S., pp. 185-194.

7. ERDA, pp. 5-20 to 5-22.

8. Advanced Composites Design Guide, Vol. IV, Materials, Air Force Materials Laboratory, (January 1973).

9. Chiao, T.T., et. al., "Lifetimes of Fiber Composites Under Sustained Tensile Loading", Proceedings of the 1977 International Conf. on Fracture Mech. & Tech., (March 1977), Hong Kong.

10. Tobler, R.L. and Read, D.T., "Fatigue Resistance of a Uniaxial Glass/Epoxy Composite at Room and Liquid Helium Temperature", J. Composite Materials, Vol. 10, (Jan 1976), p. 32.

11. Pazmany, L. "Potential Structural Materials and Design Concepts for Light Airplanes", NASA CR-73258, (Oct 1968), p. 177.

12. Cutler, M.B. and Pinckney, R.L., "Static and Fatigue Test Properties for Woven and Nonwoven S-Glass Fibers", USAAVLABS Technical Report 69-9, (April 1969).

13. Rao, M.S.M. and Dvorak, G.J., "Micro-plastic Deformation of Fibrous Composites", Final Report, AMMRC Contract DAAG46-73-0228, (September 1974).

14. Friedericy, J.A. and Raynard, A.E., "Garrett's Outlook on Vehicle Flywheels", F.S., pp. 62-75.

15. Witmer, E.A. and Holms, A.G. (ed.) "An Assessment of Technology for Turbojet Engine Rotor Failures", NASA CP-2017, (Aug 1977)

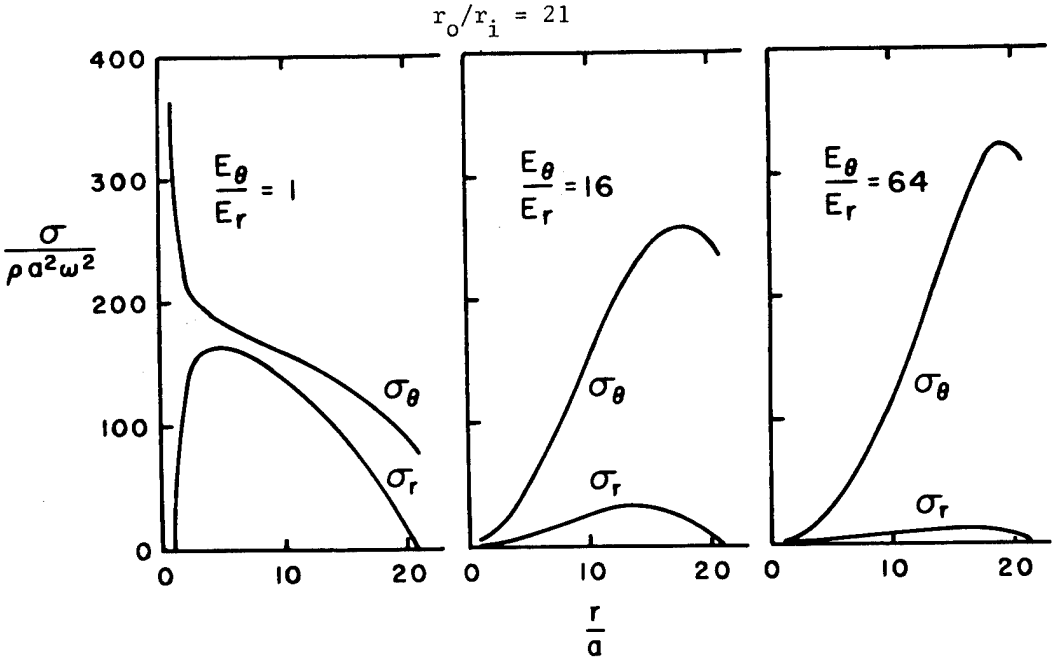


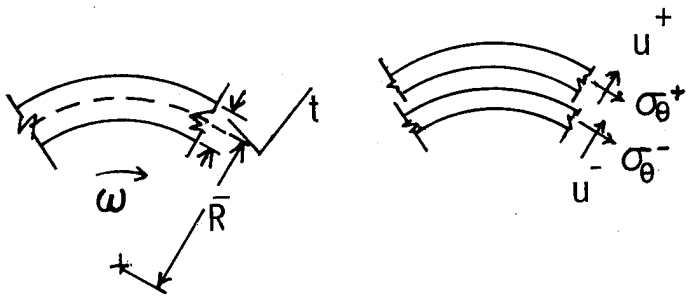
Figure 1. Hoop and radial stress distributions in flat rotating disks; $\nu = 0.3$[3]

ACKNOWLEDGMENT - This work was partially supported by funding from Benet Laboratories of U.S. Army Watervliet Arsenal on behalf of the Department of Transportation.

APPENDIX - APPROXIMATE RADIAL STRESSES IN THIN RIM WHEELS

The following calculations are developed for a thin rotating ring of hoop modulus E_θ by assuming first of all that the ring is split circumferentially along a surface located at its mean radius, determining the amount of separation that will take place between the two pieces because of differing linear speed (corresponding to a difference in mean radius of the separated pieces) which leads to a difference in hoop stress, and finally, calculating the radial stress that is needed to cancel out the separation. It is assumed that the initial thickness of the ring is so small that radial strains (and consequently radial modulus) do not enter into the calculations. Radial deflections correspond only to hoop stresses or to the effect of radial stress on hoop stress through equilibrium.

In the following the superscript + refers to the outer piece of the split ring and - to the inner ring. Thus, u^+, v^+, ε_θ^+, and σ_θ^+ are the mean displacement, mean linear speed, hoop strain and hoop stress of the outer piece while the same quantities with the - superscript refer to the inner piece. If a ring of thickness t and mean radius $\bar{R}$ (Fig. A.1) is rotating at a mean speed $\bar{v} = \omega\bar{R}$ where ω is the angular velocity, and is split along the mean radius, the outer half will have a mean radius $\bar{R} + t/4$ and the inner half a radius $\bar{R} - t/4$. The two halves having no radial stress to cause them to re-join, will assume radial displacements controlled strictly by the hoop stress and



(A) Ring In Tact (B) Ring Split

Figure A. I Thin Ring Geometry

and strain, i.e.,

$$\varepsilon_\theta^+ = \frac{u^+}{\bar{R}+\frac{t}{4}} = \frac{1}{E_\theta}\sigma_\theta^+ = \frac{1}{E_\theta}\rho v^{+2}$$

$$= \frac{\rho\bar{v}^2}{E_\theta}\,\frac{(\bar{R}+\frac{t}{4})^2}{\bar{R}^2}$$

$$\varepsilon_\theta^- = \frac{u^-}{\bar{R}-\frac{t}{4}} = \frac{\rho v^{-2}}{E_\theta}\left(\frac{\bar{R}-\frac{t}{4}}{\bar{R}}\right)^2$$

or

$$u^+ - u^- = \left(\frac{\rho\bar{v}^2}{E_\theta}\right)\frac{6\bar{R}^2\frac{t}{4} + 2\left(\frac{t}{4}\right)^3}{\bar{R}^2} \qquad (A.1)$$

i.e.

$$\Delta u = u^+ - u^- = \left(\frac{\rho\bar{v}^2}{E_\theta}\right)\left(\frac{t}{2}\right)\left[3 + \left(\frac{t}{4\bar{R}}\right)^2\right]$$

The radial stress needed to rejoin the two pieces is that required to reduce the outer ring displacement by $\Delta u/2$ and increase the inner ring displacement by $\Delta u/2$. This, in turn, requires a reduction in outer ring hoop stress by the amount

$$\Delta\sigma_\theta^+ = -\frac{E_\theta}{2}\frac{\Delta u}{\bar{R}-\frac{t}{4}} \simeq \frac{E_\theta}{2}\frac{\Delta u}{\bar{R}}$$

and an increase in inner ring hoop stress by

$$\Delta\sigma_\theta^- = +\frac{E_\theta}{2}\frac{\Delta u}{\bar{R}-\frac{t}{4}} \simeq \frac{E_\theta}{2}\frac{\Delta u}{\bar{R}}$$

A radial stress on the inner surface of the outer ring, given by

$$\sigma_R = \frac{-t}{2\bar{R}}\Delta\sigma_\theta^+ = \frac{t}{2\bar{R}}\Delta\sigma_\theta^-$$

and the same radial stress applied to the outer surface of the inner ring will establish this adjustment. Thus, the required σ_R is given by

$$\sigma_R \simeq -\frac{t}{2\bar{R}}\Delta\sigma_\theta^+$$

$$\simeq \frac{t}{2\bar{R}}\frac{E_\theta}{2}\frac{\Delta u}{\bar{R}} \qquad (a.2)$$

Substituting for Δu from Equation (A.1)

$$\sigma_R \simeq \left(\frac{t}{2\bar{R}}\right)^2\left[3 + \left(\frac{t}{4\bar{R}}\right)^2\right]\rho\bar{v}^2$$

$$\simeq \frac{3}{4}\left(\frac{t}{\bar{R}}\right)^2\rho\bar{v}^2$$

FAILURE MODES OF BI-DIRECTIONALLY REINFORCED FLYWHEELS

Donald E. Johnson
Avco Systems Division
Wilmington, Mass. 01887

and

Donald W. Oplinger
Army Materials and Mechanics Research Center
Watertown, Mass. 02172

ABSTRACT

Bi-directionally reinforced composite flywheel designs are theoretically capable of achieving the maximum energy per unit weight associated with composite flywheels. Unlike the composite ring configurations they also have the advantage of exhibiting high energy per unit volume. This paper considers the effects of several failure modes that can limit the performance of bi-directionally reinforced flywheels. These effects include potential shear failures, degraded properties and variations caused by manufacturing. Finite element analyses are carried out to determine the magnitude of both the in-plane and interlaminar shear stresses that arise from the discreteness of the individual radial reinforcements. The finite element analysis is also used to model the degradation of material properties due to high biaxial stress levels, especially the drop in shear modulus. Experiments are conducted to evaluate this property degradation. The experimental results are then factored into the finite element analysis to determine the effect of in service property degradation on the predicted failure speed. In addition, the effect of manufacturing property variations on both the specific energy of the flywheel and on its imbalance is investigated. Results are presented in parametric form in terms of predicted reductions in the theoretical specific energy of bi-directionally reinforced composite flywheels.*

INTRODUCTION

This paper summarizes the results of an investigation of bi-directionally reinforced composite flywheels. The investigation focuses on the hoop-radial type of bi-directional configuration developed by Avco and includes both analytical and experimental work. A schematic of a typical bi-directionally reinforced flywheel is shown in Fig. 1. In this work we consider the case of alternate successive layers of hoop and radial reinforcements. We are thus concerned with four basic failure modes:

1. Tensile failure of hoop reinforcements.
2. Tensile failure of radial reinforcements.
3. Interlaminar shear failure.
4. In-plane shear failure.

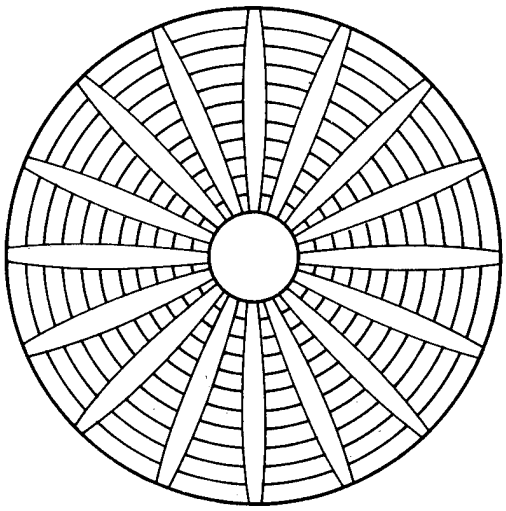


Fig. 1. Schematic of typical bi-directionally reinforced flywheel.

*This work has been carried out under Contract DAAG46-77-C-0017 from the Army Materials and Mechanics Research Center.

In addition, the effect of property degradation due to the presence of a high biaxial state of stress is considered.

Bi-directional reinforced flywheels offer potential advantages over the more conventional composite ring designs, such as greater energy per unit volume and a larger number of geometric parameters to apply to the design of hub connections. In addition, theoretical analyses show that the stored kinetic energy per unit weight of a bi-directionally reinforced wheel can be within a few percent of that obtained via ring designs.

The kinetic energy per unit weight of a composite flywheel composed of one material can be written in the following form.

$$\frac{\text{Kinetic Energy}}{\text{Weight}} = K_s \frac{\sigma}{\rho g}$$

where

K_s = shape factor

σ = allowable tensile stress of a 1-D ply in the 0^o direction

ρ = weight/unit volume of the wheel.

For a given material, σ and ρg are known and the primary problem is to configure the wheel to achieve the highest possible value of K_s. Analyses based on neglecting the very low 90^o tensile strengths indicate that the maximum K_s obtainable for a composite is 0.5. (For a simple ring $K_s = 0.5$.) Design experience at Avco indicates that some deviation from the optimum is necessary to prevent excessive hoop radial interlaminar shear stresses, and that the shape factor K_s must be slightly reduced from 0.5 to 0.474. It should be noted that since the formula cited for kinetic energy per unit weight involves only the strength in the 0^o direction, the formula applies to a flywheel which has been designed so that other failure modes will not occur before the 0^o tensile failure.

The Avco bi-directional flywheel design consists of a stacked sequence of hoop and radial layers. The hoop layers are approximately 0.017-inch thick and essentially axisymmetric. The radial layers each contain 144 radial members, 0.008-inch thick and of tapered width to provide optimum efficiency. The material is Kevlar 49. This design is used as a reference point for the current investigations. Consequently, it is appropriate to review some of the basic parameters that controlled the reference design.

At the onset we introduce appropriate nondimensional stress nomenclature as follows:

$$\hat{\sigma} = \frac{\sigma}{\rho \Omega^2 R^2}$$

where

σ = stress

$\hat{\sigma}$ = nondimensional stress

ρ = mass density of a ply

Ω = angular velocity in radians/sec.

R = outside radius of the flywheel

The nondimensionalization symbol $\hat{}$ is applied to various stress components.

The dominant feature of an efficient bi-directional flywheel is a biaxial state of stress with approximately equal stresses in the hoop and radial directions. For Kevlar the 0^o and 90^o failure strains, ε_0 and ε_{90} form the following ratio

$$\frac{\varepsilon_{90}}{\varepsilon_0} = \frac{0.22\%}{1.6\%} = .138$$

This implies that the transverse (90^o) properties of the Kevlar will be degraded, and crazing will occur well before the 0^o failure strains are reached. For this reason the radial configuration of the reference Kevlar flywheel was designed on the basis of $E_{90} = 0$ in each hoop and radial ply. To implement the iterations required during the design process a "smeared out" axisymmetric finite element model is used to obtain the optimally shaped radial reinforcements that yielded the highest shape factor K_s. The nondimensional stresses derived from the axisymmetric model are shown in Fig. 2. This figure clearly shows the dominant features of the problem: nearly biaxial ($\sigma_R = \sigma_\theta$) stresses over the interior of the wheel and very much smaller shear stresses σ_{RZ} and $\sigma_{R\theta}$. (See separate scale on right side of the figure.) Unfortunately the shear allowables are correspondingly smaller, as

Table 1. Stresses in reference flywheel design.
For $E_{90} = 0$ (crazed)

Type of stress	Equivalent axisymmetric analysis		2-D finite element		
	Nondimensional	At Ω = 5685 radians/sec.	Nondimensional	At Ω = 5630 radians/sec.	Allowables
σ_R	.516	200 Ksi	.514	200 Ksi	188-211 Ksi
σ_θ	.516	200 Ksi	.530	200 Ksi	188-211 Ksi
σ_{RZ}	.00401	1.55 Ksi	.00355	1.34 Ksi	1.45-7.9 Ksi
$\sigma_{R\theta}$	.00982	3.81 Ksi	.01032	3.90 Ksi	7.9 Ksi

may be seen from Table 1 which summarizes the maximums of the stresses shown in Fig. 2 together with the corresponding stresses from a more complex two-dimensional finite element model of the same problem in which the discreteness of the radials is accounted for.

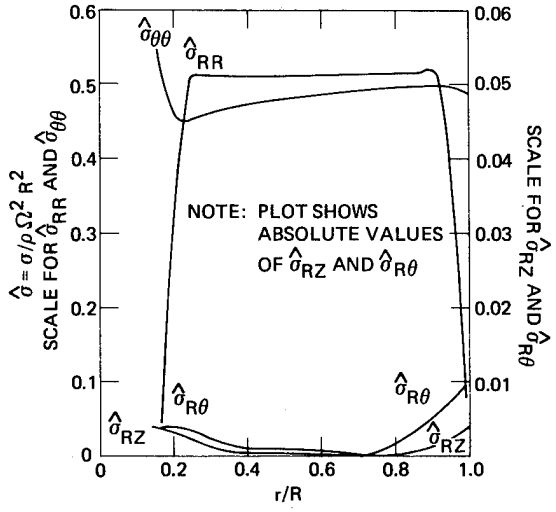


Fig. 2. Nondimensional stresses from equivalent axisymmetric model.

MATERIAL PROPERTIES

The following Kevlar 49 mechanical properties were used:

Property	Equivalent Nomenclature	Values Used Uncrazed	Crazed
E_1	$E_0 = E$	12 x 10^6 psi	12 x 10^6 psi
$E_2 = E_3$	E_{90}	0.8 x 10^6	0
$\nu_{12} = \nu_{13}$		0.34	0
$\nu_{21} = \nu_{31}$		0.0227	0
ν_{32}		0.48	0
G_{12}	G	0.3 x 10^6 psi	0.3 x 10^6 psi or reduced

These properties are derived from the properties given in Ref. (1).* As pointed out in the previous section the "crazed" properties were used in the flywheel design because of the very low transverse (90^o) strain capability of Kevlar. It should also be noted that the linear elastic nature of the problem is such that the resulting stresses are unchanged if the moduli E_1, E_2, E_3 and G are multiplied by the same scalar constant.

Finite Element Models. Three different types of finite element models were used in this work:

1. Axisymmetric Model
2. 2-D Model including Discrete Radials
3. 2-D Model using "Smeared Out" Properties

In the 2-D model with discrete radials the nodes in the hoop-radial overlap region each have one set of planar displacements, i.e., in spite of the over-lapping the model remains planar. This model uses 2488 nodes and 3410 elements to represent a very slender representative angular section of the wheel. The 2-D model using "smeared out" properties is shown in Fig. 3.

The axisymmetric model and the 2-D model with the discrete radials give almost identical results for the σ_θ, σ_R, and $\sigma_{R\theta}$ stresses. However, the σ_{RZ} interlaminar stresses obtained from these two models differ as shown in Fig. 4. This latter difference is not accountable from the circumferential variations in the 2-D model but appears to be caused by a fundamental difference between the two models. Because of the planar nature of the 2-D model it gives a $\sigma_{R\theta}$ that does not approach zero at the edge of a radial. This can violate the shear-free condition actually present at the lateral free edge of a radial. It is believed that the differences shown in Fig. 4 can only be resolved by a local 3-D finite element analysis in the region of

*1. Hunter, R. L., "Characteristics and Uses of Kevlar 49 High Modulus Organic Fiber," Dupont Report, revised 9/18/73, page 36.

the edge of the radial. However, since the maximum σ_{RZ} stresses shown in Fig. 4 differ by only 13 percent, the differences between the models do not present a serious obstacle in designs.

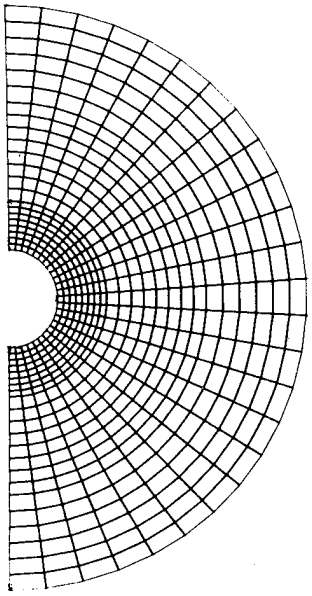


Fig. 3. Finite element grid used for asymmetric property variations.

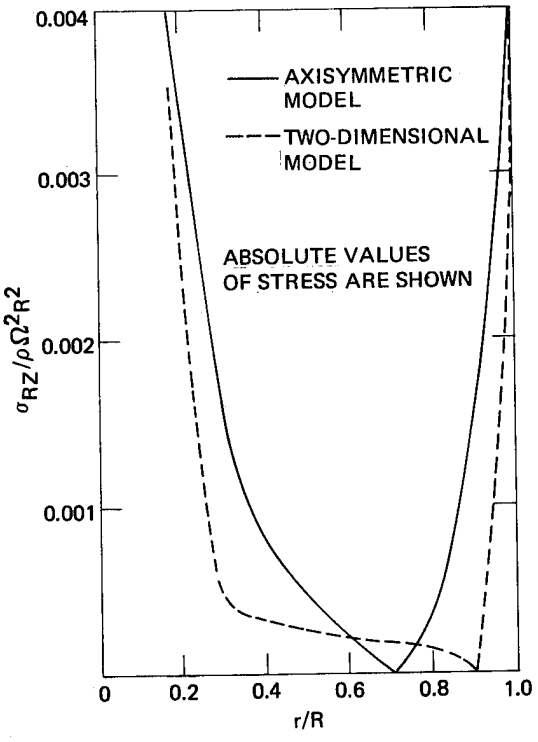


Fig. 4. Original flywheel with crazed properties comparison of shear stresses σ_{RZ}.

ANALYTICAL ASSESSMENT OF EFFECT OF DEGRADED PROPERTIES

We next investigate the effect of degraded material properties caused by the high biaxial stresses in the flywheel. The analytical results are obtained by using the 2-D finite element model with discrete radials.

Preliminary Investigation: Crazed Versus Uncrazed. As previously mentioned, the flywheel is designed and optimized using the $E_{90} = 0$, $\nu = 0$ crazed properties because of the low transverse (90°) strain allowable of Kevlar. If the same configuration is analyzed using uncrazed properties, the stress distributions are as shown in Figs. 5 and 6. Note that the maximum hoop stress in the uncrazed condition is substantially larger than that in the design crazed condition as is shown in the following table.

Results for 2-D finite element analysis.

	Crazed	Uncrazed
$\frac{\sigma_{R\ max}}{\rho\ \Omega^2\ R^2}$	.514	.470
$\frac{\sigma_{\theta\ max}}{\rho\ \Omega^2\ R^2}$	.530	.605
K_s (2-D Anal.)	.461	.404

The table also shows the shape factor K_s computed for these two cases and indicates a 12 percent lower K_s (and hence lower energy density) for the uncrazed condition than for the crazed condition used to optimize the design.

Effect of Degraded Shear Modulus. A series of two-dimensional finite element runs was made to determine the effect of reducing the shear modulus G for the crazed properties. The results shown in Table 2, are somewhat startling. They indicate that the maximum stresses and shape factor K_s are almost unaffected by reductions in the shear modulus down to one-tenth of the original. The distributions of the stresses shown in Table 2 are given in Figs. 2 through 9 for the two cases $G/G_{orig} = 1$ and $G/G_{orig} = 0.1$. Although the figures show very little change in the maximum stresses with the reduction of G/G_{orig} to 0.1, they do indicate the beginnings of changes in the stress pattern. Figure 7 shows that as the shear

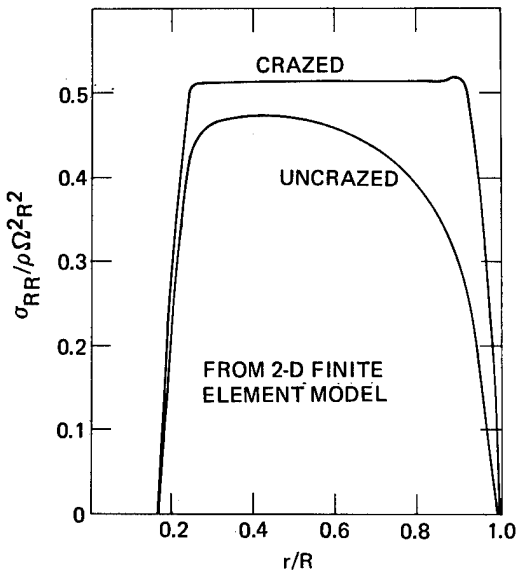


Fig. 5. Crazed versus uncrazed comparison of radial stresses in fiber direction σ_{RR} in the center of the radial layer.

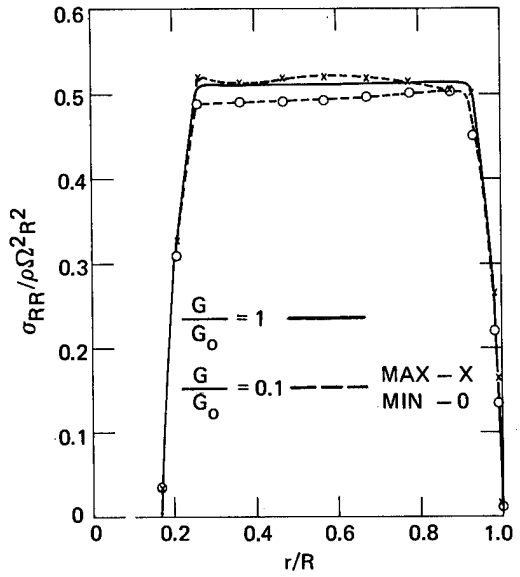


Fig. 7. Comparison of radial stress distribution for undegraded and degraded shear moduli.

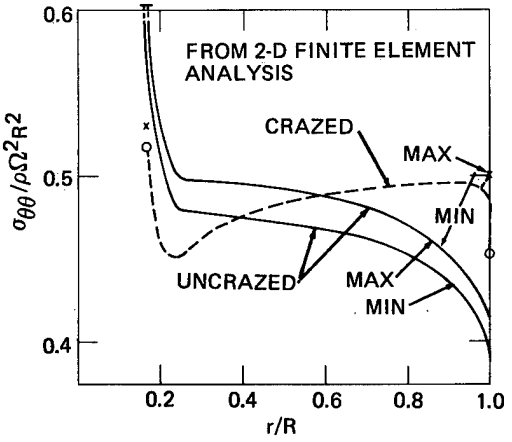


Fig. 6. Crazed versus uncrazed comparison of hoop stresses in fiber direction $\sigma_{\theta\theta}$ in the hoop layer.

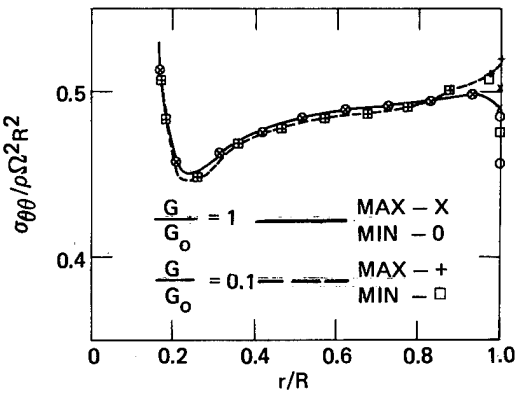


Fig. 8. Comparison of hoop stress distribution for undegraded and degraded shear moduli.

modulus is lowered, the distribution of σ_r stresses in the circumferential direction across a radial becomes increasingly nonuniform. At $G/G_{orig} = 0.1$, as shown in Table 2, the nonuniformity is already sufficiently great for the radial stresses to become the maximum stresses in the wheel. Figure 8 shows a similar circumferential nonuniformity in the hoop stresses near the outside of the wheel as the shear modulus is reduced. These trends would indicate that the σ_r and σ_θ stresses will increase as G is reduced below 0.1.

Table 2. Effect of degraded shear modulus.

(From 2-D finite element analysis)

$G/G_{original}$	1.0	0.5	0.1
$\frac{\sigma_{R\ max}}{\rho\ \Omega^2\ R^2}$	0.514	0.517	0.526
$\frac{\sigma_{\theta\ max}}{\rho\ \Omega^2\ R^2}$	0.530	0.529	0.523
$\frac{\sigma_{RZ}}{\rho\ \Omega^2\ R^2}$	0.00355	0.00356	0.00354
$\frac{\sigma_{R\theta}}{\rho\ \Omega^2\ R^2}$	0.01032	0.00958	0.00947
K_s	0.461	0.462	0.465

Implications of this result are as follows. First, within the range of G degradations considered it indicates that the dominant effect of flywheel efficiency will come from reduced shear stress allowables rather than from the reduced modulus. Secondly, the results indicate that G/G_{orig} must be reduced below 0.1 to alter the stresses σ_r and σ_θ sufficiently to effect the overall flywheel shape factor K_s. Further evaluation of extremely degraded G cases is being continued at the present time.

Correlation of Predictions with Measured Degradation. We now correlate the analytical predictions with the property degradation measured experimentally and reported in a subsequent section. The experimentally determined shear modulus ratio $G/G_{original}$ is 0.825 and falls within the range covered by Table 2. This indicates that the wheel stresses are essentially unaffected. The reduction in shear strength of 0.728, however, indicates lower margins of safety with respect to shear failure for the degraded case. The margin of safety on the $\sigma_{R\theta}$ stress, computed from the values shown in Table 1, is (7.9/3.9)-1 = 1.02. For the experimentally measured degraded shear strength it is (5.75/3.9)-1 = 0.47, so that the margin is reduced roughly by half but nevertheless remains positive. Since the experimental results apply to the case of 52 percent of the ultimate 0^o stress, it is possible that the degradation of in-plane shear strength may limit the flywheel performance at high percentages of the ultimate load. Such a problem, if it occurs, could be ameliorated by increasing the number of radials and thereby reducing the $\sigma_{R\theta}$ stresses.

SENSITIVITY STUDIES

Sensitivity studies were carried out to evaluate the effect of property variations and geometric variations associated with manufacturing and fabrication.

Variations of Hoop Thickness. Results obtained by varying the hoop thickness are shown in Figs. 10-12. Fig. 10 shows the changes in stress distribution that occur as the hoop thicknesses are perturbated away from the design configuration. The figure indicates that as the hoops are thickened (+20%) the radials become overstressed and the hoops understressed. When the hoop thickness is reduced (-20%) the reverse occurs: the hoops are overstressed and the radials become understressed. These results also show the optimal feature of the unperturbed (0%) original design thickness combination in which the hoop and radial failures are expected to occur at approximately the same spin rate. The corresponding changes in shape factor K_s are shown in Fig. 11. The wheel appears to be more sensitive to decreases in hoop thickness because of the tendency for high hoop stresses to occur at the inside edge of the wheel. These calculations also apply to changes in radial thickness, that is, the results are dependent on the ratio of hoop to radial thickness.

In Fig. 12, the corresponding σ_{RZ} hoop to radial interlaminar shear stresses are plotted. The special nondimensional form of stress shown in the figure relates the shear stress to the maximum 0^o stress so that the significance of the shear stress changes can be evaluated. We presume that the wheel will be spun up to a speed Ω for which the maximum σ_r or σ_θ stresses reach the material allowable - consequently the ratio σ_{rZ}/σ_{Max} is a key

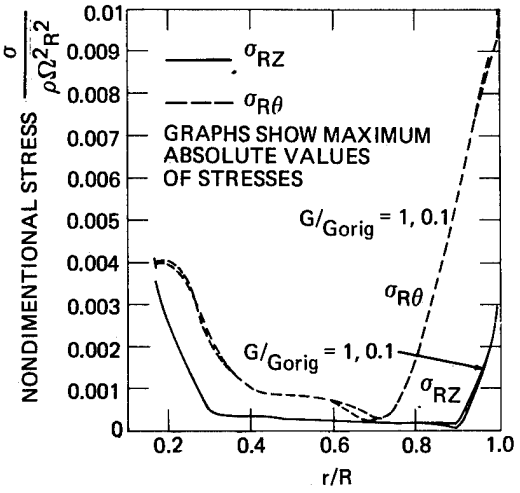


Fig. 9. Effect of reduction in shear modulus on shear stresses σ_{RZ} and $\sigma_{R\theta}$.

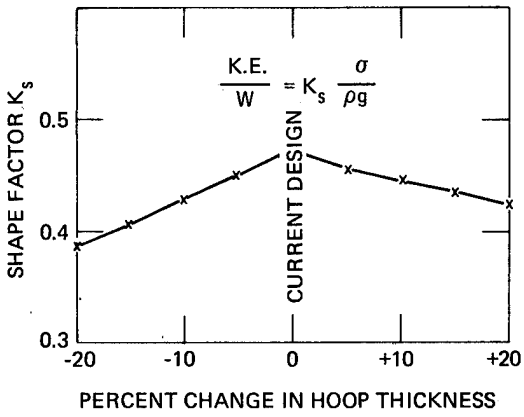


Fig. 11. Sensitivity of shape factor to hoop layer thickness.

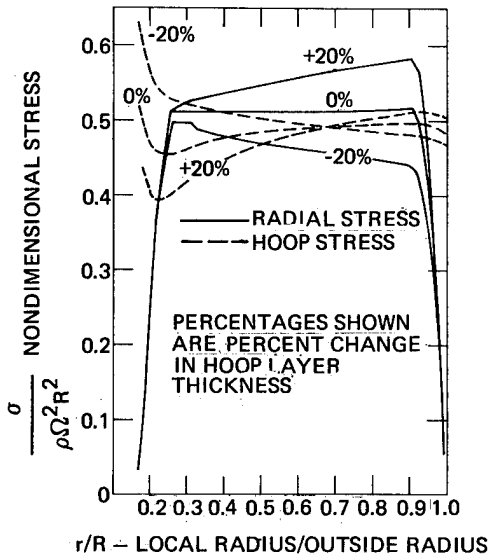


Fig. 10. Sensitivity of stresses to hoop layer thickness.

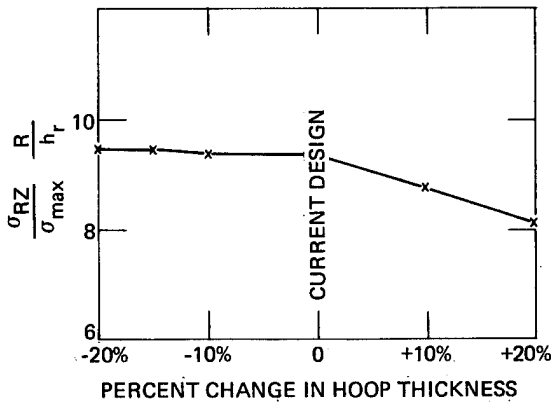


Fig. 12. Sensitivity of interlaminar shear stresses to hoop layer thickness.

parameter. Figure 12 shows that the effect of changing hoop thicknesses of ±20% does not substantially influence the σ_{RZ} shear stresses.

Changes in Radial Width. Parametric studies were also conducted for changes in radial width. It was found that the σ_{RZ} interlaminar shear stresses are strongly affected by changes in radial width because it directly changes the shear area available for transfer of load from radials to hoops.

Variations in Fiber Volume. Here we consider the effect on the flywheel stresses and efficiency of axisymmetric variations in the fiber volume ratio V_f. The case presented here is that of one constant value of V_f for the radial layers and another constant value for the hoop layers.

The following properties were used for the Kevlar 49 fiber and epoxy matrix:

Modulus of fiber	$= E_f = 20 \times 10^6$ psi
Modulus of matrix	$= E_m = 0.5 \times 10^6$ psi
Fiber weight/volume	$= \rho_f g = 0.053$ lbs/in^3
Matrix weight/volume	$= \rho_m g = 0.0426$ lbs/in^3

The mechanical properties for a composite are formulated by using a simple rule of mixtures, namely:

$$E_l = E_f V_f + E_m (1-V_f)$$
$$\rho g = \rho_f g V_f + \rho_m g (1-V_f)$$

The resulting values of E as a function of V_f are given in Fig. 13. It should be pointed out that for $V_f = 0.59$ one has the reference properties $E_l = 12 \times 10^6$ psi and $\rho g = 0.0487$. In this case we fix $V_f = 0.59$ for the radial reinforcements and vary V_f for the hoop reinforcements. Results obtained from the axisymmetric model are shown in Fig. 13.

In order to determine the effect of V_f on the wheel efficiency it is necessary to postulate the dependence of the strength on V_f. This was determined on the basis of an allowable strain criterion. Consequently the 0^o strength is assumed to be proportional to the modulus, which is shown in Figure 13. To define the value of K_s given in Figure 13, the density and stress allowable were taken as those corresponding to the reference value of $V_f = .59$.

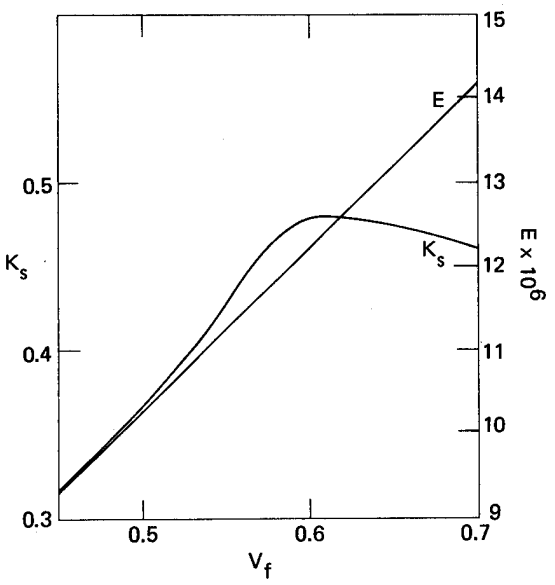


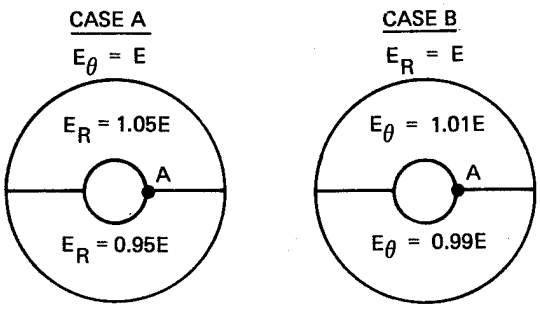
Fig. 13. Variation of modulus and shape factor K_s with volume fraction V_f.

Evaluation of Asymmetric Property Variations. Asymmetric property variations were evaluated using the finite element grid shown in Fig. 3. The model "smears out" the radials in the circumferential direction. Two cases of asymmetric variations of the modulus, as shown in Fig. 14, were analyzed. In Case A the modulus of the radials is varied; in Case B the modulus of the hoops. The change in stresses for these cases is as follows:

Case	Change in modulus	Change in maximum stress
A	±5%	+3.9%
B	±1%	+.1%

A major reason for carrying out these asymmetric property variation studies is to compute the imbalance due to deformation of the wheel. To do this we evaluate the shift in centroid of the wheel (relative to point A of Fig. 14) that would exist when $\sigma_{Max} = 200$ ksi. The results shown below apply to a 19.5" O.D. wheel weighing 16.86 pounds:

Case	Change in modulus	Distance of centroid shift (inch)	Imbalance (inch-grams)
A	±5%	0.00416	36.19
B	±1%	0.000904	6.9



KEY

E_θ = Modulus of hoops

E_R = Modulus of radials

E = Reference modulus, 12.0×10^6 psi

Fig. 14. 2-D models used to evaluate asymmetric property variations.

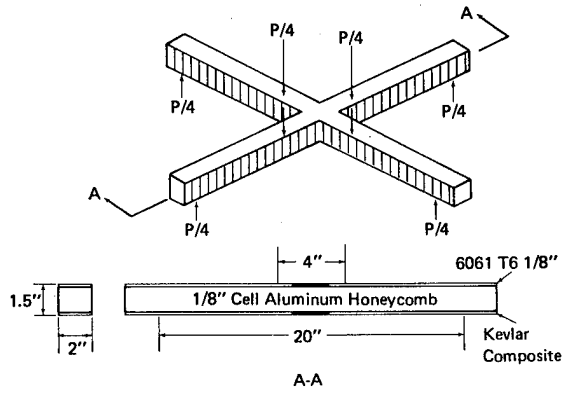


Fig. 15. Biaxial beam schematic.

The resulting imbalances are considerably in excess of the imbalances ordinarily achieved after balancing which are of the order of 1 inch-gram. It should be recognized that the ±5% and ±1% variations used in the study are highly unlikely to occur because they represent averages of all the deviations in modulus through the thickness as well as in the in-plane directions. The variations used in this study are conservative estimates of asymmetries in an individual layer. Random layer orientation during assembly and inter-layer load sharing during operation will tend to distribute displacement more evenly. The method of fabricating the hoops is more likely to generate axisymmetric rather than asymmetric variations in modulus. Similarly, the radials are stamped out of sheets of Kevlar tape and are expected to be very regular.

Testing for Degraded Property Effects. Degraded shear modulus and shear strength are determined experimentally as a function of $\sigma = \sigma_x = \sigma_y$ biaxial stress level using the honeycomb sandwich beam test arrangement shown in Fig. 15. After loading the sandwich beams to a percent of ultimate, 45^o tensile tests on the degraded material are used to determine modulus and strength. The test program is unfinished at this time. However initial results at 52 percent of ultimate load indicate a 17 percent reduction in shear modulus and a 27 percent reduction in shear strength. Further tests are being carried out in the range of 50 to 70 percent of ultimate load.

CONCLUSIONS

Major conclusions from this work are as follows:

1. The analysis indicates that reductions in in-plane shear modulus of up to 90 percent have a small effect on the maximum stresses. Preliminary biaxial test data at 52 percent of ultimate indicates only 27 percent degradation of shear modulus, and, consequently, positive margins in stress. Biaxial tests at higher load levels are being prepared during the writing of this paper.

2. The efficiency of a bi-directionally reinforced flywheel is sensitive to variations in fiber volume, and variations in hoop and radial reinforcement geometry. The relationship between variations in efficiency and variations in property and geometric inputs differ from case to case. The type of predicted failure mode also depends on variations in property and geometric inputs. Asymmetric variations in material properties can also lead to substantial wheel imbalances which depend on the degree of nonuniformity present.

PREDICTION OF CREEP BEHAVIOR FOR FILAMENTARY COMPOSITES UNDER STRESS CONDITIONS ENCOUNTERED IN FLYWHEELS

C.W. Bert and T.L.C. Chen
School of Aerospace, Mechanical and Nuclear Engineering
The University of Oklahoma, Norman, OK

ABSTRACT

A method of analyzing the creep behavior of a filamentary composite is presented. The approach is based on an approximate creep micromechanics analysis using creep data of the fibers and matrix material tested individually at the temperature of interest. The validity of the present analysis is verified by comparison with test data on a unidirectional Kevlar 49-ERLA 4617 epoxy composite in uniaxial longitudinal tension at room temperature. Numerical results are presented for the above mentioned composite under the following four loading cases: longitudinal tension, transverse tension, biaxial tensions and generalized plane-stress distribution, i.e. biaxial tension and shear stress. Creep constitutive equations are fitted by using the creep version of Hill's theory of orthotropic plasticity.

INTRODUCTION

There have been only a relatively few investigations that have been concerned with predicting the creep behavior of unidirectional filamentary composites. This is perhaps due to the complexities of time-dependent phenomena and lack of significant creep observed prior to failure in longitudinal loading of composites reinforced with fibers of glass, boron or graphite. However, if a composite material is reinforced by some new organic polymer fibers such as Kevlar 49, which exhibits creep under longitudinal tension, an appreciable amount of creep may be observed, depending on the state of stress and temperature.[1-3] Such materials may exhibit a certain amount of creep even at room temperature. This is in contrast to most structural metallic alloys which do not exhibit significant creep at least up to a few hundred degrees.

To the best of the present investigators' knowledge, the first significant work concerning creep of composite materials was due to McDanels, et al.[4], who suggested a rule-of-mixtures approach to estimate the creep-rupture strength. For linear viscoelastic composites, Hashin[5] used a self-consistent model, and DeSilva[6] presented a more elaborate mathematical model. Lou and Schapery[7] used a constitutive equation based on a thermodynamic theory to describe nonlinear viscoelastic composites, while Bert[8] presented a unified method to analyze time-independent plastic deformation and creep deformation of a filamentary composite.

There is considerable interest in advanced composite materials for flywheels in hybrid vehicles because of their desirable combination of high stiffness, high strength and low density and their less catastrophic failure characteristics than structural alloys. It is believed to be rather important to be able to predict creep behavior of flywheels rotating at a relatively high speed[9]. Since significant shear, radial and circumferential stresses occur when a flywheel rotates about an axis which is eccentrically offset from the geometric center of the flywheel[10], a creep analysis under generalized plane stress is needed.

In the present investigation, a method of analyzing the creep behavior of a filamentary composite is presented. The approach is based on an engineering approach to the micromechanics of creep and creep data of fibers and matrix materials obtained in uniaxial longitudinal tension tested by Ericksen[11] at room temperature. The validity of the present analysis is verified by comparison with test data on a unidirectional Kevlar 49-ERLA 4617 epoxy composite in longitudinal tension. Numerical results are presented for the above mentioned composite material under the following four loading conditions: longitudinal tension, transverse tension, biaxial tensions and generalized plane-stress distribution, i.e. biaxial tensions and shear stress. Creep constitutive equations are proposed by fitting the above obtained data with the creep analog of Hill's orthotropic plasticity theory[12].

MICROMECHANICS MODEL OF COMPOSITE

For purpose of analysis, the composite is assumed to be unidirectional. By longitudinal, we mean uniaxial loading parallel to the fibers; transverse loadings refer to loadings perpendicular to the fibers. In the present work, a mechanics-of-materials approach is adopted. The prominent assumption (Voigt's hypothesis) of this model is that the longitudinal strains in the fibers and in the matrix are equal to each other. If one uses superscripts f and m to refer to the fiber and matrix properties, respectively, one has

$$\epsilon_1 = \epsilon_1^f = \epsilon_1^m \qquad (1)$$

where ϵ_1, ϵ_1^f, and ϵ_1^m are longitudinal strains for the composite, fibers, and matrix, respectively.

In view of Eq. (1) and longitudinal equilibrium, the following equation should be satisfied:

$$\sigma_1 = V_f\sigma_1^f + V_m\sigma_1^m \qquad (2)$$

where σ_1 is the applied longitudinal stress; σ_1^f and σ_1^m are respectively the internal stresses in the fibers and matrix; V_f is the fiber volume fraction and $V_m(= 1-V_f)$ is the matrix volume fraction.

In the mechanics-of-materials approach, the same transverse stress, σ_2, is assumed to exist in both the fibers and the matrix (Reuss's hypothesis), i.e.,

$$\sigma_2 = \sigma_2^f = \sigma_2^m \qquad (3)$$

where σ_2^f and σ_2^m are transverse stresses for the fibers and matrix, respectively. The total transverse strain in the composite is

$$\epsilon_2 = V_f\epsilon_2^f + V_m\epsilon_2^m \qquad (4)$$

where ϵ_2^f and ϵ_2^m are transverse strains for fibers and matrix, respectively.

If one assumes that the in-plane shear stress, σ_6, in the composite is equal to that in fibers and matrix (σ_6^f and σ_6^m), one has

$$\sigma_6 = \sigma_6^f = \sigma_6^m \qquad (5)$$

and

$$\epsilon_6 = V_f\epsilon_6^f + V_m\epsilon_6^m \qquad (6)$$

where ϵ_6, ϵ_6^f and ϵ_6^m are respectively the in-plane shear strains for the composite, fibers, and matrix. It is noted that Eqs. (1) through (6) are true regardless of the applied stress state.

BEHAVIOR OF CONSTITUENTS

Since we consider the case where both of the constituents exhibit creep, it is necessary to characterize the creep behavior of both constituents.

If a material is incompressible and orthotropic, a creep potential can be expressed as a function of the following quadratic form previously used by Hill[12] to describe anisotropic plasticity.

$$g = C_{11}(\sigma_2-\sigma_3)^2 + C_{22}(\sigma_3-\sigma_1)^2 + C_{33}(\sigma_1-\sigma_2)^2 + 2(C_{12}\sigma_6^2+C_{23}\sigma_4^2+C_{31}\sigma_5^2) \qquad (7)$$

If the material is transversely isotropic with respect to the 2-3 plane, one has $C_{22} = C_{33}$ and $C_{12} = C_{31}$. Thus, Eq. (7) can be simplified as follows for a generalized plane stress state on the 1-2 plane.

$$g = C_{11}\sigma_2^2+C_{11}\sigma_1^2+C_{33}(\sigma_1-\sigma_2)^2+2C_{12}\sigma_6^2 \qquad (8)$$

The component of the total strains under creep is equal to the sum of elastic and creep strains. Hence the components of the total strains for each constituent are given by the following:

$$\epsilon_1^i = S_{11}^i\sigma_1^i+S_{12}^i\sigma_2^i+\left[A_i\bar{\sigma}_i^{N_i-1}(\log_{10}\frac{t}{t_o})^{K_i}\right](\sigma_1^i + \bar{\nu}_{12}\sigma_2^i)$$

$$\epsilon_2^i = S_{12}^i\sigma_1^i+S_{22}^i\sigma_2^i+\left[A_i\bar{\sigma}_i^{N_i-1}(\log_{10}\frac{t}{t_o})^{K_i}\right](\bar{\nu}_{12}^i\sigma_1^i + C_{i2}\sigma_2^i)$$

$$\epsilon_6^i = S_{66}^i\sigma_6^i+\left[A_i\bar{\sigma}_i^{N_i-1}(\log_{10}\frac{t}{t_o})^{K_i}\right](C_{i6}\sigma_6^i)$$

$$i = f, m \qquad (9a\text{-}9c)$$

where S_{ij} are elastic compliance constants; A_i, N_i, K_i are constants to be determined from experiment; t is time; t_o is a small time and

$$C_{i2} \equiv \left[\frac{S_{22}^i}{S_{11}^i}\right]_{creep} \quad i=f,m \; ; \; C_{f6} \equiv \left[\frac{S_{66}^f}{S_{11}^f}\right]_{creep}$$

$$\bar{\nu}_{12}^{i} \equiv \left[\frac{S_{12}^{i}}{S_{11}^{i}}\right]_{creep} \qquad i=f,m \qquad (10a\text{-}10c)$$

$$\bar{\sigma}_i \equiv \left[\sigma_1^{i\,2}+\sigma_1^i\sigma_2^i+\frac{C_{33}^i+C_{11}^i}{2\,C_{33}^i}\,\sigma_2^{i\,2}+\frac{C_{12}^i}{C_{33}^i}\,\sigma_6^{i\,2}\right]^{1/2}; \quad i = f,m \qquad (11)$$

It is noted that in writing the above equations, we assumed that it is suitable to characterize fibers and matrix as transversely isotropic and isotropic materials, respectively.

The three coefficients in Eq. (11) have to be determined from a series of creep tests under various loading conditions (including longitudinal, transverse and shear). Unfortunately, only longitudinal uniaxial creep data are available in the literature; thus, an alternative approach must be considered. A reasonable engineering approximation for Eq. (11) is one known as the Hill-Tsai failure criterion[13].

$$\bar{\sigma}_i = \left[\sigma_1^{i\,2}-\sigma_1^i\sigma_2^i+\frac{X_i^2}{Y_i^2}\,\sigma_2^{i\,2}+\frac{X_i^2}{Y_i^2}\,\sigma_6^{i\,2}\right]^{1/2}; \quad i = f,m \qquad (12)$$

where X, Y, S are the respective longitudinal, transverse, and shear strengths.

DETERMINATION OF CREEP CONSTANTS OF CONSTITUENTS IN LONGITUDINAL TENSION

The creep constants in Eq. (9) can be determined by fitting them with experimental data obtained for the material needed at the temperature of interest. In the present work, Kevlar 49 fibers and ERLA 4617 epoxy are chosen for presentation, since they are potential materials for advanced composite flywheels currently under investigation. The only experimental data for such materials reported in the literature were obtained under uniaxial longitudinal loading. In order to fit experiment results, Eq. (9) has to be reduced to the uniaxial longitudinal tension case. Under longitudinal tension, one has $\sigma_2 = \sigma_6 = 0$. Thus Eq. (9) becomes

$$\epsilon_1^f = S_{11}^f\sigma_1^f+S_{12}^f\sigma_2^f+A_f\sigma_1^{N_f}(\log_{10}\frac{t}{t_o})^{K_f} \qquad (13a)$$

$$\epsilon_1^m = S_{11}^m\sigma_1^m+S_{12}^m\sigma_2^m+A_m\sigma_1^{N_m}(\log_{10}\frac{t}{t_o})^{K_m} \qquad (13b)$$

where t_o can be any small time scale. In the present work, it is chosen to be $1.0\text{x}10^{-8}$ hrs. Since the test data presented in Ericksen's work[11] are concerned with the creep strain only, the elastic strains in Eq. (13) are ignored. Due to the linear nature of the room-temperature creep versus $\log_{10}t$ plot as given by Fig. 2 in [11], the value of K_f is equal to unity. The value of N_f can be determined by using the creep ratio for two different applied loadings at any given time. Once N_f is determined, value of A_f can be determined at any stress level. For completeness, a sample calculation is presented. From Fig. 3 in [11], one has the following data:

$$\epsilon_1^f = 0.033\% \text{ @ } \sigma_1^f = 240 \text{ MPa and } t = 10 \text{ hrs}$$

$$\epsilon_1^f = 0.11\% \text{ @ } \sigma_1^f = 1940 \text{ MPa and } t = 10 \text{ hrs}$$

By using Eq. (13a) and recalling that only creep strains are needed, one can find the creep ratio as follows:

$$\frac{0.033}{0.11} = \left(\frac{240}{1940}\right)^{N_f}$$

The value of N_f then is determined as 0.576. By using the first set of data given above, one has

$$0.033\% = A_f(240)^{0.576}\log_{10}\frac{10}{1.0\text{x}10^{-8}}$$

or

$$A_f = 1.56 \times 10^{-6}\ [\text{MPa}]^{-N_f}$$

The same calculation procedure can be applied to determine N_m and A_m by using Fig. 4 in [11]. However, due to the creep versus $\log_{10}t$ plot, the value of K_m is no longer equal to unity. Its value can be determined from two sets of data obtained at the same stress level but different times. For example,

$$\epsilon_1^f = 0.09\% \text{ @ } \sigma_1^m = 34 \text{ MPa and } t = 10 \text{ hrs}$$

$$\epsilon_1^f = 0.19\% \text{ @ } \sigma_1^m = 34 \text{ MPa and } t = 100 \text{ hrs}$$

Thus, one has

$$\frac{0.09}{0.19} = \left[\frac{\log_{10}\frac{10}{1.0\text{x}10^{-8}}}{\log_{10}\frac{100}{1.0\text{x}10^{-8}}}\right]^{K_m}$$

or

$$K_m = 7.09$$

In summary, we have determined all the uniaxial creep constants and they are summarized as follows:

Fiber	Matrix
$N_f = 0.576$	$N_m = 1.84$
$A_f = 1.56\times10^{-6}[\text{MPa}]^{-N_f}$	$A_m = 2.35\times10^{-13}[\text{MPa}]^{-N_m}$
$K_f = 1.0$	$K_m = 7.09$

METHOD OF CALCULATION

If a desired set of values for σ_1, σ_2 and σ_6 are given and held constant, initially (at t=0), the constituents exhibit no creep strain. Thus, the total strain at this instant is equal to the elastic strain. In view of Eq. (1), (3) and (9), we have the following relation:

$$S_{11}^f\sigma_1^f(0) + S_{12}^f\sigma_2 = S_{11}^m\sigma_1^m(0) + S_{12}^m\sigma_2 \quad (14)$$

From Eq. (2), we have the following equation which holds for any time:

$$\sigma_1^m = \frac{\sigma_1 - V_f\sigma_1^f}{1 - V_f} \quad (15)$$

Substituting Eq. (15) into Eq. (14) and solving for $\sigma_1^f(0)$, one has

$$\sigma_1^f(0) = \frac{(S_{12}^m - S_{12}^f)\sigma_2 + S_{11}^m\sigma_1/(1-V_f)}{S_{11}^f + \frac{V_f}{1-V_f}S_{11}^m} \quad (16)$$

The initial transverse strains of the constituents can be obtained from the following equations and Eqs. (15) and (16):

$$\epsilon_2^f(0) = S_{12}^f\sigma_1^f(0) + S_{22}^f\sigma_2$$
$$\epsilon_2^m(0) = S_{12}^m\sigma_1^m(0) + S_{22}^m\sigma_2 \quad (17)$$

Thus, the initial strains in the composite can be expressed as follows by using Eqs. (1), (4), (5) and (6):

$$\epsilon_1(0) = S_{11}^f\sigma_1^f(0) + S_{12}^f\sigma_2$$

$$\epsilon_2(0) = V_f\left[S_{12}^f\sigma_1^f(0) + S_{22}^f\sigma_2\right] + V_m\left[S_{12}^m\sigma_1^m(0) + S_{22}^m\sigma_2\right]$$

$$\epsilon_6(0) = V_fS_{66}^f\sigma_6 + V_mS_{66}^f\sigma_6 \quad (18)$$

In view of Voigt's hypothesis, one can obtain the following equation from Eqs. (2) and (9) at some time t.

$$S_{11}^f\sigma_1^f + S_{12}^f\sigma_2 + \left[A_f\bar{\sigma}_f^{N_f-1}(\log_{10}\frac{t}{t_o})^{K_f}\right](\sigma_1^f + \bar{\nu}_{12}^f\sigma_2^f) - S_{11}^m(\sigma_1 - V_f\sigma_1^f)/(1-V_f) - S_{12}^m\sigma_2 - \left[A_m\bar{\sigma}_m^{N_m-1}(\log_{10}\frac{t}{t_o})^{K_m}\right]\left[(\sigma_1 - V_f\sigma_1^f)/(1-V_f) + \bar{\nu}_{12}^m\sigma_2\right] = 0 \quad (19)$$

For a given stress state, a step-by-step method can be used to compute the creep strain components in the composite by using Eqs. (1) through (6) and (9) through (19). The method is summarized as follows:

1. A stress state is given.
2. For a given time t, one solves for σ_1^f in Eq. (19) by using the trial-and-error technique*.
3. Equation (15) is now used to compute σ_1^m.
4. In view of Eqs. (1), (3) and (5), the total strains in each of the constituents can be determined from Eq. (9).
5. Total strains in the composite are computed according to Eqs. (1), (4) and (6).
6. The initial strains for the composite are calculated by using Eqs. (15), (16) and (18).
7. The creep strain components in the composite are determined by subtracting the initial strains (step 6) from the total strains (step 5).

*The advantage of solving for $\sigma_{1_f}^f$ instead of solving for time, in which σ_1^f has to be assumed, is that the complexity due to load-transfer pheonomna can be eliminated.

NUMERICAL RESULTS

The influence of anisotropy on the creep behavior of Kevlar 49/epoxy are demonstrated by calculating some numerical results. The elastic material properties of fibers and epoxy are given in Table 1.

Table 1. Constituent material properties of Kevlar 49/epoxy*.

	Fiber (Kevlar 49)	Matrix (Epoxy)
$S_{11}(MPa)^{-1}$	7.15×10^{-6}[11]	265.12×10^{-6}[11]
$S_{12}(MPa)^{-1}$	-2.30×10^{-6}[14]	-95.43×10^{-6}**
$S_{22}(MPa)^{-1}$	145.03×10^{-6}[14]	265.12×10^{-6}[11]
$S_{66}(MPa)^{-1}$	456.13×10^{-6}[15,16]	684.12×10^{-6}[17]

*Fiber volume fraction = 0.5

**$\nu_m = 0.36$, thus $S^m_{12} = -\nu_m S^m_{11}$

The values were obtained from various sources as shown in the table. Since only limited creep deformation data are available for the constituent materials, we do not know the creep compliances corresponding to transverse normal and in-plane shear loadings. As an engineering approximation, we assume that the compliance ratio in creep deformation is equal to that in elastic deformation. Thus, Eqs. (10) become

$$C_{i2} = \left[\frac{S^i_{22}}{S^i_{11}}\right]_{elastic} \quad i=f,m \; ; \; C_{f6} = \left[\frac{S^f_{66}}{S^f_{11}}\right]_{elastic} \qquad (20)$$

Also, incompressibility of the constituent materials implies that $\nu^i_{12} = -0.5$*.

Another assumption used in the present calculation due to insufficient experimental data is that the strength ratio for both constituent materials are equal to the ratios of corresponding stiffnesses. That is

$$\frac{X_i}{Y_i} = \frac{S^i_{22}}{S^i_{11}} \; ; \; i=f,m \; ; \; \frac{X_i}{S_i} = \frac{S^i_{66}}{S^i_{11}} \; ; \; i=f,m \qquad (21)$$

With these assumptions, the creep components can be computed step by step as shown in the preceding section. Fig. 1 presents a comparison of experimental

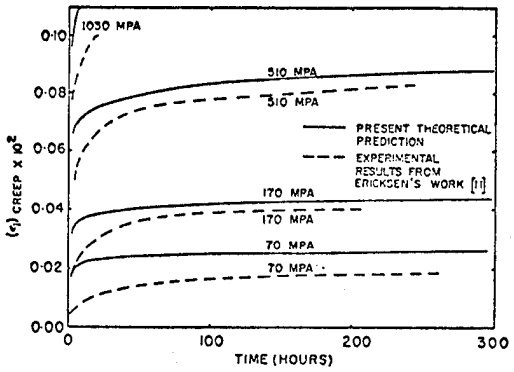


Fig. 1. Comparison of present theoretical results with experimental results in longitudinal tension.

results from [11] and theoretical results from the present work in uniaxial longitudinal tension. It is seen that the similarity of the results is encouraging at least for engineering purposes. The creep deformation under uniaxial transverse tension is shown in Fig. 2. Com-

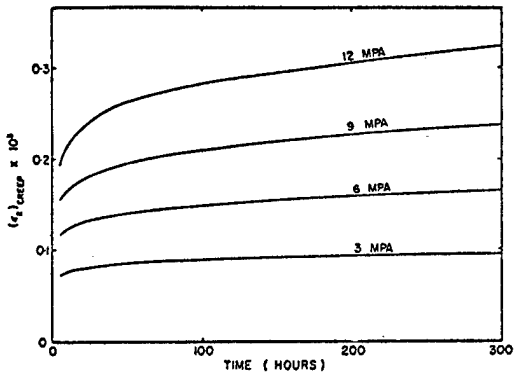


Fig. 2. Creep curves for Kevlar 49/epoxy in transverse tension.

paring Figures 1 and 2, one sees that the creep in transverse loading is much more pronounced than that in longitudinal loading.

Creep curves under various biaxial stress states are given in Figures 3 and 4. It is interesting to see that creep in the transverse direction decreases as longitudinal loading increases if transverse loading remains unchanged. This is not surprising, since the same phenomenon is found in isotropic material. For example, the creep in direction 2 for epoxy decreases about 47% if the stress ratio σ_1/σ_2 is increased from 1 to 1.5 (with σ_1 fixed). Fig. 5 shows creep deformations

*In obtaining this value, the transverse isotropic and isotropic characteristics of fibers and matrix material have been used.

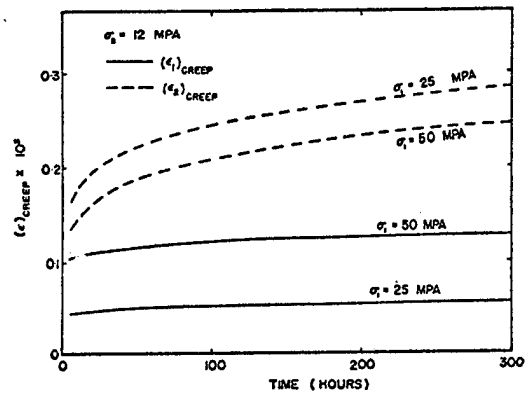


Fig. 3. Creep curves for Kevlar 49/epoxy under various biaxial stress states with σ_2 = 12 mpa.

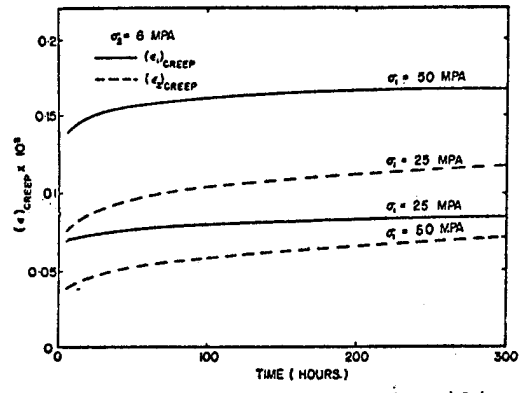


Fig. 4. Creep curves for Kevlar 49/epoxy under various biaxial stress states with σ_2 = 6 mpa.

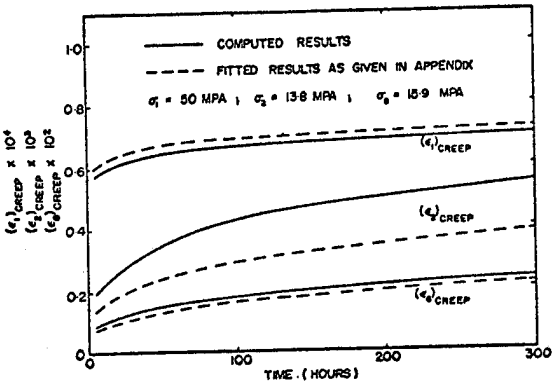


Fig. 5. Creep under generalized plane-stress condition with σ_1=50 mpa, σ_2=13.8 mpa, and σ_6=15.9 mpa.

corresponding to a generalized plane-stress state. The solid curves in Fig. 5 are obtained by the method presented in the preceding section, while the dashed curves are obtained by fitting the present analysis with a creep version of Hill's theory of orthotropic plasticity. (The procedure used for fitting curves is presented in the Appendix.)

CONCLUSIONS

A rational approach was used to derive equations for predicting creep behavior of a filamentary composite under a generalized plane stress state. These equations were used in conjunction with constituent material behavior information. Numerical results were presented for Kevlar 49/epoxy at room temperature for the following four loading cases:

1. Longitudinal tension
2. Transverse tension
3. Biaxial tension, i.e. cases 1 and 2 superimposed.
4. Generalized plane stress, i.e. case 3 with superimposed shear load.

Good agreement was obtained by comparing the present theoretical results with existing experimental results in case 1. No experimental data for the last three stress-state cases are available in the literature. More tests in addition to uniaxial longitudinal tension are strongly recommended to characterize the creep behavior of constituent materials as well as the composites.

ACKNOWLEDGMENT

The research reported here was sponsored by Sandia Laboratories, Albuquerque, NM, with Dr. Frank Gerstle as project monitor.

REFERENCES

1. Hanson, M.P., "Effect of Temperature on the Tensile and Creep Characteristics of PRD-49 Fiber/Epoxy Composites", NASA Technical Memorandum TM X-68053, 1972.

2. Moore, J.W., "PRD-49 A New Organic High Modulus Reinforcing Fiber", Proc. 27th Annual Technical Conference, Society of the Plastics Industry, Inc., 1972, Sec. 17-F.

3. Kevlar 49 DP-01 Data Manual, E.I. duPont & Co., Textile Fibers Department, Wilmington, Delaware, 1974.

4. McDanels, D.L., Signorelli, R.A., and Weeton, J.W., "Analysis of Stress-Rupture and Creep Properties of Tungsten Fiber Reinforced Copper Composites", Fiber-Strengthened Metallic Composites, American Society for Testing and Materials, Spec. Tech. Publ. 427, 1967, pp. 124-148.

5. Hashin, Z., "Viscoelastic Fiber Reinforced Materials", AIAA Journal, Vol. 4, No. 8, August 1966, pp. 1411-1417.

6. De Silva, A.R.T., "A Theoretical Analysis of Creep in Fiber Reinforced Composites", Journal of Mechanics and Physics of Solids, Vol. 16, June 1968, pp. 169-186.

7. Lou, Y.C. and Schapery, R.A., "Viscoelastic Behavior of a Nonlinear Fiber-Reinforced Plastic", Journal of Composite Materials, April 1971, pp. 208-234.

8. Bert, C.W., "Plasticity and Creep Analysis of Filamentary Metal-Matrix Composites", Tech. Report, Sandia Laboratories, Albuquerque, NM, SC-DR-720055, March 1972.

9. Bert, C.W., "Dynamic Problems in Composite-Material Flywheels for Energy Storage in Hybrid Vehicles", presented at the 47th Shock and Vibration Symposium, Albuquerque, New Mexico, October 19-21, 1976.

10. Bert, C.W. and Niedenfuhr, F.W., "Stretching of a Polar-Orthotropic Disk of Varying Thickness under Arbitrary Body Forces", AIAA Journal, Vol. 1, June 1963, pp. 1385-1390.

11. Ericksen, R.H., "Room Temperature Creep of Kevlar 49/Epoxy Composites", Composites, Vol. 7, July 1976, pp. 189-194.

12. Hill, R., The Mathematical Theory of Plasticity, Oxford University Press, London, 1950.

13. Tsai, S.W., "Strength Theories of Filamentary Structures", Fundamental Aspects of Fiber Reinforced Plastic Composites, R.T. Schwartz and H.S. Schwartz ed., Wiley Interscience, New York, 1968, pp. 3-11.

14. Allred, R.E. and Gerstle, F.P., Jr., "The Effect of Resin Properties on the Transverse Mechanical Behavior of High-Performance Composites", Proceedings, 30th Tech. Conference, Reinforced Plastics/Composites Institute, Soc. of the Plastics Industry, Inc., 1975, Section 9-B.

15. Kulkarni, S.V., Rice, J.S. and Rosen, B.W., "An Investigation of the Compressive Strength of Kevlar 49/Epoxy Composites", Composites, Vol. 6, September 1975, pp. 217-225.

16. Kashin, Z. and Rosen, B.W., "The Elastic Moduli of Fiber-Reinforced Materials", Journal of Applied Mechanics, Trans. ASME, Vol. 31, Series E, No. 2, June 1964, pp. 223-232.

17. Novak, R.C. and Bert, C.W., "Theoretical and Experimental Bases for More Precise Elastic Properties of Epoxy", Journal of Composite Materials, Vol. 2, No. 4, October 1968, pp. 506-508.

APPENDIX - CURVE FITTING

In view of Hill's plasticity theory one can write the following general creep equations for orthotropic material:

$$(\epsilon_1)_{creep} = A_\ell \bar{\sigma}_c^{N_\ell - 1} t^\ell (\sigma_1 - 0.5\sigma_2)$$

$$(\epsilon_2)_{creep} = A_p \bar{\sigma}_c^{N_p - 1} t^p \left(-0.5\sigma_1 + \frac{S_{22}^c}{S_{11}^c}\sigma_2\right)$$

$$(\epsilon_6)_{creep} = A_s \bar{\sigma}_c^{N_s - 1} t^s \left(\frac{S_{66}^c}{S_{11}^c}\sigma_6\right) \qquad (A.1)$$

where $\bar{\sigma}_c$ is the so-called effective stress. If the material is transversely isotropic, one can write the effective stress as follows (see Eq. 9):

$$\bar{\sigma}_c = \frac{1}{\sqrt{2}}\sqrt{(\sigma_1 - \sigma_2)^2 + \sigma_1^2 + a\sigma_2^2 + b\sigma_6^2} \qquad (A.2)$$

The constants A_ℓ, A_p, A_s, N_ℓ, N_p, N_s, ℓ, p, S, a and b can be determined as follows:

1. Determine ℓ from longitudinal tension: find the ratio of two different (ϵ_1) creep strains for two different times at the same applied tension.

2. Determine N_ℓ from longitudinal tension: find the ratio of two different (ϵ_1) creep strains for two different loadings at the same time.

3. Once ℓ and N_ℓ are determined, A_ℓ can be determined by using longitudinal data.

4. Determine p from transverse tension: same as 1 except use transverse loading instead of longitudinal loading.

5. Determine N_p from transverse tension: same as 2, except use transverse loading.

6. Determine A_p and a by using two sets of data; one in transverse tension and one in biaxial loading.

7. Determine s from pure shear loading: same as 1 and 4 except use pure shear loading.

8. Determine N_s from pure shear loading: same as 2 and 5 except use pure shear loading.

9. Determine A_s and b by using two sets of data: one in pure shear, one in shear plus longitudinal loadings.

In order to determine compliance of the composite material in terms of constituent material properties, a micromechanics theory should be used. For engineering purposes, the following equations are accurate enough to determine composite compliances.

$$S_{11}^c = \left[\frac{V_f}{S_{11}^f} + \frac{V_m}{S_{11}^m}\right]^{-1}$$

$$S_{22}^c = S_{11}^m V_m + S_{11}^f V_f \qquad \text{(A.3)}$$

and from [16] one has

$$S_{66}^c = S_{66}^m \frac{\eta V_m + (1+V_f)}{\eta(1+V_f) + V_m} \; ; \; \eta = \frac{S_{66}^m}{S_{66}^f} \qquad \text{(A.4)}$$

In the present paper, the values of constants used are summarized as follows:

$\ell = 0.0438$; $p = 0.253$; $s = 0.253$

$N_\ell = 0.582$ $N_p = 1.661$ $N_s = 1.661$

$A_\ell = 1.724\times10^{-5}$; $A_p = 1.40\times10^{-8}$; $A_s = 1.40\times10^{-8}$

$(\text{MPa})^{-N_\ell}$ $(\text{MPa})^{-N_p}$ $(\text{MPa})^{-N_s}$

$a = 350$; $b = 1500$

CONSTANT RADIAL DISPLACEMENT, THICK WALL, FILAMENT WOUND FLYWHEELS

R. Z. Naar, R. A. Panora, Jr., Dept. of Chemical Eng. Tufts University, Medford, MA.
B. M. Halpin, Jr., Army Materials & Mechanics Research Center, Watertown, MA.

ABSTRACT

A new type of composite flywheel rotor design is proposed for use in an energy storage system. The design is based on filament winding manufacturing techniques with Kevlar Aramid® fibers as the reinforcing fiber in an epoxy matrix. The concept is a variation of the so-called "Modular Ring" concept with the elastomer ring to ring attachment eliminated by varying the modulus of elasticity (in the circumferential direction) with radial position in the flywheel cylinder. By proper adjustment of the modulus of elasticity with radial position, each annulus of the flywheel will expand equally in the radial direction thus eliminating radial stresses and the need for a modular design. The modulus of elasticity is varied radially by continuously changing the orientation of the fibers from the inside to the outside diameter of the flywheel rotor by suitably programming the filament winding machine. To verify the theoretical predictions, flexure tests on filament wound rings were carried out on angle-ply specimens wound at various orientations. This testing provided data as to modulus changes with fiber orientation. The samples were also strength tested using a hydroburst apparatus to allow a prediction of the energy storage capabilities of this design. Based on the experimental results the proposed flywheel could store 20 W.-hr./lb. and .75 W.-hr/in^3 of energy. Further optimization of this design is also proposed, which would greatly improve the design's energy storage capacity.

I. INTRODUCTION

In composite flywheels the existence of both radial and hoop stresses on rotation presents a problem. Generally in a composite flywheel, the strength bearing member (the reinforcing fiber) is oriented circumferentially, the rotor possessing little strength in the radial direction (i.e. only the strength of the resin). The maximum RPM is thereby limited, hence limiting the energy storage capacity. A number of designs have been proposed to overcome this limitation. Some are based on the fact that if the thickness of a rotor is much less than its diameter, radial stresses are very small and can be supported by the matrix resin. Flywheels have been built on that principle (i.e. thin rim). The volumetric efficiency of such flywheels is low. Other flywheels have been constructed to make use of the same principle but attempting to increase the volumetric efficiency. For instance, a flywheel composed of many concentric thin rings would have a higher volumetric efficiency. The problem in such a flywheel is: a. joining the thin rings, b. each ring expands under the influence of centrifugal forces by a different absolute amount, the outermost ring expanding the greatest amount.

One proposed solution to the concentric ring problem is a flywheel design with the rings jointed by a compliant elastomeric matrix allowing for differential expansion. Problems with this concept include:

a. complicated construction
b. inability to accelerate or decelerate at high rates because of the considerable shear forces generated in the elastomeric layers.

We have developed a new concept based on the idea that no elastomer would be necessary, in a modular design, if the displacement of each ring during rotation were the same. If the modulus of elasticity of each ring in the hoop direction were suitably altered, then the radial expansion of each ring could be controlled. Thus we could construct a one-piece, thick-walled flywheel which could be visualized as a series of extremely thin rings in contact with each other (no compliant adhesive being necessary). All rings would expand by the same absolute amount on rotation generating essentially no radial stress. Composite materials technology allows us to do just that, by utilizing filament winding techniques with Kevlar/epoxy as one selection. The

modulus can be varied at will, by the proper choice of the wrap angle (helix angle) of the reinforcing fiber, and this can be achieved by suitably programming a continuous filament winding machine.

II. THEORY

A. MODULUS OF ELASTICITY REQUIREMENTS:

On the basis of the above, we calculated for a given geometry (i.e. solid flywheel of outside radius R and inner radius R/2):

a. The appropriate values of the modulus as a function of radial position.

b. The proper wrap angle to achieve the required modulus value.

It is well known (1) that the hoop stress experienced by a thin ring, of radius r, upon rotation varies with the square of its radius:

$$\sigma_r = \rho \frac{r^2 \omega^2}{g_c} \qquad (1)$$

where: σ_r = hoop stress
ρ = density of the ring
r = radius of the ring or lamina
ω = angular velocity of the ring
g_c = gravitational constant

For a flywheel composed of a series of concentric laminae in contact with each other, the condition that all laminae expand by the same amount (i.e. that their radial displacements be the same) is

$$\Delta r = \Delta R \qquad (2)$$

Now, the strain in each lamina is, by definition, $\varepsilon_r = \frac{\Delta r}{r}$ (and $\varepsilon_R = \frac{\Delta R}{R}$) hence taking the ratio $\frac{\varepsilon_R}{\varepsilon_r}$ and using Eq. (2) we have

$$\frac{\varepsilon_r}{\varepsilon_R} = \frac{R}{r} \qquad (3)$$

Finally, assuming the materials to be Hŏokean and using Eq. (1) we obtain by substitution in (3),

$$\frac{E_r}{E_R} = \left(\frac{r}{R}\right)^3 \qquad (4)$$

Equation (4), where E_r and E_R are the Young's moduli, describes how the modulus must vary with radial position in order for the individual laminae to expand by the same amount under rotationally induced hoop stress.

Next Eq. (4) needs to be translated into the proper inclination angle. (Figure 1 shows how the angle of wrap, α, is defined). This was done by first applying classical laminate theory (2) to determine how the elastic modulus varies with angle α, and is shown in Fig. 2. Using Fig. 2 and Eq. (4), the winding program for constructing the proposed flywheel is readily obtained and is shown in Fig. 3.

B. STRENGTH LIMITATIONS

Since the adjustment in fiber orientation results in loss of strength relative to the 90° orientation, the hoop strength at each radial position in a flywheel constructed per Fig. 3 must be estimated. A loss in strength is acceptable, of course since stresses will be considerably lower in the inner portions of the wheel, as indicated by Eq. (1). Three predictions as to how strength varies with radial position were utilized, shown in Fig. 4. The curve labeled Author's approximation refers to a simplified, "maximum strain" approach. The other two predictions are from the so-called "maximum stress theory" (2) and from a computer solution from the literature (3).

To calculate the energy storage ability of our design, the predictions of strength may be used to calculate the level of stress where failure would occur. As an example, consider the "author's" strength prediction. Based on the winding program of Fig. 3, and the above prediction, the strength of this flywheel as a function of radial position can be estimated. This is shown in Fig. 5 by the curve labelled "stress before failure". The level of stress as a function of radial position is also shown in Fig. 5, labeled: "working stress". Of course, the working stress level can be shifted by changing the RPM of the flywheel. At the stress level, or RPM, where tangency of the two curves occurs, failure will take place. Based on Fig. 5, the proposed design can store 55 W-hr/lb of energy. The other, less optimistic predictions indicate failure will

occur at a lower RPM, when the wheel is storing 30 w-hr/lb.

III. EXPERIMENTAL

To test our hypothesis we conducted experiments on suitably constructed filament wound ring specimens, and determined the actual modulus as well as the strength of the rings. The rings were wound at different angles and corresponded to specific radial locations in the proposed composite flywheel.

Experiments were performed on separate rings 8" in diameter, 1" wide and approximately 0.060" thick containing 60% fiber by volume. The experimental rings were sufficiently thin that, if they were spun, minimal radial stresses would be generated. The rings were filament wound on a programmable winder from Kevlar 49 and Dow XD 7818 epoxy cured with Jeffamine T-403, and were cut from 12" long cylinders wound on an 8" mandrel. The helix angles selected for winding were 90°, ± 80°, ± 60° and ± 50°.

The specimens prepared in this manner developed a resin "skin" during cure on the mandrels. Their actual thickness, t, was taken to be the total ring thickness measured with a micrometer, less the resin "skin". The thickness of the skin was measured with the aid of a microscope. Numerous measurements were made at several points around the ring and averaged.

Also a new technique for measuring fiber concentration, based on elemental analysis of specimens, was developed and will be published in Fiber Science and Technology.

A. MODULUS EXPERIMENTS

Each ring was tested in flexure by applying point loads at diametrically opposed locations on the ring and measuring the resultant deflections. Each ring was tested twice, 90° apart. The tests were performed on an Instron machine. Care was taken to insure that the imposed deformations were within the elastic range. This was evidenced by the perfect reversibility of the loading and unloading curves (no hysteresis). The modulus was then calculated according to Timoshenko Strength of Materials: Part II Advanced Theory and Problems using the theory of stiffness of curved bars.

The results are shown in Fig. 6. The agreement with the theory is good, one experimental point which is not in agreement is attributed to a possible error in measuring the thickness. The calculations of modulus depend on the third power of the thickness and a small error would be magnified.

B. STRENGTH EXPERIMENTS

We did not have a capability for determining fiber strength in rotation. Hoop strength was determined in a simple apparatus that subjected the specimens to hoop stress generated by hydraulic pressure. Although this is not an ideal method for strength determination because of the edge effects imposed on the 1" wide specimens, it had the overwhelming asset of being available and the specimens could be rapidly prepared.

A detailed drawing of the apparatus is shown in Fig. 7. A photograph of the apparatus disassembled is shown in Fig.8. In this apparatus each ring is subjected to stress with the aid of a hydraulically pressurized elastomeric bladder (a bicycle tire bladder shortened and glued to the proper dimensions). A fixture restrains the rings on top and bottom in an attempt to insure that they are subjected to hoop stress only. In practice considerable manipulation was necessary to insure that the rings were not compressed by the restraining fixture, thereby generating frictional forces at their edges that would require additional pressure to fracture them and thus lead to erroneous (artificially high) strength values. To that effect, shims were used in each test so that after assembly of the apparatus, but prior to pressurization, the ring could be moved about easily by hand. This, however, led to another difficulty: because of the Poisson contraction of the rings under test, the bladder at high pressures tended to extrude between the ring edges: this effect will be discussed below and was particularly pronounced with the 90° specimens.

Once the ring was mounted on the apparatus and suitably shimmed as described above, pressure was applied and increased until failure of the ring occurred. The pressure at failure, P_f, was

recorded and the corresponding hoop failure stress σ_f was calculated using thin walled vessel theory

$$\sigma_f = \frac{P_f r}{t} \qquad (5)$$

The results of strength, as a function of helix angle are shown in Fig. 9. The three predictions are also compared to the experimental results.

In general our strength results conform well to the predictions of Yao and Abildskov [3]. Since strength is an end property, it is notoriously difficult to predict. This is evidenced by the great number of models proposed by various authors on these complex systems. Our major difference with the published results occurred at the helix angle of 90° where our strengths were well below those reported in the literature by workers using specially constructed vessels to eliminate or minimize end effects (e.g. T.T. Chiao's work on Organic Fiber/Epoxy pressure vessels done for NASA Contract No. C-13980-C). We have no reason to believe that the filament wound rings contained defects responsible for the observed lower strength values. The observed values are believed to be lower than the true strength of the specimens and we attribute them to artifacts and end effects resulting from the rather unrefined apparatus.

The 90° specimens, as did most others, presented the problem that the pressurizing bladder in the hydroburst apparatus tended to extrude over the top of specimen. Based on this observation, a mechanism for the early failure of 90° specimens is proposed. As shown in Fig. 10, the bladder extrudes over the specimen at high pressures resulting in a bending of the ring. Bending, of course, is accompanied by tension which would act perpendicular to the fibers, causing a splitting of the ring. Visual inspection of the failed 90° specimens shows that they do appear to have failed from tension applied transversely to the fibers. Moreover (and this is true of the 90° specimens only) in 10 separate fracture experiments we were never able to fracture a specimen through: only one half (usually the top) would fail as described above. Specimens wound at other angles would be able to resist bending because of the inclination of the fibers; hence they did not split as the 90° specimens did.

IV SUMMARY & CONCLUSIONS

Based on the experimental strength values which we obtained and which we believe to be conservative, an estimate of the energy storage capacity of our design can be made. The stress where failure would occur at each radial position is shown in Fig. 11, and is marked "Failure Stress". The stress distribution at 3 different RPM is also shown. A flywheel of 4 inches inner and 8 inches outer diameter using a winding program determined from experiment (i.e. modified version of Fig. 3) will fail at 62000 RPM. The stress level will be of such that the flywheel would be storing 20 w hr/lb and .75 w-hr/in^3 of energy. This compares with values reported in the literature shown in Table 1.

The design can be improved by making the angle of wrap steeper to increase the tensile strength of the inner portions of the rotor. This should be possible if the system will tolerate certain levels of radial stresses.

Other areas for future work include the investigation of hybrid composites to optimize the design by allowing for greater strength in the inner portions of the wheel.

REFERENCES

1. Toland, R.H., "Transfer Matrix Analysis of Composite Flywheels with Reliability Applications", Proceedings of the 1975 Flywheel Technology Symposium, Berkeley, California, Nov. 10-12, 1975.

2. Jones, R.M., "Mechanics of Composite Materials", Scripta Book Co., Washington, D.C. 1975.

3. Yao, S., and Abildskou, D., "Low-Radar-Cross-Section Section OH-6A Helicoptor Tail Rotor Blade", USAAMRDL - TR - 74 - 31, Final Report prepared for Eustic Directorate U.S. Army Air Mobility Research Development Lab. Fort Eustis, VA.

4. William M. Brobeck & Associates, Berkeley, California "Investigation of Multi-Ring-Fiber-Composite Flywheels for Energy Storage", EPRI EM-227, Project 269-2, Final Report, Sept. 1976.

5. Whitaker, R., and Birk, J., EPRL Journal, Vol. I, No. 8, Oct. 1976,pp.6-13.

6. Rinde, J.A., Chiao, T.T., and Stone, R.G., "Composite Fiber Flywheel for Energy Storage", paper presented at 8th SAMPE Technical Conference, October 12-14, 1976.

7. Crandall, S.H., and Dahl, N.C., "An Introduction to the Mechanics of Solids", McGraw Hill, New York, N.Y.

Table 1. A Comparison of Flywheels to batteries.

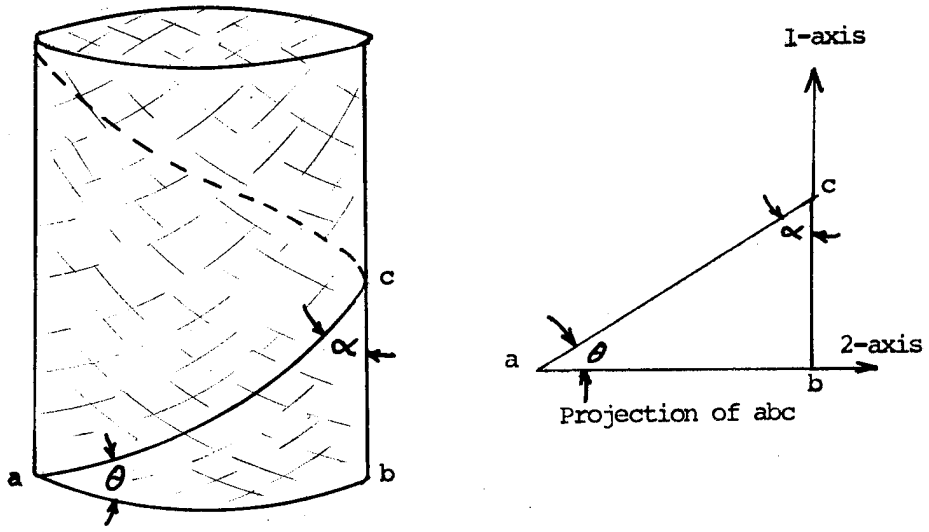
System	Energy Storage (W-hr/lb)	Energy Storage ($W\text{-hr/in}^3$)
Sodium Antimony Tricholoride Battery*	50	2
Lithium Metal Sulfide Battery*	85	3.5
Lead Acid Batteries*	9	.75
Garrett's Flywheel†	20	.65
Multirim Flywheel**	14.1	not given
Thin Rim (estimate)	55	.45
Proposed Design A	20	.75

*Whitaker, R., and Birk, J., EPRI Journal Vol, I. No. 8, Oct. 1976, pp. 6-13.

†Rinde, J.A., Chiao, T.T., and Stone,R.G., "Composite Fiber Flywheels for Energy Storage", paper presented at 8th SAMPE Technical Conference, Oct. 12-14, 1976.

**William M. Brobeck & Associates, Berkeley, California "Investigation of Multi-Ring Fiber-Composite Flywheels for Energy Storage", ERPI EM-227, Project 269-2, Final Report, Sept. 1976.

A. Orientation of fibers in a filament wound composite cylinder



B. Orientation of fibers in a cross-ply composite laminate

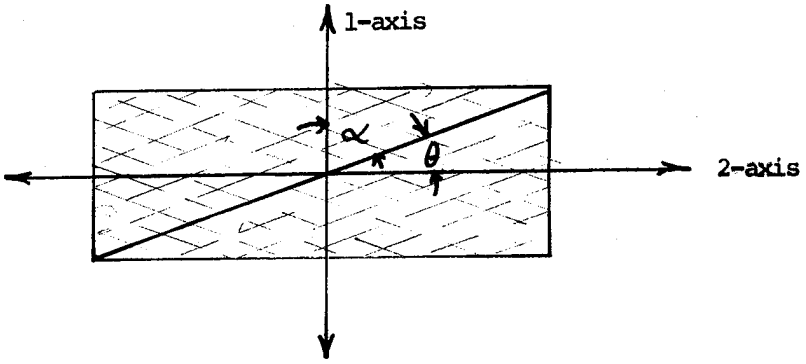


Figure 1. Definition of Fiber Orientation

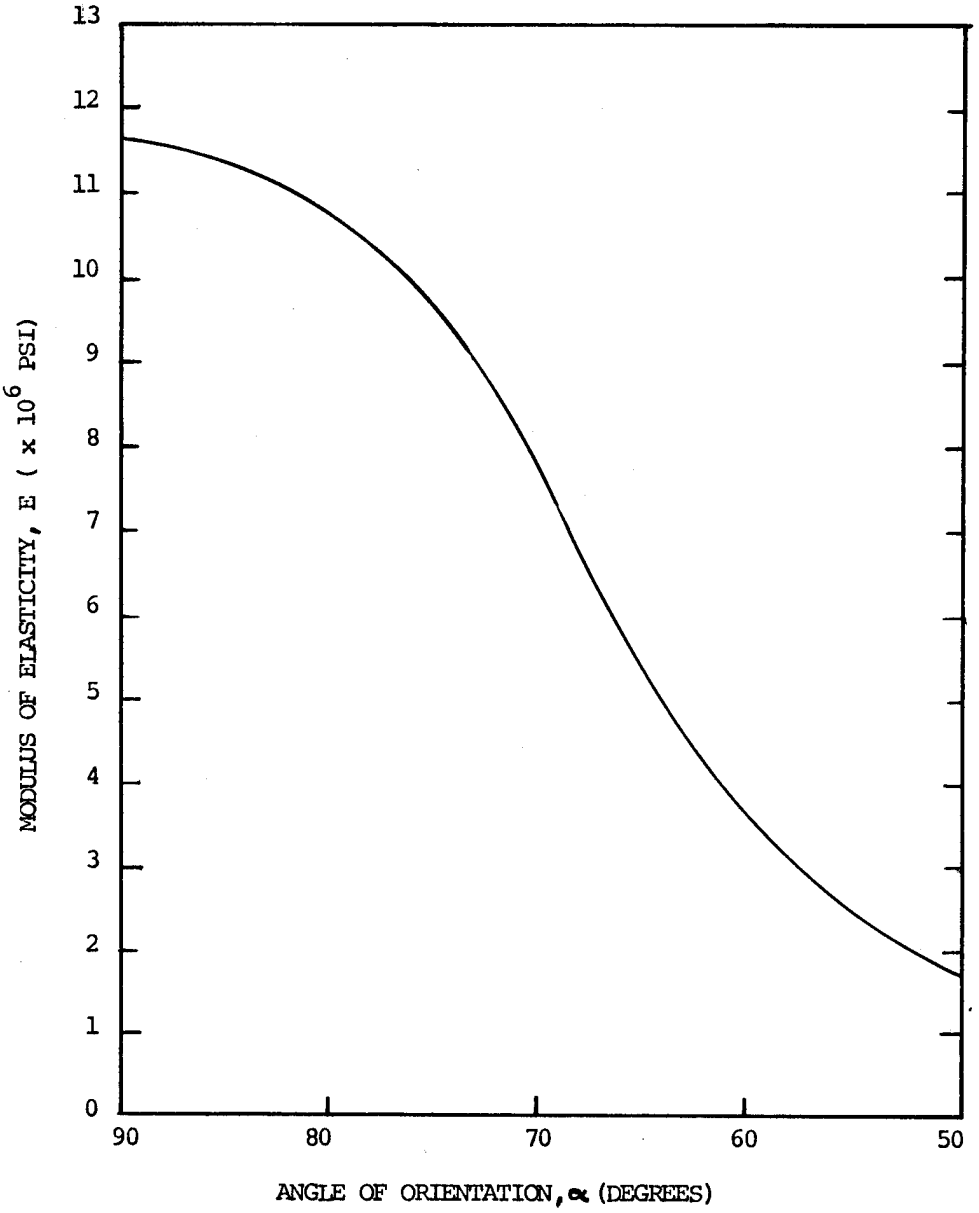


Figure 2. Variation of Modulus with Fiber Orientation for Kevlar Composites

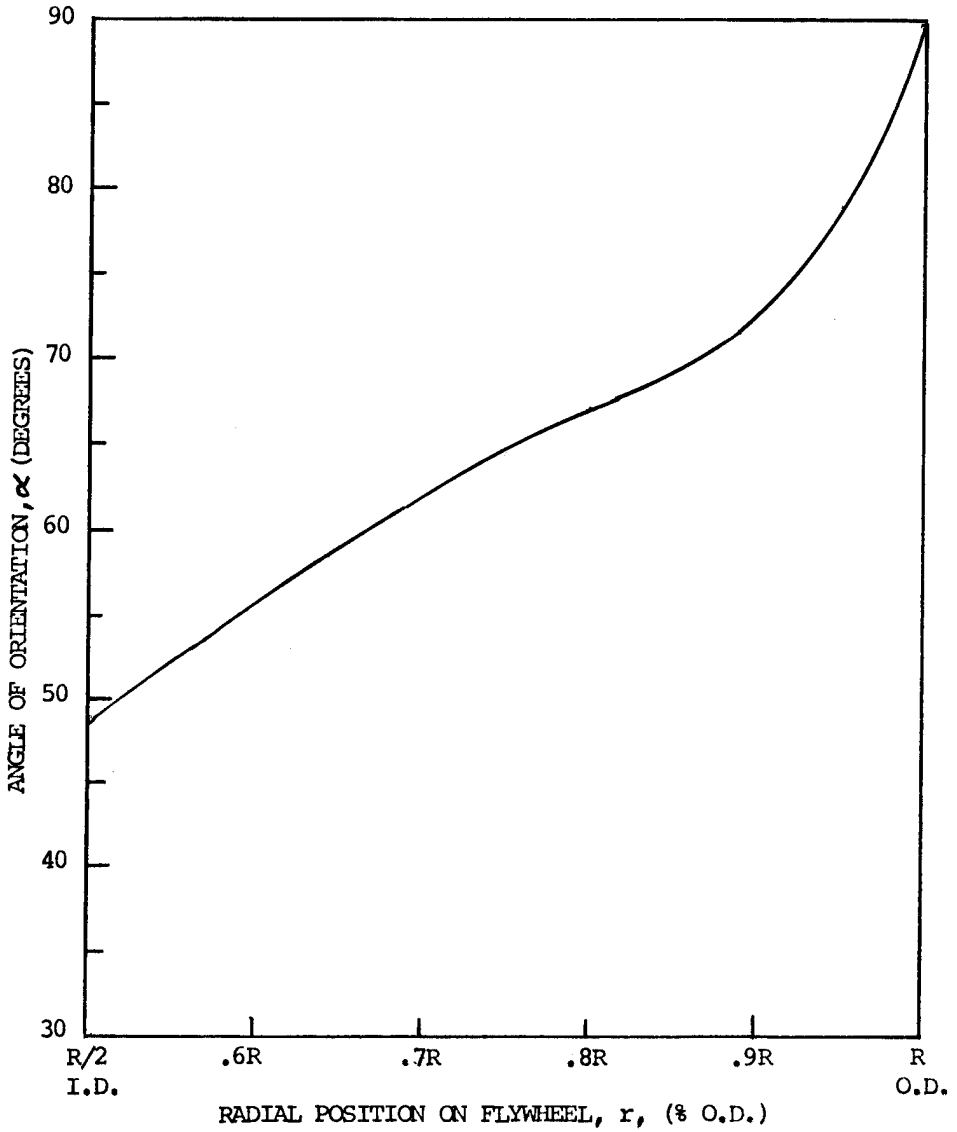


Figure 3. Fiber Orientation vs. Radial Position for Proposed Flywheel Design

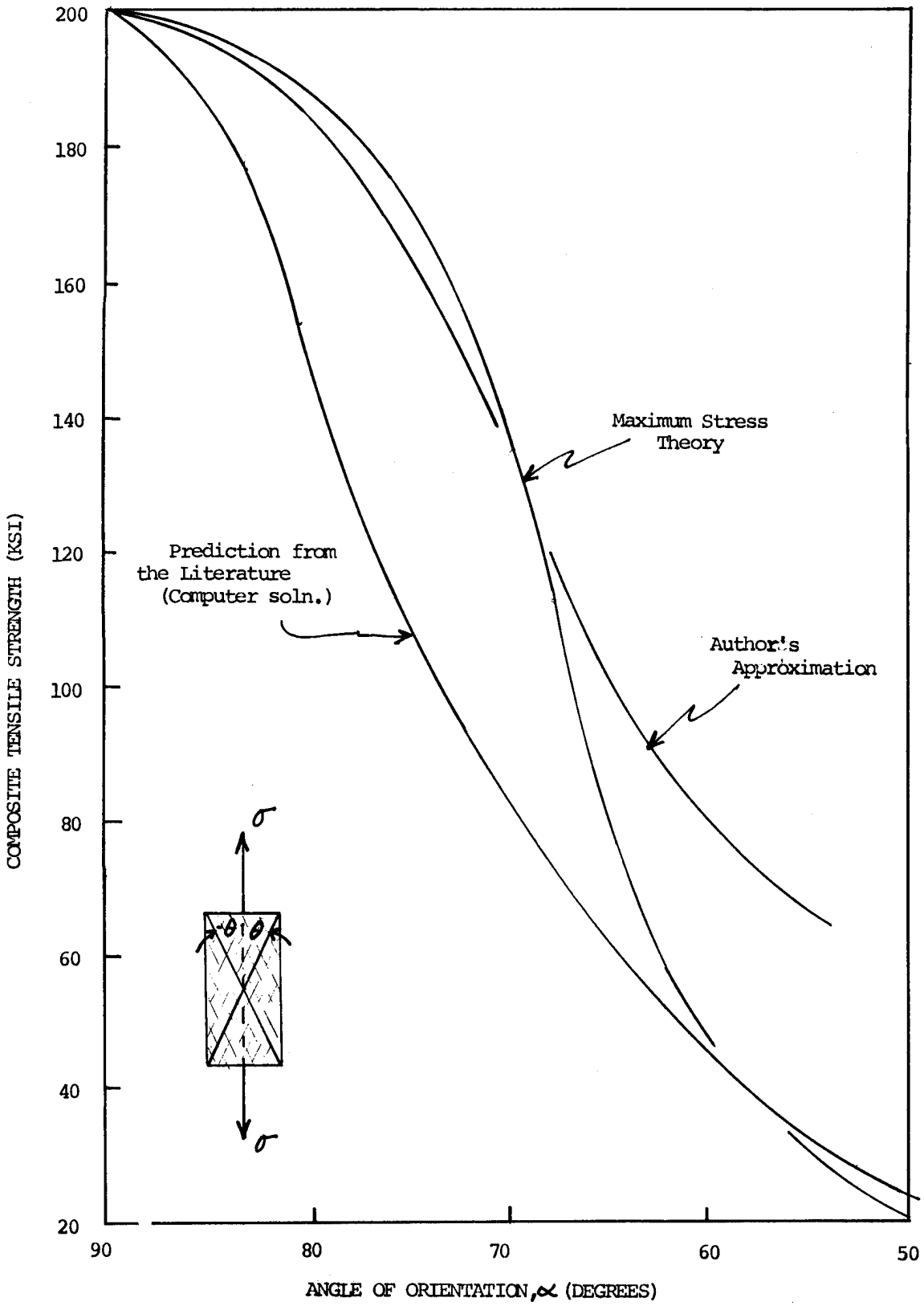


Figure 4. Prediction of Strength Variation with Fiber Orientation

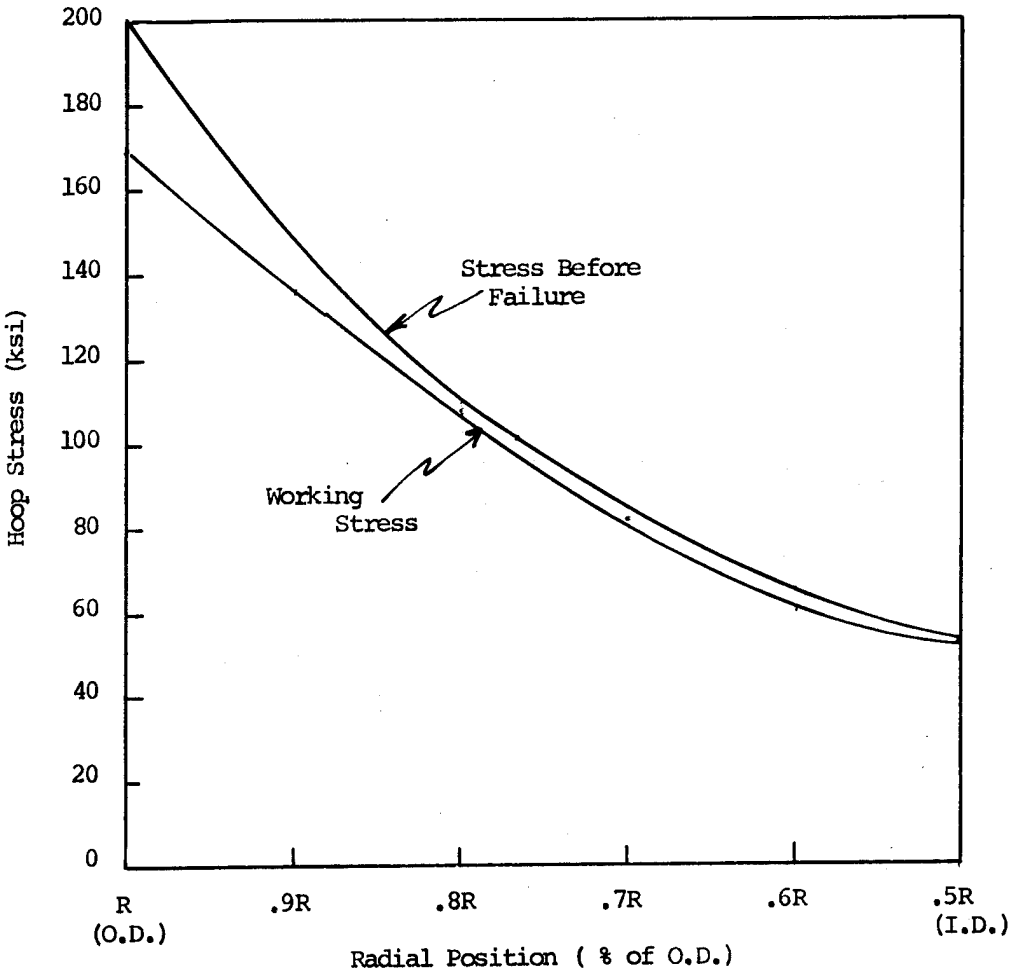


Figure 5. Working and Maximum Stress in Proposed Flywheel on Rotation

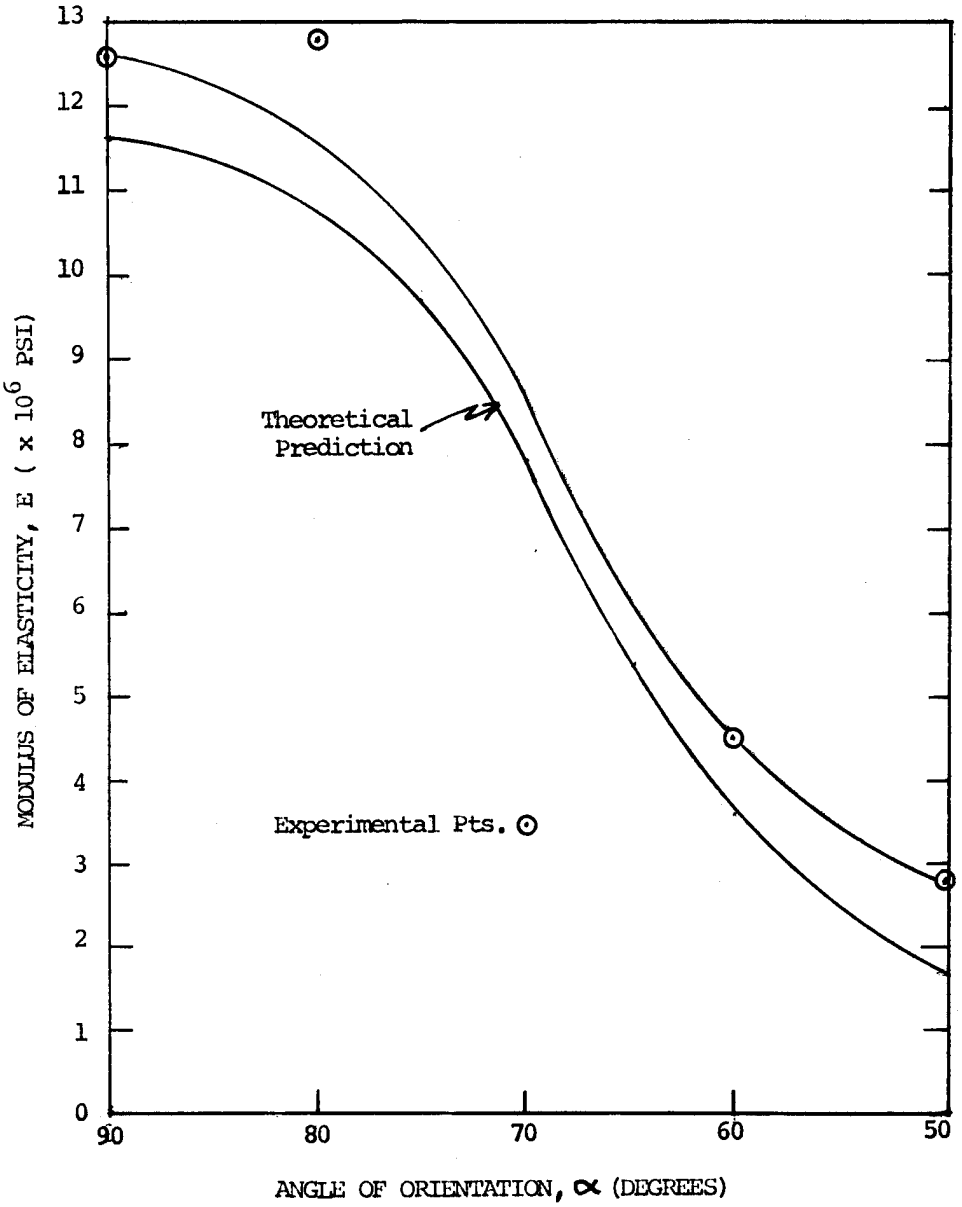


Figure 6. Variation in Modulus with Orientation

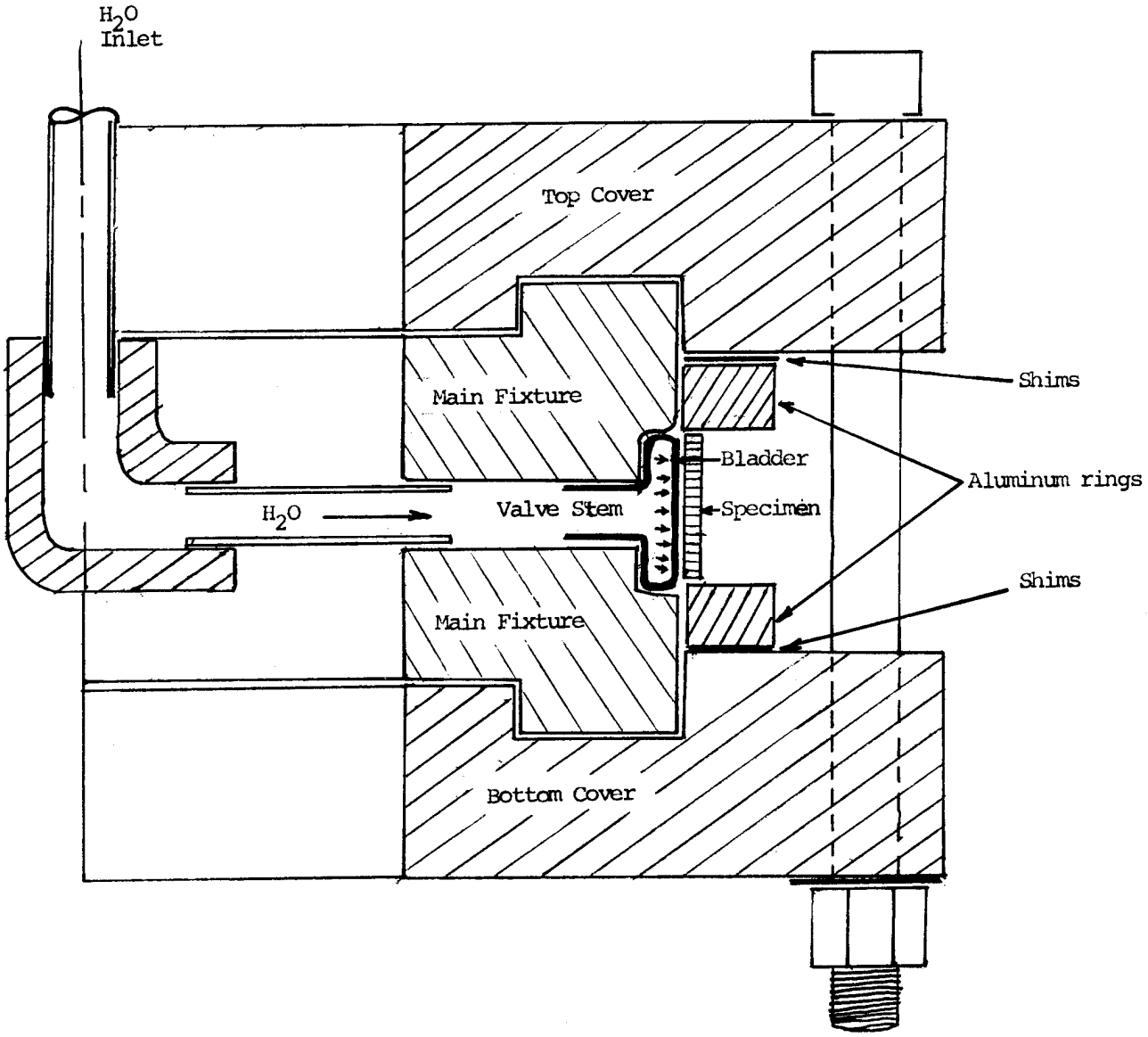


Figure 7. Cross Section of Hydroburst Apparatus



Figure 8. Hydroburst Apparatus (Disassembled)

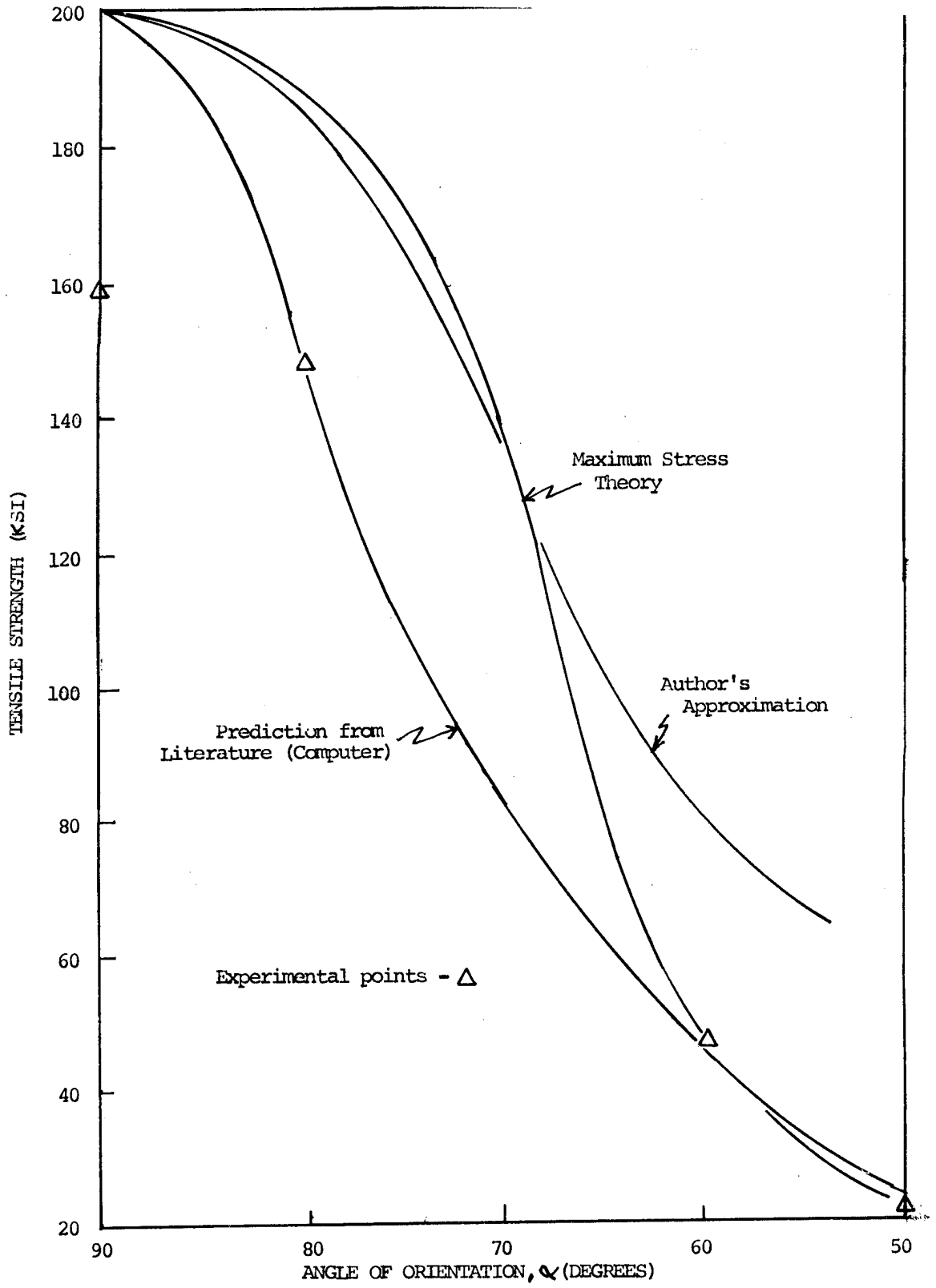


Figure 9. Experimental Strength Results vs. Predictions

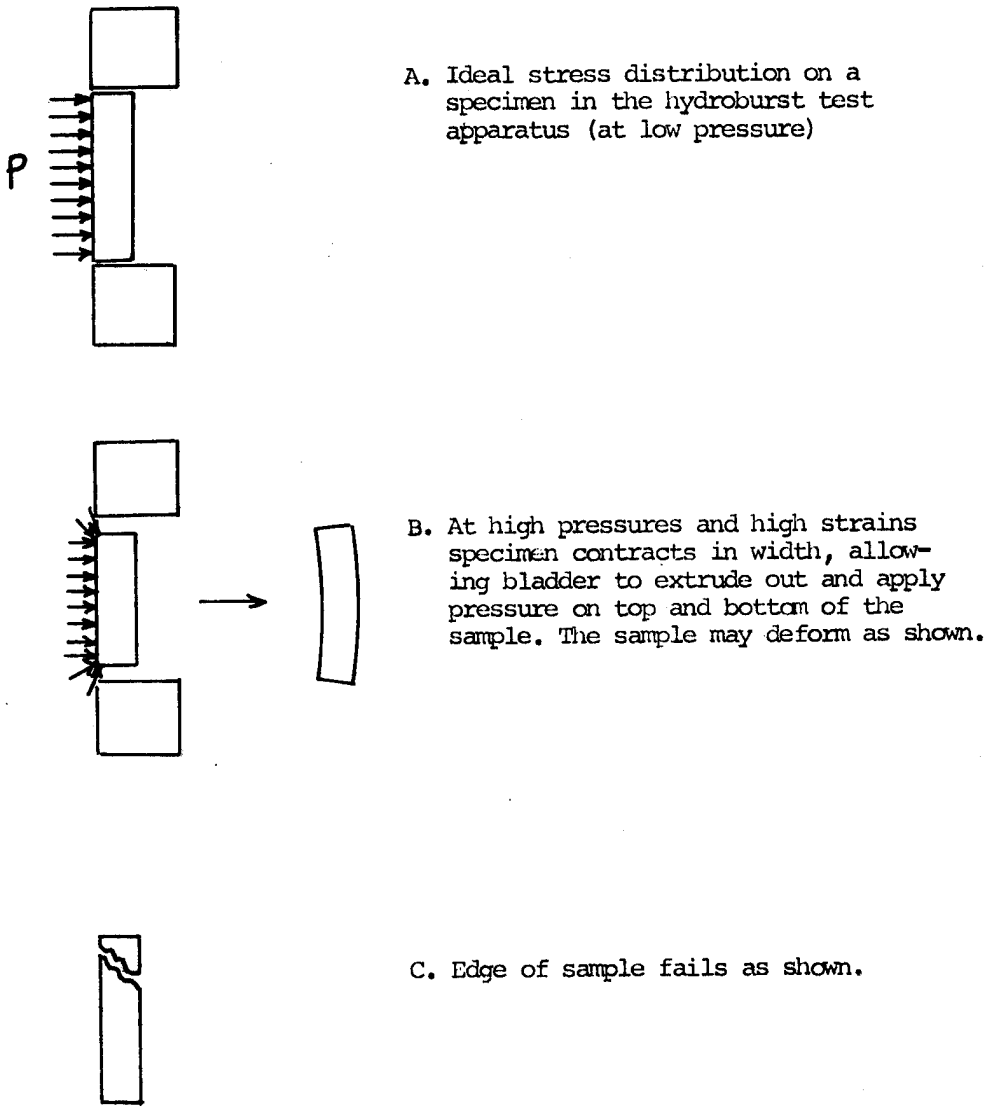


Figure 10. Possible Failure Mechanism for Hoop Wound Specimens

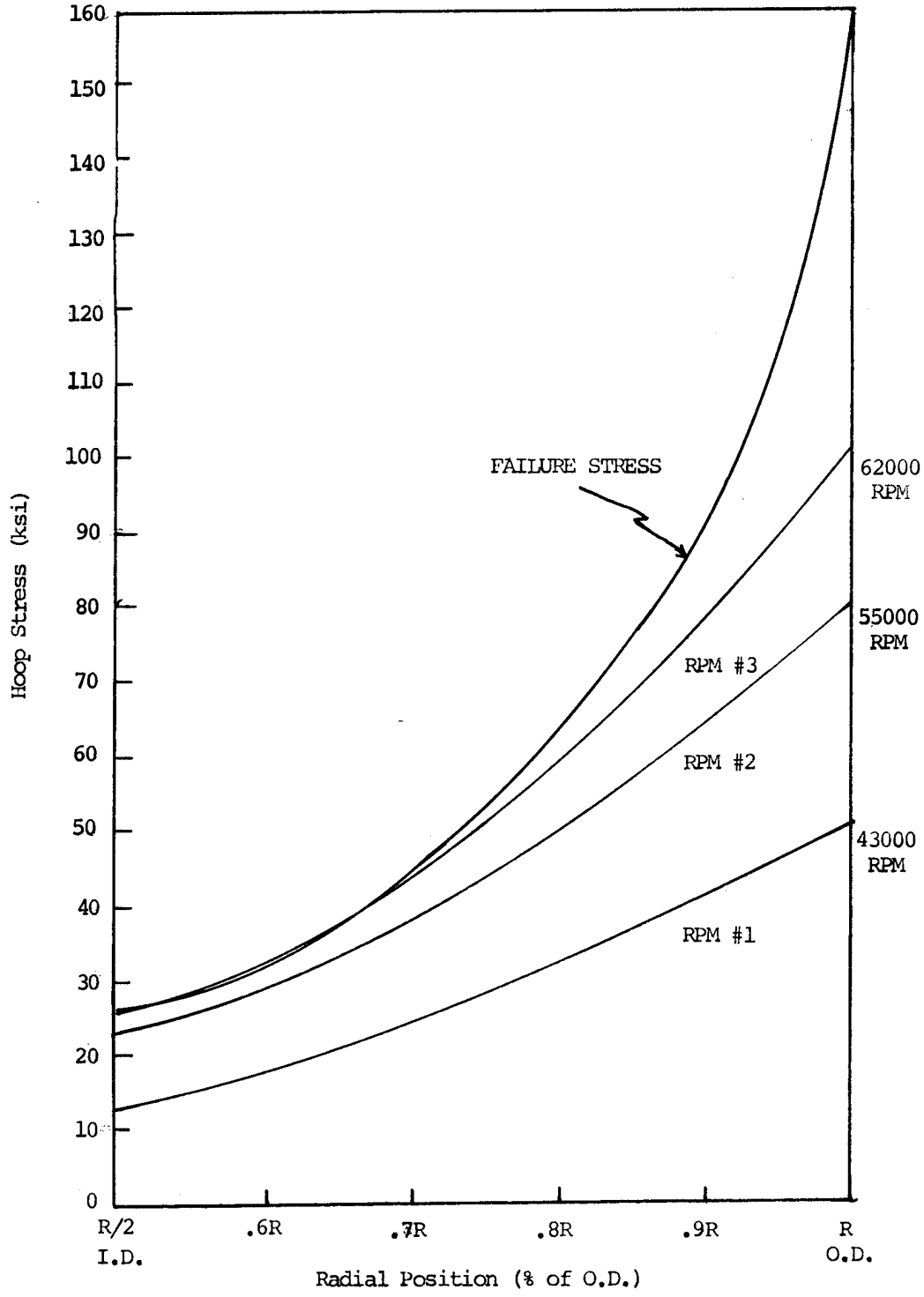


Figure 11. Stress Level as a Function of RPM vs. Radial Position for Proposed Flywheel

SANDIA BASIC FLYWHEEL TECHNOLOGY STUDIES

R. O. Woods
F. P. Gerstle, Jr.
Sandia Laboratories
Albuquerque, New Mexico 87115

ABSTRACT

Sandia has been assigned lead-laboratory status by ERDA, charged with advancing the technology of flywheel energy storage systems. At the outset, particular emphasis has been placed upon systems which might be used in vehicular applications. Other presentations at this symposium by Reedy and Gerstle; Allred, Foral, and Dick; and Bert and Chen describe our work on composite flywheels - an effort which still comprises the bulk of our in-house activity. In this talk, we will list all of the technological problems which we are (or will be) investigating. These are the components of a unified program which grew out of our initial effort with composite wheels.

INTRODUCTION

The economic success of a technology rarely springs from a single innovation. In most cases, the governing factors are quantitative rather than qualitative. Thus, for example, although manned flight had been taking place for a century, aviation did not become commercially feasible until a lengthy evolution had produced an internal combustion engine with power-to-weight ratio high enough to allow its use in flight.

Energy storage technology is in much the same state as early aviation. No question exists concerning the technical feasibility of energy storage. The problems which we now face are matters of degree. They are concerned with making systems smaller, lighter, more efficient, more reliable, safer and cheaper. Failing any dramatic innovations, the components of a successful flywheel energy storage system can be easily identified by their function (Viewgraph 1). Great latitude exists, however, as to the choice of the specific hardware which is to perform each of the given functions. The first objective of our program will be to characterize potential system components in order to allow tradeoff studies to be performed. These studies will allow an optimum permutation of components to be selected for given applications. Thus, the best compromise for a hybrid vehicle might be a composite wheel, rolling contact bearings, and electrical input and output; a stationary application may be best served by a metal wheel, air bearings, and a mechanical drive. The permutations are numerous and, without data characterizing each element of the system, no rational basis exists for decision making.

Each of the ten components identified in Viewgraph 1 will be discussed in turn, with a commentary on Sandia's efforts relating to that item. The subject of "Wheel Design" (Viewgraph 2) will be adequately treated by companion papers mentioned in the abstract. This viewgraph lists the aspects of wheel design which actually involve efforts by Sandia Laboratories as of the present writing.

Under the heading of "Heat Transfer" (Viewgraph 3), a study is being performed which treats aerodynamic heating of the wheel. This problem is particularly severe in the case of a resin matrix composite wheel because, not only is the material temperature sensitive, but also its poor thermal conductivity tends to allow the temperature rise to be concentrated at the periphery rather than be mitigated by radial conduction. A first analysis has already shown that the problem is more severe than was generally recognized, hence placing stringent requirements upon the vacuum system.

Viewgraph 4 shows the equilibrium temperature which will be assumed by the periphery of a one foot radius disk rotating at 40,000 RPM in air or helium at pressures between 10^{-2} and 10^{-4} Torr. These curves were calculated assuming that the temperature is established by a balance between heating due to skin friction and cooling by radiation. This assumption is conservative, but not radically so in view of the low thermal conductivity of composites. The calculations were performed using an algorithm which had been developed at Sandia Laboratories for reentry problems. Note that air pressures on the order of 10^{-4} Torr will be required if wheel temperatures

are to be kept below a realistic value of about 150°F. This work is currently being extended to account for conduction and to produce a computer code which will give internal temperature distributions.

Bearings are treated in Viewgraph 5. "Data for Tradeoff Studies" lists the parameters which will have to be defined in order to allow a choice of bearing types to be made for any given application. This sort of data will be understood wherever the heading, "Tradeoffs" appears on subsequent viewgraphs. "Types" lists the developmental efforts which we will be sponsoring in industry, with the exception of hydrodynamic bearings, to which we have assigned a lower priority.

The first two types of shaft seal listed in Viewgraph 6 should be familiar to most readers. The "Dynamic", however, is a fairly unique bit of technology which incorporates a molecular drag pump into the rotating seal. The "Hydrodynamic" involves pumping the clearance volume between a shaft and the surrounding cylinder. We are sponsoring efforts in all four types listed here.

A number of vacuum pumping schemes are listed in Viewgraph 7. Of these, only turbomolecular pumps are currently being investigated. The requirements which a pump must meet in a flywheel application are not stringent as vacuum technology goes, but high premiums are placed on reliability and energy economy. Ultimately, we plan an intensive effort in the field of pumping.

No effort is currently being exerted per se upon "Containment" (Viewgraph 8). A certain amount of relevant data will be generated during spin tests, where efforts are to be made to photograph the wheel at break-up and during subsequent interactions with the walls of the container.

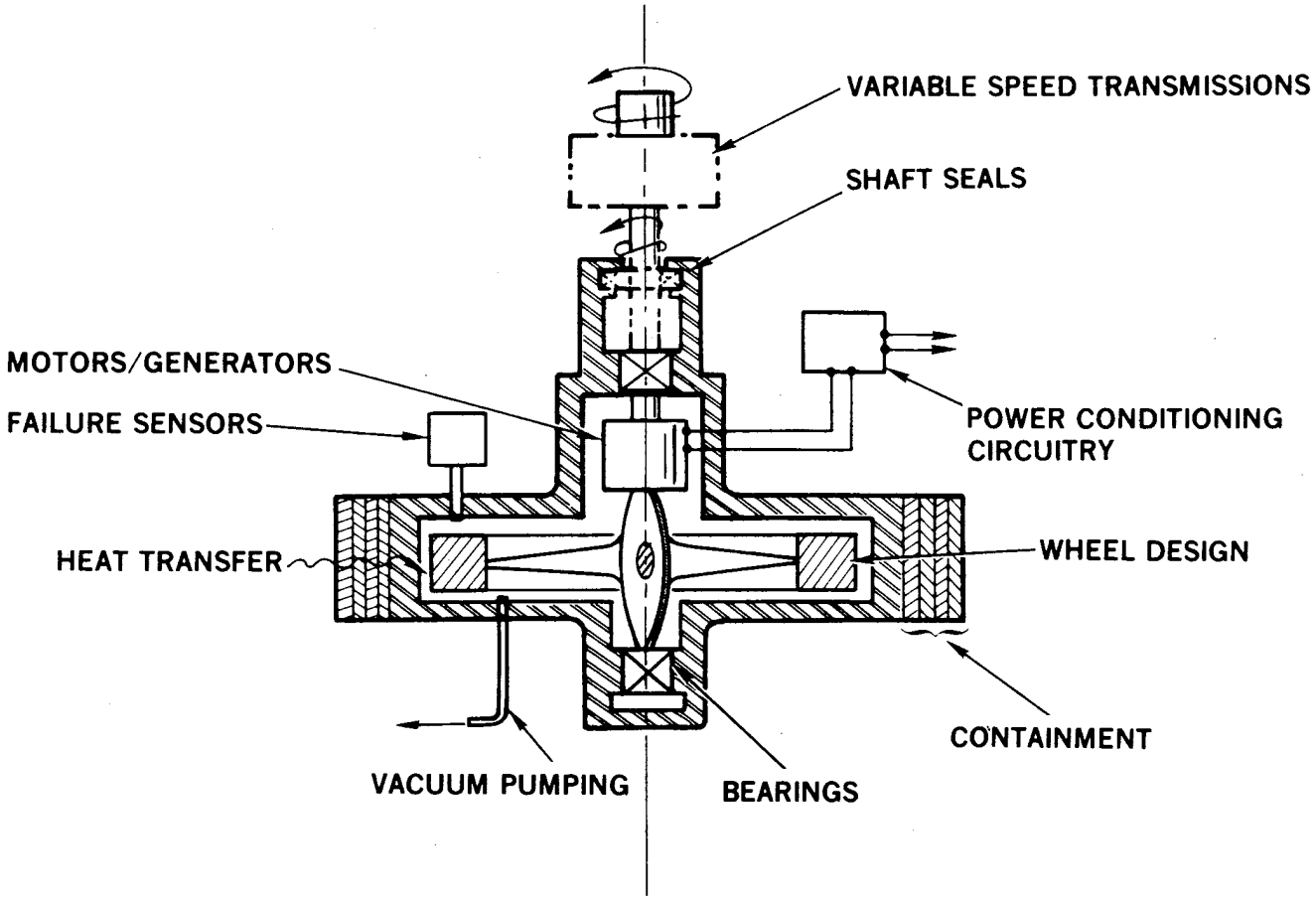
"Power Conditioning" (Viewgraph 9) is listed for completeness, although Sandia is not currently funding any studies of this problem.

Creating "Failure Sensors" (Viewgraph 10) which are reliable and cheap enough to be economically usable will present an interesting technical challenge. Monitors are needed which will indicate deterioration of the vacuum due to leaks or outgassing. Similar detectors would also respond to the pressure pulse which is generated when a wheel fractures and exposes a fresh surface covered with volatile products. In some cases this pulse may preceed catastrophic failure of the wheel by a period long enough to allow emergency shutdown.

Mechanical deterioration of the wheel might be detected by particle impact sensors around the periphery. Accelerometers on the bearings can detect unbalance of the wheel due to creep, as well as the vibration of an impending bearing failure. Temperature monitors looking at the wheel periphery would provide another check on abnormal aerodynamic heating due to poor vacuum and might sense energy being dissipated at a fracture in the wheel.

Bearing instrumentation is self explanatory, except for "Specifics" such as deterioration of lubricating oil or abnormalities in the behavior of servo electronics in magnetic bearings.

"Variable Speed Transmissions" (Viewgraph 11) and "Motors/Generators" (Viewgraph 12) are included, again, for completeness, although we have no efforts in progress under either of these headings.



"BACKGROUND TECHNOLOGY"

SANDIA FLYWHEEL PROGRAM

WHEEL DESIGN

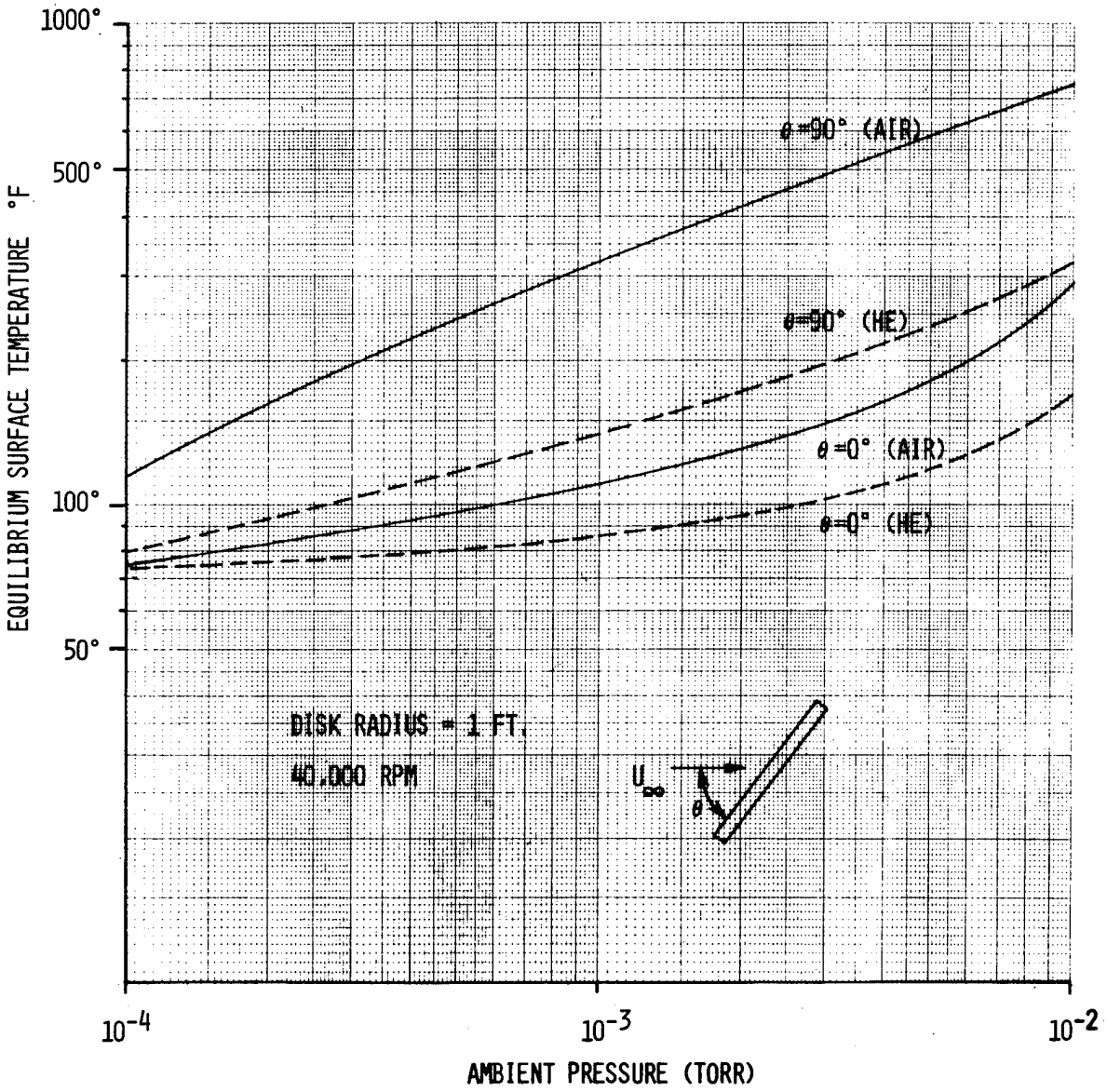
- COMPOSITES STUDIES
  - FABRICATION STRESSES
  - THERMAL STRESSES
  - CREEP AND TEMPERATURE EFFECTS
  - UPGRADING TRANSVERSE PROPERTIES
- DESIGN AND ANALYSIS
  - GEOMETRY
  - MATERIALS COMPATIBILITY
  - DYNAMICS
- TESTING
  - PERFORMANCE (SPEEDS, VIBRATION, CREEP)
  - FAILURE MODES
  - DIAGNOSTICS
  - CONTAINMENT

VIEWGRAPH 2

HEAT TRANSFER

- AEROTHERMODYNAMICS
- INTERNAL TEMPERATURE FIELD
  - MAXIMUM TEMPERATURE
  - THERMAL STRESSES

VIEWGRAPH 3


1000°
500°
100°
50°
EQUILIBRIUM SURFACE TEMPERATURE °F
θ=90° (AIR)
θ=90° (HE)
θ=0° (AIR)
θ=0° (HE)
DISK RADIUS = 1 FT.
40,000 RPM
U∞
θ
10-4
10-3
10-2
AMBIENT PRESSURE (TORR)

VIEWGRAPH 4

BEARINGS

- DATA FOR TRADEOFF STUDIES
  - POWER LOSSES
  - OPERATING RANGES (LOAD AND SPEED)
  - LIFETIMES
  - COST
  - SPECIAL REQUIREMENTS
- TYPES
  - ROLLING CONTACT
  - MAGNETIC
  - HYDRODYNAMIC
  - HYDROSTATIC
  - "HYBRID"

VIEWGRAPH 5

SHAFT SEALS

- TRADEOFFS
- TYPES
  - MECHANICAL (SLIDING CONTACT)
  - FERROFLUIDIC
  - "DYNAMIC"
  - HYDRODYNAMIC

VIEWGRAPH 6

VACUUM PUMPING

- TRADEOFFS
- SCHEMES
  - OFFBOARD
  - DISPLACEMENT PUMPS
  - TURBOMOLECULAR PUMPS
  - EXOTIC

VIEWGRAPH 7

CONTAINMENT

- WHEEL FAILURE MODES
  - COMPOSITE
  - METAL
- PARTICLE PENETRATION
- MOMENTUM DUMPING
- TEMPERATURE EFFECTS

VIEWGRAPH 8

POWER CONDITIONING

- TRADEOFFS
- DC/AC (CONVERTERS, INVERTERS)
- ENERGY BUDGETING
- SYSTEM OPTIMIZATION (MECHANICAL/ELECTRICAL)

VIEWGRAPH 9

FAILURE SENSORS

- VACUUM
  - LEAKAGE
  - GAS PULSE FROM WHEEL FRACTURE
- WHEEL
  - SPALLATION
  - FRACTURING
  - UNBALANCE
  - TEMPERATURE
- BEARINGS
  - VIBRATION
  - TEMPERATURE
  - SPECIFICS

VIEWGRAPH 10

VARIABLE-SPEED TRANSMISSIONS

- TRADEOFFS
- FRICTIONAL CONTACT
- HYDRAULIC
- V-BELT
- EXOTIC

VIEWGRAPH 11

MOTORS/GENERATORS

VIEWGRAPH 12

ADVANCED ELECTRICAL CONVERSION SYSTEMS FOR FLYWHEEL APPLICATIONS

David Eisenhaure, Stephen O'Dea,
William Stanton
The Charles Stark Draper Laboratory, Inc.
555 Technology Square
Cambridge, Massachusetts 02139

ABSTRACT

The development of low-cost, brushless rotating machine systems with high broad band efficiency is critical for the production of effective flywheel modules for electric vehicles. The Charles Stark Draper Laboratory has been developing a variety of brushless machine systems which appear to have the potential for both low cost and high broad band efficiency. The rotating machines utilized in these systems include wound rotor, induction, inductor, permanent magnet, and special purpose machines. The converters considered for use with these machines include D.C. link inverters, phase controlled rectifiers, cycloconverters, and special purpose switching system. This paper will review work recently and/or currently funded at the Draper Laboratory in the flywheel conversion area by NSF, DOT, and NASA. Emphasis will be placed on several unique machine concepts developed at the Draper Laboratory for flyhweel application. These include a field modulator inductor motor alternator, an optimum slip induction motor, and a permanent magnet brushless D.C. motor controlled for optimum torque angle. The results of experiments and analytical studies indicated that these approaches result in both overall system simplification and cost reduction as well as increasing broad band efficiency.

TEXT

SUMMARY

An economic need has been generally recognized for systems which would allow transient storage of electrical energy. Flywheel energy storage is a potentially promising solution to this need. It is characterized by high reliability, long life, and low cost and has the potential, with proper development, of storing energy efficiently at relatively high energy densities. The Draper Laboratory feels that the most difficult problem associated with the use of flywheels may be the development of low-cost electrical conversion systems at suitable power densities. These subsystems require state-of-the-art advancement to make flywheel energy storage cost effective. Flywheels in vehicle applications require special emphasis on the conversion system because of the typical power and energy requirements of these applications.

This paper describes efforts by the Draper Laboratory (CSDL) in the conceptualization and development of advanced concept energy conversion systems for use in conjunction with flywheel energy storage. These energy conversion studies were directed toward the utilization of flywheel energy storage for utility load leveling during peak power periods, storage for alternate energy sources, and electric vehicles.

The Charles Stark Draper Laboratory has been developing a variety of brushless machine systems suitable for flywheel applications which appear to have the potential for both low cost and high broad band efficiency. The rotating machines considered for these systems include wound rotor, induction, inductor, permanent magnet, and special purpose machines. The converters considered for use with these machines include D.C. link inverters, phase controlled rectifiers, cycloconverters, and special purpose switching systems. Emphasis will be placed on several unique machine concepts developed at the Draper Laboratory for flywheel application. These include a field modulator inductor motor alternator, an optimum slip induction motor, and a permanent magnet brushless D.C. motor controlled for optimum torque angle.

SYSTEM REQUIREMENTS

In order to evaluate conversion system alternatives it is first necessary to develop electrical interface requirements for the flywheel storage system which would allow it to effectively fulfill its function in the system. Since the function of the flywheel storage system is to manage power flow, the flywheel system could perform the following independent functions.

1. Long term power averaging
2. Short term power regulation

Based on these generalized functions, a detailed set of subsystem requirements was generated for the energy conversion system which would allow interface between the flywheel shaft and electrical bus. The subsystem requirements toward which conversion system developments have been directed are based on the following overall requirements for the flywheel conversion system:

1. Handle independently controlled amounts of real and reactive power
2. Motor/generator operation
3. Interface with a variable speed shaft
4. Provide controlled output frequency
5. Power factor correcting
6. Capable of running in either a stand-alone or line-coupled mode
7. Provide acceptable output waveform quality
8. Cost effective

SUBSYSTEM DEVELOPMENT

The Draper Laboratory has reviewed existing conversion concepts to determine their applicability to the flywheel storage conversion problem. Consideration was given to the following classes of conversion systems:

1. Variable speed mechanical drives
2. Conventional machines coupled with rectifier/inverter sets
3. Conventional machines and cycloconverters
4. Multiple machines
5. Existing special-purpose conversion systems

After reviewing these conventional approaches to the conversion problem, it was felt that all had enough deficiencies when compared to the desired subsystem requirements to warrant the development of a conversion system specifically tailored to this application.

Efforts at the Laboratory have been directed toward the development and evaluation of special purpose conversion systems. This development may be summarized as follows:

1. Rotating machine/switching systems have been defined which appear to have significant advantages over conventional approaches for the flywheel application.
2. Rotating machine designs have been generated to satisfy the above conversion systems.
3. A novel approach to computer modeling the rotating machine has been taken which will allow quantitative evaluation of design alternatives.
4. The control equations have been generated to allow the conversion system to satisfy the overall flywheel system requirements.

DEVELOPMENT OF OPTIMUM BACK EMF DRAPER LABORATORY FLYWHEEL CONVERSION SYSTEM

It was felt that an alternative to the conventional approaches to the conversion problem that considered all of the system requirements was needed. The result of this study was a conversion system which uses a special purpose machine to generate the optimum back EMF for the power switching stage.

Currently efforts at the Draper Laboratory are being directed toward the development and evaluation of this special purpose conversion system. However, before beginning a detailed description of this system, some general discussion seems warranted regarding the philosophy behind its development. The conventional approach to this type of conversion problem would be

to treat it as two separate engineering tasks. The first of these tasks would be to select a conventional rotating machine. The design of a power conditioning stage to interface between the rotating machine and the line would comprise the second task. In the view of the Draper Laboratory the proper approach to this problem is to consider all components between the shaft and the electrical line as a single system. This integrated approach to the conversion problem using system engineering techniques results in substantial system level advantages compared to more conventional approaches. This approach uses mathematical techniques, combined with the desired system requirements, to synthesize an optimum conversion system from a general machine and power switching model.

The CSDL system was synthesized so as to satisfy the engineering requirements previously stated for the flywheel conversion system. In order to arrive at a system which uses the machine and SCR switches more efficiently, the following additional requirements were imposed.

CSDL Approach. Design integrated rotating machine power switching system.

System Approach to Design Includes Generator:

Design machine so that its generated voltage will:

1. Drive current continuously in each of its phases -- Improved Efficiency
2. Cause zero crossings of current to be coincident with SCR switchings -- Lower EMI
3. Utilize output impedance of machine to limit current amplitude for parallel operation -- Simplified Control Schemes

The Draper Laboratory technique uses waveform requirements, switching characteristics, and machine impedance to determine the required back EMF for an optimal performance defined by the above requirements. The particular analysis that follows is for two-phase field modulation that controls the amplitude and phase of a single-phase output of lower frequency. In general, more than one phase at the generator frequency would be summed to reduce the harmonic content of the lower frequency output. This frequency conversion concept is best summarized by Fig. 1. For two phases of high frequency generation converted to a single phase of lower frequency, the system would be as is diagrammed in Fig. 2.

With reference to Fig. 2, the 1 subscript in each case refers to the voltage due to one phase of the field. The 2 subscript refers to the second phase of the field. The two fields are in quadrature as are the phase A and phase B outputs. For a resistive load, it turns out that the modulation signal for the two field phases are in phase. The output waveform for different power factor loads are shown in Fig. 3. The waveforms in Fig. 3 correspond a generator with two stator phases. To more easily portray the concept, the back EMF's drawn are for the case when $(f_g/f_L) = \infty$. This case exists if the output is D.C., for which no modulation is required, or is approximately true when $f_g >> f_L$. Although the technique of defining an optimal back EMF to generate a given output waveform, is applicable in general, it may be impractical to implement. Resorting to an approximation as is displayed in Fig. 3 is consistent with the desired system operation since only a minor amount of harmonics are generated by the approximation.

OPTIMUM SLIP FREQUENCY, VARIABLE SPEED INDUCTION MOTOR(*)

Background. An induction motor is a simple, rugged, and easily driven heavy duty motor. Traditionally it has been used for fixed speed applications, or those applications needing a limited range of speed control. Potentially, it is capable of being a full-range, variable speed motor, and in many situations may be a more cost effective choice. In recent years induction motors have been used over a wider speed range, but existing speed control systems still leave a lot to be desired.

The Draper Laboratory is developing concepts for state-of-the-art improvements in induction motor speed control, such that an induction motor can be used efficiently at all speeds. The concepts relate to advances in electronics and thyristor switching stage for use with a heavy duty

(*)"Full-Range, Variable Speed, Linearized Induction Motor Controls", W. Curtiss, June 1, 1976.

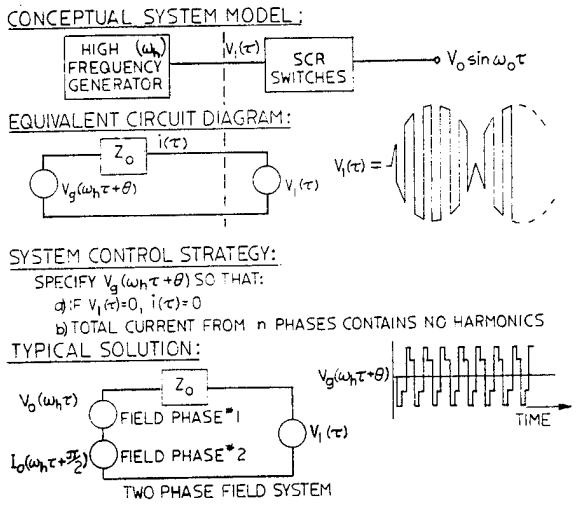


Fig. 1 Conceptual Development of Special Purpose Flywheel Conversion System

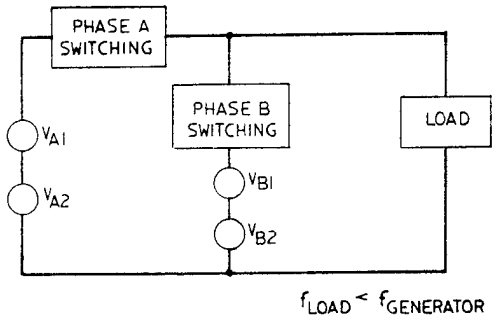


Fig. 2 System for Two Phases of High Frequency Generation Converted to a Single Phase of Lower Frequency

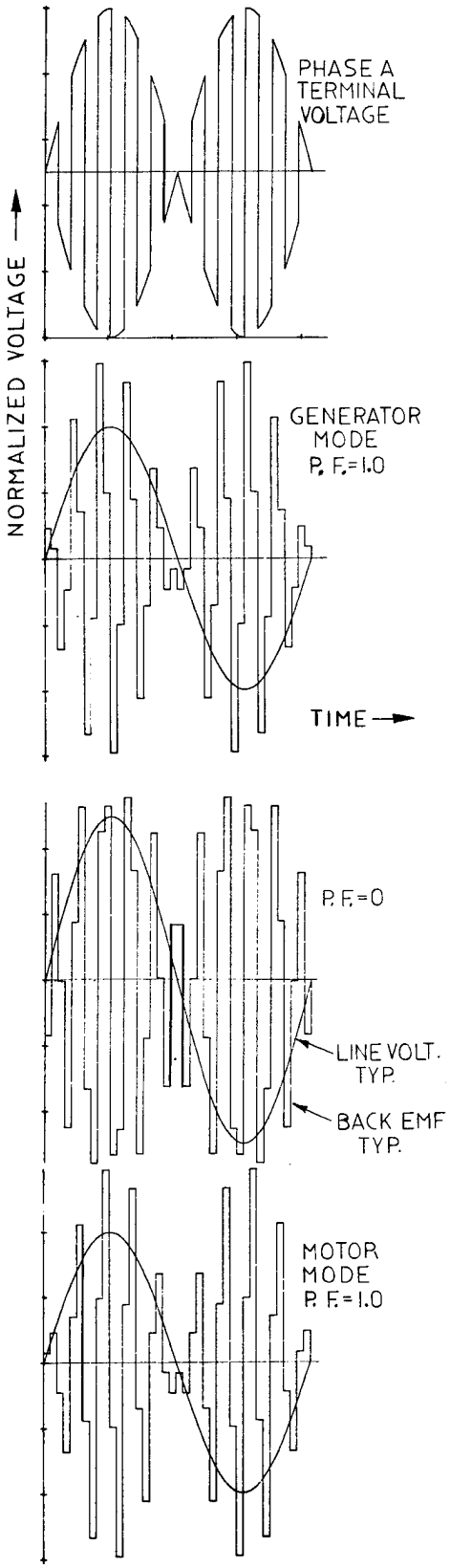


Fig. 3 Two Phase System Voltages

induction motor. New pulse-width modulation and SCR commutation techniques are incorporated in the power stage.

Induction Motor Advantages. An induction motor has competitive advantages over a brushless permanent (PM) D.C. motor in several situations; namely,

1. More rugged - no demagnetization problems
2. Easily driven by switching supplies. High efficiency switching supplies can more easily drive an induction motor, because the high inductance smooths the excitation.
3. Induction motor drive requirements are less critical as induction motors are phase insensitive.
4. For wide speed range, constant or declining torque applications, an induction motor can be driven with minor variations in voltage supply. In contrast, the voltage supply for a PM motor must increase linearly with speed to provide a constant torque.
5. In high speed, low torque conditions an induction motor has low losses, whereas a conventional PM motor tends to have high magnetic drag losses at high speed regardless of torque output. Rotating the back iron of the PM motor, however, reduces this advantage.

Control System. The control system uses a closed commutating loop for slip control, and current feedback to slave the amplitude of the smoothed motor excitation current to the input command. Except for operation near low values of torque, the motor slip would be fixed by the commutation loop to optimize some predetermined combination of efficiency and/or torque sensitivity.

At low values of commanded torque the characteristics of both the commutating loop and current command are modified to linearize the input-to-torque relationship and provide "glitch free" operation through null. The linearization is accomplished by holding the stator current constant and linearly modulating slip with the command input.

Figure 4 is a block diagram of the linearized, variable speed controller. The input command controls the amplitude of all the motor excitations. The frequency of the motor excitations is slaved by the commutation loop to be a controlled frequency difference higher than the shaft speed for positive torque, and a controlled frequency difference lower than the shaft speed for negative torque. The frequency difference is picked for the best combination of motor efficiency and/or torque constant. At low values of command torque the controller is linearized by holding the current constant, and making the frequency difference a linear function of the input command. Figure 5 is a sketch of the resulting locus of torque versus slip for several excitation amplitudes.

This commutation loop requires an angle transducer to sense the shaft speed. Many possible angle transducers could be used. The preferred types would have no electrical connections to the rotor: possibilities include optical, reluctance, magnetostrictive, and magnetostrictive transducers.

The commutation circuit includes two multiplying functions:

1. The shaft frequency and command slip frequency must be mixed to produce the stator frequency, probably in a single-sideband operation.
2. The stator signals must be amplitude modulated by the input command.

OPTIMUM TORQUE ANGLE D.C. BRUSHLESS MOTOR COMMUTATION

This section provides a brief summary of brushless D.C. motor commutation techniques for polyphase machines. Only linear first order effects of the machine will be treated and these will be described on the basis of the machines equivalent electrical circuit.

To provide a basis for discussing brushless commutation techniques as well as the so-called optimum torque angle drive, the equivalent electrical circuit in Fig. 6 will be developed.

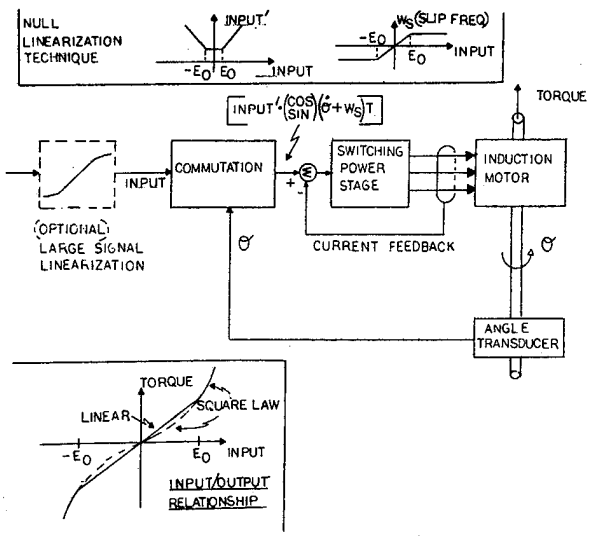


Fig. 4 Full-Range, Variable Speed, Linearized, Induction Motor Controller With Closed Loop Slip Control

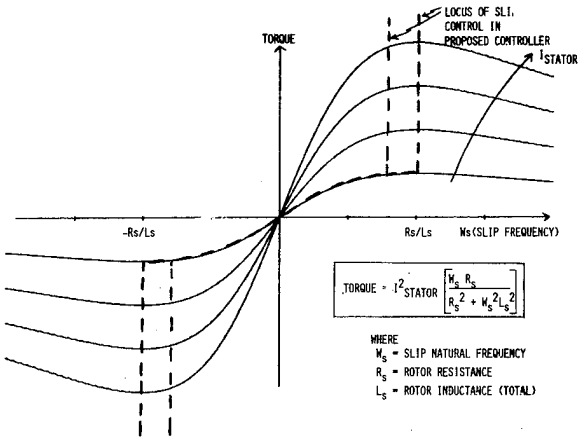


Fig. 5 Induction Motor Torque vs Slip

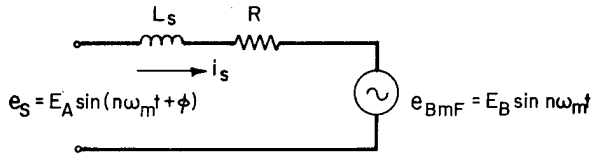


Fig. 6 Equivalent Electrical Schematic of One Phase of a Polyphase D.C. Motor

where ω_m mechanical frequency
n half the number of machine poles
e_s stator applied voltage
i_s stator current

The current which flows in the stator winding is i_s and can be written as $I\sin(n\omega t+\theta)$ where the value of I is dependent on the motor parameters. For a given value of I, maximum mechanical power delivered by the motor will be obtained when the phase difference, θ, between i_s and e_{BEMF} is zero. Since the ratio of delivered power to losses will be maximized for this value of θ, the efficiency will be maximized. Motor torque is by definition the mechanical power divided by the rotation rate and is easily derived using the above discussion.

Now, since the BEMF leads the rotor field by 90^o and since the stator field is in phase with the stator current, the torque angle which is defined as the angle between these two fields is at its optimum value of 90^o. The optimum torque angle drive technique is therefore reduced to the requirement of driving a stator current through the stator coils so that the BEMF and stator current are in phase.

To provide stator current at the proper phase implies having an excitation which is phase locked to rotor position. This requirement can also be stated as the necessity of providing a stator current whose amplitude is $I\sin n\theta_m$ where θ_m is zero when the BEMF is zero. The net result of either of these statements is that a position sensor which measures the relative angle between rotor and stator must be provided.

Position sensing can be provided in a number of ways. Hall devices sensing, hopefully, only the rotor magnetic field and providing an output which is $E_H \sin n\omega_m t$ that is nominally in phase with BEMF could with proper amplitude and power scaling be used to drive the stator current. Similarly a resolver with same number of poles as the motor with a single phase excitation (one by two) provides an output on one secondary which is $E_R \sin W_{ext} \sin n\omega_m t$ which when demonstrated at the excitation frequency, Wex, would provide a signal $KE_r \sin n\omega t$ which could be scaled to drive the stator current. The block diagram for this commutation is in Fig. 7.

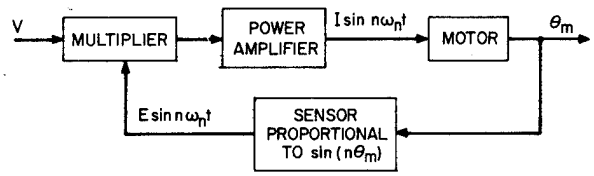


Fig. 7 Commutation With Continuous Angle Encoding

The appropriately shifted multi-phase excitations are implied in Fig. 2. A voltage applied at V in Fig. 2 would cause a specific rotational rate; it is therefore essentially a torque command. An incremental encoder, such as an optical sensor, that provides a pulsed output at some multiple of mechanical rate could be used with proper conditioning to drive stator current. The conditioning would include angle interpolation and a sin $n\theta_m$ scaling and would require that the output be locked to a zero in BEMF. A block diagram of this system is in Fig. 8.

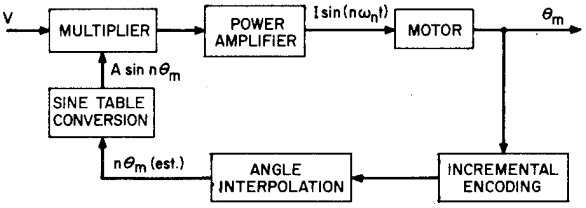


Fig. 8 Commutation With Incremental Encoding

A resolver with a two phase excitation provides a somewhat different measure of rotor position in the form A sin $(\omega_{ex}t+k\theta_m)$ where k is the resolver speed. The angle information can be extracted from this signal by sampling at a multiple of the excitation frequency. A convenient method of angle extraction is with a phase locked loop sampled at the excitation frequency. The extracted angle is then used in a manner similar to that in Fig. 8 to provide a stator excitation current. This complexity of this scheme is reduced if k is equal to n or integrally divisible by n.

For any of the commutation methods, there are many electronics methods for signal handling such as pulse position or amplitude multiplication instead of linear multiplication. It was not the intent of this summary, however, to provide a coverage of those techniques, but rather to provide an overview of brushless commutation techniques for D.C. motors. Basic angular sensing methods were developed along with the concept of optimum torque angle drive.

A final point is that when the R/L break frequency of the motor is sufficiently above the maximum expected stator excitation frequency ($n\omega_m$), a voltage source can replace the stator current source since negligible phase shift between stator current and voltage will be introduced because of the stator impedance.

COMPUTERIZED DESIGN OF ROTATING MACHINES FOR FLYWHEEL APPLICATIONS

Background. Generally, the design of electric machines for specialized applications has been achieved by "cut and try" methods. The designer, aiming at a design which will meet specific requirements, bases his initial design on past experience, analyzes the performance of the initial design and makes changes iteratively until the specifications are satisfied. This approach becomes very difficult for flywheel applications because of the unusual design considerations.

Although digital computers have been employed for many years in the area of electrical-machine design with few exceptions these computers have been used for design analysis. Design analysis represents the determination of the performance of a device, given the designer's estimate of the various independent parameters. The designer could then modify his estimates in the light of the calculated performance. The program being developed at the Draper Laboratory differs from this in that it would be capable of design synthesis. In design synthesis the machine parameters are determined from the performance requirements utilizing non-linear programming techniques and a detailed machine model. In most cases performance requirements will not uniquely specify a machine design. In these cases non-linear programming techniques may be applied to the machine model in order to synthesize an optimum design. An optimum design is one where some figure of merit is maximized or minimized; typical figures of merit would include torque/weight, efficiency, material cost, etc.

The computer approach to be followed makes it possible to meet unusual performance requirements, where experienced

designers have great difficulty using more conventional methods. Whenever a design does not meet all the requirements, the computer itself can find out what corrective action is to be taken, without this specifically being built into the program.

The Model for the Rotary Machine. Many different parameters: geometrical, magnetic, mechanical, electrical outputs, etc. are necessary to describe the machine. Most of these parameters, because of their definition and the nature of the machine, are interrelated, and therefore, cannot be treated as independent quantities. Others are completely specified from the outset according to the characteristics desired of the machine. Finally, some restrictions have to be imposed so as not to violate physical limits, such as stress, thermal, and magnetic saturation, that would prevent acceptable machine performance.

All these internal relations, specifications and constraints are written in the form of mathematical equations in terms of the basic parameters defining the machine. These equations are catalogued according to their origin, as geometrical, electrical, magnetic, thermal, mechanical and specified inputs.

Solution of Equation Set. Most of the equations describing the system are non-linear so that conventional methods for solving systems of linear equations cannot be used. The most suitable approach seems to be the use of the multidimensional form of the Newton-Raphson equations coupled with successive numerical iterations. Initial guesses are made for all the unknown parameters. Reasonable estimates result in a realizable system otherwise an iterative procedure results. Since the system of Newton-Raphson equations is linear, every numerical iteration requires the solution of a linear system of equations, which is done in a straight-forward manner.

In the optimization phase of the problem the task is to obtain a design having a minimum figure of merit. For this study the term "figure of merit" is defined as the nearness of a design to an optimum feature, like minimum material cost, minimum weight or maximum efficiency. Optimization in the design of electrical machines has been approached as a problem in non-linear programming. The prescribed figure of merit of the machine is minimized subject to constraints like temperature rise, mechanical stresses, efficiency.

CONCLUSIONS

This paper has covered several areas of research associated with flywheel energy conversion systems that are currently in process at the Draper Laboratory. From these studies, the Laboratory believes that the most difficult technological problem associated with the use of flywheels is the development of light-weight, low cost electrical conversion systems with particular emphasis on low cost. Special consideration must be given to the conversion systems for use with flywheels in vehicle applications because of the characteristic power and energy requirements of these applications. Although some research has been funded in this area, it is our impression that no consensus exists among the major sponsoring agencies regarding the need for research in this area. The Draper Laboratory feels that it is essential to the success of the Flywheel Program that research on systems of advanced machines and converters be expanded significantly.

"AN ULTRA-WIDE SPEED RANGE HIGH EFFICIENCY HYDRAULIC PUMP/MOTOR POWER TRANSMISSION"

Robert C. Clerk
Research Consultant
20 Whitehill Road
Whitehill Industrial Estate
Glenrothes, Fife
Scotland

ABSTRACT

Hydrostatic power transmission has been disadvantaged until now by unacceptable noise, high relative cost, poor part-load efficiencies, low power/weight ratio, and bulky control ancillaries. Eight years of fundamental research and composite development covering fourteen problem areas primarily to achieve characteristics complementary to an energy storage flywheel have resulted in a hydraulic pump and identical motor of unusual capability, performance, ease of manufacture, and above all, controllability by virtue of a modular, programmable, hydro-computing element, inserted within the pump/motor casing, and replacing all the usual control impedimentia, excepting the operators command transmitter. Extremely low zero-load running losses, in continuous 200% overspeed operation, advantage applicability to flywheel energy systems as does its reciprocal capability as a motor which will accept hydraulic power and transmute it into rotary flywheel energy or which will serve as vehicle wheel-driving motor offering real time individual wheelslip control whether accelerating or being used as a hydraulic retarder. It can operate entirely without bulky and costly ancillary equipments such as pressure relief valves, filters, heat exchangers and system control valves. Its power rating can be stretched almost 100%, its operating speed range 300% and its life expectancy 1200% without production change other than materials specification. Yet perhaps its most outstanding characteristic is its simple smoothly modulated instantly responsive control.

PREFACE

In another paper[1] presented in this symposium, we have discussed a high energy accumulator in which a storage flywheel is associated with a specially developed pump. But although the accumulator is a complete product in its own right, it is only half the story in any application of flywheel energy to a vehicle or other mechanism which might be powered by rotary motor output. This paper describes development of the special characteristics necessary to achieve functioning and performance complementary to storage flywheel operation and to application in a vehicle as automatic power transmission which with the power unit or units and controls form an integrated propulsion system.

THE COMMISSIONAL BRIEF

As no hydraulic power pump existed, or was in prospect, which could in any way operate in function complementary to a storage flywheel, a specification was drawn up of indispensable and expedient characteristics which appeared feasible and could serve as a commissional brief.

What was required was a vertical axis variable pump having the following characteristics:

(1) consistent operation within the 200% overspeed range above rated power speed at rated power or less.
(2) ultra-low rotation drag loss in zero-load running at 200% overspeed or less.
(3) mechanically and hydraulically quiet running and pulseless intake and delivery
(4) high mechnical and hydraulic power transmutation efficiencies whether pumping or motoring.
(5) as a motor,displacement must go over-center for reverse driving.
(6) wholly internal all-hydraulic control system with data processing capability which will operate in harmony with other similarly equipped elements of a complex, as an intigrated system exercising perfect

control modulation and response.
(7) optinum commonality between pumps, motors and pump/motors, vertical or horizontal axes, and right or left handed rotation.
(8) high power/weight and power/bulk ratios.
(9) low cost per horsepower rated thruput or per torque unit.
(10) minimal or zero dependence on external ancilleries; e.g. circulation filters, pressure relief valves, oil heat exchangers, actuators, etc.
(11) simple installation; all hydraulic connections into manifold facing on pump (top) end opposite driving end. Driveshaft to be only mechanical connection. Smooth exterior devoid of screws and flanges.
(12) pump/motor to be stretchable in power rating and/or life expectancy merely by changing materials and treatments of basic design.
(13) eschewing empirical factors, design principles to be based on logical variation of accepted engineering practices, so reducing development costs of a range or family of pumps and motors.

Unfortunately no established hydraulics manufacturer would accept what they considered to be an "impossible" commission, so it landed back in our own project office.

HISTORICAL RESEARCH

Unfortunately one must pass over the capable work of Thoma and Hele-Shaw and go back to Williams-Janney, 1907, for logical precepts applied to a ported axial pump, instead of a melange of inconsistent empirical factors.

Thoma's fixed displacement bent-axis pump is a real gem, but the variable displacement development is a real Rube, but no ruby. The Williams-Janney variable design, with no notable improvement, is still being manufactured for marine application, offering a dependability and reliability not found in modern slipper-pad pumps.

MARKET RESEARCH

Market research showed there was real need, outside of the low power bracket, for a pump embodying many of the characteristics in our commissional brief, but more importantly, automotive hydrostatic transmission was awaiting the viability of just such characteristics. This provided our first go-ahead decision point.

FEASIBILITY STUDY

This pinpointed the problem areas in which normal pump design was deficient, and the study areas for which classic engineering and commercial solutions had to be found. These were:

1) Compatible working fluids
2) Filtration - necessity or fetish?
3) Internal hydrodynamic "churning" losses
4) Manufacturing precisions and operating strain distortions. Rigidity or conformability
5) Transmission of driving torques from or to the mainshaft.
6) Transmission of driving thrust to and from the pistons.
7) Cylinder barrel: the costly heart of a pump.
8) Curbing fluid-shear losses at high rotational speeds.
9) Portface fluid-shear, flutter and port area control by clearance modulation.
10) Port-flow compatibilities.
11) Hydraulic decompression shock and mechanical noise.
12) Flow ripple and pressure pulsation.
13) Hydraulic data processing and actuating controls
14) Integration of problem solutions into a commercially acceptable composite adaptable to both high and low volume production techniques.
15) Elemental commonality and integration of complex systems.
16) Materials technology as affecting life expectancy and cost effectiveness.

RESEARCHED SOLUTIONS

Each of the above areas was exhaustively studied and the possible solutions short listed to those most suitable to production processes and communal integration.

COMPATIBLE WORKING FLUIDS

Hydrocarbon hydraulic oils are like a sponge, absorbing upwards of 8% air into solution at standard temperature and pressure, more at higher pressures, and will release this as discrete bubbles at any sudden pressure drop within the pump circulating system. This leads to premature cavitation and subsequent pressure hammer, both of which have destructive effect.

The working fluid should retain minimal discrete or dissolved gases and, needless to say, must also be non-corrosive and a reasonable lubricant; such as Losorb Silicone for atmospheric application or vacuum-stripped

Hydrocarbon for evacuated applications. An hermetic reservoir, circuits and sealed systems would be a distinct advantage. Surface dissipation should keep the reduced waste heat with 45° C above ambient.

FILTRATION

Axial piston pumps are notoriously sensitive to anything less than perfect filtration - some so sensitive that just breathing the word "grit" will cause them a seizure. I just am not a believer in hydraulic circuit full-flow filtration - suction or pressured. The one clogs, unless regularly serviced, with results which can be more disastrous than unfiltered flow; the other is too heavy, bulky and costly, yet never 100% safe.

The aim should be to design a pump or motor which will digest anything which will negotiate the induction and delivery passages and galleries without physically jamming up the works. The advanced pump under discussion must be so designed that by a change of material specification any (lack of) filtration requirement can be met. Sensitive flow impedences and bearing surfaces should be individually guarded by self-clearing porous elements.

INTERNAL CHURNING LOSSES

All pumps run with their casings full of oil (at least until my earlier published work seven years ago) in order to damp mechanical and hydraulic noises and to ensure adequate lubrication. Any internal ullage results in severe aeration and real trouble, but even with zero ullage hydrodynamic "churning" creates a resistance drag and heat problem.

The only answer, for a pump particularly, is to go "dry sump" and scavenge internal leakage oil as quickly as possible; or go further and evacuate the air/oil mist as well. At the speeds entertained for the energy storage application, oil churning would waste literally hundreds of horsepower as embarrassing heat. As regards the undamped mechanical noises, these must be eradicated at source.

PRECISIONS: RIGIDITY VS. CONFORMABILITY

Pump design is normally based on very precise relationships within a rigid structure. Unfortunately rigidity can never be absolute, depending upon the applied load relative to mass and modulus. Precision also is relative, and the closer it approaches absolute the more rapidly do manufacturing costs escalate according to inverse cube law.

By adopting the principle of flexible or articulated component inter-relationships in association with comformable structuring, the precision requirement and also the mass modulus (weight) requirement can both be reduced by an order of magnitude, particularly if the ancillary equipment items are designed as insertable modular sub-assemblies.

As example, if all the components connecting the upper casing assembly to the lower case assembly are articulated (e.g. ball ended connecting rods) this seeming extravagance will allow of very thin and flexible casing skirts which if compressively prestressed by end-to-end elastic tie-rods will be audio-frequency stiffened and otherwise competent so long as the displacement tilt-box is not gimbal-journalled in the casing skirt.

This applies to all component inter-relationships except the portface which in any event is at the inter -face between the only two deep sectioned masses, the cylinder block and the casing head. The cylinder sleeves float in the block, the short pistons in the sleeves, the con-rods in the pistons and to the swash-plate which floats in the tilt-box which floats on rockers in a rocker journal which floats in the lower half casing. The mainshaft also is spherically journalled in upper and lower casings and employs a floating link drive to the swash plate, so is free to bend or run misaligned without ill effect. As a result no spigot or dowel location or bolting flange is required at the inter-casing joint face, and casing skirt sectional thickness is foundry determined.

TRANSMISSION OF DRIVING TORQUE

In most axial pumps the drive from the mainshaft is through the attached cylinder barrel via the pistons, the cantilevered ends of which carry articulated slipper-pads which apply the loads to an angled swash-plate. Load reaction and friction, of that part of the piston remaining in the cylinder, is enormous. At high loads and swash angles the leveragefrictions and the bending of the pistons provide a definite limitation to torque and horsepower transmitted. What is more the cylinder barrel

is tipped over at the port-face causing wear at the contact edge and pressure leakage at the open edge.

Driving direct from the mainshaft to a tiltable rotating swash-plate overcomes all these deficiencies. Williams-Janney did it with double-Hooke's gimbal with limited angle of tilt, Hele-Shaw with spherical ball universal with torque Brinelling limitation. We opt for a spider-link universal Fig. 1 and Fig. 2, allowing not only high torque and large tilt angle but tying the swash-plate radially to the mainshaft yet allowing it free axial float and tilt

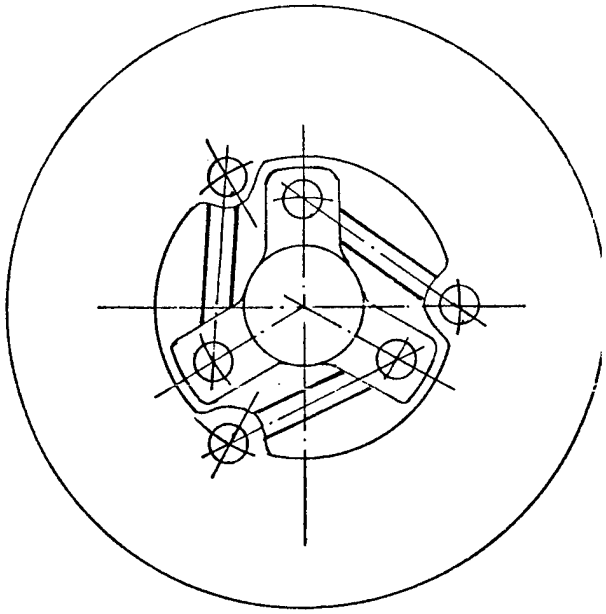


Fig. 1. Universal Spider Drive: open links.

But the piston pressure loads, acting on the tilted swash-plate, generate a combined lateral component, effective as torque at a mean 0.707 of active radius, whereas the entire lateral load must be located, in a slipper-pad pump by the shaft via the cylinder barrell and the extended pistons, in our case directly by the mainshaft which can bend to the strain without affecting the cylinder barrel in which is rotated in synchronism by three resilient fingers.

At large angles of tilt, the geometry corrections to improve compliance and life of the spherical link joints cause a slight epitrochoidal variation from true concentric rotation of the swashplate, but its only effect is the inertia harmonic transmitted by the "tight" links to the mainshaft.

The calculated efficiency loss of this universal drive was 0.75%; proved in tests as 0.86% using off-the-shelf Unibal joints instead of the intended Tungsten carbide/cast iron(molybdenum flashed) joints. These are a press/adhesive fit in the light alloy swashplate and in the cast lugs of the modular iron mainshaft, the drive pin through each joint ball being connected by a parallel pair of strain-compensating links to the complementary joint pin as a closed loop.

TRANSMISSION OF DRIVE THRUST

As there is no torque transmission between cylinder block and swashplate, the pistons can be short light-alloy die-castings Fig. 3 thrusting via ball ended connecting rods to the rotative swash-plate

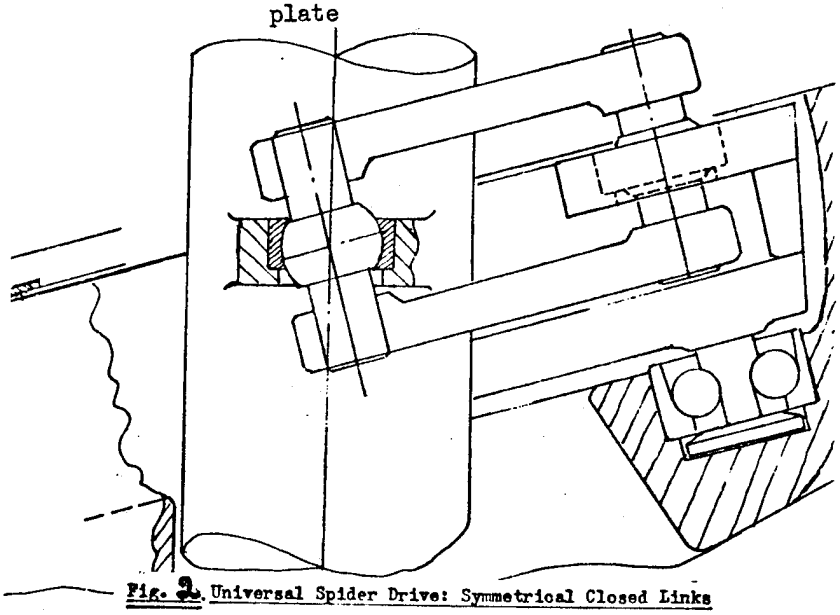


Fig. 2. Universal Spider Drive: Symmetrical Closed Links

The piston/con-rod compliance never exceeds 2° angle whereas the con-rod/swashplate compliance approximates to the tilt angle and is accommodated by standard Glacier DX cup and truncated cap lubricated and semi-floated by cylinder pressure transmitted via the drilled connecting rod.

The angle-contact paralleled thrust bearings shown in Fig. 2 have given way to an all-hydrostatic thrust pad arrangement which has the advantage of "floating" any tilt-box distortion and of being retractile to reduce shear-drag at low piston thrust loads. Thrust compliance and support efficiency losses amount to 0.65% using Carbon steel connecting rods, unplated.

The tilt-box is supported on a pair of rocker journals which are hydrostatically floated in a turret assembly Fig. 4 itself floated in the lower half casing so that it can be rotated the few degrees necessary for port-face control of decompression energy as later discussed. Tilt-box rocking actuation for displacement control is effected by a parallel pair of cylinder/piston /con-rod assemblies identical to the pumping assemblies but having the cylinders inserted in the upper casing.

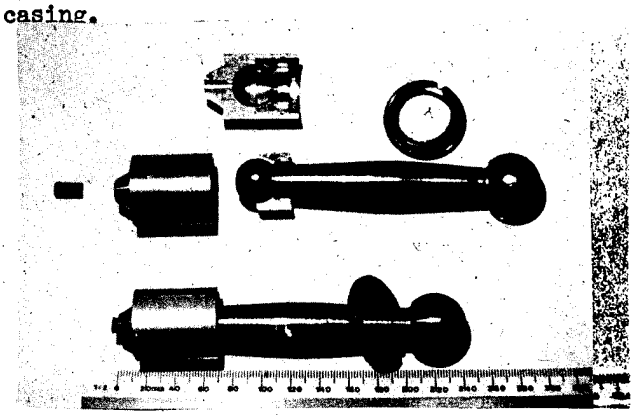


Fig. 3. Piston/Con-Rod Sub-Assembly.

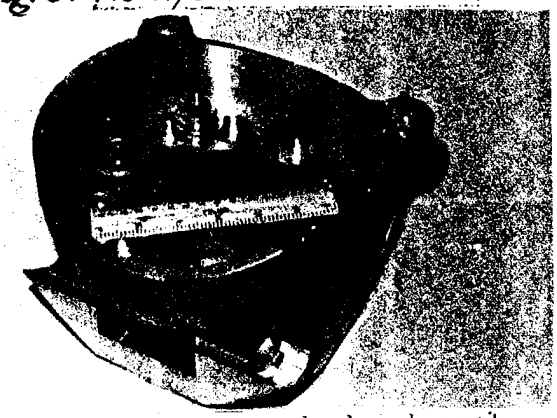


Fig. 4. Swash Carrier on Rocker Journal

CYLINDER BARREL

Normally the most expensive part of a pump, and having the highest reject percent scrap, whether the cylinders are honed in situ or pressed-in liners. The repeated hydraulic pressures and shock waves induce hoop strains which can lead to crazing and break up of the bore surface.

We have developed a fully-floating wet liner Fig. 5 which, being subject to the same pressures outside as inside, is always in some degree of compression. This allows a wide choice of tensile-sensitive fabricated cylinder liners, appropriate to life and application, e.g. ceramic or iron sinters, cast white irons, or low cost cold-extruded finished steel tubular sleeves.

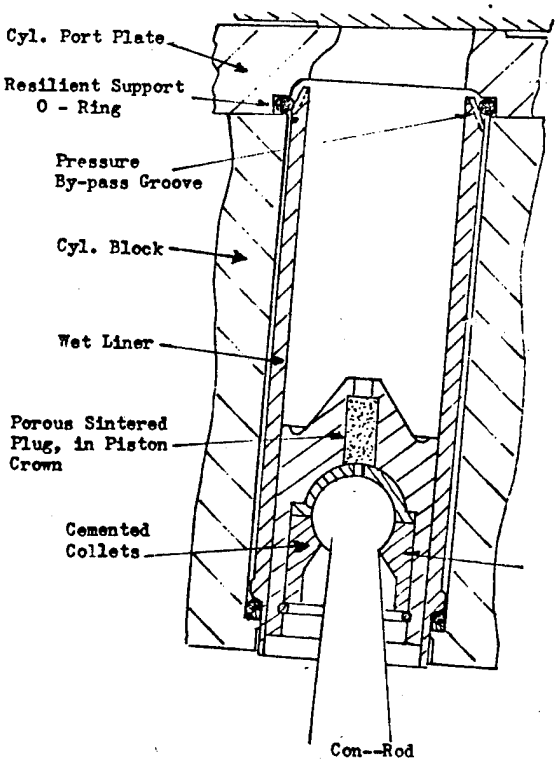


Fig.5. Floating Sleeve Cylinder

The "as-cast" cylinder barrel is assembled to the port-plate with the O-ring floated liners entrapped within the rough bores, and is located and secured by a circlip and a filler adhesive. The only metal removal would be on the dynamic balancing rig.

Apart from the production and life advantages, the pressure floated sleeves are perhaps more important operationally, as they are not subject to hoop strain expansion by the pressures within the cylinder and therefore to the clearance cubed leakage law. On the contrary they can be designed to close up under pressure so that leakage is neither pressure related nor a function of piston length.

Although the high-alumina ceramic sleeves, in association with plasma-sprayed hard coat pistons, were intended primarily for infinite life applications, their inertness to fire resistant or non-flam hydraulic fluids is opening up new avenues of application activity.

The $6\frac{1}{2}^{o}$ radial splay of the cylinder is a convenient way of accommodating the optinum portface diameter to the most effective swashplate socket-circle diameter for the connecting rods, but it has minor advantages in that the centrifugal component of the splay angle reduces piston pull-out forces and assists the fluid flow into the cylinders during the intake stroke.

CURBING FLUID SHEAR LOSSES

Having come to the conclusion that ball bearings were too noisy and put an effective limit on pump performance and therefore on rating "stretch", also that roller bearing though less noisy were at a disadvantage in overspeed running, it became necessary to find ways of reducing the film-shear drag of fluid film bearings and raising the frequency response without affecting the excellent noise damping characteristic.

Hydrodynamic bearings were found unsuitable in several areas, so hydrostatic bearings were chosen, and researched in great depth to minimise both shear and circulating eddy losses and to reduce the pressure-leakage power. Hydrostatic journal bearings posed a greater problem than thrust bearings and so were treated separately, but the biggest problem was the portface which being rateless would not respond to any direct application of the hydrostatic art.

Portface Shear Drag This is a function of shearing surface area of the sealing lands, the mean operating radius, differential surface speed, and the running clearance. Having optimised the portface dimensions, and being required to maintain the wide overspeed range, we could only work on the running clearance.

Portface Clearance Control At high pumping pressures, prevention of port-face leakage demand a close precise running clearance, allowing only sufficient leakage across the lands to flush away the shear heat-quite considerable for a largish pump running at really high revolutions. At lower pressures the same clearance would not allow enough flushing leakage to prevent a hot spot or worse, when running "free". We therefore contrived a floating counter-thrust arrangement Fig. 6 whereby the clearance varies inversely with pressure and in fact at very low pressures or "free" running, it opens a bit extra to reduce the shear loss to negligible proportions.

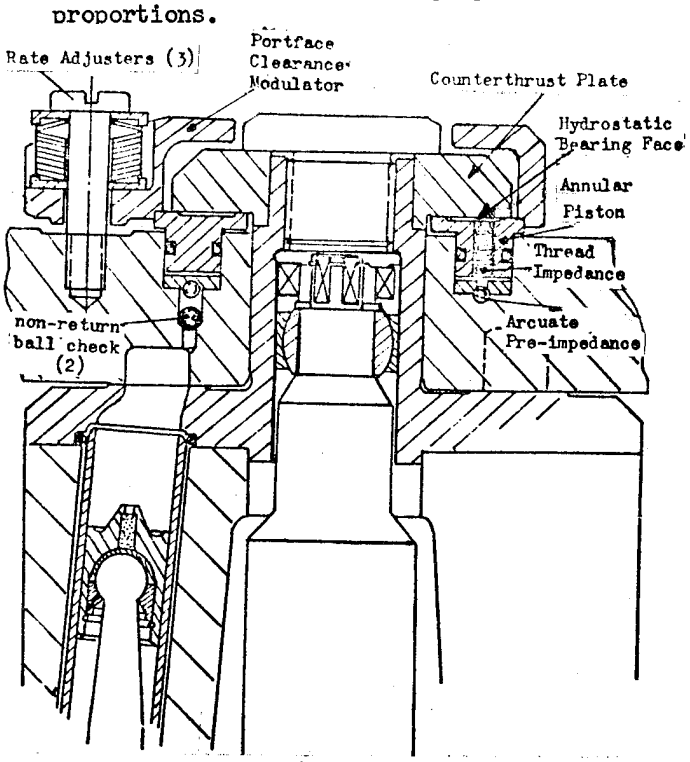


Fig.6. Port-Face Counterbalance and Clearance Modulation.

In any normal pump, the port sizes are very definitely limited by the hydraulic forces holding the port-face in balance. The contrived counter-thrust provides sufficient control over these forces to allow doubling or trebling the port areas as may be necessary to prevent induction cavitation at the flow rates consonant with a large power throughput.

Piston/cylinder Shear Drag As discussed earlier, the floating ambience cylinder sleeve allows an inversion of normal practice, in that we can start with a generous sliding clearance which closes up with pressure to reduce leakage and shear drag in a controlled manner.

Hydrostatic Thrust Bearings Primarily the portface counter-thrust and the swashplate thrust support bearing, which posed different problems. The former being a continuous annular arrangement was difficult in that it demanded 30 k Hertz response with minimal leakage from the working pressure bleed supply and was achieved by triple phased impedences with the float pressure taken after the first stage. This was so successful that a similar arrangement was adopted for the swashplate support bearing though initially this is fragmented into 10 floating circular pads, five on the intake semicircle and five on the delivery side, three on each side being retractile at low pressures to reduce no-load shear drag; but these will later be replaced by a pair of semicircular pads having lower overall drag.

Hydrostatic Journal Bearings

Primarily the portplate sleeve-shaft juxtaposed journal pair, and the mainshaft spherical main journal bearings, the shear drag of the former has been reduced mainly by tailoring the land running clearances inversely as and the land widths directly as the maximum operating pressure drop across the lands. The spherical main bearing Fig. 7 has been similarly treated but the greater diametral surface speed generated severe eddy current losses now controlled by chevron bar lands and recirculating perimeter channels. Each bearing has only three unequal pad areas as the loadings are unidirectional.

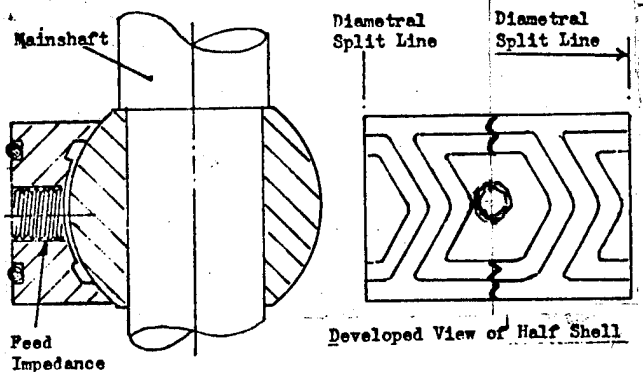
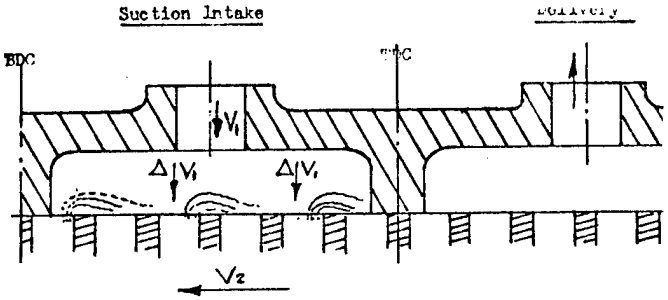


Fig.7. Spherical Hydrostatic Main Journal Bearing.

PORT-FLOW COMPATIBILITIES

Because the pistons induce axially, most other pump port galleries have axial entry. Unfortunately, in any pump and particularly in a high speed pump, the passing speed of the cylinder ports around the port-face Fig 8 can be a whole order of magnitude greater than the axial velocities, resulting in spill-wave formations which deflect, and can effectively choke, the axial flows into the following cylinder, causing disastrious cavitations.



Ratio $\frac{\text{Port Passing Velocity}}{\text{Diffused Intake Velocity}} \propto \frac{V_2}{\Delta V_1} = \frac{2\pi RN}{\Delta V_1} = 10\alpha \text{ @ } \phi$

ϕ = Swash Plate Angle Δ = Diffusion Factor

Fig.8. Spill Wave Formation Due To Velocity Mismatch

We have designed the portface with tangential inflows accelerated by a convergent gallery to the mean passing speed of the cylinder ports. Fig. 9

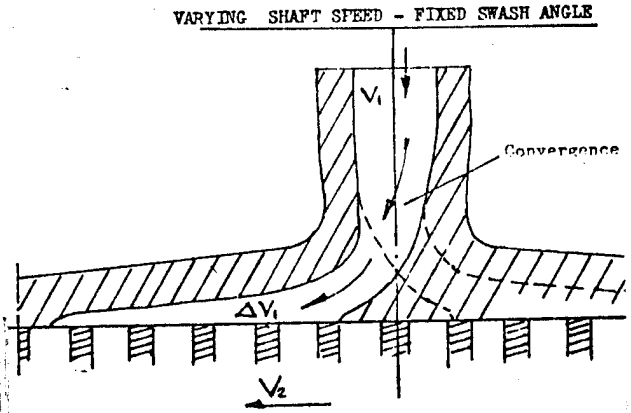
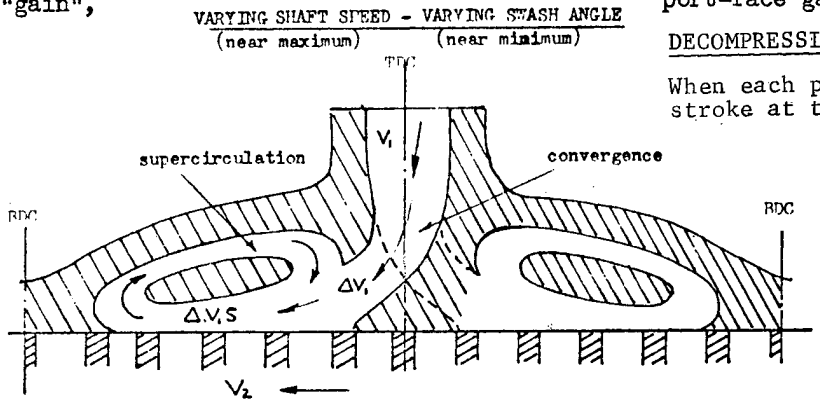


FIG 9 VELOCITY MATCH AT FIXED DISPLACEMENT AND CONVERGENCE

However, to cater for wide variation of flow at constant speed, or wide ranges of speed at constant flow, even this is not enough. It has been necessary to develop a portface with internal supercirculation, forced by the passing cylinder ports, and

amplified by a controlled vortex. Fig. 10 shows this for the overspeed case with positive supercirculation "gain",



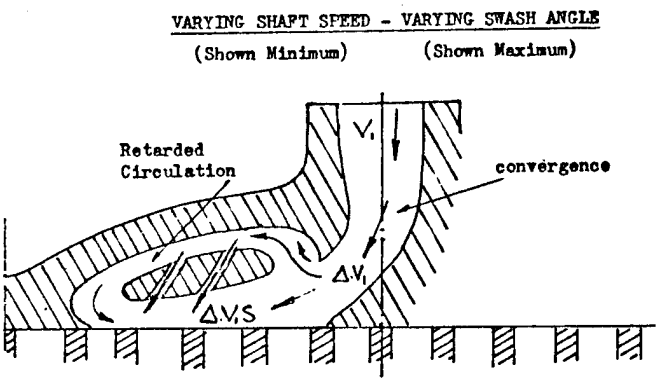
Δ = Venturi-Accelerated Flow Factor

S = Supercirculation Gain (Auto-Variable)

where $V_2 > \Delta V_1 S$

Fig.10. Velocity Match by Supercirculation at Low Angles

and Fig. 11 for under speed "negative gain".



i.e. Motor or 'FLYDRAULIC' Pump where $V_2 < \Delta V_1 S$

S = Retarded Circulation Factor (Auto Variable)

Fig.11. Velocity Match by Retarded Circulation at High Displacement Angles.

The internal profile has a self-polishing fluidized-bed deposited finish.

Radial Splay of Cylinder Port-tracts

Even with the large cylinder-ports, the acceleration of the oil into and through the port-tracts might need to be greater than can be effected by the residual absolute intake pressure. Splaying of the port-tracts provides a centrifugal component acting to accelerate the oil column in the port-tract, aided by the centrifugal pressure generated by the supercirculating flow in the arcuate port-face gallery.

DECOMPRESSION SHOCK AND NOISE:

When each piston completes its pumping stroke at top-dead-centre, and its cylinder port passes from the pressure portface, across the sealing land to the intake portface, the residual pocket of high pressure oil is released into the intake with a resounding shock-front which is difficult to control at differing flow rates and passing speeds. Conversely when passing across bottom dead centre the cylinder full of low pressure intake oil is suddenly in communication with the pressurised portface, and an even greater shock-wave will enter the cylinder, travel down it and hammer the piston and cylinder walls. This is the reason for the peculiar shape of the piston crown Fig. 3 adopted as a result of experience of high-energy-rate explosive forming.

A simple but effective way of dissipating this pent-up pressure energy is to "bleed" the dead-centre sealing land via a porous impedance which will allow fluid to pass, but not a shock-wave, so that there is no pressure differential when the cylinder port reaches the next portface area. Unfortunately the pent energy is wasted by this ploy.

A more efficient arrangement is to adjust the port-face timing so that opening to the next portface area is delayed beyond top dead centre until the piston has retreated (been forced back) until the compressed oil has expanded to intake pressure, or conversely delayed beyond bottom dead centre until the piston has advanced far enough to pre-compress the cylinderful of fluid to delivery pressure.

This has long been recognised as difficult of achievement, but is now effected quite simply by rotating the tilt-box rocker turret to the appropriate lag angle, automatically, manually or by preadjustment dependent upon application.

FLOW RIPPLE AND PRESSURE PULSATION

Every piston pump has a volumetric variation, dependent upon the number of cylinders and their displacement.

The result of this flow ripple in a "hard" hydraulic circuit (as distinct from a spongy one) is a pressure pulsation the amplitude of which increases with "hardness" to destructive proportions. Adding a small air/oil accumulator to the circuit will serve as a palliative up to choking frequency, a line-damper "accumulator" will raise the safe frequency of the closed system as a whole, though less so at the source point.

For frequencies of the order of 1500 pulse Hertz (9 cylinders at 10,000 RPM) it becomes obligatory to control the pulsations substantially at source point. Even less appreciated is the necessity to control the induced pulsations in the intake port as even a low amplitude can be the source point of suction cavitations. Fig. 12 shows the solution to the problem, incorporated in our new pump design, a modular air/oil pulse absorber, inserted into a cavity galleried with one port or the other and precharged to two thirds of the limiting pressure above and below ambient respectively.

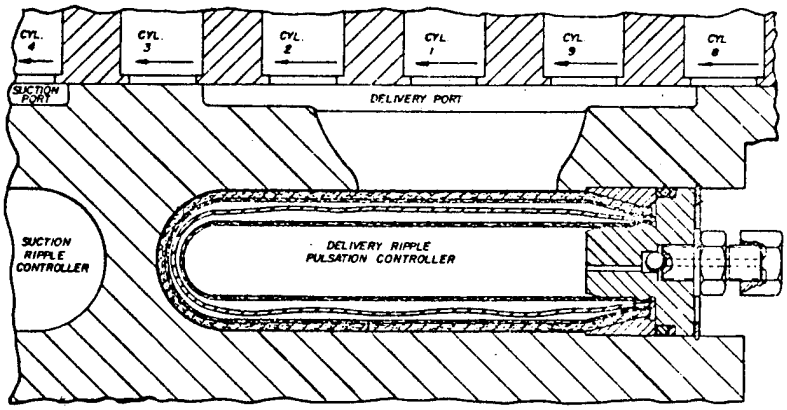


Fig.12. Delivery Ripple Pulsation Controller.

HYDRAULIC DATA COMPUTING CONTROL

Where one or more variable pumps is operating in association with one or morevariable hydraulic motors, the interrelationships can be quite complex, even for a simple duty cycle.

For complex operations the control system can be nightmare, like a well known hydrostatic transmission for light tractors, where the pump and motor are lost within a whelter of links, levers, cams, cranks, servos and other appendages.

We have developed a small computing valve module, Fig. 13 which is inserted into a cast pocket within the pump/motor unit, and serves to prescribe all the operational functions in relation to like-programmed computing valves inserted in the pumps or motors elsewhere in the system.

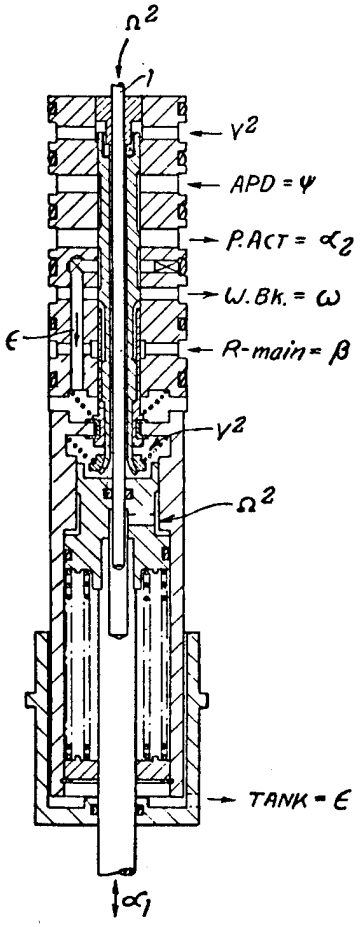


Fig. 13. COMPUTING CONTROLLER.

Except for the operators (driver's) pedal and lever control inputs Fig. 14 (which provide fluid pilot signals), there are NO mechanical appendages or interconnections in the system, only the minimum of data or pilot-line connections between the pre-designated master valve and the slaves. In fact, where there is only one slave unit and therefore no ambiguity this minimum can be zero - NONE.

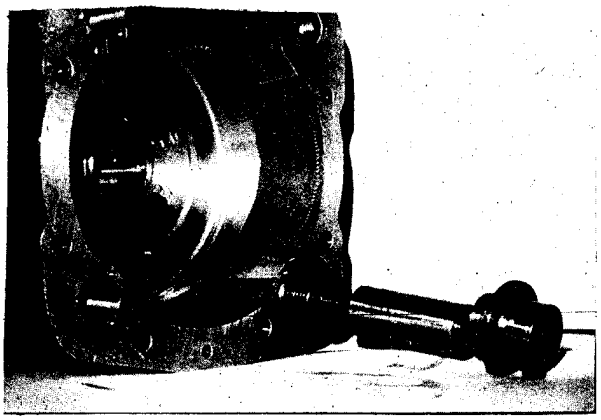


Fig.13a. Computing module being inserted into upper casing joint face.

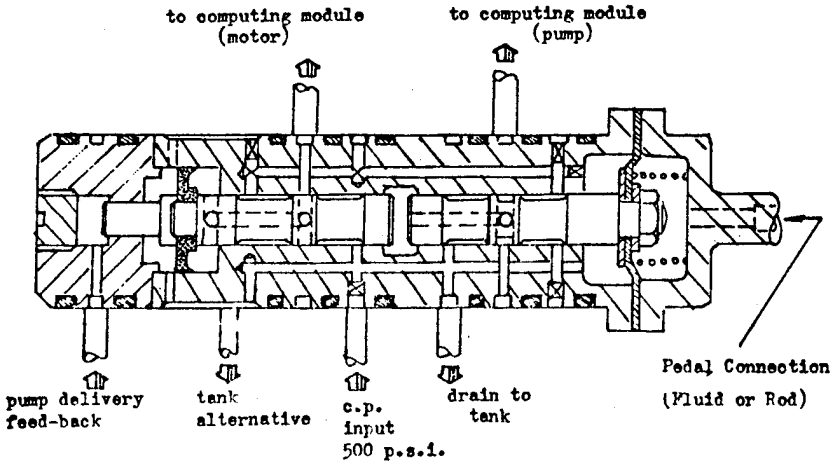


Fig. 14. Operator's Command Transducer.

This computing valve, with up to 8 input/outputs, can handle quite complex operational requirements. The most complex application so far considered is for a kinetic accumulator boosted vehicle transmission, where the master valve in the accumulator pump resolves and controls all but two of the 19 operational requirement functions, even including the mass energy summation equation; $K = mV^2 + I(\Omega_2^2 - \Omega_1^2) = (\text{Konstant})$ in the regenerative braking and charging modes. Except in "Neutral", it controls the vehicle engine absolutely, ensuring optimun b.m.e.p. in all regimes, and it provides instantaneous modulated response to operator demand, regardless of engine response characteristic. All this and much, much more, with a charming simplicity.

COMPOSITE DESIGN INTEGRATION

As each problem solution had been selected on a basis of interrelating compatibility, their integration into a composite design Fig. 15 did not prove difficult.

FIG. 15 A

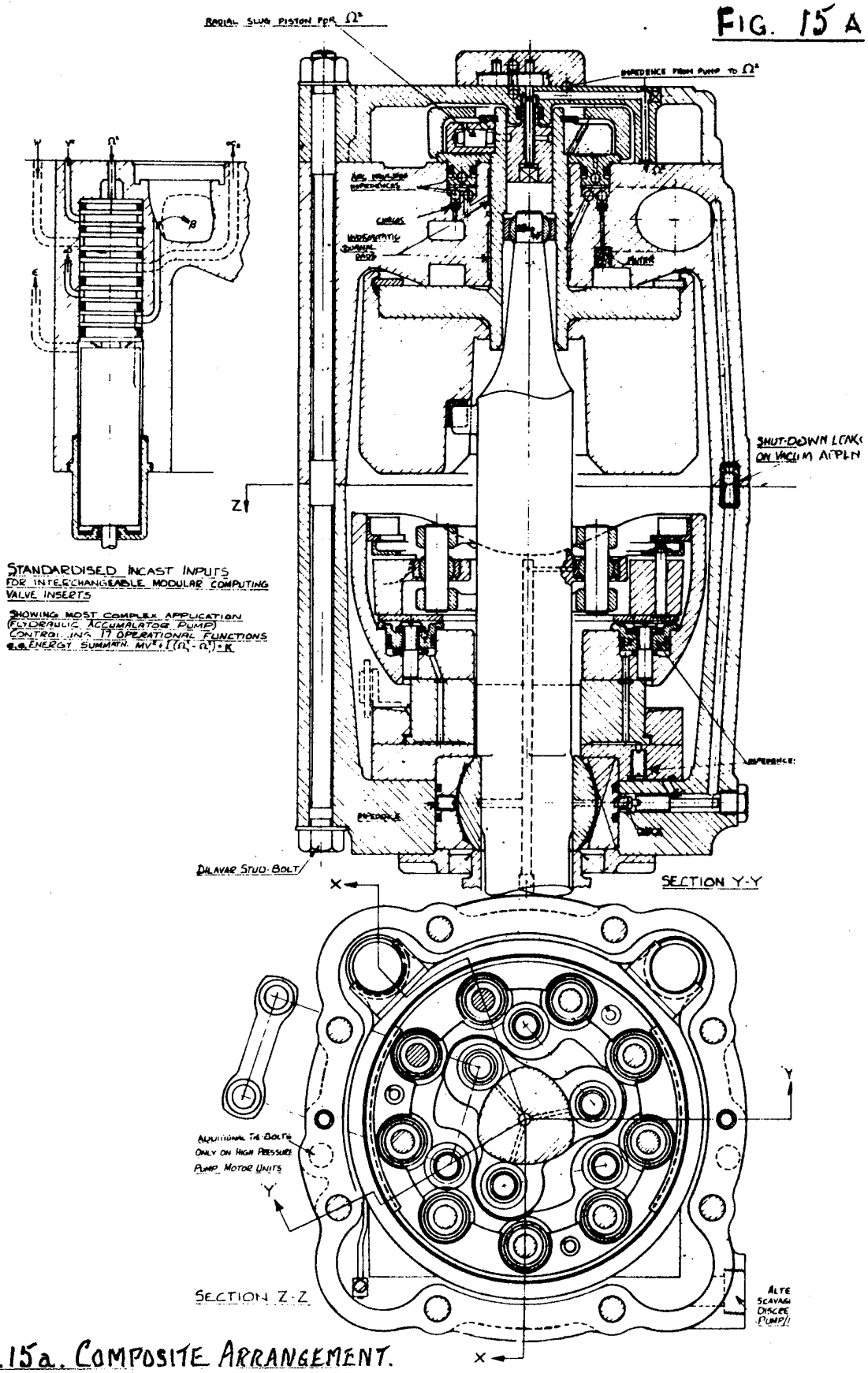


FIG. 15a. COMPOSITE ARRANGEMENT.

FIG. 15 B.

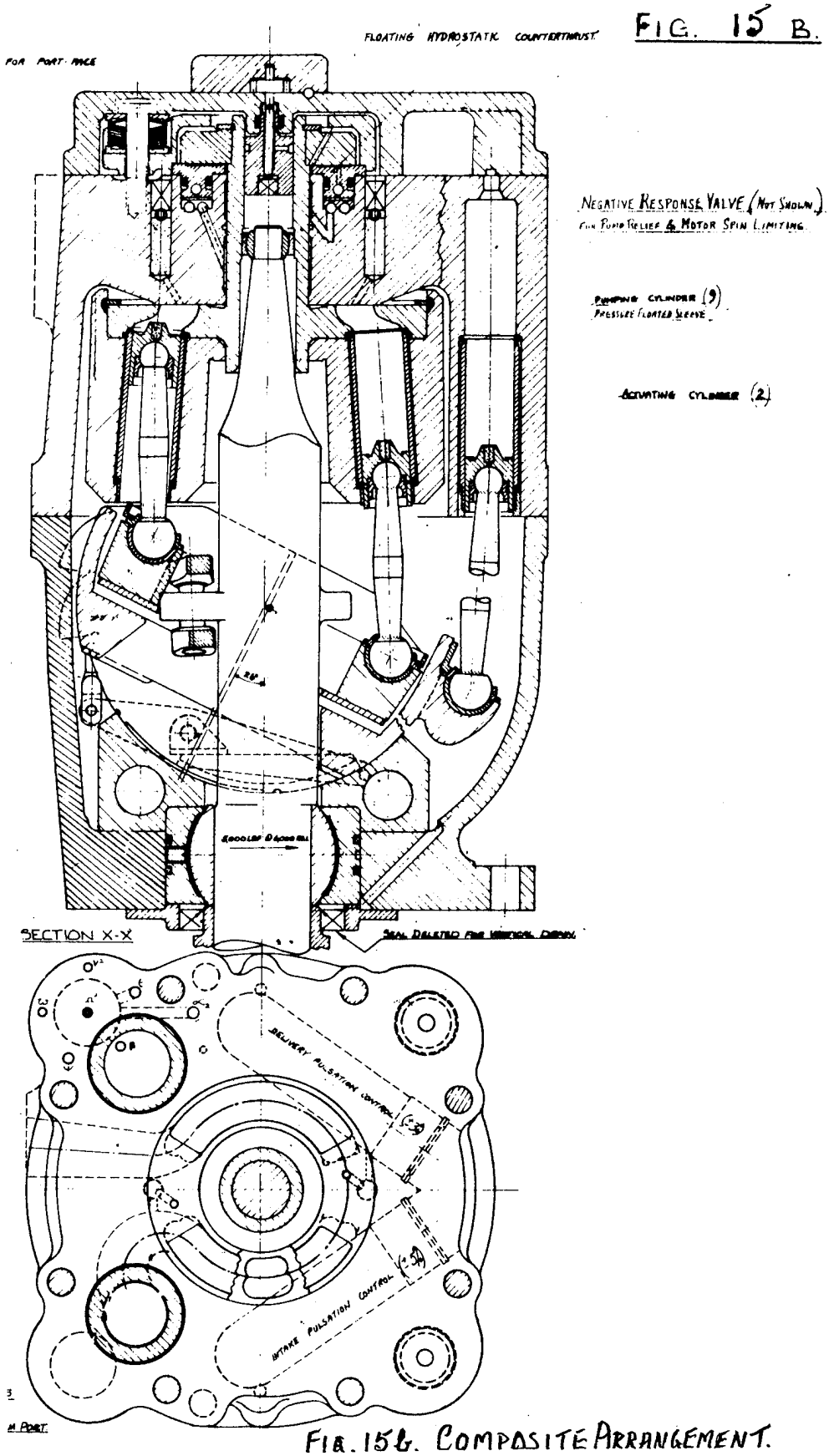


FIG. 15b. COMPOSITE ARRANGEMENT.

Of course they would not necessarily all be incorporated together, but it would perhaps be cost effective for the same production arrangement to allow this.

For example, the supercirculating intake gallery Fig. 16 has special relationships to flywheel systems, but equally a pump so equipped could be driven from a higher ancillary drive gear stage of a gas turbine; or directly by a high speed gasoline engine, merely by programming the hydro-computing insert to the appropriate speed and delivery parameters. Or the pulsation controllers may be an application luxury and the cavities plugged.

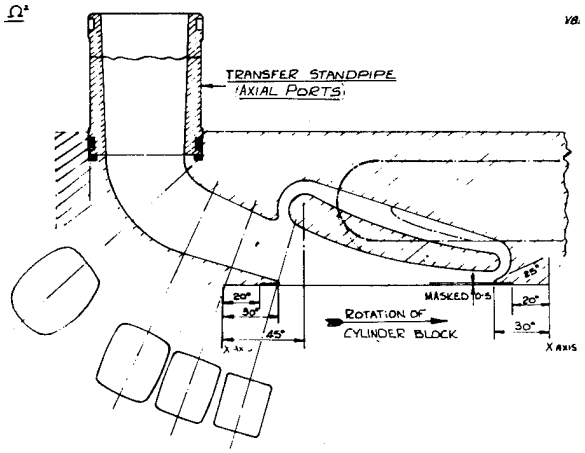


Fig. 16. DEVELOPMENT OF SUCTION PORT

Excepting the port galleries in the upper casing all casting dies (or alternative sand patterns) can be straight drawn and will accommodate alternative materials despite differing shrinkage, working stresses being calculated to the lowest factor. The lowest cost cylinder sleeves are from cold-extruded carbon steel tube, with bores unmachined but ballized, and cost a few cents each, whereas at the other extreme high-alumina sleeves cost a few dollars each, but well worth it for some applications. The lowest cost pistons are pressure die cast and pushed through a plain broach before anodizing, those at the other extreme are plasma sprayed complementary to the cylinder sleeves.

COMMONALITY IN COMPLEX SYSTEMS

Pumps and motors are identical except for the inserted hydrocomputing element which determines their characteristics and except for the priming mini-pump which is not always necessary. Handing, where necessary, if effected when machining the portface and by fitting a handed priming pump if required.

Every unit, pump or motor, generates a pressure signal varying the square of speed and this provides an element of data for computer processing. Another data element can signal displacement tilt angle. Modulation of return line pressure will provide further data which together with a common basic response to the system operating pressure provides identical-twin or family interrelationship between any number of units programmed to similar basics. Response can be immediate and sharp or allowed a fixed or proportioned time rise.

APPLYING MATERIALS TECHNOLOGY

Although this pump or motor is designed for low cost production in high or low volume, and the basically rated unit utilises low cost material for limited life requirement, we have established that it is generally more cost-effective to increase rated thruput and life by substituting better but more expensive materials treatments and finishes within the same design dimensions and on the same production and assembly tools and fixtures than to have to design develop, tool up and provide additional spares holdings for a larger size of pump or a more closely spaced range of pumps.

The basic "Lo" rated pump can be "stretched" to a "Normal" rating 40% higher, or further to "Hi" rating 80% to 90% higher; alternatively its operating overspeed range can be "stretched" to 200% higher, all with appropriate life ratings, by change of materials specification. For example, connecting rods can be carbon steel, plated Aluminium or Magnesium alloys, or Titanium alloy, depending upon operating pressures and overspeeds. Cylinder sleeve and piston alternatives have already been mentioned; as have casing materials which can be cast iron for underground application, high-damping bronze for undersea,

Aluminium for normal above ground use, or Magnesium for ultra-quiet or ultra-light special requirements, all from the same patterns or dies without shrinkage corrections. The port-tract supercirculating centerbody which complicates castings is being developed as an optional insert but we are researching a controlled vortex without centerbody, also a precast port-face and tract burnt into the light alloy casting.

MODERNISED ASSEMBLY METHODS

In this design, production screw threading has been generally tabooed, and fixings are by elastic tierods, self-loading bevel circlips and spring circlips, and interference or adhesive filled permanent fits: these may even be used in combination to provide "belt and braces" security; the adhesive located piston collets have a back-up wire circlip, and bevel circlip for a high frequency location has an adhesive security bond.

EXEMPLARY PUMP/MOTOR PERFORMANCE

A 25 mm bore 9 cylinder axial piston pump (or motor) having a displacement variable up to 16.8 cu. in. per revolution, scales 152 lbs with all ancillaries built in, and measures $10\frac{1}{2}$" x 11" x 18" overall excluding the driveshaft projection. In "Lo" rating it is controlled to a maximum delivery of 162 GPM (US) and 4400 p.s.i. (416HP) at 2500 RPM but may be programmed to give a higher pressure at commencement of delivery to a motor, allowing greater starting torque.

In "Normal" rating it is controlled to 195 GPM maximum and 5140 p.s.i. (570HP) at 2800 RPM and in "Hi" rating will deliver 216 GPM at 6100 p.s.i. and 3000 RPM or above. When being motored with zero delivery, the driving torque is only 1.03 lb. ft. at 2500 RPM and 1.43 lb. ft. at 3000 RPM rising to 4.2 lb. at 9000 RPM with heavy "Lo" rated internals at present state of development. Leakage (including lubrication) is 2.48 GPM at 4400 p.s.i. falling to 0.6 GPM at 1000 p.s.i. below which it remains constant. Mechanical efficiency of approximately 98% is suspect until our new back-to-back dynamometer is commissioned. Noise is entirely related to port timing adjustment which is not yet in automatic mode.

The pump features are protected by ten U.S. patents and the initial production range is exemplified in Table A.

TABLE A: INITIAL PUMP/MOTOR SIZE-RANGE

Coded Rating Cyls/Bore/ccpr/Duty	Dimensions (in. (B x W x L)	Weight lbs & Matl.	Displacement (cipr/ccpr)	Pressure (Op.psi)	Torque 100% (lbf. ft.)	R.P.M. (Rated)	G.P.M. (Rated)	Hyd.Output (Rated H.P.)
7/12/20/Norm.	$4\frac{1}{4}$" x $4\frac{1}{2}$" x $7\frac{1}{2}$"	10 Al.	1.22/20	5140	83	6000	31	92
9/12/27/Lo	$5\frac{1}{4}$" x $5\frac{1}{2}$" x $8\frac{3}{4}$"	32 C.I.	1.65/27	4400	96	5250	37	95
9/12/30/Norm.	$5\frac{1}{4}$" x $5\frac{1}{2}$" x $8\frac{3}{4}$"	17 Al.	1.83/30	5140	124	5750	45	135
9/12/33/Hi	$5\frac{1}{4}$" x $5\frac{1}{2}$" x $8\frac{3}{4}$"	12 Mg.	2.01/33	6100	162	6250	54	190
9/15/60/Norm.	$6\frac{1}{4}$" x $6\frac{1}{2}$" x $10\frac{3}{4}$"	33 Al.	3.66/60	5140	249	4600	72	210
9/18/100/Norm.	$7\frac{1}{2}$" x 8" x 13"	50 Al.	6.1/100	5140	415	4000	103	303
9/21/155/Norm.	$8\frac{3}{4}$" x $9\frac{1}{2}$" x 15"	90 Al.	9.5/155	5140	647	3300	133	392
9/25/250/Lo	$10\frac{1}{2}$" x 11" x 18"	280 C.I.	15.25/250	4400	888	2500	162	400
9/25/265/Norm.	$10\frac{1}{2}$" x 11" x 18"	152 Al.	16.35/265	5140	1115	2800	195	570
9/25/280/Hi	$10\frac{1}{2}$" x 11" x 18"	99 Mg.	17.0/280	6100	1375	3000	216	750
9/36/820/Norm.	15" x $15\frac{3}{4}$" x $25\frac{1}{2}$"	450 Al.	50/820	5140	3400	2000	425	1250
9/50/2130/Norm.	21" x 22" x 36"	1215 Al.	130/2130	5140	8850	1500	830	2440
9/60/3800/Mar.	$25\frac{1}{4}$" x $26\frac{1}{4}$" x 43"	2100 Al.	232/3800	5140	15800	875	717	2500
9/72/6600/Norm.	30" x $31\frac{1}{2}$" x 52"	3620 Al.	403/6600	5140	27400	1000	1709	5100
9/100/17200/Norm.	42" x 44" x 72"	9700 Al.	1050/17200	5140	71500	750	3360	10000

ROTOR DESIGN IMPLICATIONS FOR COMPOSITE MATERIAL PROPERTIES*

Richard H. Toland
Lawrence Livermore Laboratory, University of California
Livermore, California 94550

ABSTRACT

The role and needs of materials research and characterization are defined within the context of the rotor design and analysis process. In particular, we see that material/geometry tailoring permits design optimization, composites can be utilized most efficiently when fiber properties govern rotor performance and reliability, and time-dependent properties are essential for practical and reliable rotor design.

INTRODUCTION

It is of interest to step back from the details of specific rotor designs and reflect upon the general principals of flywheel rotor mechanics and their implications for composite materials usage and research needs. A good place to begin is the classical performance index for rotors made of homogeneous, isotropic materials. Here,

$$(KE/M) = C\ (\sigma/\rho)\ , \qquad (1)$$

where KE is the kinetic energy, M is mass, C is the shape factor, σ is a usable (allowable) strength, and ρ is the mass density. This is a convenient measure which appears trivial but is actually elegantly simple. The independent measures of geometry, C, and materials properties, σ/ρ, are noninteracting, allowing the designer to easily and independently compare different materials and designs, thus greatly facilitating design development. Examples of the shape factor, C, and the strength-to-density ratio, σ/ρ, are given in Fig. 1 and Table 1, respectively.

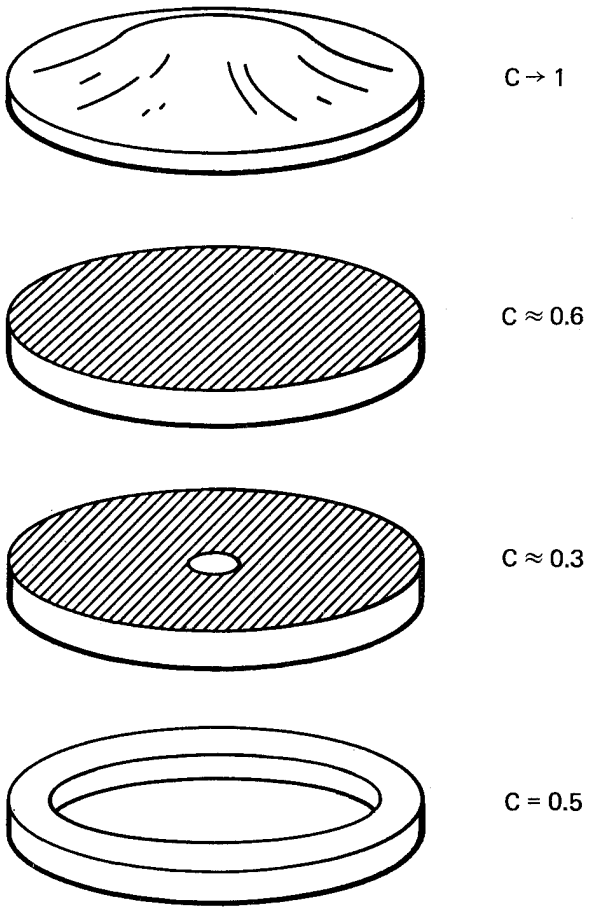


Fig. 1. Flywheel shapes and corresponding shape factor C.

A quick evaluation of the energy densities that are possible with rotors made of these materials reveals that little gain over battery performance is achieved. Instead, flywheel applications to date have been exploiting the significantly better power density. However, the question remains whether, when energy losses and system complexity are also integrated into the design, this mechanical energy storage device offers sufficient advantages over conventional batteries. The answer obviously depends on both the application and the near-future development of advanced flywheel technology. In the latter case, the use of advanced fiber composites in rotor construction offers the promise of major gains in rotor energy density. When their potential value to this application

*This work was performed under the auspices of the U.S. Department of Energy, under contract No. W-7405-Eng-48.

Table 1. Representative strength-to-density ratios for three metals.

Material	Usable strength, σ, MPa (ksi)	Strength/density, σ/ρ, MJ/kg (Wh/lb)
Steel	6.9 (100)	0.08 (10)
Aluminum	1.85 (27)	0.06 (7.5)
Titanium	3.45 (50)	0.07 (9)

is evaluated, these materials are compared on the basis of their strength-to-density ratios; however, only the strength of the unidirectional laminate in the fiber direction, S_1, is considered. Table 2 lists the representative static strengths, S_1, the energy density, $[0.5(S_1/\rho_c)]$, a range for material cost, and a representative cost per unit of energy. The potential of these materials for advanced flywheels is apparent. The E-glass/epoxy is cheapest in terms of cost per unit energy, whereas Kevlar/epoxy offers the highest performance.† While there is reason for optimism, we must recall that these materials have distinctive and more complex behavior including anisotropy and heterogeneity. We must consider that:

- When measuring rotor perrormance, the orthotropy in elastic moduli can introduce a strong coupling between geometry and material properties.
- Fiber composites have low strengths in failure modes which are not controlled bv the fiber properties.
- Time-dependent properties can be significantly different than the usually quoted static values.

†Reference to a company or product name does not imply approval or recommendation of the product by the University of California or the U.S. Department of Energy to the exclusion of others that may be suitable.

EVALUATION

Now we must ask, how can we evaluate the roles of geometry and materials as a measure of performance of composite rotors? One generalized performance index which recognizes the greater complexity of these materials and the rotors constructed from them is

$$(KE/M)_{max} = \min \left[C_i (K_{i_{min}} S_i/\rho_c) \right] , \qquad (2)$$

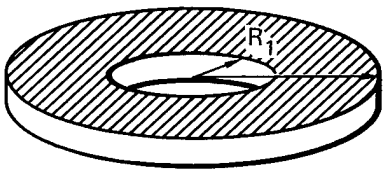
where i is the i^{th} failure mode for a given design concept, C_i is a shape factor, incorporating geometry, material orthotropy, type of fabrication, and type of failure mode, S_i is a base strength for the i^{th} failure mode, and K_i is the appropriate material "knockdown" factor which considers time-dependency and other possible service conditions. The expression in brackets is a string of numerical values, the smallest of which will be the maximum achievable energy density for that material system and design. The shape factor now permits coupling between materials properties and geometry; the allowable (or usable) strength is represented as $(K_{i_{min}} S_i)$ where K can be likened to a ratio between practical reality and unrestrained optimism. As an example, consider the class of rotor geometries defined by Fig. 2. For these systems we can define

$$(KE/M) = [(1 + b^2)/4]\omega^2 R_2^2 . \qquad (3)$$

To determine the maximum (KE/M) we must evaluate the system for maximum ω. The hoop and radial stresses are functions of r, b, n^2, and $\rho\omega^2 R_2^2$. Then we can evaluate their maximum values for given b and n^2 as

Table 2. Comparison of materials.

Material	S_1, MPa (ksi)	Specific gravity	$0.5(S_1/\rho c)$, MJ/kg (Wh/lb)	Unit cost, \$/kg (\$/lb)	Unit energy cost, \$/MJ (\$/kWh)
E-glass/epoxy	1100 (160)	2.1	0.26 (33)	1-5 (0.4-2.3)	3.9 (12)
S2-glass/epoxy	1750 (255)	2.0	0.44 (55)	3-10 (1.4-4.5)	6.8 (25)
Kevlar/epoxy	1800 (260)	1.35	0.67 (84)	13-25 (6-11)	19 (71)
HS graphite/epoxy	1800 (260)	1.6	0.56 (71)	28-55 (13-25)	50 (183)



$b = R_1/R_2$

$n^2 = E_\theta/E_r$

Fig. 2. Class of rotor geometries which includes thin rings, thick rings, and disks.

$$\sigma_{\theta_{MAX}} = C_\theta \rho \omega^2 R_2^2, \quad \sigma_{r_{MAX}} = C_r \rho \delta^2 R_2^2 , \qquad (4)$$

where C_θ and C_r are numerical values defined for each given case of b and n^2 to give the maximum stress in the rotor. Then

$$(KE/M)_{max} = \min \left\{ \left[(1 + b^2)/4C_\theta \right] (K_\theta S_\theta/\rho_c) , \right.$$

$$\left. \times \left[(1 + b^2)/4C_r \right] (K_r S_r/\rho_c) \right\} . \qquad (5)$$

The quantities $[(1 + b^2)/4C_\theta]$ and $[(1 + b^2)/4C_r]$ are the "shape" factors for the hoop and radial failure modes.

To examine these aspects of composite rotor design in light of the above example and to look for directions to materials development, we specifically consider material/geometry tailoring for high rotor performance, the role of matrix-controlled strengths in limiting design performance, and the effect of time-dependent properties on the usable energy density and the cost per unit of energy.

MATERIAL/GEOMETRY TAILORING

Consider a parametric study in which we evaluate C_θ for varying b and n. We find (Fig. 3) that a minimum value for C_θ can be obtained for each b, resulting in the maximum of $[(1 + b^2)/4C_\theta]$. Therefore, if the hoop strength controls rotor failure, optimal values of n exist which produce the maximum (KE/M) for given values of b. Interestingly, we find in these cases that $(KE/M)_{max}$ is approximately $[0.5(K_\theta S_\theta/\rho_c)]$ and that the hoop stress distribution is nearly constant with r (an optimal condition). It has been shown previously that $[0.5^+(S_1/\rho_c)]$ is the upper bound for the energy density of rotors made of anisotropic (composite) materials. (The plus recognizes a possible matrix contribution in some designs.) It is apparent now that material properties can be tailored (when

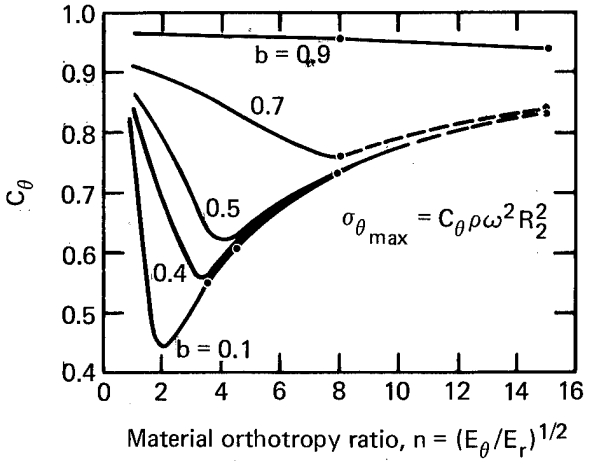


Fig. 3. Factor C_θ for maximum hoop stress as a function of material orthotropy n and geometry b.

possible) to achieve maximum rotor performance within this class. Alternately, Christensen and Wu discuss, in this proceedings, how the geometry can be tailored for a given material system to achieve maximum performance.

MATRIX-CONTROLLED COMPOSITE STRENGTH

We now consider the possible role of matrix-controlled composite strengths (transverse tensile strength) in limiting rotor performance. Continuing the previous parametric study by evaluating C_r for varying b and n, we find (Fig. 4) that significant radial stresses exist in the disks (b = 0.1) and thick rings (b = 0.7) which could potentially control rotor performance. Only in the thin ring (b > 0.9) do we find negligible radial stresses. Because we can tailor our material for optimal performance relative to S_θ, we

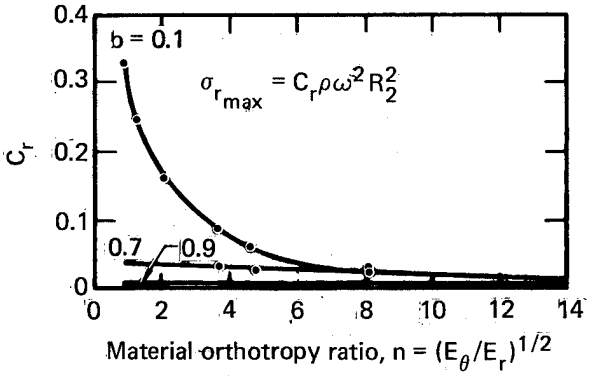


Fig. 4. Factor C_r for maximum radial stress as a function of material orthotropy n and geometry b.

Table 3. Transverse tensile strengths for composites.

Material	S_2, MPa (ksi)	b	C	S_r, MPa (ksi)	S_2/S_r
E-glass/epoxy	7.5 (1.1)	0.1	0.385	424 (61)	0.018
		0.7	0.04	44 (6.4)	0.17
S2-glass/epoxy	42.5 (6.2)	0.1	0.375	656 (95)	0.065
		0.7	0.04	70 (10.2)	0.62
Kevlar/epoxy	15 (2.2)	0.1	0.19	342 (50)	0.044
		0.7	0.038	68 (9.9)	0.22
HS graphite/epoxy	45 (6.5)	0.1	0.135	243 (35)	0.18
		0.7	0.036	65 (9.4)	0.69

wish to define the condition for which radial strength S_r does not limit performance. The condition for simultaneous failure in both hoop and radial modes can be defined by specifying a "breakeven" radial strength as

$$\bar{S}_r = \bar{C}\, S_\theta ,$$

where

$$\bar{C} = C_r/C_\theta .$$

To examine this condition relative to a specific situation, we consider the hoop-wound rotor which can have the geometry of a thin ring, a thick ring, or a disk. The relative ease of fabrication of this type of flywheel suggests possible low cost and high production rates. These rotors, however, must sustain the radial stresses in the matrix-dependent transverse tensile mode. Representative values of transverse tensile strength for the four previous material systems now must be compared to the S_r breakeven strength for b = 0.7 (thick ring) and b = 0.1 (disk) geometries (Table 3). None of these material systems possesses 20% of the required strength for the disk rotor. Even for the thick ring (b = 0.7), we cannot obtain more than 69% of the breakeven strength. The S2-glass and HS-graphite/epoxy come the closest. Thus, only the thin ring is a logical choice for hoop-wound construction at this point. By plotting C vs b for varying n (Fig. 5), we can better define the role of radial strength on rotor design and material construction.

For the material systems considered ($n \leq 4.5$), we see that hoop-wound construction is readily achieved for thin rings ($b > 0.9$), but a laminated construction appears to be necessary for disks ($b < 0.7$). The in-between ground ($0.7 < b < 0.9$) presently is not attractive for simple hoop-wound designs; however, the general class of "nested" rings (including the ballasted and multimaterial rings) seems promising. The multimaterial ring uses a high-stiffness outer ring and an inner ring of lower stiffness to achieve a significant reduction in the peak radial stress. Both Union Carbide/Oak Ridge and Sandia Laboratories have discussed such designs in this symposium.

We also can see from Figs. 4 and 5 that a higher orthotropy ratio n^2 or a lower radial modulus (transverse modulus of hoop wound rotor) would reduce the required radial breakeven strength. However, several problems confront this approach. First, from a design standpoint for disks (b = 0.1) with a lower radial modulus, the optimal material orthotropy ratio for hoop-controlled rotor performance is no longer obtainable. However for the thick ring (where b = 0.7), this does appear to be a

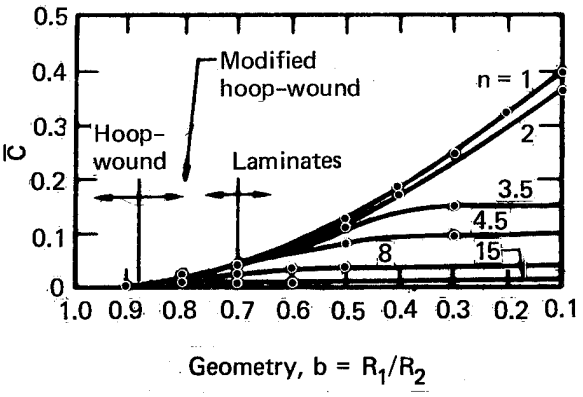


Fig. 5. Parameter $\bar{C}$ (equal to C_r/C_θ) used to evaluate the hoop and radial breakeven condition as a function of material orthotropy n and geometry b.

reasonable approach. Second, material systems with low transverse moduli suffer significant reductions in the longitudinal strength S_1, the prime motivator for composites. In addition, a reduction in the transverse modulus must be accompanied by increases in total elongation in this mode. We can estimate this by defining

$$\bar{e}_r = n^2 \bar{C} e_\theta \ . \qquad (6)$$

From Fig. 5, we see that transverse tensile strains approximately twice that of the fiber strain at failure are required for breakeven. This is not possible with any engineering material system available. At this point, we must conclude that designs where matrix properties control rotor performance will be limited to below the potential of the fiber.

TIME-DEPENDENCY OF COMPOSITE PROPERTIES

While we have emphasized performance in rotor design, successful applications of these energy storage systems require that the emphasis be shared with design practicality and reliability. Thus, the definition of the time-dependent properties of composites is necessary for developing reliable rotors. Because the data required for this purpose have not yet been generated, we can obtain an estimate by adjusting the material strengths to reflect the effects of cyclic fatigue and stress-rupture. In effect, we attempt to design a rotor to a specified minimum life.

Table 4 provides the "knockdown" factors for fiber-controlled and transverse tensile strength. Admittedly, these are engineering "judgement" values, based on available stress-rupture and fatigue data. A minimum 10-year and 500,000-cycle lifetime is assumed and $K1_{min}$ is taken as the minimum of two values for the above conditions. The selection of K_2 is based on an estimate of the time-dependent "endurance limit" of the epoxy matrix properties of the composite, using epoxy adhesive and composite creep data. It is evident that fibers must control not only the performance aspects of rotor design but also the reliability. Thus we must define reasonable time-dependent allowable strengths.

Table 4. Time-dependent "knockdown" factors.

Material	$K_{1_{min}}$	K_2
E-glass/epoxy	0.3	0.25 → 0.33
S2-glass/epoxy	0.4	for all materials
Kevlar/epoxy	0.55	
HS graphite/epoxy	0.75	

It also is of interest to compare materials on both the short-term and long-term basis for fiber- and matrix-controlled designs (Table 5). The effect of time dependency clearly suggests that graphite/epoxy should be considered as a prime material candidate, especially if the fiber cost drops below $10/lb as projected. Also, S2-glass is a reasonable candidate on a cost per unit performance basis.

Table 5. Materials comparison for short- and long-term use.

	Short term	Long term	
Material	$[0.5(S_1/\rho_c)]$,[a] MJ/kg (Wh/lb)	$[0.5(K_1S_1/\rho_c)]$,[a] MJ/kg (Wh/lb)	$[(1+b^2)/4C_r](K_2S_2/\rho_c)$,[b] MJ/kg (Wh/lb)
E-glass/epoxy	0.26 (32.8)	0.08 (10.1)	0.01 (1.3)
S2-glass/epoxy	0.44 (55.4)	0.175 (22.0)	0.075 (9.5)
Kevlar/epoxy	0.67 (84.4)	0.36 (45.3)	0.04 (5.0)
HS graphite/epoxy	0.56 (70.6)	0.42 (52.9)	0.12 (15.1)

[a] Replace the 0.5 factor with 0.42 for the b = 0.7 case.

[b] Here, b = 0.7.

EPOXY MATRICES FOR FILAMENT-WOUND FLYWHEELS*

J. A. Rinde, E. T. Mones, and T. T, Chiao

Lawrence Livermore Laboratory, University of California
Livermore, California 94550

ABSTRACT

Epoxies are popular as matrix materials for composite flywheels. Depending on the design, the required matrix properties may differ greatly. In this study, we recommend a moderate-temperature-curable epoxy as well as a rubberized, high-temperature-resistant epoxy to meet specific requirements for composite flywheels. In addition, preliminary data on flexible long-elongation epoxies for flywheel applications are not encouraging.

INTRODUCTION

Epoxies, because of their high performance, have been the key matrix materials for filament-wound composite flywheels. Present promising flywheel designs essentially fall into three types: (1) hoop-wound thin rims (either single or multirims) with an inside-to-outside radius ratio of about 0.9; (2) thick-rims or versions of spoke-rim designs with a radius ratio around 0.7; and (3) solid disk designs, either hoop-wound or laminated. Depending on the design and the fiber selected, the required matrix properties are different. As shown in Fig. 1, the demands placed on the matrix of a thin-rim composite flywheel are not very severe. The only critical property required for the matrix here is temperature resistance at the operating conditions. For a hoop-wound, thick-rim aramid fiber/epoxy flywheel, however, additional critical properties are required of the matrix, including a low-temperature cure to reduce fabrication stresses and a high transverse composite strength and strain to prevent delamination failure. In addition, there are other flywheel designs for which engineers request flexible or rubber-like epoxies. Thus, to satisfy the various design philosophies without necessarily endorsing any particular design, the LLL study of epoxy resins has concentrated on three areas: (1) a moderate-temperature-curable epoxy formulation; (2) a rubberized high-temperature-resistant epoxy formulation; and (3) flexible (low modulus) and high-elongation epoxy formulations.

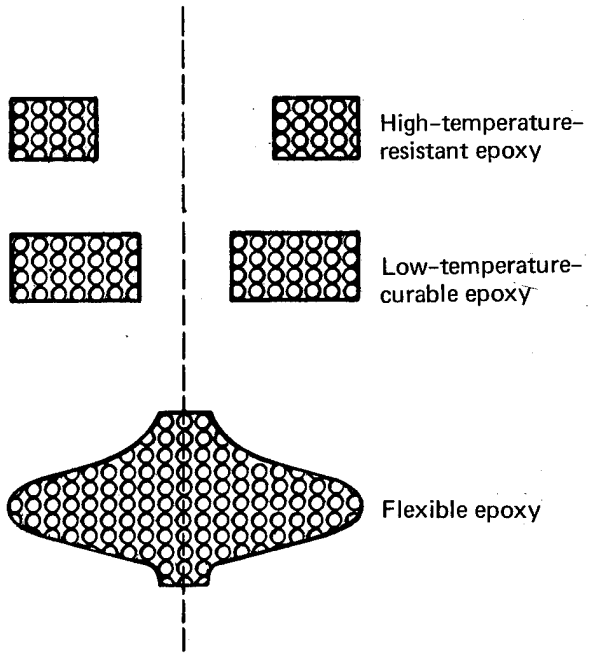


Fig. 1. Diagram of fiber-epoxy resin arrangements for different flywheel designs.

MODERATE-TEMPERATURE-CURABLE EPOXY FORMULATION

The main use for a moderate-temperature-curable epoxy resin system is in very large flywheels that might be fabricated in the field. This epoxy formulation also can be used for small thick-rim flywheels which may delaminate during a high-temperature

*This work was performed under the auspices of the U.S. Department of Energy under Contract No. W-7405-Eng-48.

cure due to high residue composite stresses. Our recommended formulation[1] is 100 parts (by weight) DER 332 (Dow Chemical) and 45 parts Jeffamine T-403 (Jefferson Chemical).† The system is gelled at room temperature and cured for 16 h at 60°C. The advantages of this system include low composite residue stresses, reasonable mechanical properties, a large available data base, and suitability for on-site fabrication. However, this moderate-temperature-curable system does have two major drawbacks: it has a low service temperature range (65 to 80°C) and has a low composite transverse strain (ε = 0.1 to 0.16%) to failure.

RUBBERIZED HIGH-TEMPERATURE-RESISTANT EPOXY FORMULATION

Depending on the air pressure in a flywheel containment chamber, the operating temperature of a flywheel may exceed 70°C. For this reason, the epoxy matrix used for flywheel must be resistant to high temperatures. Recent research work on the fracture mechanics of epoxies has indicated that a rubberized epoxy could substantially improve the fracture resistance of epoxy resins. Work on simple hoop-wound flywheels also qualitatively verified the benefit of the rubberized epoxy matrix in the composite. Therefore, we recommend the following rubberized epoxy formulation: 100 parts XD 7575.03 (Dow Chemical), 65 parts XD 7114 (Dow Chemical), and 35 parts Tonox 60-40 (UniRoyal), cured for 4.5 h at 60°C plus 3 h at 130°C. The tensile stress-strain curves of this epoxy and the moderate-temperature-curable epoxy are compared in Fig. 2. Note that the high elongation at maximum stress is approximately 6% for the rubberized formulation. Additional unique features of this epoxy include high fracture resistance, high service temperature (105°C), ease of processing (800 cps, 29.3-h pot life), and good modulus (377 ksi). Scanning electron microscope pictures of the cured rubberized epoxy confirmed expectations that the material has two phases: rubber and epoxy. We are continuing our study of this epoxy formulation in an attempt to realize its full potential.

†Reference to a company or product name does not imply approval or recommendation of the product by the University of California or the U.S. Department of Energy to the exclusion of others that may be suitable.

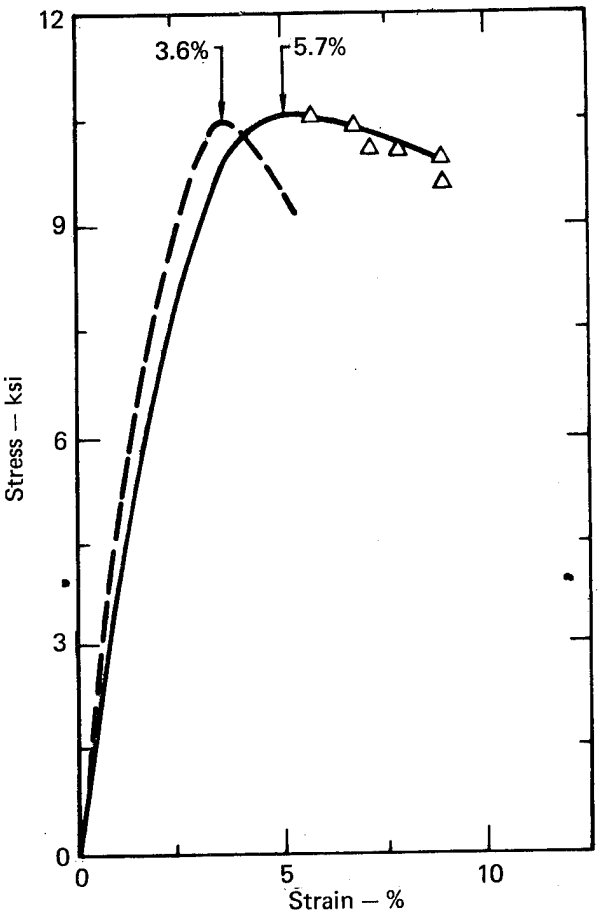


Fig. 2. Comparison of stress-strain curves for the moderate-temperature-curable epoxy (dashed curve) and the rubberized, high-temperature-resistant epoxy (solid curve).

FLEXIBLE EPOXIES

Our work on flexible epoxies[2] covers three groups: (1) epoxies with relatively high tensile strength and low elongation to failure (see Fig. 3); (2) epoxies with moderate strength and moderate elongation (see Fig. 4); and (3) rubber-like materials with low strength and high elongation (see Fig. 5). To verify the utility value of the flexible resin concept in fiber composites, we selected four resin systems from the three groups, prepared simple S2-glass/epoxy composites, and measured the composite transverse properties. This work is reported in more detail in these proceedings by R. M. Christensen. From the practical point of view, preliminary data on flexible epoxies do not seem to offer any obvious unique advantages for composite flywheel designs.

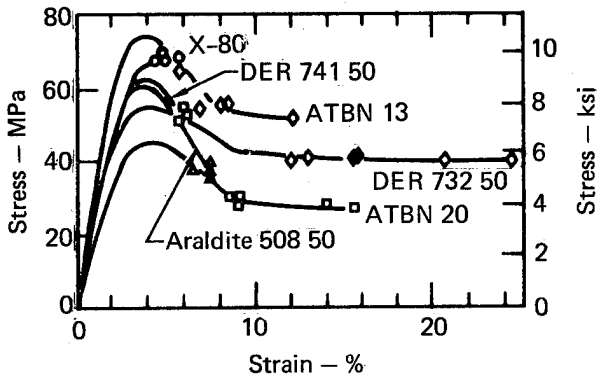


Fig. 3. Tensile stress-strain curves for epoxies with relatively high strength and low elongation.

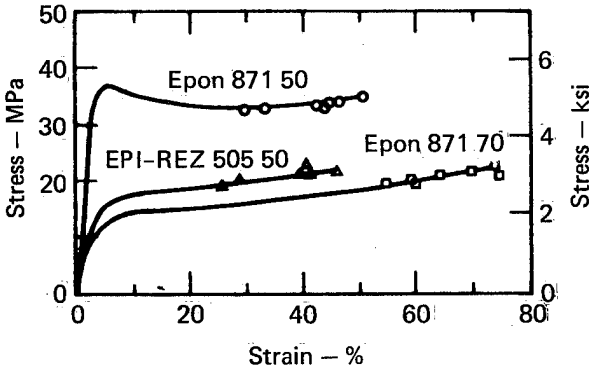


Fig. 4. Tensile stress-strain curves for epoxies with intermediate strength and high elongations.

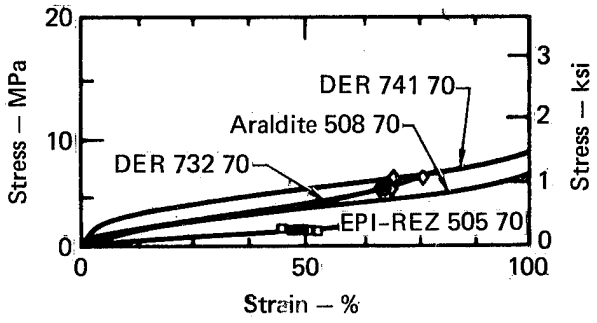


Fig. 5. Tensile stress-strain curves for epoxies with low strength and high elongation.

REFERENCES

1. T. T. Chiao and R. L. Moore, "A Room-Temperature-Curable Epoxy for Advanced Fiber Composites," in Proc. 29th Annual Technical Conference, SPI (Washington D.C., February 5-7, 1974).

2. J. A. Rinde, E. T. Mones, and H. A. Newey, "Flexible Epoxies for Wet Filament Winding," in Proc. 32nd Annual Conference, SPI (Washington D.C., February 8-11, 1977).

TRANSVERSE TENSILE CHARACTERISTICS OF FIBER COMPOSITES USING FLEXIBLE RESINS*

R. M. Christensen, J. A. Rinde, and E. T. Mones

Lawrence Livermore Laboratory, University of California
Livermore, California 94550

ABSTRACT

Fiber composite structures are often designed and fabricated using a laminate construction built by stacking individual lamina at various angles. When testing such laminates to failure, it typically is found that resin failure occurs before fiber failure. The reason for this is quite obvious; for an individual lamina in a state of transverse tension, the presence of the fiber phase causes a stress/strain concentration effect which induces premature failure of the resin phase. An appealingly simple means to prevent premature resin failure has been suggested. This method is to employ a flexible resin in the composite that can withstand the high local elongations caused by the strain concentration effect. Although this remedy has been widely discussed, there has been little quantitative data available to support the thesis. However, we have recently obtained specific data which will now be described.

In a state of transverse tension and in the case of rigid fibers at a volume concentration of two-thirds, the corresponding strain concentration factor has been shown to be very nearly ten. One implication of this phenomenon is that a lamina in a state of transverse tension is expected to fail at a strain ten times lower than that of the neat resin. This hypothesis assumes that there is no change in the mode of failure. To verify the hypothesis, several flexible resins have been tested. Figure 1 shows the stress-strain characteristics of the four resins whose composition is shown in Table 1. The corresponding composite transverse tension test results are shown in Fig. 2. In all cases, the composite fails at a lower strain level than was predicted by the simple factor-of-ten scaling. It should be noted, however, that the increasingly flexible resins do indeed give increased elongation at failure in the composite, although not as much as is expected from the strain concentration rationale.

The reason for the inability of the strain concentration factor to accurately predict the composite failure level appears to be related to change in the mode of failure between the neat resin and the composite. There seems to be a brittle failure mode in the composite whereas the failure mode in the resin is of a more ductile type. The mechanism of brittle fracture in composites employing flexible resins is now being investigated to verify the governing mechanism. Next, following the brittle failure mechanism rationale, further flexible resins will be examined in an attempt to obtain a further increase in elongation at failure. Also, the effect of flexible resins on other composite properties must be investigated.

At this point, the preliminary results indicate that the use of flexible resins, although simple in concept, involves complicated behavioral aspects in composite form. The performance of composites using the flexible resins tested to date does not warrent immediate application in laminate flywheels.

This report is abstracted from work in progress: completed study will be submitted for formal journal publication.

*Work performed under auspices of U,S. Department of Energy, under contract No, W-7405-Eng-48.

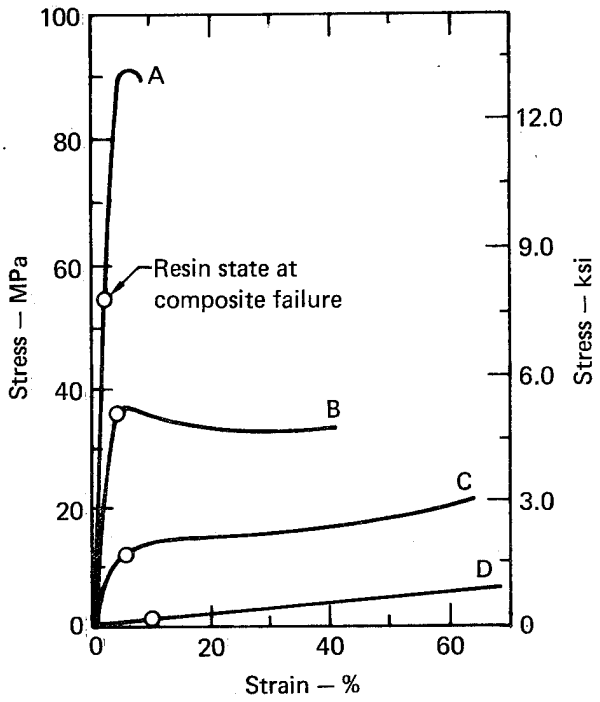


Fig. 1. Transverse tensile stress-strain curves for the four resins (composition of the resins is listed in Table 1).

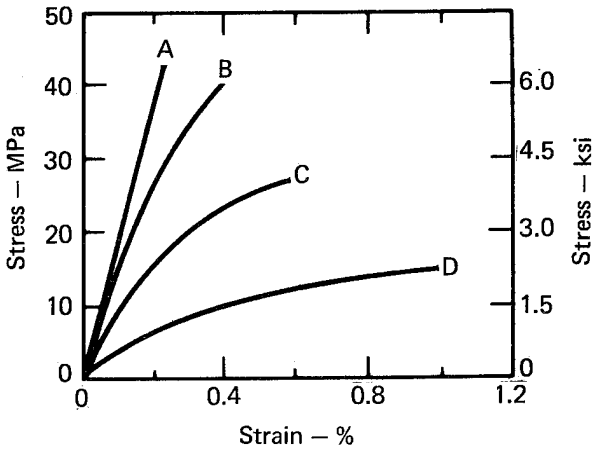


Fig. 2. Transverse tensile stress-strain curves for the composites made from the flexible resins (composition of the resins is listed in Table 1).

Table 1. Resin system components.[a]

Resin	Components	Ratio
A	XD 7818[b]/XD 7114[b]/Tonox 60-40[c]	100/30/30.7
B	Epon 871[d]/XD 7818/XD 7114/Tonox 60-40	50/30/20/16.4
C	Epon 871/XD 7818/XD 7114/Tonox 60-40	70/20/10/13.3
D	DER 732[b]/XD 7818/Tonox 60-40	70/30/15.0

[a]References to a company or product name does not imply approval or recommendation of the product by the University of California or the U.S. Energy Research and Development Administration to the exclusion of others that may be suitable.

[b]Dow Chemical Company.

[c]UniRoyal Chemical Company.

[d]Shell Chemical Company.

COMPARATIVE PROPERTIES OF FIBER COMPOSITES FOR ENERGY-STORAGE FLYWHEELS. PART A: EVALUATION OF FIBERS FOR FLYWHEEL ROTORS*

Lynn S. Penn
Lawrence Livermore Laboratory, University of California
Livermore, California 94550

ABSTRACT

Four fiber-composite systems (Kevlar 49/epoxy, Kevlar 29/epoxy, S2-glass/epoxy, and E-glass/epoxy) were studied for use in flywheel rotors. We compared not only the performance of the materials, but also the relationship of the results of conventional tests (e.g., NOL ring hydroburst) to the results of flywheel rotor spin tests. We found that the relatively inexpensive hydroburst test gives failure stress results statistically identical to those obtained from the costly spin tests. Thus, at a given fiber volume, NOL ring burst data can be used to predict rotor performance. A comparison of materials performance revealed that in terms of energy storage potential, the Kevlar 49/epoxy composite ranks highest, but in terms of energy storage per unit cost, E-glass/epoxy is best.

INTRODUCTION

A study of four fiber-composite systems for use in flywheels (Kevlar 49/epoxy, Kevlar 29/epoxy, S2-glass/epoxy, and E-glass/epoxy†) has been carried out. We at LLL wish not only to compare the performance of the materials but also to obtain the relationship between results of conventional tests on composite materials and flywheel rotor spin tests. Establishing such a relationship would permit the use of conventional materials tests in place of spin tests to screen fibers and composites for flywheel applications. For each material, we carried out strand-tensile tests, NOL ring hydroburst, thin-rim rotor hydroburst, and thin-rim rotor spin. All of these test configurations presumably evaluate the longitudinal tensile strength of the fiber composite.

Table 1 identifies the fibers used and gives their densities, numbers of filaments per strand, and cost. All specimens were filament-wound and impregnated with DER 322 (Dow Chemical) epoxy resin cured with Jeffamine T-403 (Jefferson Chemical). The composites were cured 16 h at 35° plus 4 h at 80°C. Strands and NOL rings of several different fiber volume fractions were prepared for test. Because of their considerable expense, the composite rotor specimens were fabricated at a single fiber content rather than over a range.

Table 1. Fiber information.

Fiber	Density, Mg/m^3	Filaments/ strand	Current cost, $/lb
Kevlar 49 (DuPont)	1.45	1000	8.50
Kevlar 29 (DuPont)	1.44	1000	8.00
E-glass type 30 (Owens-Corning Fiberglas)	2.57	2052	0.40
S2-glass, 20-end roving (Owens-Corning Fiberglas)	2.43	4080	2.00

*This work was performed under the auspices of the U.S. Department of Energy, under contract No. W-7405-Eng-48.

†Reference to a company or product name does not imply approval or recommendation of the product by the University of California or the U. S. Department of Energy to the exclusion of others that may be suitable.

EXPERIMENTAL PRODCEDURE

Hydroburst tests of both NOL rings and rotors were done using hydrostatic pressure. In the pressuring chamber, the seal between the fluid and the ring was formed with an elastomeric ring of square cross section. Strain gages on the NOL rings showed that there was no undesirable bending moment on the specimens during pressurization.

For spin tests, the rotors were mounted on the spiked hub shown in Fig. 1. The rotors were slightly deformed into a square shape for mounting. The rotors had inside diameters of nominally 407 mm, varying from 400 to 408 mm, depending on the fiber used. The slight diameter differences originate from the radial growth differences of each material due to different moduli under the stress of a spin test. A starting diameter was chosen for each rotor such that at its failure speed, the rotor would grow into a circular shape and yet still fit the hub. The wall thickness of the rotors was about 25 mm in all cases. The rotors were spun to failure in a vacuum chamber. Burst could be detected audibly and by changes in rotor speed, chamber pressure, shaft motion, and chamber temperature.

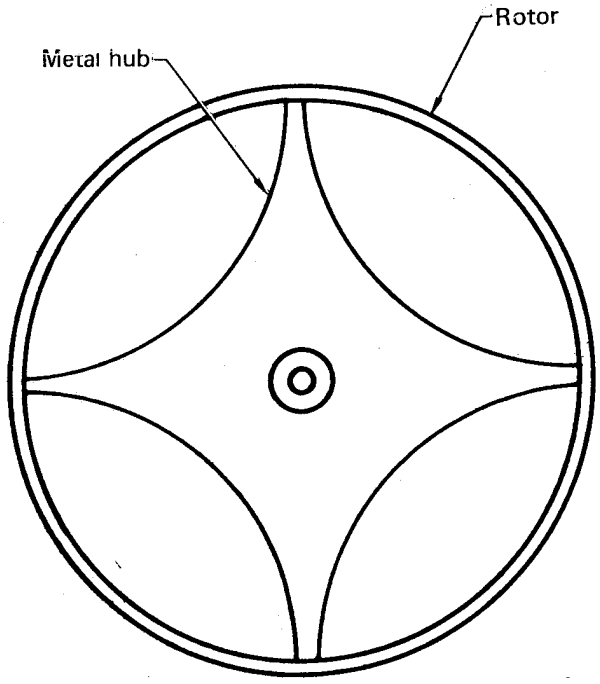


Fig. 1. Hub and rotor assembly.

RESULTS

The results of strand tensile tests, obtained on a universal testing machine, are shown in Fig. 2. There is an optimum in composite performance between 60 and 75 vol% fiber. When these results are presented as fiber stress (Fig. 3), not composite stress, they reveal that the fiber itself does not give its best performance when the composite is low in resin. This indicates that increasing the fiber volume beyond 75% may not necessarily result in the increase in composite performance expected by many.

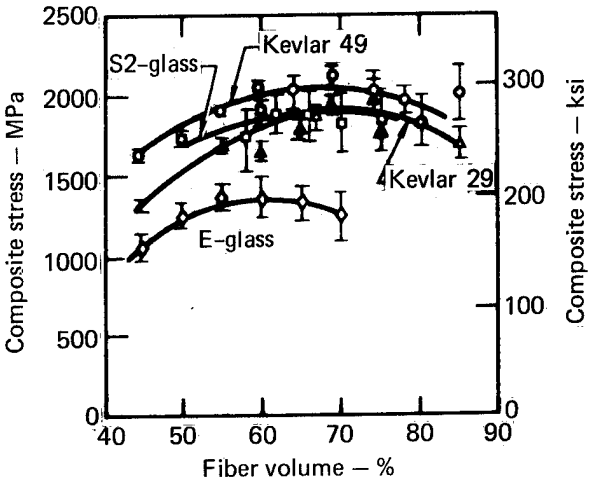


Fig. 2. Strand test results plotted as composite failure stress.

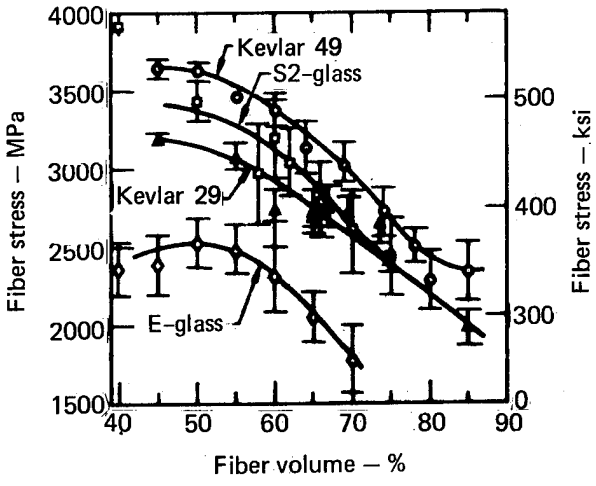


Fig. 3. Strand test results plotted as fiber failure stress.

Figures 4 and 5 show the NOL ring hydroburst test results, plotted as composite stress and fiber stress, respectively. In most cases, the NOL rings show lower failure stresses than do the strands. However, the rank order of the four fiber composites is the same in both tests.

Table 2 gives the hydroburst and spin test results for composite rotors. High speeds were achieved and the failure

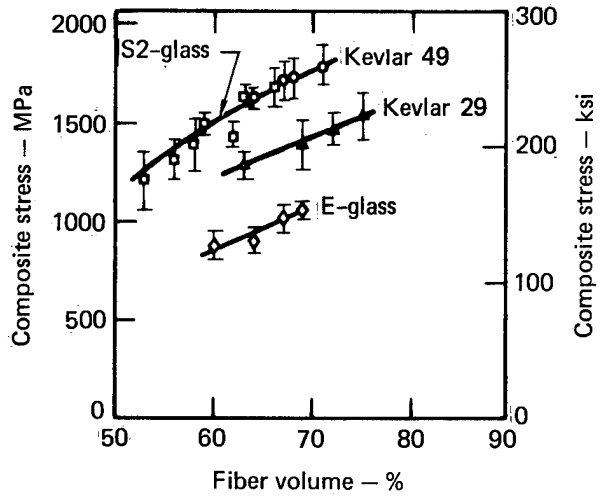


Fig. 4. NOL ring hydroburst test results plotted as composite failure stress.

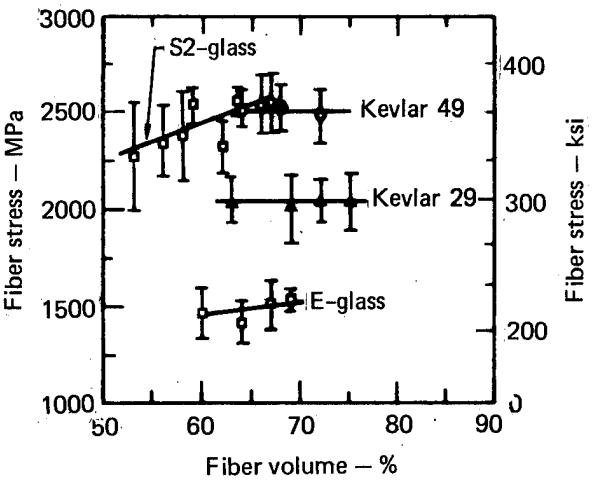


Fig. 5. NOL ring hydroburst test results plotted as fiber failure stress.

stresses in the spin tests are essentially the same as those in the hydroburst test. This means that the less expensive rotor hydroburst test can be used to determine failure stress in spin. Figure 6 shows the failed (pulverized) rotors from the spin tests. This pulverization during failure vividly demonstrates the increased safety of fiber composites over metal flywheels.

Comparison of the NOL ring hydroburst results with the rotor hydroburst and spin results shows that they are the same within one standard deviation, so long as the data from specimens of the same fiber volume are compared. Thus, this conventional laboratory test, i.e., the NOL ring burst, can serve as a good indicator of spin failure stress. Care must be taken, however, when using strand test data as a failure stress indicator because strands usually perform better than larger specimens. From Fig. 2 and Table 2, we see that a factor is required to relate strand data to rotor data; this factor may vary with fiber volume.

When a failure stress criterion alone is used to compare materials, Kevlar 49 and S2-glass composites rank the highest. Table 3, however, compares the materials on criteria more pertinent to flywheel applications: strength-to-density, energy density, and strength-to-density per unit cost. Thus, Kevlar 49/epoxy ranks highest in energy density but E-glass/epoxy ranks highest when cost is included.

CONCLUSION

In summary, we have shown that the relatively inexpensive hydroburst test gives failure stress results statistically the same as those obtained from the costly spin tests. Hydroburst results of NOL rings were in excellent agreement with rotor burst and spin test results. Thus, at a given fiber volume, NOL ring burst data can be used to predict rotor performance. Good performance was obtained in spin tests from all four materials and the pulverizing failure mode in spin was demonstrated. In terms of energy storage potential, Kevlar 49/epoxy ranks highest, but in terms of energy storage per unit cost, E-glass/epoxy is best.

Table 2. Test results for composite rotors.

Composite	Fiber volume, % (±1 std. dev.)	No. of Specimens	Composite failure stress, MPa[a,b]	C.V., %[c]	Fiber failure stress, MPa	C.V., %[c]	Initial modulus of elasticity, GPa[d]
Hydroburst Test							
Kevlar 49/ epoxy	71.3 ± 1.4	5	1810	5	2540	4	92.2
Kevlar 29/ epoxy	73.2 ± 0.9	5	1700	6	2320	6	50.8
S2-glass/ epoxy	70.4 ± 1.6	5	1810	4	2570	3	56.0
E-glass/ epoxy	74.1 ± 0.6	5	986	8	1330	9	51.2

Spin Test							Burst speed, rpm	C.V., %[c]
Kevlar 49/ epoxy	70.3 ± 1.5	5	1720	11	2450	12	51,100	6
Kevlar 29/ epoxy	73.0 ± 2.1	5	1540	12	2110	14	48,300	6
S2-glass/ epoxy	69.5 ± 1.1	5	1880	3	2710	4	43,600	0.2
E-glass/ epoxy	73.7 ± 1.4	5	1520	11	1520	12	32,400	6

[a] Composite stress calculated using stress = 8 × gage pressure/cross-sectional area.
[b] To convert from pascals to pounds per square inch, divide by 6.894×10^3.
[c] C.V. = coefficient of variation, std. dev./average × 100.
[d] Based on one sample.

Table 3. Energy density and cost of the fiber composite rotors.

Composite	$\frac{\text{Composite stress } (\sigma), \text{ MPa}}{\text{Composite density } (\rho), \text{ Mg/m}^3}$	Energy density, J/kg[a]	$\frac{\sigma/\rho}{\$}$
Kevlar 49/epoxy	$\frac{1720}{1.36} = 1260$	6.32×10^5	$\frac{1260}{6.25} = 202$
Kevlar 29/epoxy	$\frac{1540}{1.36} = 1130$	5.64×10^5	$\frac{1130}{2.46} = 459$
S2-glass/epoxy	$\frac{1880}{2.04} = 922$	4.60×10^5	$\frac{922}{1.35} = 683$
E-glass/epoxy	$\frac{1120}{2.19} = 511$	2.53×10^5	$\frac{511}{0.56} = 913$

[a] To convert to watt-hours per pound, multiply by 12.6×10^{-5}.

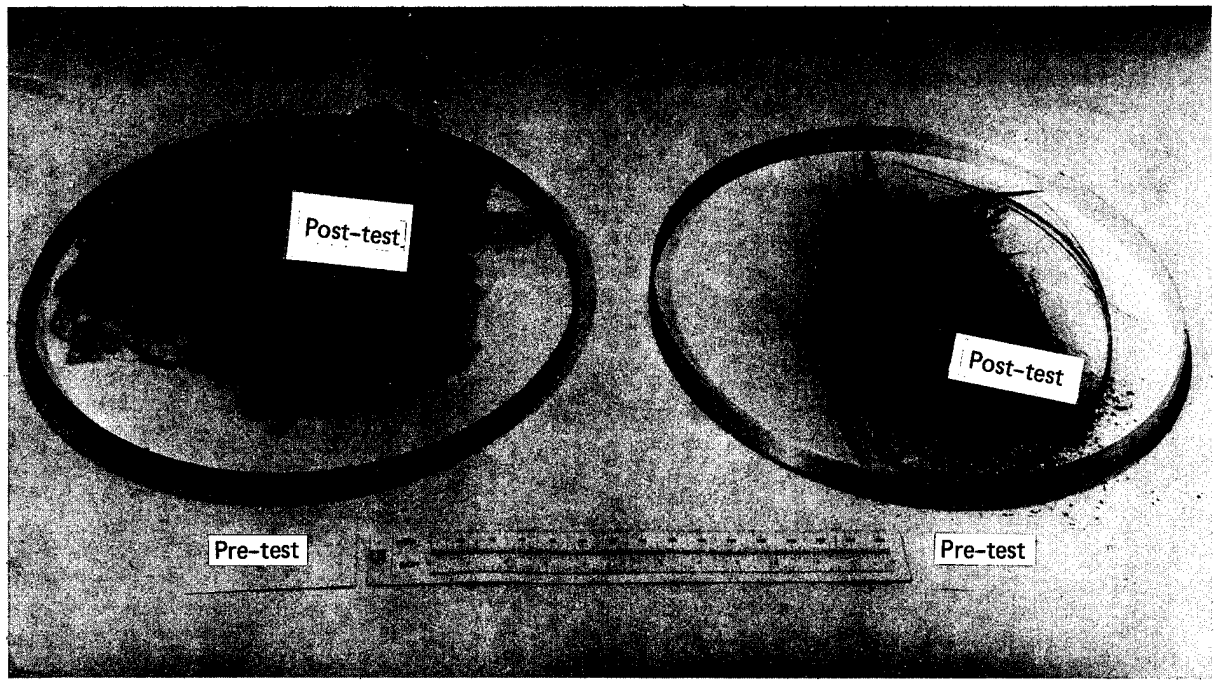


Fig. 6. Failed and unfailed rotors, illustrating the pulverization mode of failure.

COMPARATIVE PROPERTIES OF FIBER COMPOSITES FOR ENERGY STORAGE FLYWHEELS*

PART B: ENGINEERING PROPERTIES OF COMPOSITES

Linda L. Clements
Lawrence Livermore Laboratory, University of California
Livermore, California 94550

ABSTRACT

The LLL flywheel program includes the determination of engineering properties of the composite materials which are considered most likely to be used in flywheel designs. Mechanical as well as thermal properties are determined; we have also examined the effect of the volume percent fiber on these properties. A comparison of the properties of filament-wound composites of three fibers — Kevlar 49, S2-glass, and E-glass — in the same epoxy matrix indicates that the results of engineering property tests can predict the strengths obtained in rotor spin and burst tests, if transverse as well as longitudinal properties are considered. Differences in the relative properties of the three composites enable the flywheel designer to tailor the fiber composite properties, by careful choice of materials, to the design requirements.

INTRODUCTION

After the materials are selected but before a composite flywheel can be designed, the designer requires data on the material engineering properties. The LLL materials characterization program includes the determination of thermal properties and of mechanical properties in tension, compression, and shear; it also includes an examination of the effect of the volume percent fiber on these properties. In this paper, we compare the properties of filament-wound composites made from three fibers — Kevlar 49, S2-glass, and E-glass† — in the same room-temperature-curable epoxy matrix (Dow DER 332 — Jeffamine T-403). Details of the characterization of each system have been or will be published elsewhere[1-3]; thus it is our purpose here to summarize and compare the more important results. Detailed property information is given in Appendix A for the 60-vol% Kevlar 49 composite, and in Appendices B-D for the 60-, 65-, and 70-vol% E-glass composite. Appendix E gives partial data for the 60-vol% S2-glass composite.

RESULTS

The longitudinal tensile properties of the three 60-vol% composites are compared in Fig. 1 and in Table 1. The relative strengths of the three composites are the same as those reported for strand and NOL-ring burst tests in Part A of this report.[4] Table 2 compares data for 70-vol% composites with rotor burst and spin test results. This comparison indicates that the composite engineering data accurately predict the rotor burst and spin test results for all but the Kevlar 49 composite (i.e., the strengths statistically overlap for all composites except Kevlar 49). It is possible that the Kevlar 49 composite performs poorer as a rotor than is predicted from the longitudinal tensile results alone because of its poor transverse tensile properties. The transverse tensile data for all 60-vol% composites are compared in Fig. 2 and in Table 3. As can be seen, the Kevlar 49 composite has extemely low transverse tensile properties, particularly in comparison to the S2-glass composite. This is significant because transverse tensile properties are

*This work was performed under the auspices of the U.S. Department of Energy, under contract No. W-7405-Eng-48.

†Mention of a company or product name does not imply approval or recommendation of the product by the University of California or the U.S. Department of Energy to the exclusion of others that may be suitable.

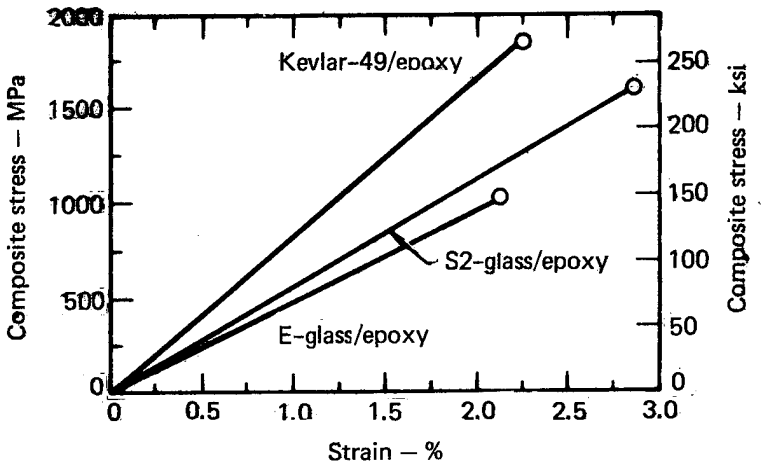


Fig. 1. Comparison of longitudinal tensile stress-strain curves for 60-vol% fiber composites.

Table 1. Comparison of longitudinal tensile properties of 60-vol% fiber composites. Limits are for 95% confidence; numbers of specimens tested are given in parentheses.

Fiber composite	Modulus		Strength		Strain
	GPa	Msi	MPa	ksi	%
Kevlar 49/epoxy	81.8 ± 1.5 (5)	11.9 ± 0.2	1850 ± 50 (5)	268 ± 7	2.33 ± 0.06 (5)
S2-glass/epoxy	56.2 ± 2.7 (25)	8.2 ± 0.4	1615 ± 127 (25)	234 ± 18	2.9 (estimated)
E-glass/epoxy	48.1 ± 0.8 (24)	7.0 ± 0.1	1022 ± 23 (22)	148 ± 3	2.16 ± 0.11 (7)

Table 2. Comparison of composite strengths from longitudinal tensile tests with those from rotor spin and burst tests.[4] All values are normalized to 70-vol% fiber. Limits are for 95% confidence; numbers of specimens tested are given in parentheses.

Fiber composite	Longitudinal tensile tests		Rotor spin		Rotor burst	
	MPa	ksi	MPa	ksi	MPa	ksi
Kevlar 49/epoxy	2160 ± 60 (5)	313 ± 9	1710 ± 260 (5)	248 ± 38	1780 ± 120 (5)	258 ± 17
S2-glass/epoxy	1884 ± 148 (25)	273 ± 22	1890 ± 70 (5)	274 ± 10	1800 ± 100 (5)	261 ± 15
E-glass/epoxy	1183 ± 29 (22)	171 ± 4	1060 ± 170 (5)	154 ± 25	930 ± 100 (5)	135 ± 15

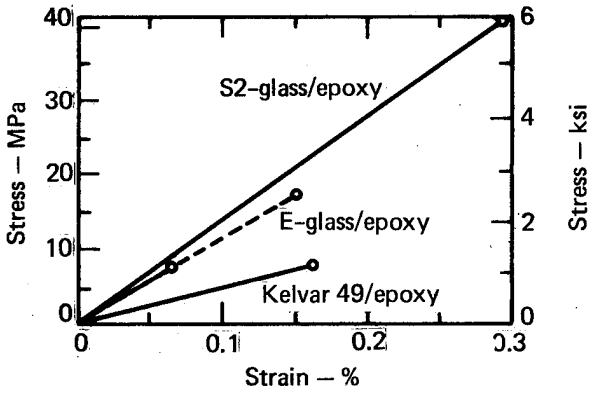


Fig. 2. Comparison of transverse tensile stress-strain curves for 60-vol% fiber composites. The dashed line indicates the performance of "high quality" E-glass composites.

particularly important in some flywheel designs. Also in Fig. 2 we see the effect of processing upon the properties of composites. The solid line for the E-glass/epoxy composite represents the result of tests on the average composite obtained by using commercially feasible processing techniques, whereas the dashed line represents the results for occasionally obtained composites of "high quality." These "high quality" composites also have longitudinal strengths 15% higher than those of the "average" E-glass composite (Fig. 1, Table 1).* Obviously, predictable property results can be expected only if flywheel material processing is well controlled and consistent.

*In the time since our work on the E-glass composites was completed, we have developed some simple techniques that enable us to produce "high quality" composites consistently in a commercially feasible manner.

In Fig. 3 and in Table 4 we compare the in-plane shear properties of the three composites. As with the other properties, the shear properties vary considerably among the three composites. In some cases, the designer may wish to choose the material with these and other property variations in mind. Another way to tailor the composite properties to the design (Table 5) is to alter the volume percent fiber. Unlike the strand test results reported in Part A, but similar to the results of the NOL-ring burst tests, we have found that the dependence of composite longitudinal tensile strengths follows the rule of mixtures. Losses in strength due to factors such as composite dryness do occur, however, above 75 vol% fiber (70 vol% for E-glass composites).

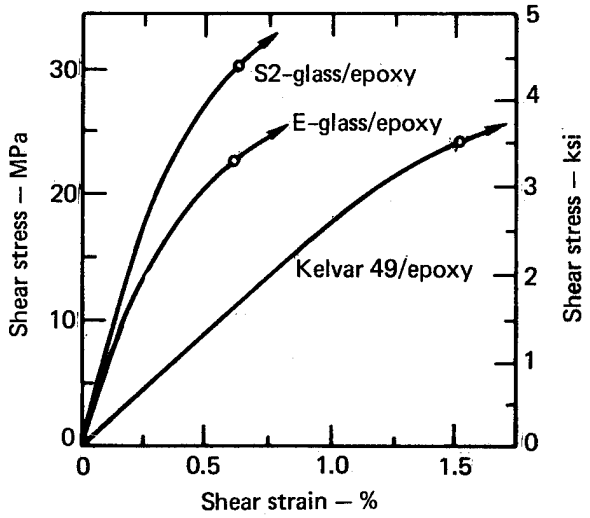


Fig. 3. Comparison of in-plane shear stress-strain curves for 60-vol% fiber composites. The open circles indicate the stress and strain values at 0.2% strain offset.

Table 3. Comparison of transverse tensile properties of 60-vol% composites. Limits are for 95% confidence; numbers of specimens tested are given in parentheses.

Fiber composite	Modulus		Strength		Strain
	GPa	Msi	MPa	ksi	%
Kevlar 49/epoxy	5.10 ± 0.10 (5)	0.740 ± 0.015	7.9 ± 1.1 (8)	1.15 ± 0.16	0.161 ± 0.023 (8)
S2-glass/epoxy	15.7 ± 1.0 (25)	2.28 ± 0.15	41.0 ± 6.3 (11)	5.95 ± 0.91	0.292 ± 0.064 (11)
E-glass/epoxy	12.2 ± 0.7 (5)	1.77 ± 0.10	7.7 ± 0.5 (7)	1.12 ± 0.07	0.064 ± 0.019 (5)

Table 4. Comparison of in-plane shear properties of 60-vol% composites. Limits are for 95% confidence; numbers of specimens tested are given in parentheses.

Fiber composite	Modulus		Stress[a]		Strain[a]
	GPa	Msi	MPa	ksi	%
Kevlar 49/epoxy	1.82 ± 0.09 (5)	0.264 ± 0.013	24.4 ± 2.4 (5)	3.51 ± 0.35	1.55 ± 0.16 (5)
S2-glass/epoxy	7.41 ± 0.56 (14)	1.07 ± 0.08	30.4 ± 1.0 (14)	4.41 ± 0.14	0.620 ± 0.041 (14)
E-glass/epoxy	5.8 ± 0.3 (5)	0.84 ± 0.04	22.8 ± 1.1 (5)	3.31 ± 0.16	0.600 ± 0.040 (5)

[a]At 0.2% strain offset.

Table 5. Comparison of tensile strengths at three volume percentages of fiber for S2-glass and E-glass fiber composites. Limits are for 95% confidence; numbers of specimens are given in parentheses.

Fiber content, vol%	Longitudinal tensile strength		Transverse tensile strength	
	MPa	ksi	MPa	ksi
S2-glass/epoxy				
60	1615 ± 127 (25)	234 ± 18	41.0 ± 6.3 (11)	5.95 ± 0.91
65	1750 ± 138 (25)	254 ± 20	42.5 ± 3.1 (6)	6.17 ± 0.50
70	1884 ± 148 (25)	273 ± 21	43.6 ± 3.4 (5)	6.32 ± 0.49
E-glass/epoxy				
60	1022 ± 23 (22)	148 ± 3	7.7 ± 0.5 (7)	1.12 ± 0.07
65	1107 ± 25 (22)	161 ± 4	7.5 ± 1.1 (6)	1.09 ± 0.16
70	1192 ± 27 (22)	173 ± 4	6.2 ± 0.5 (3)	0.90 ± 0.07

Table 6 compares the room-temperature thermal properties of 60-vol% Kevlar 49 and E-glass composites. The values are quite different, again indicating that it is possible to tailor the composite to meet the design needs by the choice of material and of winding pattern. This is especially true of Kevlar 49 composites, where the unusual negative longitudinal coefficient of thermal expansion can be used to advantage in certain designs.

CONCLUSIONS

From our comparison of the engineering properties of composites made from three fibers in the same room-temperature-curable epoxy matrix, we conclude that engineering property tests can predict the composite strengths obtained in rotor spin and burst tests if transverse and longitudinal properties are considered. Also, if composite processing is precisely

Table 6. Comparison of thermal properties at room temperature for single samples of 60-vol% Kevlar 49 and E-glass fiber composite.

Thermal property	Kevlar 49/epoxy	E-glass/epoxy
Linear coefficient of thermal expansion:		
Longitudinal, 10^{-6}/K (10^{-6}/°F)	-4.0 (-2.2)	6.57 ± 0.53 (3.65 ± 0.29)[a]
Transverse, 10^{-6}/K (10^{-6}/°F)	79 (44)	30.0 (16.7)
Thermal conductivity:		
Longitudinal, W/m•K (BTU/h•ft•°F)	3.22 (1.86)	1.17 (0.68)
Transverse, W/m•K (BTU/h•ft•°F)	0.35 (0.20)	0.55 (0.32)
Heat capacity, J/kg•K (cal/g•°C)	1120 (0.268)	850 (0.20)

[a]Three samples tested; limits are for 95% confidence.

controlled to produce consistent properties, careful materials selection can enable the designer to tailor composite properties to the design requirements.

REFERENCES

1. Linda L. Clements and Richard L. Moore, Composite Properties of an Aramid Fiber in a Room-Temperature-Curable Epoxy Matrix, Lawrence Livermore Laboratory, Rept. UCRL-79549 (1977).

2. L. L. Clements and R. L. Moore, "Composite Properties for E-Glass in a Room-Temperature-Curable Epoxy, " Composites (1978), to be published.

3. Linda L. Clements and Richard L. Moore, "Composite Properties for S2-Glass in a Room-Temperature-Curable Epoxy," in preparation (1977).

4. Lynn S. Penn, Comparative Properties of Fiber Composites for Energy Storage Flywheels. Part A: Evaluation of Fibers for Flywheel Rotors, Lawrence Livermore Laboratory, Rept. UCRL-80016, Part A (1977).

Appendix A. Summary of preliminary engineering design data for a nominally 60-vol% system of Kevlar 49 fiber (1420 denier, DuPont), 100 parts by weight DER 332 (bisphenol-A-based epoxy resin, Dow Chemical), and 45 parts by weight Jeffamine T-403 (polyether triamine, Jefferson Chemical). The composite system was cured for 24 h at room temperature plus 16 h at 85°C. Where more than one specimen was tested, the number of specimens is given in parentheses. Limits are for 95% confidence; data without confidence limits are taken from a single specimen. Data in brackets are estimated from results for Kelvar 49 in an XD 7818/T-403 epoxy matrix. See Ref. 1 for details of the characterization.

Mechanical properties

Elastic constants[a]:		
Longitudinal Young's modulus, E_{11}, GPa	81.8 ± 1.5	(5)
Transverse Young's modulus, E_{22}, GPa	5.10 ± 0.10	(8)
Shear modulus, G_{12}, GPa	1.82 ± 0.09	(5)
Major Poisson's ratio, ν_{12}	0.310 ± 0.035	(5)
Minor Poisson's ratio, ν_{21}	0.0193 ± 0.0014	(8)

Ultimates:	Tension		Compression		Shear	
Longitudinal strength, MPa	1850 ± 50	(5)	[235 ± 3]	(6)	—	
Longitudinal ulitmate strain, %	2.23 ± 0.06	(5)	[0.48 ± 0.3]	(6)	—	
Transverse strength, MPa	7.9 ± 1.1	(8)	[53 ± 3]	(10)	—	
Transverse ultimate strain, %	0.161 ± 0.023	(8)	[1.41 ± 0.12]	(6)	—	
Shear stress at 0.2% offset, MPa	—		—		24.4 ± 2.4	(5)
Shear strain at 0.2% offset, %	—		—		1.55 ± 0.16	(5)

Thermal properties

Linear coefficient of thermal expansion, 10^{-6}/K	-50°C	-25°C	0°C	25°C	50°C	75°C	100°C	125°C
Longitudinal	-3.8	-3.8	-3.8	-4.0	-4.7	-6.0	—	—
Transverse	61	66	72	79	87	150	214	214
Thermal conductivity, W/m•K								
Longitudinal	2.62	2.84	3.05	3.22	3.31	3.34	—	—
Transverse	—	0.27	0.33	0.35	0.37	0.39	—	—
Heat capacity, J/kg•K	840	930	1020	1120	1190	1300	—	—

[a] Elastic constants are valid for both tension and compression.

Appendix B. Summary of preliminary engineering design data for a nominally 60-vol% system of E-glass fiber (type 30, 410AA-450, Owens-Corning), 100 parts by weight DER 332 (bisphenol-A-based epoxy resin, Dow Chemical), and 45 parts by weight Jeffamine T-403 (polyether triamine, Jefferson Chemical). The composite system was cured for 16 h at 60°C. Where more than one specimen was tested, the number of specimens is given in parentheses. Limits are for 95% confidence; data without confidence limits are taken from a single specimen. Data in brackets are estimated from results of a 70-vol% composite of the same system. See Ref. 2 for details of the characterization.

Mechanical properties

Elastic constants[a]:		
Longitudinal Young's modulus, E_{11}, GPa	48.14 ± 0.82	(24)
Transverse Young's modulus, E_{22}, GPa	12.2 ± 0.7	(5)
Shear modulus, G_{12}, GPa	5.8 ± 0.3	(5)
Major Poisson's ratio, ν_{12}	0.191 ± 0.015	(24)
Minor Poisson's ratio, ν_{21}	0.0482 ± 0.0059	(5)

Ultimates:	Tension		Compression		Shear	
Longitudinal Strength, MPa	1022 ± 23	(22)	490 ± 100	(4)	—	
Longitudinal ultimate strain, %	[2.16 ± 0.11]	(7)	[1.11 ± 0.27]	(4)	—	
Transverse strength, MPa	7.7 ± 0.5	(7)	[78 ± 4]	(11)	—	
Transverse ultimate strain, %	0.064 ± 0.010	(5)	[0.68 ± 0.10]	(6)	—	
Shear stress at 0.2% offset, MPa	—		—		22.8 ± 1.1	(5)
Shear strain at 0.2% offset, %	—		—		0.600 ± 0.040	(5)

Thermal properties

Linear coefficient of thermal expansion, 10^{-6}/K	-60°C	-20°C	20°C	50°C	80°C
Longitudinal	6.57 ± 0.53 (3) →				
Transverse	23.4	25.9	30.0	35.3	104
Thermal conductivity[b] W/m•K					
Longitudinal	—	1.06	1.17	1.36	1.46
Transverse	—	~0.5	~0.55	~0.6	~0.65
Heat capacity, J/kg•K	[640]	[750]	[850]	[900]	[950]

[a] Elastic constants are valid for both tension and compression.

[b] Approximations, valid to within about ±20%.

Appendix C. Summary of preliminary engineering design data for a nominally 65-vol% system of E-glass (type 30, 410AA-450, Owens-Corning), 100 parts by weight DER 332 (bisphenol-A-based epoxy resin, Dow Chemical), and 45 parts by weight Jeffamine T-403 (polyether triamine, Jefferson Chemical). The system was cured for 16 h at 60°C. Where more than one specimen was tested, the number of specimens is given in parentheses. Limits are for 95% confidence; data without confidence limits are taken from a single specimen. Data in brackets are estimated from results of a 70-vol% composite of the same system. See Ref. 2 for details of the characterization.

Mechanical properties

Elastic constants[a]:	
Longitudinal Young's modulus, E_{11}, GPa	52.15 ± 0.89 (24)
Transverse Young's modulus, E_{22}, GPa	14.03 ± 0.61 (6)
Shear modulus, G_{12}, GPa	6.3 ± 0.5 (12)
Major Poisson's ratio, ν_{12}	0.207 ± 0.016 (24)
Minor Poisson's ratio, ν_{21}	0.056 ± 0.011 (6)

Ultimates:	Tension	Compression	Shear
Longitudinal strength, MPa	1108 ± 25 (22)	530 ± 110 (4)	—
Longitudinal ultimate strain, %	[2.16 ± 0.11] (7)	[1.11 ± 0.27] (4)	—
Transverse strength, MPa	7.5 ± 1.1 (6)	[78 ± 4] (11)	—
Transverse ultimate strain,%	0.054 ± 0.009 (6)	[0.68 ± 0.10] (6)	—
Shear stress at 0.2% offset, MPa	—	—	22.4 ± 1.7 (12)
Shear strain at 0.2% offset, %	—	—	0.546 ± 0.045 (12)

Thermal properties

Linear coefficient of thermal expansion, 10^{-6}/K	-60°C	-20°C	20°C	50°C	80°C
Longitudinal	6.31 ± 0.51 (3)	→			
Transverse	20.2	22.4	25.6	30.5	90
Thermal conductivity[b] W/m•K					
Longitudinal	—	1.14	1.26	1.35	1.44
Transverse	—	0.53	0.59	0.63	0.68
Heat capacity, J/kg•K	[640]	[750]	[850]	[900]	[950]

[a] Elastic constants are valid for both tension and compression.

[b] Approximation, valid to within about ±20%.

Appendix D. Summary of preliminary engineering design data for a nominally 70-vol% system of E-glass fiber (type 30, 410AA-450, Owens-Corning), 100 parts by weight DER-332 (bisphenol-A-based epoxy resin, Dow Chemical), and 45 parts by weight Jeffamine T-403 (polyether triamine, Jefferson Chemical). The system was cured for 16 h at 60°C. Where more than one specimen was tested, the number of specimens is given in parentheses. Limits are for 95% confidence; data without confidence limits are taken from a single specimen. See Ref. 2 for details of the characterization.

Mechanical properties

Elastic constants[a]:		
Longitudinal Young's modulus, E_{11}, GPa	56.16 ± 0.96	(24)
Transverse Young's modulus, E_{22}, GPa	17.30 ± 1.04	(12)
Shear modulus, G_{12}, GPa	7.4 ± 0.5	(4)
Major Poisson's ratio, ν_{12}	0.233 ± 0.017	(24)
Minor Poisson's ratio, ν_{21}	0.0681 ± 0.0091	(12)

Ultimates:	Tension		Compression		Shear	
Longitudinal strength, MPa	1183 ± 29	(22)[a]	570 ± 120	(4)	—	
Longitudinal ultimate strain, %	2.16 ± 0.11	(7)[b]	1.11 ± 0.27	(4)	—	
Transverse strength, MPa	6.2 ± 0.5	(3)[c]	78 ± 4	(11)	—	
Transverse ultimate strain, %	0.042 ± 0.030	(3)	0.68 ± 0.10	(6)	—	
Shear stress at 0.2% offset, MPa	—		—		26.8 ± 1.5	(4)
Shear strain at 0.2% offset, %	—		—		0.568 ± 0.023	(4)

Thermal properties

Linear coefficient of thermal expansion, 10^{-6}/K	-60°C	-20°C	20°C	50°C	80°C
Longitudinal	6.07 ± 0.49 (3)				
Transverse	17.1	18.9	21.6	25.8	76
Thermal conductivity,[d] W/m•K					
Longitudinal	—	1.23	1.35	1.44	1.53
Transverse	—	0.50	0.56	0.58	0.61
Heat capacity, J/kg•K	640	750	850	900	950

[a] Elastic constants are valid for both tension and compression.

[b] The longitudinal tensile strength and ultimate strain value do not include those from four specimens of a single, very clear (i.e., good resin impregnation) composite which gave average ultimates of 1370 ±75 MPa and 2.4 ±0.2%.

[c] The transverse tensile strength data exclude four specimens from two separate windings that gave an average ultimate strength of 17 ±5 MPa.

[d] Approximations, valid to within about ±20%.

Appendix E. Summary of preliminary engineering design data for a nominally 60-vol% system of S2-glass fiber (type P263A-750, Owens-Corning), 100 parts by weight DER 332 (bisphenol-A-based epoxy resin, Dow Chemical), and 45 parts by weight Jeffamine T-403 (polyether triamine, Jefferson Chemical). The system was cured for 16 h at 60°C. Where more than one specimen was tested, the number of specimens is given in parentheses. Limits are for 95% confidence; data without confidence limits were taken from a single specimen. See Ref. 3 for details of the characterization.

Mechanical properties

Elastic constants[a]:		
Longitudinal Young's modulus, E_{11}, GPa	56.2 ± 2.7	(25)
Transverse Young's modulus, E_{22}, GPa	15.7 ± 1.0	(11)
Shear modulus, G_{12}, GPa	7.41 ± 0.56	(14)
Major Poisson's ratio, ν_{12}	0.282 ± 0.031	(25)
Minor Poisson's ratio, ν_{21}	0.079 ± 0.014	(11)

Ultimates:	Tension		Compression		Shear	
Longitudinal strength, MPa	1615 ± 127	(25)	460 ± 60	(3)	—	
Longitudinal ultimate strain, %	~2.9		0.92 ± 0.06	(3)	—	
Transverse strength, MPa	41.0 ± 6.3	(11)	111.8 ± 2.2	(5)	—	
Transverse ultimate strain, %	0.292 ± 0.064	(11)	2.93 ± 0.32	(5)	—	
Shear stress at 0.2% offset, MPa	—		—		30.4 ± 1.0	(14)
Shear strain at 0.2% offset, %	—		—		0.620 ± 0.041	(14)

[a]Elastic constants are valid for both tension and compression.

TIME-DEPENDENT PROPERTIES OF FIBER COMPOSITES FOR ENERGY-STORAGE FLYWHEELS*

E. M. Wu and L. S. Penn
Lawrence Livermore Laboratory, University of California
Livermore, California 94550

ABSTRACT

Time-dependent deformation and time-dependent strength are being characterized for several candidate polymeric composites for flywheels. This presentation highlights the motivation and the philosophy of the characterization adopted by the authors in establishing the ongoing programs at LLL. This overview is intended to provide a basis for inferring the type of engineering data being generated for different aspects of flywheel design. The details of these data can be obtained from the published reports and articles. Two aspects of flywheel design data are addressed: those dealing with time-dependent statistical strength, and those dealing with deformation and strength under time-varying history.

DISCUSSION

Time-dependent statistical strength data are needed to predict failure probabilities for a flywheel operating under various stresses associated with input, storage, and output of energy. Stress-rupture tests at constant load levels are used as baseline benchmarks. Such tests are required because even a nominal variation in static strength (typically less than 5%) can lead to large scatter in stress-rupture life (in excess of 100%), as shown in Fig. 1 To provide the necessary statistical parameters for reliability design, large data samples from long-term testing are now being accumulated in testing facilities capable of simultaneous testing of 100 samples (Fig. 2). The type of data being generated is typified in Fig. 3. From curves such as these, we can determine the amount of derating in stress level that is required to attain

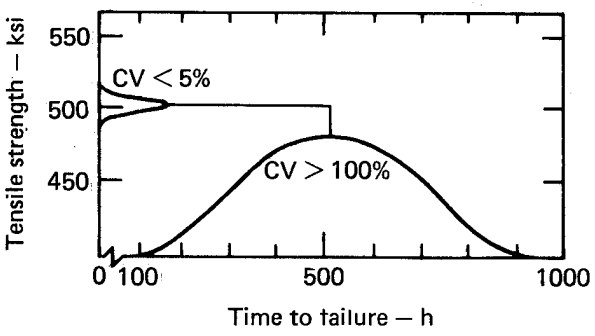


Fig. 1. Nominal scatter in static strength data which can result in large scatter of lifetime predictions.

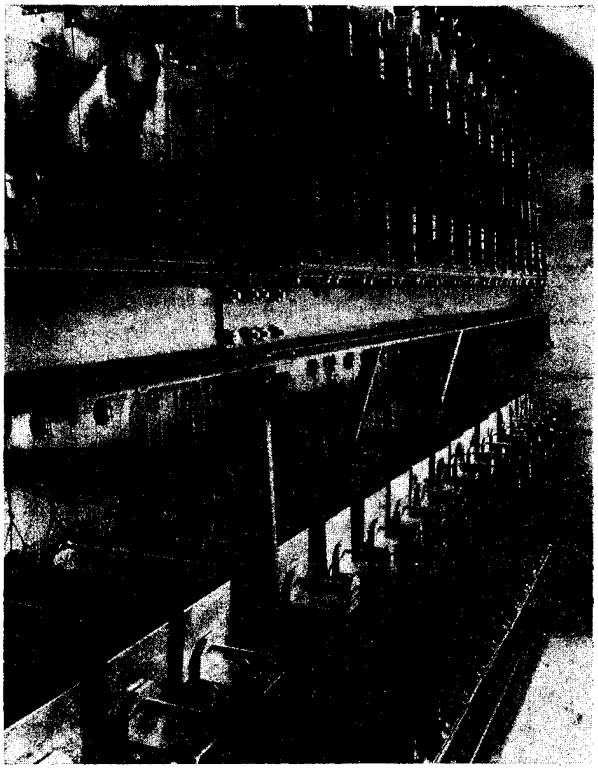


Fig. 2. Stress-rupture test for facilities; 100 stations are available for simultaneous testing of many samples.

*This work was performed under the auspices of the U,S. Energy Research and Development Administration, under contract No. W-7405-Eng-48.

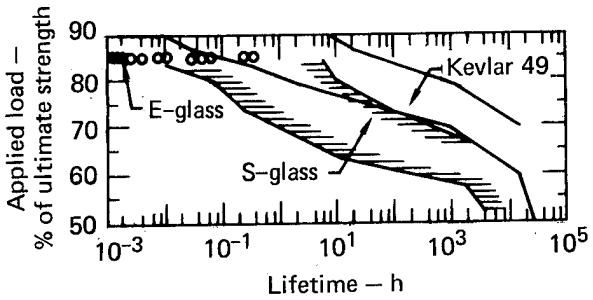


Fig. 3. Stress-rupture lifetime data for several composite materials being considered for flywheels. For S-glass and Kevlar 49 composites,* 2 to 100% failure bands are displayed.

the desired degree of reliability in the operating life.

Deformation and strength under time-varying history are pertinent in assessing the dimensional stability and fatigue sensitivity of materials employed in flywheel application. For a flywheel, dimensional stability is directly related to the hub attachment and containment design; it is also indirectly related to strength augmentation through prestressing and hybrid designs. Deformation under time-varying history can be estimated from load-deformation constitutive relations. We are adopting the convolution integral form for such reactions:

$$\varepsilon(t) = \int_0^t J(t - \tau) \frac{d\sigma}{d\tau} d\tau \ .$$

In this program, we record the time-varying stress-history $\sigma(t)$ and the time-varying strain history $\varepsilon(t)$. With these data, we establish the limits of linearity and qualitatively determine the creep compliance $J(t)$.

The characterization of strength under time-varying load history depends on the identification of damage parameters which provide meaningful engineering sensitivity. A damage parameter may be regarded as a failure criterion in time. For example, under stress-rupture conditions, the creep strain $\varepsilon(t)$ may be used as a damage criterion (Fig. 4a). However, creep strains for polymeric composites often approach an asymptotic limit and this, combined with the usual material scatter, leads to a large uncertainty, Δt, in life prediction (Fig. 4a). Hence, we seek a damage function Ψ of the form,

$$\Psi = \int_{t_0}^{t} f(\sigma,\varepsilon,t,\theta)dt \ ,$$

such that Ψ would exhibit the property depicted in Fig. 4b, providing a higher sensitivity or a smaller uncertainty of life prediction. The exploratory effort to identify such damage function requires comprehensive instrumentation for recording the multitude of time-varying parameters, i.e., $\sigma(t)$, $\varepsilon(t)$, t, θ(environment). The comprehensive instrumentation and mechanical testing are provided by five servo-hydraulic testers and 44 creep and program-interruptable creep machines serviced by three computers for data acquisition and data processing. A sample of the data being recorded is shown in Fig. 5; some intermediate cycles are expanded in Fig. 6.

The overall objective of these programs is to provide time-dependent deformation and material strength data in sample sizes that are large enough to be statistically meaningful as well as to present data in quantitative forms amenable to design applications.

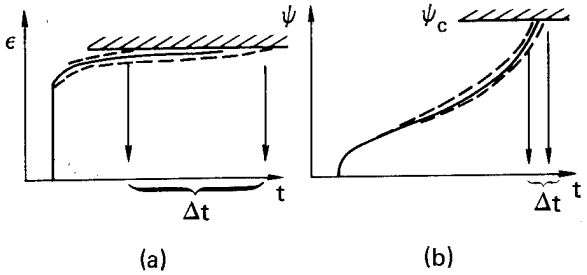


Fig. 4. Damage parameters: (a) use of creep strain as a damage parameter may result in a large uncertainty in the lifetime prediction; however, in (b) a damage parameter is being constructed to reduce the uncertainty in the lifetime predictions.

*Reference to a company or product name does not imply approval or recommendation of the product by the University of California or the U.S. Department of Energy to the exclusion of others that may be suitable.

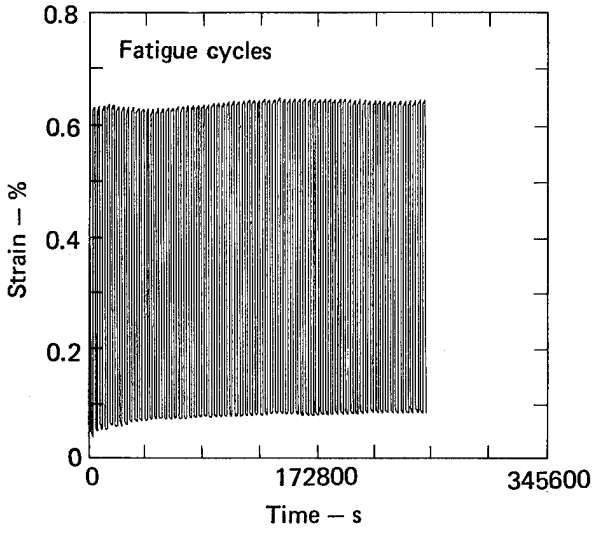


Fig. 5. Time-dependent strain history in fatigue of an aramid fiber strand composite exhibiting accelerated creep strain.

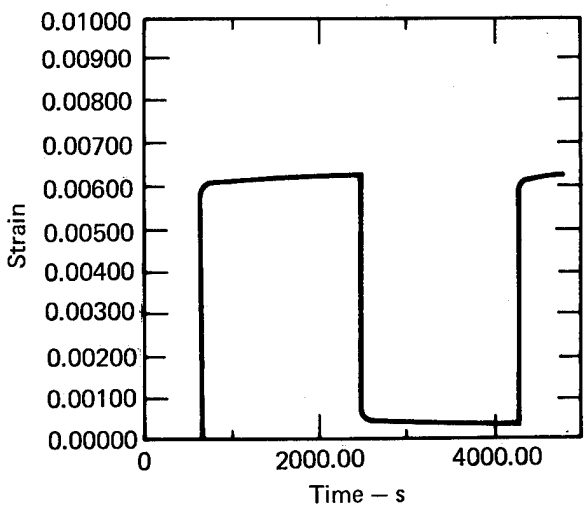


Fig. 6. Expanded plot of the strain history in fatigue of Kevlar 49 strand composite exhibiting creep and recovery within each stress-cycle.

IMPROVED PERFORMANCE FOR HOOP-WOUND COMPOSITE FLYWHEEL ROTORS

R. E. Allred
Sandia Laboratories
Albuquerque, New Mexico 87115

R. F. Foral
Dept. of Engineering Mechanics
University of Nebraska
Lincoln, Nebraska 68588

W. E. Dick
Brunswick Corporation
Lincoln, Nebraska 68504

ABSTRACT

Developmental work to date has shown the performance of hoop-wound composite flywheel rotors to be severely limited by composite transverse strength. This problem is addressed in a joint experimental - analytical effort aimed at improving transverse properties and assessing the impact of this improvement on flywheel performance. An improved test fixture designed to test hoop-wound cylinders in axial tension is developed. Test results show this specimen and test fixture produce more consistent data than do flat tensile bars cut from hexagonal cylinders. Initial experimental results from the improved specimen indicate that the transverse strength of Kevlar 49/epoxy composites could be improved by 30 percent by copolymerizing the epoxide matrix with an elastomer. The impact of these data on flywheel performance is predicted by a computer program which identifies optimum designs for given material properties on an energy-stored-per-swept-volume basis. A substantial improvement in performance is predicted - the attained 30 percent strength improvement of Kevlar 49/epoxy is shown to produce a 15 percent increase in energy stored. The analysis also permits multiple-material designs. Hybrid designs appear to have considerable potential for increasing storage capacity compared to single-material designs.

INTRODUCTION

The theoretical potential of high strength filament-wound flywheels has been well publicized. It is recognized, however, that in practice the performance of these flywheels is significantly limited by the transverse properties of the material. Kevlar 49 composites in particular exhibit a high degree of strength anisotropy due to the poor transverse strength of the fiber and its poor wetability. Two approaches can be considered for dealing with this problem. The first and possibly the most obvious is to increase the transverse strength of the composite. Surprisingly, little effort has been spent in this area.

The second approach is to design the flywheel to minimize the effects of transverse strength. A considerable amount of work has been done in trying to create designs which avoid premature transverse failure. Of the designs that attempt to address practical energy storage needs, most tend toward the exotic and do not appear to be practical from a fabrication or operational standpoint.

This paper is a joint experimental-analytical effort. The experimental effort is aimed at improving transverse properties of composites and, in the process, developed a test fixture and test procedures which produce consistent results. The analytical effort is aimed at determining the effect of improved transverse properties on flywheel performance. A computer program was developed which predicts optimum designs for either single-material or hybrid, multiple-material configurations. The program predicts optimized designs on a swept-volume, mass or total-energy-stored basis.

*This work was jointly supported by the United States Dept. of Energy, the University of Nebraska, and Brunswick Corporation.

PART I. TEST SPECIMEN AND MATRIX DEVELOPMENT

INTRODUCTION

Composite material systems for rotor applications exhibit longitudinal-to-transverse strength ratios from 25 to near 200. Because of its high longitudinal specific strength, Kevlar 49/epoxy is one of the most promising composite systems for rotor applications; however, it falls in the high end of the strength anisotropy range due to the low transverse strength of the filament itself and its poor wetability. Attainment of Kevlar/epoxy composite flywheels which are both mass and volume efficient would then be facilitated by increased transverse strength or strain carrying capacity of the composite.

Before materials studies aimed at transverse strengthening can be conducted or reliable design data obtained, however, an accurate test specimen is required. Typically, either flat rectangular bars cut from filament-wound plates or circumferentially-wound tubes have been used for this type of test. Scatter in the data has been excessive in most cases. High coefficients of variation in test data can exceed property improvement values which result from materials variations and, thus, can mask important trends. Each of the above specimens has inherent disadvantages. The bar specimen suffers from difficulties in winding tension control during fabrication which, in turn, affects fiber spacing and volume fraction. The bar specimen is also subject to damage during machining and from the stress concentrations present at the corners and edges.

The cylindrical specimen is superior to the rectangular bar because it is axisymmetric. It is also more representative of the manufacturing conditions which would be employed for a hoop-wound flywheel rotor. In addition, it is thought that the large amount of data scatter seen with this specimen is due to misalignment in the testing machine. The tubes are generally bonded into rigid end caps or overwrapped on the ends with a glass fabric composite which is threaded prior to testing. Misalignment can be introduced in these bonding operations which will result in the application of a bending moment to the specimen during testing. This type of misalignment cannot be fully compensated for by the universal joint employed on most mechanical test machines.

In Part I is described a self-aligning specimen fixture which reduces scatter in the properties obtained from circumferentially wound composite tubes tested in axial tension. Stress-strain data are given for composites of Kevlar 49 filaments in a common, room-temperature curable epoxide and an elastomer toughened formulation. In Part II, the impact of these data on the design of a hoop-wound flywheel rotor is discussed.

EXPERIMENT

A schematic of the self-aligning test fixture is shown in Fig. 1. Self-alignment is attained by the incorporation of ball-and-socket joints in the end caps. The additional degrees of freedom compensate for the inherent misalignment of the specimen. The bearing surfaces (sockets) are on threaded stainless steel cylinders so that only one set of joints is required to test a number of specimens. Stainless steel is also used as the ball material. Bearing surfaces were machined to a number 16 finish and coated with silicone grease prior to each test. The 11.1 mm diameter hole in the socket allows the 9.5 mm diameter rod on the ball to circumscribe a cone angle of 1.3 degrees on each end of the specimen.

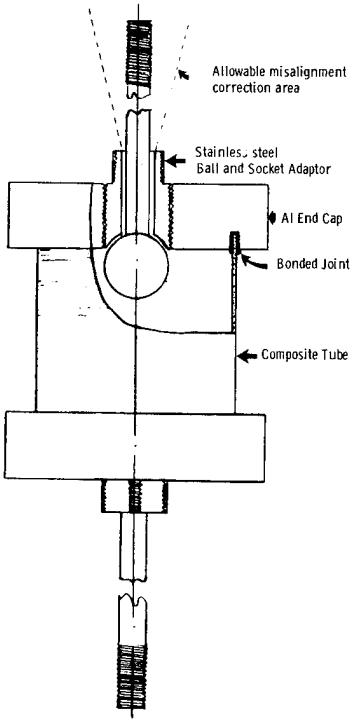


Figure 1. Schematic of self-aligning test fixture for the determination of composite transverse tensile properties.

The actual components of the test specimen are shown in Fig. 2. The composite cylinders were bonded into a 6 mm deep, 2.8 mm wide slot in the aluminum end caps with an aluminum-filled room temperature cureable epoxy adhesive. A square was used to attain alignment between the tube and end caps. One end cap was bonded in place and allowed to cure overnight before attachment of the second endcap. It should be noted that at no time during testing did the rod assume the full 1.3 degree angle and contact the sides of the socket cylinder; thus, the opening in the socket cylinder is adequate to compensate for the amounts of misalignment created through the bonding procedure.

The composite test specimens were fabricated by wet filament winding on a 77.2 mm diameter aluminum mandrel. 4560 denier Kevlar 49 filament was impregnated with DER 332/Jeffamine T403 (100:36) epoxy in a resin bath and wound under 13.7 N tension. The yarn was dried 12 hours at 150°C and stored in a dessicated box prior to use. Winding was accomplished from the dessicated box such that contact with ambient conditions lasted only a few seconds. The composites were cured 3 days at room temperature and removed by chilling the mandrel from the inside with liquid nitrogen. The differential thermal expansion between the composite and mandrel allowed the composite to be easily removed. A toughened version of the matrix resin was also combined with the Kevlar 49 filament. Toughening was accomplished by the addition of either 6 or 15 parts by weight of amine-terminated butadiene/acrylonitrile (ATBN) and 1 part DMP-30 (tridimethyl aminomethyl phenol) accelerator per 100 parts DER 332. All other winding parameters were held constant. Filament volume fractions of 52-55 percent were determined by dissolution.[2]

For purposes of comparison, an equivalent set of rectangular specimens was fabricated by winding on an hexagonal Al mandrel with 150 mm flats. The bar samples were machined to 12.5 and 25.0 mm widths by 6.3 mm thickness. Castings of the neat resins were also prepared and machined into 6.3 mm diameter cross-section tensile specimens for the determination of matrix properties. The as-wound composite tubes were machined to a wall thickness of 2.5 mm and a length of 90 mm. All machined surfaces were sealed with 332/T403 epoxy before testing. Three uniaxial strain gages were mounted at the midpoint of the cylindrical specimens, 120° apart. Tensile load was applied to the gaged specimens in 222 N increments by manual movement of the testing machine crosshead. Strains were recorded at each load increment up to failure. All ungaged specimens were tested in tension at a crosshead rate of 0.5 mm/min. Strains of the neat resin samples were monitored with a strain gage extensometer. The rectangular composite specimens were tested for strength only.

RESULTS AND DISCUSSION

The specimen fixturing discussed above is designed to impart a uniform stress state and thus reduce the misalignment inherent to tubular specimens. Misalignment of a test specimen, which results in an applied moment, will be observed as a large deviation in the strain gage readings at a given applied load. To provide a basis for comparison with the self-aligning fixture, the data from Ref. 3 were examined for the rigid-end loading condition. An average coefficient of variation (CV) for the gage readings on the Kevlar 49/epoxy tube tests was found to be 7.8 percent. Thornel 75/epoxy exhibited a CV of 7.5 percent and Thornel 400/epoxy was 6.4 percent. These data result in an average CV of 7.2 percent for the rigid loading condition based upon 30 specimens. Strain gage readings from specimens tested with the self-aligning fixture show an average agreement (CV) within 3 percent. The impact of reducing bending moments on the specimen is seen in the strength data given in Table I. A comparison of the 332-T403 matrix tube data shows that scatter has been reduced nearly 50 percent with the improved fixture. The more uniform stress-state also produces a 40% improvement in the determined transverse strength over the rigid-end samples. The high scatter and lower strength determined with the bar specimens is probably due to the stress concentrations and handling difficulties previously discussed for that specimen.

The value of the improved specimen is illustrated in experiments conducted on

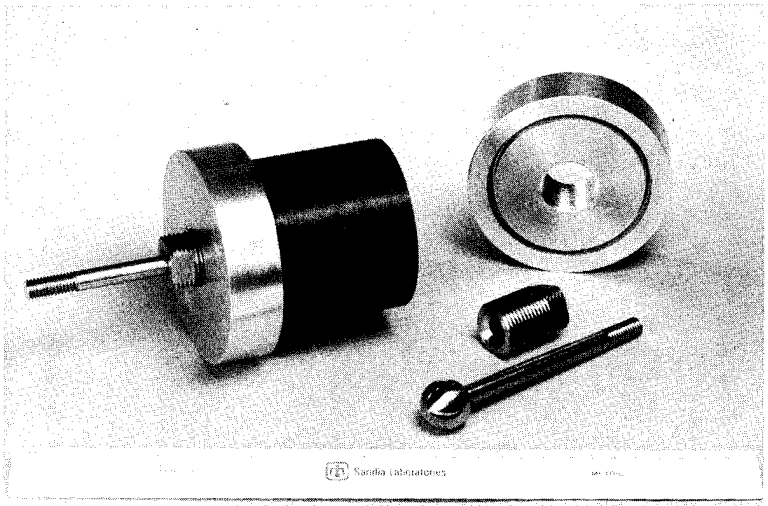
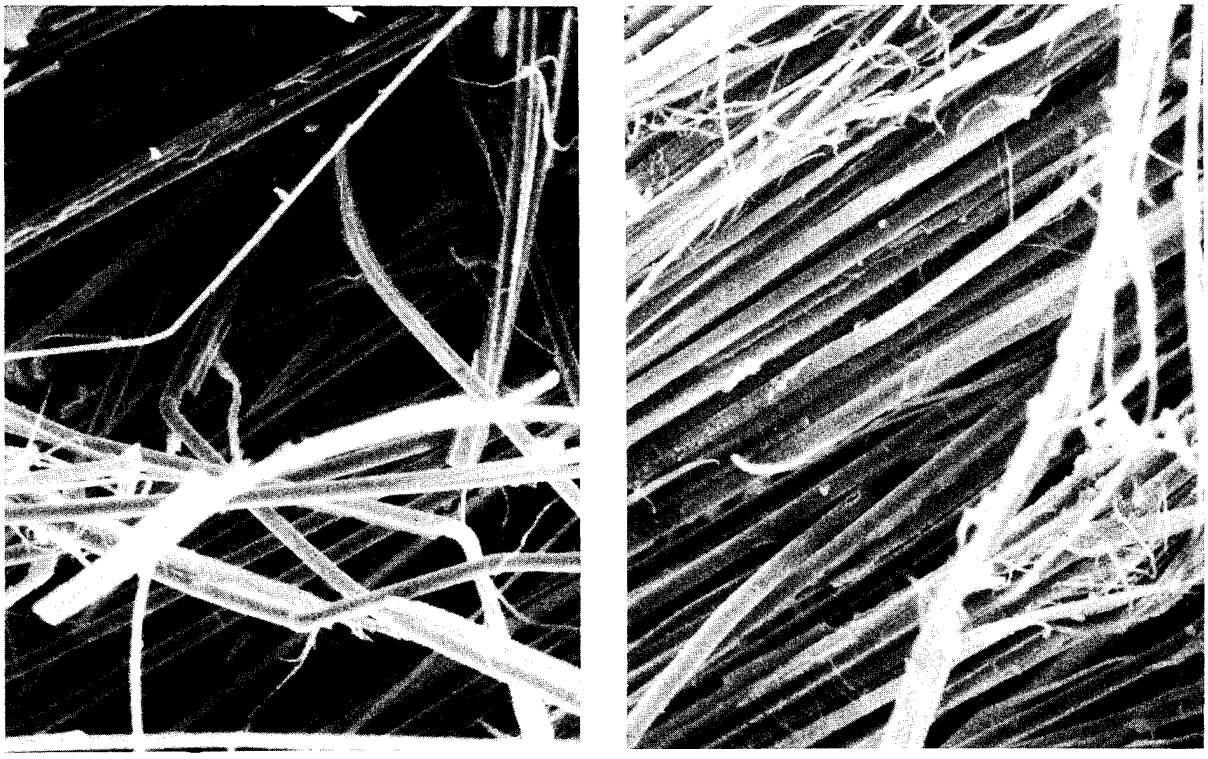


Figure 2. Components of self-aligning fixture showing end caps, ball and socket joint and composite specimen.



(a) (b)

Figure 3. Scanning electron micrographs of Kevlar 49/epoxy transverse fracture surfaces. (a) 332/T403/ATBN/DMP-30 (100:36:6:1) matrix. (b) 332/T403 (100:36) matrix. (200X)

the toughened matrix. The addition of ATBN increased the measured strength and reduced scatter in the data with each type specimen. However, only with the improved specimen does the effect appear statistically significant. The effect of ATBN on the transverse strength of Kevlar/epoxy has a significant effect upon the storage capacity of Kevlar-reinforced flywheels (discussed in Part II of this paper). The consistency from specimen to specimen with the self-aligning fixture is also evident in other mechanical properties as shown in Table II.

Based on the data presented in Table II, several observations may be made. The reduction in composite transverse stiffness due to the addition of ATBN is very slight compared to the increases seen in strength and ultimate elongation. The data in Table II indicate that these changes occur with small additions of ATBN to 332/T403. Apparently, ATBN reduces the sensitivity of the composite to filament winding flaws or filament splitting and allows the transverse strength of the composite to approach that of the resin. One would also expect that such an increase in toughness would also raise the fatigue endurance limit of the composite.

Visual examination of composites containing ATBN exhibit much cleaner fracture surfaces. The reduced number of exposed filaments would indicate less fiber splitting or better wetting with the ATBN. A detailed examination of the surfaces with the scanning electron microscope failed to resolve a mechanism. As seen in the micrographs shown in Fig. 3, the ATBN seems to exhibit better wetting; however, it is more likely that the increased toughness of the ATBN matrix allows the composite near the fracture plane to remain intact, whereas the more brittle matrix (without ATBN) shatters and releases the filaments near the fracture zone.

From the neat resin data given in Table III and the composite data in Table II, it can be determined that the composites containing ATBN fail at 72 percent of the resin strength on a net section basis. Also, the composite is virtually linear elastic to failure (Table II). These observations lead to the conclusion that further additions of ATBN would not increase the transverse strain carrying capacity of this composite system because of the reduction in strength of the neat resin. Other materials improvements such as filament coatings, better wetting matricies, or lower void content may further enhance the properties developed in this study.

PART II. FLYWHEEL PERFORMANCE

INTRODUCTION

To judge the impact of improved transverse properties on flywheel performance, we choose a flywheel of simple hoop-wound, constant thickness configuration. This design, essentially a flat rim, has important cost, manufacturing, and efficiency advantages. We use it as a study vehicle and propose to proportion and configure the wheel to produce maximum performance. To measure performance of a design, kinetic energy per swept volume (U/V) is used as the object function. A computer program is developed which can work for either single material or hybrid, multiple material designs. The computer program is used to numerically study performance characteristics, the importance of transverse properties, and the impact of improved transverse properties and hybrid configurations on optimized flywheel performance.

COMPUTATIONAL PROCEDURE

In this section, the basic equations and logic of the optimization program are described as well as some fundamental results. The basic element in the analysis is a symmetrical ring of uniform thickness with mass density ρ rotating at a constant speed ω. At the radius r, the radial and tangential stresses σ_r and σ_θ satisfy force equilibrium

$$\frac{d}{dr}(r\sigma_r) - \sigma_\theta + \rho\omega^2 r^2 = 0 \qquad (1)$$

and the corresponding strains are

$$\varepsilon_r = \frac{du}{dr}, \quad \varepsilon_\theta = \frac{u}{r} \qquad (2)$$

in terms of the radial displacement u. For the conditions of plane stress, the stresses and strains are related by

$$\varepsilon_r = \frac{\sigma_r}{E_r} - \nu_{\theta r}\frac{\sigma_\theta}{E_\theta}$$

$$\varepsilon_\theta = \frac{\sigma_\theta}{E_\theta} - \nu_{r\theta}\frac{\sigma_r}{E_r} \qquad (3)$$

in terms of radial and hoop elastic moduli E_r and E_θ and Poisson's ratios $\nu_{r\theta}$ and $\nu_{\theta r}$.

The flywheel is assumed to be stress free at its inner and outer edges, r=a and r=b, so that

$$\sigma_r\Big|_{r=a} = 0, \quad \sigma_r\Big|_{r=b} = 0 \quad . \qquad (4)$$

When more than one material is used in the flywheel design, there must be stress and displacement continuity between material layers. Thus

$$\sigma_r\Big|_{r_i^-} = \sigma_r\Big|_{r_i^+}$$

$$u\Big|_{r_i^-} = u\Big|_{r_i^+} \qquad (5)$$

must be satisfied at the interface radius r_i.

Closed-form solutions for single material flywheels (Eqs. (1)-(4)) are avaliable in the literature.[5] Other sources[6,7] consider layered constructions of more than one material and produce numerical solutions.

The programming of Newhouse[6] is used as our core routine; given the wheel geometry, material properties, temperature change* and angular speed, the program calculates stresses, strains, etc., at points radially through the wheel. For given material properties and geometry, the stresses are first calculated for unit angular speed. Since the stresses vary as the square of angular speed, the critical angular speed ω_c can then be found knowing the allowable radial, S_r, and hoop, S_θ, stresses. Once the critical speed is found, other quantities of interest can be calculated.

The optimization routine is a simple, straight-forward procedure. For given material properties, an incremental sequence of geometries is analyzed. The program automatically selects the a/b ratio and, if appropriate, the hybrid material radial thicknesses that result in the maximum energy per unit swept volume. The neighborhood around this geometry is then reanalyzed with a finer mesh, repeating as often as desired.

This sort of optimization routine is satisfactory as an initial estimate. The equations are simple enough that such a sequence of runs can be made at a relatively low cost. Examining behavior as geometry is sequenced provides insight into design change effects. Until knowledge of design change effects is sufficiently developed, this procedure provides some protection against selecting an incorrect local maximun in the presence of multiple maximums.

The performance calculations are conducted for unit outer radius b. Sequencing the geometry involves varying the a/b ratio and thus the inner radius a, but at constant swept volume. With swept volume thus established, maximizing U/V is the same as maximizing the energy stored within the envelope.

The effect of geometry sequencing is seen in Fig. 4., where, for a given material, energy per swept volume is plotted vs radius ratio. Relatively thick rings (low a/b ratio) show a radial failure. As material is removed (a/b increases), U/V increases and reaches a maximum, at which point simultaneous radial and hoop failure occur. All a/b values to the right of the peak in Fig. 4 show hoop failures. Thus, given a volume envelope, material may be added to increase energy but there is a limit at which the energy peaks. Adding material past this limit produces an energy loss. At the energy peak, simultaneous hoop and radial failure occur.

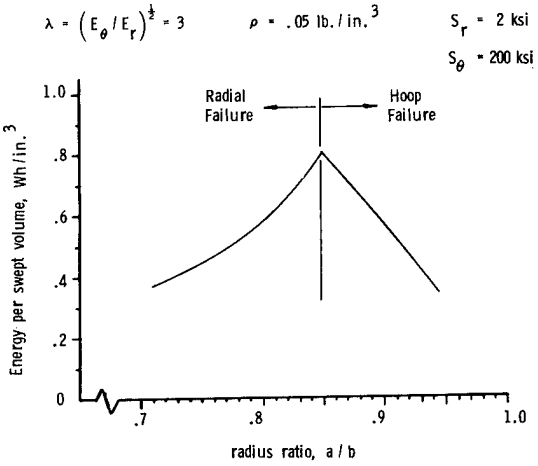


Figure 4. Single-Material Flywheel Performance as a Function of Radius Ratio.

IMPORTANCE OF TRANSVERSE PROPERTIES

It is well known that flywheel designs have been severely limited by the material transverse properties. In this section the computer program discussed above is used to show the importance of transverse properties on flywheel performance.

*Except for a brief discussion later, the effects of temperature change will be neglected here.

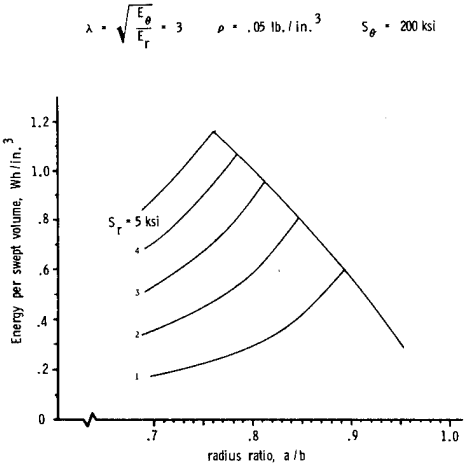


Figure 5. Single-Material Flywheel Performance for Various Transverse Strength Values.

Figure 5 shows energy per swept volume vs radius ratio for a sequence of transverse strength values S_r, all other material properties remaining constant. Each transverse strength shows a maximum U/V at a specific a/b ratio. As transverse strength increases, the maximum energy increases, occurring at decreasing a/b ratios (i.e. thicker rings). In each case, the peak represents occurrence of simultaneous radial and hoop failures.

Figure 6 plots predicted energy per swept volume vs transverse strength for a sequence of anisotropy ratios, λ ($\lambda = \sqrt{E_\theta/E_r}$). The energy values plotted in Fig. 6 are maximum attainable values such as are plotted in Fig. 5. In fact, the values of the peaks from Fig. 5 (λ=3) are plotted as one of the curves in Fig. 6.

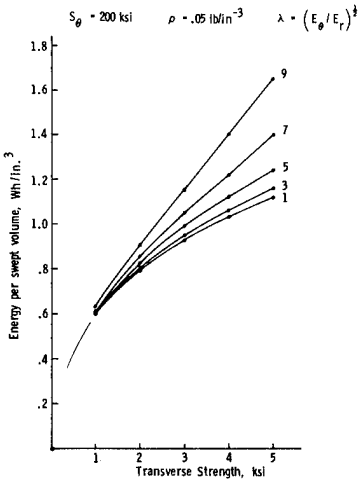


Figure 6. Effect of Transverse Strength and Anisotropy on the Potential Performance of Optimized Thick-Ring Flywheels.

From Fig. 6 we note that attainable performance is increased if either transverse strength S_r is increased or anisotropy ratio λ is increased. The latter can be accomplished by either decreasing the transverse modulus of elasticity E_r or increasing the hoop modulus E_θ.

The range of S_r and λ depicted in Fig. 6 covers the range of probable values encountered in existing composites. All of the calculations upon which Fig. 6 are based, except for the highest λ and S_r values, showed peak hoop stress σ_θ occurring at the inner edge of the wheel. Using existing solutions which express σ_θ as a function of r (Ref. 5) we can write

$$\sigma_\theta\Big|_{r=a} = S_\theta \qquad (6)$$

Maximum radial stress occurs at intermediate radius r_m, where the derivative of σ_r with respect to r is zero. Thus, once again using the solution in Ref. (5), we can write

$$\sigma_r\Big|_{r_m} = S_r \qquad (7)$$

and

$$\frac{d\sigma_r}{dr} = 0 \qquad (8)$$

Equations (6), (7) and (8) are a set of three equations requiring simultaneous radial and hoop failure. These equations were solved numerically using Newton-Raphson iteration to produce a solution for the radius ratio a/b, the critical angular velocity ω_c, and the location r_m. These a/b and ω_c values are those to which the optimization routines converge. Thus the above analysis provides a direct solution for the best performance in cases where the maximum hoop stress does indeed occur at the inner edge.

FLYWHEEL PERFORMANCE IMPROVEMENTS

Table IV summarizes material properties of the high performance composites which will be considered. Included in the table are the improved properties attained by ATBN modification of Kevlar 49-Epoxy, as reported in Part I. These materials will be used in both single material designs and hybrid, multiple material designs.

Single Material Designs. We first consider Kevlar 49 flywheels and the performance improvements accomplished by the

transverse property improvements due to adding ATBN. The results are plotted in Fig. 7 as energy per swept volume vs radius ratio a/b. As reported in Part I, adding ATBN increases the transverse strength S_r from 2.28 ksi† (15.7 MPa) to 2.96 ksi (20.4 MPa), a 30% increase; the transverse modulus E_r decreases from 685 ksi to 661 ksi, about a 4% decrease. Due to these changes, we note in Fig. 7 that performance has improved from .841 Wh/in^3 to .966 Wh/in^3, a 15% improvement.

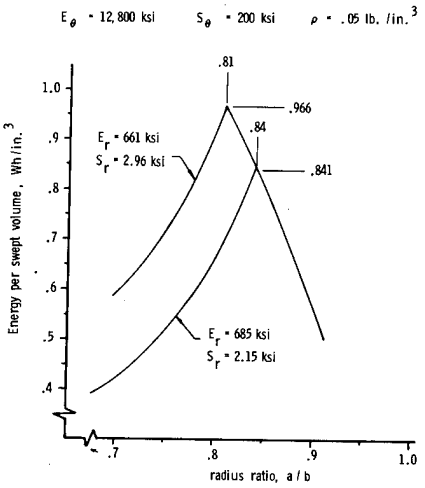


Figure 7. Effect of the Improved Transverse Properties on the Performance of a Kevlar 49 Flywheel.

Predicted performances on an energy-per-swept-volume basis for the Kevlars and for Thornel 300 and S Glass are listed in Table V along with the corresponding a/b ratios. We note that the Thornel and S Glass wheels performed better than Kevlar according to the energy-per-swept-volume criteria. Energy per unit mass often is proposed as a performance measuring criteria. With these single-material wheels, however, this criteria produces the thinnest wheels (highest a/b ratio) as best, which is not a practical solution. For the proportions determined by the energy-per-swept-volume criteria, we list in Table V the corresponding energy per unit mass. The Kevlars attain highest performance under this criteria, although adding ATBN has actually decreased this parameter.

The critical angular velocity ω_c listed in Table V is the angular velocity which produces the best attained performance. The values shown correspond to a unit outer radius b=1. Corresponding values for other outer radii can be obtained by simply dividing the value given in Table V by the desired radius. As an example, a 1 inch radius Kevlar 49 wheel has a critical angular velocity of 388,000 RPM, as given in Table V. A 10 inch radius Kevlar 49 wheel spins at 38,800 RPM for best attained performance. Of course, the energy-per-swept-volume parameter is independent of outer radius.

†Early results indicated this value to be about 2.5 ksi. As such, the computer analysis was conducted for 2.15 ksi rather than the final average value of 2.28 ksi.

Hybrid Designs. Considerable improvement in performance can be attained by combining materials in a flywheel design. We have conducted preliminary studies of optimized designs for two and three layer configurations. The logic and some results are presented below.

The proper scheme of material placement is demonstrated by a simple analysis using Eqs. (1) through (4). With the idea that performance can be severely restricted by transverse properties, we first investigate the condition where transverse strain ε_r is zero. Analytical manipulation, not shown here, produces the requirement that hoop modulus to density ratio E_θ/ρ must vary as the radius squared, i.e.,

$$\varepsilon_r = 0 \rightarrow E_\theta/\rho = \frac{\omega^2(1 - \nu_{\theta r}\nu_{r\theta})}{\varepsilon_\theta} r^2 \quad . \quad (9)$$

Requiring transverse stress to vanish produces

$$\sigma_r = 0 \rightarrow E_\theta/\rho = cr^{(3+\nu_{\theta r})} \qquad (10)$$

where c is a constant of integration. Equations (9) and (10) imply that materials should be placed so that E_θ/ρ increases with increasing r. This criteria is used in the hybrid designs below.

The computer program handles multiple material designs in a manner similar to single material designs, i.e., a sequence of geometries is scanned and the best performer selected, the process being repeated at a finer mesh as often as desired. With a two material hybrid design, however, the radius ratio a/b as well as the thickness ratio t_2/t_1 must be scanned. Here, t_2 is the radial thickness of the outer material layer, t_1 the thickness of the inner material.

A scan of performance variation with geometry is shown in Fig. 8, where, for a

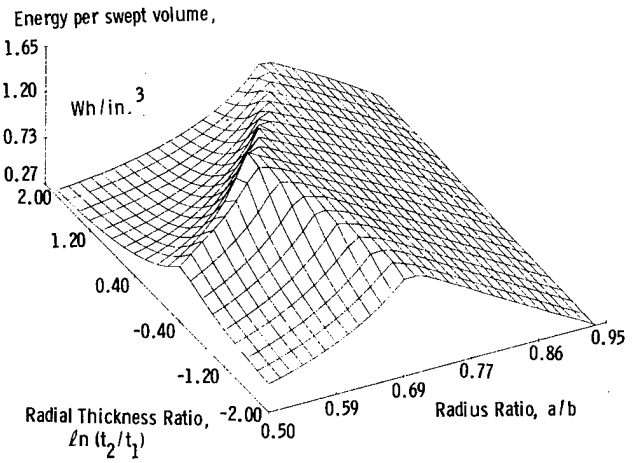


Figure 8. Performance Surface for a Kevlar 49/S Glass Reinforced Hybrid Flywheel.

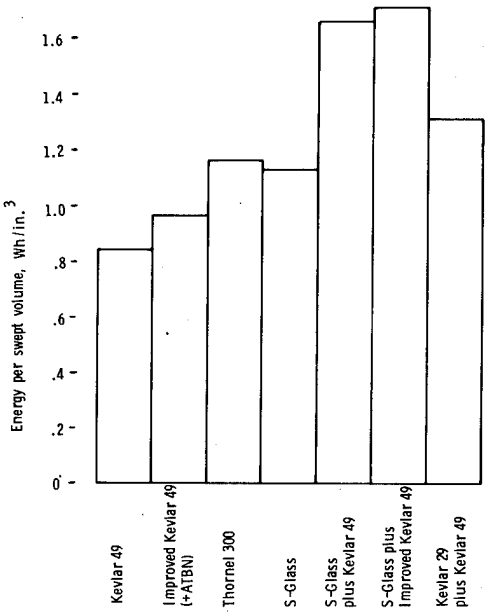


Figure 9. Attainable Performance - Single-Material and Two-Material Designs.

configuration with S Glass on the inside, Kevlar 49 on the outside, U/V is plotted vs a/b and the natural logarithm of the thickness ratio, ln t_2/t_1. As is apparent in Fig. 8, the grid is somewhat coarse, but the plot does show the configuration of the energy surface, indicating a region of geometries producing best performance. The maximum attained with this mesh is reached at a/b = 0.605 and ln t_2/t_1 = 0.20 (i.e. $t_2/t_1 = e^{-0.20} = 0.819$) with the performance being 1.659 Wh/in^3.

Table VI shows predicted performance and corresponding geometry for three hybrid designs. The maximum performance design for the hybrid systems is not so clear cut as with a single material. Almost equal maximums for slightly different configurations were noticed in the numerical output, introducing the possibility of multiple solutions. Analytical studies are planned to produce a more complete knowledge of the energy surface, similar to what was done for the one material configurations.

Comparing the results in Table V and VI shows that a significant improvement in attained energy per swept volume is accomplished by hybrid wheels over single material wheels. This improvement is shown in bar graph form in Fig. 9. Table VI lists the energy per unit mass for each design, even though the designs have not been configured to optimize this parameter. When optimized with respect to energy per unit mass, the two-material wheels with a given t_2/t_1 approach a zero thickness ring. As with the case of single-material wheels, this solution does not provide practical energy storage capacity. The critical angular speeds, ω_c shown in Table VI are analogous to those given in Table V.

The two S Glass-Kevlar 49 designs listed in Table VI attained their performance with essentially simultaneous hoop and radial failure in both inner and outer rings. The Kevlar 29 - Kevlar 49 design does not attain this condition. Simultaneous hoop and radial failure is attained in the Kevlar 49 outer ring, and, while radial failure does occur in the inner ring, the maximum hoop stress is 40 ksi below the allowable 180 ksi value for Kevlar 29. Why simultaneous failure is accomplished for one material combination and not for another is not completely understood. Further study is in progress to resolve this anomaly.

Preliminary numerical runs have been made with hybrid flywheels containing three materials. One indication produced by the work so far is that, with particular materials ordering, a two material configuration is chosen in preference to any three material design; one of the materials is discarded in the optimization procedure. This indication also points to the need for further understanding of material placement effects on hybrid flywheel performance. Temperature change will affect flywheel performance, perhaps significantly in some designs. Capability to calculate temperature change effects has been incorporated into the computer program and numerical investigations are in progress.

CONCLUSIONS

The results of this joint experimental-analytical study on the effect of transverse composite properties on flywheel rotor performance allow the following conclusions:

(1) The addition of amine-terminated butadiene/acrylonitrile (ATBN) into a Kevlar 49/epoxy composite system in small amounts increases the composite transverse strength and elongation by 30 percent. Such increases can have a significant effect on the energy storage capacity of a Kevlar-reinforced flywheel. Higher concentrations of ATBN reduce these properties in proportion to the strength reduction of the neat resin. Further increases in the transverse strain carrying capability of Kevlar 49/epoxy will probably have to be based on improving the filament-matrix interfacial bond.

(2) The experimental results were obtained with the use of an improved fixture for testing transverse tensile properties of filament-wound tubes. The improved fixturing incorporates ball-and-socket adaptors to compensate for the inherent misalignment of tubular specimens with rigid-end caps. The more uniform tensile stress state produced by this fixture greatly decreases scatter in the composite data and results in increased determined strengths and elongations for Kevlar 49/epoxy.

(3) A computer program has been developed to calculate optimum hoop-wound flywheel proportions for given material properties in either single-material or multiple-material designs. Analytical results indicate that transverse properties, specifically modulus and strength, have a significant effect on the performance of hoop-wound composite wheels and that substantial improvements in performance can be accomplished with hybrid, multiple-material designs.

(4) Additional analytical and experimental work should be undertaken to understand hybrid flywheel performance. Particular topics to investigate include material properties optimization, materials placement optimization and temperature effects.

ACKNOWLEDGEMENT

The authors are indebted to H. K. Street for his contributions to the development of the self-aligning fixture and for conducting the experimental aspects of this study.

REFERENCES

1. D. L. Hagen and A. G. Erdman, "Flywheels for Energy Storage: A Review with Bibliography," Proc. of ASME Design Engr. Conf., Quebec, Sept. 1976, paper 76-DET-96.
2. R. E. Allred and N. H. Hall, "Volume Fraction Determination of Kevlar 49/Epoxy Composites," to be submitted to J. Comp. Mat'ls.
3. R. E. Allred and F. P. Gerstle, Jr., "The Effect of Resin Properties on the Transverse Mechanical Behavior of High-Performance Composites," Proc. of Society of the Plastics Institute 30th Technical Conference, Washington, DC, Feb. 1975, paper 9-B.
4. L. L. Clements and R. L. Moore, "Fiber-Composite Flywheel Program, Quarterly Progress Report Jan-March 1977," UCRL-50033-77-1, May 1977, p. 8.
5. G. F. Morganthaler and S. P. Bonk, "Composite Flywheel Stress Analysis and Materials Study," Proc. of 12th Nat'l. SAMPE Symp., Oct. 1967, paper D-5.
6. N. L. Newhouse, "A Computerized Analysis of Axisymmetric Flywheels," Proc. of 1977 Flywheel Technology Symposium, San Francisco, October 1977.
7. E. L. Donfelt, S. A. Hewes and T. Chou, "Optimization of Composite Flywheel Design," Int. J. Mech. Sci., 19, 1977 pp. 69-78.

Table I.

Transverse Tensile Strength Results for Kevlar 49/Epoxy in Various Specimen Configurations

	Test Specimen Type				
	12.5 mm Bar	25 mm Bar	25 mm Bar [4]	Rigid Tube [3]	Self-aligning Tube
Matrix: 332/T403 (100:36)					
Ultimate Strength, MPa	9.7	12.2	7.9	11.3	15.7
Standard Deviation, MPa	3.6	3.1	1.1	2.6	2.0
Coefficient of Variation, %	37.4	25.1	13.9	23.0	12.9
Sample Size	(4)	(4)	(-)	(12)	(5)
Matrix: 332/T403/ATBN/DMP-30 (100:36:6:1)					
Ultimate Strength, MPa	10.9	13.0	--	13.5	20.4
Standard Deviation, MPa	1.2	1.2	--	3.0	0.7
Coefficient of Variation, %	11.0	9.0	--	22.1	3.5
Sample Size	(4)	(4)	(-)	(4)	(5)

Table II.

Transverse Mechanical Properties of Kevlar Composite Tubes Tested with Self-Aligning Fixture

Matrix (mix ratio)		Young's Modulus GPa	Ultimate Strength MPa	Elongation to Failure, %
332/T403 (100:36)	Value	4.72	15.7	.33
	Std. Dev.	.01	2.0	.04
	Coef. Var.	0.2 %	12.9%	11.2 %
	Sample Size	(5)	(5)	(5)
332/T403/ ATBN/DMP-30 (100:36:6:1)	Value	4.56	20.4	.45
	Std. Dev.	.07	0.7	.02
	Coef. Var.	1.5 %	3.5%	5.3 %
	Sample Size	(5)	(5)	(5)
332/T403/ ATBN/DMP-30 (100:36:15:1)	Value		17.1	.41
	Std. Dev.		0.6	.03
	Coef. Var.		3.5%	6.3 %
	Sample Size		(5)	(5)

Table III.

Tensile Properties of 332/T403 Epoxy as a Function of ATBN* Content (RT Cure)

Percent ATBN	Young's Modulus GPa	Ultimate Strength MPa	Ultimate Elongation Percent
0	3.2	71.7	3.1
6	2.6	62.9	3.7
15	2.1	52.3	4.2
25	1.7	43.9	4.8

*amine-terminated butadiene/acrylonitrile

Table IV.

Material Properties of Fiber - Epoxy Composites

Reinforcement	E_θ 10^3 ksi	E_r 10^3 ksi	$\nu_{\theta r}$	ρ lb/in^3	S_θ ksi	S_r ksi
Kevlar 49	12.8	.685	.3	.05	200	2.28
Improved Kevlar 49 (+ATBN)	12.8	.661	.3	.05	200	2.96
Kevlar 29	6.9	.685	.3	.05	180	2.28
Thornel 300	18	1.34	.314	.054	200	4.8
S Glass	8	2.5	.25	.072	180	6

Table V.

Predicted Performance for Single-Material Composite Flywheels

Reinforcement	Radius Ratio a/b	Critical Speed 10^6 RPM	$\frac{\text{Energy}}{\text{Swept Volume}}$ Wh/in^3	$\frac{\text{Energy}}{\text{Mass}}$ Wh/lb
Kevlar 49	.840	.388	.841	57.1
Kevlar 49 (+ATBN)	.810	.390	.966	56.1
Thornel 300	.759	.379	1.152	50.3
S Glass	.724	.312	1.130	33.0

Table VI.

Predicted Performance for Two-Material Hybrid Composite Flywheels

Reinforcement	Radius Ratio a/b	Radial Thickness Ratio t_2/t_1	Critical Speed ω_c 10^6 RPM	Energy / Swept Volume Wh/in^3	Energy / Mass Wh/lb
S Glass + Kevlar 49	.595	.755	.381	1.659	42.0
S Glass + Kevlar 49 (+ATBN)	.585	.880	.389	1.710	43.1
Kevlar 29 + Kevlar 49	.677	1.01	.388	1.321	48.8

BIBLIOGRAPHIC AND NUMERIC DATA BASES FOR FIBER COMPOSITES AND MATRIX MATERIALS*

F. E. McMurphy and T. M. Quick
Lawrence Livermore Laboratory, University of California
Livermore, California 94550

ABSTRACT

We have been conducting research leading to the creation of bibliographic and numeric data bases of material properties, under contract with ERDA's† Division of Energy Storage Systems (ERDA/STOR). We have created both bibliographic and numeric data bases for fiber composites and matrix materials, with particular emphasis to their application to modern flywheel technology. The bibliographic data base was created to provide a direct means to visually examine pertinent literature. The numeric data base is being created to provide evaluated materials properties data for direct input to applications programs. These and related data bases are being prepared to serve ERDA/STOR administrators and their contractors in the expanding field of energy storage. Data bases and their evaluation programs will be stored on a PDP-11/70 computer system at LLL and be available for interactive use over the ARPAnet and by telephone dialup.

SUMMARY

The Data Management Group at the Lawrence Livermore Laboratory (LLL) is conducting research leading to the creation of data bases for energy storage systems. These data bases are computer-based and will contain bibliographic information, material properties data, and data on essential criteria for energy storage systems. Access to these central files will be from remote terminals over computer networks and by telephone dialup, in addition to the more conventional means of computer-generated reporting, and dissemination on magnetic tapes.

To validate the material properties data, a working agreement has been established between LLL and the National Bureau of Standards (NBS). The Office of Standard Reference Data at NBS coordinates and monitors data evaluations by recognized national data evaluation centers. One of the five data requests, for molten salts and molten salts systems (battery and thermal energy storage materials), has been completed and the data is being entered into a data bank for molten salts and thermal energy storage materials. Other data requests for selected properties of metal alloys (flywheel materials), and metallic hydrides (hydrogen storage materials) are currently being worked on by several data evaluation centers. A bibliographic data base for flywheel energy storage has been created and published. In addition, a comprehensive bibliography for molten salts and TES materials is in preparation.

INTRODUCTION AND BACKGROUND

"Research Leading to the Production and Early Use of Numeric Data Banks of Material Properties and System Analysis" has been carried out since February 1976, by the Data Management Group of LLL under contract to the U. S. Energy Research and Development Administration, and the Division of Energy Storage Systems (ERDA/STOR) under contract number E(49-1)-3835.[1]

Many alternate energy storage systems are undergoing continued research and development: thermal, chemical, electrochemical, battery, physical, etc. The technological efficiency of these systems and their cost effectiveness often depend in large measure upon the properties of

*Work performed under the auspices of the U. S. Department of Energy under contract number W-7405-Eng-48.

†Now called Department of Energy.

materials and substances in heretofore uncharted operational domains. Technical and economical feasibility is the central issue in the decision-making process. Basic data on material properties, and on characterizations of energy storage systems, are required to provide a reliable foundation for these activities.

Data bases of this type are being created as an essential part of this project. When completed, they will contain evaluated physical and chemical properties for materials used in energy storage systems and information and data to characterize the validity domains of the systems. The NBS and selected data evaluation centers are collaborating. These computerized data banks are being made available to industry and to universities. As such, they will serve as a public resource for the scientific and technological research community. It is anticipated that data bases of this type will provide a solid and expanding basis for the accelerating research activities in energy storage. They should help to eliminate discrepancies and should be a valuable aid to channel work into promising directions.

A staff of up to five professionals are participating in the project at LLL. Their academic backgrounds and experience are in chemistry, metallurgy, and computer science. Dr. Terrence Quick, material scientist, is project leader.

Project activity during the past year has centered around the publication of a bibliographic data base for flywheel energy storage,[2] the computerization of evaluated molten salts data received from NBS, and acquisition of a PDP-11/70 computer system on which energy-storage-related data will reside. General energy storage data will be made available on the PDP-11/70 computer system over the ARPAnet, a national computer network, and by telephone dialup later in FY 1978.

TECHNOLOGICAL DATA BASE ACTIVITIES

Our major technological data base activities include the identification and the evaluation of materials and their properties required for energy storage systems, and the creation of bibliographic and evaluated material properties data banks for user-oriented manipulation and dissemination. During the past year, we have acquired a computer system that is being prepared to handle these data banks for ERDA's Division of Energy Storage.

IDENTIFICATION OF MATERIALS AND PROPERTIES FOR FLYWHEEL ENERGY STORAGE SYSTEMS

The identification of materials and properties for flywheels was carried out in collaboration with the flywheel research activities at LLL and with Sandia Laboratories. Based on an initial survey and on feedback obtained directly from users and researchers, requests for data on flywheel metals and composite materials have been sent to the NBS for evaluation (see next section).

CRITICAL EVALUATION OF MATERIAL PROPERTIES

The critical evaluation of material properties is now in progress through a formal working agreement between LLL and NBS. Under this agreement the NBS Office of Standard Reference Data, which manages the National Standard Reference Data System (NSRDS), acts as the mandated monitoring agency for the evaluation of material properties. The actual evaluations are carried out by nationally recognized evaluation centers affiliated with the NSRDS/NBS. Computerization of the data and its transfer into the public domain is carried out by LLL. The data will also be published in a special series by NSRDS/NBS.

BIBLIOGRAPHY ON FLYWHEEL TECHNOLOGY

A selected bibliography for flywheel energy storage and fiber composites has been published.[2] It contains 382 citations on the properties and mechanics of fibers, fiber composites, matrix materials and on flywheel energy storage systems. The materials and flywheel systems citations were derived from the world literature. The bibliography is machine produced and is generated in two parts: A concordance on keywords and phrases, and the chronological listing of all bibliographic citations (see section on FLYWHEEL AND FIBER COMPOSITES BIBLIOGRAPHY).

MOLTEN SALTS/TES BIBLIOGRAPHY

A comprehensive molten salts/TES bibliographic data base is being created in a similar way as the flywheel bibliography. Major sources of machine readable citations have been received from

Dr. George Janz of the Molten Salts Data Center at the Rensselaer Polytechnic Institute (approximately 4000 citations) and from Sandia Laboratories Fused Salt Bibliography (approximately 3000 citations). Sources of hardcopy citations include a M.S. thesis by L. S. Charnoff (approximately 4000 citations) and other citations from ongoing literature searches at LLL. These bibliographic sources[3-6] are being combined into a single data bank which will be completed during FY 1978 for general use.

MOLTEN SALTS/TES MATERIAL PROPERTIES DATA BASE

A molten salts/TES material properties data base is under development for interactive use on our dedicated PDP-11/70 computer system. In addition to the inorganic salts data already computerized,[7,8] we have added the evaluated molten salts/TES material properties data received during the past year from Dr. George Janz. These data include values of up to 16 properties on 82 salt systems.

COMPUTER SYSTEM TO HANDLE STORAGE DATA

A PDP-11/70 computer system is being set up on the ARPAnet for storage, manipulation, and dissemination of energy-storage-related data. The basic computer system was procured and tested during the past year. In FY 1978, additional capability will be installed to enable both technological data bases, and other energy-storage related data bases, to be accessed directly over the ARPAnet or by telephone dialup.

DESCRIPTION OF FLYWHEEL-RELATED DATA BASES

We are creating both bibliographic and evaluated materials properties data bases for flywheel-related applications as previously mentioned. A flywheel bibliography has been published for the 1977 Flywheel Technology Symposium in San Francisco. A numeric data base for flywheel materials is currently being developed in anticipation of the receipt of evaluated data from NBS.

FLYWHEEL AND FIBER COMPOSITES BIBLIOGRAPHY

The flywheel and fiber composites bibliography consists of two sections: (1) A concordance that serves as a subject and author index, containing key words and phrases, authors, and organizations; and (2) the bibliographic listing of citations. This format is planned for future bibliographies and other subjects in the field of energy storage.

The entire bibliography owes its existence to computer technology. It is, in a sense, merely a printed copy of part of a computerized data base. As a printed copy it is static, the data base itself is not. Several advantageous aspects of computerization are reflected in this publication.

One aspect of computerization is the opportunity to quickly look up specific information, such as what authors may have published articles on a certain subject in a given time period. Such information can be retrieved in a fraction of the time it would take to do a literature search. It should be noted that other information exists in the data base, but is not pertinent for this bibliography.

A second aspect is the ease with which statistics can be generated; for example, the number of publications by author in a certain field or by center of research in a given subject.

A third aspect is the advantage of using a computer to create the concorded bibliography. Rapid updating is possible merely by adding new entries as they appear in the literature. In fact, whole blocks of records from other data bases can be transferred by computer. Upgrading the concordance then creates a new edition ready for printing, a process much faster than conventional publishing methods. Thus, vast amounts of readily accessible data become available to the user quickly.

A final aspect is that professional value judgements play a very important role throughout the whole process. Specific terms are included or rejected, editing rules are defined, and a report structure is set up. In this manner, human intelligence and decisions are reflected in the final product.

FLYWHEEL MATERIALS NUMERIC DATA BASE

An entirely different class of data bases is represented by the numeric data base. Lists of materials pertinent to the subject, in this case flywheels, are evaluated through processess described in IDENTIFICATION OF MATERIALS AND PROPERTIES

FOR FLYWHEEL ENERGY STORAGE SYSTEMS. A spectrum of material properties is then compiled; properties included are mechanical, chemical, thermodynamic, electromagnetic, nuclear, etc. These properties are then evaluated by NBS-affiliated data evaluation centers (see CRITICAL EVALUATION OF MATERIAL PROPERTIES). The evaluated property data are subsequently computerized at LLL.

Two flywheel-related data requests have been made. The first consists of a list of 22 metals and alloys, together with nine properties for each material. The second data request contains 16 fiber materials (16 properties each), 13 epoxy resins (27 properties each), and six resins (27 properties each). Evaluation of the flywheel metals data request is close to completion. The evaluations for the fibers and matrix materials data request are still in progress. (See Appendix for detailed lists of materials and properties.)

We are placing particular emphasis on making numeric data bases interactive. Our goal is to allow the uninitiated user to sit down at a terminal and be able not only to retrieve specific data, but to do on-line manipulations of the data as well. Another goal is to allow the user to do on-line calculations with functional equations, since many of the properties are reported in functional form i.e., as empirical equations with sets of coefficients which fit the data within specific bounds of temperature, pressure, etc. Finally, we intend to make the data bases interactive so that the user, by a simple keyboard command, can print or otherwise display entire tables of data.

Computer graphics is also being pursued actively. Often, a graphical representation, such as a phase diagram, is the only form of information available for a property or relationship. Digitizing such graphical material, and reconstructing it on television monitors or x-y plotters, is a current project.

Other minor sophistications such as conversions between systems of units of measurement are being built into the computer system to provide additional convenience to the user.

In general, an interactive numeric data base, such as the one proposed for flywheels, can be a powerful research tool, potentially very versatile, easily maintained, and updated.

We welcome your comments and suggestions.

REFERENCES

1. T. M. Quick and E. A. Henry, Research Leading to the Production and Early Use of Numeric Data Banks of Material Properties and System Analyses, Quarterly Progress Report, Lawrence Livermore Laboratory, Report UCRL-50038-76-3 (March, 1977). See also Second Quarterly Progress Report, UCRL-50038-76-2 (September, 1976) and First Quarterly Progress Report, UCRL-50038-76-1 (May, 1976).

2. E. A. Henry, K. W. Johnson, F. E. McMurphy, and T. M. Quick, Bibliography of Flywheel Energy Storage Systems, Lawrence Livermore Laboratory Report, UCID-17592 (Sept. 30, 1977).

3. G. J. Janz, R. P. T. Tomkins, J. R. Downey. Jr., and C. B. Allen, Editors, "Molten Salts Awareness Bulletin, Annotated Bibliography," RPI, Troy, NY (1975).

4. G. J. Janz, C. B. Allen, J. R. Downey, Jr., and R. P. T. Tomkins, "Eutectic Data: Safety, Hazards, Corrosion, Melting Points, Compositions and Bibliography," ERDA Division of Energy Storage Systems, TID-27163-P1 and -P2 (2 volumes), July, 1976.

5. M. Shalit, Editor, "Fused Salt Bibliography," Sandia Laboratories Report, SLA-73-0053 (December, 1972).

6. L. S. Charnoff, "An Annotated Bibliography of Molten Salts," M. S. Thesis, New York University (1958), University Microfilms, Inc., Ann Arbor, MI

7. A. Borucka, "Survey & Selection of Inorganic Salts for Application to Thermal Energy Storage," ERDA-59, June, 1975.

8. G. A. Lane, D. N. Glew, E. C. Clarke, S. W. Quigley, and H. E. Rossow, "Isothermal Solar Heat Storage Materials - Phase 1," Technical Report, ERDA-117, May, 1975.

APPENDIX. Tables of flywheel-related materials and properties submitted to NBS for evaluation.

Table 1. Priorities for properties of fibers in flywheel rotors.

Property	Priority
Density	1
Elastic modulus	1
Tensile stress	1
Strain at ultimate stress	1
Usable (design) tensile strength	1
Upper use temperature	1
Creep	1
Elongation	1
Surface treatment	2
Filament diameter	2
Filaments per tow	2
Moisture absorbency	2
Thermal expansion coefficient	3
Poisson's ratio	3
Thermal conductivity	3
Specific heat	3
Electrical and magnetic properties of the amorphous, glass-like, metal alloys	3

Table 2. Priorities for fibers in flywheel rotors.

Fibers	Priority[a]
Kevlar 49	1
Kevlar 29	1
S-glass, 901	1
S-glass, 903	1
S2-glass	1
E-glass, type 30, 410	1
E-glass, type 30, 475	1
E-glass, multiend rovings	1
Carbon fiber Magnamite AS1 (Hercules, Inc.) Magnamite AS2 (Hercules, Inc.) Morganite, Type 1 (Morganite Modmor, Inc.) Morganite, Type 2 (Morganite Modmor, Inc.) Morganite, Type 3 (Morganite Modmor, Inc.) Panex 30 C (Stackpole Fibers Co.)	2
Graphite fiber Thornel 300 (Union Carbide) Thornel 50 (Union Carbide) Thornel 75 (Union Carbide) Magnamite HTS (Hercules, Inc.) Fortafil CG5 (Great Lakes Carbon Corp.) Celion 2000 (Celanese Research Corp.) GSCY 2.10 (Carborundum Co.)	2
Quartz fiber	2
Dacron, Hi Tenacity (Polyester)	3
Nylon 6, Hi Tenacity	3
Nylon 6,6, Hi Tenacity	3
Rayon, Hi Tenacity (Fortisan - 36)	3
Amorphous glass-like metal alloys METGLASS Alloy 2826 (Allied Chemical) METGLASS Alloy 2605 (Allied Chemical) METGLASS Alloy 2605A (Allied Chemical) METGLASS Alloy 2204 (Allied Chemical)	3

[a]The priorities refer to the fact that a particular fiber will probably be used in a system (1), that it might be used (2), and that it probably won't be used (3).

Table 3. Priorities for matrix systems in fiber composite flywheels.

Epoxy resin systems	Priority
XD 7818/XD 7575.02/ERL 4206 Tonox 60-40	1
DER 332/T-403	1
XD 7818/XD 7114/Tonox 60-40/DAP	1
Epon 826/RD-2/Tonox 60-40	
XD 7818/T-403	1
XD 7818/XD 7114/Epon 871/Tonox 60-40, a & b	1
XD 7818/XD 7575.02/XD 7114/Tonox 60-40/DAP	2
XD 7818/XD 7575.02/ERL 4206/Tonox 60-40/DAP	2
XD 7818/XD 7114/Epirez 505/Tonox 60-40, a & b	2
XD 7818/DER 732/Tonox 60-40, a & b	2
XD 7818/XD 7114/ATBN/Tonox 60-40	2
ERE 1359/RD-2/DAP	2
Polyester resins	
DeraKane 411C	1
EPOCRYL 480	1
Atlac 382	1
Koppers 1010-5	2
Koppers 1201-5	2
Koppers 6030-5	2

Table 4. Properties of cured resins.

Property	Priority
Composition (types and amount) Resins Diluent Curing agents	1
Cure schedule	1
Tensile properties Maximum stress Stress at failure Strain at maximum stress Strain at failure Elastic modulus in tension	1
Compressive properties Maximum compressive strength Strain at maximum strength Secant modulus	1
Shear properties Stress at failure Shear modulus	1
Viscosity at 25°C	1
Time for viscosity to reach 2.0 Pa·s	1
Gel time	1
Exotherm of 500 g from 25°C	2
Density (uncured) at 25°C	1
Density (cured) at 25°C	1
Shrinkage (% volume) After gelation After cure	1
Water absorption	1
Glass transition temperature	1
Heat distortion temperature	1
Specific heat	2
Heat capacity	2
Thermal coefficient of linear expansion	2
Thermal conductivity	2

Table 5. Priorities for metals and metal alloys in flywheel rotors.

Material	Priority
Aluminum 6061-T6	1
Aluminum 7075-T6	1
Stainless steel, 15-7Mo	1
Steel 4340	1
Maraging steel 18 Ni-300	1
Titanium 6Al-4V	1
Aluminum 2024-T851	2
Stainless steel cast AM 355	2
Stainless steel custom 455	2
Stainless steel 440C	2
Steel 1020	2
Steel 1040	2
Steel H-11	2
Cobalt MP 35N	3
Stainless steel 216	3
Steel C1141	3
Maraging steel 18 Ni-400	3
Steel, Unitemp 212	3
Steel, V-57	3
Titanium, 6Al-4V-2.5Sn	3
Titanium, 8Mo-8V-2Fe-3Al	3
Titanium, 2Mo-0.25Si	3

Table 6. Priorities for properties of metals and metal alloys in flywheel rotors.

Property	Priority
Young's modulus	1
Shear Modulus	1
Bulk modulus	1
Poison's ratio	1
Yield strength	1
Ultimate strength	1
Creep strength	1
Fatigue strength	1

GLASS FIBER FOR ENERGY STORAGE FLYWHEELS

Stewart N. Loud
Equipment Manufacturers Marketing and
Manager, Advanced Composites Section
Owens-Corning Fiberglas Corporation
Fiberglas Tower
Toledo, Ohio 43659

ABSTRACT

This paper discusses the benefits of two glass fiber candidates for energy storage flywheels manufactured from composites. Some background from other uses, test results and test programs are reviewed.

INTRODUCTION

Economically viable and commercial flywheel energy storage systems will be successful only if materials can be found with the right combination of cost and performance. Low cost, high performance S-2 Glass* and Type 30* E Glass are materials offering great promise in the energy storage system area.

BENEFITS OF GLASS FIBER

S-2 Glass is an excellent material where high performance is most important, but cost is a serious consideration versus higher priced options such as S901 Glass fiber, aramid fiber and carbon fiber composites. Type 30 E Glass is offered where low cost is paramount. Both fibers offer excellent processibility and are used regularly in commercial composites manufactured by filament winding and prepreg processes. There is a known technical base of information on both products for other application markets, which should be translatable to this market. Both products are offered with epoxy compatible sizings for optimum bonding to the matrix resin. Both can be manufactured with compatibility with polyester. Sizings compatible with polyimide and other resins which might be used could be developed if product demand justifies such an effort.

Both products are commercially available in large quantities. The base material is silica, which is in plentiful supply. S-2 Glass is produced in quantities of hundreds of thousands of pounds at the present time, with projected volumes well above that. E Glass is produced in the hundreds of millions of pounds annually. Therefore, there is a known availability and reliability of manufacturing sources. S-2 Glass Roving sells for $2.25 per pound in its most common package. Type 30 E Glass sells for $.49 per pound. Both are truckload pricing.

Lawrence Livermore Laboratories, in their contract number W-7405-ENG-48 with Energy Research and Development Administration (now part of the new Department of Energy) has done considerable work on fiber composite systems for energy storage flywheels. Their work indicates that S-2 Glass offers high composite failure stress performance, high fiber failure stress capability, good burst speed performance and a very low coefficient of variation in laminate performance. This work also indicates that Type 30 E Glass should perform well at the lower end of the performance and cost spectrum. Neither product is recommended as a candidate if the ultimate in performance or lightest possible weight is desired, and cost is little or no object. See Tables II and III from a paper given by Lawrence Livermore Laboratories personnel at the Society For the Advancement of Materials and Process Engineering Conference in San Diego in April 1977.

*Trademarks of Owens-Corning Fiberglas Corporation, Toledo, Ohio.

Some prior work on S901 roving composites, also done by Lawrence Livermore Laboratories, indicates that glass fiber composites degrade over time through a process known as stress rupture. The cause of the gradual degradation is believed to be related to deterioration of the glass/resin interface as a result of low level moisture absorption from the ambient test conditions. In past work done by Owens-Corning Fiberglas Corporation, composites have shown significant degradation after humidity conditioning. But other work has indicated that S Glass composites can be dried out and will revert to their original strength. Based on this, it is believed that glass will perform very well in a flywheel system, because the composite is operating in vacuum. Therefore, no moisture can get to the composite (the composite can be preconditioned prior to installation in the vacuum system, if it has been subjected to humid conditions) to contribute to the stress rupture phenomenon. In order to establish reliability, testing is required on glass fiber composites in the vacuum environment of an operational flywheel system.

NEW PRODUCT DEVELOPMENTS

During 1975 through 1977 Owens-Corning Fiberglas Corporation developed a new version of S-2 Glass, with 449 sizing (formerly P283A). The initial research work began in early 1975 on an unrelated S Glass program. 449 was found to be more efficient in manufacturing and to exhibit laminate performance superior to the older versions of S-2. Improvement was made in resistance of S-2 laminates to degradation under a variety of long term moisture and temperature testing. This improved sizing has resulted in a higher strength retention after water boil and temperature/humidity cycling, typically around 91 to 93% retention, which is superior to any E Glass candidates and former S Glass products known. (See Table III).

In addition to the above test results one manufacturer now scaling up on 449 S-2 Glass roving for a tactical weapon application found that 449 had 93% strength retention, compared with only 85% strength retention with the former S-2 product. Three different E Glass candidates were compared with P262B Type 30 E Glass having 88% retention and conventional rovings from two glass fiber manufacturers having only 81% retention of original values.

New Uses

Pressure Tanks -- Filament wound S-2 Glass/epoxy composites have been gaining rapid acceptance in pressure tanks for fire, police and medical rescue breathing apparatus, aircraft jet engine starter bottles and mountain climbing oxygen tanks. In October 1976 S-2 Glass tanks were carried to the top of Mt. Everest by the American Bicentennial Expedition. The much lighter weight and longer air supply available with the S-2 Glass/epoxy overwrapped aluminum tanks is credited with being a major contributor to the success of that expedition.

Tactical Weapon Launch Tubes -- S-2 Glass yarn is braided into a sleeve for reinforcement of epoxy launch tubes for the Dragon anti-tank weapon. The objective of this conversion from filament wound E Glass or metal is the desire for lighter weight, while retaining high strength to withstand the pressures of rocket launch or misfire.

Tactical Weapon Motor Cases -- We recently developed the new 449 sizing for S-2 Glass roving for filament winding into epoxy for the rocket motor nozzle on the new Viper anti-tank weapon system to be produced in 1979. Here, the high strength, light weight, competitive cost and percentage retention of original strength of S-2 after moisture conditioning, beat out maraging steel for the application.

Helicopter Blades -- We offered the new 449 sizing more recently to this market, to accelerate the acceptance and penetration of S-2 glass for helicopter rotor blades. This material is now gaining rapid acceptance with all of the major helicopter producers, including: Boeing-Vertol, Bell, Kaman and Hughes. S-2 Glass/epoxy prepreg is used for blade skins and spars. Filament winding is also being used for prototypes of spars. Rapid displacement of metal and former glass candidates is expected.

Wind Energy Blades -- Wind energy conversion systems are being prototyped under the sponsorship of NASA and ERDA. Composites are competing with metal blades for this application. Aluminum blades must be very carefully designed in order to prevent metal fatigue, which has been known to shorten their life. Composite blades offer the chance for equally light weight and far better resistance to fatigue than metal. Type 30 E Glass is the prime candidate for prototyping of a 150 foot blade in 1978, to be tested for use in the largest wind turbine yet produced in this country.

Aircraft Flooring -- Recently S-2 Glass was selected by Boeing as the reinforcement for prepreg skins to be used over Nomex* honeycomb cores to replace aluminum skinned balsa flooring now used. It is anticipated that the S-2 flooring will rapidly accelerate in growth for use in new production aircraft and later for retrofitting of older aircraft. The material is lighter in weight, offers greater ease in fabrication and is competitive in cost. Boeing is considering this flooring for all of their aircraft, as are other commercial aircraft manufacturers.

Future Development

To prove the benefits of glass fiber for composite flywheels, we as an industry must utilize the material in flywheel prototypes in their operating environment, under vacuum and zero humidity. We recommend that this be done by the various companies pursuing flywheel hardware at the present time. We also recommend that research and development be continued by the new Department of Energy on these materials so that potential users of composite materials for flywheels will receive continuing guidance on material selection for their technical programs.

Owens-Corning Fiberglas Corporation feels that it too can assist in this area. As a means of screening current products and assessing the benefits of new developments we have installed a spin test chamber at our technical center in Granville Ohio. The equipment is capable of spinning only an NOL ring test specimen, as we consider this sufficient for our purposes at this time. Also this is the size specimen used for shear testing. Equipment specifications are as follows:

Chamber size -- 8½" height, 15" diameter 2" thick wall, 1" thick bottom, 2" thick plastic ballastic-tolerant viewing plate.
Limiting Speed -- 180K RPM
Spin-up Rate -- 4 Hours
Limiting Weight -- ½ pound current specimen, range to 2 + pounds based on bearing wear.
Magnetic Centering and Support Device for Start-up.
Limiting Vacuum -- 50 microns or .0009 PSI.
Humidity -- Controlled by vacuum.
Counters -- Photo cells/automatic printout.
Failure Detection -- via counter.
Strain/Growth -- telemicroscopes -- .0001 resolution.

Conclusion

In summary, Type 30 E Glass offers a low cost candidate for future flywheel applications where economics are most critical, such as in an electrical utility storage system. S-2 Glass roving offers an economical approach to higher strength composite flywheels and is recommended for markets such as battery/flywheel hybrid commuter cars of the future, where performance and economics are critical. Performance testing programs to be conducted in 1978 and beyond by Owens-Corning Fiberglas Corporation and others in the composites and flywheel industries should be able to prove the viability.

*Nomex is a trademark of DuPont.

reliability and economy of glass fiber composites for energy storage flywheels.

References

Proceedings of the 22nd National SAMPE Symposium and Exhibition -- Volume 22, April 26-28, 1977 pp. 449 and 451 -- "Fiber-Composite Systems for Energy-Storage Flywheels" by Lynn S. Penn and E. S. Jessop.

Table I

Composite	Fiber volume, % (± 1 std dev)	N	Composite failure stress, MPa[a,b]	C.V.[c]	Fiber failure stress, MPa	C.V.[c]	Initial modulus of elasticity, G GPa
HYDROBURST TEST							
Kevlar 49/epoxy	71.3 ± 1.4	5	1810	5.0%	2540	3.8%	92.2
Kevlar 29/epoxy	73.2 ± 0.9	5	1700	6.0%	2320	6.2%	50.8
S2-glass/epoxy	70.4 ± 1.6	5	1810	3.9%	2570	3.4%	56.0
E-glass/epoxy	74.1 ± 0.8	5	986	8.1%	1330	8.8%	51.2
SPIN TEST							Burst speed, rpm / C.V.
Kevlar 49/epoxy	70.3 ± 1.5	5	1720	10.8%	2450	11.7%	51 100 / 5.5%
Kevlar 29/epoxy	73.0 ± 2.1	5	1540	12.4%	2110	13.9%	48 300 / 6.3%
S2-glass/epoxy	69.5 ± 1.1	5	1880	2.8%	2710	4.3%	43 600 / 0.2%
E-glass/epoxy	73.7 ± 1.4	5	1120	11.2%	1520	12.1%	32 400 / 5.6%

[a]Composite stress calculated using: stress = 8 x gauge pressure/cross-sectional area.

[b]To convert from Pa to psi, divide by 6.894×10^3.

[d]Based on one sample.

Table II

Composite	Composite stress (σ), MPa / Composite density (p),[a] Mg/m^3	Energy density, J/Kg[b,c]	σ/p / $[d]
Kevlar 49/epoxy	$\frac{1720}{1.36} = 1260$	6.32×10^5	$\frac{1260}{6.25} = 202$
Kevlar 29/epoxy	$\frac{1540}{1.36} = 1130$	5.64×10^5	$\frac{1130}{2.46} = 459$
S2-glass/epoxy	$\frac{1880}{2.04} = 922$	4.60×10^5	$\frac{922}{1.35} = 683$
E-glass/epoxy	$\frac{1120}{2.19} = 511$	2.53×10^5	$\frac{511}{0.56} = 913$

[a]Based on the fiber-volume fraction in table 4 (70%).

[b]Rim only (not hub) at failure.

[c]To convert J/kg to W.h/lb multiply by 1.26×10^{-4}.

[d]Cost of the composite per pound using manufacturers projected prices for fiber (Table 1) and $1/lb for resin.

TABLE III

	449 S-2 Glass Roving	P262B Type 30* E Glass	456 E Glass Conventional Roving
Shear NOL Ring			
KSI Dry	9.66	10.8	9.93
72 Hr.. Boil	9.00	9.77	8.79
% Retention	93.2%	90.5	88.5
Strand Tensile KSI	545	206	345

THE PROPERTIES OF NATURAL CELLULOSIC MATERIALS PERTAINING TO FLYWHEEL KINETIC ENERGY STORAGE APPLICATIONS

David L. Hagen
Mechanical Engineering Department
University of Minnesota
111 Church Street S.E.
Minneapolis, Minnesota 55455

ABSTRACT

Natural cellulosic materials have been shown to have moderately high tensile strengths, low densities and thus reasonably high specific energies, making them promising for flywheel energy storage applications where volume and total mass are not in question. An overview of the existing technology is discussed with special attention given to wood and wood laminates. Suggestions for further investigation are presented. Preliminary sorting of species by specific energy has revealed at least twenty five woods with axial intrinsic energy densities of over 200 kJ/kg (25 wh/lb.) Reductions in moisture and in veneer thickness do not appear to give the improvements previously anticipated. Increases in molding pressure may increase the specific energies, but double the cost. Conventional fatigue tests show high endurance, but critical energy release rates at zero moisture are significantly lower than under ambient conditions indicating greater brittleness and lower fatigue endurance. Large flywheels would appear to be readily fabricated and balanced at reasonable costs. The existing theories and data indicate the need for further experimentation to evaluate the material and fatigue properties of cellulosic materials at zero moisture under vacuum conditions. Assembled rotor costs are on the order of 3 to 5 wh/$.

INTRODUCTION

Flywheels constructed of natural cellulosic materials have been proposed for use in kinetic energy storage systems. Cellulosic materials offer high specific strengths, are readily available, have an established technology, and are low in cost. The wide variety of materials suggested for this application includes well known domestic hardwoods; wood products such as paper, pressboard, and plywood; and exotic materials such as bamboo. This paper discusses the numerous properties that affect the design, assembly, and useable operating conditions of a cellulosic flywheel.

Low cost per unit of energy stored is crucial for stationary flywheels since mass and volume are not primary considerations. The energy storage capacity is directly proportional to the strength to density ratio of the flywheel material. Thus materials with high working strengths and low densities and costs are desirable. High strength steels have been used for flywheels but have the serious disadvantage of shattering into large fragments upon failure. High tensile strength fibers and composites have recently enjoyed much popularity in flywheel research. In addition to potentially very high energy storage capabilities, these materials tend to fail by shredding, making them far safer than steel. Glass fibers and plastic aramid fibers, e.g., Kevlar, have been investigated extensively. Graphite fibers are also being considered in light of expected cost reductions in the near future.

Cellulosic fibers such as wood and bamboo have been suggested as flywheel materials by D. W. Rabenhorst[1] because of their surprisingly high strength to density ratios and low costs. He discussed the comparative advantages and potential applications of compressed wood in a vacuum, and suggests areas for further research. Another investigating team[2] has cited estimates of tensile strengths of natural fibers and of costs for small scale production. A comprehensive review of current flywheel research revealed that no work has been done to clearly establish the technical and economic practicality of wood or cellulosic fibers as flywheel

materials.[3]

This paper presents an overview of the existing technology, especially for wood, as it relates to flywheel applications; the need for further research in various areas is described. The characteristics of different species, and the effects of environmental conditions and assembly methods on energy storage capabilities are discussed. Special attention is given to the moisture content of wood as it relates to use in a vacuum. The working strengths of wood are discussed, including the effect of fatigue loading. Fracture theories and related empirical data on crack propagation are presented. Finally, methods of flywheel fabrication and the economic desirability of cellulosic materials are discussed with numerous suggestions made for additional investigation.

ENERGY STORAGE CAPABILITIES

The maximum specific energy* E_{MAX} that can be stored in a flywheel is directly proportional to the ratio of the working tensile strength σ to density ρ of the rotor material. This may be written:

$$\hat{E}_{max} = K_m(\sigma_{max}/\rho)$$

where the constant of proportionality K_m is the shape factor and varies between 0 and 1. The shape factor is typically 0.6 for a cylindrical homogeneous rotor and 0.3 for anisotropic rotors such as the multirim or brush rotors (or for a cylindrical homogeneous rotor with a hole through its axis).

The characteristics of different species, and the effects of environmental conditions and assembly methods on the specific strengths are discussed below.

* The strength to density ratio (σ/ρ) has the units of N m kg^{-1} or kJ kg^{-1} or m^{2}s^{-2}, and is here called the specific (per unit mass) energy. This has also been called the energy density by Rabenhorst. When engineering units are used, the ratio has the units of length when the acceleration of gravity is surpressed. This is called the breaking length and is equal to the length of material that can support itself under standard gravity.

Wood and other plants can be broadly defined as a composite of cellulose and hemicellulose fibers bonded together by lignin and other compounds. They are usually characterized by alternating cylindrical areas of fibers of slow and rapid growth which have large differences in strengths and elastic moduli between them. These in turn have crystalline and non crystalline regions. Because of the natural distribution of properties and defects, and the cylindrical orthotropy, statistical methods are required to accurately characterize wood. Furthermore, wood exhibits nonlinear time dependent elastic, viscoelastic, viscous (creep), and plastic behavior to various degrees at all levels of stress. These in turn depend on the previous thermal, moisture, and stress history. An excellent review of these effects was made by Schniewind[4]. The development of comprehensive constitutive equations for wood is still in the formative stages. Wood is often considered an elastic cartesian orthotropic solid with a yield point to approximate commercially available boards, veneers, and composites. At low stresses more rigorous approaches assume a linear viscoelastic model. The strengths of wood along the grain are typically twenty to forty times greater than in the tangential or radial directions. Values of the orthotropic coefficients for birch are given in the appendix.

Pure cellulose has a density of 1500 kg m^{-3} and a theoretical static tensile strength on the order of 18.9 GPa (2 x 10^6 psi) for continuous chains.[5] The stress intensity in cell walls is approximately 8.3 times the applied stress, reducing the theoretical strength of individual tracheids to 2.28 GPa (330,000 psi). Average strengths of up to 1.2 GPa (180,000 psi) for individual Douglas fir tracheids have been measured by Kersavage.[6] These are bound together in the plant to form a porous composite with a distribution of inhomogeneities and defects.

The average tensile strengths along the grain of large clear samples is typically 140 MPa (20,000 psi) or an order of magnitude lower than the fiber strength; small samples of wood and numerous species of bamboo are often two or three times this strong.

The densities of wood are typically

on the order of 700 kg m^{-3} which results in an expected specific energy of 200 kJ kg^{-1} (25 wh lb^{-1})(intrinsic).

SPECIES

The numerous species of wood exhibit a tenfold variation in both strengths and densities. The specific energies, however, only vary by a factor of two to three. The strengths of various plywoods, averaged parallel and perpendicular to the grain, and the corresponding specific energies are listed in Tables A1 and A2 in the Appendix. Similar values, measured along the grain, of a number of tropical woods are listed in Table A3. Separate tables are provided in order to distinguish the comparatively older data of Table A1 since those values do not correspond to more recent experimental results.

Note that over twenty-five species have specific energies of greater than 200 kJ kg (25 wh lb^{-1}) along the grain, or averaged specific energies parallel and perpendicular to the grain of greater than 100 kJ kg^{-1}, under ambient conditions. Thus these values of specific energy appear to be reasonably attainable and will be used as base values, even though individual species are far stronger. Further data is available in the Holzatlas.[7]

These values are more than a factor of two larger than experimental values obtained by Rabenhorst.[8,9] Further experimentation is needed to see if the strengths are reduced this much when operating in a vacuum, or if defects or experimental stress concentrations (e.g. from rapid drying) cause these reductions.

The bamboos are another natural cellulosic species with very high strengths. Experimental studies by Glenn[10] showed average tensile strengths of 277 MPa (40,200 psi) for sections without nodes for 57 species of seasoned bamboo. These ranged from 378 MPa (54,800 psi) down to 152 MPa (22,000 psi). For sections containing a node, the tensile strengths are somewhat less with an average of 196 MPa (28,4000 psi), varying from 320 MPa (46,500 psi) down to 79 MPa (11,500 psi). Strength changed little with seasoning, though it increased somewhat with age, leveling off with four year old culms.

Some species of bamboo grow over 30 m (100 ft) tall and up to 25 cm (10") in diameter with walls up to 2 cm (3/4") thick. A list of eleven species of bamboo that grow to 15 cm (6") in diameter or larger is given in Table A4. It may be possible to veneer these large species. (The Hokusan Company in Japan is currently producing ornamental bamboo veneers.) The decrease in strength at the nodes and the short lengths in between would appear to limit the applicability of bamboo to small flywheels, hardboard type composites, or multiring rotors from laminated strips. The comparatively high strengths do, however, invite further consideration. Though no densities are listed, a conservative value of 1200 kg m^{-3} implies that half these species have specific energies along the grain of more than 225 kJ/kg for clear sections.

MOISTURE CONTENT

The tensile strength of wood parallel to the grain increases fairly linearly from the fiber saturation point of 30% moisture content (m.c.) down to ambient conditions of 10% m.c. Kuch[11] gives some evidence that the tensile strengths of wood parallel to the grain peak between 8 and 10% m.c. though the data is scattered due to the natural variability of properties. Measurements of the tensile strengths of individual Douglas fir tracheids by Kersavage show a distinct peak between 8 and 12% m.c.[6] The regression curve through the points is given by eqs. (1).*

The tensile strength of dry tracheids was 65% of those at 12% m.c. Wood may have a similar reduction in strength as it drys completely.

Wood is very hydroscopic, thus difficult to dry and keep dry. Oven drying of wood gives a slight degradation of properties as compared with vacuum freeze drying. More experimentation is needed to better understand the strengths of cellulosic materials at 0% m.c. in a vacuum.

LAMINATES

The tensile strength of laminated wood or plywood increases as the thickness of the veneers decreases and more

---

* Numbered equations are listed sequentially at the end of the text.

laminates are used. However, the density also increases due to greater volume of adhesive per volume of veneer, and to a corresponding increase in compression. The resulting strength to density ratio (σ/ρ) tends to decrease as the veneers become thinner.

The average of the specific strengths of three ply Gibbon plywood are shown in Figure 1 for five thicknesses and three adhesives. The sapwood was measured separately from the hardwood plywood.[44] Similar results are obtained from the data of Preston[12] on yellow poplar with four thicknesses and six adhesives. That data is more scattered with several of the thinnest veneers showing greater specific energies. The overall trend, however, is downward.

Measurements of the strength of microtome sections of wood by Biblis[13] show that the tensile strength decrease fairly linearly with thickness below about 200μm (.008"). The tensile strength at 100μm was about half that measured in a modified ASTM Standard tensile test for the same zones. This is apparently caused by cutting the tracheids, and by the greater incidence of shear failure within the sample due to shorter fibers.

The costs will increase with increasing number of veneers and larger volume adhesives used with the thinner veneers. Greater uniformity and smaller defects would result from the thinner veneers. However, the existing data does not provide sufficient incentive to use veneers thinner than 1 mm (1/25").

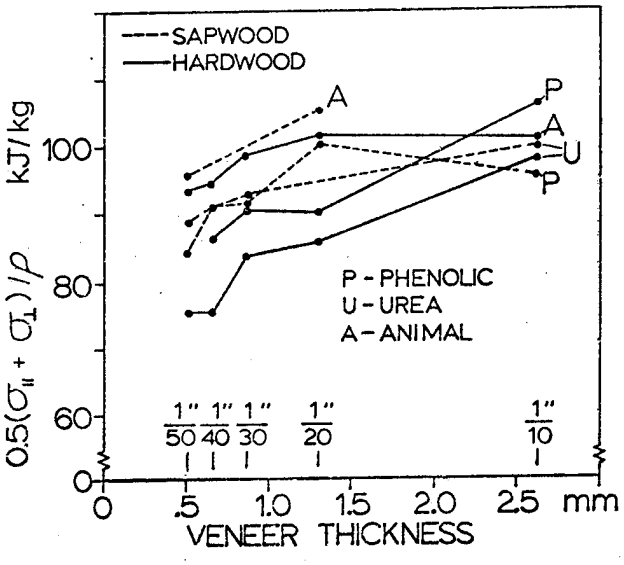


Figure 1. Average Intrinsic Specific Energies of 3 ply Gibbon Plywood versus Adhesive and Veneer thickness. Data from Princes Risborough Labs.(1974)[44]

The strength of the adhesive bond is usually greater than the shear strength of the wood so that failure generally occurs in the wood. Penetration of the adhesive and its toughness affect the overall strength, the amount of compression and the density of the veneer - adhesive combination. (See Figure 1) Phenolic resin adhesives are found to generally give greater specific strengths than urea resins. Surprisingly the animal glue appears even stronger.

The data by Preston suggests that resorcinol phenolic and phenolic resins gave the largest specific energies and strengths. Resorcinol and melamine bonded laminates were about 25% lower. These differences in specific strengths need to be compared with the resulting changes in overall costs. The comparative specific energies and fatigue properties should be tested at 0% m.c. before a final selection of adhesive can be made.

WORKING STRENGTHS

STATIC LOAD FATIGUE

A constant stress or constant strain will cause failure in wood, distinct from the more familiar cyclic fatigue fracture. Comparatively little data exist on these effects under pure tensile stresses, since in most applications wood will fail in shear before it does in tension. The existing literature is reviewed by Gerhards.[14] The constant tensile stress that wood can sustain decreases in proportion to the log of the time under load. (eqs.2) A load of 60% of the static strength will cause failure in bending in about ten years. There is considerable scatter in actual results due to the natural distribution of defects in wood. Experimental research in progress at Washington State University is investigating the effects of constant tensile loads.[15]

Wood is often considered as linearly viscoelastic. At high strain levels or with careful measurements, distinctly nonlinear behavior is observed. Echenique-Manrique[16] shows that a non Newtonian

hyperbolic sine stress rate function fits the measured data of stress relaxation much better than a linear function. He noted that the rate of permanent strain retention begins to rapidly increase at strain levels between 0.25 and 0.30%. Sugiyama[17] also noted this onset of increasingly rapid plastic deformation in creep under constant load and called it the creep limit.

Ivanov[18] noted the correlary phenomena of a sharp increase within the rate of permanent deformation under cyclic ramp loading to increasingly higher stress levels. This observation was reasonably independent of rate of loading as distinct from a "proportional limit" or 5% offset since these change with rate of loading and accuracy of experimental instruments. This point is usually reached between 50 and 60% of the static tensile strengths. Ivanov called this point the "limit of plastic flow of wood" and suggested it as the lower bound on the long term strength. King[19] presented further data along these lines. Additional long duration tensile testing will be needed to verify this proposition, but the phenomena are worth noting.

CYCLIC LOAD FATIGUE

Sugiyama conducted bending tests with a loading cycle of one day on, one day off. In the first one hundred days this resulted in less reduction in strength than an equal but constant stress. Comparatively rapid cyclic tensile testing by Kellogg[20] revealed no significant decrease in strength up to 100 cycles. Thus for low frequency tensile stress, creep due to the stress history predominates over the number of cycles in causing failure.

Fatigue studies by Lewis on Douglas fir with rapid tensile loading parallel to the grain indicate that the average working tensile strength is 85% of the static strength at 10^4 cycles and 65% at 10^6 cycles.(Fig.2)[21] Lewis recommended useable working stresses at 50% of static strengths at 30 million cycles. At 10^4 cycles, 70% would probably be suitable. (Note that 10^4 cycles is diurnal cycling for 27.4 years). Similar results were found by Egner and Rothmund.[22] In the Wood Handbook, the discussion on fatigue cites, without reference, "tests in fatigue in tension parallel to the grain indicate an endurance

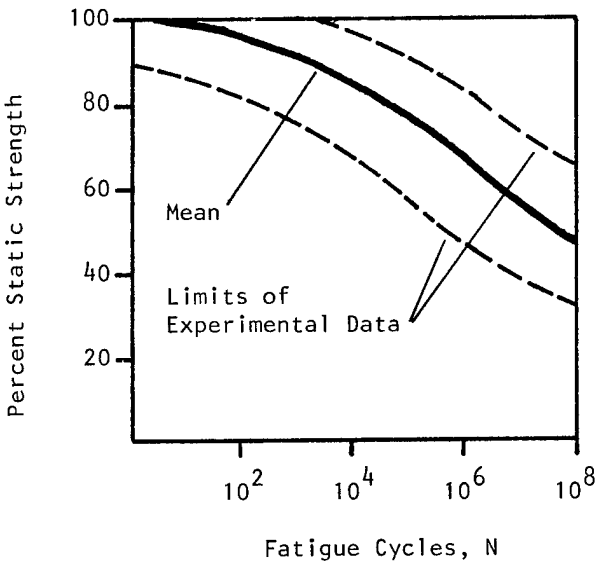


Figure 2. Strength of Birch under Cyclic Tensile Fatigue Parallel to Grain.

Data from Lewis (1951)[21]

limit of about 40% of the strength of air-dry wood as determined by the standard static test."

It is unclear what the combination of cyclic fatigue and high stress is on a cellulose rotor. Rapid cyclic fatigue will increase the internal temperature somewhat, decreasing the strength. The magnitude of this effect should be further investigated.

PRESSURE

The combination of high pressures, moisture, and elevated temperature will compress woods or laminates toward the ultimate density of 1500 kg/m^3. This has the advantage of reducing the volume of the rotor by almost a factor of two, but also increases its price due to the additional processing required. There is some evidence that the high pressures increase the specific energy by increasing the strength faster than the density.[23] Further study is needed to better understand these effects and the associated production costs to determine if the use of compressed woods or laminates for flywheels is economically promising. (See Table A5)

FAILURE THEORIES AND FRACTURE MECHANICS

The fracture mechanics theories of

Griffith modified by Irwin to include plasticity (see Knott[24]) were first applied to wood in the early 1960's and experiments are continuing to test the validity of the results with greater accuracy.

A comprehensive study of the effects of geometry, humidity, and temperature on the critical strain energy release rate G_{IC} was first conducted by Porter[25] in his doctoral thesis.* The measured values of G_{IC} were found to be reasonably independent of geometry over the wide ranges of width, height, and specimen length chosen, considering the natural distribution of properties.

At -195°C, G_{IC} was almost independent of moisture content, while for the oven dried samples G_{IC} increased only about 20% over the temperature range. Increases in moisture content, however, essentially doubled the strain energy release rate. Porter suggested that the changes due to moisture were due to viscoelastic energy losses. DeBaise, Porter and Pentoney[26] monitored acoustic emissions during studies of the fracture of White Pine in tangential-longitudinal and radial-longitudinal Mode I (opening) crack propagation. Measurements of this critical strain energy release rate G_{IC}* over a wide range of temperatures and moisture levels were fit by the expression in eqs. (2). This would indicate that under vacuum conditions, the fatigue strength of wood may be substantially less than under ambient conditions.

CRACK GROWTH

Crack growth as evidenced by acoustic emissions was initially observed at tensile stresses between 5 and 20 percent of the stress at failure. A rapid increase in the emission rates was observed during tensile loading near the maximum stress at failure. Similar increases just before failure were noticed in creep under constant load. The fracture history could also be followed in micrographs of the RL plane fracture surface. These coupled with acoustic emissions indicated numerous short crack growths caused by local stress concentrations and arrested by regions of lower stress or higher resistance.

Upon correlation with temperature and moisture data, these results indicated primarily slow fracture propagation above approximately 10% m.c. and -10°C where the material is more plastic. Below 10% m.c. the wood is more brittle and the crack exhibits numerous short jumps. Below -10°C and above 10% m.c. growth was characterized by a few long jumps.

Schniewind and Pozniak[27] have applied fracture mechanics methods to studying failure due to natural defects and cracks ("checks" resulting from drying stresses) in wood. Crack lengths of cell dimensions gave fracture toughness of 40 kPa $m^{1/2}$ (37 psi $in^{1/2}$) indicating that very little stress is required for microscopic crack growth as evidenced by the acoustic emission studies of DeBaise, et al.

Further experiments by Schniewind and Lyon[28] indicated a theoretical inherent flaw size of 2.5 mm (0.10") which was calculated from the average failure stress of samples without notches. Approximately 40% of the samples with checks of this size or smaller failed away from the checks.

Schniewind and Centeno[29] then made a detailed study of the fracture toughness in all six principal systems of crack propagation and of the duration factor for cracks propagating parallel to grain in air dried Douglas fir. These results are displayed in Table 1. The values of the critical stress intensity K_{IC} in the LT and LR systems for Mode I crack propagation were almost an order of magnitude greater than in the other systems. All differences (except between the TR and RT systems) were found to be statistically significant at the 1% level. Tests over four orders of magnitude in time showed a gradual increase in K_{IC} with the rate of loading in the TL system (but with considerable scatter in the data). The empirical expression for K_{IC} is given in eqs. (4).

The effects of size on fracture due to heterogeneity in material strength was developed by Weibull[30]. The non negative coefficient s relates the nominal stress at fracture σ_o to a characteristic length L by

$$\sigma_o = A/L^s$$

* The first subscript, I, refers to values of the critical strain energy release rate measured during Mode I crack propagation.

Table 1. Critical Stress Intensity Factors for the Six Principal Systems of Crack Propagation in Douglas Fir

Crack Propagation System[a]	Tensile Strength MPa	Critical Intensity psi $\sqrt{inch}$	Stress Factor kPa $\sqrt{m}$
LT	69	2200	2420
LR	69	2450	2690
TL	3.9	281	309
RL	3.2	373	410
TR	3.9	323	355
RT	3.2	323	355

[a] L = Longitudinal, T = Tangential, R = Radial directions; the first index refers to the normal to the crack plane, the second to the propagation direction.

in which A is a constant. Leicester[30] has calculated theoretical values of s for orthotropic materials as a function of notch angle.

Weibull's weakest link theory was used by Barrett[31] to describe the significant dependence of tensile strengths on volume and the stress distribution within specimens. Further studies by Barrett[32] showed that the critical stress intensity decreased with increasing crack width. Regression analysis of all existing data using the weakest link model gives the expression for critical stress intensity written in eq. (5). These size effects take on major importance in extrapolating laboratory results to large structures.

Large specimens demonstrated considerable nonlinearity and slow crack growth under tension. Predicted values of the critical stress intensity correlated reasonably well with experiments using the ASTM 5% offset procedure for critical load but were much lower than values derived from the maximum load.

This slow crack growth in Douglas Fir was studied by Mindess, Nadeau, and Barrett[33] by the double torsion method. At low velocities, the crack growth rate V in the RL Mode I crack geometry was related to the stress intensity K_I by

$$V = a(K_I)^m$$

in which m and a are the empirically determined slope and rate. A plot of log V versus log K_I was reasonably linear over four orders of magnitude in velocity. Critical stress intensity factors were calculated using orthotropic elastic compliances. These compared reasonably with values obtained by other studies when crack widths were included.

The time to failure under a constant applied stress, found by integration, is given in eq. (6). This theory gives reasonable comparisons with strength reductions in long term loading experiments but postulates a more gradual slope.

The rapid increase in crack growth with stress intensity described by Mindness et al. is strikingly similar to the rapid increase in acoustic emissions at about 90% of the stress at failure reportedby DeBaise, Porter and Pentoney.[26] Both these effects seem to parallel the increasing deviation from viscoelastic models under stress. A detailed correlation of these three parameters could provide convenient identification of material properties which could be used to predict the effects of stress on the fracture of wood.

The strain energy release rate G is strictly limited to linear elastic materials. Rice[24] has proposed a J integral for nonlinear elastic materials which is path independent and equal to the rate of change of potential energy with crack extension. This theory seems to be more directly applicable to wood with possible modifications for the time dependent properties. The data from preliminary tests on birch plywood proved too scattered to be useful; future investigation will require more stringent controls and larger sample sizes.

Creep-rupture tests by Bach[34] and ramp loading to fracture tests by Bach and Pentoney[35] indicate that work to failure appears to be a constant for the material. Bach has proposed a modification of Reiner-Weisenberg theory of failure to predict time dependent fracture of wood.[36] This allows any general viscoelastic model and mode of mechanical loading. It predicts failure when the viscoelastic stored energy reaches a material dependent constant. Recently, a damage theory for wood has been formulated by C. C. Gerhards[37] who is conducting experiments to test it.

ASSEMBLY METHODS

Each of the major flywheel configurations can conceivably be built with natural cellulosic materials. Veneers are commonly cut in 2.4 m (8 ft) widths, but lathes exist which can cut veneers up to 6.7 m (22 ft) wide. Paper similarly comes in standard widths of 1.8 m (72") and hardboard in 1 m (40") widths. These could easily be made larger. Manufacturing pseudoisotropic cylinders 1 to 2 meters (3' to 6') in diameter and 1 to 3 m (3' to 10') in length weighing one to ten tons out of veneer or paper should be relatively straightforward.

Glue bonds are generally as strong as the wood or paper. Continuous stips could be made for a multiring or brush type rotor while eliminating defects. Natural fibers such as flax, jute, cotton, hemp or sisal could be used in many high performance composites. A laminated plywood cylinder has been used initially as a simple straightforward configuration. This can be used as a base to compare other configurations within later developments.

Birch and beech have some of the highest specific strengths and best grain uniformity of the temperate woods. Currently 45.000 m^3 of Baltic birch plywood made of continuous plys are imported each year, while overall production is possibly 200,000 m^3. In the U.S. there are 137 x 10^6 m^3 of standing yellow birch timber and 185 x 10^6 m^3 of standing beech.† With planned replanting, one million m^3 of timber would be harvestable per year on a renewable basis. Suitable tropical woods such as Philippine mahogany are even more abundant. Thus there is an adequate supply of material.

The immediate feasibility of a cellulose rotor can readily be demonstrated by laminating commercially available solid birch plywood or tempered hardboard to form a block of material. This can be rough cut into a disk with a bandsaw, then turned on a lathe. Shafts and hubs can be glued on and aligned concentrically and the flywheel balanced by sanding material off the surface.

To demonstrate this, a small flywheel weighing 28 kg (62 lbs) has been assembled using 19 mm (3/8") commercially available Baltic birch available at a cost of $0.50 kg. This flywheel is 35 cm (14") in diameter and 38 cm (15") long. Three spin tests of 9.5 cm (3/8") thick, 73 cm (25 3/8") diameter disks of the same material demonstrated a static specific energy of 33 kJ/kg (42 wh/lb) by spinning to 11,700 rpm.*

For experimental studies the flywheel was turned on a lathe till uniform to ± .05 mm (.002"). Recessed wells were turned in a 1 cm deep and 15 cm wide to accommodate the hubs and provide a physical support in case of adhesive failure. The ends of the rotor were turned down as a truncated cone so that the increased stress from the hub recession was eliminated by halving the radius. Similarly, slightly oversize steel shafts were press fit into aluminum hubs, and bonded to the rotor with an epoxy adhesive. After assembly the shafts were turned down on a lathe to 19.05mm (0.750").

The rotor had a static imbalance of 5 g-m (7 in oz) which is equivalent to the center of mass being 0.18 mm off axis. This can be eliminated by sanding off a strip of 10 cm wide, 1 mm deep, the length of the rotor. The complete dynamic imbalance will be considered in balancing the rotor. Tests will be needed to determine the extent of imbalance caused by uneven expansion and creep of the rotor during operation.

A number of immediate improvements can be made. For example, the plywood could be made with an interply angle of 60° instead of 90° to raise the minimum strength found halfway between the primary grain directions. The average tensile strength $\sigma_{x\theta}$ at an angle θ to the face ply for 90° cross plywood is written in eq. (7)[38,47]

Experiments on fiberglass composites indicate overall specific strengths of 45% of the uniaxial fiber strengths for 60°plys as compared to 35% for 90°plies.**

† Forest Economics and Marketing Research Division of U.S. Forest Service

* Private communication with D. W. Rabenhorst, Applied Physics Lab., Johns Hopkins University

** Private communication from Dennis McGuire, Lord Corporation, 1977

This could increase the experimental static burst specific energies 28% to 45 kJ/kg (5.6 wh/lb). In addition, the press fit between shaft and hub could be replaced by an inertially forged joint which could have 90% of the original strength at nominal cost in quantity.

The elastic moduli of cold-rolled steel and birch plywood are 203 GPa (29.5×10^6 psi) and 8.5 (1.2×10^6 psi) respectively. This large difference in the elastic moduli usually causes failure at the hub to rotor bond with conventional adhesives. An elastomeric bonding layer developed by the Lord Corporation appears to have solved this problem.[9]

Conventional machining and balancing methods of removing or adding material are time consuming and expensive. Rabenhorst has proposed the use of a mechanically adjustable hub to balance a rotor. An alternative possibility is to support a flywheel with viscoelastic restraints, and spin it above its critical speed. The rotor will then spin about its true inertial axis. The rotor could be attached with a fluid bonding material and allowed to rotate on this axis as the bond becomes rigid. Various adhesives and elastomers, or inertial welding or brazing might be used.

For commercial production plywood or hardboard could be cut accurately into disks using high pressure water jets or carbon dioxide lasers. Alternatively, pulp could be molded directly into hardboard disks. These disks could be rapidly weighed to locate inherent imbalance, and then assembled so as to eliminate the gross imbalances.

Currently plywood and hardboard are designed for visual appeal, moderate strength and good weathering. The adhesives and forming methods could be reformulated for optimum specific energy and toughness at 0% m.c. Immediately after pressing, in the conventional fabrication process, the hardboard has very little moisture. Maintaining this low moisture content rather than steaming the hardboard to ambient conditions as is currently the practice, could eliminate much of the problem of later removing this water, and of the subsequent stresses involved in changing the moisture content. Production costs would also be reduced.

Tempered hardboard is made by applying pressure and heat longer to further polymerize the adhesives. This gives considerably higher tensile strengths with only moderate increase in cost. Further experimentation and better adhesives could most likely provide substantial improvement in the specific energy.

Cellulose materials, especially wood, appear to have the potential for commercial production using existing, or soon to be developed, methods. Wood science and technology have been rapidly expanding to meet the demand for more accurate measurements of wood's physical properties and for better methods to characterize the performance of wood structures. This is exemplified by recent texts on wood and composites by Kollman[39,40] and Jayne.[41]

ECONOMICS

The cost of the cellulose materials and assembly is a very strong function of the abundance of the material, the quality of the product, and the demand for production. Most paper, hardboard, and plywood is manufactured to meet the requirements of the printing and construction industries. As such they must meet stringent moisture endurance and visual standards. On the other hand interior defects and interior laminations of inferior woods are widely tolerated.

Plywoods used in aircraft, patternmaking, and other specialized industries must be uniform throughout and have good dimensional stability. About 45,000 m^3 (33,000 tons) of solid Baltic birch plywood are imported to the U.S. annually. Local prices for this fairly high quality birch are given in Figure 3 for carload quantities (i.e. for production runs of approximately 100 residential-sized flywheels). This product has knots in the interior, and exterior knots are removed and plugged. If these are located near the center of the wheel the effective useable strength could be halved, as spin tests by Rabenhorst reveal.

Plywood made without knots, or with knots away from the center, would probably double the cost. For example, a high quality beech plywood suitable for patternmaking costs $1.00/kg.* Compressing

* Manufactured in Germany by Blomberg Holtz Industry

this beech to its ultimate density of 1370 kg/m^3 raises the cost to $2.00/kg in carload quantities. Standard hardboard (masonite) by comparison costs on the order of $0.20 - 0.25/kg, while Kraft wrapping paper costs $0.45/kg in carload (25 ton) quantities.

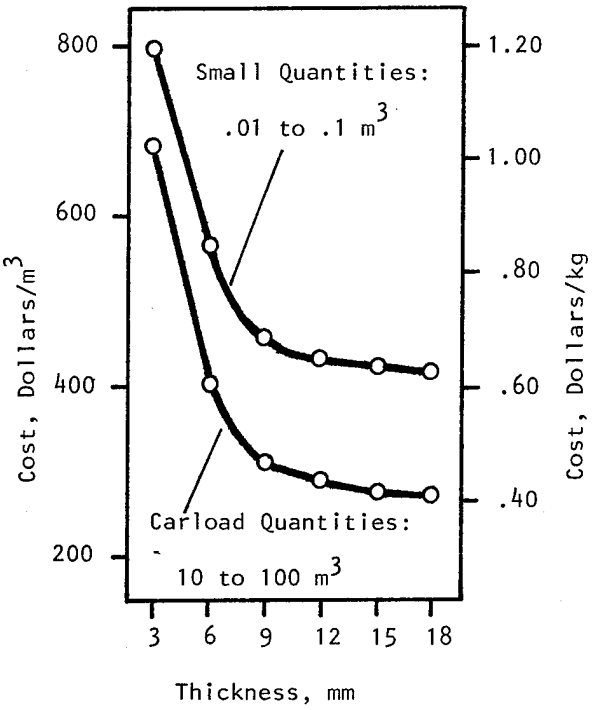


Figure 3. Retail Prices of Solid Baltic Birch Plywood Grade BB (1977)

Knots on both surfaces are removed and plugged; interior layers are continuous birch veneers with knots.

To estimate the energy storage potential of a laminated rotor, we assume an average static specific energy of 100 kJ/kg for clear plywood, or 50 kJ/kg for plywood with small knots near the center. Working strength at 10^4 cycles is estimated at 70% of static. A safety factor S of 70% is assumed together with a shape factor K_m of 0.6 for a cylinder giving an overall energy storage potential of 30 kJ/kg (3.8 wh/lb) for clear plywood or 15 kJ/kg (1.9 wh/lb) for plywood with knots. Assuming plywood costs of $1.00/kg and $0.50/kg respectively and estimating assembly costs at $1/kg, we obtain 15 kJ/$ (4.2 wh/$) and 10 kJ/$ (2.8 wh/$) as the material cost for plywood rotors in small production runs (e.g. 100 units @ 1 ton). For comparison, recent costs of Kevlar[2] and S-Glass in quantity are estimated at $15/kg and $2/kg respectively. Assembly costs are estimated to be $4/kg by virtue of the relative difficulties of construction, machinery and labor involved. The relative energy storage potentials for these materials are summarized in Table 2. The storage potentials presented for birch plywood are intended to be conservative, as are values for other species given in Tables A1 - A3. However, as discussed above, the working strengths in a vacuum might be much lower than nominal static strengths thus lowering the storage potentials. The static strengths assume plywood with 120° interply angles has a pseudoisotropic strength of the average of the axial and tangential tensile strengths.

Thus wood rotors appear to compete favorably in cost with Kevlar and fiberglass as a rotor material on the basis of preliminary material and economic estimates. More detailed studies are needed of the entire system since the greater

Table 2 Energy Storage Potential and Costs

Material	Strength σ_o[a] MPa	Density ρ kg/m^3	Fatigue Factor f[b]	Specific Energy[c] kJ/kg	Material $/kg	Costs Labor[d] $/kg	Storage $/kJ
Birch Plywood Clear	160	700	0.7	34	1.0	1.0	0.06
Knotted	80	700	0.7	17	0.5	1.0	0.09
Kevlar Composite	1380	1400	0.7	145	15.0	4.0	0.13
S-Glass Composite	1650	2000	0.3	52	2.0	4.0	0.12

a. Tensile Strengths Parallel to Fibers
b. Fatigue Factor $f = \sigma_{10^4}/\sigma_o$
c. Specific Energy = $SKf\sigma_o/\rho$

Safety Factor f = 0.7
Shape Factor K = 0.3

d. Assumed

volume and mass may decrease efficiencies and increase the cost of associated equipment more than the savings.

SUMMARY

The established technology, low cost and moderately high intrinsic specific energies of natural cellulosic materials appear to make them competitive for low cost stationary flywheels where mass and volume are not critical. A third of the species studied had initial axial tensile strength to density ratios of greater than 200 kJ/kg (25 wh/lb). These values will probably be reduced somewhat as all the moisture is removed. Thinner veneers appear to reduce the intrinsic energy densities of plywood though they provide greater uniformity. High pressure during assembly improves the intrinsic specific energy somewhat and doubles the density, but may also double the cost. Removing the moisture, and high temperature assembly may prestress the rotor causing premature failure. The magnitude of all these effects needs to be further clarified.

Tensile fatigue tests under ambient conditions indicate that wood has a high endurance similar to other polymeric materials. However fracture mechanics studies indicate that wood is more brittle at zero moisture with significantly lower strain energy release rates. Creep in wood under constant stress also reduces the strength and can result in eventual failure. The combined effects of cyclic fatigue and sustained stress over long periods at zero moisture is unknown and needs further study.

A pseudoisotorpic cylindrical cellulose rotor made of plywood with 120° interply angles should be able to store 30 kJ/kg (3.8 wh/lb) over 10,000 cycles. It appears possible to readily fabricate and balance large flywheels weighing one to ten tons at reasonable costs. Medium quality homogeneous plywood is available for $0.50 to $1.00/kg. With assembly costs of similar magnitude, overall costs for the rotor on the order of 3-5 wh/$ seed commercially feasible, making cellulose competitive with stationary Kevlar or S-glass rotors.

These results indicate poorer performance than previously expected but that cellulose rotors still appear to compete realistically with expensive high performance fibers. Further experimentation is required to reliably define the properties of cellulosic rotors over the flywheel's life cycle operating conditions, and to demonstrate cost effectiveness.

ACKNOWLEDGEMENTS

Financial support for this work was kindly provided by the Minnesota Energy Agency and the University of Minnesota's IT Corporate Fellowship Program.

EQUATIONS

Tensile strength of individual summerwood Douglas fir trachieds as a function of percent moisture content x:

$$\sigma_o = 774.8 + 53.0x - 1.97\,x^2 \quad \text{MPa}$$
$$= 112{,}500 + 7{,}683 - 289\,x^2 \quad \text{psi} \qquad (1)$$

Empirically the tensile strength σ_t at time t under constant stress decreases logrithmically from the initial strength σ_i as:

$$\sigma_t = \sigma_i - A \ln t \qquad (2)$$

Critical strain energy release rate G_{IC} as a function of the absolute temperature T in degrees Kelvin, and the moisture content x, in percent of oven-dry weight:

$$G_{IC} = 224 + 1.97(T-243)(1-e^{-x/6}) \quad \text{kJ/m}^2$$
$$= 1.28 + 0.01125(T-243)(1-e^{-x/6}) \quad \text{psi} \qquad (3)$$

Critical stress intensity K_{IC} as a function of time to failure under ramp loading t in seconds:

$$K_{IC} = 304.4 - 10.1 \log t \quad \text{kPa m}^{1/2}$$
$$= 276.1 - 9.2 \log t \quad \text{psi in}^{1/2} \qquad (4)$$

Critical stress intensity K_{IC} as a function of total crack width B in inches:

$$\log K_{IC} = 2.55 - 0.135 \log B \qquad \text{psi in}^{\frac{1}{2}} \qquad (5)$$

Time to failure τ under constant applied load σ_a as a function of critical stress intensity K_{IC}, and fracture strength σ_f, in which m and a are the slope and intercept of the ln V^{IC} versus ln K_I plot where V is the crack velocity:

$$\tau = 2[K_{IC}\ \sigma_a/\sigma_f]^{(2-m)}/[(m-2)Y^2\sigma_a{}^2\ a] \qquad (6)$$

Average tensile strength $\sigma_{x\theta}$ at angle θ to the face ply of 90° cross plywood in which θ_x and θ_y are the ultimate tensile strengths parallel and perpendicular to the grain, and θ_{xy} is the ultimate shear strength:

$$\sigma_{x\theta} = \left(\frac{\cos^4\theta}{\sigma_x^2} + \frac{\sin^4\theta}{\sigma_y^2} + \frac{\sin^2\theta\ \cos^2\theta}{\sigma_{xy}^2} \right)^{-\frac{1}{2}} \qquad (7)$$

REFERENCES

1. D. W. Rabenhorst, "The Applicabilty of Wood Technology to Kinetic Energy Storage," Johns Hopkins University--Applied Physics Lab., APL/JHU Tech. Dig., 11(5) 2-12 (May-June 1972).

2. Rockwell International Space Division, "Economic and Technical Feasibility Study for Energy Storage Flywheels," Fianl report to E.R.D.A. div. Conservation Research and Tech., No SD75-SA-0166, Contract AT(04-3)-1066 (Dec. 1975).

3. D. L. Hagen & A. G. Erdman,"Flywheels for Energy Storage:A Review with Bibliography," Design Eng. Tech. Conf., Montreal, ASME Paper No. 76-DET-96 (Sept. 26-29,1976).

4. A. P. Schniewind, "Recent Progress in the study of the rheology of wood," Wood Sci. Tech.,2,188-206(1968).

5. R. Mark, "Cell Wall Mechanics of Tracheids," Yale Univ. Press, New Haven, Conn., (1967).

6. Paul C. Kersavage, "Moisture Content Effect on Tensile Properties of Individual Douglas-Fir Latewood Tracheids," Wood & Fiber, 5(2),105-117 (Summer 1973).

7. Rudi Wagenfuhr,ed., Holzatlas,(Fachbuchuerlag, Leipzig, 1975)

8. D. W. Rabenhorst & T. R. Small, "Composite Flywheel Development Program Progress Report: March-September, 1976," Johns Hopkins University-Applied Physics Lab., APL/JHU No. SDO-4616, N.S.F. Grant No. AER75-20607 (October 1976).

9. D. W. Rabenhorst, "Composite Flywheel Development Program-Final Report," Johns Hopkins University-Applied Physics Lab. APL/JHU SDO-4616A, N.S.F. Grant No. AER75-20607 (1977).

10. H. E. Glenn, "Seasoning, Preservative and Water-Repellent Treatment and Physical Property Studies of Bamboo," Eng. Expt. Sta. Clemson Agricultural College, The A & M College of So. Carolina, Bulletin No. 8 (July 1956).

11. W. Kuch, "Der Einfluss Des Feuchtigkeitsgehalts auf Die Festigkeit von Voll- und schichtholz." Holz Als Roh- und Werkstoff 6,157-161 (1943)

12. Stephen B. Preston, "The Effect of Synthetic Resin Adhesives on the Strength and Physical Properties of Wood Veneer Laminates," Yale University:School of Forestry, Bulletin No. 60, (1954).

13. Evangelos J. Biblis, "Effect of Thickness of Microtome Sections on their Tensile Properties," Wood and Fiber,2(1) 19-30(Spring 1970).

14. Charles C. Gerherds, "Effect of Duration andRate of Loading on Strength of Wood and Wood-Based Materials," USDA Forest ServiceRes. Paper FPL283 (1977).

15. C. C. Gerhards, J. D. Barrett, B. Madsen, M. D. Strickler, & R. Pellerin, "Proposed Studies of Time-Related Load Effects on Wood Materials: An Invitation to Participate in Research," For. Prod. J. 26(12), 39-40 (1976).

16. Ramon Echenique-Manrique, "Stress Relaxation of Wood at Several Levels of Strain," Wood Sci. and Tech. 3,49-73(1969).

17. Hideo Sugiyama, "On the Effect of the Loading Time on the Strength Properties of Wood: A Review of Japanese Research," Wood Science and Tech. 1, 289-303 (1967).

18 Iu. M. Ivanov, "The Limit of Plastic Flow of Wood," U.S.D.A. Forest Prod. Lab. Translation No. 111 by H. P. Kipp (August 1955).

19. Edward G. King Jr., "Creep and Other Strain Behavior of Wood in Tension Parallel to the Grain," Forest Prod. J. 7, 324-330 (1957).
20. R. M. Kellogg, "Strain Behavior of Wood: Subjected to Repetitive Stressing in Tension Parallel to the Grain," Forest Prod. J. 8,301-307 (October 1958).
21. Wayne C. Lewis, "Fatigue of Wood and Glued Joints Used in Laminated Construction," Forest Prod. Res. Soc. 5,221-229 (1951).
22. K. Egner & A. Rothnund, "Zusammenfassender Bericht über Dauerzugversuche mit Hölzern," Materialprufungsanstalt Tech. Hochschule Stuttgart, (1944).
23. R. M. Seborg, Harold Tarkow & A. J. Stamm, "Modified Woods," U.S.D.A. Forest Service, For. Prod. Lab. Report No 2192, Revised (November 1962).
24. J. F. Knott, Fundamentals of Fracture Mechanics, (John Wiley & Sons, 1973).
25. Andrew W. Porter, "On the Mechanics of Fracture in Wood," Forest Prod. J. 14(8),325-331 (August 1964).
26. G. R. DeBaise, A. W. Porter, R. E. Pentoney, "Morphology and Mechanics of Wood Fracture," Materials Research & Standards, 6(10), 493-499 (October 1966).
27. A. P. Schniewind and R. A. Pozniak, "On the Fracture Toughness of Douglas Fir Wood," Engineering Fracture Mechanics 2 223-233, (1971).
28. A. P. Schniewind & D. E. Lyon, "A Fracture Mechanics Approach to the Tensile Strength Perpendicular to Grain of Dimension Lumber," Wood Science and Technology, 7, 45-59, (1973).
29. A. P. Schniewind & J. C. Centeno, "Fracture Toughness and Duration of Load Factor I. Six Principal Systems of Crack Propogation and the Duration Fact Cracks Propogating Parallel to Grain." Wood & Fiber 5(2),152-159 (1973)
30 R.H. Leicester, "Effect of Size on the Strength of Structures", Forest Prod. Lab. Div. Bldg. Res. Tech. Paper No. 71 Comm. Sci. & Ind. Res. Org. Australia(1973)
31 J.D. Barrett, "Effect of Size on Tension Perpendicular-to-grain Strength of Douglas-Fir", Wood & Fiber 6(2),126-143, (1974).
32 J.D. Barrett "Effect of Crack-front Width on Fracture Toughness of Douglas-Fir." Engr. Fracture Mechanics 8(4),711-718 (1976)
33 Sidney Mindess, John S. Nadeau, & J. D. Barrett, "Slow Crack Growth in Douglas-Fir." Wood Sci. 8(4),389-396,(1975).
34. Lars Bach, "Static Fatigue of Wood under Constant Strain," Inform. Rep. For. Prod. Lab. Vancouver, No. VP-x-24(1967).
35. Lars Bach & R. E. Pentoney, "Non-Linear Mechanical Behavior of Wood," Forest Prod J. 18(3), 60- (1968).
36. L. Bach, "Reiner-Weisenberg's theory applied to time-dependent fracture of wood subjected to various modes of mechanical loading," Wood Science 5(3),161-171 (1973).
37. Charles C. Gerhards, "Time Related Effects of Loads on Strengths of Wood," Proc. Conf Environmental Degredation of Engineering Materials, Virginia Polytechnic Inst., State Univ. Blackburg, VA. (October 10-12, 1977).
38. E. C. O. Erickson & K. H. Boller, "Strength and Related Properties of Forest Products Laboratory Laminated Paper Plastic (Papreg) at Normal Temperature," U.S.D.A. Forest Service, Forest Prod. Lab.No.R1319 (May 1945).
39. F. F. P. Kollman & W.A. Côté, Jr., Principles of Wood Science and Technology I. Solid Wood, (Springer-Verlag, Inc.,New York, N.Y., 1967).
40. F. F. P. Kollmann, E.W. Kuenzi & A. J. Stamm, Principles of Wood Science and Technology II Wood Based Materials, (Springer-Verlag, New York, N.Y. 1975).
41. Benjamin A. Jayne, Theory and Design of Wood and Fiber Composite Materials, (Syracuse University Press, 1972).
42. D. V. Doyle, J. T. Drow, & R. S. MacBureney, "The Elastic Properties of Wood," U.S. Dept. Agr. For. Prod. Lab. Mimeo 1528 and supplements A to H, Madison, Wisconsin, (1945/1946).
43. A. E. Elmendorf, ed., "Data on the Design of Plywood for Aircraft," National Advisory Committee for Aeronautics Ann. Rpt.(1920) Tech. Rpt. 84 (1921).
44. Princes Risborough Laboratories, The Strength Properties of Timber, Section 3, (1974).
45. Robert M. Kellogg & Geza Ifju, "Influence of Specific Gravity and Certain Other Factors on the Tensile Properties of Wood," Forest Products J. 12(10), 463-470 (October 1962).
46. F.A. McClure, "Bamboo as a Building Material," Foreign Agricultural Service, U.S.D.A., (May 1953).
47. Note: See also the Army-Navy-Civil Committee on Aircraft Design Criteria ANC Bulletin 18 (June 1944).

APPENDIX

HOOKE'S LAW FOR ORTHOTROPIC MATERIALS

Hooke's law for orthotropic materials can be written according to the matrix equations

$$\underline{\varepsilon} = \underline{\underline{S}}\,\underline{\sigma} \quad \text{and} \quad \underline{\sigma} = \underline{\underline{C}}\,\underline{\varepsilon} \quad \text{where } \underline{\underline{C}} = \underline{\underline{S}}^{-1}$$

$\underline{\varepsilon}$ = the strain vector, $\underline{\sigma}$ = the stress vector

$\underline{\underline{S}}$ = the compliance matrix $\underline{\underline{C}}$ = the stiffness matrix

Values of the compliance matrixes are sumarized by Kollmann[39-42]. The values for Yellow Birch for instance as measured by Doyle, Drow and McBurney[42] are as follows where the tangential direction is first, longitudinal second and radial third. The compliances S_{ij} are in units of 10^{-10} Pa^{-1}.

$S_{11} = 13.87$ $S_{44} = 9.43$ $S_{12} = S_{21} = -0.324$ All other $S_{ij} = 0.0$

$S_{22} = 0.700$ $S_{55} = 41.7$ $S_{13} = S_{31} = -6.12$

$S_{33} = 8.93$ $S_{66} = 10.30$ $S_{23} = S_{32} = -0.343$

The Youngs moduli $\underline{E}$ and the shear moduli $\underline{G}$ in units of GPa are:

$E_{TT} = 1/S_{11} = 0.721$ $G_{LR} = 1/S_{44} = 1.060$

$E_{LL} = 1/S_{22} = 14.3$ $G_{RT} = 1/S_{55} = 0.239$

$E_{RR} = 1/S_{33} = 1.119$ $G_{TL} = 1/S_{66} = 0.971$

The bulk Poisson's ratio $= -\dfrac{S_{31} + S_{12} + S_{23}}{S_{11} + S_{22} + S_{33}} = 0.288$

The directional Poisson's ratios can be obtained by taking ratios of the appropriate compliances. Further correlations and equations can be found in Kollmann[39] or Jayne[41].

METRIC CONVERSION FACTORS

1 lb (avoirdupois) = 0.4535924 1 psi = 6.894757×10^3 Pa

1 kgf/cm^2 = 1 kp/cm^2 = 9.806650×10^4 Pa 1 wh/lb = 7.93664 x kJ/kg

1 wh = 3.6 kJ

TABULATED DATA

Tables A1 through A5 appear on the following pages.

Table A1. Average Tensile Strengths and Specific Energies of Common Hardwoods[a]

Species (Common Name)	Density ρ kg /m^3	Moisture Content %	Tensile Strength[b] σ_{av} MPa	Psi	Specific Energy $\sigma av/\rho$ kJ/kg
Mohagany, Philippine (Tanguile)	530	10.7	57.4	8,330	108.4
Birch, Yellow	670	8.5	72.1	10,460	107.6
Beech	670	8.6	70.0	10,150	104.4
Basswood	420	9.2	38.5	5,590	91.8
Magnolia	580	8.8	51.5	7,475	88.9
Cherry, Black	560	9.1	49.6	7,190	88.5
Cottonwood	460	8.8	39.7	5,760	86.3
Maple, Hard	680	8.0	57.6	8,360	84.8
Poplar, Yellow	500	9.4	41.8	6,055	83.5
Maple, Soft	570	8.9	46.8	6,780	82.0
Sweetgum	540	8.7	44.1	6,390	81.6
Sycamore	560	9.2	45.7	6,625	81.6
Walnut, Black	590	9.1	46.6	6,755	78.9
Elm, Cork	620	9.4	48.1	6,970	77.5
Mahogany, True	480	11.4	35.1	5,085	73.0
Douglas Fir	480	8.6	34.8	5,050	72.5
Tupelo, Black (Blackgum)	540	10.6	38.9	5,640	72.0
Ash, Black	490	9.1	34.9	5,060	71.2
Hackberry	540	10.2	37.7	5,470	69.8
Elm, White	520	8.9	34.0	4,925	65.3
Ash, White	600	10.2	37.4	5,430	62.4
Mahogany, African (Khaya)	520	12.7	31.5	4,570	60.6
Oak, White	640	9.5	37.7	5,465	58.9
Oak, Red	590	9.3	31.3	4,545	53.1

[a]Elmendorf, A. E., ed., "Data on the Design of Flywood for Aircraft", National Advisory Committee for Aeronautics Ann. Rpt. (1920)

[b]Average of tensile strengths parallel and perpendicular to face grain of three equal plies .1 to .5 inch thick.

Table A2. Average Tensile Strengths and Specific Energies of Tropical Hardwoods[a]

Species	Density ρ kg /m^2	Moisture Content %	Average Tensile Strength σ_{av} Psi	MPa	Specific Energy σ_{av}/ρ kJ/kg
Birch, Yellow (Betula Alleshani)	710	10.3	13,605	93.8	132.0
Kawang Jantong (Shorea Macrophyl)	415	9.1	7,535	52.0	125.3
Nkobakoba (Triplochiton scl)	815	9.3	13,880	95.7	117.5
Gagil (Hopea Sangal)	656	8.6	10,711	73.8	112.5
Seraya, White (Sterculia Rhinop)	477	8.8	7,709	53.2	111.4
Seraya, Red (Parashorea Malaa)	483	9.5	7,658	52.8	109.2
Keruing, Sabah (Protium Decandru)	725	9.0	11,472	79.1	109.1
Seraya, White (Parashorea Spp.)	627	10.2	9,507	65.6	104.5
Pterygota, African (Gonystylus Banca)	671	9.5	9,971	68.8	102.5
Maho (Khaya Nyasica)	631	12.0	9,355	64.5	102.2
Kurokai (Anigeria Robusta)	698	9.8	10,160	70.0	100.4
Ramin (Entandrophragma)	667	10.6	9,652	66.5	99.8
Kapur, Saba (Bryobalanops Ian)	646	9.9	9,275	64.0	99.0
Agba (Gossweilerodend)	577	11.2	7,934	54.7	94.8
Selangan, Red (Shorea Sp.)	825	8.7	11,335	78.2	94.7
Sepetir (Shorea Sp.)	640	10.1	8,753	60.3	94.4
Kauri, Fijian (Agathis Vitiensi)	552	8.1	7,527	51.9	94.0
Seraya, Red (Shorea Spp.)	469	11.7	6,324	43.6	93.0
Baromalli (Catostemma Commu)	819	11.9	10,863	74.9	91.5
Afrormosia (Pericopsis Elata)	748	9.6	9,848	67.9	90.8
Chile Pine (Araucaria Arauca)	552	12.7	7,223	49.8	90.2
Mora (Newtonia Buchana)	969	10.1	12,575	86.7	89.5

continued next page

[a]Princes Risborough Laboratories, The Strength Properties of Timber, Section 3 (1974)

Table A2 Continued

Species	Density ρ kg /m^3	Moisture Content %	Average Tensile Strength σav Psi	MPa	Specific Energy σav/ρ kJ/kg
Binuan (Octomeles Sumatr)	415	14.0	5,337	36.8	88.8
Landosan (Sterculia Prurie)	556	9.6	7,085	48.9	87.8
Sterculia, Brown (Sterculia Oblong)	862	10.5	10,936	75.4	87.4
Poon (Pterygota Bequae)	554	12.3	6,991	48.2	87.0
Kembang (Dipterocarpus Ca)	704	7.8	8,855	61.0	86.7
Sterculia, Yellow (Oxystigma Oxyphy)	808	9.3	10,153	70.0	86.6
Pine, Scots (Pinus Sylvestris)	598	11.2	7,506	51.8	86.6
Adwea (Dacryodes Klaine)	802	9.7	10,051	69.3	86.4
Gaboon (Aucoumea Klainea)	465	11.4	5,765	39.8	85.6
Kapur, Saba (Dryobalanops Bec)	750	9.2	9,290	64.0	85.4
Obeche (Daniellia Ogea)	375	9.8	4,627	31.9	85.1
Saple (Shorea Guiso)	677	10.5	8,035	55.4	81.8
Berlinia (Berlinia Cónfusa)	740	10.4	8,688	59.9	81.0
Tchitola (Entandrophragma)	625	7.0	7,324	50.5	80.8
Mahogany, A. Rican (Khaya Ivorensis)	679	8.5	7,890	54.4	80.1
Danta (Nesogordonia Psp)	735	12.9	8,535	58.9	80.0
Muchenche (Tarrietia Utilis)	629	8.7	7,201	49.7	78.9
Abura (Mitragyna ciliat)	602	9.2	6,773	46.7	77.6
Makore (Mora Excelsa)	592	10.0	6,628	45.7	77.2
Greenheart (Ocotea Rodiaei)	998	11.1	11,023	76.0	76.2
Utile	617	15.0	6,744	46.5	75.4
Douglas Fir (Pseudotsuga Menz)	523	10.8	5,714	39.4	75.3
Afara (Terminalia Super)	604	11.5	6,541	45.1	74.6
Mahogany, A. Rican (Tiehgemella Heck)	560	13.9	6,019	41.5	74.1
Niangon (Baikiaea Insigni)	685	12.0	7,201	49.7	72.4
Selangan Batu (Pseudosindora Pa)	917	8.2	9,442	65.1	71.0
Cebia (Ceiba Pentandra)	412	15.3	3,989	27.5	66.7
Ogea (Calophyllum Tone)	410	12.7	3,909	27.0	65.7

Table A3. Tensile Strengths and Specific Energies of Tropical Woods Parallel to the Grain[a]

Common	Botanical	Density ρ kg/m^3	Moisture Content %	Modulus of Elasticity GPa	Tensile Strength σ_u Psi	MPa	Specific Energy kJ/kg
Chewstick	Syphonia Globulifera	724	10.0	24.0	34,500	238	329
Hickory	Carya Sp.	859	11.3	22.4	36,500	252	293
Copaia	Jacaranda Copaia	354	8.7	12.3	14,900	102	290
White Pine	Pinus Strobus	380	10.5	13.2	15,900	110	289
Cedro Granadino	Cedrela Tonduzii	389	12.4	11.1	14,700	101	261
Timbauba	Enterolobium Schomburgkii	965	11.3	24.8	35,200	243	252
Laurel Blanco	Cordia Alliodora	555	9.9	11.9	19,800	137	246
My Lady	Aspidosperma Cruentu	742	10.4	18.4	25,700	177	239
Roble Blanco	Tabebuia Pentaphylla	589	10.4	14.7	18,800	130	220
Acapu	Vouacapoua Americana	846	11.1	20.1	26,500	183	216
Espave	Anacardium Excelsum	485	9.2	12.4	14,500	100	206
Nargusta	Terminalia Amazonia	714	11.2	12.3	21,200	146	205
Brazil Nut	Bertholletia Excelsa	640	10.7	13.5	18,300	126	197
Simaruba	Simaruba Smara	403	9.0	9.2	10,900	75	186
Kaneelhart	Licaria Cayennensis	1,006	11.2	25.0	27,000	186	185
Bannia	Swartzia Bannia	1,180	7.9	29.5	31,200	215	182
Redwood	Sequoia Sempervirens	327	9.2	7.3	7,810	54	165
Sapupira	Diplotropis Purpurea	811	8.4	21.1	19,100	132	162
Ceiba	Ceiba Pentandra	262	13.3	4.4	6,010	41	158
Determa	Ocotea Rubra	543	9.0	10.7	11,800	81	150
Ceibai	Ceiba Pentandra	222	11.9	2.9	3,300	23	103

[a]Kellogg, R. M., and Ifju, G., "Influence of Specific Gravity and Certain Other Factors on the Tensile Properties of Wood," Forest Products Journal, Vol. 22, No. 10, October 1962, pp. 463-470.

Table A4. Species of Large Bamboos[a]

Bambusa balcooa: Balku Bans (Bengali), Baluka (Assam), Borobans, Sil Barua, Teli Barua, Wamnah, Beru, Betwa. INDIA. 15 to 21 m by 8 to 15 cm.

Bambusa polymorpha: Kyathaungwa (Burmese), Betua (Assam), Jama Betua (Bengali). INDIA (E. Bengal) and BURMA. 15 to 24 m by 8 to 15 cm.

Dendrocalamus asper: Bulah Betong, B. Panching (Malay), Kuur (Sakai), Deling Petung, Jajang Betung, Pring Petung (Java), Awi Betung, Bitung (Sudan), Bambu Batueng, Pering Betung (Sumatra), Bontong (P.I., teste Hugh Curran, Jr.) MALAYSIA: Java. 30 m by 15 to 20 cm.

Dendrocalamus brandisii: Kyellowa, Waya, Wapyu (Burmese), Wakay (Warren), Waklu. INDIA and BURMA. 24 to 36 m by 12 to 20 cm.

Dendrocalamus giganteus: Wabo (Burma), Worra (Assam). INDIA. 24 to 30 m by 20 to 25cm.

Dendrocalamus hookerii: Seiat, Ussey, Sejasai, Sigong, Denga, Ukotang, Patu, Tili, Kawa Ule. INDIA to UPPER BURMA. 15 to 18 m by 45 to 50 cm.

Dendrocalamus sikkimensis: Pugriang (Lepcha), Wadah (Garo Hills), Tiria, Vola (Nepal). INDIA and BHUTAN. 15 to 18 m by 13 to 18 cm.

Gigantochloa levis: Kawayan-bó-o, K. Sina, K. Puti, Bohó (Tagalog), Bokó, Bolo, Botong (Bisaya), Butong (teste Hugh Curran, Jr.). PHILIPPINE ISLANDS. 20 m by 15 to 20 cm.

Gigantochloa verticillata: Whorled Bamboo, Bamboo Andong (Malay), Pring Soorat (Java), Andong Kekes, Awi Andong, A. Gambong, A. Liah, A. Soorat (Sunda). JAVA. 21 m by 15 cm to 2 cm thick.

Guadua angustifolia: Guadua. ECUADOR, COLOMBIA, and PERU. 27 m by 15 cm to 2 cm thick.

Phyllostachys bambusoides: Giant Timber Bamboo, Madake (Japanese), Kam Chuk (Chinese). CHINA and JAPAN. 23 m by 15 cm.

[a]McClure, F. A., "Bamboo as a Building Material", Foreign Agricultural Service, U. S. Department of Agriculture, May 1953, pp. 32-39.[46]

Table A5. Molding Pressure and Specific Energy[b]

Resin	Resin Content %	Density kg m^{-3}	Tensile Strength MPa	Specific Energy kJ kg^{-1}
At 4.1 Mpa (600 psi)				
A	28.0	1200	301	246
B	32.0	1240	300	242
C	28.5	1240	330	266
			Average	252
At 10.3 Mpa (1500 psi)				
A	28.5	1360	370	272
B	31.5	1360	377	277
C	28.0	1370	354	258
			Average	269

[b]Tensile strength parallel to grain of parallel laminated birch Compreg made from 1.6 mm veneers. Data from Seborg, Tarkow and Stamm (1962)[22].

CRITICAL SPEED FOR STANDING-WAVE INSTABILITY IN A FILAMENT-WOUND-COMPOSITE RING-TYPE FLYWHEEL

C.W. Bert
School of Aerospace, Mechanical and Nuclear Engineering
The University of Oklahoma
Norman, Oklahoma 73019

ABSTRACT

Two different solid-mechanics analyses are made to predict the lowest critical speeds associated with so-called standing-wave instability for ring-type flywheels constructed of filament-wound composite material. This type of instability has been found to occur when the angular speed of a backward-traveling transverse wave coincides with the disk's forward rotational speed, so that the wave becomes a standing wave with respect to a fixed reference frame. In one analysis, thin-plate theory is employed; in the other thin-ring theory, including both twisting and out-of-plane deformation, is used.

INTRODUCTION

For over fifty years, the following facts about transversely vibrating disks spinning at constant rotational speed (Ω) have been known from experimental observations[1]: The transverse motion consists of a backward traveling wave and a forward traveling wave of smaller amplitude. Under a constant, steady axial force, critical speed instability occurs when the angular speed of the backward wave (ω_n/n) coincides with Ω. Here n is the circumferential wave number and ω_n is the lowest frequency associated with that wave number. Thus, the critical speed is given by

$$\Omega_{cr} = (\omega_n/n)_{min} \qquad (1)$$

Additional experiments have been reported on isothermal spinning disks[2-4] on circular saws which undergo edge heating[5] and on automobile tires[6].

Most analyses of transverse vibration of spinning disks have neglected the flexural rigidity of the disk, i.e., the disk was considered to be a membrane, either linear isotropic[7-10], linear cylindrically orthotropic[11-12], or isotropic with geometric nonlinearity[2,4,13-15].

Plate flexural rigidity was included in the formulation by Goldberg and Setlur[16], but they gave no significant numerical results. Barasch and Chen[17] included flexural rigidity in their numerical analysis and confirmed the following simple relation among the natural frequencies of the same model numbers, first hypothesized by Lamb and Southwell[7]:

$$\omega^2 = \omega_{rm}^2 + \omega_{np}^2 \qquad (2)$$

where ω is the frequency predicted for a rotating plate, ω_{rm} is that of a rotating membrane, and ω_{np} is that of a nonrotating plate. Dugdale[3] used an energy approach, which is equivalent to the use of Eq. (2). Nowinski[18] considered both flexural rigidity and geometric nonlinearity, but considered only a solid disk.

So far as is known by the present investigator, there have been no critical-speed analyses of rotating disks of cylindrically orthotropic material. In view of the current interest in flywheels constructed of such materials by means of the filament-winding process, an analysis of this problem is presented here. The plate geometry considered is that of a concentric circular annular plate such as could be used in a ring-type flywheel.

The present work also considers the same problem by application of linear thin-ring theory including twisting of the ring cross section as well as out-of-plane displacement.

Finally numerical results are presented for some typical flywheels under consideration for energy storage application in hybrid automotive vehicles.

ANALYSIS USING THIN-PLATE THEORY

The basis for the present analysis is Eq. (2). For determining ω_{rm}, Ghosh's analysis[11-12] of a cylindrically orthotropic spinning membrane is used. The numerical results obtained by Ramaiah and Vijayakumar[19] for the natural frequencies of a nonrotating cylindrically orthotropic plate are used for ω_{np}. After inserting ω_{rm} and ω_{np} into Eq. (2) to obtain ω, Eq. (1) is utilized to obtain the critical speed Ω_{cr}.

The frequency expression derived by Ghosh may be written in the following form:

$$\omega_{rm}^2(m,n) = \Omega^2 K(m,n) \qquad (3)$$

where m and n refer to the respective radial and circumferential mode numbers and

$$K(m,n) \equiv [(3Q_{rr}+Q_{r\theta})(k_1-m\alpha)(k_1-m\alpha+2) - (3Q_{r\theta}+Q_{rr})n^2](9Q_{rr}-Q_{\theta\theta})^{-1}$$

$$k_1 \equiv -\tfrac{1}{2}(\alpha+2)+\tfrac{1}{2}[(\alpha+2)^2+4\xi n^2]^{\frac{1}{2}} \qquad (3a)$$

$$\xi \equiv (qQ_{r\theta}+Q_{\theta\theta})(qQ_{rr}+Q_{r\theta})^{-1}$$

$$q \equiv (Q_{\theta\theta}/Q_{rr})^{\frac{1}{2}}$$

Here the Q_{ij} are the plane-stress-reduced stiffness coefficients which are related to the engineering elastic properties as follows:

$$Q_{\theta\theta} = E_\theta/\lambda \; ; \; Q_{r\theta} = \nu_{\theta r}E_r/\lambda$$
$$Q_{rr} = E_r/\lambda \; ; \; \lambda = 1-\nu_{\theta r}\nu_{r\theta} \qquad (4)$$

where E_θ and E_r are the Young's moduli in the circumferential and radial directions, $\nu_{\theta r}$ is the Poisson's ratio associated with uniaxial loading in the circumferential direction, and it is assumed that $\nu_{r\theta} = \nu_{\theta r}E_r/E_\theta$.

The lowest value of m for which K(m,n) is positive governs. For the material properties for aramid fiber-epoxy composite material as listed in Table 1, the governing value is m = 1 and K(1,1) = 0.357.

From Ref. 19, we find that for n=1, the ratio of ω_{pn} to the corresponding frequency for isotropic plates, $(\omega_{pn})_{iso}$, is 0.508 for a disk with a small hole (ID/OD = 0.1) and 0.270 for a disk with a large hole (ID/OD) = 0.9. From Table 2.30 of Leissa's monograph[20], we find that k_{cr} = 27.3 for ID/OD = 0.1 and 2189 for ID/OD = 0.9 at mode numbers m = n = 1. Here $k_{cr} \equiv (\omega_{pn})_{iso} R^2(\rho h/D_\theta)^{\frac{1}{2}}$.

Table 1. Material Properties of Composite Materials Considered.

Property	Aramid -epoxy	Graphite -epoxy
E_θ, psi	11.0×10^6	18.0×10^6
E_r, psi	0.8×10^6	1.28×10^6
$G_{r\theta}$, psi	0.3×10^6	0.85×10^6
$\nu_{\theta r}$	0.34	0.27
ρg, pci	0.050	0.054

Thus, by applying the above in Eqs. (1) and (2), one obtains

$$\Omega_{cr}(\text{rpm}) = (60/2\pi)(h/R_0)(Q_{\theta\theta}/12\rho)^{\frac{1}{2}}k_{cr} \qquad (5)$$

Applying Eq. (5), we obtain for R_0 = 10 in., Ω_{cr}(rpm) = 80,670 hk_{cr}. Then Ω_{cr}(rpm) is $1.39 \times 10^6 h$ for ID/OD = 0.1 and $59.5 \times 10^6 h$ for ID/OD = 0.9. This indicates that even for disks as thin as 0.125 in., the critical speed predicted is well above the operating speed associated with ultimate material failure.

ANALYSIS USING THIN-RING THEORY

In some ring-type flywheels, the flywheel rim is very compact and it is apparent that ring theory is more appropriate than plate theory. The analysis developed herein includes the preloading due to centrifugal action and twisting of the ring cross section as well as out-of-plane deflection.

First it is necessary to determine the steady hoop-tension force N_c resulting from centrifugal action. The equilibrium equation is:

$$(N_c/R) + K_R U_c = \rho A R \Omega^2 \qquad (6)$$

where A ≡ cross-sectional area, K_R ≡ radial elastic foundation constant of the connection between the ring and the hub, R ≡ radius measured to the centroid of the ring cross section, U_c ≡ steady radial displacement, and ρ ≡ ring-material density.

The constitutive relation for in-plane stretching of the ring is

$$N_c = (AE_\theta/R)U_c \tag{7}$$

Substituting U_c from Eq. (7) into Eq. (6) and solving for N_c, one obtains the following result:

$$N_c = \frac{\rho A\Omega^2 R^2}{1 + (K_R R^2/AE_\theta)} \tag{8}$$

Using Ojalvo's linear thin-ring theory[21] as a basis, one can write the following equations of motion. For out-of-plane (axial) displacement w:

$$\frac{1}{R}\frac{\partial Q_0}{\partial\theta} - \frac{N_c}{R^2}\frac{\partial^2 w}{\partial\theta^2} = -\rho A\frac{\partial^2 w}{\partial t^2} \tag{9}$$

where $Q_0 \equiv$ out-of-plane shear force, and $t \equiv$ time.

For rotation about a radial axis, neglecting the rotatory inertia, one may write:

$$\frac{1}{R}\frac{\partial M_0}{\partial\theta} + \frac{M_6}{R} - Q_0 = 0 \tag{10}$$

where $M_6 \equiv$ twisting moment (torque).

For angular motion about a circumferential axis, one has

$$\frac{1}{R}\frac{\partial M_6}{\partial\theta} - \frac{M_0}{R} + K_t\phi = -I_m\frac{\partial^2\phi}{\partial t^2} \tag{11}$$

where $I_m \equiv$ mass polar moment of the cross section about its centroid, $K_t \equiv$ twisting stiffness of the rim-to-hub connector, and $\phi \equiv$ angle of twist.

Using Eq. (10) to eliminate Q_0 in Eq. (9), one obtains

$$\frac{1}{R^2}\frac{\partial^2 M_0}{\partial\theta^2} + \frac{1}{R^2}\frac{\partial M_6}{\partial\theta} - \frac{N_c}{R^2}\frac{\partial^2 w}{\partial\theta^2} = -\rho A\frac{\partial^2 w}{\partial t^2} \tag{12}$$

The constitutive relations for the moment and torque are

$$M_0 = -D_{00}\left(\frac{\phi}{R} - \frac{1}{R^2}\frac{\partial^2 w}{\partial\theta^2}\right)$$
$$M_6 = -D_{66}\left(\frac{1}{R^2}\frac{\partial w}{\partial\theta} + \frac{1}{R}\frac{\partial\phi}{\partial\theta}\right) \tag{13}$$

Substituting Eqs. (13) into Eqs. (12) and (11), one gets the following coupled displacement equations of motion:

$$\begin{bmatrix} L_{11} & L_{12} \\ L_{12} & L_{22} \end{bmatrix}\begin{Bmatrix} w \\ \phi \end{Bmatrix} = \begin{Bmatrix} 0 \\ 0 \end{Bmatrix} \tag{14}$$

where the L_{ij} are linear differential operators defined as follows:

$$L_{11} \equiv D_{00}R^{-4}d_\theta^4 - (D_{66}R^{-4}+N_cR^{-2})d_\theta^2 + \rho Ad_t^2$$
$$L_{12} \equiv -(D_{00}+D_{66})R^{-3}d_\theta^2 \; ; \; L_{22} \equiv -(D_{66}d_\theta^2 - D_{00})R^{-2} + K_t + I_m d_t^2 \tag{15}$$
$$d_\theta \equiv \partial/\partial\theta, \text{ etc.}$$

The solution of Eqs. (14) for a backward-traveling wave solution (with $\omega = n\Omega$ for a standing wave with respect to fixed space) can be expressed as

$$w = W\cos(n\theta+\omega t) \; , \; \phi = P\cos(n\theta+\omega t) \tag{16}$$

Substituting Eqs. (16) into Eqs. (14) leads to the following frequency determinant:

$$\begin{vmatrix} C_{11} - (1-C_n)\rho An^2\Omega^2 & C_{12} \\ C_{12} & C_{22} - I_m n^2\Omega^2 \end{vmatrix} = 0 \tag{17}$$

where

$$C_{11} \equiv D_{00}R^{-4}n^4 + D_{66}R^{-4}n^2$$
$$C_{12} \equiv (D_{00}+D_{66})R^{-3}n^2$$
$$C_{22} \equiv (D_{66}n^2+D_{00})R^{-2} + K_t \tag{18}$$
$$C_n \equiv [1+(K_RR^2/AE_\theta)]^{-1}$$

The solution of Eq. (17) may be written as

$$\Omega = (1/n)[A_1 \pm (A_1^2 - B_1^2)^{\frac{1}{2}}]^{\frac{1}{2}} \tag{19}$$

where

$$A_1 \equiv (1/2)[(C_{11}/\rho A)(1-C_n)^{-1} + (C_{22}/I_m)]$$
$$B_1^2 \equiv (C_{11}C_{22} - C_{12}^2)/[\rho AI_m(1-C_n)] \tag{20}$$

As a first example, Eq. (19) is applied to an aramid-epoxy ring having a rectangular cross section. Then

$$A = hd \; ; \; I_m = (\rho hd/12)(d^2+h^2)$$
$$D_{00} = E_\theta dh^3/12 \; ; \; D_{66} = \beta G_{r\theta} dh^3 \quad (21)$$

where d ≡ radial depth of cross section, h ≡ axial thickness of cross section, and β ≡ a dimensionless factor which depends upon the d/h ratio[22]. It is assumed here that the composite material is transversely isotropic with its plane of isotropy coinciding with the cross-sectional plane. Thus, $G_{r\theta} = G_{\theta z}$.

For the example design, R = 9.50 in., d = 1.00 in., h = 0.25 in. Thus, the mean radius and cross section are identical to those considered by plate theory in the preceding section, except that now h is set at the specific value of 0.25 in.

Inspecting Eqs. (18) and (20), one notes that the radial stiffness K_R of the connection between the ring and hub must be specified in order to calculate the critical speed. If $K_R = 0$, centrifugal action allows the ring to expand radially so as to exactly counteract the transverse inertia effect and thus results in $(1 - C_n) = 0$ and a critical speed that has no bound. At the other limit, if K_R has no bound, the ring is fully restrained against centrifugal action and the full transverse inertia takes effect. This results in $C_n = 0$ and a minimum critical speed. The resulting critical speed occurs at a circumferential wave number of 2 and is equal to 1,723 rpm. This is a drastic decrease from that predicted by plate theory in the preceding section. Evidently this decrease is due to the strong effect of the twisting flexibility as well as the omission of beneficial centrifugal expansion in the present calculation.

For another example, Eq. (19) is applied to a Type AS graphite-epoxy ring having a semi-elliptic cross section. The flat portion of the cross section is at the inside radius and the curved portion is at the outside radius. Then

$$A = (\pi/2)ab$$
$$I_m = \rho[(\pi/8)ab(a^2+b^2) - A\bar{x}^2]$$
$$D_{00} = (\pi/8)E_\theta ab^3 \; ; \; D_{66} = \frac{16}{9\pi}\frac{a^3b^3G_{r\theta}}{a^2+b^2} \quad (22)$$
$$R = R_i + \bar{x} \; ; \; \bar{x} = 4a/3\pi$$

where a ≡ radial depth of cross section, b ≡ axial semi-axis, and $\bar{x}$ is the distance between the centroidal radius R and the inside radius R_i.

For this example design, a = 2.375 in., b = 1.500 in., R_i = 7.625 in. In this design the rim is attached to the hub by twelve radial band-type spokes of unidirectional aramid-epoxy. These bands are estimated to provide an equivalent radial foundation stiffness of K_R = 53,600 psi. Using the graphite-epoxy properties listed in Table 1 and Eqs. (22), the lowest critical speed for this design is found to be 45,600 rpm, which is about 14% above the predicted burst speed based on static strength considerations.

CONCLUSIONS

Two different analyses were presented to predict the lowest critical speed of "standing-wave instability" of a ring-type flywheel. The thin-plate-theory analysis is most appropriate for a flat ring, i.e. one that is axially thin. The thin-ring-theory analysis is most appropriate for a ring of compact cross section. In this latter analysis, drastically lower critical speeds are predicted when the radial stiffness of the ring-to-hub connector is large. On the other hand, if this stiffness is negligible, the lowest critical speed increases without bound. Numerical results were presented for some typical flywheel designs of current interest for application in hybrid automobiles.

ACKNOWLEDGMENT

The research reported here was sponsored by Sandia Laboratories, Albuquerque, with Dr. Frank Gerstle as project monitor.

REFERENCES

[1] W. Campbell, Trans. ASME 46, 31 (1924).

[2] S.A. Tobias and R.N. Arnold, Proc. I. Mech. E. 171, 669 (1957).

[3] D.S. Dugdale, J. Mech. Phys. Solids 14, 349 (1966).

[4]A.I. Krauter and P.Z. Bulkeley, J. Appl. Mech. 37, 1037 (1970).

[5]C.D. Mote, Jr. and J.E. Rakowski, Exp. Mech. 9, 1 (1969).

[6]W. Soedel, J. Sound Vib. 41, 233 (1975).

[7]H. Lamb and R.V. Southwell, Proc. Roy. Soc., London, Ser. A, 99, 272 (1921).

[8]R.V. Southwell, Proc. Roy. Soc., London, Ser. A, 101, 133 (1922).

[9]J.G. Simmonds, J. Aerosp. Sci. 29, 16 (1962).

[10]W. Eversman, AIAA J. 6, 1395 (1968).

[11]N.C. Ghosh, Czech. J. Phys. 23, 506 (1973).

[12]N.C. Ghosh, Ind. J. Phys. 47, 693 (1973).

[13]C.J.H. Williams and S.A. Tobias, J. Mech Eng. Sci. 5, 325 (1963).

[14]S.H. Advani, Int. J. Mech. Sci. 9, 307 (1967).

[15]P.Z. Bulkeley, J. Appl. Mech. 40, 133 (1973).

[16]J.E. Goldberg and A.V. Setlur, Developments in Mechanics 3 (Proc. 9th Midwestern Mech. Conf.), Pt. 2, 229 (1965).

[17]S. Barasch and Y. Chen, J. Appl. Mech. 39, 1143 (1972).

[18]J.L. Nowinski, J. Appl. Mech. 31, 72 (1964).

[19]G.K. Ramaiah and K. Vijayakumar, J. Sound Vib. 26, 517 (1973).

[20]A.W. Leissa, "Vibration of Plates", NASA SP-160, p. 245 (1969).

[21]I.U. Ojalvo, Int. J. Mech. Sci. 4, 53 (1962).

[22]S.G. Lekhnitskii, Theory of Elasticity of an Anisotropic Elastic Body (Holden-Day, San Francisco, CA, 1963).

INFLUENCE OF BEARING STIFFNESS ON FLYWHEEL-ROTOR SYSTEM

J.S. Hickey
Corporate Research and Development
General Electric Company
Schenectady, New York

ABSTRACT

When a rotating shaft is not symmetric with respect to its bearings, the choice of each bearing stiffness is important to the shaft critical speeds. The design of a simple machine is illustrated to give a rationale for choosing bearing stiffnesses. The effect of shaft rigidity on those shaft critical speeds involving the bearings is also demonstrated.

DISCUSSION

The major components of a flywheel energy storage system usually receive a great deal of design attention. How these components are supported on their bearings should be considered carefully, for the bearings are usually a major factor in determining how well the machine actually performs. The bearings have a considerable effect on the critical speeds of the rotor and are crucial with respect to the operating life of the machine. The friction losses in the bearings are equally important since they represent a continuous power drain for the storage system.

A typical example of the design problem is illustrated for an inductor-alternator-flywheel combination. Because the electrical machine is attached to the flywheel on a common shaft, the resulting rotor is asymmetric. A considerably simplified sketch of the rotor is shown in Fig. 1. In a practical machine, the shaft is not a uniform cylinder, but has poles and flanges. Consequently, the actual stiffness is not easily calculated accurately. A design which is not extremely critical to shaft stiffness is then desirable.

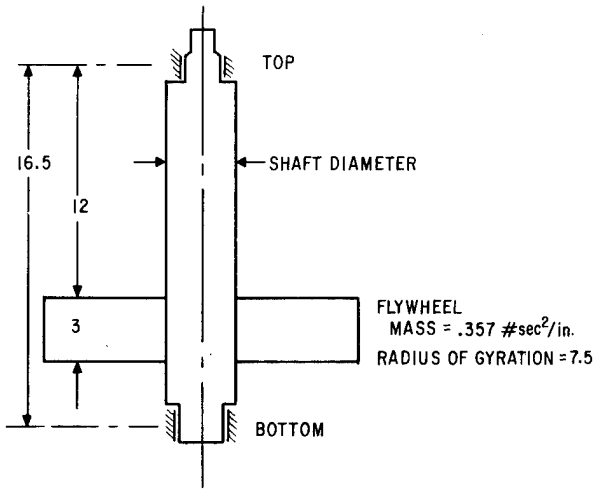


Fig. 1. Rotor Dimensions (inches).

The bearings for this machine should be chosen with the following criteria in mind:

- Shaft critical speeds to fall outside the operating range with a suitable safety factor
- Shaft criticals not to be a strong function of shaft stiffness near the operating range
- Bearing friction to be as low as possible
- Bearing life to suit the machine application—3000 hours at operating speed in this case

To keep the friction loss low, ball bearings are chosen. For the size machine in question, with an upper operating speed of 15,000 rpm, the maximum radial stiffness available with an expected bearing life of over 3000 hours is approximately 2×10^6 lb/in. Less stiff bearings can be obtained, or the bearing housing made resilient to simulate any lower stiffnesses required. The lower limit on bearing stiffness is given by the permissible rotor motion in relation to air-gap clearances. Low stiffness bearings are desirable since they also have lower losses.

Shaft diameters over 4 inches would not be feasible with the constraints imposed by the electrical design of the inductor alternator. Within the above limits, the range of bearing stiffnesses 2×10^4 to 2×10^6 and the range of shaft diameters $1\frac{1}{2}$ to 4 inches were investigated.

A computer program, Link III, was used to calculate the shaft critical speeds. This program includes gyroscopic effects, and considers the effect of resilient bearing mounts as well as the mass of the bearing assembly. Figure 2 shows schematically the properties that are entered into the computer program for each bearing. In the case under consideration, the stiffnesses in the X and Y directions are easily made equal. A portion of the stator and housing mass was assigned to each bearing, as bearing mass, and the stiffness of the proposed vibration isolation was used for the spring stiffness from pedestal to ground. It was determined that this spring had no practical effect upon the shaft critical speeds.

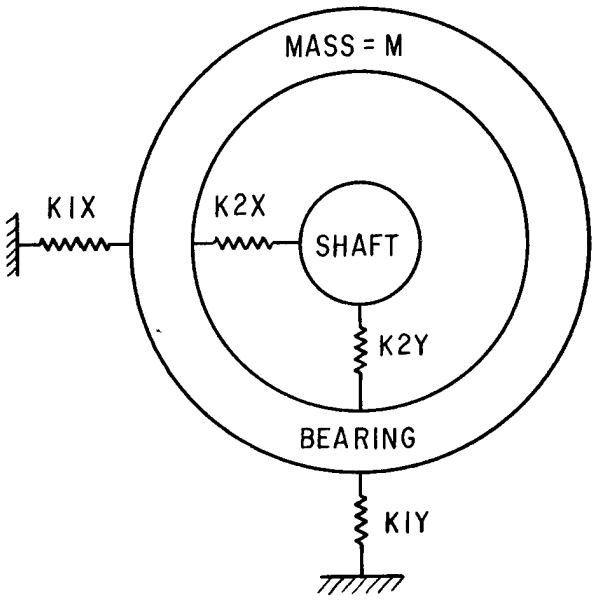


Fig. 2. Shaft bearing configuration (top) bearing m = 0.4 #sec^2/inch; bottom bearing, m = 0.3 #sec^2/inch; KIX = KIX = 2000 #/inch).

The results of the computer investigation are shown in Fig. 3. Each of five separate bearing combinations was investigated for the forementioned range of shaft diameters, $1\frac{1}{2}$ to 4 inches. The five cases are juxtaposed in this figure to allow easy comparisons. At the bottom of each plot, the abscissa is shaft diameter, and below this the bearing stiffnesses for each plot are given. The ordinate is shaft speed, with the desired machine range shown as a heavy line.

Case 5, at the right side, is for a very stiff bearing near the flywheel, and a soft one at the free end. As can be seen, the lowest critical speed is near the lower speed range of the machine for any shaft diameter. This bearing combination is obviously not suitable.

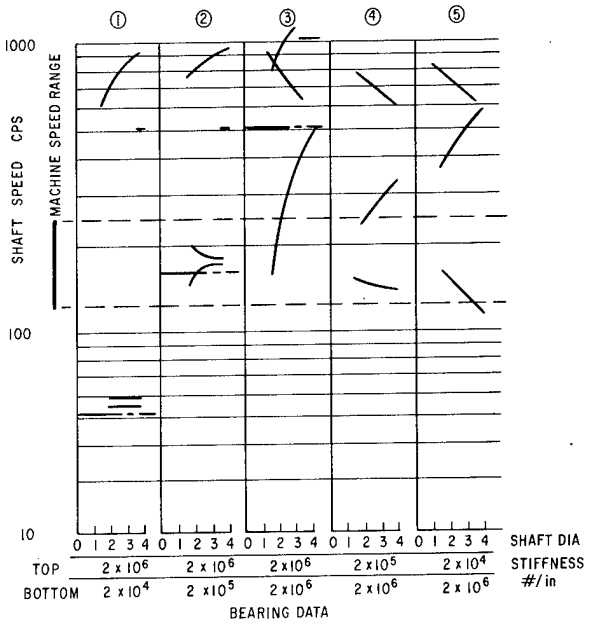


Fig. 3.

Case 4, which has a stiffer upper bearing, shows no improvement in the lowest critical, and the second critical has been brought down into the machine range.

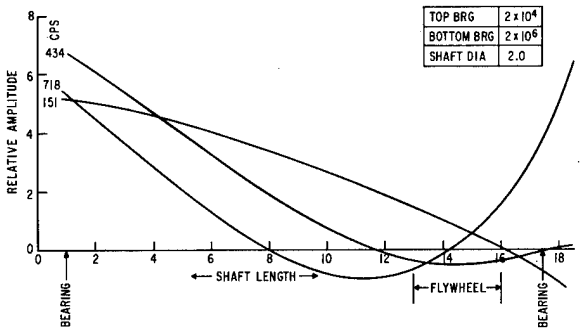
Stiffening the upper bearing to the practical limit is done in Case 3. Here, for stiff shafts, the lowest critical is well over the highest machine speed. This bearing-shaft combination is acceptable, but is not ideal. Two stiff bearings have the highest friction losses, and the lowest mode is very sensitive to shaft stiffness.

The lower bearing is made softer. In Case 2, the lower bearing is made 1/10th the stiffness of the upper. A doublet lower mode appears in the middle of the operating range. Softening the lower bearing still more, as in Case 1, gives a mode pattern with a doublet mode well below the operating range and the next highest mode well over the highest operating speed.

Case 1 has a mode-free range that goes from 1/2 to 2 times the operating range. The soft lower bearing has low friction losses. The low speed mode is associated with the soft bearing, and is not a dangerous mode. Essentially, this mode is the boundary between low-speed solid body rotation about the shaft mechanical axis and high-speed rotation about the shaft balance axis. In a well balanced machine, this transition would not be noticeable.

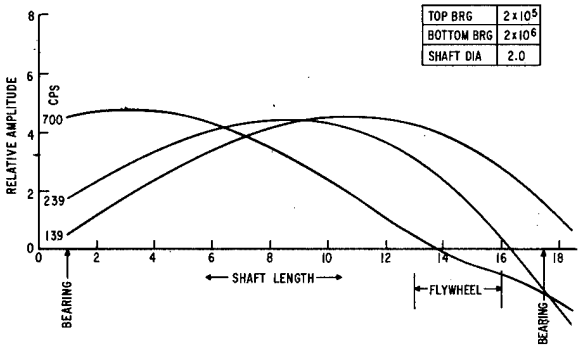
MODE SHAPES

The mode shapes for the critical speeds less than 1100 cps are of interest in assessing the operation of the rotor. Higher critical speeds are not determined with accuracy by the computer program, and are of little practical value since it is not desirable to operate above the first shaft flexure mode. The mode-shape plots give the relative deflection of the shaft at the critical speed in question. There is no correlation in amplitude between the deflection at one speed and the deflection at another. Only representative mode plots are shown, as the variation in mode pattern with shaft diameter is not very striking.



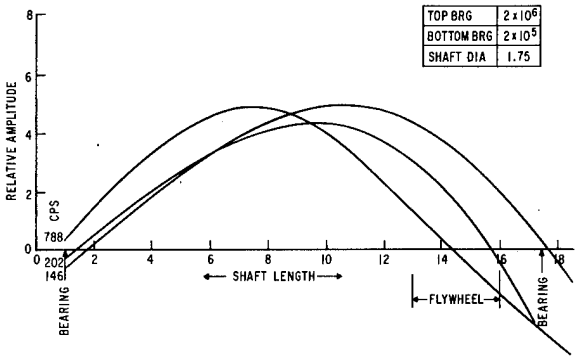
Case 5 - Mode Shapes

The mode plots for this case show that the soft upper bearing is involved in all three modes. The lowest frequency mode, at 151 cps, is one wherein the flywheel and upper bearing vibrate in phase, while the lower bearing is almost stationary. The middle mode, at 434 cps, is associated with shaft flexure and the upper bearing vibrating. Note that the flywheel does not wobble in this mode, as the slope of the curve at the flywheel position is essentially zero. The upper mode, as 718 cps, is associated with in-phase vibration of both bearings and considerable flexure of the shaft. Note that in this mode the flywheel wobbles at shaft frequency.

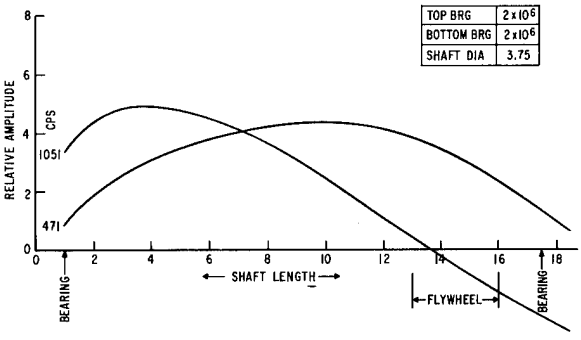


Case 4 - Mode Shapes

In this case the increased upper bearing stiffness shows its effect. The lowest mode, 139 cps, is the classic "both bearings in phase," while the second, at 239 cps, has "both bearings out of phase." These two modes show flywheel wobble. The third mode, at 700 cps, shows shaft flexure. Since the upper bearing is now more rigid, the force needed to displace it is so great that the shaft deflection shows an inflection point at the flywheel.



The second mode plot for Case 4 is for a soft upper bearing and a very limber shaft. Note that for all modes the upper bearing displacement is small. The doublet mode is now at 146 and 202 cps, and a difference in the mode shapes is discernible. Whether the 202 cps mode is the upper one of the doublet or the "lower bearing stationary" mode of the previous plot is moot. There is no practical difference, but the data taken at intermediate shaft stiffnesses indicate that the latter mode does not appear for shaft diameters below 2.75 inches, while the doublet does. Below the 1.75-inch diameter, the doublet also disappears. The first shaft critical is now at 788 cps.

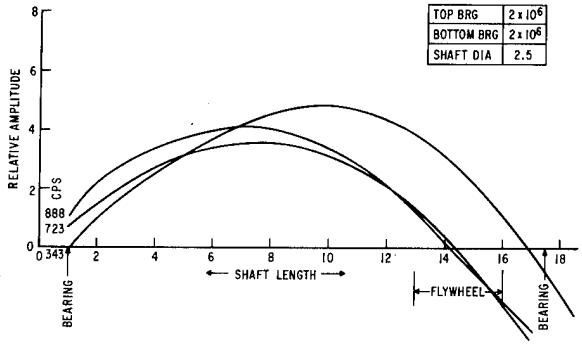


Case 3 - Mode Shapes

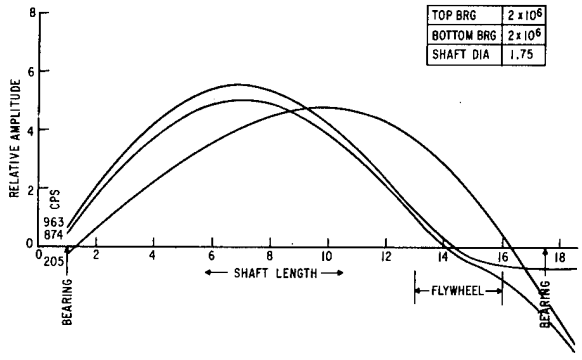
This case, for two very stiff bearings, is more complex than the two previous cases. Three mode plots are shown to completely demonstrate the effect of shaft stiffness.

First, consider the plot for a very stiff shaft. The only two modes found in the range of interest are the classic "bearings in phase" at 471 cps, and "bearings out of phase" at 1051 cps. The 471 cps mode is exactly at the calculated frequency for a system composed of rotor mass, spring, and bearing mass with no rotary effects at all. This frequency is shown as a dashed line in Fig. 3.

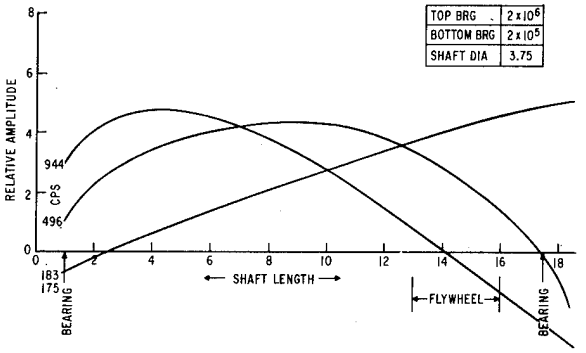
The sharp curvature at the left edge of the 1051 cps mode is due to the reduced shaft diameter for the bearing.



The second plot for Case 3 is for a shaft of intermediate stiffness. The lowest mode has decreased in frequency to 343 cps. The upper mode of the first plot has decreased in frequency, and a third mode has become apparent. This mode is the same one that was the highest mode in Cases 4 and 5. On this plot, it is difficult to tell which is which. Since the frequencies are close, this is of no practical concern.



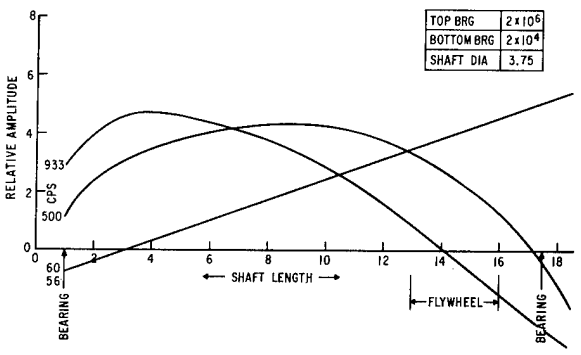
The third example of Case 3 is for a very limber shaft. Here the upper bearing is seen to be always almost completely rigid. The lowest mode, at 205 cps, is still the "bearings in phase" mode, and the two higher modes are almost identical from flywheel to upper bearing. They differ only in the amplitude of the lower bearing vibration and the amount of flywheel wobble. If we associate the mode having the greatest wobble with the shaft flexure mode, we see that at 874 cps it is lower than the "bearings out of phase" mode at 963 cps.



Case 2 - Mode Shapes

This case, with the lower bearing 1/10th the stiffness of the upper, shows a marked difference in the mode plots from the previous three cases. Here the lowest plot, for 175 or 183 cps, shows essentially no shaft deflection, only vibration of the lower bearing. This mode doublet is slightly higher in frequency than the calculated resonance of rotor, lower bearing spring, and lower bearing mass. It is a doublet because of the effects of shaft mass and shaft stiffness.

The next mode, at 496 cps, is one with the lower bearing stationary and the upper bearing vibrating, and the highest mode, at 944 cps, is the usual first shaft critical. Notice that the 496 cps mode agrees closely with the 471 cps mode in Case 3. The fact that the shaft vibration amplitude at the bearing is small indicates that the bearing housing vibration must be large.

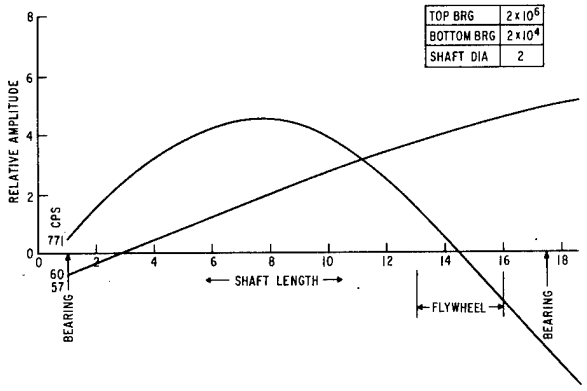


Case 1 - Mode Shapes

This case, which is the one of most practical interest, is for the least stiff lower bearing. Note that the low frequency doublet mode, at 56 and 60 cps, shows absolutely no shaft deflection. There is still a doublet because of the shaft distributed mass. The frequency of this mode again agrees with the calculated resonances as in Case 2.

The next mode, at 506 cps, is again in agreement with the upper bearing resonance calculation and, again, has a large upper bearing housing vibration amplitude.

The last mode, at 933 cps, is the first shaft critical. Note that these last two modes are essentially unchanged from Case 2.



The last mode plot is for Case 1 and a shaft diameter of 2 inches. This departure from the diameter of 1.75 inches, used as the limber shaft case in previous plots, is because the low frequency doublet disappears for smaller diameters. For the 1.75-inch diameter shaft, the only mode found is the first shaft critical.

In this plot, the doublet is present at 57 and 60 cps and shows some shaft deflection. The first shaft critical mode is at 771 cps, lowered somewhat by the flexible shaft.

It is evident that this bearing configuration is the best one to use with a very limber shaft.

CONCLUSIONS

In many practical flywheel applications, the shaft length and bearing positions are not symmetric with respect to the wheel. For many asymmetric mountings, there is a clear design procedure. The bearing farthest from the wheel is made much stiffer than the bearing near the wheel. For a wide range of stiffnesses, the only bearing resonance present concerns the shaft mass and the near bearing mode. This mode can usually be made so low in frequency that it is unobjectionable. For too stiff shafts, the far bearing and flywheel resonance may be present. A properly designed mount will have no resonances between the aforementioned near bearing mode and the first shaft critical.

OVALIZATION CRITICAL SPEEDS IN ANISOTROPIC ROTATING DISKS

Giovanni Belingardi - Giancarlo Genta - Muzio Gola
Istituto della Motorizzazione - Politecnico di Torino
Corso Duca degli Abruzzi 24 - Torino - (Italy)

This work was sponsored by C.N.R. (Italian National Research Council)

ABSTRACT

The use of materials characterized by a ultimate strength over Young Modulus ratio far higher than for conventional materials in the construction of flywheels, leads to consider the potential danger due to the critical speeds of ovalization. Flywheels of high strength composite materials can be subjected to quite large displacements, both in radial and circumferential (if the material is not axially simmetrical) direction. Such rotors, even considered with rigidly fixed axis of symmetry can show a behavior similar to the one encountered in the study of flexible rotating shafts, and usually referred to as "critical speeds".

In fact, the rotating disk can displace from the current configuration of equili - brium taken under centrifugal forces, and take a configuration of indifferent equilibrium in the centrifugal field characterized by one or more lobes.

The single lobe configuration is obviously associated with the lowest "critical speed" and displaces the center of mass of the system from the axis of rotation while at higher "criti cal speeds" only the change in the form of the disk does occur.

The calculation of such "critical speeds" was performed through a modification the Raleygh - Ritz procedure, originating generalized stiffness matrix and mass matrix having as unknowns the coefficients of interpolation polynomial of the displacements over the whole field.

The chosen interpolation procedure has proven to be a convenient one also from the point of view of the structure of the solving matrices.

AIM OF THE WORK

During a research program concerning the design and construction of composite material flywheels it was thought convenient to calculate, besides the stress state in the disks, also their possible ovalization "critical" speeds.

In fact flywheels built using high strength and low elastic modulus materials (such as some composite materials; particularly those having an elastomeric matrix) can be subject to quite large displacements both in radial and circumferential direction (if the material is not axially sim - metrical).

This fact leads to consider the potential danger due to the critical speeds of ovalization.

A numerical solution has been searched for, by the well known method of expressing radial and circumferential displacements through polynomials, whose coefficients are calculated by means of energy principle methods[1 2 3 4 5].

As only rotors obtained by filament winding technique were considered, the material is assumed to be axially simmetrical, but also other cases can be solved with small changes.

Only basic assumptions are the usual ones of plane stress state and of elastic behaviour of the material. All geometrical and mechanical parameters are considered variable with the radius.

MATHEMATICAL PROCEDURE

BASIC EQUATIONS

A critical speed is present when the disk undergoes a system of displacements in the centrifugal field for which the virtual work of the centrifugal forces is equal to the one of the stresses:

$$\int_V E_v \, dV + \int_V E_v' \, dV = \int_V \omega^2 (r+u) s \, dm. \quad (1)$$

Since for equilibrium obviously:

$$\int_V E_v \, dV = \int_V \omega^2 \, r \, s \, dm, \qquad (2)$$

equation (1) yields:

$$\int_V E'_v \, dV = \int_V \omega^2 \, u \, s \, dm. \qquad (3)$$

The disk is studied as a two-dimensional circular body, on every point of which a radial displacement u and a circumferential displacement v are defined.

Between the outer radius r_e and the centre, a system of M equally spaced circles is defined, whose radial distance is:

$$\Delta r = r_e/M \, . \qquad (4)$$

Thus the radius of the k-th (k =1,M) circle will be:

$$r_k = r_e \, k/M. \qquad (5)$$

The points of the k-th circle undergo a radial displacement u_k and a circumferential displacement v_k, that can conveniently be expressed through periodic functions.

Since during "critical" deformation the disk becomes multi-lobed, the number of lobes being dependent on the order of the speed, the period of functions u_k and v_k can be an angle $\Theta = 2\pi/n$ (n = 1, 2, 3, ...) according to the first lowest speed to be determined.

Thus:

$$\begin{cases} u_k = \sum_{i=o}^{L} u_{ik} \cos (i \, 2 \, \pi \, \theta/\Theta) \\ v_k = \sum_{i=1}^{L} v_{ik} \sin (i 2 \, \pi \, \theta/\Theta), \end{cases} \qquad (6)$$

where L is the highest harmonic order taken into consideration.

It is well known[6] that given M+1 equally spaced values of a function y(x) over the interval (x = 0,1), the following Bernstein interpolation formula holds:

$$y(x) = \sum_{k=o}^{M} \binom{M}{k} y(x_k) x^k \, (1-x)^{M-k}. \qquad (7)$$

Thus, after neglecting for convenience the constants $\binom{M}{k}$, and using the non-dimensional vector radius x instead of r, eq.(6) can be written:

$$\begin{cases} u = \sum_{k=1}^{M} \sum_{i=o}^{L} u_{ik} \, x^k (1-x)^{M-k} \cos(i 2\pi\theta/\Theta) \\ v = \sum_{k=1}^{M} \sum_{i=1}^{L} v_{ik} \, x^k (1-x)^{M-k} \cos(i 2\pi\theta/\Theta), \end{cases} \qquad (8)$$

or, in matrix notation:

$$\{^{u}_{v}\} = [U] \, \{S\} \, . \qquad (8')$$

Calculating the virtual strains:

$$\begin{cases} \varepsilon_{uu} = \dfrac{\partial u}{\partial r} \\ \varepsilon_{vv} = \dfrac{u}{r} + \dfrac{1}{r} \dfrac{\partial v}{\partial \theta} \\ \varepsilon_{uv} = \dfrac{1}{r} \left(\dfrac{\partial u}{\partial \theta} - v + r \dfrac{\partial v}{\partial r}\right) \end{cases} \qquad (9)$$

by using the shorthand symbols:

$$X(k) = x^k \, (1-x)^{M-k}$$

$$DX(k) = \frac{x^k (1-x)^{M-k}}{r_e} \left(\frac{k}{x} - \frac{M-k}{1-x}\right)$$

$$CT(i) = \cos \left(i \, 2\pi \frac{\theta}{\Theta}\right),$$

$$ST(i) = \sin \left(i \, 2\pi \frac{\theta}{\Theta}\right)$$

the deformations become:

$$\varepsilon_{uu} = \sum_{k=1}^{M} \sum_{i=0}^{L} u_{ik} \, DX(k) \, CT(i) \qquad (11)$$

$$\varepsilon_{vv} = \sum_{k=1}^{M} \sum_{i=o}^{L} u_{ik} \, \frac{X(k)}{r} \, . \, CT(i) +$$

$$+ \sum_{k=1}^{M} \sum_{i=1}^{L} v_{ik} \, \frac{X(k)}{r} \left(i \, \frac{2\pi}{\Theta}\right) CT(i)$$

$$\varepsilon_{uv} = \sum_{K=1}^{M}\sum_{i=o}^{L} u_{ik}\frac{X(k)}{r}\left(-\,i\,\frac{2\pi}{\hat{\theta}}\right) ST(i) +$$

$$+ \sum_{k=1}^{M}\sum_{i=1}^{L} v_{ik}\left[DX(k) - \frac{X(k)}{r}\right] ST(i)$$

Since the stress strain relationships is written:

$$\{\sigma\} = [E]\ \{\varepsilon\} \qquad (12)$$

substituting eq. (9) into eq. (12) the stresses are easily obtained.

GENERALIZED STIFFNESS MATRIX

Having defined a generalized displacement vector

$$\{S\} = \begin{Bmatrix} u_{ik} \\ v_{ik} \end{Bmatrix}, \qquad (13)$$

using eq. (8) in matrix notation, eq. (9) can be written as:

$$\{\varepsilon\} = [A]\ \{S\}. \qquad (14)$$

In the same way the stresses can be expressed as:

$$\{\sigma\} = [B]\ \{S\}.$$

Using the principle of virtual work, and choosing as compatible strain state the same chosen for the equilibrium stress state, it is obtained:

$$\{\varepsilon\}^T\ \{\sigma\} = \{S\}^T\ [A]^T\ [B]\ \{S\}. \qquad (15)$$

The product $[A]^T\ [B]$ gives a square symmetric matrix $[C]$, that is the generalized stiffness matrix.

This matrix can be ideally divided as follows:

$$[C] = \left[\begin{array}{c|c} C_{uu} & C_{uv} \\ \hline \text{symm.} & C_{vv} \end{array}\right] \qquad (16)$$

Coefficients C_{uu} are produced by the coefficients of only variables u_{ik}

Coefficients C_{vv} are produced by the coefficients of only variables v_{ik}.

Coefficients C_{uv} are produced by the coefficients of variables u_{jh} times those of variables v_{ik}.

The general forms of these coefficients are:

C_{uu}:

$$DX(h)\ .\ CT(j)\ .\ \left[E_{cc}\ .\ DX(k) + E_{cr}\ .\ \frac{X(k)}{r}\right]$$

$$.\ CT(i) + \frac{X(h)}{r}\ .\ CT(j)\ .\ \left[E_{cr}.DX(k) +\right.$$

$$\left. + E_{rr}\ .\ \frac{X(k)}{r}\right].\ CT(i) + \frac{X(h)}{\hat{r}}\ .\ ST(j)\ .$$

$$\left(-j\,\frac{2\pi}{\theta}\right) E_{ss}.\ \frac{X(k)}{r}\ .\ \left(-i\,\frac{2\pi}{\theta}\right)\ .\ ST(i)$$

Cv:

$$\frac{X(h)}{r}\left(j\,\frac{2\pi}{\theta}\right).\ CT(j)\ .\ E_{rr}\ .\ \frac{X(k)}{r}\ .\ \left(i\frac{2\pi}{\theta}\right).$$

$$CT(i) + \left[\ DX(h) - \frac{X(h)}{\hat{r}}\right]\ .\ ST(j)\ .\ E_{ss}\ .$$

$$\left[\ DX(k) - \frac{X(k)}{\hat{r}}\right]\ .ST(i)$$

C_{uv}:

$$DX(h)\ .\ CT(i)\ .\ E_{cr}\ .\ \frac{X(k)}{r}\ .\ \left(i\,\frac{2\pi}{\theta}\right)\ .$$

$$CT(i) + \frac{X(h)}{r}\ .\ CT(j)\ .\ E_{rr}\ .\ \frac{X(k)}{r}\ .$$

$$\left(i\frac{2\pi}{\theta}\right).\ CT(i) + \frac{X(h)}{\hat{r}}\ .\ \left(-j\,\frac{2\pi}{\theta}\right) ST(j)\ .$$

$$E_{ss}\ .\ \left[\ DX(k) - \frac{X(k)}{\hat{r}}\right]\ .\ ST(i).$$

As the disk was assumed to be axially symmetrical, it is possible to integrate the coefficients of $[C]$ along θ. Moreover the matrix $[C]$ takes a particular band-form, since the integrals

$$\int_o^{\Theta} \cos\left(j2\pi\theta/\Theta\right)\ \cos\left(i2\pi\theta/\Theta\right)d\theta$$

$$\int_o^{\Theta} \sin\left(j2\pi\theta/\Theta\right)\ \sin\left(i2\pi\theta/\Theta\right)d\theta \qquad (17)$$

are zero when $i \neq j$, only the fewer for

which i = j are then to be calculated.

If the geometrical or elastic parameters are not constant with θ, the integration of the coefficients of [C] can be performed numerically, but in this case all terms of [C] can be different from zero.

GENERALIZED MASS MATRIX

The virtual work of the additional centrifugal forces due to displacement from the equilibrium position is calculated through:

$$u \cdot \omega^2 \cdot u \cdot dm \qquad (18)$$

that is more generally written:

$$\begin{Bmatrix} u_{jh} \\ v_{jh} \end{Bmatrix}^T \omega^2 \left[\begin{array}{c|c} 1 & 0 \\ \hline 0 & 0 \end{array}\right] \cdot \begin{Bmatrix} u_{ik} \\ v_{ik} \end{Bmatrix} \cdot dm, \qquad (19)$$

which leads to:

$$\{S\}^T \cdot \omega^2 [F] \{S\} . \qquad (20)$$

Matrix [F] is symmetric, and has the role of a generalized mass matrix: only its coefficients coming from products of u_{jh} by u_{ik} terms are nonzero. These coefficients have the form:

$$\int_m X(h)\, CT(j)\, X(k)\, CT(i)\, dm, \qquad (21)$$

and thus only the ones with j = i give a non zero integral.

Taking into account eq. (15) and eq. (20), it is obtained

$$[C] \cdot \{S\} = \omega^2 [F] \cdot \{S\} \qquad (22)$$

Observing that [C] can be inverted while [F] cannot, eq. (22) can be written as:

$$\{S\} = \omega^2 [C]^{-1} [F] \{S\} \qquad (23)$$

and thus:

$$\frac{1}{\omega^2} \{S\} = [C]^{-1} [F] \{S\} \qquad (24)$$

that with:

$$[C]^{-1} \cdot [F] = [D] \qquad (25)$$

takes the canonical eigen values form:

$$\left[[D] - \frac{1}{\omega^2} [1] \right] \{S\} = \{0\} \qquad (26)$$

DISCUSSION OF THE RESULTS

In order to test the correctness of the generalized stiffness matrix, it is possible to calculate the stress state in the stable configuration, according to equation:

$$[C] \{S\} = \{Q\} \qquad (27)$$

where the vector {Q} due to centrifugal forces comes from:

$$\begin{Bmatrix} u \\ v \end{Bmatrix}^T \{Q\} = \{S\}^T \cdot [U] \cdot \{\omega^2 \, r_o\} \qquad (28)$$

The general term of Q is thus

$$\int_m X(h)\, CT(j) \cdot \omega^2 . r \, dm \qquad (29)$$

The stress state was calculated for various disks, and compared with the corresponding solution obtained by a modified Manson's method[7].

For the disk under consideration, composed by a fiberglass - epoxy filament wound rim supported by a quasi-constant stress Ertalon 6 disk (fig. 1) the stress state is shown in fig. 2 with full lines.

This solution was obtained using a M = 6 degree polynomial along the radius.

The reference solution (dotted lines) was obtained by the method shown in ref.7.

After this test, the calculation of critical speeds was started employing several values for the degree M of the polynomial and for the maximum harmonic order L.

It was found:

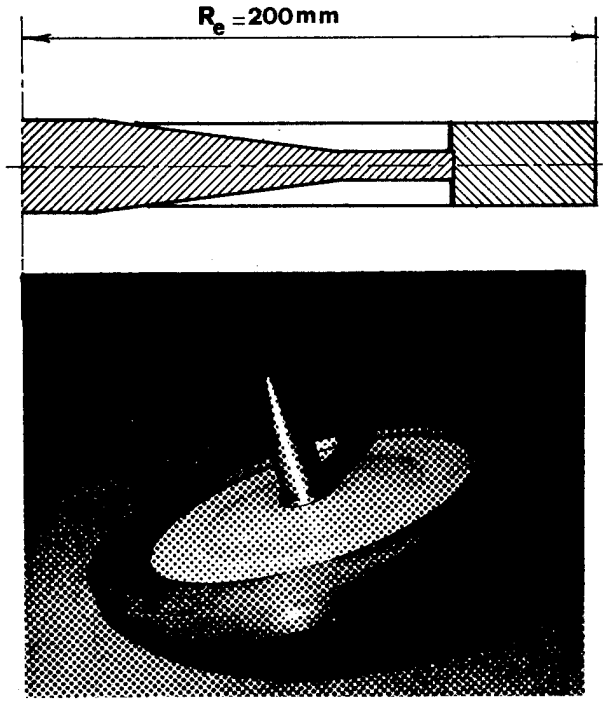


Fig. 1 - View and section of the disk taken into consideration.

1. the solutions are not influenced at all by the choice of maximum harmonic order L, apart of course from the maximum obtainable number lobes.

2. the solutions were dependent on the degree M of the polynomials, and a satisfactory value was found to be M = 7 (fig. 3)

3. in the eigen vectors that give the coefficients of the displacement functions only the coefficients related to one harmonic at a time are non zero. This of course is due to the axialsymmetry of the disk.

The first three deformed configurations are shown in fig. 4.

The maximum radial and circumrerential stresses in the rim at the first critical speed are respectively 1205 MN/m^2 and 28 MN/m^2.

If the usual delamination problems (which caused failure at a far lower speed of the flywheel shown in fig. 1) can be

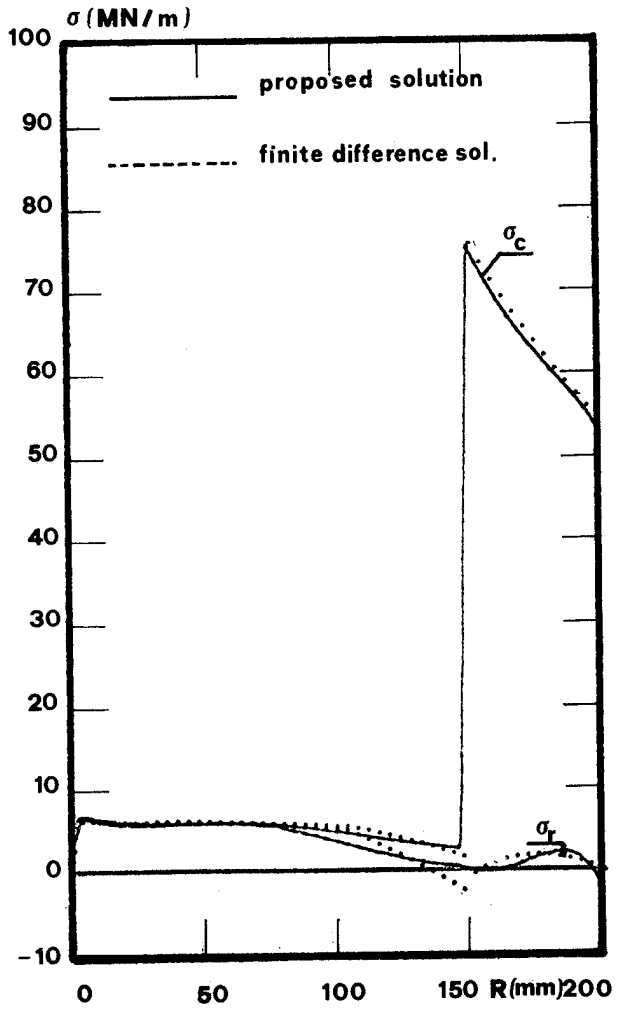


Fig. 2. Stress state at 1000 rad/s in the considered disk.
Full lines: proposed methods solution with M = 6.
Dotted lines: finite differences solution (Manson)

overcome, these values of the circumferential and radial stresses arelow enough to allow the flywheel to reach the first critical speed.

If the rim were built using a composite material with elastomeric matrix, the critical speed can even be lower, and the danger due to the first critical speed can be reale

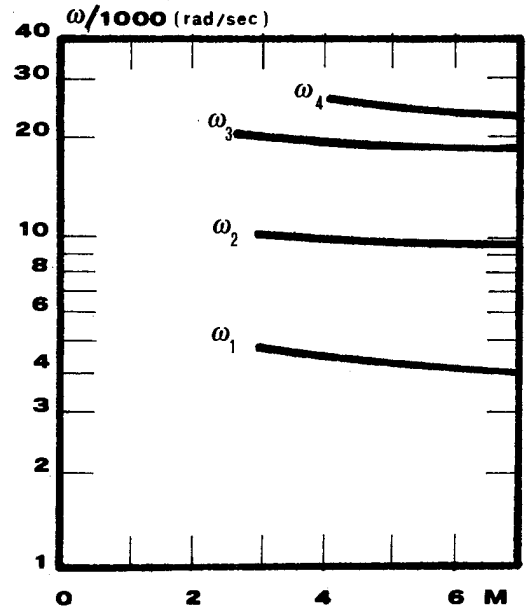


Fig. 3 - First four critical speeds in function of the degree M of interpolating polynomials.

CONCLUSIONS

The proposed method allows to calculate the ovalization critical speeds of rotating disks.

A generalized stiffness matrix is obtained that has a triple-band structure, most of the elements being zero.

Results are presented for an already constructed disk; the first critical speed was found to be lower then the speed at wich the flywheel would burst, provided that delamination problems ennountered during spin tests are solved.

SYMBOLS

m	mass
r	radius
r_e	outer radius
s	general virtual displacement
x	nondimensional vector radius $x = r/r_e$
[E]	plane stress stiffness matrix of the material

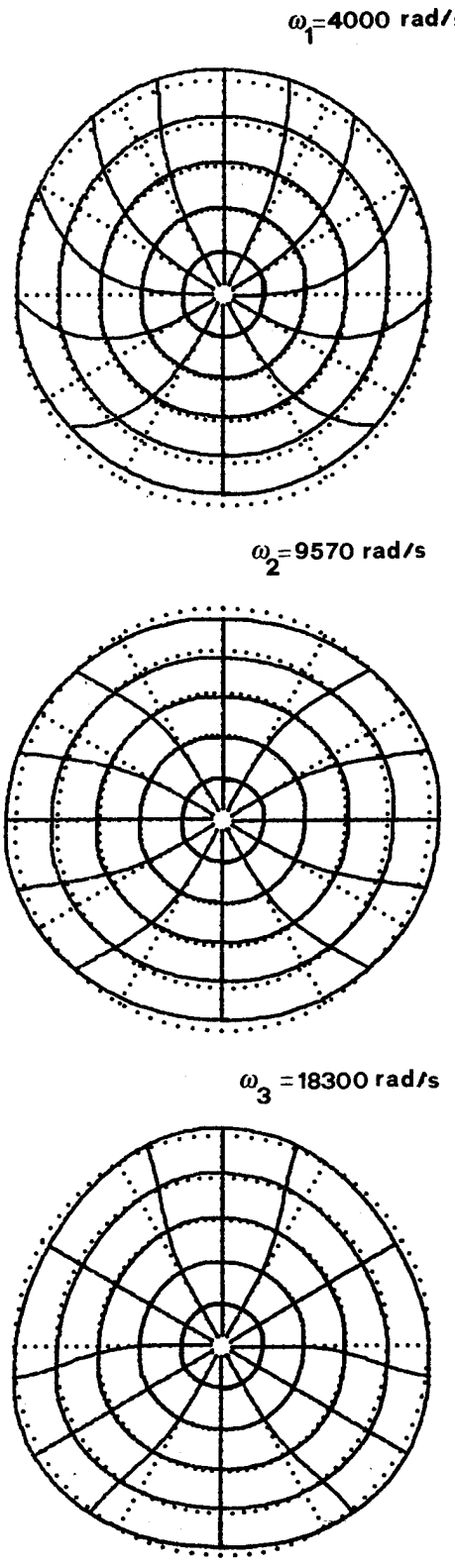


Fig. 4 - The deformed configurations at the first three critical speeds.

E_v volume energy for basic equilibrium configuration

E'_v volume energy for additional "ovalization" deformation

L maximum harmonic order

M order of interpolation polynomials

V volume

θ vector angle

ω angular velocity

REFERENCES

[1] Ritz W. - "Zeisch. Reine und Angew. Math.", vol. 135, p. 1-61, 1902.

[2] Ritz V. - "Ann. Physik" vol. 28, p. 737, 1909;

[3] Pflügen A. - "Stabilitäts probleme den Elastostatik", Springer, Berlin 1960.

[4] Szabò J.: "Hohere Technische Mechanik" Springer, Berlino 1956.

[5] J.S. Przemieniecki -"Theory of matrix structural analysis", Mc Graw Hill, New York, 1968.

[6] Cheney E.W.:"Introduction to Approximation theory"- Mc Graw-Hill, 1966.

[7] Belingardi G., Genta G. -"Generalizzazione del metodo di Manson, per il calcolo di corpi a simmetria cilindrica in parete spessa in materiale ortotropo assialsimmetrico non lineare". La meccanica italiana, June 1977 , n. 108.

EFFECT OF HUB TO RIM STIFFNESS ON SPIN-WHIRL DYNAMICS OF PENDULOUS ROTORS

Charles N. McKinnon, Jr.
Systems, Science and Software, Inc.

ABSTRACT

The principal advantage of spin testing prototype composite material rotors in the pendulous mode is the high tolerance to mass unbalance. The rotor safely whirls at the end of an elastic shaft. The two degrees of freedom in the usual spin-whirl analysis are tilt angle and radial displacement of the rigid rotor.

If the hub and rim are separate bodies coupled by finite stiffness, say in the form of spokes, a three degree of freedom system results: tilt angle of hub, tilt angle of rim, and the common radial displacement. The steady state dynamical equations are cast in nondimensional form and result in a frequency equation which is quadratic in spin and sixth order in whirl. Solutions using typical rotor parameters produce two real quadratic spin roots for a range of assigned whirl frequencies. The resulting spin-whirl maps cover four decades of spoke stiffness and are similar to those for a rigid rotor with the addition of an upper branch.

On this branch; self-excited vibrations that arise at discrete spin frequencies are unstable due to the direction of spoke hysteresis force. A stability criteria is derived which is a function of the spoke to shaft stiffness ratio and of the hub polar to diametral inertia ratio. As the desired spin operating frequency increases, there is an increase in the minimum stiffness ratio required. At a given spin frequency, higher stiffness ratios are required for lower hub inertia ratios. The model has confirmed experimental results, predicting the maximum stable spin frequency within 5% of actual.

Although the study was prompted by a spoked configuration, the results are applicable to any pendulous rotor with finite connection stiffness.

(Paper Not Submitted)

ADVANCED FLYWHEEL DEVELOPMENT

P. W. Hill
A. A. Vicario
T. C. White
T. L. Waltz
Hercules Incorporated
Allegany Ballistics Laboratory
Cumberland, MD 21502

ABSTRACT

Design studies were conducted to define performance potential of near optimum composite flywheels using commercially acceptable material property values and safety factors. Investigation included three classes of flywheels: (1) disks (hoop wound), (2) shell (helical wound), and (3) spoked. Fibers studied included glass, Kevlar, and graphite. Optimization of thickness contours for disk flywheels was accomplished using a nested ring model. Highest performance in a contoured hoop wound disk was provided by a variable modulus graphite design with a computed operational rated energy density of 19.4 wh/lbm. Finite element stress analyses of helical shell type flywheels with hoop wound rims were conducted. A variety of failure mechanisms involving intralaminar shear and transverse tension were identified, opening new questions regarding the degree of severity of micromechanics type failures (resin crazing) in non-critical locations. Rated performance approaching 40 wh/lbm was computed for the best configuration. A series of advanced concept spoke/rim designs were identified and screened. The pin wrapped concept was selected as most promising. Two wheels of this type are being built for delivery to Sandia Laboratories. Results of stress analyses and a description of the fabrication are provided. The paper covers work on contour optimization initiated in 1975 through fabrication efforts continuing through September 1977.

INTRODUCTION

Kinetic energy storage in the form of rotating masses has been practiced for a very long time. Today's interest is characterized by a much longer cycle period, extending to many hours, and/or much higher energy density. This interest brings the flywheel into competition with electrical, chemical, thermal, and other forms of mechanical energy storage for some applications. However, the flywheel in all forms retains two attributes not easily provided by other storage means - the ability to deliver very high power density and a characteristic resistance to performance degradation throughout its lifetime. It is therefore appropriate to examine means by which the energy density may be improved while retaining other advantages.

Modern concepts of composite energy storage flywheels include many different forms. Among these are radial bars, brushes, thin spokeless rims, multiple concentric rings, thin shells, as well as flat or contoured wheels. Each class requires a different approach for optimum design synthesis, and no one class is universally superior to date.

For these problems, uniqueness of the optimum is not assured in the real world, and certainly the formulation of the math model will introduce assumptions and restrictions that probably exclude the real optimum from the region of search, even if it exists. Therefore we seek near-optimum, compromised solutions that lead to operationally practical designs at an acceptable cost. The law of diminishing returns applies.

OBJECTIVES

The objectives of this study may be concisely stated as follows:

1. Evaluation of performance potential of commercially acceptable composite flywheels in simple and innovative designs.

2. Definition of benefit from contouring circumferentially wound disk type flywheels.

3. Screening and ranking of materials in practical configurations.

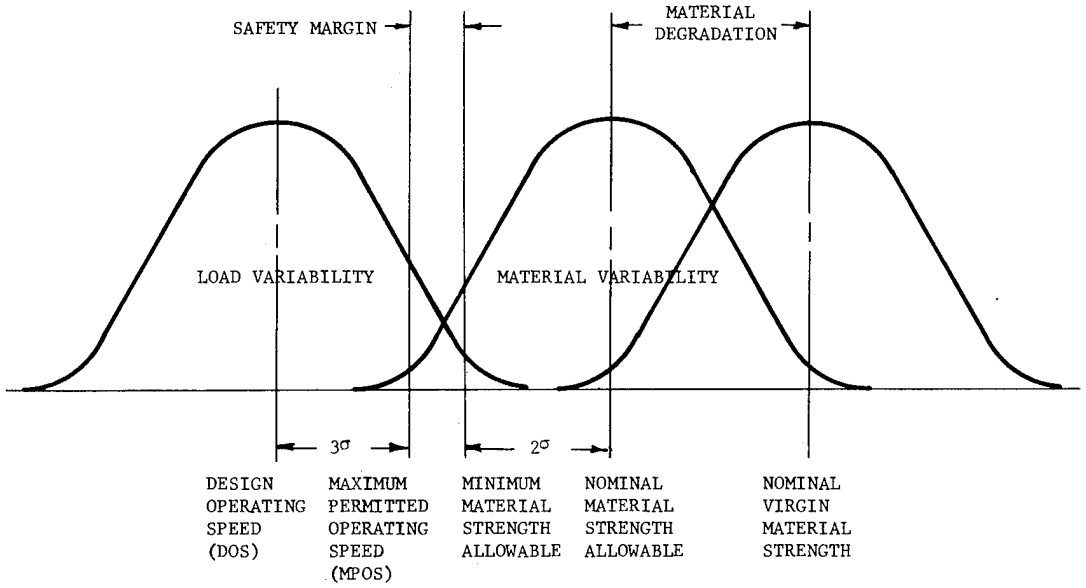
COMMERCIALLY ACCEPTABLE RATING

Performance potential for composite flywheels is quoted on a variety of bases, ranging from system delivery values to theoretical fiber strength/density ratio (σ/ρ). Numbers associated with a given material (Kevlar-49) may range from 10 to 140 W-hr/lb), and there seems to be little hesitation in comparing the theoretical fiber strength of composites to the system delivery value of batteries or even steel flywheels. Standard terminology is urgently needed.

in load, analysis, material, manufacturing, etc. and factors of safety representing general social, professional, and commercial acceptance. Figure 1 illustrates the approach.

CONTOURED DISK FLYWHEELS

Although the contoured disk may be the least sophisticated of all flywheel types and has been dismissed by many as having performance potential too low to merit deep study, characteristic advantages include:



DEGRADATION TO DESIGN ENVIRONMENT

Material	Material Variation* (-2σ) (%)	200°F Temperature Degradation (% of Ultimate)			Degradation Due to Static Fatigue (% of Ultimate)		
		Long.	Trans.	Shear	Long.	Trans.	Shear
Kevlar-49 Composite	10	3	21	15	40	40	40
Type ASMS Graphite Composite	20	0	15	15	3	20	20
S-2 and E-Fiberglass Composite	10	10	15	15	50	55	50

*(-2σ) variation includes material handling, fabrication, test data.

Fig. 1. Design criteria.

For the purposes of this paper, energy densities are compared on the basis of energy stored in the rotor and hub at the maximum permissible operating speed (MPOS). The MPOS is set by due consideration of stress distribution, material strength as degraded by the operating environment, uncertainties

(1) Simple fabrication, low cost.

(2) Simple mechanical coupling to other system components.

(3) Dynamic stability.

(4) Compactness.

A design synthesis study was conducted seeking the best contour for disk type flywheels made from fiber reinforced epoxy composite material. The method combined a two-dimensional stress analysis, modeling the variable width disk as a series of concentric contiguous rings of differing width, with an automated search procedure to adjust the width of each ring until the energy density was a maximum.

The objective of the study was to achieve a realistic appraisal of the performance that could be expected from different materials when practical constraints inherent in the materials and designs were considered as in a commercial product. The design was limited to filament winding in the circumferential direction, leading inevitably to failure predictions in the radial (transverse to the fiber) direction. Thus the transverse strength of the material became critical.

DESIGN SYNTHESIS STRATEGY

The framework of the strategy used herein to study the filament wound flywheel was as follows. Given the outer and inner radii, the material properties and the boundary conditions (prescribed stresses or deformations at the inner and outer surfaces), find the contour of the sides that yields the highest energy density without initiating a material failure or violating a minimum thickness established by manufacturing or extraneous operating conditions (vibration, static creep, etc.). An extension of the problem when more than one material is used is to find the best placement of each material.

The critical parameter is the failure condition at every point in the wheel which must be determined by comparing the stress state with a prescribed failure criteria. The design variables are the thicknesses, or contour description, and the radial location of the interfaces between different materials. The constraints are the prescribed inner and outer radii and the minimum thickness. The measure of value is the energy density which is computed such that failure is impending at the point where the failure condition is the highest. A dummy load (spin velocity) is applied initially to compute the stress distribution, after which the failure velocity and energy density can be computed.

THE STRESS SOLVER

Compromise is immediately encountered when selecting a stress solution to incorporate in the model. Closed form solutions generally require restriction of geometry or material variation to simple analytic forms that do not include the optimum in most cases.[1,2,3,4]

Finite element methods can model both geometry and mathematics to a high degree of satisfaction, including in this axisymmetric problem, a full three-dimensional treatment, but are very expensive to use in parametric exploration of wide ranging design features. However, for use as a final design procedure to refine a predetermined, near-optimum solution and provide accurate stresses, this method is satisfactory and has been used by the authors.

Numerical integration, using a piecewise linear approximation for the contour, was successfully applied by Gerstle and Biggs[5] for design synthesis of a disk flywheel of one material. This procedure minimizes the incompatibilities at the segment interfaces, and may be extendible to multiple materials.

For the method described herein, the disk is modeled with a series of straight sided concentric ring segments (Fig. 2), similar to the approach of Seireg and Surana,[6] but which may be of any prescribed material having polar orthotropy. The solution proceeds similarly to that of Toland,[7] but with an extension to admit variable width to the segments.

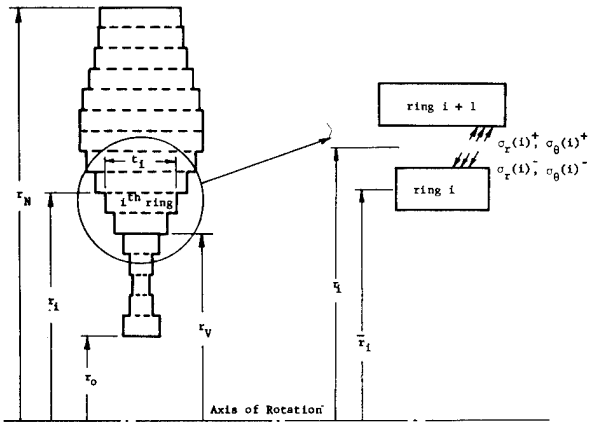


Fig. 2. Transfer matrix model for disk of variable thickness.

RESULTS

It is important to note here than an objective of this study was to sense the best that might be expected from flywheels of inherently simple design and manufacture—a circumferentially wound wheel—recognizing in advance that the full potential of the fiber strength cannot be realized in such designs. The fact that the material strength perpendicular to the fiber is of order 25-100 times weaker than that parallel to the fiber and the stress ratio is of order 10 for wheels with $r_o/r_N < 0.5$ causes the critical stress invariably to be σ_r.

Design properties for composite materials were established using commercial allowances for temperature, creep, fatigue, statistical variations, and factors of safety. The assumptions used to determine the design properties are:

1. Flywheel to operate in a vacuum. Temperature not to exceed 200°F.

2. Flywheel to be capable of withstanding load cycles between 100% and 70% of design operating loads for 10^6 cycles.

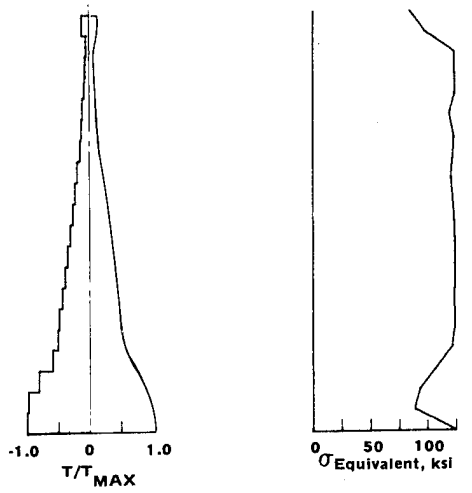
3. Flywheel to be cycled between 10% and 100% of design operating load for 3.2×10^3 cycles.

4. Flywheel to be capable of sustained loading at design operating conditions for 2.5×10^4 hours.

Based on available data to date on static and dynamic fatigue, static fatigue at 2.5×10^4 hours is the most critical condition on the composite flywheel under transverse tensile loading conditions (σ_r).

Nominal static properties at 77°F are shown in Table I for candidate materials. The design criteria are summarized in Fig. 1 and the design allowables for Kevlar-49, ASMS graphite*, S-2 fiberglass and E-glass composites are presented in Table 2.

The optimization of the steel flywheel was performed as a test case to verify the operation of the optimization routine. The resultant energy density, 12.9 watt hours/lb, and the optimum shape (Fig. 3) are comparable with those presented by Davis.[8]



η = 12.9 W-hr/lbm

Fig. 3. Steel flywheel.

Results of the parametric study (Energy Density vs. Radius Ratio) for composite disk flywheels of a single material are presented in Table 3. The significant results of the study, those for which $R_i/R_o = 0$, are energy densities representative of a complete rotor. The energy densities for $R_i/R_o = 0.2, 0.5$, on the other hand, are representative of the composite rim only (no hub or hub attachments). For $R_i/R_o = 0$, the contoured graphite disk flywheel exhibits the highest energy density, 12.5 watt-hours/lbm. It should be noted that the material ranking, ASMS graphite, Kevlar-49, and S-2 fiberglass, (based upon the energy density) results from the transverse stress critical condition which is common to all contiguous hoop wound designs. Typical optimum flywheel shape and resulting stress distributions for the composite solid disk flywheels ($R_i/R_o = 0$) are presented in Fig. 4. Note that the thin sections might require thickening to withstand lateral loads or improve dynamic characteristics.

Table 3. Energy density: watt-hours/lb (kJ/kg) vs. radius ratio R_i/R_o.

R_i/R_o	Material		
	S-2 Fiberglass	Kevlar-49	ASMS Graphite
0	2.13 (16.91)	4.42 (35.09)	12.54 (99.57)
0.2	2.81 (22.31)	4.41 (35.02)	12.20 (96.87)
0.5	11.11 (88.13)	9.04 (71.78)	25.21 (200.17)

*Hercules' Magnamite® Graphite Fiber Type ASMS

Table 1. Nominal static properties at room temperature for candidate materials.

Property	Kevlar-49 Composite	Type ASMS Graphite Composite	S-2 Fiberglass Composite	E-Glass Composite
Longitudinal Tensile Modulus, E_{11}, psi (GPa)	11.0×10^6 (75.8)	18.0×10^6 (124.1)	7.8×10^6 (53.8)	6.0×10^6 (41.4)
Transverse Tensile Modulus, E_{22}, psi (GPa)	0.6×10^6 (4.1)	1.0×10^6 (6.9)	3×10^6 (20.7)	2×10^6 (13.8)
Poisson's Ratio, ν_{12}	0.34	0.27	0.25	0.25
In-Plane Shear Modulus, G_{12}, psi (GPa)	0.30×10^6 (2.1)	0.85×10^6 (5.9)	0.9×10^6 (6.2)	1.0×10^6 (6.9)
Longitudinal Tensile Strength, F_{11_T}, ksi (MPa)	200 (1380)	220 (1520)	226 (1560)	150 (1030)
Transverse Tensile Strength, F_{22_T}, ksi (MPa)	2.5 (17.2)	6 (41.4)	5.8 (40.0)	4 (27.6)
Longitudinal Compressive Strength, F_{11_C}, ksi (MPa)	45 (310)	160 (1100)	86 (595)	90 (620)
Transverse Compressive Strength, F_{22_C}, ksi (MPa)	14 (96.5)	18 (124.1)	18 (124.1)	20 (137.9)
In-Plane Shear Strength, F_{12}, ksi (MPa)	2.9 (20.0)	8 (55.2)	5 (34.5)	6 (41.4)
Composite Density, lb/in.^{3} (kg/m^3)	.050 (1.38×10^3)	.054 (1.50×10^3)	.072 (1.99×10^3)	.075 (2.08×10^3)

Table 2. Design allowables.

Property	Kevlar-49 Composite	Type ASMS Graphite Composite	S-2 Fiberglass Composite	E-Glass Composite
Longitudinal Tensile Modulus, $E_{11} \times 10^6$ psi (GPa)	10.7 (73.8)	18.0 (124.1)	7.2 (49.6)	5.4 (37.2)
Transverse Tensile Modulus, $E_{22} \times 10^6$ psi (GPa)	0.5 (3.4)	0.9 (6.2)	1.7 (11.7)	1.7 (11.7)
Poisson's Ratio, ν_{12}	0.33	0.27	0.24	0.24
In-Plane Shear Modulus, $G_{12} \times 10^6$ psi (GPa)	0.25 (1.7)	0.8 (5.5)	0.7 (4.8)	0.8 (5.5)
Longitudinal Tensile Strength, F_{11_T}, ksi (MPa)	122 (840)	170.5 (1175)	102.0 (703)	61.2 (421)
Transverse Tensile Strength, F_{22_T}, ksi (MPa)	1.3 (9.0)	3.9 (26.9)	2.7 (18.6)	1.5 (10.3)
Longitudinal Compressive Strength, F_{11_C}, ksi (MPa)	25.0 (172)	140.0 (965)	24.3 (168)	36.7 (253)
Transverse Compressive Strength, F_{22_C}, ksi (MPa)	6.0 (41.4)	11.0 (75.8)	11.0 (75.8)	7.7 (53.1)
In-Plane Shear Strength, F_{12}, ksi (MPa)	1.3 (9.0)	5.0 (34.5)	2.7 (18.6)	2.3 (15.9)

(1) Assume: $\nu_{12} = \nu_{13} = \nu_{23}$

$G_{12} = G_{13} = G_{23}$

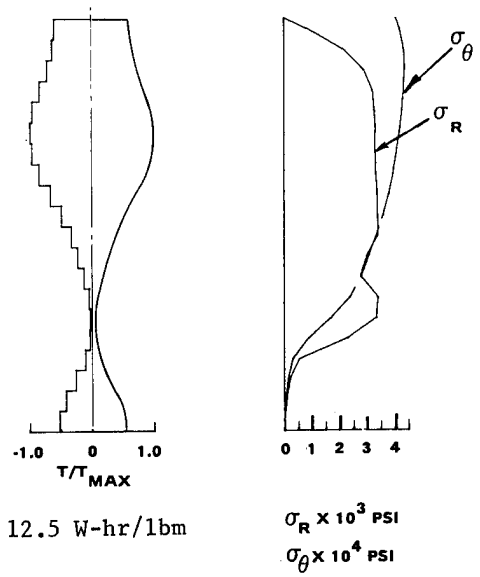


Fig. 4. ASMS graphite flywheel.

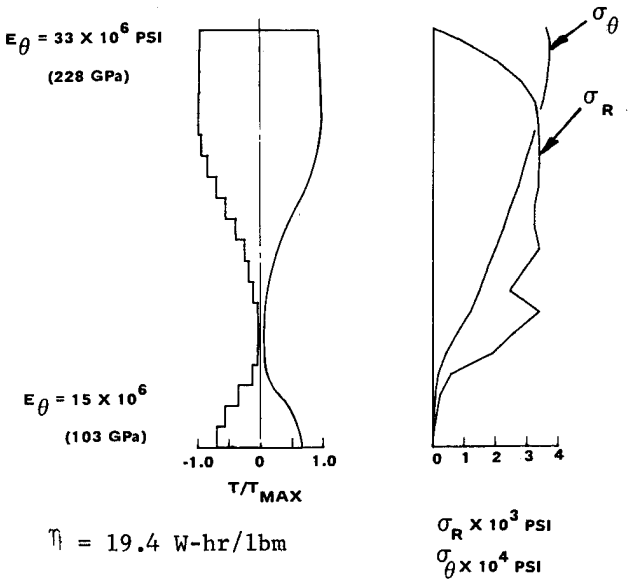


Fig. 5. Variable modulus graphite flywheel.

Calculations were also performed to determine the optimum graphite disk flywheel with a linear circumferential composite modulus (E_θ) distribution along the radius. The graphite flywheel was assumed to have a hoop modulus variation of 15 x 10^6 psi at the center to 33 x 10^6 psi at the outer radius.* The energy density for the variable modulus graphite disk flywheel, 19.4 watt-hrs/lb, was the highest energy density calculation for a solid disk flywheel (R_i/R_o = 0). Results for this flywheel are presented in Fig. 5.

In addition to the single material disk flywheels, multi-material flywheels can be optimized using the same approach. An additional variable, the radius to the interface between the materials, can be adjusted to determine the optimum location for each material. Initial results indicate little value in utilizing anything other than graphite in a contour optimized hoop wound disk flywheel due to their reduced transverse strength.

*One of the unique properties of graphite fiber is the ability to control the modulus by adjusting the manufacturing process for the fiber.

HELICAL SHELL FLYWHEELS

DESCRIPTION

Combinations of hoop wrapped rims and various forms of shells which contain the rim and connect it to the hub have been proposed; e.g., Ref. 8. Preliminary investigation into the state of stress in one such design was conducted using a specialized finite element code providing for laminate analysis of axisymmetric bodies. The shell considered was formed from helical windings in the conventional geodesic pattern, but with the build-up at the hub distributed symmetrically with respect to the shell mid-plane. Hoop wound rims were studied, both internal and external to the shell in several thicknesses. No optimization of shell or rim was attempted. Figure 6 illustrates the geometry.

A series of eight cases was examined, including variations of material and configuration as noted below:

- Materials:

  Shell: S-2 Fiberglass or ASMS Graphite

  Hoops: ASMS Graphite

- Winding angle of helicals (R_i/R_o ratio):

  α_s = 10.5°, 30.0°

- Number of hoops:

  Thickness of hoop layers, both on the inside and outside, varied from t_H = 0 to 1.25 in.

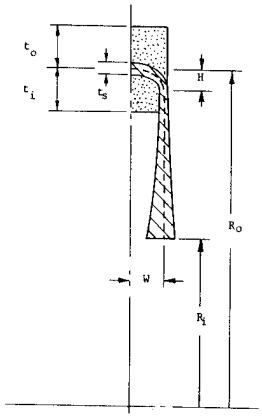


Fig. 6. Shell flywheel geometry.

RESULTS

Table 4 summarizes the results of the finite element stress computations.

Table 4. Summary of results.

Case No.	Description		Energy Density (W-hrs/lbm) Matrix Failure	Fiber Failure
1	Shell: S-2 Fiberglass Rim: None	$\alpha_s = 10.5^o$	1.4	17.0
2	Shell: S-2 Fiberglass Rim: ASMS Graphite	$\alpha_s = 10.5^o$ $t_i = t_o = 1.25"$	14.4	24.8
3	Shell: S-2 Fiberglass Rim: ASMS Graphite	$\alpha_s = 10.5^o$ $t_i = t_o = .625$	10.4	18.1
4	Shell: S-2 Fiberglass Rim: None	$\alpha_s = 30^o$	2.2	22.6
5	Shell: S-2 Fiberglass Rim: ASMS Graphite	$\alpha_s = 30^o$ $t_i = t_o = 1.25$	11.4	35.3
6	Shell: S-2 Fiberglass Rim: ASMS Graphite	$\alpha_s = 30^o$ $t_i = t_o = .625$	9.6	32.2
7	Shell: ASMS Graphite Rim: ASMS Graphite	$\alpha_s = 30^o$ $t_i = t_o = 1.25$	8.4	44.0
8	Shell: ASMS Graphite Rim: ASMS Graphite	$\alpha_s = 30^o$ $t_i = 1.25$ $t_o = 0$	22.4	38.9

The need for stiffness in the shell is apparent from these results. The matrix failure in case 7 occurred at the rim-shell juncture in the outside hoop winding, a point of known design deficiency correctable by eliminating hoop windings in that region.

These results emphasize the need for more detailed study of micromechanics failure control and experimental evaluation of these failure effects, but also show the attractive potential of this simple design concept.

In Fig. 6 the details of results from case No. 8 are presented. Note the progression of failure levels associated with matrix failure in regions of low fiber stress. These results are typical of pressure vessels also, and are not catastrophic in that case. The effect of this resin "crazing" on flywheels needs to be investigated if shell concepts are to merit further development.

A transverse failure indication at location 4 would be deemed "serious"; however, corrective design via containment is possible, leading to increased performance as indicated by the next failure level. Details of the stress distribution showed changes in shell contour to reduce bending at the perimeter and increase radial stiffness are needed. High stiffness of the shell relative to the rim is desirable. Additional ballasting of the rim or adding rim material by contouring the inner surface will increase energy density.

SPOKED FLYWHEELS

A variety of rim and spoke concepts have been proposed for composite flywheels. One concept in which the spokes are attached to the hub by pins is the subject of this section, and is illustrated in Fig. 7. General advantages of this concept include:

1. Positive centering.

2. High radial natural frequencies.

3. Flexibility in number of spokes to control rim bending.

4. Clear center for shaft or hub adapters.

5. No spoke buildup at the hub.

6. Continuous circuit spoke winding program.

SHELL FLYWHEEL MODEL

COMPUTER RUN DESCRIPTION

Case No. 8

Description:

Shell - ASMS Graphite

Hoops - ASMS Graphite

Dimensions

R_o = 10.0"

R_i = 5.0"

W = 1.0"

H = 0.5"

α_s = 30°

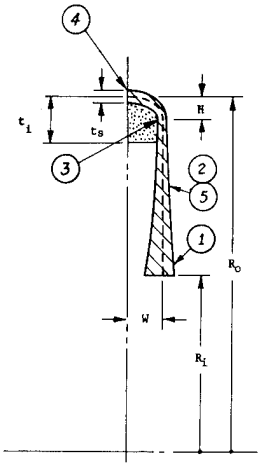
t_s = 0.25

t_1 = 0

t_2 = 0

t_3 = 0.625

t_4 = 0.625



Mass - 9.55 lbm

Moment of Inertia - 513.1 lbm-in.^{2}

Failure Location	Stress Type	Value (psi)	Speed (rpm)	Energy Density (wh/lbm)
1	Transverse	3,400	10,930	2.86
2	Shear	4,400	23,643	13.38
3	Shear	4,400	26,738	17.1
4	Transverse	3,400	30,602	22.4
5	Fiber	148,300	40,322	38.9

Fig. 6. Shell flywheel model - case 8.

Difficulties common to spoked designs include:

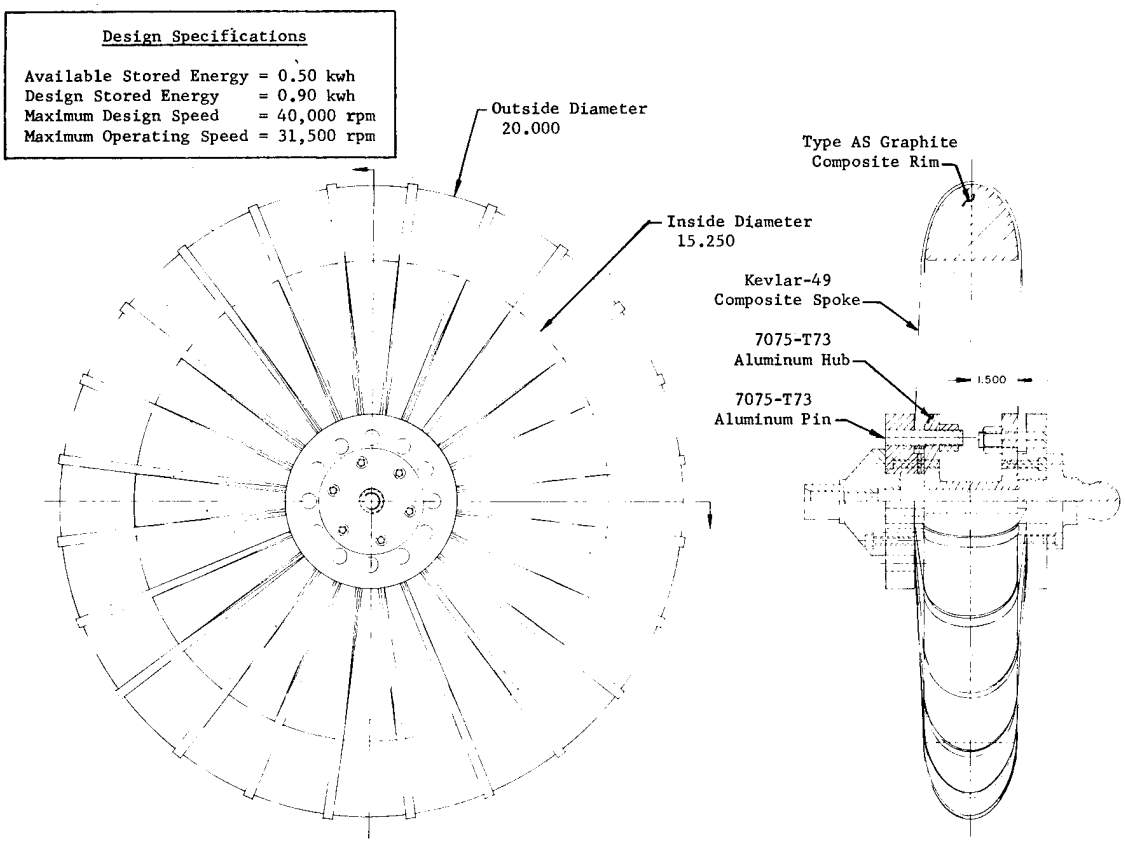
1. Low axial stiffness.

2. Maintaining concentricities during sequential winding and curing steps.

3. Stress concentrations at component interfaces.

Some compromises to cost and schedule in this design; e.g., suboptimum rim contour, and hub configuration constrained by testing interface requirements are apparent.

Stress analyses were conducted in three steps using three finite element grid models. The first step consisted of an axisymmetric analysis of the overall flywheel configuration. The finite element grid network, boundary and loading conditions used in this analysis are shown in Fig. 8. In order to model the spokes in this analysis, a special "zero hoop stress" element was employed. The procedure consists of modeling each section of the spoke from the rim to the pin by segments of ring elements so formulated that axial, radial and shear stress gradients can occur within the element but the circumferential or hoop stress is zero. From this analysis the stress, strain and displacements in the rim and spokes can be determined.



*Design prepared by Sandia Laboratories.

Fig. 7. Pin-wrapped spoke flywheel.

The second step of the analysis consisted of a finite element model to determine the stress distribution in the region where the spoke is wrapped around the pin. A plane stress representation was assumed and the model, boundary and loading conditions are illustrated in Fig. 9. Displacements obtained from the axisymmetric analysis are applied to the plane stress model at a 4-in. radial location on the spoke.

The third step of the analysis consisted of determining the stress distribution in the aluminum pin and hub. The finite element model for the analysis is shown in Fig. 10. The loading condition consists of a pressure distribution equivalent to the spoke load determined from the results of the previous analysis plus a radial acceleration load equivalent to 40,000 rpm.

Results of the analyses are summarized in Fig. 11. The critical stress occurs in the spoke where it is wrapped around the pin. The stress distribution at this location is very non-uniform and is highly dependent upon the spoke thickness.

The stress distributions in the graphite rim are illustrated in Figs. 12 and 13. The concentrations of transverse stress near the initial contact point of the spoke indicate potential for improvement by optimizing bond location.

CONCLUSIONS

DISKS

1. Contiguous hoop wound flywheels are controlled by transverse tensile strength; graphite provides superior performance (12.5-19.4 wh/lb).

2. Combination of optimum contour and modulus variation provides a marketable graphite disk flywheel provided system cost is competitive.

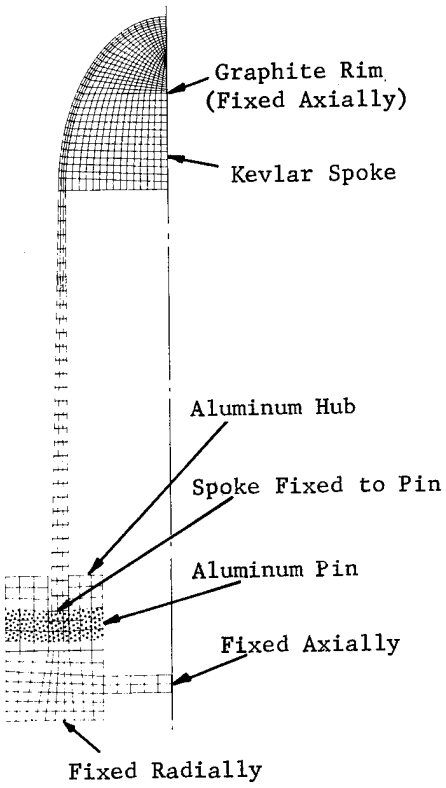


Fig. 8. Axisymmetric model of flywheel assembly.

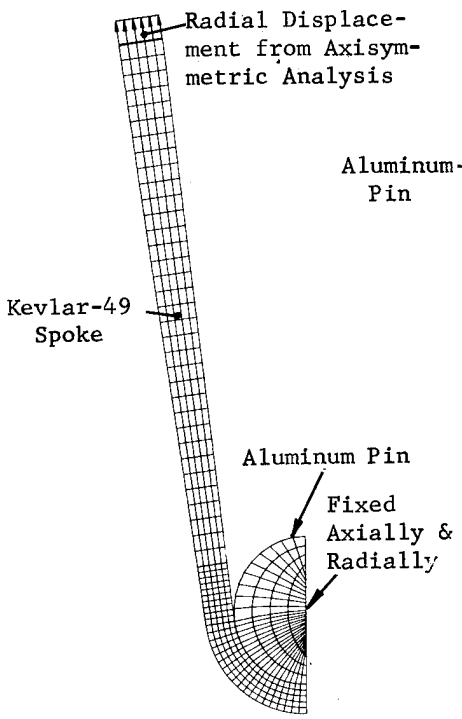


Fig. 9. Plane stress model of spoke and pin.

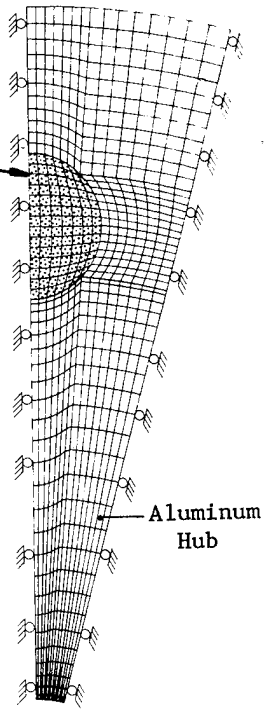
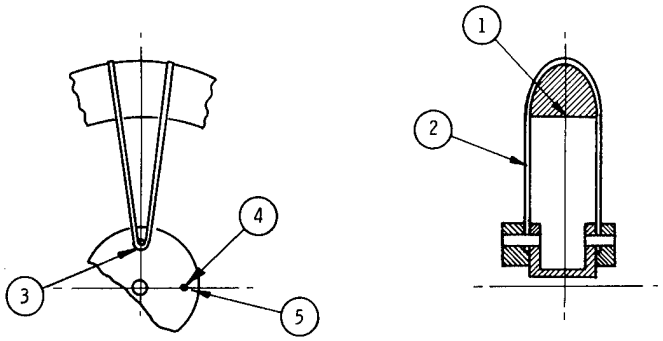


Fig. 10. Plane stress model of aluminum pin and hub.



LOCATION	FLYWHEEL COMPONENT	TYPE OF STRESS	MAX. STRESS @ 31,500 RPM (KSI)	MARGIN OF SAFETY
1	TYPE AS GRAPHITE RIM	HOOP OR LONGITUDINAL COMPOSITE	130.0	0.69
		RADIAL OR TRANSVERSE COMPOSITE	3.0	1.00
2	KEVLAR-49 SPOKE	LONGITUDINAL COMPOSITE	81.2	1.46
3	KEVLAR-49 SPOKE	LONGITUDINAL COMPOSITE	145.1	0.38
4	ALUMINUM PIN	EQUIVALENT	17.0	2.29
5	ALUMINUM HUB	EQUIVALENT	19.2	1.92

Fig. 11. Summary of results of pin-wrapped flywheel structural analysis @ 40,000 rpm.

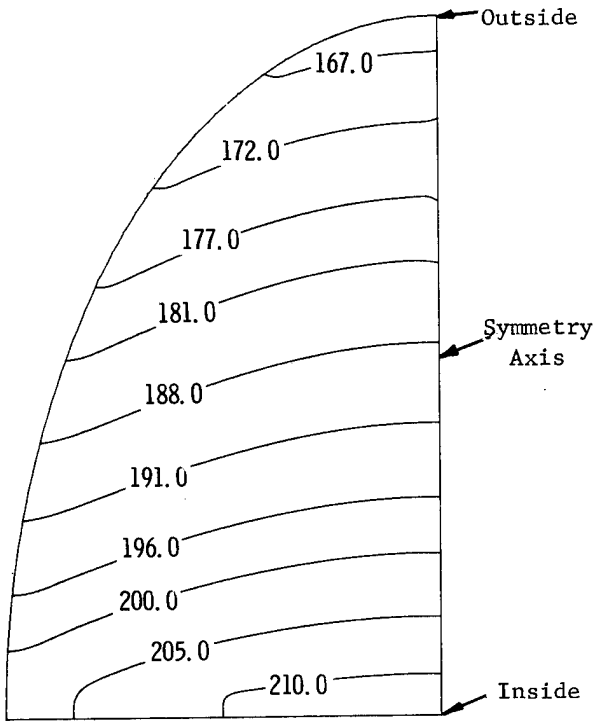


Fig. 12. Hoop stress iso-plot through graphite rim @ 40,000 rpm.

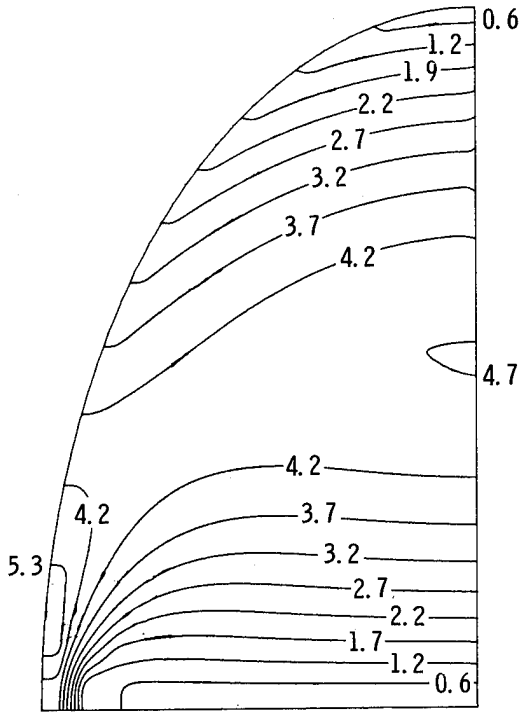


Fig. 13. Radial stress-iso-plot through graphite rim @ 40,000 rpm.

SHELLS

1. Calculated graphite shell performance was higher than any composite rotor demonstrated to date on a commercial rating basis (22 wh/lb).

2. Modest redesign should provide 40 wh/lb.

3. 100% filament wound fabrication should provide manufacturing advantage.

4. Failure mechanism needs definition.

SPOKED RIMS

1. Spoked rims provide a direct approach to high energy density on a weight basis, volumetric improvement will come with optimization.

2. Stresses and deformations can be managed to provide a workable product.

3. Manufacturing of several designs has been demonstrated.

4. Additional study of dynamic response and secondary loads is now needed.

In all studies, results emphasized the necessity to consider the micromechanics (transverse stresses) for all composite flywheel designs, and the urgent need for more material data in the transverse direction under sustained loads, cyclic loads, and elevated temperatures.

REFERENCES

[1] Chang, C. I., "Stresses and Displacements in Rotating Disks with Variable Densities," AIAA Journal, Volume 14, No. 1, January 1976, pages 116-118.

[2] Murthy, D. N. S., and Sherbourne, A. N., "Elastic Stresses in Anisotropic Disks of Variable Thickness," International Journal of Mechanical Sciencies, Pergammon Press, Volume 12, 1970, pages 627-640.

[3] Sen Gupta, A. M., "Stresses in Some Aeolotropic and Isotropic Circular Disks of Varying Thickness Rotating About the Central Axis," Bulletin Calcutta Mathematical Society, Volume 31, No. 3, September 1949, pages 120-139.

[4]Reddy, T. Y., and Sinrath, H., "Elastic Stresses in a Rotating Anisotropic Annular Disk of Variable Thickness and Variable Density," International Journal of Mechanical Sciences, Pergammon Press, Volume 16, 1974, pages 85-89.

[5]Gerstle, F. P., Jr., and Biggs, F., "On Effective Use of Filamentary Composites in Flywheels," Proceedings 1975 Flywheel Technology Symposium, pages 146-150.

[6]Seireg, Ali, and Surana, K. S., "Optimum Design of Rotating Disks," Journal of Engineering for Industry, ASME, February 1970, pages 1-10.

[7]Toland, R. H., "Transfer Matrix Analysis of Composite Flywheels with Reliability Applications," Proceedings of the 1975 Flywheel Technology Symposium, November 10-12, 1975, Berkeley, California, Energy Research and Development Agency, ERDA 75-85. See also J. Composite Materials, Volume 10, July 1976, pages 258-260.

[8]Davis, D. E., "The USA-MEDRC High Energy Storage Homogeneous Flywheel Module," Proceedings of the 1975 Flywheel Technology Symposium, November 10-12, 1975, Berkeley, California, Energy Research and Development Agency, ERDA 76-85, pages 117-122.

THE VARIABLE INERTIA FLYWHEEL (VIF), AN INTRODUCTION TO ITS POTENTIAL

David G. Ullman
Department of Mechanical Engineering
Union College
Schenectady, N.Y. 12308

Henry R. Velkoff
Department of Mechanical Engineering
The Ohio State University
Columbus, Ohio 43210

ABSTRACT

Designs of flywheels which vary their inertia in an effort to reduce the transmission requirements of flywheel energy storage are presented. The physical laws which govern these Variable Inertia Flywheels (VIFs) regardless of configuration are explained and the implications of these laws stated with conclusions and recommendations for future work.

INTRODUCTION

Due to its very simplicity, the concept of storing energy in the rotating mass of a flywheel seems very attractive. A closer look, however, reveals subleties which significantly complicate the implementation of an operational system. Primary among these complicating factors is the difficulty of transferring the energy to and from the energy storage flywheel.

The governing energy storage relation for a flywheel is: energy stored $=\frac{1}{2}*$(moment of inertia)*(rotational rates squared). This states that in order to retrieve stored energy from a flywheel the rotational rate must decrease. This decrease in rotational rate is not desirable as systems being powered by flywheels require a rotational rate which is constant or even increasing. This mismatch in rotational rate is usually handled with the use of a variable ratio transmission such as a traction drive, a hydraulic pump and motor, or an electric generator and motor. Each of these systems have drawbacks either in terms of cost, reliability or, most importantly, efficiency. Specifically, the electric and hydraulic systems (the most technically developed systems) are inefficient and costly enough to possibly hamper the practical development of commercial systems.

If the equation for stored energy is reconsidered another approach to the problem becomes evident. It may be possible to alter the moment of inertia of the flywheel to gain added control of the release of stored energy.

The resulting mechanism is called a Variable Inertia Flywheel (VIF). This mechanism combines the duties of energy storage and load matching on one package.

In a program begun at the Ohio State University and continuing at Union College, the potential of the VIF is being studied. Previous work in the area and potential designs have been identified. The basic governing equations of motion have been developed and verified with a fully controllable proof-of-concept experimental model.[1]

In this paper the basic variable inertia flywheel configurations are itemized and comments on their potential offered. The laws of physics which describe the operation of VIFs regardless of configuration, are developed and discussed. This particular ordering is taken as it is easier to understand the physics with some configurations in mind. As the paper progresses various conclusions will be stated. These results and recommendations will be summarized at the end of the paper.

POTENTIAL VIF DESIGNS

The design of fixed inertia flywheels with a reasonable energy density is still the subject of much research. The design

of variable inertia flywheels will, by necessity, be more complex than that of a fixed inertia design. To enable the flywheel to vary inertia about its spin axis, the goemetry about that axis must be variable. This means moving parts on a high speed rotating body which is definitely a complicating factor. This will probably result in a VIF with lower energy storage capability than a comparable fixed inertia flywheel. However, the VIF with its combination of storage and transmission may be able to meet the requirements of a specific application better than a fixed inertia flywheel coupled to a separate transmission system. It is still too early to tell if competitive VIF systems are developable but, as will be shown there are many potential VIF configurations and one in particular which appears to have great potential.

In compiling a list of VIF configurations many were found in the U.S. patent literature,[2,3,4,5] one in the USSR patent[6] and periodical[7] literature, and others conceived by the authors. Basically the designs presented fall into two groups, fluid filled VIFs and mechanical geometry changing VIFs.

FLUID FILLED VIFs

Whenever the subject of varying the inertia of a rotating body is broached one idea always suggested is a fluid filled cylinder with the capability to pump the fluid in and out to alter the moment of inertia. References 2, 3, and 4 are all patents on variations of this concept. However, there are two major drawbacks to fluid filled VIFs. Any swirling of the fluid which will occur during radial rate variation results in an energy loss. The second drawback is left until the discussion of the equations of motion where it will be concluded that the fluid filled VIF will be no more efficient than a fixed inertia flywheel with a hydrostatic transmission.

MECHANICAL GEOMETRY CHANGING VIFs

Possibly the oldest VIF design is the James Watt type flyball governor. This apparatus, Figure 1, was originally designed as a constant speed control device where a variation from the desired speed caused an imbalance between a spring or counter-poise weight force and the centrifugal force on the flyweights. This imbalance was cancelled by a shift in the flyweights to a new equilibrium position thus actuating a control linkage correcting the throttle position of the governed prime mover. With a VIF the force of the spring or counter-poise weight would be replaced by an actuation force such that its variation resulted in an inertia change and a change in energy and/or rotational rate state. Obviously since swept area is small the energy density is low, however this configuration is relatively simple to build and actuate and thus was used as the basis for the two experimental apparatus built to date.[1]

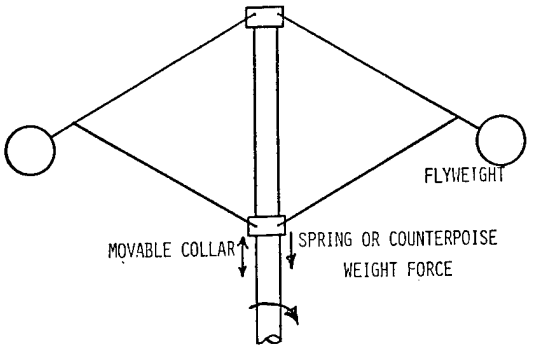


FIGURE 1
THE FLYBALL VIF

Four other mechanical geometry change VIFs are shown in Fig. 2.

Figure 2a shows a Bar Type Variable Inertia Flywheel design. This flywheel has as its inertia members bars pivoted on an axis normal to the axis of shaft rotation. These bars may be simple circular in cross section or of constant stress shape with tapering ends. The moment of inertia of the system is changed by pivoting the bars in a symetric manner to assure dynamic balance. Although the energy density for this type of configuration is not high, large variations in moment of inertia can be obtained.

Another potential type of variable inertia flywheel is shown in Figure 2b. This is called the Disk Type Variable Inertial Flywheel and is composed of a series of disks which pivot in a manner similar to that of the rods above. The disk design is capable of higher energy density than the rod design but does not afford as great a variation of moment of inertia. Not shown in the Figure multiple disks can be pivoted in such a way as to insure dynamic balance for the entire system.

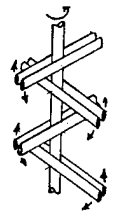


FIGURE 2a
BAR TYPE VIF

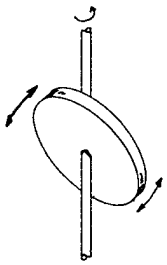


FIGURE 2b
DISK TYPE VIF

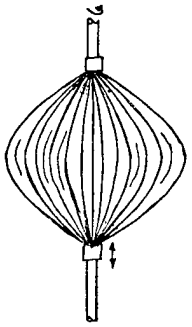


FIGURE 2c
ISOTENSOID TYPE VIF

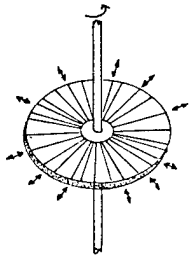


FIGURE 2d
BRUSH TYPE VIF

FIGURE 2
MECHANICAL GEOMETRY
CHANGE VIFs

In Figure 2c a flywheel is presented which is composed of elements attached to the shaft at their end points. The shape of the elements and their mass properties (cross section and material mass distribution) are designed to maximize the energy density and yet retain constant stress throughout the elements. The inertia of the flywheel is changed by moving the end points on the shaft. As can be seen, great variations in moment of inertia are available with this design making it suitable for application in a variable inertia flywheel system. There has been some work on fixed inertia flywheels of this type where the elements were filaments of constant size and designed for equal tension. This has been called an isotensoid design[8]. Thus, the Variable Inertia Flywheel design of similar properties will be hereafter referred to as the Isotensoid Type Variable Flywheel.

Lastly in figure 2d is a variable brush type Super Flywheel. In this design the radial filaments are drawn into the shaft to alter the moment of inertia. This design is effectively a two dimensional isotensoid design.

Probably the most interesting concept in the area of variable inertia flywheels has been subject of at least one United States patent,[5] two Soviet patents and at least two Soviet publications or articles[6,7]. This is the coiled band flywheel which is shown in Figure 3. This flywheel is composed of a hollow outer casing and a separate central hub. Connecting these is a band of some flexible material mounted as the mainspring in a watch. Centrifugal force pushes the band to the outer edge of the hollow casing. As the inner hub is rotated relative to the outer casing, the band is wound on the hub lowering the moment of inertia of the system. What is occurring is a balance between the centrifugal force on the band, the angular rate difference between the components and the torque flow through the mechanism supplemented by the torque given up (retained) by the change in angular momentum of the band.

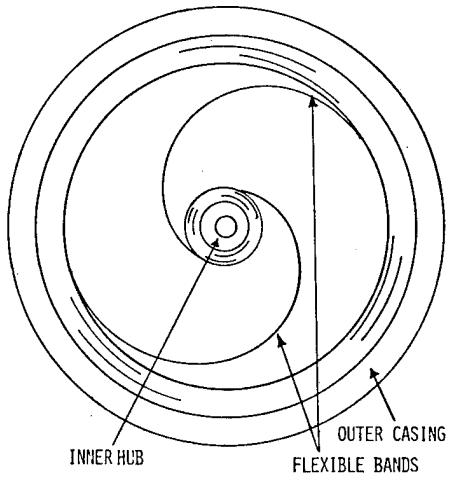


FIGURE 3
COILED BAND FLYWHEEL

The majority of the work on this type of flywheel has been done by N.V. Gulia of the Academy of Sciences of the Georgian Soviet Socialist Republic. In his work the flywheel is used as a passive device. Typically, the operation is as follows, the band begins in the stable position pressed against the outer casing. The hub is clutched to a shaft from which energy is to be absorbed (e.g. a car axle) and the band begins to wind onto the hub. The inertia of the band on the hub increases but, more importantly to Gulia, the centrifugal force on the band acts as a torque countering the rotation. Both of these effects tend to absorb energy from the shaft but, for Gulias passive device

the torque effect is dominant. As the shaft is slowed the rotational rate of the outer casing, accelerated by the reaction torque becomes greater than that of the shaft and the band starts reaccumulating in the outer casing. However, even as it is unwinding from the hub, the centrifugal force on the band is still supplying a decelerating torque to the shaft. This is a very interesting concept which is not actively being pursued in the free world. Actually there is a U.S. patent for the same mechanism awarded to O. Durouchoux of France in 1965. In this patent the basic band type flywheel is presented with many modifications. Each configuration still constitutes a passive device with the inertia change determined by the dynamics of the loading on the hub and the outer casing. In some configurations the casing and hub are geared together altering the characteristics of the flywheel, but nowhere in the literature is any form of active feedback control presented. No dynamic analysis of such a mechanism has been found in the open literature. The dynamic balance of torques, forces, and momentum is surely complex and understanding of the dynamics is required to fully understand the potential of the device.

It is also interesting to note that this concept is in complete concert with the anisotropic rim Super Flywheel. The band is loaded uniaxially and in the high energy configuration (the band centrifugally pressed in the casing) the band resembles the rim rotor. Also, as Durouchoux points out, the band may be designed with a high surface friction coefficient such that in the high energy configuration a majority of the hoop stress is carried by the band and, the casing need not be as substantial as might originally be thought.

THE PHYSICS OF THE VIF

Without regard to the exact configuration a set of general equations for the VIF can be derived. The original derivations[1] were made considering a point mass a distance from the spin axis. Here the results are presented in terms of the moment of inertia for ease of understanding. For a complete derivation of the equations see Reference 1.

Although the torque-angular acceleration characteristics of a flywheel are usually written in the common form of Newtons Law, $T = I\dot{\omega}$. For a VIF the conservation of momentum form is more applicable, namely

$$T = \frac{d}{dt}(I_f\omega_f) = I_f\dot{\omega}_f + \dot{I}_f\omega_f \qquad (1)$$

In this form a negative torque (energy out of the flywheel) can be developed even with an angular acceleration ($\dot{\omega}_f > 0$) simply by forcing a decrease in moment of inertia at a rate such that $|\dot{I}_f\omega_f| > I_f\dot{\omega}_f$. This is like the ice skater spinning on her toes losing energy to friction yet increasing her angular rate dramatically by bringing her arms to her sides.

There are two ways of modeling the VIF as a part of a system. First the VIF can be considered as an open loop device where the power for inertia variation, P_I, enters from some external source, Fig. 4a. Secondly, the VIF can be modeled as a power recirculation device where some of the power flowing from the VIF, P_F, is recirculated to change the inertia, P_I, and the remainder is output to the load P_L.

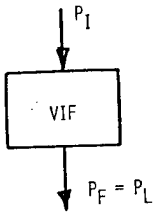


FIGURE 4a
OPEN LOOP VIF POWER FLOW

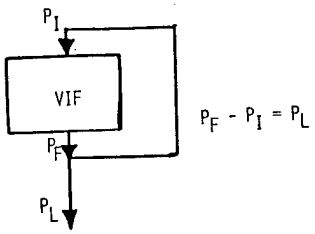


FIGURE 4b
RECIRCULATING VIF POWER FLOW

The concept of recirculating power is, by far the most appealing as then the VIF is truly a system with the only power flow in or out going to the load. As this case is readily reduceable to the open loop case the equations for power recirculating VIF will be presented.

Using conservation of angular momentum and energy laws the powers and associated torques are:

$$P_I = \tfrac{1}{2}\dot{I}_f\omega_f^2 \quad (2) \qquad T_I = \tfrac{1}{2}\dot{I}_f\omega_f \quad (3)$$

$$P_F = I_f\dot{\omega}_f\omega_f + \dot{I}_f\omega_f^2 \quad (4)$$

$$T_F = I_f\dot{\omega}_f + \omega_f\dot{I}_f \quad (1)$$

$$P_L = P_F - P_I = I_f\omega_f\dot{\omega}_f + \tfrac{1}{2}\dot{I}_f\omega_f =$$

$$\tfrac{1}{2}\frac{d}{dt}(\omega_f I_f) \quad (6)$$

$$T_L = T_F - T_I = I_f\dot{\omega}_f + \tfrac{1}{2}I_f\omega_f \quad (7)$$

Note that Eq. (1) is the torque produced by the VIF as discussed earlier.

The only assumption made in the derivation of these equations is that the acceleration associated with inertia change is small compared to the coriolis, centrifugal, and angular accelerations. This assumption is not at all restrictive as to violate it to any significant degree requires the energy content of VIF to change by a factor of 2 in less than .001 sec^1 which is not operationally reasonable. This assumption is also equivalent to saying that the Kinetic Energy stored in the motion of inertia change is small compared to that stored in the rotating mass. The result of this can be seen by indefinitely integrating eq. (6) to find the energy content of the VIF,

$$E_{VIF} \doteq \tfrac{1}{2}I_f\omega_f^2 \quad (8)$$

Here there is no term for the kinetic energy of inertia change as it has been assumed small.

The energy states of a VIF can be plotted as isoenergy lines on a plot of I_f versus ω_f as shown in Figure 5. In this figure the VIF is at a constant energy state at any point on an isoenergy line and a change in energy level to a new energy state can be obtained through an infinite combination of inertia and angular rate change determined by the angular rate and Power demand of the load. The trajectory of a constant inertia flywheel is shown on the figure and as can be seen an angular rate decrease is associated with an energy decrease.

Other energy change trajectories on Fig. 5 and the implications of the VIF describing equations can most easily be seen by considering some examples.

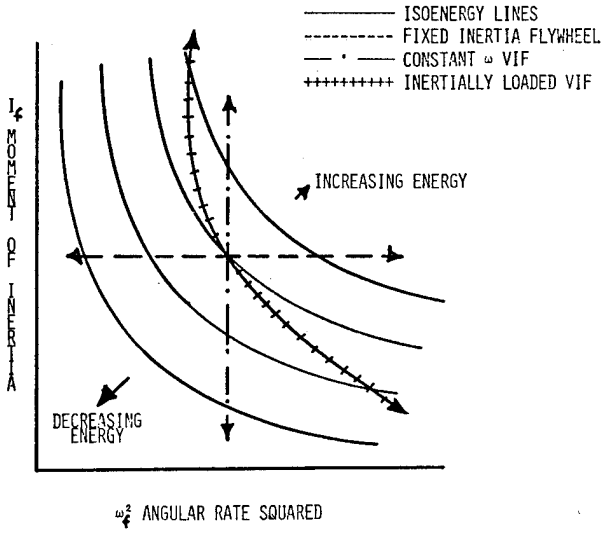


FIGURE 5
ISOENERGY LINES AND STATE
TRAJECTORIES FOR VARIOUS LOADINGS

THE VIF POWERING A CONSTANT ANGULAR RATE LOAD

One of the most interesting applications of the VIF is for a constant angular rate loading. This loading is essentially that of a vehicle cruising, an electric AC generator with a constant load or other constant friction loading. For this case Eq. (2), (4) and (6) reduce to

$$P_L = P_I = \tfrac{1}{2}P_F = \tfrac{1}{2}\dot{I}_f\omega_f^2 \quad (9)$$

Thus one half the power released by the flywheel must be recirculated to change the inertia. This is an extremely important conclusion and is totally independent of the physical design of the VIF. Further, from the torque relations, $T_L = \tfrac{1}{2}\dot{I}_f\omega_f^2$, the rate of inertia variation is uniquely prescribed as a function of the load torque and angular rate ($\omega_L = \omega_F$)[1]

$$\dot{I}_f = 2T_L/\omega_L^2 \quad (10)$$

The trajetory of the state of the VIF is shown on Fig. 5 where the rate of energy change is directly dependent on the values of T_L and ω_L relative to the energy stored in the VIF.

In light of this conclusion above the fluid filled VIFs must, for inertia variations, convert from mechanical power to fluid power the same amount of power as is supplied to the load. In this case

the inefficiency incurred is the same as if the pump were in the ouput link of fixed inertia flywheel. This along with the swirling loses mentioned previously makes the fluid filled VIF appear no more efficient than the system it is trying to replace.

THE VIF POWERING AN INERTIAL LOAD

If the loading is essentially inertial such as a vehicle accelerating at low speed, there is prescribed inertia variation required for the VIF which is different than that for constant angular rate. Consider a VIF powering a purely inertial load, I_L through a transmission of ratio R. At some time zero the inertia of flywheel and its angular rate are assumed as I_{Fo} and ω_{Fo} then the required inertia of the VIF is given by[1]

$$I_f = R^2[(\frac{\omega_{fo}}{\omega_L})^2(I_{fo} + R^2 I_L) - I_L] \quad (11)$$

Thus the moment of inertia is a direct function of the angular rate of the load. Thus if the angular rate history or acceleration history desired for a given inertial load was specified the flywheel inertia is uniquely specified. For example, let $I_{fo} = R^2 I_L$ then the trajectory is as shown in Fig. 5.

The amount of power required for inertia change in this case is not as simple as for constant angular rate. It is in fact dependent on the rate of acceleration desired for the load inertia. Although no direct relation between the power to the load and that causing inertia change is possible it can be seen from Eq. (6) that unless $\dot{\omega}_f$ is excessive P_I and P_L will be of the same order of magnitude.

LIMITATIONS OF THE VIF

As can be seen in the previous two examples the dependence of the inertia level and rate of change varies with the characteristics of load. Thus it would be most desireable to have the recirculating power flow to the inertia change, P_I, be completely controllable to allow for differing inertia change requirements. Unfortunately, complete controllability of the recirculating power, P_I, can only be had with a variable ratio transmission such as that which the VIF is proposed to eliminate. Also, it was shown that with constant rotational rate loading, the amount of power to be recirculated through the variable ratio transmission would be the same as that ouput. Thus it appears that the VIF in this configuration could have no better efficiency than a fixed inertia flywheel with the variable ratio transmission on the output shaft.

However, complete control of the recirculating power is not required for most tasks as the nature of the loading is usually reasonably well known and slight deviations from the desired are usually tolerated, thus it is possible to create a fixed power recirculation path to meet the requirements of a specific load. By using the term, "fixed power recirculation", it is implied that the mechanism carrying power P_I to create the inertia change is of fixed geometry, or at a maximum, a countably few variations of geometry. The result of this VIF with a fixed path, is a flywheel with fixed properties which differ from those of a standard fixed inertia flywheel. Another way of stating this is that now $I_f = I_f(\omega_f)$ so that the torque in eq. (1) is now totally a function of angular rate but a vastly different function than that of a standard fixed inertia flywheel. A simplistic example of such a VIF with fixed ratio power recirculation is shown in figure 6. This is a band type VIF with the inner and outer casings connected through an epicyclic gear set. In this example the exact paths of P_F and P_I are not distinct but the power recirculation loop is defined by the epicyclic gear ratio and the band/casing geometry.

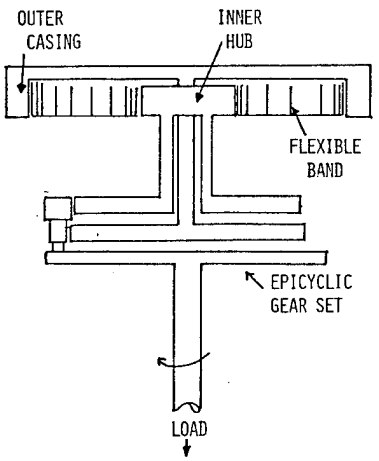


FIGURE 6

FIXED RATIO POWER RECIRCULATION VIF

CONCLUSIONS AND RECOMMENDATIONS

The primary conclusions to be drawn from this paper are as follows:

1. There are many potential VIF designs which may be suitable for differing tasks. Virtually no studies have been done on any of the designs presented to aid in determining their potential. Some seemingly inefficient designs may have potential in specific applications.

2. The band type VIF appears to have great potential as an energy intensive VIF. Work is presently under way to fully describe the dynamics of this configuration.

3. Based on the findings of this paper, fluid filled VIFs appear to have little useful potential.

4. The power required for inertia change is equal to the output power for a constant rotational rate VIF. For other loadings the power required for inertia change is the same order of magnitude as the output power.

5. A fully controllable VIF, full control over the moment of inertia irrespective of the VIF state, is not practical as the efficiency obtained can be no better than a fixed inertia flywheel with an infinitely variable ratio transmission.

6. A VIF with a fixed power recirculation results in a flywheel with a unique torque/angular rate characteristics. Whereas a fixed inertia flywheel is restricted to $T_f = I\dot{\omega}_f$ a VIF can theoretically be formed such that the torque is related to any function of angular rate. Limitations on this concept are being studied in conjunction with the analysis of the band type VIF described in item 2 above. Specifically the configuration in Fig. (6) is being pursued as a first step.

7. Based on the analysis to date the VIF concept is not the answer to all our prayers. It is however, a concept which may have a competitive potential in some applications. It does, at a minimum, deserve continued study to more fully establish its potential.

REFERENCES

1. Ullman, D.G., "A Preliminary Analytical and Experimental Investigation of Variable Inertia Kinetic Energy Storage Flywheels", to be published as a Dissertation at the Ohio State University, 1977.

2. Meyer, F.W., U.S. Patent #2,404,515, 1951.

3. Lewis, O.G., U.S. Patent #3,248,967, 1966.

4. Sohon, H., U.S. Patent #2,603,103, 1952.

5. Durouchoux, O., U.S. Patent #3,208,303, 1965.

6. Gulia, N.V., USSR Patent #1182724/24-27, 1969.

7. Gulia, N.V., "A Coiled Band Mechanism for the Recovery of a Vehicle's Mechanical Energy", Journal of Mechanisms, Vol. 3, pp. 113, 1968.

8. Adams, L.R., "Application of Isotensoid Flywheels to Spacecraft Energy and Angular Momentum Storage," NASA CR-1971, Feb., 1972.

DESIGN SYNTHESIS AS APPLIED TO COMPOSITE FLYWHEELS

Milton Vagins
Battelle-Northwest Laboratories
P. O. Box 999
Richland, Washington 99352

ABSTRACT

This paper treats with the problem of design synthesis in heterogeneous elasticity, particularly as applied to flywheel design. Design synthesis is defined as the achievement of a desired design criterion, in this case, constant circumferential stress, in a flywheel by preselecting a stress pattern in the loaded flywheel and then determining the variation of the elastic moduli that is required to permit the desired effects. This accomplishment requires the solution of the governing equations of elasticity, particularly the compatibility equation, in terms of preselected and hence known stress fields in the body of the flywheel for the unknown material properties which are spatial functions.

INTRODUCTION

Using presently available design methodology, flywheels are constructed of any number of different materials and in a great variety of shapes. It is quite apparent that once the material, geometry and operating conditions for a flywheel are specified, then the stress condition in that flywheel is predetermined. All the analyst does is find the predetermined stress field and decide if the stresses are acceptable. If it is found that the stresses are unacceptable, then a change in either the material, geometry and/or the operating conditions is needed, followed by reanalysis and so on to the next iteration. When one considers that for many applications, and in particular, flywheel design, the optimum geometry and stress fields are known in general, it becomes clear that the standard design methods are really not a satisfactory way of doing things.

Composites, whether filamentary, fibrous, or sintered or fused metallics, are capable of being tailored to meet specific requirements. When considering specific structural applications for such materials, it would be logical to assume that a structure (such as a flywheel) could be optimized by varying the mechanical properties of the material throughout the structure. Furthermore, it would be logical to bypass analysis completely and define this now homogeneous structure by means of design synthesis. This paper deals with the mathematical development of the concept of design synthesis as applied to flywheel design. In essence, it deals with the solution of the plane elasticity compatibility equations in terms of known stresses and unknown, spatial dependent, material properties. An in-depth, mathematical treatment of this subject is shown in the appendix.

ROTATING ANNULAR DISK

Consider the rotating, uniform thickness annular disk as shown in Fig. 1. The equilibrium equation governing this case is:

$$\frac{d}{dr}(r\sigma_r) - \sigma_\theta + \frac{\gamma}{g}\omega^2 r^2 = 0 \ . \qquad (1)$$

The compatibility equation reduces to:

$$\frac{d}{dr}(r\epsilon_\theta) - \epsilon_r = 0 \ , \qquad (2)$$

and the stress-strain relation for an orthotropic medium is:

$$\epsilon_r = a_{11}\sigma_r + a_{12}\sigma_\theta$$
$$\epsilon_\theta = a_{12}\sigma_r + a_{22}\sigma_\theta \qquad (3)$$

where a_{11}, a_{12}, and a_{22} are functions of r. Assuming a stress function such that

$$\sigma_r = \frac{1}{r}\Psi$$
$$\sigma_\theta = \Psi' + \frac{\gamma}{g}\omega^2 r^2 . \tag{4}$$

It is possible that the material density, γ, could be a function of the radius. At this stage, such a condition introduces an unnecessary complication and will not be considered. This being the case, the governing compatibility equation becomes:

$$\Psi''(a_{22}) + \Psi'(a'_{22} + \frac{1}{r}a_{22}) + \Psi\left(\frac{a'_{12}}{r} - \frac{a_{11}}{r^2}\right) + \frac{\gamma}{g}\omega^2 r^2\left(a'_{22} + 3\frac{a_{22}}{r} - \frac{a_{12}}{r}\right) = 0 . \tag{5}$$

Assume that there exists a simple ratio relationship between the various orthotropic moduli and their first derivatives, as follows:

$$a_{22} = a_{22},\ a'_{22} = a'_{22}$$
$$a_{11} = k_1 a_{22},\ a'_{11} = k_1 a'_{22} \tag{6}$$
$$a_{12} = k_2 a_{22},\ a'_{12} = k_2 a'_{12}$$

where the prime mark indicates differentiation with respect to r. Eq. (5) becomes:

$$0 = a'_{22}\left[\Psi' + \frac{k_2}{r}\Psi + \frac{\gamma}{g}\omega^2 r^2\right] + a_{22}\left[\Psi'' + \frac{\Psi'}{r} - \frac{k_1\Psi}{r^2} + \frac{\gamma}{g}\omega^2 r(3-k_2)\right] \tag{7}$$

If we now choose that the hoop stress, σ_θ, be constant and that the boundary conditions on the disk are that the radial stresses on the inner and outer peripheries are zero, i.e., $\sigma_r(a) = \sigma_r(b) = 0$, the stress function and associated stresses become:

$$\Psi = \frac{\gamma v^2}{3g}\left(\frac{k}{k-1}\right)\left[r\left(1 - \frac{1}{k^3}\right) - a\left(1 - \frac{1}{k^2}\right) - \left(\frac{r}{b}\right)^3\left(b - a\right)\right] \tag{8}$$

$$\sigma_r = \frac{\gamma v^2}{3g}\left(\frac{k}{k-1}\right)\left[1 - \frac{1}{k^3} - \frac{1}{\rho k} + \frac{1}{\rho k^3} - \rho^2 + \frac{\rho^2}{k}\right]$$

$$\sigma_\theta = \frac{\gamma v^2}{3g}\left(\frac{k}{k-1}\right)\left[\frac{k^3 - 1}{k^3}\right]$$

where $\rho = r/b$
$k = b/a$
$v = \omega b$ = tip velocity
ω = rotational velocity, radians
g = acceleration of gravity.

Here we note that in the limits, when $k \to 1$

$$\sigma_\theta = \frac{\gamma v^2}{g} \tag{9}$$

which is the stress in a rotating thin ring, and when $k \to \infty$ (i.e., when a very small)

$$\sigma_\theta = \frac{\gamma v^2}{3g} , \tag{10}$$

which is smaller than exists for the isotropic, homogeneous case by the ratio

$$\frac{\sigma_{\theta_1}}{\sigma_{\theta_o}}_{\max} = \left(\frac{4}{3(3+\nu)}\right) \tag{11}$$

where σ_{θ_1} = hoop stress for heterogeneous case
σ_{θ_o} = hoop stress for isotropic, homogeneous case
ν = Poisson's ratio for isotropic, homogeneous case.

Substituting Eq. (8) into Eq. (7) and carrying out the required differentiation yields

$$a'_{22} - \left[\frac{Ar^3 + Br + D}{Fr^4 + Gr^2 + Hr}\right] a_{22} = 0 \tag{12}$$

where $A = (k_1 - 3k_2)$

$$B = (1 - k_1)\ \frac{b^3 - a^3}{b - a}$$

$$D = k_1(ab)(b+a)$$

$$F = k_2$$

$$G = -(1+k_2)\ \frac{b^3-a^3}{b-a}$$

$$H = k_2(ab)(b+a).$$

A digital computer program, Determination Of Modulus Variation 1 (DOMOV1), was structured for the solution of these sets of equations. A finite difference method of solution as developed by Manson[1] was used for the calculation algorithm. This program was used to solve several problems, as follows:

1. The modulus variation for an orthotropic disk with a pressurized ID for σ_θ = constant (disk not rotating).
2. The modulus variation for an isotropic disk with pressurized ID for σ_θ = constant (disk not rotating).
3. The modulus variation for an isotropic disk with pressurized OD for σ_θ = constant (disk not rotating).
4. The modulus variation for a rotating orthotropic disk with no edge loads for σ_θ = constant.
5. The modulus variation for a rotating orthotropic disk (Poisson's ratio variable) with no edge loads for σ_θ = constant.
6. The modulus variation for a rotating orthotropic disk with no edge load for constant in-plane shear stress.
7. The modulus variation for a rotating orthortopic disk (Poisson's ratio variable) with no edge loads for constant in-plane shear stress.
8. The modulus variation for a rotating orthotropic disk with 60.0 in. OD, 6.0 in. ID, turning at 2000 RPM, stressed on the OD with a uniform edge load of 10,000 psi for σ_θ = constant.
9. The modulus variation for a rotating orthotropic disk with 60.0 in. OD, 6.0 in. ID, turning at 4000 RPM, stressed on the OD with a uniform edge load of 12,000 psi for σ_θ = constant.

For the purposes of this paper, only the results of problem number 6, arising from Eq. (12) will be shown in Fig. 2 and 3.

These figures have been nondimensionalized by the expediency of plotting E/E_{max} and R/B where:

$E = E_\theta$, the modulus of elasticity in the θ direction.

E_{max} = the maximum E_θ calculated in the body of the disk.

R = the radius of the point in the disk at which the modulus is being calculated.

B = the outer radius of the disk.

K_1 = orthotropic ratio $\left(=\frac{E_\theta}{E_r}\right)$

Figure 2 clearly defines the variation of the moduli in the flat disk flywheel as a function of the radius. Note that the variation is independent of the angular velocity of the flywheel and is fully determined by the requirement that σ_θ be constant throughout the disk. For example, compare two annular flywheels, both turning at an angular velocity of 4000 RPM. Each disk has an outer diameter of 60.0 in. and an inner diameter of 6.0 in. Each disk is made of a material with a uniform density of 0.1 lb/in.^{3}. One disk's material is isotropic and the other has its material properties varied as shown by the curve in Fig. 2 with an orthotropic ratio of 2.5 and a Poisson's ratio of 0.5. The maximum hoop stress for the isotropic flywheel occurs only at the inner radius and equals:

$$\sigma_{\theta_{max}} = \frac{3+\nu}{4}\ \frac{\gamma}{g}\ b^2\omega^2\left(1+\frac{1-\nu}{3+\nu}\ \frac{a^2}{b^2}\right) \qquad (13)$$

$$= 35{,}800 \text{ psi.}$$

The hoop stress for the heterogeneous flywheel, which is uniform throughout the disk is:

$$\sigma_\theta = \frac{\gamma}{3g}\ b^2\omega^2\left(\frac{k}{k-1}\right)\left[\frac{k^3 - 1}{k^3}\right] \qquad (14)$$

$$= 15{,}121 \text{ psi.}$$

Thus, by use of design synthesis, the maximum stress in such a disk or flywheel can be reduced by a factor of 2.36 as compared to an isotropic disk of similar density. Further, Fig. 3 shows that this reduction can be achieved with a modulus

variation through the disk of approximately 1.8 from low to high value.

APPENDIX

TWO-DIMENSIONAL MATHEMATICAL FOUNDATION

Consider the following question: Given a plane elastic body with known boundary tractions and/or displacements, can the mechanical properties of the continuum be described such that an "arbitrary" stress distribution within the body is met?

The term "arbitrary" is to be understood as defining a family of stress distributions that are preselected but still conform to equilibrium requirements and boundary conditions. To answer this question, we start by making the following two basic assumptions:

(1) The classical equations of linear elasticity are valid in this application, and (2) the mechanical properties of the continuum can be expressed as spatial functions.

Following from these assumptions, the well known governing relations of generalized plane stress, given in rectangular coordinates are as follows:

Equilibrium Equations

$$\frac{\partial \sigma_x}{\partial x} + \frac{\partial \sigma_{xy}}{\partial y} + X = 0$$

$$\frac{\partial \sigma_{xy}}{\partial x} + \frac{\partial \sigma_y}{\partial y} + Y = 0 \ , \tag{A-1}$$

Strain-Displacement Equations

$$\epsilon_x = \frac{\partial u}{\partial x} \ , \ \epsilon_y = \frac{\partial v}{\partial y} \ , \tag{A-2}$$

$$\epsilon_{xy} = \frac{\partial v}{\partial x} + \frac{\partial u}{\partial y} \ ,$$

Compatibility Equation

$$\frac{\partial^2 \epsilon_x}{\partial y^2} + \frac{\partial^2 \epsilon_y}{\partial x^2} = \frac{\partial^2 \epsilon_{xy}}{\partial x \partial y} \ . \tag{A-3}$$

Assuming that the continuum exhibits orthotropic material properties and neglecting time and strain rate effects, the constitutive equations can be expressed as generalized Hooke's Law as:

$$\begin{Bmatrix} \epsilon_x \\ \epsilon_y \\ \epsilon_{xy} \end{Bmatrix} = \begin{bmatrix} a_{11} & a_{12} & 0 \\ a_{21} & a_{22} & 0 \\ 0 & 0 & a_{66} \end{bmatrix} \begin{Bmatrix} \sigma_x \\ \sigma_y \\ \sigma_{xy} \end{Bmatrix} + \begin{Bmatrix} \alpha_1 T \\ \alpha_2 T \\ 0 \end{Bmatrix} \tag{A-4}$$

where α_1 and α_2 are the coefficients of thermal expansion and T represents the temperature difference distribution.

Substituting Eq. (A-4) into (A-3), assuming that the a_{ij}'s are spatially dependent and carrying out the required differentiation yields, Eq. (A-5) as shown at:

$$\left\{a_{12}\frac{\partial^2\sigma_y}{\partial y^2} + a_{66}\frac{\partial^2\sigma_{xy}}{\partial x\partial y} + a_{11}\frac{\partial^2\sigma_x}{\partial y^2} + a_{21}\frac{\partial^2\sigma_x}{\partial x^2} + a_{22}\frac{\partial^2\sigma_y}{\partial x^2}\right.$$

$$\left. + \frac{\partial^2}{\partial y^2}(\alpha_1 T) + \frac{\partial^2}{\partial x^2}(\alpha_2 T)\right\}$$

$$+ \left\{\frac{\partial^2 a_{11}}{\partial y^2}\sigma_x + \frac{\partial^2 a_{12}}{\partial y^2}\sigma_y + \frac{\partial^2 a_{21}}{\partial x^2}\sigma_x + \frac{\partial^2 a_{22}}{\partial x^2}\sigma_y\right.$$

$$+ \frac{\partial^2 a_{66}}{\partial x\partial y}\sigma_{xy} + 2\frac{\partial^2 a_{11}}{\partial y}\cdot\frac{\partial\sigma_x}{\partial y} + 2\frac{\partial a_{12}}{\partial y}\cdot\frac{\partial\sigma_y}{\partial y} + 2\frac{\partial a_{21}}{\partial x}\cdot\frac{\partial\sigma_x}{\partial x}$$

$$\left. + \frac{\partial a_{22}}{\partial x}\cdot\frac{\partial\sigma_y}{\partial x} + \frac{\partial a_{66}}{\partial x}\cdot\frac{\partial\sigma_{xy}}{\partial y} + \frac{\partial a_{66}}{\partial y}\cdot\frac{\partial\sigma_{xy}}{\partial x}\right\} = 0 . \qquad \text{(A-5)}$$

Assume that the body forces have a potential, V, such that:

$$X = -\frac{\partial V}{\partial x} \qquad \text{(A-6)}$$

$$Y = -\frac{\partial V}{\partial y} ,$$

and choose Airy's stress function, Ψ, in the form:

$$\sigma_x = \frac{\partial^2\Psi}{\partial y^2} + V \qquad \text{(A-7)}$$

$$\sigma_y = \frac{\partial^2\Psi}{\partial x^2} + V$$

$$\sigma_{xy} = -\frac{\partial^2\Psi}{\partial x\partial y} .$$

Making the appropriate substitutions into Eq. (A-6) yields:

$$\left\{a_{22}\frac{\partial^4\Psi}{\partial x^4} + (a_{21} + a_{12} - a_{66})\frac{\partial^4\Psi}{\partial x^2\partial y^2} + a_{11}\frac{\partial^4\Psi}{\partial y^4}\right. \qquad \text{(A-8)}$$

$$\left. + (a_{11} + a_{12})\frac{\partial^2 V}{\partial y^2} + (a_{22} + a_{21})\frac{\partial^2 V}{\partial x^2} + \frac{\partial^2}{\partial y^2}(\alpha_1 T) + \frac{\partial^2}{\partial x^2}(\alpha_2 T)\right\}$$

$$+\left\{\left(\frac{\partial^2 a_{11}}{\partial y^2}+\frac{\partial^2 a_{21}}{\partial x^2}\right)\cdot\frac{\partial^2\psi}{\partial y^2}+\left(\frac{\partial^2 a_{12}}{\partial y^2}+\frac{\partial^2 a_{22}}{\partial x^2}\right)\cdot\frac{\partial^2\psi}{\partial x^2}\right.$$

$$-\frac{\partial^2 a_{66}}{\partial x\partial y}\cdot\frac{\partial^2\psi}{\partial x\partial y}+\frac{\partial^2}{\partial x^2}(a_{22}+a_{21})\cdot V+\frac{\partial^2}{\partial y^2}(a_{11}+a_{12})\cdot V$$

$$+\frac{\partial}{\partial y}(2a_{12}-a_{66})\cdot\frac{\partial^3\psi}{\partial x^2\partial y}+\frac{\partial}{\partial x}(2a_{21}-a_{66})\cdot\frac{\partial^3\psi}{\partial x\partial y^2}+2\frac{\partial a_{11}}{\partial y}\cdot\frac{\partial^3\psi}{\partial y^3}$$

$$\left.+2\frac{\partial a_{22}}{\partial x}\cdot\frac{\partial^3\psi}{\partial x^3}+\frac{\partial}{\partial y}(2a_{11}+2a_{12})\cdot\frac{\partial V}{\partial y}+\frac{\partial}{\partial x}(2a_{21}+2a_{22})\cdot\frac{\partial V}{\partial x}\right\}=0$$

and, of course, the equilibrium equations are met exactly.

Equation (A-8) can also be expressed in polar coordinates as follows:

(A-9)

$$\left\{\left[a_{22}\frac{\partial^4\psi}{\partial r^4}+2\frac{a_{22}}{r}\frac{\partial^3\psi}{\partial r^3}-\frac{a_{11}}{r^2}\frac{\partial^2\psi}{\partial r^2}+\frac{a_{11}}{r^3}\frac{\partial\psi}{\partial r}+\frac{a_{11}}{r^4}\frac{\partial^4\psi}{\partial\theta^4}\right.\right.$$

$$-\left(\frac{2a_{12}+a_{66}}{r^3}\right)\cdot\frac{\partial^3\psi}{\partial r\partial\theta^2}+\left(\frac{2a_{12}+a_{66}}{r^2}\right)\cdot\frac{\partial^4\psi}{\partial r^2\partial\theta^2}$$

$$\left.+\left(\frac{2a_{11}+2a_{12}+a_{66}}{r^4}\right)\frac{\partial^2\psi}{\partial\theta^2}\right]$$

$$+\left[a_{21}\frac{\partial^2}{\partial r^2}+\left(\frac{2a_{21}-a_{11}}{r}\right)\frac{\partial}{\partial r}+\frac{a_{11}}{r^2}\frac{\partial^2}{\partial\theta^2}\right](V_r)$$

$$+\left[a_{22}\frac{\partial^2}{\partial r^2}+\left(\frac{2a_{22}-a_{12}}{r}\right)\frac{\partial}{\partial r}+\frac{a_{12}}{r^2}\frac{\partial^2}{\partial\theta^2}\right](V_\theta)$$

$$\left.+\left[\frac{\partial^2}{\partial r^2}+\frac{2}{r}\frac{\partial}{\partial r}\right](\alpha_\theta T)+\left[\frac{1}{r^2}\frac{\partial^2}{\partial\theta^2}-\frac{1}{r}\frac{\partial}{\partial r}\right](\alpha_r T)\right\}$$

$$+\left\{\frac{\partial a_{12}}{\partial r}\cdot\left[\frac{1}{r}\frac{\partial^2\psi}{\partial r^2}+\frac{2}{r^2}\frac{\partial^3\psi}{\partial r\partial\theta^2}-\frac{2}{r^3}\frac{\partial^2\psi}{\partial\theta^2}+\frac{2\partial V_r}{\partial r}+\frac{2V_r-V_\theta}{r}\right]\right.$$

$$+\frac{\partial a_{12}}{\partial\theta}\left[\frac{2}{r^2}\frac{\partial^3\psi}{\partial r^2\partial\theta}+\frac{2}{r^3}\frac{\partial V_\theta}{\partial\theta}\right]+\frac{\partial a_{22}}{\partial r}\left[2\frac{\partial^3\psi}{\partial r^3}+\frac{2}{r}\frac{\partial^2\psi}{\partial r^2}+2\frac{\partial V_\theta}{\partial r}+\frac{2V_\theta}{r}\right]$$

$$\left.-\frac{\partial a_{11}}{\partial r}\left[\frac{1}{r^3}\frac{\partial^2\psi}{\partial\theta^2}+\frac{1}{r^2}\frac{\partial\psi}{\partial r}+\frac{Vr}{r}\right]+\frac{\partial a_{11}}{\partial\theta}\left[\frac{2}{r^4}\frac{\partial^3\psi}{\partial\theta^3}+\frac{2}{r^3}\frac{\partial^2\psi}{\partial r\partial\theta}+\frac{2}{r^2}\frac{\partial V_r}{\partial\theta}\right]\right.$$

$$- \frac{\partial a_{66}}{\partial r}\left[\frac{1}{r^3}\frac{\partial^2\Psi}{\partial\theta^2} - \frac{1}{r^2}\frac{\partial^3\Psi}{\partial r\partial\theta^2}\right] + \frac{\partial a_{66}}{\partial\theta}\left[\frac{1}{r^4}\frac{\partial\Psi}{\partial\theta} - \frac{1}{r^3}\frac{\partial^2\Psi}{\partial r\partial\theta} + \frac{1}{r^2}\frac{\partial^3\Psi}{\partial r^2\partial\theta}\right]$$

$$+ \frac{\partial^2 a_{12}}{\partial r^2}\left[\frac{1}{r^2}\frac{\partial^2\Psi}{\partial\theta^2} + \frac{1}{r}\frac{\partial\Psi}{\partial r} + V_r\right] + \frac{\partial^2 a_{12}}{\partial\theta^2}\left[\frac{1}{r^2}\frac{\partial^2\Psi}{\partial r^2} + \frac{1}{r}V_\theta\right]$$

$$+ \frac{\partial^2 a_{22}}{\partial r^2}\left[\frac{\partial^2\Psi}{\partial r^2} + V_\theta\right] + \frac{\partial^2 a_{11}}{\partial\theta^2}\left[\frac{1}{r^4}\frac{\partial^2\Psi}{\partial\theta^2} + \frac{1}{r^3}\frac{\partial\Psi}{\partial r} + \frac{1}{r^2}V_r\right]$$

$$+ \frac{\partial^2 a_{66}}{\partial r\partial\theta}\left[\frac{1}{r^2}\frac{\partial^2\Psi}{\partial r\partial\theta} - \frac{1}{r^3}\frac{\partial\Psi}{\partial\theta}\right]\Bigg\} = 0$$

with Ψ being the stress function defined by:

$$\sigma_r = \frac{1}{r}\frac{\partial\Psi}{\partial r} + \frac{1}{r^2}\frac{\partial^2\Psi}{\partial\theta^2} + V_r \qquad \text{(A-10)}$$

$$\sigma_\theta = \frac{\partial^2\Psi}{\partial r^2} + V_\theta$$

$$\sigma_{r\theta} = -\frac{\partial}{\partial r}\left(\frac{1}{r}\frac{\partial\Psi}{\partial\theta}\right) .$$

Equation (A-10) satisfies the equilibrium equations formulated in polar coordinates for plane stress, which are:

$$\frac{\partial\sigma_r}{\partial r} + \frac{1}{r}\frac{\partial\sigma_{r\theta}}{\partial\theta} + \frac{\sigma_r - \sigma_\theta}{r} + R = 0 \qquad \text{(A-11)}$$

$$\frac{\partial\sigma_{r\theta}}{\partial r} + \frac{1}{r}\frac{\partial\sigma_\theta}{\partial\theta} + 2\frac{\sigma_{r\theta}}{r} + \Theta = 0 .$$

In order for Eq. (A-10) to meet Eq. (A-11) exactly, the body functions V_r and V_θ must be defined as:

$$V_\theta - \frac{\partial}{\partial r}(rV_r) = R \qquad \text{(A-12)}$$

$$-\frac{\partial V_\theta}{\partial\theta} = \Theta ,$$

thus putting a rather narrow interpretation on the body forces.

In the classical approach to the problem of orthotropic plane elasticity, the coefficients a_{ij} are either constants, as in the case of the homogeneous condition, or as in some rare cases, are special functions of position. In the first case, all the terms within the second set of large braces, {}, in Eq. (A-8) and (A-9) are zero leaving the remainder of these two equations in the form of the well-known, homogeneous, orthotropic, compatibility equations in terms of the stress function Ψ. In the second case, all the partial derivatives of the a_{ij}'s which appear in these second sets of braces are capable of being evaluated, resulting in extremely complicated fourth order partial differential equations with variable coefficients. Proceeding along classical lines, these equations must be solved for Ψ, which contains arbitrary constants of integration. These constants are then determined by evaluating Ψ in terms of the stresses on the boundaries.

Suppose it is assumed that the material coefficients, the a_{ij}'s, are unknown but that the stress function Ψ is a fully defined function of the spatial coordinates. That is, the stresses throughout the body as well as on the boundary are known. In such a case, Eq. (A-8) and (A-9) reduce to second order partial differential equations with variable coefficients, in terms of the a_{ij}'s. The solution of these equations and the resultant determination of the magnitude and distribution of the material properties throughout the body is defined in this work as <u>design synthesis</u>.

Bert[2] derived an equation similar to Eq. (A-9) wherein he reduced the unknown material property coefficients from four to one. His formulation is as follows:

$$
\begin{aligned}
&S\left[\frac{\partial^4\Psi}{\partial r^4}+\frac{2}{r}\frac{\partial^3\Psi}{\partial r^3}-\frac{e}{r^2}\frac{\partial^2\Psi}{\partial r^2}+\frac{e}{r^3}\frac{\partial\Psi}{\partial r}+\frac{2(c-\nu)}{r^2}\frac{\partial^4\Psi}{\partial r^2\partial\theta^2}\right. \\
&\left.-\frac{2(c-\nu)}{r^3}\frac{\partial^3\Psi}{\partial r\partial\theta^2}+\frac{2(c-\nu+e)}{r^4}\frac{\partial^2\Psi}{\partial\theta^2}+\frac{e}{r^4}\frac{\partial^4\Psi}{\partial\theta^4}\right] \\
&+\frac{dS}{dr}\left[2\frac{\partial^3\Psi}{\partial r^3}+\frac{2-\nu}{r}\frac{\partial^2\Psi}{\partial r^2}-\frac{e}{r^2}\frac{\partial\Psi}{\partial r}+\frac{2(c-\nu)}{r^2}\frac{\partial^3\Psi}{\partial r\partial\theta^2}\right. \\
&\left.-\frac{2(c-\nu)+e}{r^3}\frac{\partial^2\Psi}{\partial\theta^2}\right]+\frac{d^2S}{dr^2}\left[\frac{\partial^2\Psi}{\partial r^2}-\frac{\nu}{r}\frac{\partial\Psi}{\partial r}-\frac{\nu}{r^2}\frac{\partial^2\Psi}{\partial\theta^2}\right] \\
&-\left[\nu\frac{\partial^2}{\partial r^2}-\frac{e-2\nu}{r}\frac{\partial}{\partial r}-\frac{e}{r^2}\frac{\partial^2}{\partial\theta^2}\right]\left(SV_r\right) \\
&+\left[\frac{\partial^2}{\partial r^2}+\frac{2+\nu}{r}\frac{\partial}{\partial r}-\frac{\nu}{r^2}\frac{\partial^2}{\partial\theta^2}\right]\left(SV_\theta\right)=0\ ,
\end{aligned}
\tag{A-13}
$$

with the thermal terms omitted. Equation (A-13) is equal to Eq. (A-9) with the following identities:

$$
\begin{aligned}
S &\equiv a_{22} \\
e &\equiv a_{11}/a_{22} \\
c &\equiv a_{66}/2a_{22} \\
\nu &\equiv -a_{12}/a_{22}
\end{aligned}
\tag{A-14}
$$

with S being the dependent variable and e, c, and ν being fixed ratios. It is anticipated that most real composite materials will exhibit material property characteristics as defined by Eq. (A-14).

The solution of equations such as (A-8) and (A-9) where there are four or more dependent a_{ij}'s, even where these a_{ij}'s are assumed independent of temperature, is quite difficult but certainly not impossible. The simplifying assumption made in Eq. (A-14) leading to the formulation of Eq. (A-13) reduces the problem to only one unknown parameter.

REFERENCES

1. Manson, S. S., "Determination of Elastic Stresses in Gas-Turbine Disks," NACA Technical Report No. 871, Flight Propulsion Research Laboratory, National Advisory Committee for Aeronautics, Cleveland, OH, February 27, 1947.

2. Bert, C. W., "Analysis of Nonhomogeneous Polar-Orthotropic Circular Plates of Varying Thickness," Bulletin No. 190, Engineering Experiment Station, College of Engineering, The Ohio State University, Columbus, OH, Vol. 31, No. 2 (March 1962).

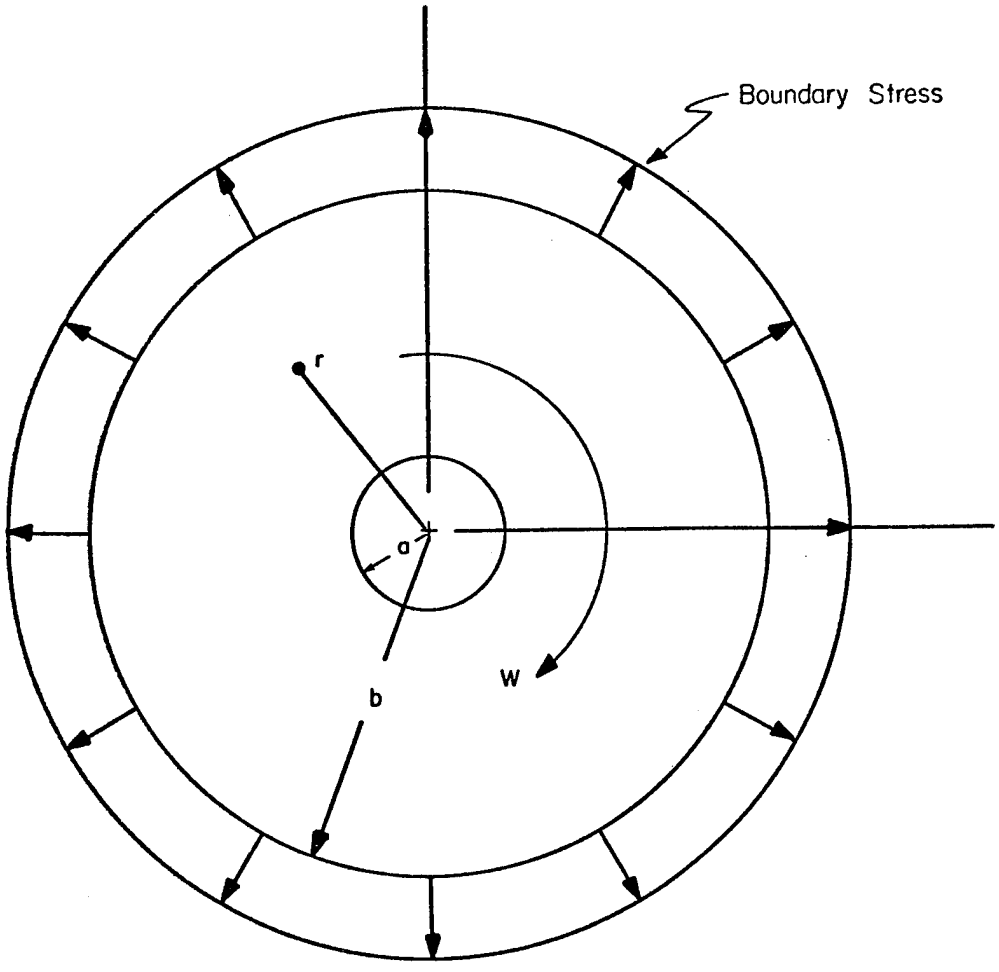
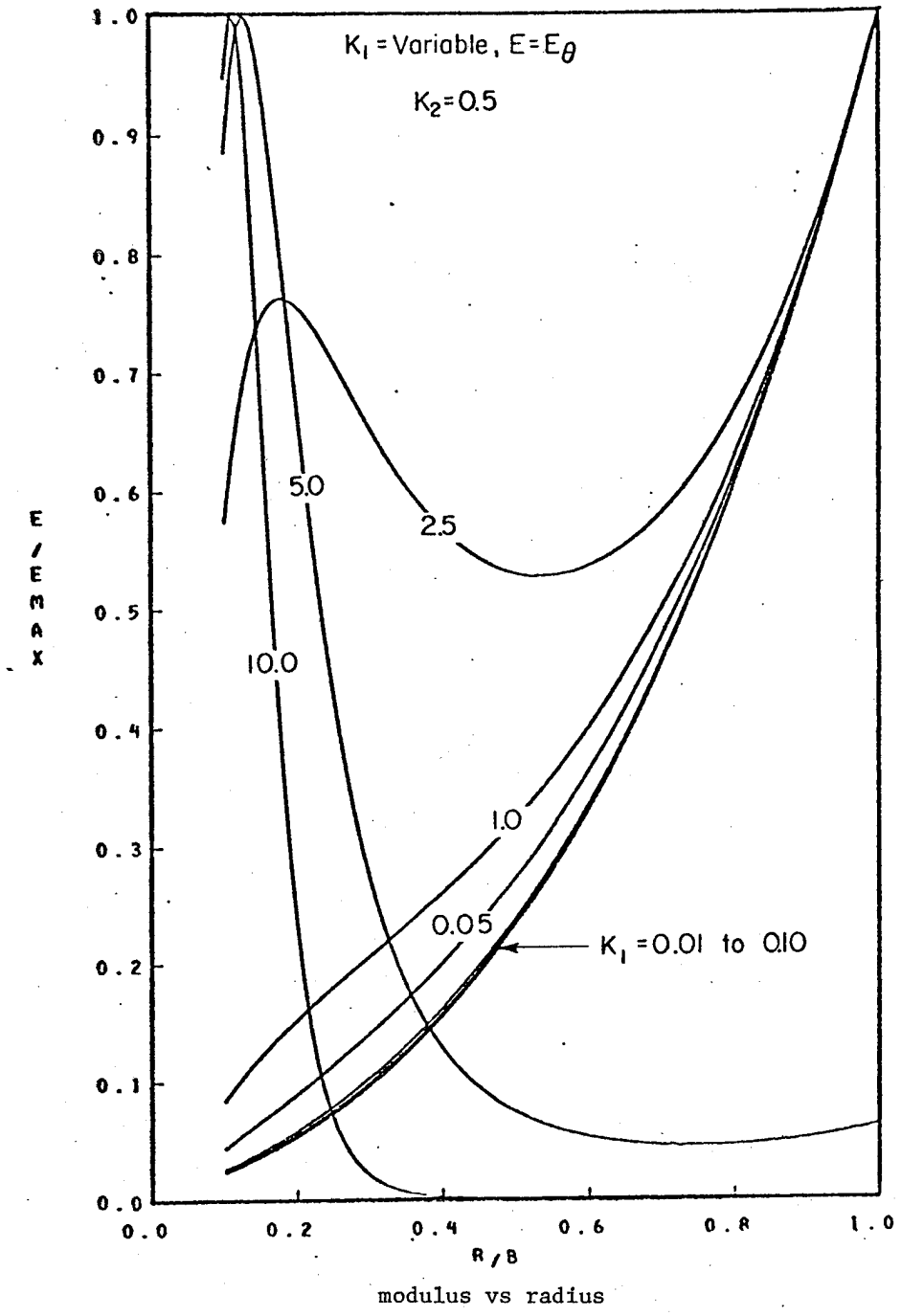


FIGURE 1. Rotating Annular Disk.



modulus vs radius

FIGURE 2. Modulus Variation for Rotating Orthotropic Disk With No Edge Loads, With σ_θ = Constant.

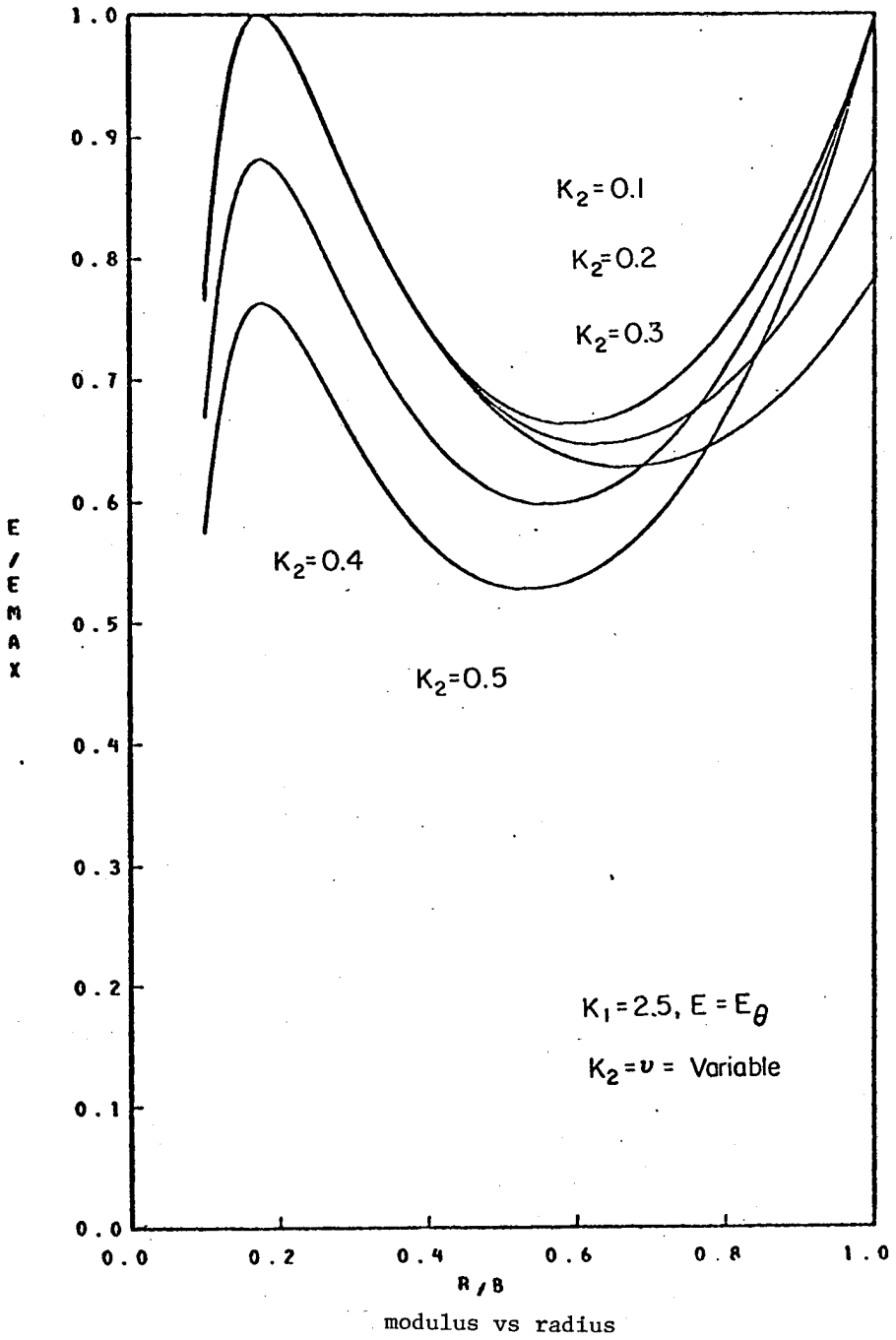


FIGURE 3. Modulus Variation for Rotating Orthotropic Disk, Orthotropic Ratio of 2.5 With No Edge Loads and σ_θ = Constant.

PANEL DISCUSSION

A Summary of the Technical Trends Versus R&D Needs

by

L. J. Lawson
Garrett AiResearch Manufacturing Company

The past two and one-half days of this symposium have served to give us all an update on flywheel technology. This afternoon I would like to briefly review the technical trends which have evolved in industry to provide flywheels to meet the needs of research and development programs.

Initially, the flywheel technology used was primarily based on one-piece metallic construction (often steel forgings) in rim or disk configurations. Because of safety considerations, these flywheels were often applied to military uses and have usually been made in small capacities or are operated at relatively low stress levels. An example is the Oerlikon Gyrobus flywheel rotor which was a 3000-lb forged steel rim with an energy density of only 2.7 Wh/lb. Relatively low-capacity, constant-stress disks of steel and titanium were built for aircraft and space applications by Rockwell International. Later modified constant-stress disks were built by Lockheed for a military helicopter hoist application in 1973 with rotor energy densities of 10 to 12 Wh/lb. The one-piece metallic flywheel continues to be used in many applications where only a small energy storage capacity is required. For example, the common internal combustion engine flywheels represent an excellent application of one-piece metallic flywheel technology. An exception to this is the relatively large flywheels (7.5 kwh/disk) being built by Rockwell International for MERADCOM.

The application of larger-capacity flywheels to transportation systems where complete burst containment is requisite led to the use of the axially-segmented metallic flywheel construction. This technique which has served to make safe, practical flywheels available for many applications probably represents an intermediate step in flywheel technology which may be largely superseded by composite flywheels in the future. The axially-segmented, fully contained steel flywheels which have been made and applied include the following examples: the 3.2-kwh flywheels used by Garrett in the NYMTA R-32 subway cars; the 4.5-kwh flywheels used in the UMTA Advanced Concept Train by Garrett; the 0.5-kwh flywheel in the University of Wisconsin Flywheel/Heat Engine Hybrid Car; and the 0.134-kwh flywheel for the U.S. Postal Service Flywheel/Battery Hybrid Jeep which were both made by Garrett. The axially-segmented steel flywheel has been shown to be well suited to transportation applications in its present form. Thus, the manufacture of axially-segmented steel flywheels is expected to continue for units up to 20 kwh capacity at least until the composite flywheel rotor technology matures.

The flywheel of the future for many applications, as we have seen at this symposium, is the composite rotor. This flywheel type, which can combine high-energy density with minimal containment requirements, is being developed by many sectors of industry to satisfy a wide-range of needs. Many different techniques of composite rotor design and fabrication have been tried with varying degrees of success as reported during the past two and one-half days. It is expected that this development activity will continue at an accelerated until fully practical, cost-effective composite rotor designs suitable for most flywheel applications evolve.

In the meantime, composite flywheels are being made to meet current research and development program needs. These flywheels show the present state of the art. The configuration which has been used for most of the development units is the multi-rim design which results in controllable levels of radial stress in the composite

rim. A relatively large composite flywheel (1.5 kwh) made by Garrett of Kevlar 49 has been tested at a peripheral speed of 2750 ft/sec. At this speed, the 72-lb flywheel (including hub) has an energy density of 21 Wh/lb. This flywheel is the first part of an assembly of axially bolted composite multi-rim flywheel segments with a total capacity approaching 30 kwh which is being built for the U.S. Army MERADCOM. A similar flywheel design technique is being employed by Garrett for a 1-kwh Kevlar flywheel for the ERDA Flywheel/Battery Hybrid car. This 44-lb, 23-in., diameter rotor operates at a peripheral speed of 2500 ft/sec with an energy density of nearly 23 Wh/lb.

In summary, industry using current flywheel technology is providing hardware which is satisfactory for many present requirements. However, the continuing increase in applications requiring higher and higher energy density along with the need for full containment has provided the impetus for extensive development activity directed toward improved composite rotors which have lower costs than metallic flywheels.

Outline of Areas in which Industry Can Act to Advance Flywheel Technology

by

Dr. D. E. Davis
Rocketdyne Division
Rockwell International

The subject that I am supposed to discuss during this afternoon's panel session is entitled "Outline of Area in Which Industry can Act to Advance Flywheel Technology." I would like to think that there is enough latitude allowed for presentations in this afternoon's panel discussion that I can modify the subject to read "Outline of Areas in Which Industry has Acted in the Past and is Presently Participating in Order to Advance Flywheel Technology." It is fairly obvious by reviewing the funding levels that have been experienced from both DoE, NASA and the Department of Defense that up until the government fiscal year 1974 the major portions of flywheel technology funding were supported by private industry and small company support groups. Examples that immediately come to mind are funding levels that have been expended from corporate resources at Rockwell International, Garrett AiResearch, U.S. Flywheel, William Brobeck and Associates, and Marshall Oil Company, the aforementioned of which are just a few of the nongovernment groups that have substantially supported flywheel technology up until the forementioned date.

It is important to note that a differentiation between advancing the flywheel technology as it exists today and what has occurred within the past five years is a representation of what can occur due to the significant technological advances that can occur in a highly interesting area. We must keep in mind that flywheel systems are a developing technology and still in its infancy with respect to high energy storage flywheel systems.

In order to assure ourselves that the area of advanced flywheel systems has evolved from the developing technolgy era to the developed technology realm of mechanical systems, several significant milestones must be successfully completed. As has been mentioned during the last three days of presentations, an important step is to identify the flywheel market itself. Errors have been made in the past and most assuredly will be made in the future with attempts to apply flywheels in areas which they are not realistically competitive. The statement has been made that "flywheel energy storage systems represent a brilliant engineering solution to energy storage, but with associated ridiculous economics". This statement becomes very obvious when one assesses the economic disadvantages of applying today's state-of-the-art flywheel systems to energy storage requirements for residential, photo-voltaic, wind-powered and private ground vehicle transportation systems. In order to be economically feasible for the aforementioned types of applications, significant economic and technological breakthroughs must be made in order to make the flywheel system competitive with state-of-the-art batteries and other low-cost energy storage systems. In order for industry to continue its advancement of flywheel technology, flywheel support systems must be aggressively pursued. The flywheel rotor system itself is fairly well defined and, except for the composite flywheel rotor, high energy storage rotor units in excess of 10 watt-hours per pound can be supplied with a very high confidence factor with respect to safety margins, cycle life capabilities, and performance characteristics.

The greatest amount of technological breakthroughs must occur in flywheel support areas such as bearings, seals, input-

output devices, containment approaches, and associated support components. In order for flywheels to be competitive with existing energy storage systems, low-loss, long-life bearing and seal components must be identified. The parasitic losses for existing flywheel systems dictate that normal half life rundown times in excess of 1-1/2 hours are very difficult to achieve. Although magnetic bearing systems have been vigorously pursued during the past several years for flywheel applications, the associated parasitic losses now being recognized with respect to magnetic bearing systems raise significant questions as to their viability as low-loss support component concepts.

Although Rockwell International has been vigorously pursuing composite rotor systems for the past several years, we are not convinced that the composite flywheel will eliminate the need for isotropic flywheels based on economics and acceptability criteria. Indications have been received during this conference that possibly the failures that have been experienced in composite rotors to date were based not primarily upon the rotor construction itself, but probably failure occurred due to a lack of understanding of the rotor dynamic characteristics of an isotropic rotating disk. It has been known for some time that a rotating disk experiences axial critical speed modes which, combined with radial critical speed problems, could create a situation which is extremely difficult, if not impossible, to predict and/or analyze. We believe that there are many severe problems that need to be solved before the composite rotor system will be totally acceptable, from both an economic and safety standpoint. The solutions to these problems we feel will be at least five years away, and possibly longer. On this basis the Rocketdyne Division of Rockwell International is vigorously making technological advances with respect to its isotropic rotor system as presented during this conference, although we are continuing our in-house efforts to support the composite rotor system.

It is very difficult to expect significant funding level increases in addressing the aforementioned problems associated with flywheels, especially when reports that seem to be less than objective are presented without taking into account the latest technological advances that have been made in flywheel systems. It is important that all reports dealing with the economic tradeoff assessments of flywheels versus other energy storage systems be carefully coordinated with the flywheel industry. To prepare studies without the benefit of the latest technology information does nothing but generate scorn and criticism from the flywheel industry and at the same time reduces the credibility of the reporting agency. A closer link between the flywheel industry, utilities and government organizations is strongly recommended in order that the aforementioned problems are not repeated.

Addressing once again the question, what can industry do to advance flywheel technology, we think that a first step toward posing an answer to this query would be to take a look in retrospect as to what has occurred in the past relating to the return on investment. Quite frankly, industry has assessed in the past that return on investment to be experienced from in-house flywheel resources being expended is practically a horror story. We believe feedbacks from organizations like Lockheed, William Brobeck and Associates, U.S. Flywheels, Marshall Oil Company, AiResearch, General Electric and other divisions of Rockwell International will confirm this.

In summary we must state that Rockwell International will continue to advance the technology with respect to flywheel systems although the cases for justifying this position are difficult to defend. There are very few potential customers standing in line waiting to buy flywheel systems, especially at the currently projected cost level of existing flywheel system development programs. We must continue above all to remember and keep in mind that flywheels are a developing technology. Applications will most assuredly be identified that heretofore were not even conceived. Therefore we strongly recommend that in order to induce industry to advance flywheel technology, the government supporting agencies must also realize that the question of return on investment is always in the forefront before company resources are committed. In order to enhance technological advancement in flywheels, the government agencies must act as a catalyst by identifying larger funding levels for both flywheel rotor and flywheel support components development programs.

Thank you.

Ways in Which Government Agencies

Can Act to Advance Flywheel Technology

by

Robert Taylor
Applied Physics Laboratory

The outline of my presentation is: the flywheel funding situation in the United States in 1977, the principles which should and do control government funding and what the government can do to advance flywheel technology.

The flywheel funding situation in the United States in 1977 is about 1/6th of the R&D funds for batteries. The total energy storage program in the U.S. received less than 1/2 of 1 percent of the total energy budget. Flywheel R&D received 29 thousandths of 1 percent of the total energy budget. Most of the flywheel R&D funding is for transportation vehicles as opposed to stationary flywheels for industrial energy storage and electric utilities.

Principles which should and do control government funding are proportional funding, parity funding, and positive feedback/negative feedback/funding response. Proportional funding is funding of a program relative to its importance and possible impact upon the problem. When we realize the importance of energy storage relative to efficient energy utilization and energy conservation, we realize that the whole energy storage program must be dramatically increased from less than 1/2 of 1 percent. The utilization of intermittent energy sources such as solar energy and wind energy, requires efficient low cost energy storage systems. Energy storage appears to have at least a 10 to 20% impact upon the whole energy problem. It should therefore be funded proportionally.

Similarly, flywheel R&D funding should also be dramatically increased from the present 29 thousandths of 1 percent. When we think of the many possible flywheel applications and the broad number of energy sources with which flywheels can be effectively utilized, 1% of the total energy funding seems far more appropriate than the present levels.

At present, the stationary flywheel for industrial energy storage and for the electric utilities is receiving very little funding; most of the flywheel funding is going for the transportation flywheel. When we realize the potential significance of the stationary flywheel, we must agree that funding should be forthcoming for this area. The Netherlands, Italy and Japan all have significant stationary flywheel programs. Why not the United States? I will mention a reason later.

Parity funding is funding equivalent technologies at approximately equal levels. When the government funds battery research at a level six times that of flywheels, they bias the results and the relative level of technology development for these two important areas of research and development. Greater balance in government funding is needed.

Another principle which does apply to funding is positive feedback and/or negative feedback. This concept is illustrated as follows:

Positive information transfer about a technology results in

Increased confidence about the technology which results in

Increased funding which results in

Increased positive results which results in

Increased positive information transfer which results in

Increased confidence, etc., etc.

This principle has inherently the chicken and the egg problem, therefore, in the very early beginnings of a program, short-term instability could generate either a positive feedback or negative feedback before the long-term results are actually determined. Unfortunately the negative

feedback response may have been excited for stationary flywheels by the 1976 report entitled: "An Assessment of Energy Storage Systems Suitable for Use by Electric Utilities".

This report rates flywheels last among the technologies considered which included: superconducting magnets, near-term lead acid batteries, thermal oil, advanced batteries, hydrogen, compressed air and hydro pumped storage.

Technology comparisons are very essential. However, they must be accomplished under very carefully formulated rules. One of the most important rules for technology comparisons is involvement of both the Protagonists and the Antagonists, without both the proponents and the detractors for each technology, an unblanced comparison is likely to occur. Unfortunately, it appears that no flywheel proponents were strongly involved in this widely distributed report on energy storage for electric utilities. This may help account for the lack of a significantly funded stationary flywheel program in this country.

What can the Government do? The government should increase its information dissemination about flywheel technology and possible flywheel applications. Information from this conference should be widely distributed within the government and to the general public. The government should fund energy programs more proportional to their expected impact upon the total energy problem. The government should fund equivalent technologies on a more equal basis and lastly, they should set strong ground rules for technology comparison studies. They should make certain that proponents and antagonists both have inputs into these important and necessary studies.

The Best Means for Commercializing Flywheels

by

David R. Phelps
General Electric Company

An examination of the history of commercializing federally-sponsored R&D in civilian markets brings quickly to mind the old quotation about what happens to those who do not learn from history. Certainly, in transit, the problems have become so readily apparent that DOT-UMTA has faced up to the situation as a crucial issue in R&D. The traditional mechanisms and market forces which would normally act to bring a new concept out of the laboratory and into production have broken down or have become grossly distorted.

There have historically been two basic scenarios in technology delivery/commercialization. There has been a purely private enterprise case, in which private investment derived from retained earnings funds R&D, which leads to a product which is sold commercially to interested customers, private or public. On the other hand, there has been the defense/aerospace case in which public investment derived from tax money funds R&D, which leads to a product which is bought by the Government - which was also the source of the R&D money.

In transit, we now have a "neither fish nor fowl" case. The market is not sufficient and tends not to have the necessary characteristics to allow the generation of much R&D money from profits, so most R&D comes from the Federal DOT. However, the customer is still largely non-Federal (Amtrak being an obvious non-transit exception), being variously O.E.M.s or operating authorities. Control over the authorities' choice is increasingly shifting to UMTA as a result of a number of factors. In time, it is conceivable that UMTA may operate with the "squadron" concept.

At the present, the funding/procurement system creates a situation in which the commercialization/delivery chain is missing the vital link which would join the researcher ultimately to the production customer. APTA has urged that this link be forged by creation of a mechanism in DOT/UMTA for completing the funding of commercialization. This immediately introduces the question of choosing which projects are to be carried through commercialization. APTA would have the choice be made by the ultimate user customers - the local authorities. This has much to commend it; one hopes the paternalism of the Federal establishment does not cause it to be rejected out of hand. No matter how the choice is made (some suggestions to assist will be made later in this discussion), the delivery process in transit needs significant improvement from the present state.

It is instructive - and perhaps even crucial - to examine the significance of the difference in the semantics attached to this process. DOT/UMTA speaks of it as "deployment", which Webster defines in almost exclusively military terms. ERDA chooses to use the term "commercialize", usually defined in a business management-for-profit context. The military concept, wherein the total resources available are spread out or arranged in a manner ordained by an overall controlling and coordinating authority, presupposes that this authority does indeed conceive of itself as the master controller of the entire industry. The significances of this attitude should not be lost on the manufacturers, local operators, and public. Lest this point be regarded as academic, it is precisely DOT/UMTA's track record in R,D&D which forces this conclusion. It is truly "deployment", not "commercialization", to force by mandate the results of R&D into production, whether justified by social concerns, the need for a return on the taxpayer's investment or any other rationale.

These activities, illustrating as they do the inevitable interconnection between politics and technology, do eventually reflect back on the question of the moment, commercializing flywheels. We are really talking about commercializing a social concern - energy conservation and pollution (noise and air) reduction. In most arenas there are competing technologies which also claim an ability to achieve these goals. Those funding the R&D - ERDA and DOT/UMTA - will eventually have to make hard decisions as to which horse to ride in the given races. Our judgment is that in some areas the flywheel will show itself to be the superior approach, and in some areas it will be inferior.

Dr. Schmitt of GE's R&D Center has pointed out recently that the nation can do what individual companies cannot, carry the options further in development before the final choice of which to commercialize. DOT/UMTA appears to believe in this, if their convictions and their funding constraints can stay in mesh.

Dr. Schmitt and his colleagues go on to offer four specific and practical suggestions in commercializing R&D. These come from the context of energy research but have more universal applicability.

"First, look for significant and measurable advantages of new developments". What is the potential market? What is the probability of success?

"Second, understand all the important factors contributing to the success of any new technology". Can it be manufactured and maintained? Is it safe? Will it appeal to the customers (at whatever level)?

"Third, consider the competitive alternatives to any new development -- including those which do not involve new technology". There may be a very good reason why the traditional technology exists at a given level.

"Fourth, realize that program selection is a continuous process, not a one-time decision which is irrevocable". Yesterday's choice may not be the right answer today.

There are general guidelines. Their applicability to commercialization of flywheels may not always give a clearcut answer, or even the presupposed answer.

Eventually, by whatever guidelines, the hard decisions must be made. Unfortunately, one immediately faces the corralory of Dr. Schmitt's Law of Energy Development, which can be stated that: assumptions about any new technology can be, and will be, extended just far enough to make the benefits/life cycle cost of that approach equal to the benefits/life cycle cost of competing approaches. That problem is presently beyond the state of the art. It can be minimized as a source of new and undesirable "history", however, by recognizing that so long as manifest social needs are met, the processes implicit in "commercializing" are preferable to the implications of "deployment".

1977 FLYWHEEL TECHNOLOGY SYMPOSIUM

LIST OF ATTENDEES

Robert K. Abbott
Lawrence Berkeley Laboratory
University of California
Berkeley, CA 94720

R. E. Allred
Sandia Laboratories
Division 5844
Albuquerque, NM 87115

Gerry B. Andeen
Stanford Research Institute
333 Ravenswood Avenue
Menlo Park, CA 94025

Maurice Audette
Transport Canada
1000 Sherbrooke St. West
P.O. Box 549
Place de I'Aviation
Montrea, Quebec, Canada

Arne J. Bang
Federal Railroad Administration
2100 Second St., S.W.
Washington, D.C. 20590

Kenneth J. Barber
Department of Energy
Washington, D.C. 20545

Thomas Barlow
Lawrence Livermore Laboratory
P.O. Box 808
Livermore, CA 94550

Raymond Beach
NASA - Lewis Research Center
21000 Brookpark Road/ M.S. 500-202
Cleveland, Oh 44135

Norman H. Beachley
University of Wisconsin
1513 University Avenue
Madison, Wisc 53706

K. R. Berg
Riggs Engineering Corp.
8245A Ronson Road
San Diego, CA 92111

Dr. Charles W. Bert
University of Oklahoma
School of AMNE, 865 Asp Avenue
Norman, Okla 73019

J. F. Biehl
Brunswick Corporation
1620 S. Lewis St.
Anaheim, CA 92803

Dr. Vernon Blackman
Systems, Science & Software
P.O. Box 1620
La Jolla, CA 92038

R. H. Braasch
Sandia Laboratories
Division 5715
Albuquerque, NM 87115

Gordon L. Bredenkamp
University of Pretoria
Hatfield
Pretoria, Rep. of South Africa 0002

W. M. Brobeck
William M. Brobeck & Associates
1235 Tenth St.
Berkeley, Ca 94710

Gregory J. Brown
FMC Corporation
P.O. Box 580
Santa Clara, CA 95050

Dallas E. Cain
General Electric Company
18 Edmel Road
Scotia, NY 12302

J. F. Campbell
Dept. of Transportation
Unit A
Second and V St. S.W.
Washington, D.C. 20590

John H. Carr
Boeing Engineering & Construction
Org. K-6180 MS/8K-50
P.O. Box 3707
Seattle, Washington 98124

Timothy Chen
University of Oklahoma
School of AMNE
865 Asp Avenue
Norman, Okla 73019

Dr. George Chang
Division of Energy Storage
Office of Conservation
Department of Energy
Washington, D.C. 20545

T. T. Chiao
Lawrence Livermore Laboratory
P.O. Box 808
Livermore, CA 94550

Edwin Chow
Jet Propulsion Laboratories
4800 Oak Grove Dr.
Pasadena, CA 91103

R. M. Christensen
Lawrence Livermore Laboratory
P.O. Box 808
Livermore, CA 94550

Linda L. Clements
Lawrence Livermore Laboratory
P.O. Box 808
Livermore, CA 94550

Merrill Cohn
San Francisco Municipal Railway
949 Presidio Avenue
San Francisco, CA 94115

A. A. G. Cooper
Babcock & Wilcox
P.O. Box 419
Alliance, Ohio 44601

D. D. Cox
Boeing Engineering & Construction
Org. K-6100 M/S 8K-39
P.O. Box 3707
Seattle, Washington 98124

Dr. Donald E. Davis
Rocketdyne Division
Rockwell International
6633 Canoga Avenue
Canoga Park, CA 91304

D. Douglas Davis
Lawrence Livermore Laboratory
P.O. Box 808
Livermore, CA 94550

A. G. DeClaire
General Motors Corporation
New Program Development Dept.
GM Technical Center
Warren, Mich 48090

Govind Deshpande
Jet Propulsion Laboratories
M.S. 169414
Pasadena, CA 91103

William E. Dick
Brunswick Corp.
4300 Industrial Avenue
Lincoln, Neb 68504

Peter R. Digiovanni
Missile Systems Division
Raytheon Company
M.S. CF1-19
Hartwell Road
Bedford, Mass. 01730

David B. Eisenhaure
The Charles Stark Draper Laboratory
555 Technology Square
Cambridge, Mass. 02139

Dr. Arthur G. Erdman
University of Minnesota
Dept. of M.E.
inneapolis, Minn. 55455

Anthony Escover
FMC Corporation
328 Brokaw Road
Santa Clara, CA 95052

Harold E. Evans
NASA/Goddard Space Flight Center
Greenbelt Road
Greenbelt, MD 20771

William Feng
Lawrence Livermore Laboratory
P.O. Box 808
Livermore, CA 94550

Ralph F. Foral
University of Nebraska
Department of Engineering Mechanics
Lincoln, NE 68588

Andrew A. Frank
Department of El. & Comp. Engineering
University of Wisconsin
Madison, Wisc 53706

Frank P. Fritchle
Beckman Instruments, Inc.
1117 California Avenue
Palo Alto, CA 94304

Giancarlo Genta
Istituto Motorizzazione
Politecnico 01
Torino, Italy

Frank Gerstle, Jr.
Sandia Laboratories
Division 5844
Albuquerque, NM 87115

Muzio Gola
Politecnico di Torino
Abruzci 25
Torino, Italy 10100

Hayden S. Gordon
William M. Brobeck & Associates
1235 Tenth Street
Berkeley, CA 94710

John M. Graham
California Brake & Clutch Parts
2607 Market St.
Oakland, CA 94607

Eugene Gray, Jr.
Owens Corning Fiberglas
U.S. 16
Granville, Ohio 43023

Fred S. Greene
Port Authority of NY & NJ
One Path Plaza
Jersey City, NJ 07036

Ronald J. Gripshover
Naval Surface Weapons Center
DF-10
Dahlgren, VA 22485

Dr. Bhagwati P. Gupta
Lord Kinematics
1635 W. 12th St.
Erie, PA 16512

David Hagen
University of Minnesota
Institute of Technology
124 Space Science Center
Minneapolis, Minn 55455

Burton D. Hatch
General Electric Company
Corporate R&D
Bldg. 37, Rm. 380
P.O. Box 43
Schenectady, NY 12301

Erich Hau
MAN
8 Munich Dachauer Str. 667
Munich, Germany

Edward S. Hickey
The Charles Stark Draper Laboratory
555 Technology Square
Cambridge, Mass. 02139

J. S. Hickey
Cryogenic Electric Programs
G.E. Company
Bldg. 37, Rm. 355
P.O. Box 43
Schenectady, NY 12301

P. Ward Hill
Hercules Incorporated
P.O. Box 210
Cumberland, MD 21502

Alfred Holzer
Lawrence Livermore Laboratory
P.O. Box 808
Livermore, CA 94550

Wilson Hull
U.S. Postal Service
11711 Park Lawn Drive
Rockville, MD 20852

Ken Ishii
Mitsui Engineering
611 West Sixth, Suite 2190
Los Angeles, CA 90017

Donald E. Johnson
Avco Systems Division
201 Lowell St.
Wilmington, Mass. 01887

J. J. Kelly
Union Carbide Corporation
Y-12 Plant
P.O. Box Y
Oak Ridge, Tenn 37830

C. E. Knight
Union Carbide Corporation
Nuclear Division (Y-12)
P.O. Box Y
Oak Ridge, Tn 37830

Gerhard Kraft
Ciba-Geigy Corporation
1004 Ciba Road
Burkburnett, TX 76354

Ken M. Kratsch
Science Applications, Inc.
201 W. Dyer Road, Unit C
Santa Ana, CA 92707

George E. Kunz
TRW (ESMD) R4-2036
1 Space Park
Redondo Beach, CA 90278

J. H. Laakso
Boeing Computer Services
M.S. 3N-18, P.O. Box 24346
Seattle, Washington 98124

Paul O. Larson
GMC Truck & Coach Division
660 South Boulevard, E.
Pontiac, MI 48053

L. J. Lawson
Airesearch Mfg. Corp.
2525 W. 190th St.
Torrance, CA 90509

R. M. Little
Boeing Engineering & Construction
Org. K-6180/M.S. 8K-50
P.O. Box 3707
Seattle, Washington 98124

Morello Lorenzo
Fiat Research Centre
145, St. Drosso
Torino, Italy 10100

Stewart N. Loud
Owens Corning Fiberglas
Fiberglas Tower
Toledo, OH 43659

Ebbe Lundgren
Division of Mechanics
Lund Institute of Technology
Fack, S-220 07
Lund 7, Sweden

E. L. Lustenader
General Electric Company
1 River Road, Bldg. 37, Rm. 311
Schenectady, NY 12345

Robert E. Medick
Ferro Corporation
8790 National Blvd.
Culver City, CA 90230

A. Keith Miller
Sandia Laboratories
Division 1281
Albuquerque, NM 87115

Alan R. Millner
M.I.T. Lincoln Lab
P.O. Box 73, Rm. C283
Lexington, Mass. 02173

Giuseppe Morandi
C.I.S.E.
P.B. 3g86
Milano, Italy

Hal M. Morgan
Airesearch Mfg. Corp.
2525 West 190th St.
Torrance, CA 90509

Dan K. McCoin
Bales-McCoin Research, Inc.
4401 Montana
El Paso, TX 79903

Molly A. McCormick
Owens Corning Fiberglas
Fiberglas Tower - T17
Toledo, Oh 43659

Prof. Alan T. McDonald
School of Mechanical Engineering
Purdue University
W. Lafayette, Ind. 47907

Henry C. McDonald
Associate Director for Engineering Support
Lawrence Livermore Laboratory
P.O. Box 808
Livermore, CA 94550

Dennis P. McGuire
Lord Kinematics
1635 W. 12th St.
Erie, PA 16512

Charles N. McKinnon, Jr.
Systems, Science & Software
P.O. Box 1620
La Jolla, CA 92038

Frederick McMurphy
Lawrence Livermore Laboratory
P.O. Box 808
Livermore, CA 94550

Thomas G. McNamara
Rockwell International
Rocketdyne Division
6633 Canoga Avenue
Canoga Park, CA 91304

Pius J. Nasvytis
Transmission Research, Inc.
10823 Magnolia Drive
Cleveland, OH 44106

Norman L. Newhouse
Brunswick Corporation
4300 Industrial Avenue
Lincoln, Neb 68504

Christer Nilsson
Lund Institute of Technology
Division of Mechanics
220 07 Fack, Sweden

T. A. Norman
U.S. Postal Service
11711 Parklawn Drive
Rockville, MD 20852

Lawrence G. O'Connell
Lawrence LIvermore Laboratory
P.O. Box 808
Livermore, CA 94550

Henry B. Odom III
Naval Surface Weapons Center
Dahlgren, VA 22448

Laura L. Omohundro
Kinergy R&D
Division of Marshall Oil Company
P.O. Box 1128
810 South Main St.
Wake Forest, NC 27587

Donald W. Oplinger
Mechanics of Materials Division
Department of the Army
Materials & Mechanics Research Center
Watertown, Mass 02172

Richard E. Ott, Executive Director
Rodale Resources Division
576 North St
Emmaus, PA 18049

Lynn S. Penn
Lawrence Livermore Laboratory
P.O. Box 808
Livermore, CA 94550

David R. Phelps, Manager
Proposals & Advanced Engineering
General Electric Company
2901 East Lake Road
Erie, PA 16531

Bruno Picasso
Universita Di Cagliari
Piazza D'Armi
Cagliari, Italy 09100

Jim Pope
Science Applications, Inc.
201 W. Dyer Road, Unit C
Santa Ana, CA 92707

Pierre C. Poubeau
Societe Nationale Industrielle
Aerospatiale BP 2
Les Mureaux
France 78130

Terrance Quick
Lawrence Livermore Laboratory
P.O. Box 808
Livermore, CA 94550

D. W. Rabenhorst
Applied Physics Laboratory
Johns Hopkins University
Johns Hopkins Road
Laurel, MD 20810

Philip W. Randles
Science Applications, Inc.
201 West Dyer Road, Unit C
Santa Ana, CA 92707

A. E. Raynard
Garrett Airesearch Mfg. Corp.
2525 W. 190th St.
Torrance, CA 90509

E. David Reedy
Sandia Laboratories
Division 5844
Albuquerque, NM 87115

Theodore J. Reinhart, Jr.
Air Force Materials Laboratory
MBC
WPAFB, OH 45433

J. A. Rinde
Lawrence Livermore Laboratory
P.O. Box 808
Livermore, CA 94550

Edoardo Robecchi
Industrie Pirelli S.P.A.
Centro Studi Speciali
P. zza Duca D'Aosta 3
Milan, Italy 20124

Samuel Romano
General Motors Corporation
Transportation Systems Division
General Motors Technical Center
Warren, MI 48090

A. S. Rubenstein
General Electric Company
1 River Road
Schenectady, NY 12345

Alan D. Sapowith
AVCO
Lowell Industrial Park
Lowell, Mass 01851

David L. Satchwell
Airesearch Mfg. Co.
2525 W. 190th St.
Torrance, CA 90509

David R. Schneider
436 No. White Road
San Jose, CA 95127

Joe Schurb
3M Company
3M Center, Bldg. 230-1F
St. Paul, Minn 55101

Martin W. Schwartz
Lawrence Livermore Laboratory
P.O. Box 808
Livermore, CA 94550

Richard D. Scott
RCA Corporation
Box 887
Camden, NJ 08101

David Shansky
Raytheon Corporation
Missile Systems Division
M.S. 24-75 Hartwell Road
Bedford, Mass 01730

David C. Sheridan
General Motors Research
Power Systems Department
Warren, MI 48090

Thomas R. Small
Applied Physics Laboratory
Johns Hopkins University
Johns Hopkins Road
Laurel, MD 20810

B. B. Smith
Union Carbide
116 Caldwell Drive
Oak Ridge, Tn 37830

M. J. Smith
British Leyland Truck & Bus
Leyland, Preston
Lancaster, England

Dennis Sobolik
Sperry Flight Systems
P.O. Box 21111, Mail Stop 1016
Phoenix, AZ 85036

J. G. Soudry
Goodyear Aerospace Corp.
1210 Massillon Road
Akron, OH 44315

Curtis H. Spenny
U.S. DoT/TSC
Kendall Sq.
Cambridge, Mass. 02142

Ellis Stair
Boeing Engineering & Construction
P.O. Box 3707
Seattle, Wash. 98124

R. G. Stone
Lawrence Livermore Laboratory
P.O. Box 808
LIvermore, CA 94550

B. E. Swartout
U.S. Flywheels, Inc.
1882 McGaw Ave-ue
Irvine, CA 92714

James H. Swisher
Department of Energy
20 Mass Avenue N.W.
Washington, D.C. 20545

Robert J. Taylor
Applied Physics Laboratory
Johns Hopkins University
Johns Hopkins Road
Laurel, MD 20810

Richard H. Toland
Lawrence LIvermore Laboratory
P.O. Box 808
Livermore, CA 94550

Dennis A. Towgood
Airesearch Mfg. Co.
2525 W. 190th St.
Torrance, CA 90509

David Ullman
Union College
Department of M.E.
Steinmetz Hall
Schenectady, NY 12308

Milton Vagins
Battelle Pacific N.W. Laboratories
P.O. Box 999
Richland, WASH 99352

John M. Vance
University of Florida
Mechanical Engineering Department
Gainesville, Fla 32607

M. Van Zanten
E.C.N.
3 Wetern Duinwes
Petten, Netherlands

Henry R. Velkoff
Ohio State University
Dept. of M.E.
206 W. 18th Avenue
Columbus, OHio 43210

Rudy Vergara
Battelle Columbus Labs
505 King Avenue
Columbus, OH 43201

C. Alfred Versailles
Transport Canada
Research & Development
1000 Sherbrooke St. W.
P.O. Box 549
Montreal, Quebec H3T1B5

William O. Wilkinson
Applied Physics Laboratory
Johns Hopkins University
Johns Hopkins Road
Laurel, MD 20810

Robert O. Woods
Sandia Laboratories
Org. 5715
Albuquerque, NM 87115

Edward M. Wu
Lawrence Livermore Laboratory
P.O. Box 808
Livermore, CA 94550

Dr. DeMarquis D. Wyatt
National Research Council
2101 Constitution Aveue N.W.
Washington, D.C. 20418

Tsuneji Yada
Mechanical Engineering Laboratory
12-1 Igusa 4-Chome
Suginamiku
Tokyo 167, Japan

Francis C. Younger
William M. Brobeck & Associates
1235 Tenth St.
Berkeley, CA 94710

Dr. John Zickel
Department of M.E.
California State University
6000 J Street
Sacramento, CA 95819

Dr. Edward S. Zorzi
General Electric Company
Corporate R&D
1 River Road
Schenectady, NY 12345

Ernest W. Schlieben
Von Research
681 South Broad St.
Trenton, NJ 08611

OUTLINES OF THE ITALIAN PROGRAMME FOR THE DEVELOPMENT OF KINETICS ENERGY STORAGE

Giuseppi Morandi
Centro Informazioni Studi Esperienze
Milano, Italy

This material was received after the balance of these Proceedings was prepared for publication; it is included here as an addendum.

In 1976 the Italian National Research Council began a three-year R&D programme (1977-79) in the field of energy-saving technologies. Among many other aspects, the programme covers also the flywheels developments. The relevant activities are grouped in two different projects: the former dedicated to mobile (transport), and the latter to stationary applications (load-leveling, and peaking supply), and involving industries as well as R&D organizations and University departments.

The present outlines refer to the second project (stationary applications).

1. Flywheels for Stationary Application

This project aims at achieving the knowledge needed to correctly evaluate the potential of the kinetic energy storage as a load leveling or peaking supply device for industrial applications (workshops, electric substations, etc.).

The total effort foreseen on the three years R&D plan is the order of 1.5×10^6 $ (at 1976 values).

The general programme of the project covers the following main areas:

--flywheel development

The activities are in progress for materials evaluations, design methods, and experimental tests on small and medium size flywheel. The materials considered are mainly: composites (epoxy or rubber matrices; kevlar, glass S and glass K as fibres), and bare filaments (kevlar, steel wires and coated fiberglass) in the subcircular arrangements. Subcircular type of flywheels have been recently successfully tested up to an energy density in the range of 30-40 wh/kg. In the next year it is foreseen also the construction of some large flywheel (in the range of some tons in weight).

-- sealing and bearing systems

As sealing system the ferromagnetic fluids is now considered. The proper laboratory tests and performance analysis are at present in progress; the pneumostatic, oleostatic and magnetic bearing are currently investigated in view of establishing the relative performances.

-- electric motors/generators

Three different electric systems to be coupled to the flywheel units are investigated: syncronous, asyncronous and homopolar motor-generators. The later one is considered for the peaking supply system, where high power is required associated to lower values of energy release: in such case the rotor of the motor acts as the flywheel itself, thus minimizing all the mechanical problems as sealed penetrations, connections between electric actuator and flywheel.

Three different prototype units (comprehensive also of the relevant

electronic regulation systems) are currently in the design or construction phase:

a) a syncronous motor, with a power of 100 kW

b) an asyncronous motor, with a power of 20 kW

c) an homopolar unit, with a storage energy capability of about 2 MW

the construction of these prototypes is foreseen within the next year, and the relevant experimental evaluation shall be started immediately afterwards.

-- complete demonstrative units

One of the programme goals is to realize a number of complete prototype units, employing the electric systems presently under construction. Those units will be connected to properly chosen dwells, in view of achieving an overall operational esperience.

Presently the activityes on this item are focused on setting up the relevant specifications for the whole assembly, taking into account the experimental goal, the identification of suitable loads and the size and performances of the flywheels which will be possible on a realistic base, to build around the end of 1978.

-- analysis of the flywheel technology's potential

An evaluation of the potential related to flywheel's technology is being presently started in view of completing the activities with an assessment of the most promising areas where to continue the effort beyond the terms of the present programme.

For most of the abovementioned items, useful cooperative interactions are already in progress between the organizations which are in charge of the R&D activities and some foreign centres.

Further and toughter contacts among the various experts from different countries and organizations, that hopefully will be encouraged by a better knowledge of what it is in progress on this subject, will surely help in developing this technology. The present very brief summary of the Italian activities is also aimed at this goal.

2. Participating Organizations

Various firms, research centres and university departments are participating in this project. The organizations involved, with the relevant task are as follows:

R&D Center:	CISE (Centro Informazioni Studi Esperienze) Milano	General Coordination Flywheel design, complete prototype systems construction & evaluation, analysis of flywheel technology's potential.
	RTM (Ist.per le Richerche di Tecnologie Meccaniche) Vico Canavese (Torino)	Seals and bearing development, construction and testing.
Industries:	PIRELLI SpA, Milano	Flywheel development, construction and testing (subcircular, composite with elastomeric matrix)
	FIAT SpA, Torino	Flywheel development, construction and testing (composite with epoxy matrix)
	ANSALDO SpA, Genova	Syncronous electric motor-generator and controls: development, construction and testing
	ENEL (Ente Nazionale per l'Energia Elettrica) Milano	Support to the analysis of the flywheel technology's potential
University Dept.:	Ist.Motorizzazione Politechnico di Torino	Flywheel design & Testing
	Ist.Meccanica Universita Cagliari	Experimental stress analysis of small scale models (spinning tests)
	Ist. Tecnologie Universita Napoli	Materials tests and evaluations
	Ist.Meccanica e Costr. Macchine Politecnico Milano	Experimental techniques for spinning tests
	Ist. Elettronica Universita Pavia	Asyncronous electric motor-generator and controls development, construction and testing.
	Ist. Elettronica Universita Padova	Homopolar electric motor-generator and controls development construction and testing.